FDD/552-89/001
CSC/TR-89/6001

Goddard Trajectory Determination System (GTDS)

Mathematical Theory

Revision 1

July 1989

Edited by

A. C. Long
J. O. Cappellari, Jr.
Computer Sciences Corporation

and

C. E. Velez
A. J. Fuchs
National Aeronautics and Space Administration/
Goddard Space Flight Center

Flight Dynamics Division
Code 550

Developed Under the Direction of R. Pajerski (GSFC/Code 552)

Through R. Luczak
Task 213
Contract NAS 5-31500
Computer Sciences Corporation

ACKNOWLEDGMENT

Acknowledgment is given to the efforts of the following people who contributed to this document or to the previous mathematical description documents cited. Affiliation with Goddard Space Flight Center (GSFC) or Computer Sciences Corporation (CSC) at the time of production of the specific document is indicated.

Goddard Trajectory Determination System (GTDS) Mathematical Theory (Revision 1), FDD/552-89/0001 and CSC/TR-89/6001, A. C. Long, J. O. Cappellari, Jr., C. E. Velez, and A. J. Fuchs (editors), July 1989

GSFC	CSC		
R. A. Gordon	D. E. Boland	T. Lee	E. J. Smith
R. S. Pajerski	J. O. Cappellari, Jr.	A. C. Long	D. B. Squier
	J. B. Dunham	R. W. Luczak	

Mathematical Theory of the Goddard Trajectory Determination System, Goddard Space Flight Center, X-582-76-77, J. O. Cappellari, Jr., C. E. Velez, and A. J. Fuchs (editors), April 1976

GSFC		CSC	
J. A. Behuncik	R. S. Pajerski	C. L. Ayres	G. P. Spears
A. J. Fuchs	C. E. Velez	J. O. Cappellari, Jr.	E. J. Smith
T. J. Grenchik		A. C. Long	H. E. Stull
F. E. McGarry		D. H. Novak	W. E. Wagner
G. D. Mistretta		J. S. Reece	W. H. Wooden

Preliminary Orbit Computation System (OCS) Mathematical Specifications, Computer Sciences Corporation, CSC/SD-83/6069, J. O. Cappellari, Jr., R. E. Shanklin, Jr., and E. J. Smith, September 1983

GSFC	CSC		
C. E. Doll	D. E. Boland	J. R. Kuhn	C. Raymond
J. Teles	B. C. Brown	T. Lee	M. V. Samii
	J. O. Cappellari, Jr.	S. Y. Liu	R. E. Shanklin, Jr.
	J. B. Dunham	A. C. Long	H. M. Sielski
	D. F. Eggert	A. S. Lyubomirsky	E. J. Smith
	B. T. Fang	F. Messing	R. L. Smith
	T. L. Gunther	B. C. Morse	D. G. Soskey
	C. Huang	Y. Nakai	S. R. Waligora

PREFACE

This document is the first revision to the National Aeronautics and Space Administration (NASA)/Goddard Space Flight Center (GSFC) document X-582-76-77, published in April 1976, which was written by Computer Sciences Corporation (CSC) and GSFC personnel and edited by J. O. Cappellari, Jr. (CSC), C. E. Velez (GSFC), and A. J. Fuchs (GSFC).

This revision reflects the operational version of GTDS associated with Release 3 of the Trajectory Computation and Orbital Products System (TCOPS). This release became operational in 1988.

ABSTRACT

This document presents a description of the mathematical theory underlying the Goddard Trajectory Determination System (GTDS) and includes an overview of the system capabilities. The basic mathematical formulations presented include mathematical descriptions of the coordinate and time systems, perturbation models, orbit propagation techniques, numerical integration techniques, measurement models, statistical estimation methods, and launch and early orbit determination techniques.

TABLE OF CONTENTS

TABLE OF CONTENTS (Cont'd)

CHAPTER 3 (Cont'd)

TABLE OF CONTENTS (Cont'd)

CHAPTER 3 (Cont'd)

TABLE OF CONTENTS (Cont'd)

CHAPTER 4 (Cont'd)

TABLE OF CONTENTS (Cont'd)

CHAPTER 5 (Cont'd)

TABLE OF CONTENTS (Cont'd)

TABLE OF CONTENTS (Cont'd)

CHAPTER 7 (Cont'd)

TABLE OF CONTENTS (Cont'd)

CHAPTER 8 (Cont'd)

TABLE OF CONTENTS (Cont'd)

CHAPTER 9 (Cont'd)

TABLE OF CONTENTS (Cont'd)

LIST OF ILLUSTRATIONS

LIST OF ILLUSTRATIONS (Cont'd)

Figure (Cont'd)

LIST OF TABLES

CHAPTER 1—INTRODUCTION

This publication presents a description of the mathematical theory for the Earth/lunar/interplanetary Goddard Trajectory Determination System (GTDS). GTDS is a multipurpose computer system designed

> *"to provide operational support for individual Earth, lunar, and planetary space missions and for the research and development requirements of the various projects of the NASA/Goddard Space Flight Center scientific community"* (Reference 1)

This orbit determination system includes many of the capabilities of previous orbit determination programs developed by the Goddard Space Flight Center (GSFC) (References 2 and 3).

GTDS is, by its very nature, an evolutionary system. The first document describing the mathematical theory of GTDS (Reference 4) corresponded to a developmental version of the system. The mathematical theory for the version of GTDS implemented at GSFC in the spring of 1976 was documented in Reference 5. Since then, GTDS has evolved through several operational versions, and a Research and Development (R&D) version has been developed to permit evaluation of promising methods for operational, nonroutine, and highly precise orbit determination. This document, which is a revision of Reference 5, corresponds approximately to GTDS Release 3.0, which was implemented at GSFC in the spring of 1988 (References 6 and 7). As additional capabilities are added to the system, this document will be updated or revised.

This document is not intended to represent a set of mathematical specifications for developing the GTDS software, but rather it is a description of the basic mathematical formulations used in GTDS. The format varies somewhat from section to section, ranging from a straightforward presentation of the basic equations used in the program to a tutorial approach that delves into some of the underlying theory, depending on the topic under discussion.

In addition to describing the basic mathematical formulations of this particular system, this document provides the reader with a comprehensive overview of the key physical and mathematical models required by orbit determination systems and describes the results of various evaluations and improvements developed at GSFC as a result of years of operational orbit determination experience.

An overview of GTDS is presented in Chapter 2. This overview includes a discussion of the programs available in GTDS, system capabilities, and schematic diagrams of the differential correction, ephemeris generation, data simulation, and error analysis processes, along with an indication of which chapters in this document contain the algorithms associated with each function.

Chapter 3 defines the coordinate and time systems necessary to accurately model the spacecraft's dynamic motion and tracking measurements. Chapter 4 describes the acceleration models that constitute the Cowell equations of motion and the variational equations. Chapter 5 gives the formulation of the orbital equations of motion, including general perturbation and special perturbation methods. Chapter 6 describes the numerical integration of the equations of motion and variational equations, while Chapter 7 describes the measurement models and systematic error corrections applied to the measurements. Chapter 8 contains a description of the estimators and statistical models, and Chapter 9 presents early orbit techniques that can be used to obtain an estimate of the vehicle state from early tracking measurements.

Several appendixes are included in this document. Appendix A gives functional descriptions of various tracking systems and preprocessing techniques. A detailed description of the time elements used in the regularized equations of motion can be found in Appendix B, and Appendix C contains a rigorous discussion of the conversion of Doppler measurements to range rate. Appendix D presents information on typical a priori standard deviations and dynamic weighting factors for several observation types, and Appendix E presents a derivation of the matrix identities associated with the sequential estimation process.

At the end of each section or appendix, references specific to that section/appendix are listed. Following the last appendix, glossaries and an index are provided for the convenience of the reader.

This mathematical theory document is specifically directed to the analyst. The *GTDS User's Guide* (Reference 6) is directed to a general user audience, which includes analysts, programmers, and data technicians. Although a brief description of the system is provided in the user's guide, the principal contents are specific requirements for using the system.

NOTATION CONVENTIONS

Major notation conventions used in the text and equations throughout this document (unless otherwise noted) are as given below.

- $\bar{\ }$ = Vector
- $\hat{\ }$ = Unit vector
- $\dot{\ }$ = First derivative or velocity
- $\ddot{\ }$ = Second derivative or acceleration
- $\mathbf{R}, \dot{\mathbf{R}}$ = Position and velocity with respect to the inertial coordinate system (this coordinate system is defined in Section 3.2)

$\mathbf{r}, \dot{\mathbf{r}}$ = Position and velocity with respect to the true of date coordinate system (this coordinate system is defined in Section 3.2)

REFERENCES

1. Goddard Space Flight Center: 1970, *Functional Requirements for the Lunar/Planetary Orbit Determination Subsystem of the Goddard Trajectory Determination System.*

2. Velez, C. E. and Brodsky, G. P.: 1969, *GEOSTAR-I, A Geopotential and Station Position Recovery System*, Goddard Space Flight Center Report X-533-69-544, December 1969.

3. Goddard Space Flight Center: 1971, *Definitive Orbit Determination Operating System Description, Edition II*, Goddard Space Flight Center Report X-544-71-296, July 1971.

4. Wagner, W. E. and Velez, C. E. (editors): 1972, *Goddard Trajectory Determination System Mathematical Specifications*, Goddard Space Flight Center Report X-552-72-244, March 1972.

5. Cappellari, J. O., Jr., Velez, C. E., and Fuchs, A. J. (editors): 1976, *Mathematical Theory of the Goddard Trajectory Determination System*, Goddard Space Flight Center Report X-582-76-77, April 1976.

6. Squier, D. and Byers, K.: 1987, *Goddard Trajectory Determination System (GTDS) User's Guide, Revision 2*, Computer Sciences Corporation Report CSC/SD-85/6738, December 1987.

7. Bacon, B. and Squier, D.: 1988, *System Description for the Trajectory Computation and Orbital Products System (TCOPS) Release 3 Goddard Trajectory Determination System (GTDS) Modifications*, March 1988.

CHAPTER 2—GTDS OVERVIEW

Orbit determination in GTDS involves a complex mathematical process that combines the disciplines of orbital dynamics, measurement modeling, and estimation theory. This process is implemented through the use of several separate programs, which are briefly described in Section 2.1.

The capabilities of the system are discussed in Section 2.2. These capabilities include trajectory generation, measurement modeling, and estimation techniques. Also included is a discussion of the early orbit determination process, which allows a crude initial estimate of the orbit to be obtained from early tracking data. In addition, the orbit determination system combines capabilities that are frequently useful in mission analysis studies when executed independently; GTDS has been provided with several modes of operation to permit utilization of these separate capabilities.

The acceleration sources that are accounted for in the GTDS dynamic model are described in Section 2.3, while Section 2.4 discusses near-realtime operation.

2.1 GTDS PROGRAMS

To meet the varying demands imposed upon the system by operational support of the research and development requirements of various projects, GTDS includes the following programs:

- Differential Correction Program
- Ephemeris Generation Program
- Ephemeris Comparison Program
- Filter Program (not currently available)
- Early Orbit Determination Program
- Data Simulation Program
- Error Analysis Program
- Data Management Program
- Permanent File Report Generation Program
- Thrust Parameter Modeling Program

This document presents the mathematical models and procedures for all of these programs except the Permanent File Report Generation Program. A brief description of each of the programs is given in the remainder of this section.

2.1.1 DIFFERENTIAL CORRECTION PROGRAM

The primary purpose of the Differential Correction Program is to estimate the satellite orbit and associated parameters. The estimation algorithm used in the Differential

Correction Program is called the weighted least-squares with a priori covariance algorithm or the Bayesian weighted least-squares algorithm. It minimizes the sum of the squares of the weighted residuals between the actual and computed measurements, while simultaneously constraining the model parameters to satisfy the a priori conditions to within a specified uncertainty. Both first- and second-order statistics (i.e., the mean and covariance matrices) are determined for the estimated variables.

2.1.2 EPHEMERIS GENERATION PROGRAM

The function of the Ephemeris Generation Program is to compute, from prescribed initial conditions, the value at a specified time of the vehicle state and, optionally, the state partial derivatives. In order to meet varying precision and efficiency requirements, several orbital theories have been provided, ranging from a first-order analytic theory to a high-precision Cowell-type numerical integration. The state partial derivatives can be computed by precision numerical integration of the variational equations. The state partial derivatives with respect to the initial state (i.e., the state transition matrix) can optionally be generated using a two-body analytic approximation.

2.1.3 EPHEMERIS COMPARISON PROGRAM

The Ephemeris Comparison Program compares two input ephemerides. The comparison can be specified over a particular arc or over the arc of overlap between the ephemerides. The radial, along-track, and cross-track differences are computed and output.

2.1.4 FILTER PROGRAM

The Filter Program, which is not currently available in the operational version of GTDS, provides an alternative to the Differential Correction Program for estimating the satellite orbit and associated parameters. The Filter Program contains sequential estimation algorithms. Sequential filters differentially correct (update) the satellite state recursively at each measurement point processed. As a result, these methods are referred to as sequential processing methods, in contrast to the batch processing method used in the Differential Correction Program. Other elements of the Filter Program, such as model parameters and measurement handling, are the same as in the Differential Correction Program.

2.1.5 EARLY ORBIT DETERMINATION PROGRAM

The Early Orbit Determination Program is designed to determine approximately an initial estimate of a satellite orbit when there is no a priori estimate available to start a differential correction process. The program provides three methods for achieving this: (1) the Gauss Method, (2) the Double R-Iteration Method, and (3) the Range and Angles Method.

2.1.6 DATA SIMULATION PROGRAM

The Data Simulation Program computes simulated tracking measurements of a spacecraft from specified ground sites. The simulated data are generated for specified measurement

intervals and sampling frequencies. The program also has the capability to simulate attitude sensor measurements. Optionally, random and bias errors can be added to the measurements. Measurements can also be modified to account for the effects of atmospheric refraction, antenna mount errors, transponder delays, and signal propagation time delays.

2.1.7 ERROR ANALYSIS PROGRAM

The GTDS Error Analysis Program provides the capability of analyzing the effect of tracking error uncertainties, solve-for vector uncertainties, and consider parameter uncertainties associated with a specified orbit and station-dependent tracking schedule. Since the Error Analysis Program functions are similar to those performed in the Differential Correction and Data Simulation programs, these programs share common mathematical processing subroutines, input processors, and data management options. The Error Analysis Program features that are common to the Differential Correction and Data Simulation programs include the use of a tracking schedule, selection of tracking stations, selection of measurement types, specification of measurement standard deviations and weights, and specification of the a priori state covariance matrix. Construction of the normal matrix and the use of the consider mode to account for the effect of consider parameter statistics on the covariance matrix of the solve-for vector are performed in the same manner as in the Differential Correction Program.

2.1.8 DATA MANAGEMENT PROGRAM

The primary function of the Data Management Program is to create working files of data to be used by other programs in GTDS.

2.2 SYSTEM CAPABILITIES

The key elements of the GTDS differential correction (DC) process are shown schematically in Figure 2-1. The chapters in this document that contain the algorithms associated with each function are indicated in this and succeeding figures in Chapter 2. Both the batch and sequential modes for estimating the orbital state are shown. The use of common modules to perform key functions is basic to the GTDS structure. For this reason, algorithms derived in this document are applicable to many areas of GTDS. As shown in Figure 2-1, an estimate of the orbital state at an initial epoch must first be specified a priori from an independent source. Measurements to be processed are retrieved from a file, and an orbit generator determines the satellite trajectory (position and velocity) at times corresponding to the measurement sampling times. In addition, at each sampling time, estimates of the measurements are computed as a function of the satellite trajectory.

In a batch mode, this process is performed sequentially from data time to data time and constitutes the inner loop of the process (see Figure 2-1). In addition to the computed measurements, partial derivatives of the measurements with respect to the epoch state

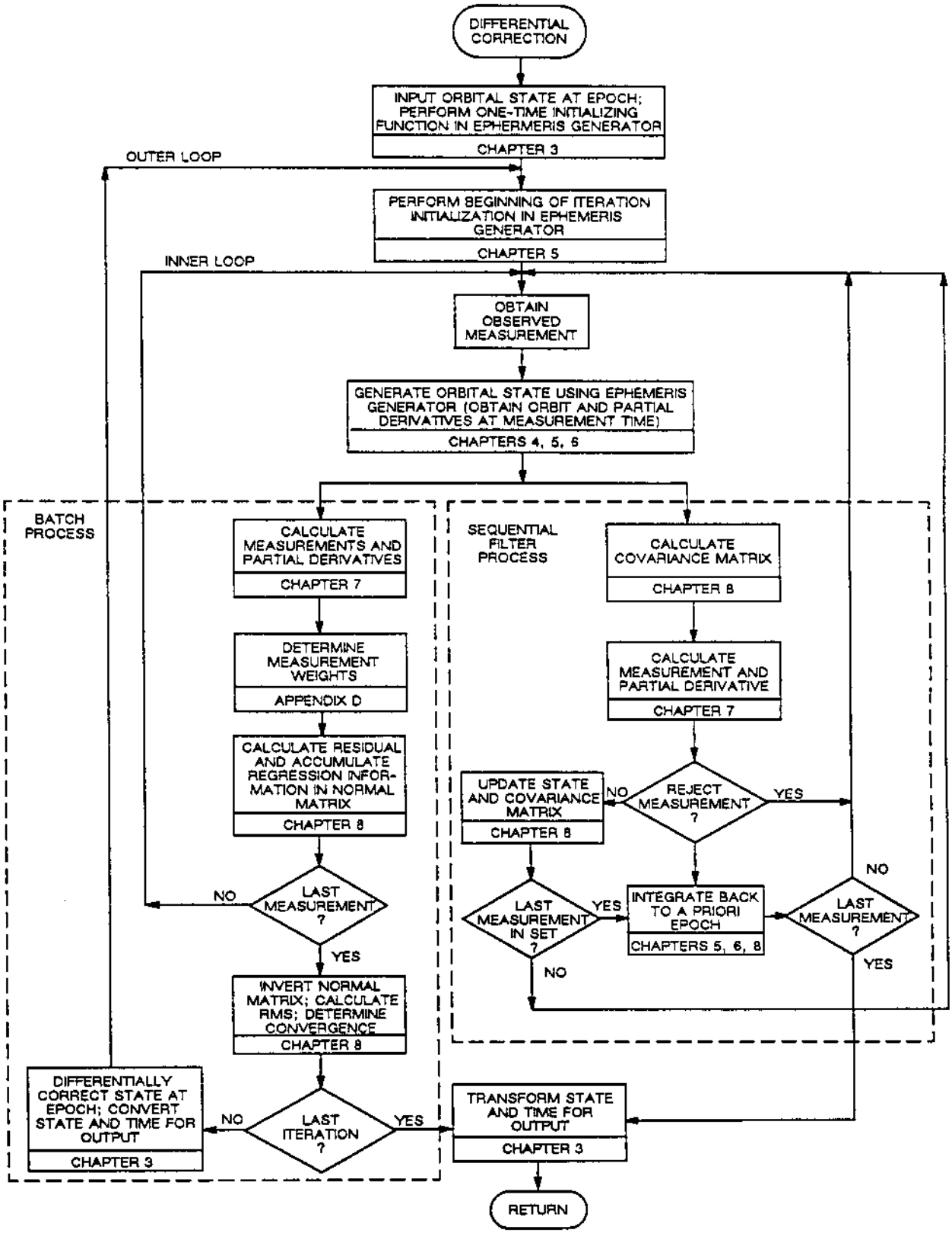

Figure 2-1. Schematic Diagram of the Differential Correction Process

must be computed in the inner loop for use in the statistical regression process. Upon completion of the inner loop processing at the measurement times, the epoch state is differentially corrected by means of a Bayesian weighted least-squares method. The updated epoch state is then used to perform another inner loop iteration. Repeated iteration of the inner loop, culminating each time with a differential correction to the epoch state, constitutes the outer loop. As the iterations proceed, the epoch state converges to the Bayesian weighted least-squares solution to the nonlinear orbit determination problem.

In the sequential filter mode, a single loop is used to perform these measurement calculations and partial derivative calculations, and the state and covariance matrices are updated after each measurement to obtain the final state. It should be noted that Figure 2-1 depicts functional relationships and not the actual GTDS structure. Within the GTDS structure, the filter mode logic is separate from the batch mode logic.

GTDS system capabilities in the areas of trajectory generation, measurement modeling, estimation techniques, early orbit determination, statistical output report modeling, and optional modes of operation are described in the following subsections.

2.2.1 TRAJECTORY GENERATION

Trajectory generation is performed through integration of the orbital equations of motion in the Ephemeris Generation Program. Ephemeris generation can be performed as a standalone function as shown in Figure 2-2. In addition, trajectory generation is a key element of the differential correction process shown in Figure 2-1. The analytic and numerical trajectory generation theories available in GTDS are discussed in this section.

The orbital equations of motion can be expressed most simply in terms of the rectangular components of the acceleration vector acting on the satellite. Considerable research has focused on the problem of transforming the orbital equations of motion into a more desirable form. The general approach is to reformulate the equations in terms of a new set of orbital elements, to solve the transformed set of equations for the value of the orbital elements at the desired time, and then to transform these elements to the desired element set (e.g., Cartesian or Keplerian).

In the general perturbation approach, this reformulation of the equations of motion yields a set of equations that can be integrated analytically. The chief advantage of such trajectory generation methods is their high efficiency. However, reformulation of the orbital equations such that an analytic solution is possible usually requires some approximations. For example, in the Brouwer theory, which is a General Perturbation Method in GTDS, the perturbation model includes only the effects of a point-mass Earth and the low-order zonal harmonics in the gravitational potential. For the generation of satellite trajectories for which these are the dominant perturbations, Brouwer theory is sufficiently accurate.

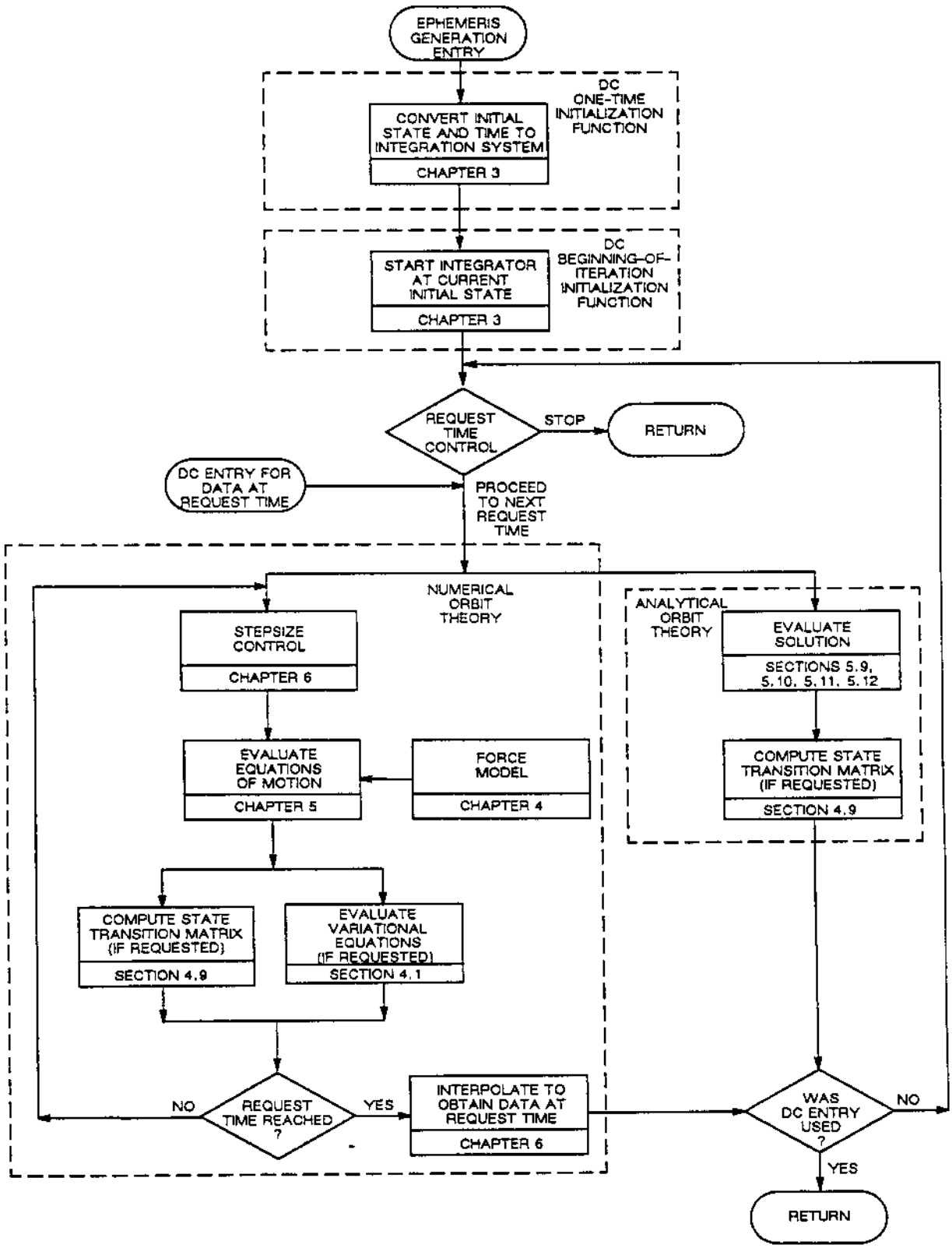

Figure 2-2. Schematic Diagram of the Ephemeris Generation Process

Solution of the equations of motion via numerical integration is classified as a Special Perturbation Method. The numerical integration techniques available in GTDS are discussed in detail in Chapter 6. In the high-precision Special Perturbation approach, the perturbing acceleration that acts on the satellite is modeled as accurately as possible. The various perturbation models and numerical integration techniques available in GTDS are discussed in Chapters 4 and 6, respectively. The chief advantage of the special perturbations approach is high accuracy; however, these methods are considerably more expensive, in terms of computer time, than the general perturbation methods.

Numerical integration of the orbital equations expressed in terms of the Cartesian components of the acceleration vector acting on the satellite is called the Cowell Method. In both the Variation of Parameters (VOP) and Intermediate Orbit approaches, the Cowell equations of motion are reformulated to obtain equations that are better conditioned for numerical integration. In the VOP approach, a transformation is made to a set of orbital elements that provides an exact solution to the two-body problem. The orbital equations expressed in terms of these elements include variations in orbital elements arising only from the perturbing acceleration vector, i.e., the point-mass effects of the Earth are integrated exactly. The VOP methods are superior for studies requiring very long propagation, such as lifetime studies.

In the Intermediate Orbit approach, an approximate solution obtained by an analytic theory is used as a reference solution, and the time rate-of-change of the difference between the the true solution and this reference solution is numerically integrated to obtain an improved solution. Intermediate Orbit methods can be developed for any analytic theory; however, only two Intermediate Orbit methods have been considered for implementation in GTDS. The first is the Brouwer Intermediate Orbit with only first-order short-period terms due to the J_2 nonspherical geopotential term or with the first-order short- and long-period terms and second-order secular terms due to the J_2 term. The second method is a similar orbit developed using Poincaré variables so that orbits of low eccentricity and low inclination can be considered. The Intermediate Orbit approach should be optimal for an orbit for which numerical inaccuracies in the integration of the element rates arising from two-body or J_2 effects are a major error source. The major drawback of both the VOP and Intermediate Orbit approaches is the computational cost associated with the required transformation of the orbital elements to and from the Cartesian state vector.

Fixed-step numerical integration is inefficient for the computation of highly eccentric orbits (i.e., eccentricity greater than 0.1) if time is used as the independent variable. For such applications, an automatic mechanism is required to force a small stepsize in the region of large perturbations and a large stepsize in the region of small perturbations. Several variable stepsize options are available in GTDS; however, stepsize changes are costly and frequently introduce errors. Therefore, an alternative analytic stepsize control

mechanism is also available. In this procedure, the equations of motion are reformulated in terms of a new independent variable s instead of time t, such that

$$ds \propto \frac{1}{r^n} dt \tag{2-1}$$

where r is the magnitude of the satellite position vector. The effect of this transformation is to "regularize" the independent variable so that fixed steps in s correspond to variable steps in t that are smaller when r is small (i.e., where the perturbations are usually larger) and larger when r is large.

Several regularized trajectory generation methods are currently implemented in GTDS. The Time-Regularized Cowell Method was developed by reformulating the Cowell orbital equations in terms of the independent variable s (with n = 3/2 as the default value) in Equation (2-1). The Kustaanheimo-Stiefel (KS) Method is a regularized VOP formulation that uses the eccentric anomaly as the independent variable (n = 1 in Equation (2-1)). The Delaunay-Similar (DS) Method is a regularized VOP formulation in which the true anomaly is used as the independent variable (n = 2 in Equation (2-1)). This form of analytic stepsize control works well when the forces vary inversely with distance from the central body. The DS approach has the strongest regularization, followed by the Time-Regularized Cowell Method, and then the KS Method. The chief disadvantage of the regularized methods is that they require numerical integration of an additional equation, the time equation. For orbits with low eccentricity (i.e., less than 0.1), analytic stepsize control is not needed and the error introduced by numerical integration of the time equation may even degrade the solution.

Special perturbation methods are also included in GTDS for generation of a mean trajectory, representing only the long-term evolution of the orbit. Numerical averaging is one such long-term orbit prediction method in GTDS. The numerical averaging method is a VOP approach in which the short-period perturbing effects are numerically averaged out of the equations of motion, leaving only the long-term motion to be integrated. The cost of each integration step is high but is usually far outweighed by the large stepsizes that are possible in the integration of the averaged dynamics. The averaged prediction model is most efficient for applications where knowledge of the short-period perturbations is not required (e.g., mission analysis or prediction of tracking station acquisition times) or where the cost of numerically integrating the precision equations of motion is prohibitively high (e.g., determination of gravitational models from large amounts of tracking data).

2.2.2 MEASUREMENT MODELING

Measurement modeling provides the means by which the estimate of the orbit of a spacecraft is compared with its true flight. The orbit estimate is expressed in terms of the

conceptual abstractions of position, velocity, and time, whereas the measurements can involve measurements of some physical property of electromagnetic wave propagations between the tracking station and the spacecraft. The propagation measurements are selected such that they can be easily related (via theoretical postulates) to the spacecraft state. This process of analytically relating the measurement quantities to the spacecraft state is referred to as measurement modeling and is vitally important to the accuracy of the orbit estimate.

The measurement models in GTDS are employed in the differential correction and data simulation processes, and, as shown in Figure 2-1, the algorithms are presented in Chapter 7. The relationship of these models to the GTDS Data Simulation Program is shown in Figure 2-3.

2.2.2.1 Measurement Types

GTDS provides for the processing of the following types of measurements:

- Goddard Range and Range-Rate (GRARR) very high frequency (VHF) and S-band radar data, including range, range-rate, and range-difference data and X and Y gimbal angle data
- C-band radar range data and azimuth and elevation angle data
- Minitrack interferometer direction cosine data
- Spaceflight Tracking and Data Network (STDN) Ranging Equipment (SRE) Unified S-band (USB) radar propagation time delay, Doppler shift, and X and Y gimbal angle data
- Applications Technology Satellites (ATS) Ranging (ATSR) propagation time delay, Doppler shift, and X and Y gimbal angle data
- Tracking and Data Relay Satellite System (TDRSS) range, Doppler shift, azimuth and elevation angle data, and TDRSS beam angles
- Laser tracking, including the range data, the azimuth and elevation angle data, and the X and Y gimbal angle data
- SRE VHF range and range-rate data
- Space Ground Link Subsystem (SGLS) range, range-difference, and azimuth and elevation angle data

2.2.2.2 Data Preprocessing

Before introduction into GTDS, the raw tracking measurements can undergo considerable preprocessing to convert from the measured quantities to estimates of the spacecraft state

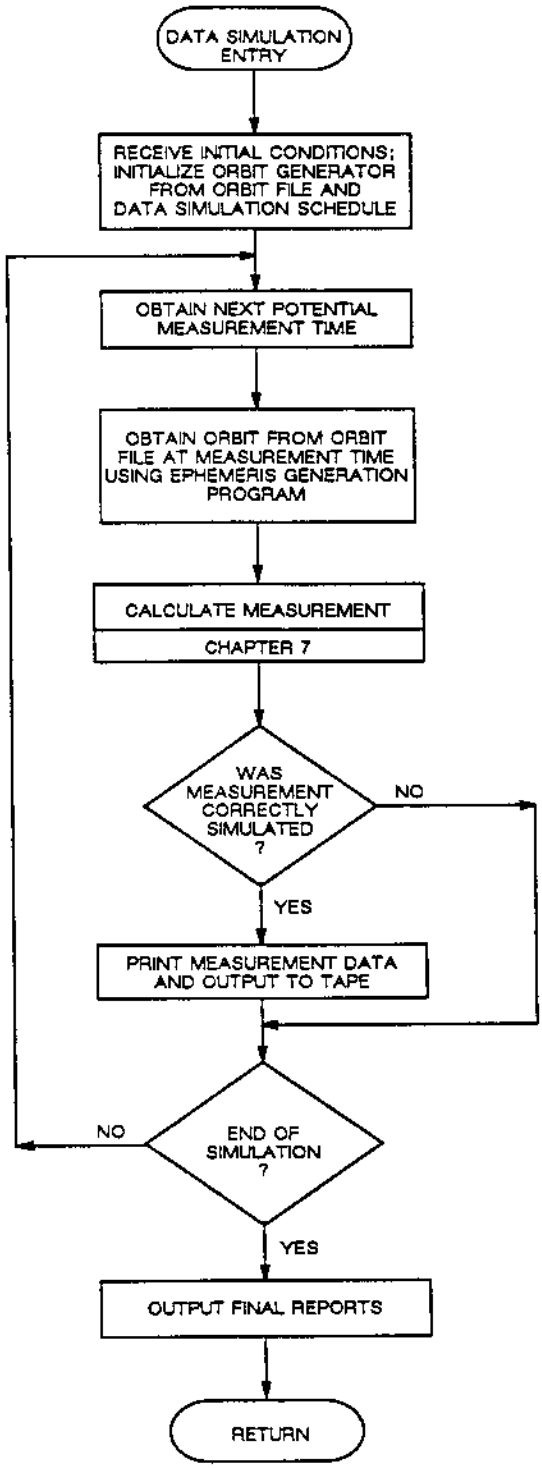

Figure 2-3. Schematic Diagram of the Data Simulation Process

components relative to the tracking station. The preprocessing of measurement data is normally done by means of a computer program completely independent of GTDS. Raw data are converted from the form received from the tracking stations to forms suitable for storage in the data base and for use in GTDS. Wild points are edited out, calibration corrections are applied to eliminate known instrumentation errors, ambiguities in the data measurement and/or recording are resolved, conversions are made from the measurement units to units that are more physically meaningful or convenient, and the data are optionally smoothed and possibly compacted if large amounts of raw data are measured. These preprocessing algorithms are discussed in Appendix A.

More specifically, this preprocessing can include the following:

- Two-way propagation time delay conversion to two-way relative ranges
- Doppler-plus-bias cycle count conversion to relative range rate
- C-band radar gimbal angle conversion to line-of-sight azimuth and elevation angles
- Minitrack interferometer fractional phase count augmentation with whole cycle counts to resolve ambiguities and conversion into line-of-sight direction cosines relative to the station east-west and north-south baselines
- Conversion of reference frequency cycle counts to time intervals

The modeling within GTDS is thus greatly simplified. It is only necessary to compute the appropriate quantity from the relative position vector between the tracking station and the spacecraft in local tangent coordinates.

2.2.2.3 Measurement Models

The GTDS measurement modeling requires rigorous iterative solutions for the two-way USB propagation paths and for the round-trip propagation path from the ground radar to the synchronous Tracking and Data Relay Satellite (TDRS) to the target satellite and back for TDRSS. These finite speed propagation paths are computed as straight lines in inertial coordinates. A round-trip circuit represents the modeling of the "range" time delay measurement, and two round-trip circuits are necessary to model the Doppler measurements in terms of the round-trip light-time difference. The USB and TDRSS Doppler measurements are implemented as a nondestruct count.

All of these measurement models assume vacuum propagation of the electromagnetic wave. Corrections to the observed measurements are computed for the refraction effects due to the presence of the atmosphere (the nondispersive troposphere and the dispersive ionosphere). In addition, other corrections to the measurements are estimated for tracking antenna location errors and spacecraft transponder delay characteristics.

The modeling of the measurements also includes the calculation of the partial derivatives with respect to the solve-for and consider variables. Variations of any of the variables except two, the tracking station locations and the tracking data biases, result in changes to the estimate of the spacecraft orbit. For the remaining variables, the partial derivatives of the measurements are computed in terms of variations of the spacecraft state at the time of the tracking signal turnaround. This variation with respect to the local state is then related back to the epoch time via the appropriate elements of the state transition matrix. This matrix maps changes in the initial state vector components into changes in spacecraft state components at any subsequent time of interest. The elements of the state transition matrix are calculated by numerical integration of the variational equations associated with the trajectory.

2.2.3 ESTIMATION TECHNIQUES

As stated in Section 2.1.1, the primary estimation algorithm available in GTDS is called the weighted least-squares with a priori or Bayesian weighted least-squares algorithm (see Chapter 8). This algorithm minimizes the sum of the squares of the weighted residuals between the actual and computed observations, while simultaneously constraining the state to satisfy an a priori state to within a specified uncertainty. The iterative estimation process differentially corrects the estimated variables and ultimately determines the weighted least-squares solution. Both first- and second-order statistics (i.e., the mean and covariance matrices) are determined for the estimated variables.

A second method, which is not currently available in the operational version of GTDS, is the Extended Kalman Filter (EKF) sequential estimator (see Chapter 8). Several features have been incorporated to prevent divergence due to model errors in the dynamics or measurements. These vary from artificially constraining the covariance gain to using adaptive techniques.

Two classes of variables can be accommodated in the statistical computations. The first class, called solve-for variables, includes model parameters whose values are known with limited certainty and are being estimated. The second class, called consider variables, includes model parameters that are not being estimated, but whose uncertainty will affect the statistics of the solve-for variables. Model parameters that can be included in either the solve-for or consider classes include the following:

- Spacecraft state vector components in Cartesian, Keplerian, or spherical coordinates (solve-for only)
- Atmospheric drag parameters
- Solar radiation pressure parameter
- Gravitational potential coefficients

- Thrust parameters
- Attitude model parameters
- Tracking station locations and timing biases
- TDRS state vector components in Cartesian, Keplerian, or spherical coordinates (solve-for only)
- Measurement biases

Specified subsets of the spacecraft position and velocity components can optionally be estimated in mean of 1950.0, mean of 2000.0, or true of date inertial Cartesian coordinates, classical orbital elements, or spherical coordinates.

GTDS can also operate in an error analysis mode, wherein only the covariance matrix of the solve-for variables is differentially corrected and propagated through the process. The error analysis process, shown in Figure 2-4, relies heavily on functions in the differential correction process, such as the computation of measurements and the update of the normal matrix. The solve-for variables are unchanged from their a priori specified values. In this mode, only the uncertainties of the tracking data, not the actual data, are required. This mode permits simulation and analysis of the uncertainties resulting from the estimation process prior to mission operations.

2.2.4 EARLY ORBIT DETERMINATION

Occasionally, a priori state value estimates of sufficient accuracy to yield convergence of the iterative process are unavailable, as when mission anomalies occur and preflight estimates of the state are no longer valid. For such cases, GTDS has the capability of rapidly determining approximations of the spacecraft's position and velocity from a limited amount of early tracking data. These approximations provide starter values for the differential correction process.

Three early orbit approximation methods, described in Chapter 9, are available in GTDS. These methods are (1) the Gauss Method, (2) the Double R-Iteration Method, and (3) the Range and Angles Method. The Gauss and Double R-Iteration Methods use three sets of radar gimbal angle measurements to estimate the state vector. The Range and Angles Method uses multiple sets of radar range and gimbal angle data to estimate the state vector.

2.2.5 STATISTICAL OUTPUT REPORT MODELING

GTDS provides the capability for validating the tracking data and calibrating the trackers through generation of the Statistical Output Report (SOR). This feature is described further in Section 8.7 of Chapter 8.

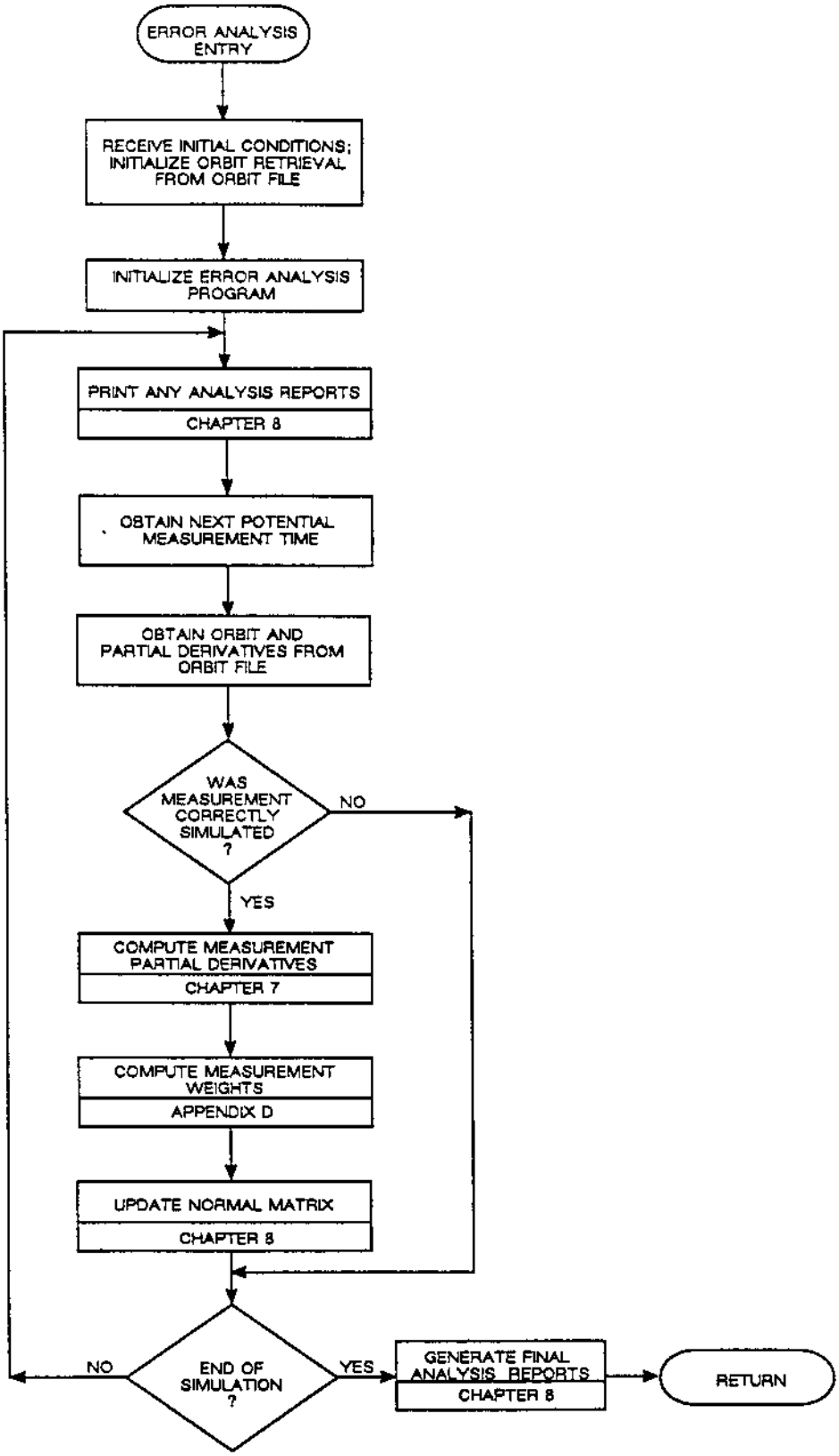

Figure 2-4. Schematic Diagram of the Error Analysis Process

2.2.6 OPTIONAL MODES OF OPERATION

Each of the programs that make up GTDS can be utilized in a number of different modes, depending on the needs of the user.

The Ephemeris Generation Program can be used to propagate a vehicle state from a given epoch to some specified time. This program is useful for several purposes:

- To generate a spacecraft ephemeris report on the online printer
- To generate a spacecraft ephemeris on disk or tape in either the ORBIT, EPHEM, or ORB1 (for Cowell integration only) File format
- To perform vehicle lifetime studies
- To generate state partial derivatives over a given timespan

The Differential Correction Program employs a Bayesian weighted least-squares algorithm to estimate the vehicle state, various force model parameters, and nondynamic parameters such as station locations and observation biases. The Differential Correction Program uses the Ephemeris Generation Program with any of the available orbit theories to satisfy integration requirements. The Differential Correction Program can also be used to do the following:

- Determine a definitive orbit during near-realtime operational mission support or during postflight support
- Determine better estimates of the gravitational harmonic coefficients, the coefficient of drag, the solar radiation constant, etc.
- Save the results of a differential correction in the form of updated elements on an elements file or an orbit history on an EPHEM or ORBIT File

The Data Simulation Program is designed to compute simulated measurements at a specified frequency for given sets of tracking stations and measurement intervals. Simulated data are useful for controlled tests that require the data to conform to certain criteria (e.g., particular force model, biases, or corrections for particular portions of the orbit). The Data Simulation Program allows the measurement tracking schedule to be specified in one of the four following forms:

- Periodic detailed schedule
- Spacecraft pass
- Function of special events
- Function of times on an actual measurement tape

The Data Simulation Program also provides for random and bias errors in the computed measurements as well as the effects of atmospheric refraction, antenna mount errors,

transponder delays, and the light-time correction. It uses the same modeling algorithms that are employed by the Differential Correction Program and data from the GTDS ORBIT File to compute measurements.

The Error Analysis Program provides the capability to perform analysis of tracking errors for an arbitrary orbit, given the station-dependent tracking schedule and other scheduling information. The program provides a variety of statistical output reports, including the following:

- The epoch covariance matrix and correlation coefficients associated with an entire tracking span are provided, along with the standard deviations associated with the elements and solve-for parameters in various coordinate systems. Sensitivity information about the consider parameters and the noise effect on the epoch state is also available.
- The user can optionally request that the epoch covariance matrix and sensitivity matrix be mapped to requested times. Trajectory standard deviations and the root sum square (RSS) of the position and velocity sigmas are provided at each mapping time. At the last mapping time, the covariance matrix and associated correlation coefficients are also printed.

The Error Analysis Program uses the Data Simulation Program tracking schedule, the differential correction matrix accumulation, and data from the GTDS ORBIT File to construct the required statistical matrices.

2.3 SPACECRAFT DYNAMICS

To accommodate the varying requirements at GSFC in near-Earth, lunar, and interplanetary mission analysis, the GTDS dynamic model includes the following acceleration sources:

- **N-Body Point-Mass Gravitational Accelerations**—These include all planets in the solar system, the Sun, and the Earth's Moon.
- **Nonspherical Gravitational Accelerations**—The nonspherical gravitational acceleration model allows the inclusion of up to a 21 $\times$ 21 potential field for the Earth and Moon.
- **Aerodynamic Force Accelerations**—The aerodynamic force acceleration model for the Earth includes a dynamic atmosphere model that accounts for the effects of variations in the solar flux on the Earth's upper atmosphere. A modified Harris-Priester model and Robert's analytical formulation of the Jacchia (1971) model are available.
- **Solar Radiation Accelerations**—The solar radiation model includes shadowing and variations with the distance from the Sun.

- **Attitude Control System Accelerations**—A generalized model is included to account for the small accelerations resulting from the use of attitude control systems (not currently available).

- **Thrusting Maneuver Accelerations**—A generalized model is included to account for the accelerations resulting from propulsive maneuvers. This includes the capability to use pregenerated mass and thrust tables.

The reference coordinate system for the equations of motion is optionally either the mean equator and equinox of B1950.0, mean equator and equinox of J2000.0, or a true of date system at a specified epoch. Coordinate transformations account for precession, nutation, and polar motion of the Earth's spin axis. Planetary positions are determined from a peripheral ephemeris file containing Chebyshev polynomial coefficients derived from Jet Propulsion Laboratory (JPL) ephemeris data.

GTDS is provided with a flight-sectioning capability, wherein the complete trajectory arc can be partitioned into multiple subarcs. The dynamic model options, numerical integration characteristics, and output quantities and frequency can be suitably tailored for each subarc. The criteria for crossover from one subarc to the next are based on either time or spatial conditions, which can be specified for each subarc.

The state transition matrix, required by the estimator algorithm, is obtained by numerically integrating the variational equations. A Cowell predictor-corrector numerical integration algorithm is used to integrate the second-order equations of motion and associated variational equations. Automatic or semiautomatic error control is provided by adjusting the integration stepsize by using a time-regularization process.

Various options are available in the dynamic models and numerical integration algorithms to provide the versatility to accommodate both high-speed near-realtime applications and precision postflight applications.

2.4 NEAR-REALTIME OPERATION

To provide operational support, GTDS includes a near-realtime capability with interactive graphics reporting and control facilities. The interactive capabilities allow the user to select and modify input parameters, to view the results of GTDS processing, and to automatically compute and monitor observation residuals.

Near-realtime operation usually necessitates a compromise in computational precision compared with that generally achieved during postflight processing. Several options are included for this purpose. These options, which permit more rapid computation without seriously jeopardizing precision, affect the orbit generator type selection, model approximation, and control over the number of variables being estimated or considered.

CHAPTER 3—COORDINATE AND TIME SYSTEMS

The orbit determination process involves measurements that are taken and forces that are modeled in several different space and time coordinate systems. This chapter defines these systems and gives the necessary transformations between them.

3.1 GENERAL COMMENTS AND DEFINITIONS

The GTDS coordinate systems consist of the fundamental astronomical reference systems and other systems that were originally borrowed from aeronautics or originated from special requirements of space exploration. Requirements for different coordinate systems occur from the following three sources:

- Input data
- Internal computations
- Output requirements

For example, the input ephemerides of the planets are heliocentric and refer to the mean equator and equinox of B1950.0* or J2000.0.† The input measurement data are in a topocentric coordinate system. The integration is done in either geocentric, selenocentric, planetocentric, or heliocentric rectangular coordinates referred to the mean equator and equinox of B1950.0 or J2000.0 or referred to the true equator and equinox of a specified epoch. The force model includes terms referred to a coordinate system that is fixed in the rotating Earth and terms that are referred to the Moon and the planets. The output requirements can be osculating elements with respect to the Earth, Moon, or planets. These specific coordinate systems are defined and discussed later in this chapter.

Since several different coordinate systems are used in GTDS, these systems must be defined and provision must be made for transforming from one coordinate system to another. A coordinate system is defined by specifying the origin of the coordinates, a reference plane, and a principal direction in the reference plane. This specification of the reference plane includes an identification of the positive, or north, or outward sense along the normal to the plane. The reference plane is an equivalence class of mutually parallel planes. For example, the equator is defined to be the plane normal to the Earth's axis of rotation. Usually, this plane contains the Earth's center of mass; however, in selenocentric

---

* The beginning of the Besselian solar year is denoted by the notation .0 after the year. The notation B1950.0 corresponds to January 0^d923, 1950 ephemeris time. For a detailed explanation, see Reference 1, pages 22, 30, and 69.

† If coordinate system axis directions are frozen with respect to the epoch 2000.0, the system is referred to as the Julian 2000.0 inertial (J2000.0) system.

equatorial coordinates, the parallel plane contains the Moon's center of mass. To avoid any such difficulty, the celestial sphere of infinite radius is introduced, and the celestial equator is defined as the intersection of the equatorial plane with the celestial sphere. This is another way of identifying the equivalence classes of parallel planes and parallel lines. The reference plane often refers to that member of the equivalence class that contains the origin of the coordinate system. The corresponding statement holds for the equivalence of parallel lines in defining a principal direction.

The designations of coordinate systems, according to the location of the origin, are given in the following table:

Origin of Coordinates	Designation of System
Observer	Topocentric
Center of the Earth	Geocentric
Center of the Moon	Selenocentric
Center of the Sun	Heliocentric
Center of mass	Barycentric

The following reference planes are used:

- **Horizon**. Without further designation, the horizon is the plane tangent to the oblate ellipsoid Earth model at a specified point on the surface. The outward normal is directed away from the Earth model. For topocentric coordinates, the reference plane is the geographic horizon corresponding to the point on the Earth model whose normal passes through the observer.

- **Equator**. The equator is the Earth's equator, unless otherwise specified. This is the plane normal to the Earth's axis of rotation, and north is in the direction of the angular velocity vector of the rotation, also called the celestial pole. The Moon's equator is defined in a corresponding way.

- **Plane of an Orbit**. The plane of an orbit is defined by two-body motion, and north is the direction of the angular momentum. In the problem of more than two bodies, the osculating plane corresponds to the state at a given epoch or the mean plane that has the periodic perturbations removed.

- **Ecliptic**. The ecliptic is the Earth–Sun orbital plane and is a special case of the plane of an orbit. North is the direction of the system's angular momentum, also called the ecliptic pole.

The principal direction is usually specified by giving the sense along the intersection of the reference plane with some other plane. The other plane can be a meridian plane, an equatorial plane, or another orbital plane. A meridian plane is defined as any plane that contains the axis of rotation of one of the principal gravitating bodies. Commonly used

meridians of the Earth and Moon that are used to determine principal directions are the following:

- **Greenwich or Prime Meridian.** The Greenwich meridian is the Earth's meridian plane that passes through the former Royal Observatory at Greenwich, England.

- **Lunar Prime Meridian.** The lunar prime meridian is the Moon's meridian plane that passes through the mean center of the apparent lunar disk (that point on the lunar surface that would be intersected by the Earth-Moon line, were the Moon to be at the mean ascending node when this node coincided with either the mean perigee or the mean apogee).

- **Local Meridian.** The local meridian is the Earth's or Moon's meridian plane that passes through the observer's position. This concept is not meaningful when the observer is situated on the axis of rotation.

Other principal directions frequently used in astronomy are as follows:

- **Vernal Equinox or Equinox.** The equinox is the fundamental principal direction used in astronomy. It is defined as the intersection of the ecliptic and the Earth's equator with the positive sense being from the Earth to the Sun as the Sun crosses the equator from south to north.

- **Ascending Node.** The ascending node is the intersection of an orbital plane and the reference plane with the positive sense being from the origin toward the orbiting body as it crosses the reference plane from the south to the north. Thus, the vernal equinox is an ascending node.

3.2 COORDINATE SYSTEM DESCRIPTIONS

The coordinate systems used in GTDS are described in the following subsections. For each system, the origin, reference plane, and principal direction are given, and the related coordinates are defined.

3.2.1 BODY-CENTERED EQUATORIAL INERTIAL (GEOCENTRIC, SELENOCENTRIC, OR PLANETOCENTRIC)

Origin:	Center of the reference body
Reference Plane:	Equatorial plane of the Earth at epoch
Principal Direction:	Vernal equinox of epoch

Rectangular Cartesian Coordinates (see Figure 3-1):

$\hat{X}$ axis = principal direction

$\hat{Y}$ axis = normal to the $\hat{X}$ and $\hat{Z}$ axes to form a right-handed system

$\hat{Z}$ axis = normal to the equatorial plane of epoch in the direction of the angular momentum vector

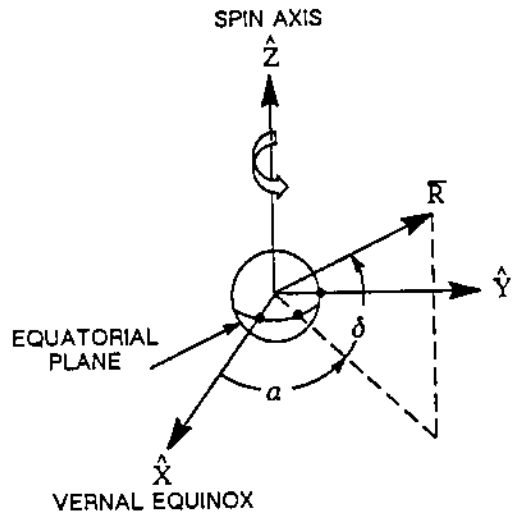

Figure 3-1. Body-Centered Inertial Coordinate System

When the reference body is the Earth, this coordinate system is referred to as the geocentric equatorial inertial (GCI) coordinate system. The origin of the GCI coordinate axes, $\hat{X}$, $\hat{Y}$, $\hat{Z}$, is the Earth's center. The $+\hat{Z}$ axis points north along the Earth's spin axis, the $+\hat{X}$ axis points to the vernal equinox direction in the Earth's equatorial plane, and the $+\hat{Y}$ axis completes the orthogonal triad so that $\hat{Y} = \hat{Z} \times \hat{X}$. Because the Earth's spin axis precesses about the ecliptic pole with a period of approximately 26,000 years, the GCI axes slowly move in inertial space at a rate of approximately 50 arcseconds per year. Therefore, a reference time has to be attached to the definition of the GCI coordinate system to make it truly inertial.

When the axis directions are frozen at their mean directions at the beginning of the year 1950 (epoch 1950.0), the system is referred to as the Besselian 1950.0 inertial (B1950.0) system. Similarly, if the axis directions are frozen at their mean directions with respect to the epoch 2000.0, the system is referred to as the Julian 2000.0 inertial (J2000.0) system. The Besselian and Julian designators refer to the associated definitions of the length of a year used in these systems.

Within the following formulation, $\bar{R}$, X, Y, and Z designate the position vector and Cartesian coordinates referred to the mean equator and equinox of B1950.0 or J2000.0 inertial coordinate frames. Similarly, $\bar{r}_E$, x_E, y_E, and z_E designate the position vector and Cartesian coordinates referred to the mean equator and equinox of epoch, and $\bar{r}$, x, y, and z designate the position vector and Cartesian coordinates referred to the true equator and equinox of epoch.

Spherical Polar Coordinates:

r = radial distance from the origin to the point being measured

α = right ascension measured east from the vernal equinox, $\tan^{-1}(Y/X)$

δ = declination measured north from the equator, $\sin^{-1}(Z/r)$

3.2.2 BODY-CENTERED ROTATING

Origin:	Center of the reference body
Reference Plane:	Equatorial plane of the reference body at epoch
Principal Direction:	Intersection of the prime meridian with the equator

Rectangular Cartesian Coordinates (see Figure 3-2):

$\hat{x}_b$ axis = principal direction

$\hat{y}_b$ axis = normal to the $\hat{x}_b$ and $\hat{z}_b$ axes to form a right-handed system

$\hat{z}_b$ axis = normal to the equatorial plane of epoch in the direction of the north celestial pole

Spherical Polar Coordinates:

r = radial distance from the origin to the point being located

λ = longitude angle measured east from the prime meridian, $\tan^{-1}(y_b/x_b)$

ϕ' = geocentric latitude angle measured north from the equator, $\sin^{-1}(z_b/r_b)$

Geodetic Coordinates:

- h = height measured normal to the local body surface to the point being located
- λ = longitude angle described above
- ϕ = geodetic latitude angle measured north from the equatorial plane to the vector normal to the ellipsoidal body surface passing through the point being located (see Figure 3-2)

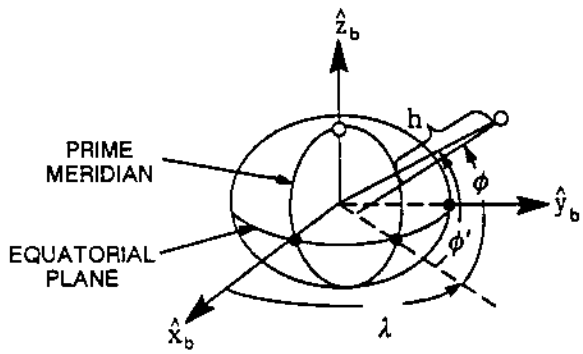

Figure 3-2. Body-Centered Rotating Coordinate System

3.2.3 LOCAL PLANE SYSTEM

Origin:	Center of the reference body (see Figure 3-3)
Reference Plane:	Plane containing $\bar{r}$, the geocentric position vector to point P, and the z axis
Principal Direction:	Geocentric position vector to point P

Rectangular Cartesian Coordinates (see Figure 3-3):

- $\hat{x}_{lp}$ axis = directed along the geocentric position vector to point P
- $\hat{y}_{lp}$ axis = axis displaced from the inertial y axis by the origin's right ascension and lying in the equatorial plane
- $\hat{z}_{lp}$ axis = north-pointed axis lying in the reference plane normal to the principal direction

Spherical Velocity Coordinates:

V = velocity vector's magnitude ($|\dot{\bar{r}}|$)

A = azimuth angle measured clockwise from the $\hat{z}_{lp}$ axis to the projection of the velocity vector onto the $\hat{y}_{lp} - \hat{z}_{lp}$ plane

β = flight path angle measured from the $\hat{x}_{lp}$ axis to the velocity vector

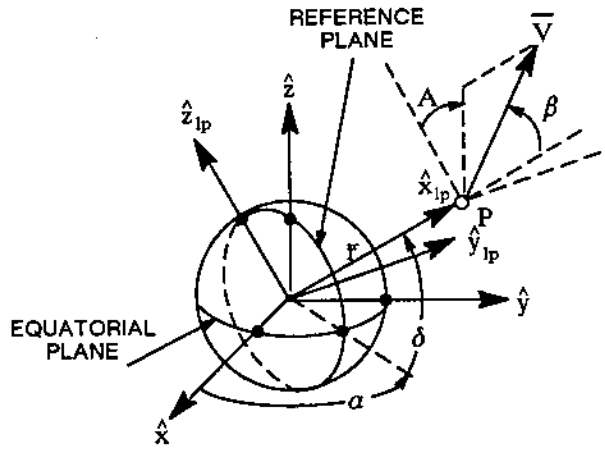

Figure 3-3. Local Plane System

3.2.4 TOPOCENTRIC LOCAL TANGENT (EAST/NORTH/UP)

Origin:	Observer (topocentric)
Reference Plane:	Plane tangent to the ellipsoidal Earth model at the observer
Principal Direction:	Vector in the reference plane, pointed north

Rectangular Cartesian Coordinates (see Figure 3-4):

$\hat{x}_{lt}$ axis = axis lying in the reference plane that points east

$\hat{y}_{lt}$ axis = principal direction

$\hat{z}_{lt}$ axis = upward direction along the geodetic vertical

Spherical Position Coordinates:

(The origin coincides with the tracking station, and $\bar{\varrho}$ is directed at the satellite.)

ϱ = station-to-spacecraft range

A = azimuth angle measured clockwise from the principal direction to the projection of the position vector in the reference plane

E = elevation angle measured from the reference plane to the station-to-spacecraft position vector

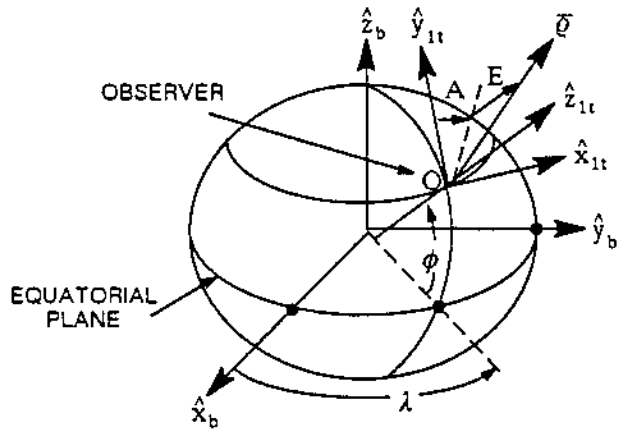

Figure 3-4. Topocentric Coordinates

3.2.5 ORBIT PLANE

Origin:	Center of the reference body
Reference Plane:	Plane of the orbit
Principal Direction:	Radius vector from the origin to the satellite

Rectangular Cartesian Coordinates:

$\hat{x}_{op}$ axis = principal direction

$\hat{y}_{op}$ axis = in the orbital plane, 90 degrees ahead of the satellite in the sense of the motion

$\hat{z}_{op}$ axis = direction along the vector $\bar{r} \times \dot{\bar{r}}$

The following two alternative orbit plane systems are defined; both have the same origin and reference plane as the basic system described above:

- The Keplerian system, which is denoted by x_p, y_p, and z_p, has its $\hat{x}_p$ axis (principal direction) directed towards the perifocus of the satellite orbit (see Figures 3-5 and 3-6).

- The equinoctial system, which is denoted by x_{ep}, y_{ep}, and z_{ep}, has its $\hat{x}_{ep}$ axis (principal direction) directed towards the "origin of longitudes." The "origin of longitudes" lies in the plane of the orbit and is displaced by the angle Ω from the ascending node $\overline{N}$, where Ω is the right ascension of the ascending node. Unit vectors along the coordinate directions x_{ep}, y_{ep}, and z_{ep} are denoted by $\hat{f}$, $\hat{g}$, $\hat{w}$, respectively.

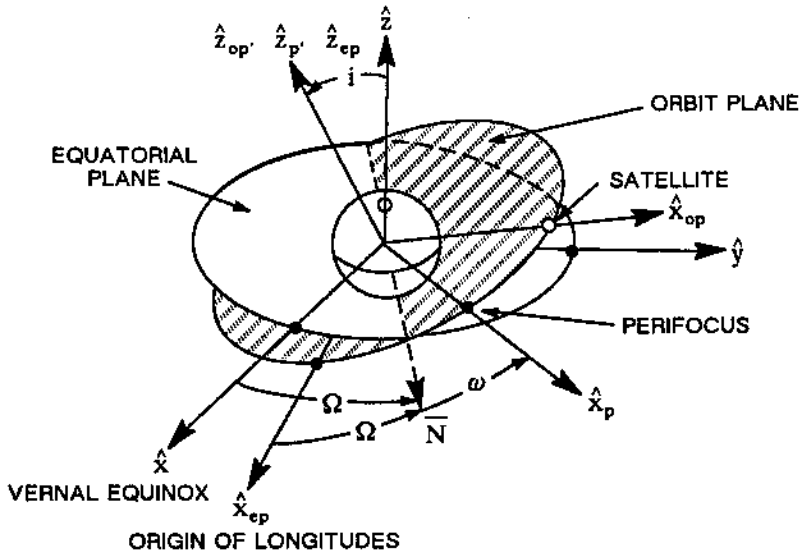

Figure 3-5. Orbit Plane Coordinates

3.2.6 ORBITAL ELEMENTS

Three types of orbital coordinates, which can be used to describe closed orbits, are presented below. Two sets of equinoctial and Herrick elements are defined such that the elements and the corresponding equations of motion are nonsingular for inclinations of both 0 degrees (direct set) and 180 degrees (retrograde set).

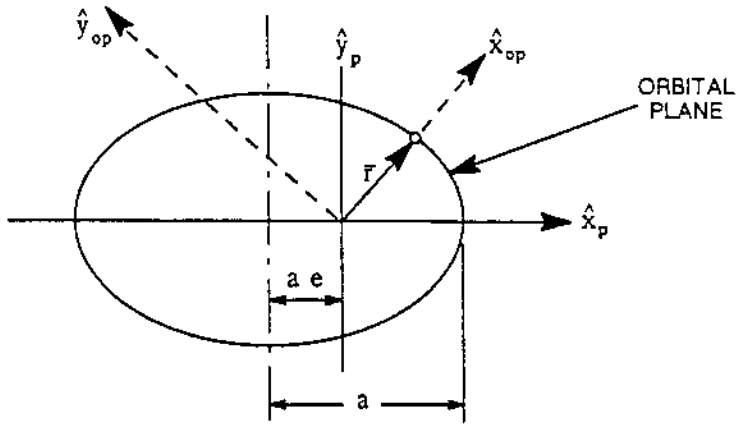

Figure 3-6. Orbital Parameters

Keplerian Elements (see Figures 3-5 and 3-6):

- a = semimajor axis
- e = eccentricity, specifying the elongation of the orbital conic section
- i = inclination, specifying the orientation of the satellite's orbital plane with respect to the equator of the central body
- Ω = right ascension of the ascending node, i.e., the angle measured eastward along the equator from the vernal equinox to the point where the satellite crosses the equator traveling in a northerly direction
- ω = argument of perigee, i.e., the angle between the ascending node and the perifocal point measured positive with increasing mean anomaly
- M = mean anomaly, i.e., the sum of the mean anomaly at epoch and the product of the mean motion and the elapsed time from epoch

Equinoctial Elements (see Figure 3-5):

- a = semimajor axis
- h = projection of the vector $\bar{e}$ on the $\hat{y}_{ep}$ axis
- k = projection of the vector $\bar{e}$ on the $\hat{x}_{ep}$ axis
- p = projection of the vector $\bar{N}$ on the $\hat{y}_{ep}$ axis

q = projection of the vector $\overline{N}$ on the $\hat{x}_{ep}$ axis

λ = mean longitude

where

$\overline{e}$ = eccentricity vector pointing in the direction of the $\hat{x}_p$ axis (perifocus) and having a magnitude equal to the eccentricity, e

$\overline{N}$ = nodal vector pointing in the direction of the ascending node and having a magnitude equal to

$$\left[\tan\left(\frac{i}{2}\right)\right]^j$$

where i denotes the orbital inclination, and j = +1 for direct orbits and −1 for retrograde orbits.

Herrick Elements:

$\overline{e}$ = eccentricity vector (defined above) expressed in inertial Cartesian coordinates

$\overline{\ell}$ = angular momentum vector divided by $\sqrt{\mu}$, where μ is the gravitational constant, i.e.,

$$\overline{\ell} = \frac{\overline{r} \times \dot{\overline{r}}}{\sqrt{\mu}}$$

and the vector $\overline{\ell}$ is expressed in inertial Cartesian coordinates

n = Kepler mean motion

λ = mean longitude

(Note: Only six of the eight scalar components above are independent. Single components of the vectors $\overline{e}$ and $\overline{\ell}$ are dependent upon the remaining six elements.)

3.2.7 VEHICLE-FIXED

Origin:	Center-of-gravity of the spacecraft
Reference Plane:	Plane containing the longitudinal and vertical axes defined by the spacecraft designer
Principal Direction:	Longitudinal axis directed toward front of the spacecraft

Rectangular Cartesian Coordinates (see Figure 3-7):

$\hat{x}_v$ axis = longitudinal (roll) axis along the principal direction
$\hat{y}_v$ axis = lateral (pitch) axis
$\hat{z}_v$ axis = vertical (yaw) axis

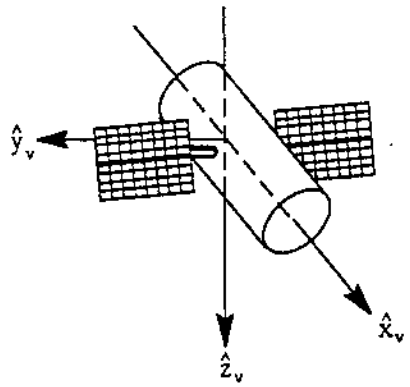

Figure 3-7. Vehicle-Fixed Coordinates

3.3 SPECIFIC TRANSFORMATIONS

The spacecraft's state vector at a given time is obtained by integrating the equations of motion. The equations of motion equate the acceleration of the vehicle to the sum of the various accelerations acting on the vehicle and are valid only in an inertial reference frame. However, the principal acceleration sources that act on the vehicle, i.e., gravity and aerodynamic drag, are most easily expressed in terms of a body-fixed system. The inertial position and velocity must therefore be transformed to body-fixed coordinates for use in computing the gravity and drag accelerations. These accelerations, expressed in terms of body-fixed axes, must then be transformed to the inertial coordinate system for use in the numerical integration process. The tracking measurement computations, used in the estimation process, also require body-fixed position and velocity coordinates of the spacecraft. Thus, one of the most basic transformations in GTDS is that between the inertial coordinate system and the body-fixed system. The following coordinate systems are also used in GTDS to express the spacecraft position, velocity, and/or acceleration for various purposes:

- **Body-Centered Equatorial Inertial.** This system, when "frozen" at a specified date, provides the basic coordinates for expressing the equations of motion

derived from Newton's laws. In GTDS, an inertial coordinate system based on the B1950.0 or J2000.0 reference date is used to locate the planets, Moon, and spacecraft.

- **Body-Centered Rotating.** This system is used to characterize the gravitational field and the atmospheric properties of the body.
- **Local Plane.** This system is used to orient the spacecraft velocity vector.
- **Topocentric Local Tangent.** This system is used to characterize ground-based radar tracking observations of the spacecraft.
- **Orbit Plane.** This system is used to characterize the spacecraft orbital position and motion.
- **Vehicle-Fixed.** This system is used to characterize propulsive and aerodynamic forces acting on the spacecraft.

In the following subsections, the transformations from the mean equator and equinox of B1950.0 and J2000.0 inertial coordinate systems to the body-fixed system are presented. This is followed by descriptions of transformations relating the inertial coordinates to the various other coordinate systems used in GTDS.

3.3.1 INERTIAL TO TRUE OF DATE

The equinox is defined as the intersection of the planes of the Earth's equator and the ecliptic. The equator is defined as being normal to the Earth's polar axis. The motion of the equinox is due to the combined motions of the two planes, the equator and the ecliptic, that define it. The motion of the celestial pole or of the equator is due to the gravitational attraction of the Sun and Moon on the Earth's equatorial bulge. It consists of two components: lunisolar precession and nutation (References 1, 2, 3). Lunisolar precession is the smooth long-period westward motion of the equator's mean pole around the ecliptic pole, and it has an amplitude of approximately 23.5 degrees and a period of approximately 26,000 years. Nutation is a relatively short-period motion that carries the actual (or true) pole around the mean pole in a somewhat irregular curve, with an amplitude of approximately 9 seconds of arc and a period of approximately 18.6 years. The motion of the ecliptic (i.e., the mean plane of the Earth's orbit) is due to the planets' gravitational attraction on the Earth and consists of a slow rotation of the ecliptic. This motion is known as planetary precession and consists of an eastward movement of the equinox of approximately 12 seconds of arc a century and a decrease of the obliquity of the ecliptic, the angle between the ecliptic and the Earth's equator, of approximately 47 seconds of arc a century. In astronomical work, the precessional motion of the equator and ecliptic, called general precession, is considered separately from the nutational motion. Thus the

"mean" equator and equinox are determined by neglecting nutation. The "true" equator and equinox can then be obtained by correcting the mean equator and equinox for nutation.

3.3.1.1 J2000.0 Inertial to Mean of Date

Transformations from the mean of J2000.0 system into other mean of date coordinate systems are given in this section (Reference 4).

The conventional expression for the Julian epoch, JE, is

$$JE = 2000.0 + \frac{JED - 2451545.0}{365.25} \tag{3-1}$$

where JED is the Julian ephemeris date. The Julian date 2451545.0 corresponds to January 1.5, 2000.

A transformation between two mean of date systems is accomplished by performing three rotations in succession. If a rotation matrix about a Cartesian z axis is denoted as $R_z(a)$ and a rotation matrix about a Cartesian x axis as $R_x(a)$, then, as functions of the rotation angle a, the elements of these rotation matrices are the following:

$$R_z(a) = \begin{bmatrix} \cos a & \sin a & 0 \\ -\sin a & \cos a & 0 \\ 0 & 0 & 1 \end{bmatrix} \tag{3-2}$$

$$R_x(a) = \begin{bmatrix} 1 & 0 & 0 \\ 0 & \cos a & \sin a \\ 0 & -\sin a & \cos a \end{bmatrix} \tag{3-3}$$

The three rotations that must be performed in sequence to transform one mean of date coordinate system with reference epoch E_1 into another with a different epoch E_2 are as follows:

$R_z(90° - \zeta_0)$ = rotation about the initial $\hat{z}$ axis that rotates the $\hat{x}$ axis to the ascending node of the mean equator at the final epoch

$R_x(\theta_p)$ = rotation of the initial equatorial plane into the final equatorial plane about an axis that coincides with the ascending node of the final mean equator of date on the initial equatorial plane

$R_z(90° + \xi_p)$ = rotation about the $\hat{z}$ axis that rotates the $\hat{x}$ axis to the descending node of the initial mean equator

The precession parameters, ζ_0, θ_p, and ξ_p, are a set of rotation angles that depend on the time. These angles are given by

$$\zeta_0 = (2306.''2181 + 1.''39656\,T - 0.''000139\,T^2)\,t + (0.''30188 - 0.''000344\,T)\,t^2 + 0.''017998\,t^3 \quad (3\text{-}4)$$

$$\theta_p = (2004.''3109 - 0.''85330\,T - 0.''000217\,T^2)\,t + (-0.''42665 - 0.''000217\,T)\,t^2 - 0.''041833\,t^3 \quad (3\text{-}5)$$

$$\xi_p = (2306.''2181 + 1.''39656\,T - 0.''000139\,T^2)\,t + (1.''09468 + 0.''000066\,T)\,t^2 + 0.''018203\,t^3 \quad (3\text{-}6)$$

where

t = time in Julian centuries between the reference epoch, E_1, and the data epoch, E_2

T = time in Julian centuries (of 36525 days) between the reference epoch, E_1, and epoch J2000.0; if E_1 = J2000.0, T = 0, such that

$$T = \frac{E_1 - 2451545.0}{36525} \quad (3\text{-}7)$$

Therefore, the total rotation matrix for precessing from the mean equator and equinox of epoch E_1 to the mean equator and equinox of epoch E_2 can be expressed as

$$A = R_z(-90 - \xi_p)\,R_x(\theta_p)\,R_z(90 - \zeta_0) = [a_{ij}] \quad (3\text{-}8)$$

Denoting the initial coordinates by $\bar{R}_1$ and the final coordinates by $\bar{r}_2$, the relationship can be expressed by

$$\bar{r}_2 = A\,\bar{R}_1 \quad (3\text{-}9)$$

where the elements of A are

$$a_{11} = -\sin \zeta_0 \sin \xi_p + \cos \zeta_0 \cos \xi_p \cos \theta_p \quad (3\text{-}10a)$$

$$a_{12} = -\cos \zeta_0 \sin \xi_p - \sin \zeta_0 \cos \xi_p \cos \theta_p \quad (3\text{-}10b)$$

$$a_{13} = -\cos \xi_p \sin \theta_p \quad (3\text{-}10c)$$

$$a_{21} = \sin \zeta_0 \cos \xi_p + \cos \zeta_0 \sin \xi_p \cos \theta_p \quad (3\text{-}10d)$$

$$a_{22} = \cos \zeta_0 \cos \xi_p - \sin \zeta_0 \sin \xi_p \cos \theta_p \quad (3\text{-}10e)$$

$$a_{23} = -\sin \xi_p \sin \theta_p \quad (3\text{-}10f)$$

$$a_{31} = \cos \zeta_0 \sin \theta_p \quad (3\text{-}10g)$$

$$a_{32} = -\sin \zeta_0 \sin \theta_p \quad (3\text{-}10h)$$

$$a_{33} = \cos \theta_p \quad (3\text{-}10i)$$

The matrix A enables a precession from the mean equator and equinox of any initial epoch E_1 within approximately one or two Julian centuries of the reference epoch J2000.0 to any final epoch E_2 within the same timespan with acceptable accuracy. Thus, a mean of date equator and equinox coordinate system can be defined for any year. Since the time derivative of A can be assumed to be negligible, the velocity coordinates are transformed as

$$\dot{\bar{r}}_2 = A \dot{\bar{R}}_1 \quad (3\text{-}11)$$

Similarly, due to the orthonormality of the transformation from mean of J2000.0 to any other mean of date coordinate system, a precession is possible from any mean of date coordinate system back to the mean of J2000.0 by simply using the transpose of the A matrix calculated above. Thus, the following relations hold for position and velocity:

$$\bar{r}_2 = A \bar{R}_1 \quad (3\text{-}12)$$

$$\bar{R}_1 = A^T \bar{r}_2 \tag{3-13}$$

where the superscript T denotes the transpose of the matrix.

3.3.1.2 B1950.0 Inertial to Mean of Date

The B1950.0 inertial coordinates are transformed into the mean equator and equinox of date by correcting only for precession. This is done by the following three rotations (see Figure 3-8):

$R_z(\pi/2 - \zeta_0)$	=	rotation about the $\hat{z}$ axis that rotates the x axis to the ascending node of the mean equator of date
$R_x(\theta_p)$	=	rotation of the B1950.0 equatorial plane into the mean equatorial plane of date about an axis that coincides with the ascending node of the mean equator of date on the B1950.0 equatorial plane
$R_z(-\pi/2 - \xi_p)$	=	rotation about the $\hat{z}_E$ axis that rotates the $\hat{x}_E$ axis to the descending node of the mean equator of B1950.0

The orthogonal transformations are defined as follows:

$$R_z(a) = \begin{bmatrix} \cos a & \sin a & 0 \\ -\sin a & \cos a & 0 \\ 0 & 0 & 1 \end{bmatrix} \tag{3-14}$$

$$R_x(a) = \begin{bmatrix} 1 & 0 & 0 \\ 0 & \cos a & \sin a \\ 0 & -\sin a & \cos a \end{bmatrix} \tag{3-15}$$

The angles ζ_0, θ_p, and ξ_p are given by (Reference 5)

$$\zeta_0 = 2304.''9969\, T_U + 0.''302000\, T_U^2 + 0.''01808\, T_U^3 \tag{3-16}$$

$$\theta_p = 2004.''2980\, T_U - 0.''425936\, T_U^2 - 0.''04160\, T_U^3 \tag{3-17}$$

$$\xi_p = 2304.''9969\, T_U + 1.''092999\, T_U^2 + 0.''019200\, T_U^3 \tag{3-18}$$

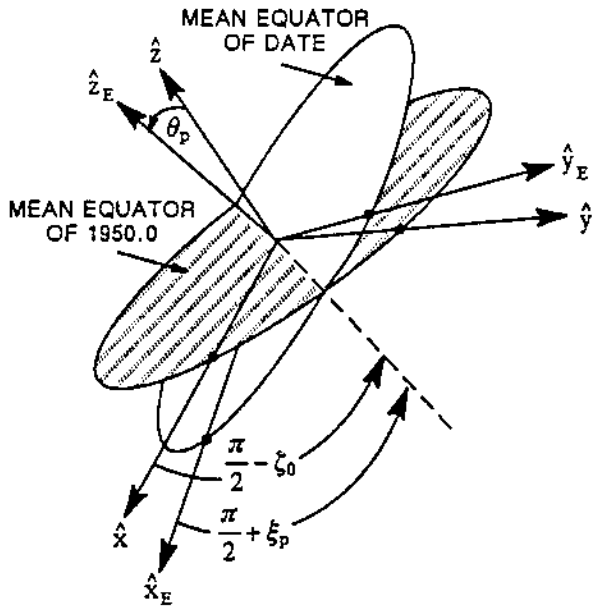

Figure 3-8. Precession Angles

where

T_U = time in Julian centuries of 36525 days elapsed from 1950.0

The total rotation matrix can be expressed as

$$A = R_z\left(-\frac{\pi}{2} - \xi_p\right) R_x(\theta_p)\, R_z\left(\frac{\pi}{2} - \zeta_0\right) = \{a_{ij}\} \tag{3-19}$$

Denoting the B1950.0 coordinates by $\overline{R}$ and the mean equator and equinox of date by $\bar{r}_E$ yields

$$\bar{r}_E = A\,\overline{R} \tag{3-20}$$

where the elements of A are

$$a_{11} = -\sin\zeta_0 \sin\xi_p + \cos\zeta_0 \cos\xi_p \cos\theta_p \tag{3-21a}$$

$$a_{12} = -\cos \zeta_0 \sin \xi_p - \sin \zeta_0 \cos \xi_p \cos \theta_p \quad (3\text{-}21b)$$

$$a_{13} = -\cos \xi_p \sin \theta_p \quad (3\text{-}21c)$$

$$a_{21} = \sin \zeta_0 \cos \xi_p + \cos \zeta_0 \sin \xi_p \cos \theta_p \quad (3\text{-}21d)$$

$$a_{22} = \cos \zeta_0 \cos \xi_p - \sin \zeta_0 \sin \xi_p \cos \theta_p \quad (3\text{-}21e)$$

$$a_{23} = -\sin \xi_p \sin \theta_p \quad (3\text{-}21f)$$

$$a_{31} = \cos \zeta_0 \sin \theta_p \quad (3\text{-}21g)$$

$$a_{32} = -\sin \zeta_0 \sin \theta_p \quad (3\text{-}21h)$$

$$a_{33} = \cos \theta_p \quad (3\text{-}21i)$$

The time derivative of A is assumed to be negligible; therefore, the velocity coordinates are transformed as follows:

$$\dot{\bar{r}}_E = A \dot{\bar{R}} \quad (3\text{-}22)$$

3.3.1.3 Mean of Date to True of Date

The transformation from the mean equator and equinox of date to the true of date system involves correcting for the nutation effect. Nutation is measured as cyclic changes in the obliquity, the angle between the equatorial plane and the ecliptic, and the longitude of the equinox. These changes in obliquity, $\delta\epsilon$, and longitude, $\delta\psi$, are assumed known. They are input to GTDS by fitting polynomials through the JPL ephemeris data (Reference 6) as described in Section 3.6.

Defining

$\delta\epsilon$ = difference between the true obliquity (ϵ_t) and the mean obliquity (ϵ_m)

$\epsilon_t = \epsilon_m + \delta\epsilon$ = true obliquity measured from the true equator to the ecliptic

$\delta\psi$ = nutation in longitude, which is the true longitude of date of the mean equinox of date

the rotation from the mean equator and equinox of date to the true equator and equinox is given by the following three rotations (see Figure 3-9):

$R_x(\epsilon_m)$ = rotation about the $\hat{x}_E$ axis through the mean obliquity to the ecliptic of date

$R_z(-\delta\psi)$ = rotation about the ecliptic pole, through the nutation in longitude

$R_x(-\epsilon_t)$ = rotation about the $\hat{x}$ axis through the true obliquity to the true equator of date

where R_x and R_z are given by Equation (3-1).

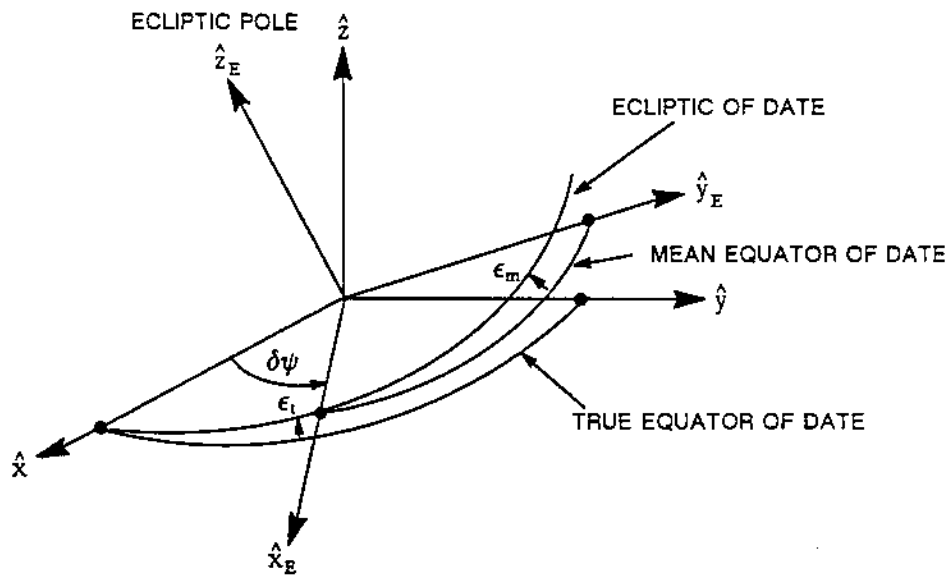

Figure 3-9. Nutation Angles

The total rotation matrix can be expressed as

$$N = R_x(-\epsilon_t)\, R_z(-\delta\psi)\, R_x(\epsilon_m) = \{n_{ij}\} \qquad (3\text{-}23)$$

Denoting the true of date coordinates by $\bar{r}$ yields

$$\bar{r} = N \bar{r}_E \tag{3-24}$$

where the elements of N are

$$n_{11} = \cos \delta\psi \tag{3-25a}$$

$$n_{12} = -\sin \delta\psi \cos \epsilon_m \tag{3-25b}$$

$$n_{13} = -\sin \delta\psi \sin \epsilon_m \tag{3-25c}$$

$$n_{21} = \sin \delta\psi \cos \epsilon_t \tag{3-25d}$$

$$n_{22} = \cos \delta\psi \cos \epsilon_t \cos \epsilon_m + \sin \epsilon_t \sin \epsilon_m \tag{3-25e}$$

$$n_{23} = \cos \delta\psi \cos \epsilon_t \sin \epsilon_m - \sin \epsilon_t \cos \epsilon_m \tag{3-25f}$$

$$n_{31} = \sin \delta\psi \cos \epsilon_t \tag{3-25g}$$

$$n_{32} = \cos \delta\psi \sin \epsilon_t \cos \epsilon_m - \cos \epsilon_t \sin \epsilon_m \tag{3-25h}$$

$$n_{33} = \cos \delta\psi \sin \epsilon_t \sin \epsilon_m + \cos \epsilon_t \cos \epsilon_m \tag{3-25i}$$

The time derivative N is assumed to be negligible. Therefore, the velocity coordinates are transformed as follows:

$$\dot{\bar{r}} = N \dot{\bar{r}}_E \tag{3-26}$$

In the J2000.0 system, the mean obliquity is given by (Reference 7)

$$\epsilon_m = 23^{\circ}.43929111 - 0^{\circ}.0130047\,T - 0^{\circ}.1639(10^{-6})\,T^2 + 0^{\circ}.5036(10^{-6})\,T^3 \tag{3-27}$$

where T = time in Julian centuries of 36525 days elapsed from J2000.0

The definition of the mean obliquity of date in the B1950.0 system (Reference 1) is given by

$$\epsilon_m = 23^\circ.445788 - 0^\circ.0130139\,T - 0^\circ.00000091\,T^2 + 0^\circ.506(10^{-6})\,T^3 \qquad (3\text{-}28)$$

where

T = time in tropical centuries (of 36524.2198 mean solar days) elapsed from the B1950.0 epoch to the date specified

3.3.1.4 Summary

The transformation matrix from inertial mean of J2000.0 or B1950.0 to true of date coordinates is given by

$$\bar{r} = C\,\bar{R} \qquad (3\text{-}29)$$

where

$$C = N(\delta\psi,\ \delta\epsilon)\ A(\zeta_0,\ \theta_p,\ \xi_p) \qquad (3\text{-}30)$$

The elements of the precession matrix, A, are given in Sections 3.3.1.1 and 3.3.1.2 for the J2000.0 and B1950.0 coordinate systems, respectively; and the elements of the nutation matrix, N, are given in Equations (3-25). In GTDS, the C-matrix is synthesized during preprocessing computations using precession angles obtained by means of Equations (3-16) and (3-17) and nutation angles obtained from an ephemeris tape provided by the Jet Propulsion Laboratory. The elements of C are stored on the Solar/Lunar/Planetary (SLP) Ephemeris File, as described in Section 3.6, for retrieval and use during program execution.

GTDS has also been provided with the optional capability to solve the equations of motion in a true of "reference date" coordinate system, designated by $\bar{r}^*$, where the reference date is specified. The orthogonal transformation in Equation (3-29) involves two times: the date of the true coordinates, denoted by t, and the epoch of the mean inertial system,

denoted by T_M (either B1950.0 or J2000.0). Therefore, using the notation defined in Section 3.2.1, Equation (3-29) can be written as

$$\bar{r} = C(t, T_M)\,\bar{R} \tag{3-31}$$

or

$$\bar{R} = C^T(t, T_M)\,\bar{r} \tag{3-32}$$

where the superscript T denotes transpose.

Specifying the reference date for the true of reference date system by t^*, then

$$\bar{r}^* = C(t^*, T_M)\,\bar{R} \tag{3-33}$$

or

$$\bar{R} = C^T(t^*, T_M)\,\bar{r}^* \tag{3-34}$$

The transformation from true of reference date to true of date coordinates is obtained from Equations (3-31) through (3-34) to be

$$\bar{r} = C(t, T_M)\;C^T(t^*, T_M)\;\bar{r}^* \tag{3-35}$$

This equation permits problems to be solved using a true of reference date coordinate system as the inertial frame but requires only the precession/nutation matrix, $C(t, T_M)$, which is available on the SLP Ephemeris File.

Note that the transformation matrix in Equation (3-35) is the identity matrix when $t = t^*$. GTDS utilizes this property and neglects precession and nutation when a true of reference date option is specified. This requires that the problem time, spanned by t, must be relatively short and in the proximity of the reference date, t^*.

3.3.2 TRUE OF DATE TO BODY-FIXED

The transformation that relates the true of date coordinates to the body-fixed coordinates accounts for two separate effects. The first relates the true vernal equinox to the prime

meridian of the rotating Earth by means of the angle a_g, the true of date right ascension of Greenwich (see Figure 3-10). The second effect, called polar motion, accounts for the fact that the pole of the body-fixed axis, $\hat{z}_b$, does not coincide with the body's spin axis, $\hat{z}$, the pole of the true of date geocentric axes. The first of these effects transforms the true of date coordinates to pseudo body-fixed coordinates, x'_b, y'_b, z'_b. These pseudo coordinates would be precisely the body-fixed coordinates, x_b, y_b, z_b, if $z'_b = z_b$, that is, if polar motion were omitted.

3.3.2.1 True of Date to Pseudo Body-Fixed

The transformation from the true of date to the pseudo body-fixed coordinates consists of a rotation about the true of date $\hat{z}$ axis through the true right ascension of Greenwich, a_g (see Figure 3-10), yielding

$$B_1 = R_z^T(a_g) = \begin{bmatrix} \cos a_g & \sin a_g & 0 \\ -\sin a_g & \cos a_g & 0 \\ 0 & 0 & 1 \end{bmatrix} \tag{3-36}$$

The true of date right ascension of Greenwich, a_g, is measured easterly from the true vernal equinox to Greenwich. A related quantity is the Greenwich hour angle, also called the true Greenwich sidereal time, which is measured westerly in the plane of the equator from Greenwich to the true vernal equinox. Thus, although their definitions differ, the right ascension of Greenwich, a_g, and the Greenwich sidereal time and hour angle are

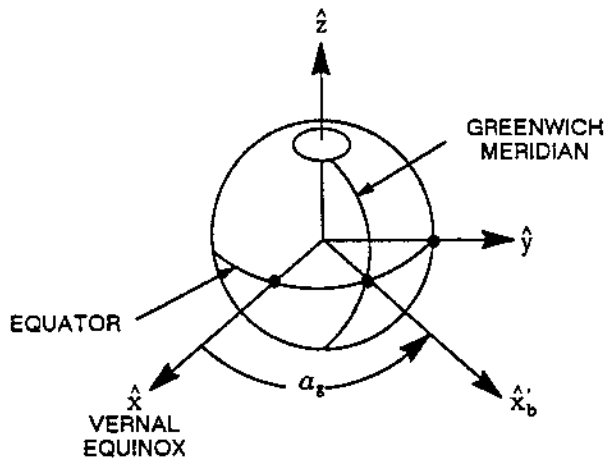

Figure 3-10. True of Date Right Ascension of Greenwich

equal in magnitude. In the B1950.0 reference frame, the true Greenwich sidereal time is obtained from the mean Greenwich sidereal time, α_{GM}, (Reference 2) as

$$\alpha_{GM} = UT1 + 6^h\,38^m\,45^s.836 + 8640184^s.542T_u + 0^s.0929T_u^2 \qquad (3\text{-}37a)$$

by applying the correction

$$\alpha_g = \alpha_{GM} + \Delta H \qquad (3\text{-}37b)$$

where

$$\Delta H = \delta\psi \cos(\epsilon_t) \qquad (3\text{-}38)$$

The nutation in longitude, $\delta\psi$, and true obliquity, ϵ_t, are discussed in Section 3.3.1.3. The times UT1 and T_u in Equation (3-37a) are

UT1 = Greenwich universal time measured from midnight (epoch) to time t; UT1 is positive for t after midnight and negative for t before midnight

T_u = number of Julian centuries elapsed from 12 hours UT1 January 0, 1900 (JD = 2415020.0) to the UT1 time of epoch

Using the J2000.0 reference frame, the mean Greenwich sidereal time, α_{GM}, is defined as the right ascension of the fictitious mean Sun minus 12 hours plus the time of day in UT1 (universal time corrected for polar motion). The mean Geenwich sidereal time is expressed in units of radians as

$$\alpha_{GM} = t\,\omega + [6^h41^m50^s.54841 + 8640184^s.812866\,T_u + 0^s.093104\,T_u^2 - 6^s.2\,(10^{-6})\,T_u^3]\left(\frac{2\pi}{86400}\right) \qquad (3\text{-}39a)$$

ω = Earth's rotation rate in radians per second

t = universal time (UT) measured in seconds from 0^h UT1 of the date of the computations

T_u = number of UT Julian centuries elapsed from epoch J2000.0 to 0^h UT1 of the date

and the superscripts h, m, s indicate hour, minutes, and seconds, respectively.

The equation consists of two parts, one a polynomial series in T_u that computes the a_{GM} at 0^h UT1 of the epoch, and a second part that computes the rotation of the Earth from the beginning of the UT1 day to the time of the computation.

The true Greenwich hour angle, a_g, is then computed by applying the correction, ΔH, from the nutation in longitude and obliquity to a_{GM}, as

$$a_g = a_{GM} + \Delta H \tag{3-39b}$$

where

$$\Delta H = (\delta\psi) \cos(\epsilon_t) \tag{3-39c}$$

The true of date coordinates transform into the pseudo body-fixed coordinates as follows:

$$\bar{r}_b' = B_1 \bar{r} \tag{3-40}$$

Differentiation yields the velocity transformation

$$\dot{\bar{r}}_b' = B_1 \dot{\bar{r}} + \dot{B}_1 \bar{r} \tag{3-41}$$

where

$$\dot{B}_1 = \begin{bmatrix} -\sin a_g & \cos a_g & 0 \\ -\cos a_g & -\sin a_g & 0 \\ 0 & 0 & 0 \end{bmatrix} \dot{a}_g \tag{3-42}$$

and where $\dot{a}_g$ is the rotation rate of the Earth and is considered constant.

3.3.2.2 Pseudo Body-Fixed to Body-Fixed (Reference 3)

The Earth's axis of figure (i.e., the principal moment of inertia) is not coincident with the spin axis, and it moves with respect to the latter causing the polar motion effect. The path

of the spin axis on the Earth's surface is "semiregular" but unpredictable due to random shifts in the Earth's crust, etc. Therefore, motion of the spin axis pole is given with respect to the pole at some established epoch. The pole at the established epoch is referred to as the adopted pole (P_A) and corresponds to the pole of the body-fixed axes, $\hat{x}_b$, $\hat{y}_b$, $\hat{z}_b$, while the present position of the spin axis pole is referred to as the true pole (P_T).

The adopted pole used in GTDS corresponds to the mean pole of 1903.0, which is consistent with that used by the International Polar Motion Service. Due to the small size of the polar motion correction (it takes place in squares of less than 30 meters), the polar region of the Earth can be considered a plane. A geocentric rectangular coordinate system is established with the $\hat{z}_b$ axis passing through P_A, the $\hat{x}_p$ axis parallel to the $\hat{x}_b$ axis and directed along the Greenwich meridian, and the $\hat{y}_p$ axis parallel to the negative $\hat{y}_b$ axis and directed along the meridian of 90 degrees west (see Figure 3-11). The coordinates of the instantaneous pole, P_T, are measured in terms of the x_p and y_p components using units of seconds of arc. (The coordinates x_p and y_p are periodically measured by the International Polar Motion Service and supplied to interested users by the United States Naval Observatory (USNO).)

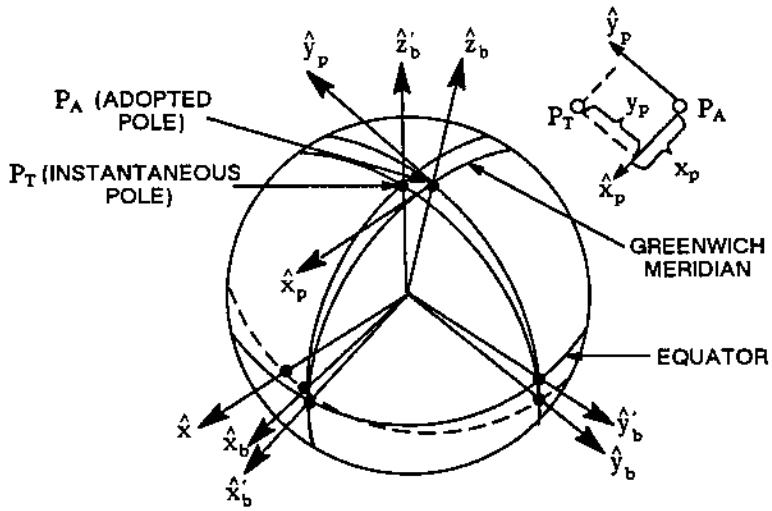

Figure 3-11. Polar Motion Schematic

To derive the expressions for the effects of x_p and y_p on a point's latitude and longitude, these two quantities are shown in relation to a regular right-handed orthogonal-rectangular coordinate system whose $\hat{z}_b$ axis passes through P_A and whose $\hat{x}_b$ – $\hat{z}_b$ plane passes

through Greenwich. In this system, the adopted longitude of a point λ_A is measured positive in an eastward direction from $\hat{x}_b$. The following notation is used:

λ_A = adopted longitude
ϕ_A = adopted latitude
λ_T = instantaneous longitude with respect to $(\hat{x}_b', \hat{y}_b', \hat{z}_b')$
ϕ_T = instantaneous latitude with respect to $(\hat{x}_b', \hat{y}_b', \hat{z}_b')$
$\Delta\phi = \phi_T - \phi_A$ = difference between the adopted and true latitude
$\Delta\lambda = \lambda_T - \lambda_A$ = difference between the adopted and true longitude

Let ϕ_T and λ_T be measured in the pseudo body-fixed coordinate system $(\hat{x}_b', \hat{y}_b', \hat{z}_b')$ whose $\hat{z}_b'$ axis passes through P_T and whose $\hat{x}_b'$ axis lies in the $\hat{z}_b - \hat{x}_b$ meridian, displaced from $\hat{x}_b$ by the angle x_p. The vector in the $(\hat{x}_b, \hat{y}_b, \hat{z}_b)$ and $(\hat{x}_b', \hat{y}_b', \hat{z}_b')$ systems can then be written as

$$\begin{bmatrix} x_b \\ y_b \\ z_b \end{bmatrix} = r_b \begin{bmatrix} \cos\phi_A \cos\lambda_A \\ \cos\phi_A \sin\lambda_A \\ \sin\phi_A \end{bmatrix} \tag{3-43}$$

and

$$\begin{bmatrix} x_b' \\ y_b' \\ z_b' \end{bmatrix} = r_b \begin{bmatrix} \cos\phi_T \cos\lambda_T \\ \cos\phi_T \sin\lambda_T \\ \sin\phi_T \end{bmatrix} \tag{3-44}$$

The two systems are related by

$$\begin{bmatrix} x_b \\ y_b \\ z_b \end{bmatrix} = R_y^T(x_p) \cdot R_x^T(y_p) \begin{bmatrix} x_b' \\ y_b' \\ z_b' \end{bmatrix} \tag{3-45}$$

where R_x is given in Equation (3-14) and R_y is

$$R_y(a) = \begin{bmatrix} \cos a & 0 & -\sin a \\ 0 & 1 & 0 \\ \sin a & 0 & \cos a \end{bmatrix} \tag{3-46}$$

The resulting transformation is

$$\vec{r}_b = \begin{bmatrix} \cos x_p & \sin x_p \sin y_p & \sin x_p \cos y_p \\ 0 & \cos y_p & -\sin y_p \\ -\sin x_p & \cos x_p \sin y_p & \cos x_p \cos y_p \end{bmatrix} \vec{r}_b' \tag{3-47}$$

The error made by neglecting the polar motion transformation defined by Equation (3-47) increases linearly with $|\vec{r}_b|$. A worst-case, order-of-magnitude indication of this error is given in Figure 3-12. The figure also shows the band of uncertainty in $|\vec{r}_b - \vec{r}_b'|$ as a result of a $\pm$2-meter uncertainty in the measurement of the polar motion coordinates, x_p and y_p.

Since x_p and y_p are small, all cosine terms are equated to unity, all sine terms equated to their angles, and all products neglected. Thus, the transformation defined by Equation (3-28) simplifies to

$$\vec{r}_b \simeq \begin{bmatrix} 1 & 0 & x_p \\ 0 & 1 & -y_p \\ -x_p & y_p & 1 \end{bmatrix} \vec{r}_b' = B_2 \vec{r}_b' \tag{3-48}$$

The worst-case error made by using the simplified transformation matrix is insignificant. For example, at lunar distances the error amounts to less than a centimeter.

In order to obtain the relationships between λ_T, λ_A, ϕ_A, and ϕ_T, the following formulas can be used:

$$\phi_T - \phi_A = \Delta\phi = x_p \cos \lambda_A - y_p \sin \lambda_A \tag{3-49}$$

$$\lambda_T - \lambda_A = \Delta\lambda = \tan \phi_A (x_p \sin \lambda_A + y_p \cos \lambda_A) \tag{3-50}$$

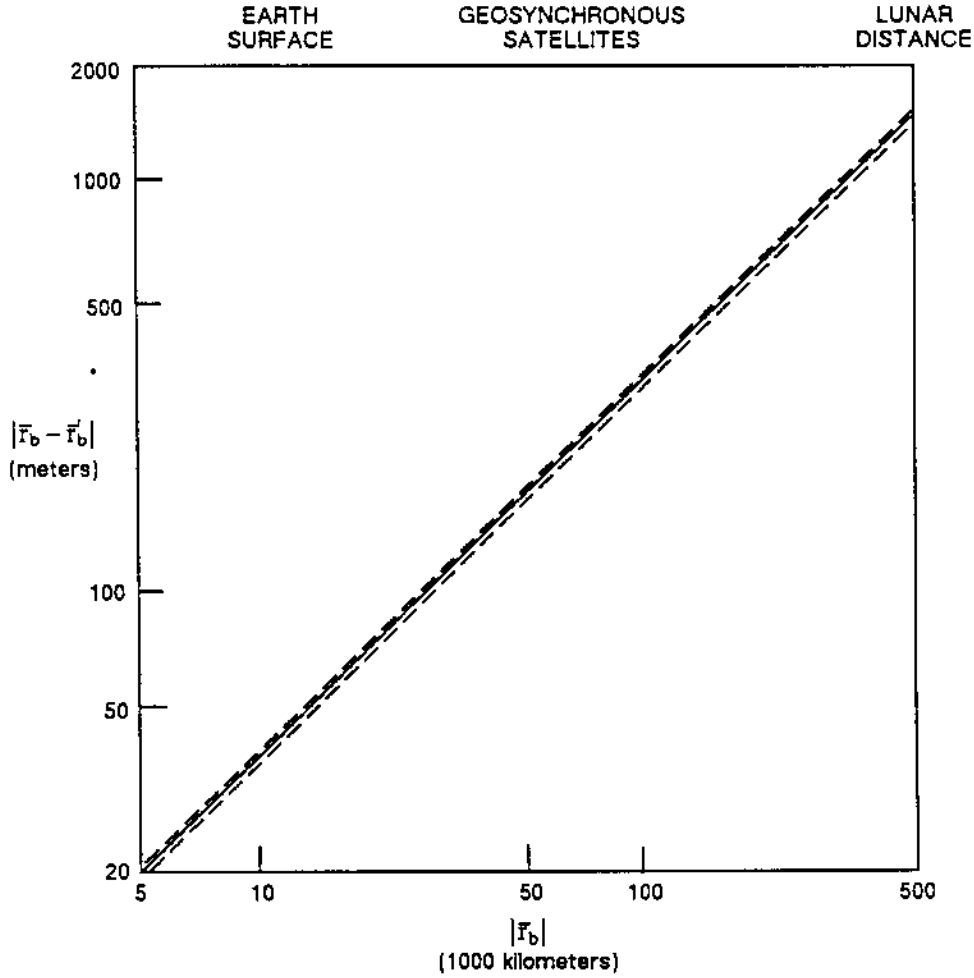

Figure 3-12. Polar Motion Errors

GTDS uses the simplified transformation matrix defined in Equation (3-48). The instantaneous coordinates of the pole, x_p and y_p, are obtained by evaluating predefined cubic polynomials at the given date, as follows:

$$x_p = a_{i1} + a_{i2}T + a_{i3}T^2 + a_{i4}T^3 \tag{3-51}$$

$$y_p = a_{i5} + a_{i6}T + a_{i7}T^2 + a_{i8}T^3 \tag{3-52}$$

where

x_p = x polar coordinate, seconds of arc
y_p = y polar coordinate, seconds of arc

and T is the number of days from the beginning of the timespan covered by the polynomial, e.g., T = 1, 2, ... For a given modified Julian date, MJD, T is given by

$$T = MJD - MJD_i + 1 \tag{3-53}$$

where MJD_i is the tabular modified Julian date that bounds the interval from below, i.e.,

$$MJD_i \leq MJD < MJD_{i+1} \tag{3-54}$$

The coefficients a_{ij} and associated timespans are determined by least-squares fitting of cubic polynomials to published daily polar motion data. The timespans are determined by constraining the maximum deviation (between the data and polynomial) to be less than 0.01 second of arc. These data are updated periodically as current data from the USNO become available. The last set of coefficients can be used to obtain extrapolated values of the polar motion coordinates for a short time in the future.

3.3.2.3 Summary

The complete transformation between the true of date coordinate system and the body-fixed system is given by

$$\bar{r}_b = B_2(x_p, y_p)\, B_1(a_g)\, \bar{r} = B\, \bar{r} \tag{3-55}$$

where $B = B_2\, B_1$, with B_1 given in Equation (3-36) and B_2 in Equation (3-48).

The time derivative of B_2 is negligible; therefore, the velocity is transformed as follows:

$$\dot{\bar{r}}_b = B_2\, B_1\, \dot{\bar{r}} + B_2\, \dot{B}_1\, \bar{r} \tag{3-56}$$

where $\dot{B}_1$ is given by Equation (3-42).

3.3.3 SELENOCENTRIC TRUE OF DATE TO SELENOGRAPHIC (REFERENCES 1, 3, 5, AND 8)

The lunar landmarks and gravitational potential are referenced to a lunar-centered, body-fixed (selenographic) coordinate system. Similar to the Earth's geographic system, the

selenographic system reference plane is the lunar equator which contains the $\hat{x}_b$ and $\hat{y}_b$ axes. The $\hat{z}_b$ axis is directed towards the lunar axis of rotation.

The Moon's mean rotation is described by the following three empirical laws of Cassini:

1. The mean axis of rotation is fixed in the Moon, perpendicular to the mean lunar equator; the mean period of rotation is equal to the mean sidereal period of revolution of the Moon around the Earth.

2. The mean lunar equator intersects the ecliptic of date at a constant inclination, I_M, for which the currently accepted value is 1 degree, 32.1 minutes.

3. The mean lunar equator, the ecliptic, and the lunar orbit plane meet in the line of modes of the lunar orbit, with the descending node of the equator at the ascending node of the orbit. The angle i, between the lunar orbit plane and the ecliptic, is a constant (the currently accepted value is 5 degrees, 8 minutes) as is the angle $i + I_M$ between the mean lunar equator and the lunar orbit plane. The ecliptic is seen to always lie between the mean lunar equator and the lunar orbit plane.

The oscillation of the actual rotational motion about the mean rotation is called the physical libration. The physical libration consists of small pendulous oscillations, never exceeding approximately 0.04 degree (in selenographic latitude and longitude), and are caused by deformations in the Moon's figure.

As a result of the first law of Cassini, the principal direction of the selenographic system ($\hat{x}_b$ axis direction) defines the lunar prime meridian and has been chosen so that it is, on the average, directed towards the center of the Earth disc. The $\hat{x}_b$ axis passes through the Sinus Medii (Central Bay) on the lunar surface. Specifically, the $\hat{x}_b$ axis is defined to be coincident with the vector pointing from the center of the Moon to the center of the Earth, if the Moon were at the mean ascending node when the node coincided with either mean perigee or mean apogee.

To transform from the inertial system to the selenographic system, a lunar-centered (selenocentric) coordinate system is defined, which is parallel to the Earth-centered Cartesian true of date system. The selenographic system ($\hat{x}_b$, $\hat{y}_b$, $\hat{z}_b$) is oriented relative to the selenocentric system ($\hat{x}$, $\hat{y}$, $\hat{z}$) by the Euler angles Ω', i_s, and Λ shown in Figures 3-13a and 3-14.

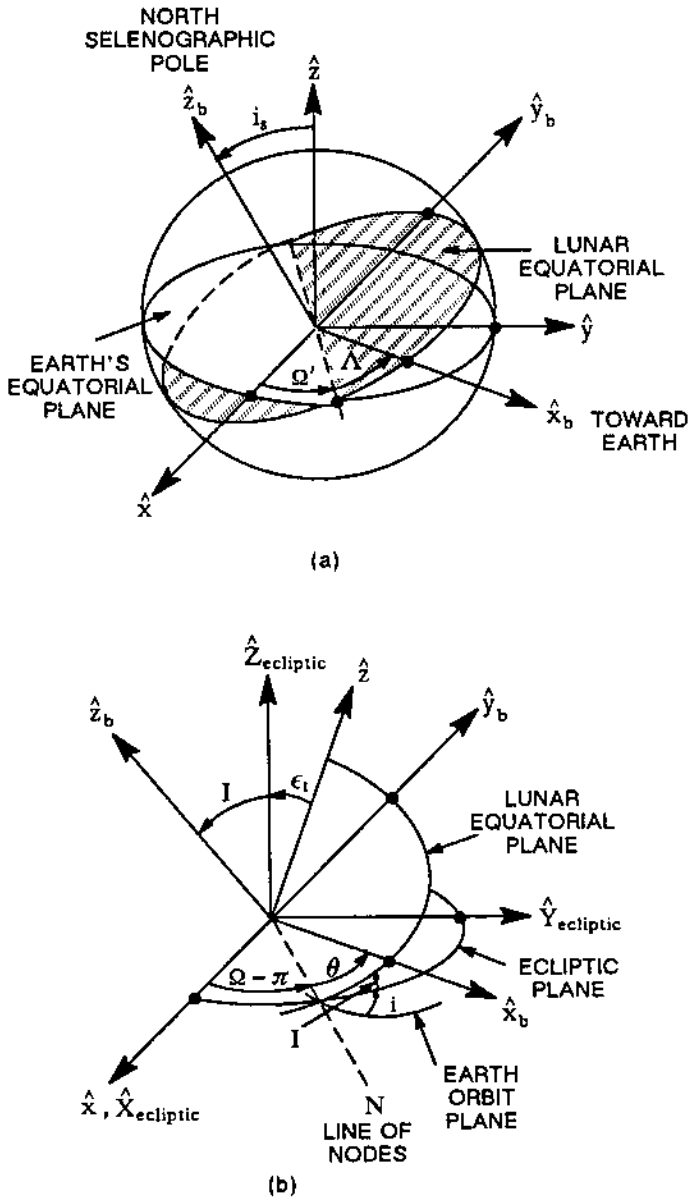

Figure 3-13. Selenocentric/Selenographic Geometry

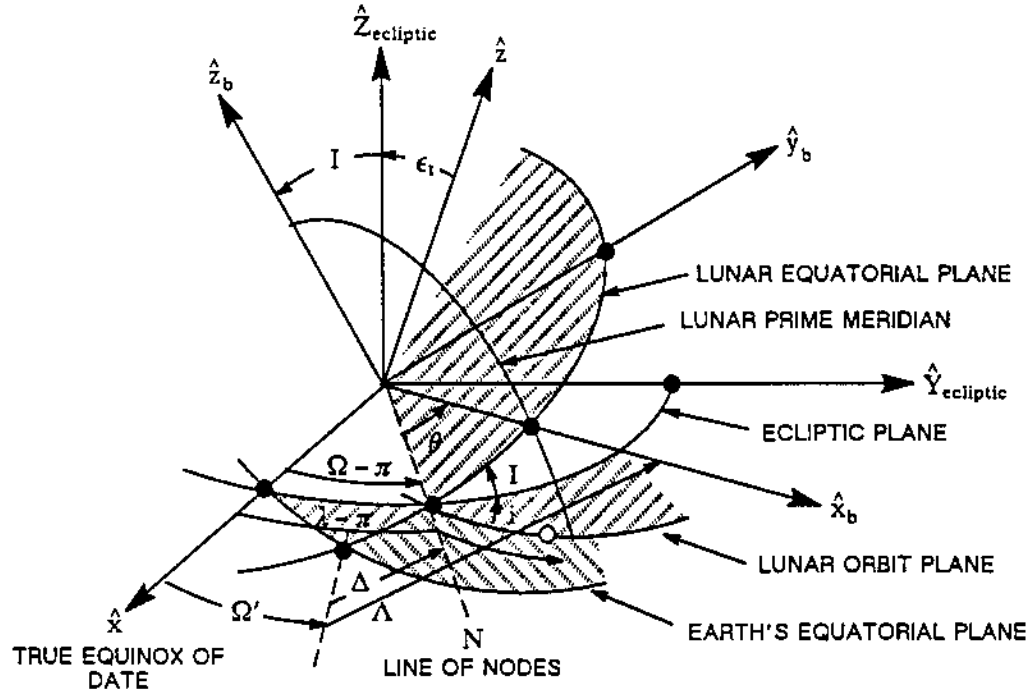

Figure 3-14. Selenographic Transformation Angles

The transformation between the selenocentric and selenographic systems is

$$\bar{r}_b = M\,\bar{r} \tag{3-57}$$

where

$$M = R_z(\Lambda)\, R_x(i_s)\, R_z(\Omega') \tag{3-58}$$

with R_x and R_z given by Equation (3-14). The elements of M are

$$m_{11} = \cos\Lambda \cos\Omega' - \sin\Lambda \sin\Omega' \cos i_s \tag{3-59a}$$

$$m_{12} = \cos\Lambda \sin\Omega' + \sin\Lambda \cos\Omega' \cos i_s \tag{3-59b}$$

$$m_{13} = \sin\Lambda \sin i_s \tag{3-59c}$$

$$m_{21} = -\sin\Lambda\cos\Omega' - \cos\Lambda\cos\Omega'\cos i_s \quad (3\text{-}59d)$$

$$m_{22} = -\sin\Lambda\sin\Omega' + \cos\Lambda\cos\Omega'\cos i_s \quad (3\text{-}59e)$$

$$m_{23} = \cos\Lambda\sin i_s \quad (3\text{-}59f)$$

$$m_{31} = \sin\Omega'\sin i_s \quad (3\text{-}59g)$$

$$m_{32} = -\cos\Omega'\sin i_s \quad (3\text{-}59h)$$

$$m_{33} = \cos i_s \quad (3\text{-}59i)$$

Because of the relationship between the Moon's mean position and the orientation of the lunar selenographic coordinates, the determination of the Euler angles Ω', i_s, and Λ necessarily involves the Moon's mean orbit.

Figure 3-13b can be used to relate orbital motion to the lunar-centered-axes system. It shows the "ecliptic" plane ($\hat{X}_{ecliptic} - \hat{Y}_{ecliptic}$), which passes through the center of the Moon and is parallel to the ecliptic. The lunar equator and orbit planes are shown intersecting in a line on the "ecliptic" plane. The $\hat{x}_b$ axis is shown in the lunar equator. In this Moon-relative coordinate frame, the Earth can be considered as orbiting the Moon (the origin) in exactly the same orbit as the Moon orbits the Earth, except that longitude angles measured in the orbit plane must be reduced by 180 degrees. For example, when the Earth is at the descending node and the $\hat{x}_b$ axis points toward N in Figure 3-13b, the Moon is, in reality, at its ascending node, 180 degrees advanced from N. Therefore, the longitude of the ascending node, Ω, and the mean longitude, λ, must be reduced by 180 degrees when used in the Moon-relative frame. The selenographic axes can be oriented to the selenocentric axes by means of the following four angles:

ϵ_t = true obliquity

$\Omega - \pi$ = longitude of the descending node

I = inclination of the lunar equator to the ecliptic planes

θ = angle measured in the lunar equator between the descending node and the Moon's prime meridian

These angles are shown in Figure 3-13b, and the transformation is

$$\bar{r}_b = M' \bar{r} \tag{3-60}$$

where

$$M' = R_z(\theta)\, R_x(I)\, R_z(\Omega - \pi)\, R_x(\epsilon_t) \tag{3-61}$$

The elements of M' are

$$m'_{11} = -\cos\theta \cos\Omega + \sin\theta \cos I \sin\Omega \tag{3-62a}$$

$$m'_{12} = -\cos\theta \sin\Omega \cos\epsilon_t - \sin\theta (\cos I \cos\Omega \cos\epsilon_t + \sin I \sin\epsilon_t) \tag{3-62b}$$

$$m'_{13} = -\cos\theta \sin\Omega \sin\epsilon_t - \sin\theta (\cos I \cos\Omega \sin\epsilon_t - \sin I \cos\epsilon_t) \tag{3-62c}$$

$$m'_{21} = \sin\theta \cos\Omega + \cos\theta \cos I \sin\Omega \tag{3-62d}$$

$$m'_{22} = \sin\theta \sin\Omega \cos\epsilon_t - \cos\theta (\cos I \cos\Omega \cos\epsilon_t + \sin I \sin\epsilon_t) \tag{3-62e}$$

$$m'_{23} = \sin\theta \sin\Omega \sin\epsilon_t - \cos\theta (\cos I \cos\Omega \sin\epsilon_t - \sin I \cos\epsilon_t) \tag{3-62f}$$

$$m'_{31} = -\sin I \sin\Omega \tag{3-62g}$$

$$m'_{32} = \sin I \cos\Omega \cos\epsilon_t - \cos I \sin\epsilon_t \tag{3-62h}$$

$$m'_{33} = \sin I \cos\Omega \sin\epsilon_t + \cos I \cos\epsilon_t \tag{3-62i}$$

The Euler angles Ω', i_s, and Λ are determined as functions of the orbital parameters ϵ_t, Ω, I, and θ by equating elements of the M and M' matrices. Equating m_{33} and m'_{33} yields

$$\cos i_s = \sin I \cos\Omega \sin\epsilon_t + \cos I \cos\epsilon_t \tag{3-63}$$

$$\sin i_s = \sqrt{1 - \cos^2 i_s} \tag{3-64}$$

Equating m_{31} and m_{32} to m'_{31} and m'_{32}, respectively, yields

$$\sin \Omega' = \frac{-\sin I \sin \Omega}{\sin i_s} \tag{3-65}$$

$$\cos \Omega' = \frac{\cos I \sin \epsilon_t - \sin I \cos \Omega \cos \epsilon_t}{\sin i_s} \tag{3-66}$$

Equating m_{13} and m_{23} to m'_{13} and m'_{23}, respectively, yields

$$\Lambda = \Delta + \theta \tag{3-67}$$

where the parameter Δ, shown in Figure 3-14, is obtained from

$$\sin \Delta = \frac{-\sin \Omega \sin \epsilon_t}{\sin i_s} \tag{3-68}$$

$$\cos \Delta = \frac{\sin I \cos \epsilon_t - \cos I \cos \Omega \sin \epsilon_t}{\sin i_s} \tag{3-69}$$

The angle θ, measured along the lunar equator from the descending node to the lunar prime meridian, must be determined from the orbital motion of the Moon. As a result of Cassini's first law, the mean rate of rotation is equated to the mean orbital rate, resulting in

$$\theta_M = \lambda_M - \Omega_M \tag{3-70}$$

where λ is the mean longitude of the Moon, Ω is the longitude of the ascending node, and the subscript M denotes mean values. Correcting Equation (3-70) for lunar physical librations gives the true value of θ

$$\theta = (\lambda_M + \tau_M) - (\Omega_M + \sigma_M) \tag{3-71}$$

Correcting Ω and I in Equations (3-63) through (3-69) for nutation and libration yields their true values

$$\Omega = \Omega_M + \sigma_M + \delta\psi \tag{3-72}$$

$$I = I_M + \varrho_M \tag{3-73}$$

The longitude of the mean ascending node of the lunar orbit is (Reference 5)

$$\begin{aligned}\Omega_M = {} & 12^{\circ}.1127902 - 0^{\circ}.0529539222\, d_e + 0^{\circ}.20795(10^{-2})\, T_e \\ & + 0^{\circ}.2081(10^{-2})\, T_e^2 + 0^{\circ}.2(10^{-5})\, T_e^3\end{aligned} \tag{3-74}$$

the inclination of the mean lunar equator to the ecliptic is

$$I_M = 1°32'.1 \tag{3-75}$$

and the geocentric mean longitude of the Moon is

$$\begin{aligned}\lambda_M = {} & 64^{\circ}.37545167 + 13^{\circ}.1763965268\, d_e - 0^{\circ}.1131575(10^{-2})\, T_e \\ & - 0^{\circ}.113015(10^{-2})\, T_e^2 + 0^{\circ}.19(10^{-5})\, T_e^3\end{aligned} \tag{3-76}$$

The T_e and d_e variables in the above equations correspond to the number of Julian centuries of 36525 Julian ephemeris days past 0^h January 1, 1950 ET, and the number of ephemeris days past the same date, respectively.

The nutation in longitude, $\delta\psi$, and the true obliquity, ϵ_t, are given in Section 3.3.1.3. The physical librations, determined by Hayn, in longitude of the ascending node, σ_M, inclination, ϱ_M, and mean longitude, τ_M, are as follows:

$$\begin{aligned}\sigma_M = {} & [-0^{\circ}.0302777 \sin g + 0^{\circ}.0102777 \sin (g + 2\omega_M) \\ & - 0^{\circ}.305555(10^{-2}) \sin (2g + 2\omega_M)]/\sin I_M\end{aligned} \tag{3-77}$$

$$\begin{aligned}\varrho_M = {} & -0^{\circ}.0297222 \cos g + 0^{\circ}.0102777 \cos (g + 2\omega_M) \\ & - 0^{\circ}.305555(10^{-2}) \cos (2g + 2\omega_M)\end{aligned} \tag{3-78}$$

$$\tau_M = -0^{\circ}.3333(10^{-2}) \sin g + 0^{\circ}.0163888 \sin g' + 0^{\circ}.5(10^{-2}) \sin (2\omega_M) \tag{3-79}$$

where the parameter g is the Moon's mean anomaly

$$g = 215^{\circ}.54013 + 13^{\circ}.064992\, d_e \tag{3-80}$$

the parameter g' is the Sun's mean anomaly

$$g' = 358^{\circ}.009067 + 0^{\circ}.9856005\, d_e \tag{3-81}$$

and ω_M is the Moon's argument of perigee

$$\omega_M = 196^{\circ}.745632 + 0^{\circ}.1643586\, d_e \tag{3-82}$$

The variables above are substituted into Equations (3-63) through (3-67) to yield the Euler angles Ω', i_s, and Λ required in the selenocentric-to-selenographic transformation given by Equations (3-57) through (3-59).

The velocity transformation from selenocentric to selenographic coordinates is obtained by differentiating Equation (3-57), yielding

$$\dot{\bar{r}}_b = M\,\dot{\bar{r}} + \dot{M}\,\bar{r} \tag{3-83}$$

The time derivative of M is obtained by differentiating its elements in Equation (3-39) with $\dot{\Omega}$ and i_s assumed zero, i.e.,

$$\dot{M} = \dot{\Lambda} \begin{bmatrix} m_{21} & m_{22} & m_{23} \\ -m_{11} & -m_{12} & -m_{13} \\ 0 & 0 & 0 \end{bmatrix} \tag{3-84}$$

The time derivative of Λ is obtained by differentiating Equation (3-67) after substituting Equation (3-71) for θ. The resulting time derivative is

$$\dot{\Lambda} = \dot{\Delta} + \dot{\lambda}_M + \dot{\tau}_M + \dot{\Omega}_M - \dot{\sigma}_M \tag{3-85}$$

where

$$\dot{\Delta} = \frac{-\cos(\Omega_M + \sigma_M + \Delta\psi)\,\sin\epsilon_i(\dot{\Omega}_M + \dot{\sigma}_M)}{\sin i_s \cos\Delta} \tag{3-86}$$

$$\dot{\lambda}_M = 0.266170762(10^{-5}) - 0.12499171(10^{-13})\, T_e \tag{3-87}$$

$$\dot{\Omega}_M = -0.1069698435(10^{-7}) + 0.23015329(10^{-13})\, T_e \tag{3-88}$$

and

$$\dot{\tau}_M = -0.1535272946(10^{-9}) \cos g + 0.569494067(10^{-10}) \cos g' + 0.579473484(10^{-11}) \cos 2\omega_M \tag{3-89}$$

$$\dot{\sigma}_M = -0.520642191(10^{-7}) \cos g + 0.1811774451(10^{-7}) \cos (g + 2\omega_M) - 0.1064057858(10^{-7}) \cos (2\omega_M + 2g) \tag{3-90}$$

3.3.4 SPHERICAL-CARTESIAN TRANSFORMATIONS (REFERENCE 9)

The coordinate transformations between the spherical and Cartesian systems are described in the following subsections.

3.3.4.1 Spherical Position and Velocity to Cartesian Coordinates

Using the spherical position coordinates, r, α, and δ, that are defined in Section 3.2.1, the transformation to Cartesian coordinates is seen from Figure 3-1 to be

$$\begin{bmatrix} x \\ y \\ z \end{bmatrix} = r \begin{bmatrix} \cos\delta \cos\alpha \\ \cos\delta \sin\alpha \\ \sin\delta \end{bmatrix} \tag{3-91}$$

To transform the spherical velocity coordinates, V, β, and A, described in Section 3.2.3, it is convenient to transform to the local plane coordinate system (see Figure 3-3) and then to the body-centered inertial Cartesian coordinate system. If the local plane coordinates, x_{lp}, y_{lp}, and z_{lp}, are fixed inertially (nonrotating), $\dot{\bar{r}}_{lp}$, can be expressed as

$$\dot{\bar{r}}_{lp} = \begin{bmatrix} \dot{x}_{lp} \\ \dot{y}_{lp} \\ \dot{z}_{lp} \end{bmatrix} = V \begin{bmatrix} \cos\beta \\ \sin A \sin\beta \\ \cos A \sin\beta \end{bmatrix} \tag{3-92}$$

The transformation between the local plane and the body-centered inertial Cartesian coordinate systems is

$$\bar{r}_{lp} = D\,\bar{r} \tag{3-93}$$

where

$$D = \begin{bmatrix} \cos\delta\cos\alpha & \cos\delta\sin\alpha & \sin\delta \\ -\sin\alpha & \cos\alpha & 0 \\ -\sin\delta\cos\alpha & -\sin\delta\sin\alpha & \cos\delta \end{bmatrix} \tag{3-94}$$

Since the local plane system is fixed inertially, the velocity vector in Equation (3-92) can be transformed to the body-centered inertial Cartesian axes by means of the transformation D, as follows:

$$\dot{\bar{r}} = D^T\,\dot{\bar{r}}_{lp} \tag{3-95}$$

The partial derivatives of $\bar{r}$ and $\dot{\bar{r}}$ with respect to r, α, δ, V, A, and β are

$$\frac{\partial \bar{r}}{\partial r} = \frac{\bar{r}}{r} \tag{3-96}$$

$$\frac{\partial \bar{r}}{\partial \alpha} = \begin{bmatrix} -y \\ x \\ 0 \end{bmatrix} \tag{3-97}$$

$$\frac{\partial \bar{r}}{\partial \delta} = \begin{bmatrix} -z\cos\alpha \\ -z\sin\alpha \\ \sqrt{x^2 + y^2} \end{bmatrix} \tag{3-98}$$

$$\frac{\partial \bar{r}}{\partial V} = \frac{\partial \bar{r}}{\partial A} = \frac{\partial \bar{r}}{\partial \beta} = \frac{\partial \dot{\bar{r}}}{\partial r} = 0 \tag{3-99}$$

$$\frac{\partial \dot{\bar{r}}}{\partial \alpha} = \begin{bmatrix} -\dot{y} \\ \dot{x} \\ 0 \end{bmatrix} \tag{3-100}$$

$$\frac{\partial \dot{\bar{r}}}{\partial \delta} = \begin{bmatrix} -\dot{z}\cos\alpha \\ -\dot{z}\sin\alpha \\ V(\cos\beta\cos\delta - \cos A\sin\beta\sin\delta) \end{bmatrix} \tag{3-101}$$

$$\frac{\partial \dot{\bar{r}}}{\partial V} = \frac{\dot{\bar{r}}}{V} \tag{3-102}$$

$$\frac{\partial \dot{\bar{r}}}{\partial A} = V \begin{bmatrix} \sin\beta(\sin A\sin\delta\cos\alpha - \cos A\sin\alpha \\ \sin\beta(\sin A\sin\delta\sin\alpha + \cos A\cos\alpha \\ -\sin A\cos\delta\sin\beta \end{bmatrix} \tag{3-103}$$

$$\frac{\partial \dot{\bar{r}}}{\partial \beta} = -V \begin{bmatrix} \cos\alpha(\cos\delta\sin\beta + \sin\delta\cos\beta\cos A) + \sin\alpha\cos\beta\sin A \\ \sin\alpha(\cos\delta\sin\beta + \sin\delta\cos\beta\cos A) - \cos\alpha\cos\beta\sin A \\ \sin\beta\sin\delta - \cos\beta\cos\delta\cos A \end{bmatrix} \tag{3-104}$$

3.3.4.2 Cartesian Position and Velocity to Spherical Coordinates

The inverse of the preceding transformations is described in the following text. The spherical radius, r, is given by

$$r = \sqrt{x^2 + y^2 + z^2} \tag{3-105}$$

From Figure 3-1, the right ascension, α, and declination, δ, of $\bar{r}$ are

$$\sin\alpha = \frac{y}{\sqrt{x^2 + y^2}} \qquad (0 \le \alpha \le 2\pi) \tag{3-106a}$$

$$\cos\alpha = \frac{x}{\sqrt{x^2 + y^2}} \qquad (0 \le \alpha \le 2\pi) \tag{3-106b}$$

and

$$\sin\delta = \frac{z}{r} \qquad \left(-\frac{\pi}{2} \le \delta \le \frac{\pi}{2}\right) \tag{3-107a}$$

$$\cos \delta = \frac{\sqrt{x^2 + y^2}}{r} \qquad \left(-\frac{\pi}{2} \leq \delta \leq \frac{\pi}{2}\right) \tag{3-107b}$$

The right ascension is measured positive east from the inertial $\hat{x}$ axis. The declination is measured positive north from the $\hat{x} - \hat{y}$ plane.

The velocity vector's magnitude is

$$V = \sqrt{\dot{x}^2 + \dot{y}^2 + \dot{z}^2} \tag{3-108}$$

and the azimuth, A, and flight path angle, β, are obtained from the local plane components of velocity as follows:

$$\sin A = \frac{\dot{y}_{lp}}{\sqrt{\dot{y}_{lp}^2 + \dot{z}_{lp}^2}} \qquad (0 \leq A \leq 2\pi) \tag{3-109a}$$

$$\cos A = \frac{\dot{z}_{lp}}{\sqrt{\dot{y}_{lp}^2 + \dot{z}_{lp}^2}} \qquad (0 \leq A \leq 2\pi) \tag{3-109b}$$

and

$$\sin \beta = \frac{\sqrt{\dot{y}_{lp}^2 + \dot{z}_{lp}^2}}{V} \qquad (0 \leq \beta \leq \pi) \tag{3-110a}$$

$$\cos \beta = \frac{\dot{x}_{lp}}{V} \qquad (0 \leq \beta \leq \pi) \tag{3-110b}$$

The azimuth and flight path angles can be obtained alternatively from the vector products of $\bar{r}$ and $\dot{\bar{r}}$ as follows:

$$\sin A = \hat{U}_{z_{lp}} \cdot \hat{U}_N \tag{3-111a}$$

$$\cos A = \frac{\hat{U}_{z_{lp}} \cdot (\hat{U}_N \times \bar{r})}{r} \tag{3-111b}$$

and

$$\sin \beta = \frac{|\bar{r} \times \dot{\bar{r}}|}{r V} \tag{3-112a}$$

$$\cos \beta = \frac{\bar{r} \cdot \dot{\bar{r}}}{r V} \tag{3-112b}$$

where $\hat{U}_{z_{lp}}$ is the unit vector in the $\hat{z}_{lp}$ axis direction and has components expressed in the body-centered Cartesian system

$$\hat{U}_{z_{lp}} = \begin{bmatrix} -\sin \delta \cos \alpha \\ -\sin \delta \sin \alpha \\ \cos \delta \end{bmatrix} \tag{3-113}$$

and $\hat{U}_N$ is the unit vector normal to $\bar{r}$ and $\dot{\bar{r}}$ given by

$$\hat{U}_N = \frac{\bar{r} \times \bar{V}}{|\bar{r} \times \bar{V}|} \tag{3-114}$$

Substituting Equations (3-87) and (3-88) into Equation (3-85) yields

$$\sin A = \frac{(x\dot{y} - y\dot{x})}{r V \sin \beta \cos \delta} \tag{3-115}$$

$$\cos A = \frac{y(y\dot{z} - z\dot{y}) + x(x\dot{z} - \dot{x}z)}{r^2 V \sin \beta \cos \delta} \tag{3-116}$$

The partial derivatives of r, α, δ, V, A, and β with respect to $\bar{r}$ and $\dot{\bar{r}}$ are

$$\frac{\partial r}{\partial \bar{r}} = \frac{\bar{r}^T}{r} \tag{3-117}$$

$$\frac{\partial a}{\partial \bar{r}} = \frac{1}{(x^2 + y^2)} \begin{bmatrix} -y \\ x \\ 0 \end{bmatrix}^T \tag{3-118}$$

$$\frac{\partial \delta}{\partial \bar{r}} = \frac{1}{r^2\sqrt{x^2 + y^2}} \begin{bmatrix} -zx \\ -zy \\ (x^2 + y^2) \end{bmatrix}^T \tag{3-119}$$

$$\frac{\partial V}{\partial \bar{r}} = [0]^T \tag{3-120}$$

$$\frac{\partial A}{\partial \bar{r}} = \frac{1}{(V^2 - \dot{r}^2)(x^2 + y^2)} \begin{bmatrix} \dot{y}(r\dot{z} - z\dot{r}) - \frac{(x\dot{y} - y\dot{x})}{r}\left(x\dot{z} - z\dot{x} + \frac{xz\dot{r}}{r}\right) \\ -\dot{x}(r\dot{z} - z\dot{r}) + \frac{(x\dot{y} - y\dot{x})}{r}\left(y\dot{z} - z\dot{y} + \frac{yz\dot{r}}{r}\right) \\ \frac{(x\dot{y} - y\dot{x})(x^2 + y^2)\,\dot{r}}{r^2} \end{bmatrix}^T \tag{3-121}$$

$$\frac{\partial \beta}{\partial \bar{r}} = \frac{1}{r^2\sqrt{V^2 - \dot{r}^2}}\left(\frac{\bar{r}^T\dot{r}}{r} - \dot{\bar{r}}^T\right) \tag{3-122}$$

$$\frac{\partial r}{\partial \dot{\bar{r}}} = \frac{\partial a}{\partial \dot{\bar{r}}} = \frac{\partial \delta}{\partial \dot{\bar{r}}} = 0 \tag{3-123}$$

$$\frac{\partial V}{\partial \dot{\bar{r}}} = \frac{\dot{\bar{r}}^T}{V} \tag{3-124}$$

$$\frac{\partial A}{\partial \dot{\bar{r}}} = \frac{1}{r(V^2 - \dot{r}^2)} \begin{bmatrix} (z\dot{y} - y\dot{z}) \\ (x\dot{z} - z\dot{x}) \\ (y\dot{x} - x\dot{y}) \end{bmatrix}^T \tag{3-125}$$

and

$$\frac{\partial \beta}{\partial \dot{\bar{r}}} = \frac{1}{r^2\sqrt{V^2 - \dot{r}^2}}\left(\dot{\bar{r}} \frac{\dot{\bar{r}}^T \bar{r}}{V^2} - \bar{r}\right)^T \tag{3-126}$$

3.3.5 BODY-CENTERED TRUE OF DATE TO ORBIT PLANE

The unit vectors in the x_{op}, y_{op}, and z_{op} directions (see Figure 3-5), measured in the body-centered true of date coordinate system, are

$$\hat{U} = \frac{\bar{r}_0}{|\bar{r}_0|} \tag{3-127}$$

$$\hat{V} = \hat{W} \times \hat{U} \tag{3-128}$$

$$\hat{W} = \frac{\bar{r}_0 \times \dot{\bar{r}}_0}{|\bar{r}_0 \times \dot{\bar{r}}_0|} \tag{3-129}$$

where $\bar{r}_0$ and $\dot{\bar{r}}_0$ are the Earth-centered position and velocity vectors used to determine the orbit plane coordinate system. If Equations (3-127) through (3-129) are expanded, they yield the following transformation relations between the orbit plane coordinates and the body-centered inertial Cartesian coordinates:

$$\bar{r}_{op} = E\,\bar{r} \tag{3-130}$$

where

$$E = \begin{bmatrix} U_x & U_y & U_z \\ V_x & V_y & V_z \\ W_x & W_y & W_z \end{bmatrix} \tag{3-131}$$

Regarding the orbit plane system as fixed inertially, the velocity transforms as follows:

$$\dot{\bar{r}}_{op} = E\,\dot{\bar{r}} \tag{3-132}$$

and the position and velocity partial derivatives are

$$\frac{\partial \bar{r}_{op}}{\partial \bar{r}} = \frac{\partial \dot{\bar{r}}_{op}}{\partial \dot{\bar{r}}} = E \tag{3-133}$$

3.3.6 BODY-FIXED TO GEOGRAPHIC TRANSFORMATIONS

The transformations between the body-centered rotating coordinate system and the geographic coordinates are described in Section 3.2.2. The transformation involves modeling the body's mean figure. The following subsections present the equations for an ellipsoidal Earth model as well as the transformations and partial derivatives relating the geodetic coordinates (h, λ, ϕ) to the body-centered rotating coordinates (x_b, y_b, z_b).

3.3.6.1 Earth Figure (Reference 9)

The shape of the Earth's surface is very nearly an ellipsoid of revolution. A satisfactory means for modeling the Earth is to characterize it as such and, where necessary, correct local deflections of the vertical (e.g., correct local astronomic zenith to ellipsoidal vertical). The polar axis of symmetry of the ellipsoid, $\hat{z}_b$, is nearly colinear with the Earth's spin axis. The ellipsoid's radius is greatest in the $\hat{x}_b - \hat{y}_b$ equatorial plane. If R_e denotes the equatorial radius, R_p the polar radius, and x_s, y_s, and z_s the coordinates of a point s on the ellipsoidal surface expressed in the body-centered rotating axis, then the coordinates of s must satisfy the following equation:

$$\frac{x_s^2}{R_e^2} + \frac{y_s^2}{R_e^2} + \frac{z_s^2}{R_p^2} = 1 \tag{3-134}$$

Two convenient parameters that describe the elliptical cross-section are the flattening coefficient, f, defined by

$$f = \frac{R_e - R_p}{R_e} > 0 \tag{3-135}$$

and the eccentricity, e, defined by

$$e^2 = 1 - \left(\frac{R_p}{R_e}\right)^2 = f(2 - f) \tag{3-136}$$

Since the ellipsoid is symmetrical about the $\hat{z}_b$ axis, there is no loss of generality in restricting the analysis to the $\hat{x}_b - \hat{z}_b$ plane. The two-dimensional analysis utilizes the symbol $x_{b'}$ or $x_{s'}$ to denote that the y_b component is omitted.

The equation of the cross-section of the ellipsoid is

$$x_{s'}^2 + \frac{z_s^2}{(1 - e^2)} = R_e^2 \tag{3-137}$$

The equation for the normal to the ellipsoid is

$$\tan \phi = - \frac{dx_{s'}}{dz_s} \tag{3-138}$$

where ϕ is the geodetic latitude shown in Figure 3-15. Differentiating Equation (3-137) and substituting the results into Equation (3-138) yields

$$\frac{z_s}{x_{s'}} = (1 - e^2) \tan \phi \tag{3-139}$$

Solving Equations (3-137) and (3-139) simultaneously for $x_{s'}$ yields

$$x_{s'} = \frac{R_e \cos \phi}{\sqrt{1 - e^2 \sin^2 \phi}} \tag{3-140}$$

From Figure 3-15, it can be shown that

$$x_{s'} = N \cos \phi \tag{3-141}$$

$$z_s = r_s \sin \phi' = N(1 - e^2) \sin \phi \tag{3-142}$$

where N is the distance from the point S to the $\hat{z}_b$ axis measured along the normal vector to the ellipsoid at point S. Substituting Equation (3-140) into Equation (3-141) yields

$$N = \frac{R_e}{\sqrt{1 - e^2 \sin^2 \phi}} = \frac{R_e}{\sqrt{1 - (2f - f^2) \sin^2 \phi}} \tag{3-143}$$

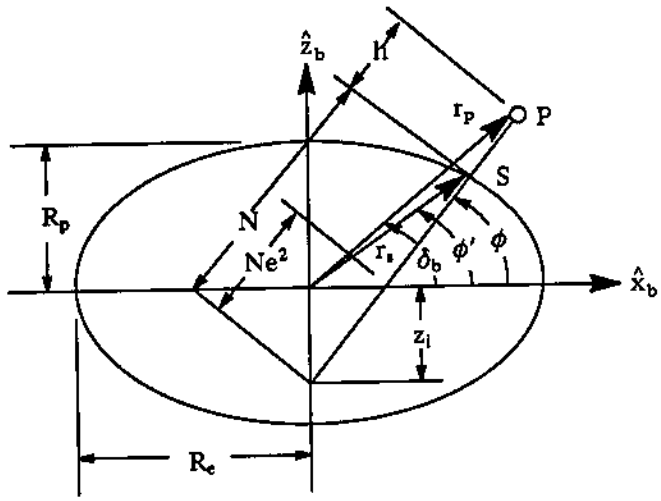

Figure 3-15. Ellipsoid Geometry

The ellipsoidal radius is

$$r_s = \sqrt{x_{s'}^2 + z_s^2} \tag{3-144}$$

Substituting Equations (3-137) and (3-142) into Equation (3-144) yields

$$r_s = \frac{R_e (1 - f)}{\sqrt{1 - e^2 \cos^2 \phi'}} \tag{3-145}$$

where ϕ' is the geocentric latitude.

3.3.6.2 Geodetic to Earth-Fixed Transformation

Assuming that point P in Figure 3-15 has the coordinates x_b, y_b, and z_b in the body-axis system and is located at a distance h from the reference ellipsoid, then, from Equation (3-139) and Figure 3-15, the x_b and z_b coordinates are

$$x_{b'} = x_{s'} + h \cos \phi = (N + h) \cos \phi \tag{3-146}$$

and

$$z_b = z_s + h \sin \phi = [N(1 - e^2) + h] \sin \phi \tag{3-147}$$

Transforming Equations (3-146) and (3-147) to three dimensions yields

$$\begin{bmatrix} x_b \\ y_b \\ z_b \end{bmatrix} = \begin{bmatrix} (N + h) \cos \phi \cos \lambda \\ (N + h) \cos \phi \sin \lambda \\ [N(1 - e^2) + h] \sin \phi \end{bmatrix} \tag{3-148a}$$

where λ, the longitude, is defined as

$$\lambda = \tan^{-1} \left(\frac{y_b}{x_b} \right) \tag{3-148b}$$

The partial derivatives of x_b, y_b, and z_b with respect to h, λ, and ϕ are

$$\begin{bmatrix} \partial x_b/\partial h \\ \partial y_b/\partial h \\ \partial z_b/\partial h \end{bmatrix} = \begin{bmatrix} \cos \phi \cos \lambda \\ \cos \phi \sin \lambda \\ \sin \phi \end{bmatrix} \tag{3-149}$$

$$\begin{bmatrix} \partial x_b/\partial \lambda \\ \partial y_b/\partial \lambda \\ \partial z_b/\partial \lambda \end{bmatrix} = \begin{bmatrix} -(N + h) \cos \phi \sin \lambda \\ (N + h) \cos \phi \cos \lambda \\ 0 \end{bmatrix} \tag{3-150}$$

$$\begin{bmatrix} \partial x_b/\partial \phi \\ \partial y_b/\partial \phi \end{bmatrix} = \left(N + h - \frac{N e^2 \cos^2 \phi}{1 - e^2 \sin^2 \phi} \right) \begin{bmatrix} -\sin \phi \cos \lambda \\ -\sin \phi \sin \lambda \end{bmatrix} \tag{3-151}$$

and

$$[\partial z_b/\partial \phi] = \left[h + N(1 - e^2) \left(1 + \frac{e^2 \sin^2 \phi}{1 - e^2 \sin^2 \phi} \right) \right] [\cos \phi] \tag{3-152}$$

3.3.6.3 Earth-Fixed to Geodetic

In transforming geodetic coordinates (h, ϕ, λ) to Earth-fixed coordinates (x_b, y_b, z_b), the point of intersection of the height normal vector and the ellipsoid (i.e., point S) is

given. In transforming from Earth-fixed to geodetic coordinates, this point is not known a priori, complicating the transformation.

Two solutions are presented. The first solution is iterative and can yield any required degree of accuracy. The second solution is a truncated binomial expansion that can be used when accuracy requirements are not so stringent.

The iterative technique is used primarily to determine the geodetic tracking station positions where high accuracy is required. For this use (and for near-Earth satellites), the approximation $h << N$ is satisfied, and since the Earth's figure is nearly spherical, $e^2 << 1$. Therefore, from Equation (3-148), the following approximation can be made:

$$N \sin \phi \approx z_b \tag{3-153}$$

Introducing z_i, the z_b intercept of the normal vector, it is apparent from Figure 3-15 that

$$z_i = -N e^2 \sin \phi \tag{3-154}$$

Combining Equations (3-153) and (3-154), the following approximation for z_i is obtained:

$$z_i = -e^2 z_b \tag{3-155}$$

Using Equation (3-155) as an initial estimate for z_i, the following sequence of equations can be solved iteratively to yield a solution for h and ϕ:

$$z_{ib} = z_b - z_i \tag{3-156}$$

$$N + h = \sqrt{x_b^2 + y_b^2 + z_{ib}^2} \tag{3-157}$$

$$\sin \phi = \frac{z_{ib}}{N + h} \tag{3-158}$$

$$N = \frac{R_e}{\sqrt{1 - e^2 \sin^2 \phi}} \tag{3-159}$$

$$z_i = -N e^2 \sin \phi \tag{3-160}$$

Upon convergence of z_i, the altitude, h, and latitude, ϕ, are obtained from Equations (3-157) and (3-158). The longitude λ is

$$\lambda = \tan^{-1}\left(\frac{y_b}{x_b}\right) \qquad (0 \leq \lambda \leq 2\pi) \tag{3-161}$$

A second, computationally simpler procedure for computing the values of ϕ and h to a specified point, P, is useful when accuracy requirements are less stringent. The latitude, ϕ, is solved for from Equation (3-139) as follows:

$$\tan\phi = \frac{z_s}{(1 - e^2)\, x_{s'}} = \frac{z_s}{(1 - e^2)\sqrt{x_s^2 + y_s^2}} \tag{3-162}.$$

where x_b, y_b, and z_b of point P are used to approximate the subvehicle point on the ellipsoid (x_s, y_s, z_s), required in Equation (3-162). This approximation yields the geodetic latitude to the normal vector of an expanded ellipse through point P. For $h << N$ and $e^2 << 1$, it is a good approximation for the geodetic latitude.

Applying the Binomial Theorem to Equation (3-145) yields

$$r_s = R_e\left[1 - \left(f + \frac{3}{2} f^2\right)\sin^2\phi' + \frac{3}{2} f^2 \sin^4\phi'\right] \tag{3-163}$$

where terms of f higher than second order are neglected. The geodetic height is nearly

$$h = r_b - r_s \tag{3-164}$$

Substituting Equation (3-163) into Equation (3-164) yields

$$h = \sqrt{x_b^2 + y_b^2 + z_b^2} - R_e + \left(R_e f + \frac{3}{2} R_e f^2\right)\sin\phi' - \frac{3}{2} R_e f^2 \sin^4\phi' \tag{3-165}$$

The geocentric latitude required in Equation (3-165) is approximated by

$$\phi' = \sin^{-1}\left(\frac{z_b}{r_b}\right) \tag{3-166}$$

The partial derivatives of h, λ, and ϕ with respect to x_b, y_b, and z_b are obtained by differentiating Equations (3-157), (3-161), and (3-158) to yield

$$\begin{bmatrix} \partial h/\partial x_b \\ \partial h/\partial y_b \\ \partial h/\partial z_b \end{bmatrix} = -\left(\frac{e^2\, a(1 - e^2)\, \sin\phi\, \cos\phi}{(1 - e^2\, \sin^2\phi)^{3/2}} + \frac{z_b\, \cos\phi}{\sin^2\phi} \right) \begin{bmatrix} \partial\phi/\partial x_b \\ \partial\phi/\partial y_b \\ \partial\phi/\partial z_b \end{bmatrix} \quad (3\text{-}167)$$

$$\begin{bmatrix} \partial\lambda/\partial x_b \\ \partial\lambda/\partial y_b \\ \partial\lambda/\partial z_b \end{bmatrix} = \frac{1}{(x_b^2 + y_b^2)} \begin{bmatrix} -y_b \\ x_b \\ 0 \end{bmatrix} \quad (3\text{-}168)$$

and

$$\begin{bmatrix} \partial\phi/\partial x_b \\ \partial\phi/\partial y_b \\ \partial\phi/\partial z_b \end{bmatrix} = \frac{(1 - e^2)}{\sqrt{x_b^2 + y_b^2}\,[(1 - e^2)^2\,(x_b^2 + y_b^2) + z_b^2]} \begin{bmatrix} -x_b\, z_b \\ -y_b\, z_b \\ (x_b^2 + y_b^2) \end{bmatrix} \quad (3\text{-}169)$$

3.3.7 EARTH-FIXED TO TOPOCENTRIC LOCAL TANGENT (EAST, NORTH, UP)

The topocentric local tangent system, described in Section 3.2.4, is used in processing ground-based measurement data. The transformation from geocentric Earth-fixed coordinates (x_b, y_b, z_b) to local tangent coordinates (x_{lt}, y_{lt}, z_{lt}) requires a translation along the geocentric radius vector to the station and a rotation of the axis through the station's longitude and latitude angles. The station parameters are defined as follows:

$\bar{r}_s$ = body-fixed coordinates of the station
ϕ_s = geodetic latitude of the station (positive north)
ϕ_s' = geocentric latitude of the station
λ_s = longitude of the station (positive east)
h_s = height of the station above the reference ellipsoid

The magnitude of the normal vector to the reference spheroid's surface at the station is given by Equation (3-143) to be

$$N_s = \frac{R_e}{\sqrt{1 - (2f - f^2)\, \sin^2\phi_s}} \quad (3\text{-}170)$$

The components of the geocentric radius vector to the station along the $\hat{x}_b$, $\hat{y}_b$, and $\hat{z}_b$ axes are given by Equation (3-148) to be

$$\begin{bmatrix} x_s \\ y_s \\ z_s \end{bmatrix} = \begin{bmatrix} (N_s + h_s) \cos \phi_s \cos \lambda_s \\ (N_s + h_s) \cos \phi_s \sin \lambda_s \\ [N_s(1 - e^2) + h_s] \sin \phi_s \end{bmatrix} \tag{3-171}$$

To bring the $\hat{x}_b$, $\hat{y}_b$, and $\hat{z}_b$ axes parallel to the $\hat{x}_{lt}$, $\hat{y}_{lt}$, and $\hat{z}_{lt}$ axes, a rotation is made about the $\hat{z}_b$ axis by the angle $(\pi/2 + \lambda_s)$ and about the new $\hat{x}_b$ axis by the angle $(\pi/2 - \phi_s)$. The resulting transformation matrix M_{lt} can be written as

$$M_{lt} = \begin{bmatrix} -\sin \lambda_s & \cos \lambda_s & 0 \\ -\sin \phi_s \cos \lambda_s & -\sin \phi_s \sin \lambda_s & \cos \phi_s \\ \cos \phi_s \cos \lambda_s & \cos \phi_s \sin \lambda_s & \sin \phi_s \end{bmatrix} \tag{3-172}$$

The local tangent coordinates of a point in space, x_b, y_b, and z_b, can be written as

$$\bar{r}_{lt} = M_{lt}(\bar{r}_b - \bar{r}_s) \tag{3-173}$$

This translates the system from the Earth's center to the station and rotates it to the local tangent system.

The Earth-fixed velocity in the local tangent system is given by

$$\dot{\bar{r}}_{lt} = M_{lt} \dot{\bar{r}}_b \tag{3-174}$$

since $\dot{M}_{lt} = 0$ and $\dot{r}_s = 0$.

The partial derivatives of the local tangent components with respect to the Earth-fixed components are the respective elements of the M_{lt} matrix given by

$$\frac{\partial \bar{r}_{lt}}{\partial \bar{r}_b} = \frac{\partial \dot{\bar{r}}_{lt}}{\partial \dot{\bar{r}}_b} = M_{lt} \tag{3-175}$$

3.3.8 KEPLERIAN-CARTESIAN TRANSFORMATIONS (REFERENCES 9 AND 10)

The coordinate transformations between the Keplerian and Cartesian systems are described in the following subsections.

3.3.8.1 Keplerian Elements to Body-Centered True of Date Coordinates

Based on the orbit geometry illustrated in Figure 3-5, the following definitions are made. The origin is the center of the reference body, the $\hat{x}$ axis points to the vernal equinox, and the $\hat{z}$ axis lies along the reference body's rotation axis. The satellite orbital plane intersects the equator at the nodes. The angle Ω is the right ascension of the ascending node. The axis $\hat{z}_{op}$ is normal to the orbital plane defining the orbit's inclination. The angle ω is the argument of perifocus. In Figure 3-6, the eccentricity, e, and the semi-major axis, a, specify the orbit's shape and size. The final element necessary to predict a body's position and velocity is the mean anomaly, M. However, the eccentric anomaly, E, or true anomaly, f, can be used instead of M to define the satellite's position in its orbit.

The transformation from the orbital elements (a, e, i, Ω, ω, M) to the orbital rectangular coordinates (x_p, y_p, z_p, $\dot{x}_p$, $\dot{y}_p$, $\dot{z}_p$) is considered first. The x_p axis is directed toward perifocus, the y_p axis is in the plane of motion advanced $\pi/2$ from the x_p axis in the direction of motion, and the z_p axis is normal to the orbit plane and completes a right-handed system. The transformations for elliptic, hyperbolic, and parabolic orbits are given below.

Ellipse: $0 \leq e < 1$

$$\begin{bmatrix} x_p \\ y_p \\ z_p \end{bmatrix} = a \begin{bmatrix} \cos E - e \\ \sin E \sqrt{1 - e^2} \\ 0 \end{bmatrix} \tag{3-176}$$

$$\begin{bmatrix} \dot{x}_p \\ \dot{y}_p \\ \dot{z}_p \end{bmatrix} = \frac{\sqrt{\mu/a}}{(1 - e \cos E)} \begin{bmatrix} -\sin E \\ \cos E \sqrt{1 - e^2} \\ 0 \end{bmatrix} \tag{3-177}$$

where

E = eccentric anomaly

μ = gravitational parameter of the reference body

The eccentric anomaly, E, is computed by Kepler's equation

$$M = E - e \sin E \tag{3-178}$$

where M is the mean anomaly defined in Section 3.2.6. This equation is solved by the following iteration scheme:

$$f(E_n) = E_n - e \sin E_n - M \tag{3-179}$$

$$D_n = 1 - e \cos [E_n - 0.5 f(E_n)] \tag{3-180}$$

$$E_{n+1} = E_n - \frac{f(E_n)}{D_n} \qquad (n = 0, 1, 2, 3, \ldots) \tag{3-181}$$

where

$$E_0 = M + e \sin M \tag{3-182}$$

Hyperbola: e > 1

$$\begin{bmatrix} x_p \\ y_p \\ z_p \end{bmatrix} = a \begin{bmatrix} \cosh F - e \\ -\sqrt{e^2 - 1} \sinh F \\ 0 \end{bmatrix} \tag{3-183}$$

$$\begin{bmatrix} \dot{x}_p \\ \dot{y}_p \\ \dot{z}_p \end{bmatrix} = \frac{\sqrt{-\mu/a}}{(e \cosh F - 1)} \begin{bmatrix} \sinh F \\ -\sqrt{e^2 - 1} \cosh F \\ 0 \end{bmatrix} \tag{3-184}$$

where F is the hyperbolic anomaly computed using Kepler's equation for a hyperbola

$$M = e \sin F - F \tag{3-185}$$

The hyperbolic Kepler equation can be solved by a Newton-Raphson iteration of the following form:

$$F_{n+1} = F_n - \frac{e \sinh F_n - F_n - M}{e \cosh F_n - 1} \quad (n = 0, 1, 2, 3, \ldots) \tag{3-186}$$

where $F_0 = M/2$. (Note: The preceding equation is singular for orbits with $e \approx 1$.)

Parabola: $e = 1$

$$\begin{bmatrix} x_p \\ y_p \\ z_p \end{bmatrix} = \begin{bmatrix} q - D^2/2 \\ \sqrt{2q\,D} \\ 0 \end{bmatrix} \tag{3-187}$$

$$\begin{bmatrix} \dot{x}_p \\ \dot{y}_p \\ \dot{z}_p \end{bmatrix} = \frac{1}{(q + D^2/2)} \begin{bmatrix} -D \\ \sqrt{2q} \\ 0 \end{bmatrix} \tag{3-188}$$

where q is the pericentric distance and D is computed from Barker's equation, that is

$$D^3 + 6q\,D = 6M \tag{3-189}$$

The orbital rectangular coordinates are transformed to inertial Cartesian position and velocity coordinates as follows:

$$\begin{bmatrix} x \\ y \\ z \end{bmatrix} = P \begin{bmatrix} x_p \\ y_p \\ z_p \end{bmatrix} \tag{3-190}$$

$$\begin{bmatrix} \dot{x} \\ \dot{y} \\ \dot{z} \end{bmatrix} = P \begin{bmatrix} \dot{x}_p \\ \dot{y}_p \\ \dot{z}_p \end{bmatrix} \tag{3-191}$$

The elements, P_{ij}, of the rotation matrix, P, are

$$P_{11} = \cos \Omega \cos \omega - \sin \Omega \cos i \sin \omega \quad (3\text{-}192a)$$

$$P_{12} = -\cos \Omega \sin \omega - \sin \Omega \cos i \cos \omega \quad (3\text{-}192b)$$

$$P_{13} = \sin \Omega \sin i \quad (3\text{-}192c)$$

$$P_{21} = \sin \Omega \cos \omega + \cos \Omega \cos i \sin \omega \quad (3\text{-}192d)$$

$$P_{22} = -\sin \Omega \sin \omega + \cos \Omega \cos i \cos \omega \quad (3\text{-}192e)$$

$$P_{23} = -\cos \Omega \sin i \quad (3\text{-}192f)$$

$$P_{31} = \sin i \sin \omega \quad (3\text{-}192g)$$

$$P_{32} = \sin i \cos \omega \quad (3\text{-}192h)$$

$$P_{33} = \cos i \quad (3\text{-}192i)$$

3.3.8.2 Keplerian to Cartesian Partial Derivatives

The functional relationships expressed in Equations (3-190) and (3-191) are

$$\bar{r} = P(\Omega, \omega, i)\, \bar{r}_p(a, e, M) \quad (3\text{-}193)$$

and

$$\dot{\bar{r}} = P(\Omega, \omega, i)\, \dot{\bar{r}}_p(a, e, M) \quad (3\text{-}194)$$

The partial derivatives of $\bar{r}$ with respect to the orbital elements can be written for ζ = a, e, and M as

$$\frac{\partial \bar{r}}{\partial \zeta} = P \frac{\partial \bar{r}_p}{\partial \zeta} \tag{3-195}$$

and

$$\frac{\partial \dot{\bar{r}}}{\partial \zeta} = P \frac{\partial \dot{\bar{r}}_p}{\partial \zeta} \tag{3-196}$$

and can be written for $\zeta = \Omega$, ω, and i as

$$\frac{\partial \bar{r}}{\partial \zeta} = \frac{\partial P}{\partial \zeta} \bar{r}_p \tag{3-197}$$

and

$$\frac{\partial \dot{\bar{r}}}{\partial \zeta} = \frac{\partial P}{\partial \zeta} \dot{\bar{r}}_p \tag{3-198}$$

The partial derivatives of $\bar{r}_p$ and $\dot{\bar{r}}_p$ for elliptical orbits are

$$\frac{\partial \bar{r}_p}{\partial (a,\ e,\ M)} = \begin{bmatrix} \frac{x_p}{a} & \left(-a - \frac{y_p^2}{r(1-e^2)}\right) & \left(-\frac{a\, y_p}{r\sqrt{1-e^2}}\right) \\ \frac{y_p}{a} & \left(\frac{x_p\, y_p}{r(1-e^2)}\right) & \left(\frac{a\sqrt{1-e^2}\,(x_p + a\, e)}{r}\right) \\ 0 & 0 & 0 \end{bmatrix} \tag{3-199}$$

and

$$\frac{\partial \dot{\vec{r}}_p}{\partial(a,\ e,\ M)} = \begin{bmatrix} -\frac{\dot{x}_p}{2a} & \dot{x}_p\left(\frac{a}{r}\right)^2\left[2\left(\frac{x_p}{a}\right) + \frac{e}{1-e^2}\left(\frac{y_p}{a}\right)^2\right] & -n\left(\frac{a}{r}\right)^3 x_p \\ -\frac{\dot{y}_p}{2a} & \frac{n}{\sqrt{1-e^2}}\left(\frac{a}{r}\right)^2\left[\frac{x_p^2}{r} - \frac{y_p^2}{a(1-e^2)}\right] & -n\left(\frac{a}{r}\right)^3 y_p \\ 0 & 0 & 0 \end{bmatrix} \tag{3-200}$$

where the mean motion, n, is

$$n = \frac{1}{a}\sqrt{\frac{\mu}{a}} \tag{3-201}$$

The partial derivatives of P with respect to Ω, ω, and i are

$$\frac{\partial P}{\partial \Omega} = \begin{bmatrix} -P_{21} & -P_{22} & 0 \\ P_{11} & P_{12} & 0 \\ 0 & 0 & 0 \end{bmatrix} \tag{3-202}$$

$$\frac{\partial P}{\partial \omega} = \begin{bmatrix} P_{12} & -P_{11} & 0 \\ P_{22} & -P_{21} & 0 \\ P_{32} & -P_{31} & 0 \end{bmatrix} \tag{3-203}$$

$$\frac{\partial P}{\partial i} = \begin{bmatrix} \sin\Omega \sin i \sin\omega & \sin\Omega \sin i \cos\omega & 0 \\ -\cos\Omega \sin i \sin\omega & -\cos\Omega \sin i \cos\omega & 0 \\ \cos i \sin\omega & \cos i \cos\omega & 0 \end{bmatrix} \tag{3-204}$$

3.3.8.3 Body-Centered True of Date Coordinates to Keplerian Elements

Given the position, $\bar{r}$, and velocity, $\dot{\bar{r}}$, at time t, the standard Keplerian elements (a, e, i, Ω, ω, M) are calculated as follows. Let the magnitude of the position, velocity, and angular momentum vectors be denoted by

$$r = |\bar{r}| \tag{3-205}$$

$$V = |\dot{\bar{r}}| \tag{3-206}$$

$$h = |\bar{h}| \tag{3-207}$$

where

$$\bar{h} = \bar{r} \times \dot{\bar{r}} \tag{3-208}$$

The equations for the orbital elements and related parameters are then the following:

Semimajor Axis

$$a = \frac{\mu r}{(2\mu - r V^2)} \tag{3-209}$$

Semilatus Rectum

$$p = \frac{1}{\mu}[(r V)^2 - (\bar{r} \cdot \dot{\bar{r}})^2] \tag{3-210}$$

Eccentricity

$$e = \sqrt{1 - \frac{p}{a}} \tag{3-211}$$

Inclination

$$\sin i = \frac{|(\bar{r} \times \dot{\bar{r}}) \times \hat{u}_z|}{|\bar{r} \times \dot{\bar{r}}|} = \frac{\sqrt{h_x^2 + h_y^2}}{h} \tag{3-212}$$

$$\cos i = \frac{(\bar{r} \times \dot{\bar{r}}) \cdot \hat{u}_z}{|\bar{r} \times \dot{\bar{r}}|} = \frac{h_z}{h} \tag{3-213}$$

where $\hat{u}_x$, $\hat{u}_y$, and $\hat{u}_z$ are unit vectors in the body-centered true of date Cartesian coordinate system, and h_x, h_y, and h_z are components of the angular momentum vector, h.

The following parameters are defined for the two cases of elliptic motion and hyperbolic motion:

Elliptic Motion ($a > 0$)

Eccentric Anomaly:

$$\sin E = \frac{1}{e}\left(\frac{\bar{r} \cdot \dot{\bar{r}}}{\sqrt{\mu a}}\right) \tag{3-214}$$

$$\cos E = \frac{1}{e}\left(1 - \frac{r}{a}\right) \tag{3-215}$$

Mean Anomaly:

$$M = E - \frac{\bar{r} \cdot \dot{\bar{r}}}{\sqrt{\mu a}} \tag{3-216}$$

Hyperbolic Motion ($a \leq 0$)

Hyperbolic Anomaly:

$$\sinh F = \frac{1}{e}\left(\frac{\bar{r} \cdot \dot{\bar{r}}}{\sqrt{-\mu a}}\right) \tag{3-214}$$

$$\cosh F = \frac{1}{e}\left(1 - \frac{r}{a}\right) \tag{3-215}$$

Mean Anomaly:

$$M = \frac{\bar{r} \cdot \dot{\bar{r}}}{\sqrt{-\mu a}} - F \tag{3-216}$$

Period:

$$P = 2\pi \sqrt{\frac{a^3}{\mu}}$$

Period not applicable for hyperbolic motion (3-217)

Energy (per unit mass):

$$\text{Energy} = -\frac{\mu}{2a}$$

Energy (per unit mass):

$$\text{Energy} = \frac{\mu}{2a} \quad (3\text{-}218)$$

The following parameters have the same definitions for both elliptic and hyperbolic motion:

Longitude of the Ascending Node:

$$\sin \Omega = \frac{h_x}{h \sin i} \quad (3\text{-}219)$$

$$\cos \Omega = \frac{-h_y}{h \sin i} \quad (3\text{-}220)$$

True Anomaly:

$$\sin f = \sqrt{\frac{p}{\mu}} \frac{(\bar{r} \cdot \dot{\bar{r}})}{r e} \quad (3\text{-}221)$$

$$\cos f = \frac{p - r}{r e} \quad (3\text{-}222)$$

Argument of Perifocus:

$$\sin\ (\omega + f) = \frac{z}{r \sin i} \tag{3-223}$$

$$\cos\ (\omega + f) = \frac{y\, h_x - x\, h_y}{h\, r \sin i} \tag{3-224}$$

Perifocal and Apofocal Radius:

$$r_p = a\,(1 - e) \tag{3-225}$$

$$r_a = a\,(1 + e) \tag{3-226}$$

Perifocal and Apofocal Height:

$$h_p = r_p - r_s \tag{3-227}$$

$$h_a = r_a - r_s \tag{3-228}$$

where r_s is the equatorial radius of the Earth.

The partial derivatives of the Keplerian coordinates with respect to the Cartesian coordinates are given by the inverse of the Keplerian-to-Cartesian partial derivatives in Equations (3-195) through (3-198), i.e.,

$$\begin{bmatrix} \partial a/\partial x & \partial a/\partial y & \cdots & \partial a/\partial \dot{z} \\ \partial e/\partial x & \partial e/\partial y & \cdots & \partial e/\partial \dot{z} \\ \partial i/\partial x & \partial i/\partial y & \cdots & \partial i/\partial \dot{z} \\ \vdots & \vdots & & \vdots \\ \partial M/\partial x & \partial M/\partial y & \cdots & \partial M/\partial \dot{z} \end{bmatrix} = \begin{bmatrix} \partial x/\partial a & \partial x/\partial e & \partial x/\partial i & \cdots & \partial x/\partial M \\ \partial y/\partial a & \partial y/\partial e & \partial y/\partial i & \cdots & \partial y/\partial M \\ \vdots & \vdots & \vdots & & \vdots \\ \partial \dot{z}/\partial a & \partial \dot{z}/\partial e & \partial \dot{z}/\partial i & \cdots & \partial \dot{z}/\partial M \end{bmatrix}^{-1} \tag{3-229}$$

3.3.9 EQUINOCTIAL-CARTESIAN TRANSFORMATIONS (REFERENCES 11 AND 12)

The following subsections present the transformations between the equinoctial elements, described in Section 3.2.6, and the inertial Cartesian system. The equinoctial elements are used only to describe closed orbits.

3.3.9.1 Equinoctial Elements to Cartesian Coordinates

Conversion from equinoctial elements, a, h, k, p, q, λ, to inertial Cartesian coordinates, $\bar{r}$ and $\dot{\bar{r}}$, is performed in the following manner. First, the generalized Kepler equation for equinoctial elements,

$$\lambda = F + h \cos F - k \sin F \tag{3-230}$$

is iteratively solved for the eccentric longitude F, which is the sum of the eccentric anomaly, the argument of perigee, and the right ascension of the ascending node.

Next, the position and velocity coordinates in the equinoctial coordinate system (x_{ep}, y_{ep}, z_{ep}) are obtained as follows for both the direct and retrograde cases:

$$X_1 = a[(1 - h^2 \beta) \cos F + h k \beta \sin F - k] \tag{3-231}$$

$$Y_1 = a[(1 - k^2 \beta) \sin F + h k \beta \cos F - h] \tag{3-232}$$

$$\dot{X}_1 = \frac{n a^2}{r}[(h k \beta \cos F - (1 - h^2 \beta) \sin F] \tag{3-233}$$

$$\dot{Y}_1 = \frac{n a^2}{r}[(1 - k^2 \beta) \cos F - h k \beta \sin F] \tag{3-234}$$

where

$$\beta = \frac{1}{1 + \sqrt{1 - h^2 - k^2}} \tag{3-235}$$

The transformation from the equinoctial system to the inertial Cartesian system is given by

$$\bar{r} = X_1 \hat{f} + Y_1 \hat{g} \tag{3-236}$$

$$\dot{\bar{r}} = \dot{X}_1 \hat{f} + \dot{Y}_1 \hat{g} \tag{3-237}$$

where $\hat{f}$ and $\hat{g}$ are unit vectors directed along the $\hat{x}_{ep}$ and $\hat{y}_{ep}$ axes, respectively (see Figure 3-5). These vectors are computed in inertial Cartesian coordinates as follows:

$$[\hat{f},\ \hat{g},\ \hat{w}] = \frac{1}{1 + p^2 + q^2} \begin{bmatrix} 1 - p^2 + q^2 & 2p\,q\,j & 2p \\ 2p\,q & (1 + p^2 - q^2)\,j & -2q \\ -2p\,j & 2q & (1 - p^2 - q^2)\,j \end{bmatrix} \tag{3-238}$$

where

$j = 1$ for direct orbits $(0 \leq i \leq 180°)$

$j = -1$ for retrograde orbits $(0 < i \leq 180°)$

In GTDS, the operational choice of direct elements was made for $0 \leq i \leq 90$ degrees and of retrograde elements for 90 degrees $< i \leq 180$ degrees.

3.3.9.2 Cartesian Coordinates to Equinoctial Elements

The equinoctial orbit elements, a, h, k, p, q, λ, are calculated from the Cartesian position, $\bar{r}$, and velocity, $\dot{\bar{r}}$. The semimajor axis is computed as follows:

$$a = \left(\frac{2}{r} - \frac{|\dot{\bar{r}}|^2}{\mu} \right)^{-1} \tag{3-239}$$

The eccentricity vector is given by

$$\bar{e} = -\frac{\bar{r}}{r} - \frac{(\bar{r} \times \dot{\bar{r}}) \times \dot{\bar{r}}}{\mu} \tag{3-240}$$

The unit vector $\hat{w}$ is defined as follows (see Section 3.2.5):

$$\hat{w} = \frac{\bar{r} \times \dot{\bar{r}}}{|\bar{r} \times \dot{\bar{r}}|} \tag{3-241}$$

The unit vectors $\hat{f}$ and $\hat{g}$ can then be computed as follows:

$$f_x = 1 - \frac{w_x^2}{1 + w_z^j} \tag{3-242}$$

$$f_y = -\frac{w_x w_y}{1 + w_z^j} \tag{3-243}$$

$$f_z = -w_x^j \tag{3-244}$$

where j is as defined following Equation (3-238), and

$$\hat{g} = \hat{w} \times \hat{f} \tag{3-245}$$

The equinoctial elements h, k, p, and q are given by

$$h = \bar{e} \cdot \hat{g} \tag{3-246}$$

$$k = \bar{e} \cdot \hat{f} \tag{3-247}$$

$$p = \frac{w_x}{1 + w_z^j} \tag{3-248}$$

$$q = -\frac{w_y}{1 + w_z^j} \tag{3-249}$$

The mean longitude is computed using the generalized Kepler equation

$$\lambda = F + h \cos F - k \sin F \tag{3-250}$$

where

$$F = \tan^{-1}\left(\frac{\sin F}{\cos F}\right) \tag{3-251}$$

with

$$\cos F = k + \frac{(1 - k^2 \beta) X_1 - h k \beta Y_1}{a\sqrt{1 - h^2 - k^2}} \tag{3-252}$$

$$\sin F = h + \frac{(1 - h^2 \beta) Y_1 - h k \beta X_1}{a\sqrt{1 - h^2 - k^2}} \tag{3-253}$$

The parameter β in Equations (3-252) and (3-253) is given by Equation (3-235).

Finally, the position coordinates x_{ep} and y_{ep}, relative to the equinoctial coordinate system, are given by

$$X_1 = \bar{r} \cdot \hat{f} \tag{3-254}$$

$$Y_1 = \bar{r} \cdot \hat{g} \tag{3-255}$$

3.3.10 HERRICK-CARTESIAN TRANSFORMATIONS (REFERENCES 13 AND 14)

The coordinate transformations between the Herrick and Cartesian systems are described in the following subsections.

3.3.10.1 Herrick Elements to Cartesian Coordinates

The following method is used for conversion from Herrick elements, $\bar{e}$, $\bar{\ell}$, n, and λ, to inertial Cartesian coordinates. The unit vectors $\hat{f}$, $\hat{g}$, and $\hat{w}$ along the equinoctial

orbit plane coordinate directions (see Section 3.2.5) must first be determined. The unit vector $\hat{w}$ is given by

$$\hat{w} = \frac{\bar{\ell}}{|\ell|} \tag{3-256}$$

The unit vectors $\hat{f}$ and $\hat{g}$ are determined from Equations (3-242) through (3-245) as functions of $\hat{w}$.

The Kepler equation for Herrick elements is solved by iteration for the eccentric longitude F,

$$\lambda = F + h \cos F - k \sin F \tag{3-257}$$

where h and k are calculated from Equations (3-246) and (3-247) as functions of the known vectors $\bar{e}$, $\hat{f}$, and $\hat{g}$.

The coordinates of position and velocity in the direct equinoctial system, X_1, Y_1, $\dot{X}_1$, $\dot{Y}_1$, are given by Equations (3-231) through (3-234), with

$$a = \left(\frac{\mu}{n^2}\right)^{1/3} \tag{3-258}$$

Finally, the position and velocity in the inertial Cartesian system are computed via the following transformations:

$$\bar{r} = X_1 \hat{f} + Y_1 \hat{g} \tag{3-259}$$

$$\dot{\bar{r}} = \dot{X}_1 \hat{f} + \dot{Y}_1 \hat{g} \tag{3-260}$$

3.3.10.2 Cartesian Coordinates to Herrick Elements

Given the Cartesian position and velocity vectors, $\bar{r}$ and $\dot{\bar{r}}$, the Herrick variables $\bar{e}$, $\bar{\ell}$, n, and λ are computed as described below.

The eccentricity, e, is given by

$$\bar{e} = -\frac{\bar{r}}{r} - \frac{(\bar{r} \times \dot{\bar{r}}) \times \dot{\bar{r}}}{\mu} \tag{3-261}$$

The angular momentum vector is

$$\bar{\ell} = \frac{\bar{r} \times \dot{\bar{r}}}{\sqrt{\mu}} \tag{3-262}$$

and the Kepler mean motion is

$$n = \sqrt{\frac{\mu}{a^3}} \tag{3-263}$$

where the semimajor axis, a, is given by

$$a = \left[\frac{2}{r} - \frac{|\dot{\bar{r}}|^2}{\mu}\right]^{-1} \tag{3-264}$$

The mean longitude, λ, is computed from the generalized Kepler equation given in Equation (3-250) to be

$$\lambda = F + h \cos F - k \sin F \tag{3-265}$$

where the variables h and k are determined from Equations (3-246) and (3-247), with vectors $\hat{w}$, $\hat{f}$, and $\hat{g}$ calculated from Equations (3-256) and Equations (3-242) through (3-245). The eccentric longitude, F, is determined from Equations (3-251) through (3-253), β is determined from Equation (3-235), and X_1 and Y_1 are determined from Equations (3-254) and (3-255).

3.3.11 KEPLERIAN TO EQUINOCTIAL AND HERRICK TRANSFORMATIONS

The coordinate transformations between the Keplerian and the equinoctial or Herrick systems are described in the following subsections.

3.3.11.1 Keplerian to Equinoctial Elements

The conversion from Keplerian elements (a, e, i, Ω, ω, M) to equinoctial elements is performed via the following equations:

Direct Set ($0° \leq i < 180°$)	Retrograde Set ($0° < i \leq 180°$)	
$a = a$	$a = a$	(3-266)
$h = e \sin(\omega + \Omega)$	$h_r = e \sin(\omega - \Omega)$	(3-267)
$k = e \cos(\omega + \Omega)$	$k_r = e \cos(\omega - \Omega)$	(3-268)
$p = \tan(i/2) \sin \Omega$	$p_r = \cot(i/2) \sin \Omega$	(3-269)
$q = \tan(i/2) \cos \Omega$	$q_r = \cot(i/2) \cos \Omega$	(3-270)
$\lambda = M + \omega + \Omega$	$\lambda_r = M + \omega - \Omega$	(3-271)

3.3.11.2 Keplerian to Herrick Elements

Conversion from Keplerian to Herrick elements is performed using the following equations:

$$e_x = e \cos \Omega \cos \omega - e \sin \Omega \sin \omega \sin i \quad (3\text{-}272)$$

$$e_y = e \sin \Omega \cos \omega + e \cos \Omega \sin \omega \cos i \quad (3\text{-}273)$$

$$e_z = e \sin \omega \sin i \quad (3\text{-}274)$$

$$|\ell| = \sqrt{a(1 - e^2)} \quad (3\text{-}275)$$

$$\ell_x = |\ell| \sin \Omega \sin i \quad (3\text{-}276)$$

$$\ell_y = -|\ell| \cos \Omega \sin i \tag{3-277}$$

$$\ell_z = |\ell| \cos i \tag{3-278}$$

$$n = \sqrt{\mu/a^3} \tag{3-279}$$

$$\lambda = M + \omega + \Omega \tag{3-280}$$

where j is as defined following Equation (3-238). The Herrick elements are not currently used in GTDS.

3.3.12 VEHICLE-FIXED TO BODY-CENTERED TRUE OF DATE TRANSFORMATIONS

The propulsive and aerodynamic accelerations are modeled in the vehicle-fixed coordinate system described in Section 3.2.7. These vehicle-oriented accelerations must be transformed to the inertial Cartesian system to be consistent with other terms in the dynamical equations of motion.

The following three angular transformations are required to orient the vehicle-fixed coordinates with respect to the inertial Cartesian axes:

$R_z(\alpha_v)$ = rotation about the inertial $\hat{z}$ axis, through the right ascension, α_v, of the vehicle's (longitudinal) $\hat{x}_v$ axis.

$R_y(-\delta_v)$ = negative rotation about the new $\hat{y}$ axis, through the declination, δ_v, of the vehicle's (longitudinal) $\hat{x}_v$ axis.

$R_x(\phi_v)$ = rotation about the new $\hat{x}$ axis (which is aligned with the $\hat{x}_v$ axis), through the roll angle, ϕ_v, to the vehicle-fixed axes

where R_x and R_z are given by Equation (3-14), and R_y is

$$R_y(\alpha) = \begin{bmatrix} \cos \alpha & 0 & -\sin \alpha \\ 0 & 1 & 0 \\ \sin \alpha & 0 & \cos \alpha \end{bmatrix} \tag{3-281}$$

If an arbitrary vector is denoted by $\bar{\xi}_v$ when expressed in vehicle-fixed coordinates and by $\bar{\xi}$ when expressed in inertial Cartesian coordinates, then the transformation between coordinates can be written as

$$\begin{aligned} \bar{\xi} &= [R_x(\phi_v)\, R_y(-\delta_v)\, R_z(a_v)]^T\, \bar{\xi}_v \\ &= Q\, \bar{\xi}_v \end{aligned} \tag{3-282}$$

where the elements of Q are

$$q_{11} = \cos \delta_v \cos a_v \tag{3-283a}$$

$$q_{12} = -\sin \phi_v \sin \delta_v \cos a_v - \cos \phi_v \sin a_v \tag{3-283b}$$

$$q_{13} = -\cos \phi_v \sin \delta_v \cos a_v + \sin \phi_v \sin a_v \tag{3-283c}$$

$$q_{21} = \cos \delta_v \sin a_v \tag{3-283d}$$

$$q_{22} = -\sin \phi_v \sin \delta_v \sin a_v + \cos \phi_v \cos a_v \tag{3-283e}$$

$$q_{23} = -\cos \phi_v \sin \delta_v \sin a_v - \sin \phi_v \cos a_v \tag{3-283f}$$

$$q_{31} = \sin \delta_v \tag{3-283g}$$

$$q_{32} = \sin \phi_v \cos \delta_v \tag{3-283h}$$

$$q_{33} = \cos \phi_v \cos \delta_v \tag{3-283i}$$

3.3.13 GEOGRAPHIC COORDINATES TO SPHERICAL COORDINATES

The right ascension, a, in spherical coordinates is obtained as follows:

$$a = a_g + \lambda_E \tag{3-284}$$

where

λ_E = geographic east longitude, measured positive west ($-2\pi \leq \lambda \leq 0$)

a_g = Greenwich hour angle

The declination, δ, in spherical coordinates is computed as follows:

$$\delta = \phi' + \arcsin\left[\frac{H_s}{r} \sin(\phi - \phi')\right] \tag{3-285}$$

where

$$\phi' = \arctan[(1 - f^2)\tan\phi] \tag{3-286}$$

$$e^2 = 2f - f^2 \tag{3-287}$$

$$r_s = \frac{R_e\sqrt{(1 - e^2)}}{\sqrt{1 - e^2\cos^2\phi'}} \tag{3-288}$$

$$H_s = \sqrt{r^2 - r_s^2\sin^2(\phi - \phi')} - r_s\cos(\phi - \phi') \tag{3-289}$$

and

f = inverse flattening coefficient of the central body [defined in Equation (3-135)]

e = eccentricity of the central body

ϕ = geodetic latitude

ϕ' = geocentric latitude

R_e = equatorial radius of the central body

r_s = distance of the subsatellite point from the center of the Earth

H_s = height above the mean spheroid, normal to the ellipsoidal surface

r = magnitude of the position vector

The bank angle, ν, in spherical coordinates, is then determined from

$$\nu = -\Gamma + \frac{\pi}{2} \tag{3-290}$$

where Γ, the flight path angle, is the angle between $\bar{R}$ and $\dot{\bar{R}}$, the spacecraft inertial position and velocity vectors, where $-\pi/2 \leq \Gamma \leq \pi/2$.

3.3.14 INERTIAL TO ROTATING LIBRATION COORDINATES

The L_1 (libration) point lies on the vector between the Sun and the Earth-Moon barycenter. If $\bar{R}_B$ and $\bar{V}_B$ are the inertial position and velocity vectors of the barycenter with respect to the Sun, then the $\hat{x}'$, $\hat{y}'$, $\hat{z}'$ axes of the rotating libration point coordinate system are aligned along the vectors $\bar{R}_B$, $(R_B \times V_B) \times R_B$, and $R_B \times V_B$, respectively.

The transformation from either ecliptic or equatorial inertial coordinates, $\bar{R}$, $\bar{V}$, to this rotating Libration Coordinate System is computed as follows:

$$\begin{bmatrix} \bar{R}_L \\ \bar{V}_L \end{bmatrix} = \begin{bmatrix} Q & 0 \\ \dot{Q} & Q \end{bmatrix} \begin{bmatrix} \bar{R} \\ \bar{V} \end{bmatrix} \tag{3-291}$$

$$Q = \begin{bmatrix} \hat{x}' \cdot \hat{x} & \hat{x}' \cdot \hat{y} & \hat{x}' \cdot \hat{z} \\ \hat{y}' \cdot \hat{x} & \hat{y}' \cdot \hat{y} & \hat{y}' \cdot \hat{z} \\ \hat{z}' \cdot \hat{x} & \hat{z}' \cdot \hat{y} & \hat{z}' \cdot \hat{z} \end{bmatrix} \tag{3-292}$$

$$\dot{Q} = \begin{bmatrix} \dot{\hat{x}}' \cdot \hat{x} & \dot{\hat{x}}' \cdot \hat{y} & \dot{\hat{x}}' \cdot \hat{z} \\ \dot{\hat{y}}' \cdot \hat{x} & \dot{\hat{y}}' \cdot \hat{y} & \dot{\hat{y}}' \cdot \hat{z} \\ \dot{\hat{z}}' \cdot \hat{x} & \dot{\hat{z}}' \cdot \hat{y} & \dot{\hat{z}}' \cdot \hat{z} \end{bmatrix} \tag{3-293}$$

The libration coordinate axes are defined as

$$\hat{x}' = \frac{\bar{R}_B}{|\bar{R}_B|} \tag{3-294}$$

$$\hat{z}' = \frac{\bar{R}_B \times \bar{V}_B}{|\bar{R}_B \times \bar{V}_B|} \tag{3-295}$$

$$\hat{y}' = \hat{z}' \times \hat{x}' \tag{3-296}$$

The quantities $\hat{x}$, $\hat{y}$, and $\hat{z}$ are the inertial axes. The inertial position and velocity of the Earth/Moon barycenter with respect to the Sun are given by

$$\bar{R}_B = \frac{\frac{M_E}{M_M}\bar{R}_E + \bar{R}_M}{\frac{M_E}{M_M} + 1} \tag{3-297a}$$

$$\bar{V}_B = \frac{\frac{M_E}{M_M}\bar{V}_E + \bar{V}_M}{\frac{M_E}{M_M} + 1} \tag{3-297b}$$

where

$\bar{R}_E$ = inertial position vector of the Earth with respect to the Sun

$\bar{V}_E$ = inertial velocity vector of the Earth with respect to the Sun

$\bar{R}_M$ = inertial position vector of the Moon with respect to the Sun

$\bar{V}_M$ = inertial velocity vector of the Moon with respect to the Sun

M_E = mass of the Earth

M_M = mass of the Moon

The rate of change of the libration coordinate axes is given by

$$\dot{\hat{x}}' = \frac{\bar{V}_B}{|\bar{R}_B|} - \frac{\bar{R}_B \cdot \bar{V}_B}{|\bar{R}_B|^3} \bar{R}_B \tag{3-298}$$

$$\dot{\hat{z}}' = \frac{\bar{R}_B \times \bar{A}_B}{|\bar{R}_B \times \bar{V}_B|} - \frac{[(\bar{R}_B \times \bar{V}_B) \cdot (\bar{R}_B \times \bar{A}_B)]}{|\bar{R}_B|^3} \bar{R}_B \times \bar{V}_B \tag{3-299}$$

$$\dot{\hat{y}}' = \frac{[(\bar{R}_B \times \bar{A}_B) \times \bar{R}_B + \bar{R}_B \times \bar{A}_B]}{|(\bar{R}_B \times \bar{V}_B) \times \bar{R}_B|} \tag{3-300}$$

$$\frac{-(\bar{R}_B \times \bar{V}_B) \times \bar{R}_B \cdot [(\bar{R}_B \times \bar{A}_B) \times \bar{R}_B + \bar{R}_B \times \bar{A}_B]}{|\bar{R}_B|^3} (\bar{R}_B \times \bar{V}_B) \times \bar{R}_B$$

where

$$\bar{A}_B = -GM_{SUN} \frac{\bar{R}_B}{|\bar{R}_B|^3} \tag{3-301}$$

3.4 TIME SYSTEMS

The GTDS orbit determination program uses the atomic time system, A.1, in the integration of the equations of motion. However, the system must interface with external input/output data sets that are referenced to other time systems, such as ephemeris time (ET) for the solar/lunar/planetary (SLP) ephemerides, UT1 for computing the Greenwich sidereal time, and coordinated universal time (UTC) for input/output epochs and tracking data. A brief description of the relevant time systems and their interrelationships follows (References 1, 15, and 16).

3.4.1 EPHEMERIS TIME, ET

Ephemeris time (ET) is the uniform measure of time, which is the independent variable of the equations of motion, and the argument for the ephemerides of the planets, the Moon, and the spacecraft. The units of ET is the ephemeris second, which is defined as the fraction 1/31,556,925.9747 of the tropical year for 12^h ET of January 0^d, 1900. Ephemeris time is determined from the instant near the beginning of the calendar

year 1900 when the geometric mean longitude of the Sun referred to the mean equinox of date was $279^h\,41'48''.04$, at which instant the measure of ephemeris time was 1900 January $0^d\,12^h$.

3.4.2 ATOMIC TIME, A.1

Atomic time (A.1) is one of several types of atomic time. It is obtained from oscillations of the United States Cesium Frequency Standard located at Boulder, Colorado. In 1958, the United States Naval Observatory established the A.1 system based on an assumed frequency of 9,192,631,770 oscillations of the isotope 133 of the cesium atom per A.1 second. The reference epoch of A.1 was established such that on January 1, 1958, $0^h0^m0^s$ UT2 the value of A.1 was $0^h0^m0^s$, January 1, 1958.

3.4.3 UNIVERSAL TIME, UT

Universal time (UT) is the measure of time that is the theoretical basis for all civil timekeeping. UT is related to the rotation of the Earth on its axis. Compared with ephemeris time, which is uniform time, UT does not take into account the irregularities of the Earth's rate of rotation.

The quantity UT is defined as 12 hours plus the Greenwich hour angle (GHA) of a point (representing the fictitious mean Sun) on the mean equator of date whose right ascension measured from the mean equinox of date is

$$R_u = 18^h38^m45^s.836 + 8,640,184^s.542\,T_u + 0^s.0929\,T_u^2 \qquad (3\text{-}302)$$

where T_u is defined following Equation (3-38).

The Greenwich hour angle of this point, denoted by S_u in Figure 3-16, is

$$\text{GHA of } S_u = a_{GM} - R_u \qquad (3\text{-}303)$$

where a_{GM} is the Greenwich mean sidereal time; hence,

$$UT = 12^h + a_{GM} - R_u \qquad (3\text{-}304)$$

Adding 12 hours to both sides of the above equation yields

$$UT + 12^h = a_{GM} - R_u \qquad (3\text{-}305)$$

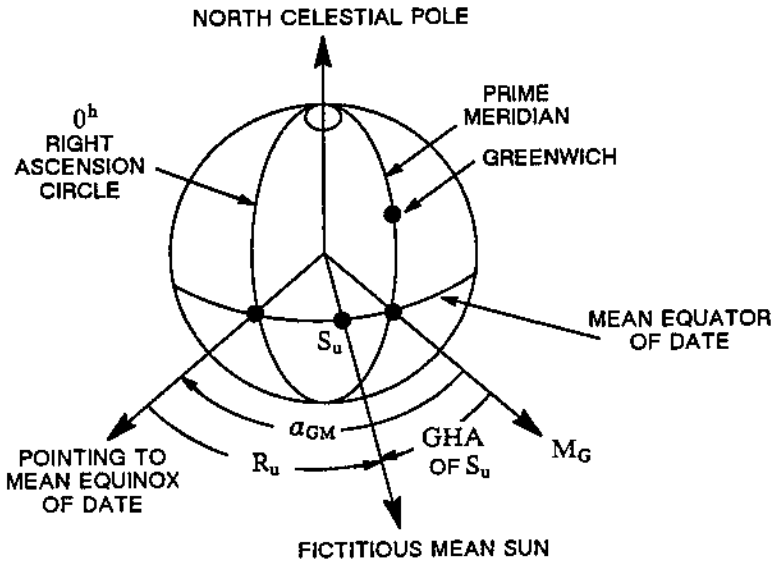

Figure 3-16. Greenwich Hour Angle

and solving for a_{GM}

$$a_{GM} = 12^h + UT + R_u \tag{3-306}$$

In practice, the point whose right ascension is R_u cannot be observed. Consequently, the practical determinations of UT are obtained, through the intermediary of sidereal time, from observations of the diurnal motion of the stars. Sidereal time is a measure of the rotation of the Earth relative to the stars and is defined as the hour angle of the vernal equinox. Therefore, the meridian transit of a star occurs at a sidereal time equal to its right ascension.

Universal time varies from uniform time due to variations of the meridian, arising principally from polar motion, and variations in the rotational rate of the Earth, consisting of secular, irregular, periodic seasonal, and periodic tidal terms. The tidal variations are very small; the secular variation is significant only over large time intervals; and the irregular variations, while they may be relatively large, are highly erratic. The periodic seasonal variation appears stable enough to be predictable.

There are three measures of UT in common usage: (1) UT0, which is determined from observations of the local mean sidereal time; (2) UT1, obtained by correcting UT0 for polar motion; and (3) UT2, which results from the removal of the seasonal inequality from UT1.

3.4.4 UNCORRECTED UNIVERSAL TIME, UT0

Uncorrected universal time (UT0) is obtained by assuming an adopted conventional value λ_A of the longitude of each observing station (see Section 3.3.2.2). The local mean sidereal time at transit is generally determined through observation of meridian transits of stars, omitting from the apparent right ascension the nutation terms that are independent of the coordinates of the star (the equation of the equinoxes). Subtracting the east longitude of the observing station gives a_{GM}, the Greenwich mean sidereal time or Greenwich hour angle of the mean equinox of date. UT0 is then obtained from Equation (3-304) by adding 12 hours and subtracting R_u from this value. Since the motion of the pole causes variations in the meridian, UT0 is dependent on the location of the observing station.

3.4.5 UNIVERSAL TIME, UT1

UT1 universal time is obtained from UT0 by applying an appropriate correction in longitude due to the motion of the pole. UT1 is the form of universal time used in GTDS. This measure of time reflects the actual orientation of the Earth with respect to the vernal equinox at that instant. UT1 will be the same for all observatories. In contrast, UT0 time, as determined by different observatories using their adopted longitude in calculations, results in a different value of UT0 for each observatory.

Then

$$UT1 = UT0 - \Delta\lambda \tag{3-307}$$

where $\Delta\lambda$ is given in Equation (3-50).

UT1 time is used by GTDS to compute the a_{GM} as given in Equation (3-38).

3.4.6 UNIVERSAL TIME, UT2

If the extrapolated value of UT1 time is corrected for periodic seasonal variations, SV, in the Earth's speed of rotation, the resulting time is UT2. UT2 does not represent the actual orientation of the Earth with respect to the vernal equinox. UT1 should always be used when the actual orientation of the Earth is required. UT2 is often referred to as Greenwich Mean Time (GMT) or ZULU time. The equation for UT2 is

$$UT2 = UT1 + SV \tag{3-308}$$

where

$$SV = 0^s.022 \sin 2\pi t - 0^s.017 \cos 2\pi t - 0^s.007 \sin 4\pi t + 0^s.006\, 4\pi t \quad (3\text{-}309)$$

or

$$SV = 0^s.022 \sin 2\pi t - 0^s.012 \cos 2\pi t - 0^s.006 \sin 4\pi t + 0^s.007\, 4\pi t \quad (3\text{-}310)$$

Equation (3-309) was used prior to 1962 and Equation (3-310) has been in use since 1962. The quantity t equals the fraction of the tropical year elapsed from the beginning of the Besselian year for which the calculation is made. (One tropical year equals 365.2422 days.) Since seasonal variations can be known precisely only after their occurrence, UT2 itself is rarely used. The Bureau International de l'Heure also issues corrections for $\Delta\lambda$ and SV.

3.4.7 COORDINATED UNIVERSAL TIME, UTC

Coordinated universal time (UTC) is the standard time scale to which tracking stations are synchronized. UTC time is derived from atomic time, A.1, in a manner that makes it almost synchronous with UT2. Up to January 1, 1972, the UTC time scale operated at a frequency offset from the atomic time scale. The value of the offset was periodically changed by international agreement so that the UTC scale would correspond more closely to UT2. On January 1, 1972, a new improved UTC system, adopted by the International Radio Consultative Committee (CCIR), was internationally implemented by the timekeeping laboratories and time-broadcast stations.

The new UTC system eliminates the frequency offset from atomic time, thus making the UTC second constant and equal in duration to the A.1 second (References 17 and 18). The new UTC time scale is now kept in synchronism with the rotation of the Earth to within $\pm$ 0.7 second by step-time adjustments of exactly 1 second, when needed.

3.4.8 STATION TIME, ST

This measure of time is obtained at each station by counting cycles of a rubidium atomic frequency standard. The difference between ST and UTC is tabulated by each station. The observables are recorded in ST and then transformed to UTC.

3.5 TRANSFORMATIONS BETWEEN TIME SYSTEMS

Desired transformations between the time systems ET, A.1, UTC, and UT1 are carried out in GTDS by evaluating either a standard formula or an appropriate time polynomial.

3.5.1 TRANSFORMATIONS BY STANDARD FORMULA

For most purposes, the difference between A.1 and ET can be considered a constant. The suspected discrepancy is roughly two parts in 10^9. The actual transformation between A.1 and ET time is given by

$$(\mathrm{ET} - \mathrm{A.1}) = \Delta T_{1958} - \frac{(\mathrm{JD} - 2,436,204.5)(86,400)}{9,192,631,770} \times \Delta f_{\mathrm{cesium}} + \frac{2e(\mu a)^{1/2} \sin E}{c^2} \tag{3-311}$$

where

ΔT_{1958}	=	ET – UT2 on 1 January 1958, $0^h0^m0^s$ UT2, minus the periodic term in Equation (3-311) evaluated at this same epoch
JD	=	Julian date
2,436,204.5	=	Julian date on 1 January 1958, $0^h0^m0^s$
$\Delta f_{\mathrm{cesium}}$	=	correction to f_{cesium} = 9,192,631,770 cycles of cesium per ephemeris second
μ	=	gravitational constant of the Sun = $1.32715445 \times 10^{11}$ kilometers^3/second^2
a	=	semimajor axis of the heliocentric orbit of the Earth-Moon barycenter = 149,599,000 kilometers
e	=	eccentricity of the heliocentric orbit of the Earth-Moon barycenter = 0.01672
c	=	speed of light at an infinite distance from the Sun = 299,792.5 kilometers/second
E	=	eccentric anomaly at the heliocentric orbit of the Earth-Moon barycenter

The first term of Equation (3-311) arises because A.1 was set equal to UT2 at the beginning of 1958. The second term accounts for the difference between the lengths of ET and A.1 seconds (if $\Delta f_{\mathrm{cesium}}$ is nonzero). The periodic term arises from general relativity. It accounts for the fact that A.1, UTC, and ST times are measures of the proper time observed on Earth and that ET is a measure of the coordinate time in the heliocentric (strictly barycentric) space-time frame of reference. The contribution of the last two terms in Equation (3-311) is negligible for the range of applications currently contemplated for

GTDS. Hence, the transformation between ET and A.1 is accomplished using the approximate formula

$$ET - A.1 = 32^{s}.15 \tag{3-312}$$

3.5.2 TRANSFORMATIONS BY TIME POLYNOMIALS

The remaining transformations between the time systems A.1, UTC, and UT1 are accomplished using the time difference data, A.1-UTC and UT1-UTC, supplied in Earth Orientation Bulletins by the United States Naval Observatory. These data have been conveniently reduced by quadratic polynomial fits to improve the efficiency of the transformation procedure. The time difference polynomials derived for use by GTDS have the form

$$(A.1 - UTC)_i = a_{i1} + a_{i2}\,T + a_{i3}\,T^2 \tag{3-313}$$

$$(A.1 - UT1)_i = a_{i4} + a_{i5}\,T + a_{i6}\,T^2 \tag{3-314}$$

where

A.1-UTC = difference between A.1 and UTC time (in seconds)
A.1-UT1 = difference between A.1 and UT1 time (in seconds)

The quantity T is the number of days from the beginning of the timespan covered by the polynomial, T = 1, 2, ... For the given modified Julian date, MJD,

$$T = MJD - MJD_i + 1 \tag{3-315}$$

In this expression, MJD_i is the tabular modified Julian date that bounds the interval from below, i.e.,

$$MJD_i \leq MJD < MJD_{i+1} \tag{3-316}$$

The coefficients a_{ij} and the associated timespans are determined by least-squares fitting second-order polynomials to published time difference data. The timespans are determined by constraining the maximum deviation (between the data and polynomial) to be less than 0.0005 second for A.1-UTC and less than 0.005 second for A.1-UT1. Provision is made for inserting future A.1-UTC offsets (leap seconds) as predicted by the USNO. Extrapolation of A.1-UT1 time is achieved by performing a linear least-squares fit on the data for the last 6 months to obtain a_{i5}, the A.1-UT1 rate. The second-order coefficient, a_{i6}, is set equal to zero. This extrapolation is used for 1 year from the date of the last available observation; after this, both a_{i5} and a_{i6} are set equal to zero.

3.6 POLYNOMIAL REPRESENTATION OF EPHEMERIS DATA

In GTDS, planetary and lunar positions and velocities, as well as the Earth's nutation and precession data, are determined by evaluating multiple-day-arc Chebyshev polynomials whose coefficients are derived from ephemeris data contained on tapes supplied by the Jet Propulsion Laboratory (JPL) (References 6 and 19). The data contained on the JPL tapes are Chebyshev coefficients for polynomial fits to the positions and velocities of the planets Mercury, Venus, Earth-Moon barycenter, Mars, Jupiter, Saturn, Uranus, Neptune, Pluto, and the Earth's Moon, as well as the nutation rates in longitude and obliquity. These data are generated by weighted least-squares estimation of the appropriate orbital models using source positions obtained on the basis of current planetary theories. Positions and velocities on the tapes are referenced to the rectangular equatorial system of the mean equator and equinox of B1950.0 or mean equator and equinox of J2000.0, with planetary data being heliocentric and lunar data being geocentric.

The software used to retrieve data from a JPL ephemeris tape provides interpolated values of position and velocity vectors of any requested set of bodies relative to the Earth. The data obtained are ephemerides of the Sun, Moon, and planets (SLP) in a mean reference frame on a dynamical (ephemeris) time base. The time base is related to the A.1 time base, as discussed in Section 3.5. Optionally, they can be coverted to data in a true of date reference frame, as discussed in Section 3.3.1. In addition, the precession and nutation data, for the same timespans as the SLP data, are generated, as discussed in Section 3.3.1.

The Chebyshev polynomial coefficients are obtained from the JPL ephemeris data in the following manner. If the function values provided by the JPL software at requested times t_i (i = 1, 2, ..., m + 1) for a single component of position, velocity, or nutation is

designated y_i, then an mth-order interpolating function in the interval $[t_1, t_{m+1}]$ can be obtained as a linear combination of basic functions $F_j(t)$ as follows:

$$Y_m(t) = \sum_{j=1}^{m+1} c_j F_j(t) \tag{3-317}$$

by requiring that the differences between the data and the function be a minimum, where the following is the function to minimize:

$$Q = \sum_{i=1}^{m+1} \left[y_i - \sum_{j=1}^{m+1} c_j F_j(t_i) \right]^2 \tag{3-318}$$

The choice of the functions $F_j(t)$ $(j = 1, 2, ..., m + 1)$ in Equation (3-317) has important ramifications both on the obtainable accuracy of $Y_m(t)$ for $t \neq t_i$ and the ease of determining the values of c_j.

The interval $[t_1, t_{m+1}]$ is transformed to $[1, -1]$ by the linear transformation of variables

$$x = \frac{2t - (t_{m+1} + t_1)}{t_{m+1} - t_1} \tag{3-319}$$

The functions F are then chosen as the orthogonal Chebyshev polynomials of degree $j - 1$, i.e.,

$$T_j(x) = \cos [(j - 1) \cos^{-1} x] \tag{3-320}$$

where

$$T_1(x) = 1 \tag{3-321a}$$

$$T_2(x) = x \tag{3-321b}$$

$$T_3(x) = 2x^2 - 1 \qquad (3\text{-}321c)$$

$$T_{j+1}(x) = 2x\,T_j(x) - T_{j-1}(x) \qquad (3\text{-}321d)$$

Under these conditions, Equations (3-317) and (3-318) can be reformulated as

$$Y_m(x) = \sum_{j=1}^{m+1} c_j\,T_j(x) \qquad (3\text{-}322)$$

and

$$Q = \sum_{i=1}^{m+1} \left[y_i - \sum_{j=1}^{m+1} c_j\,T_j(x_i) \right]^2 = 0 \qquad (3\text{-}323)$$

All data are fit over the same interval. Data reduction can be achieved by selecting the least number of coefficients for which

$$\underset{x}{\text{Max}} \left\{ \left| y - \sum_{j=1}^{m+1} c_j\,T_j(x) \right| \right\} < \epsilon \qquad (3\text{-}324)$$

for x in [1, −1]. This is satisfied if the coefficient of the truncated term, c_{m+2}, is less than ϵ, because of the minimum-maximum property of Chebyshev polynomials. For a given interval $[t_1, t_{m+1}]$, the discrepancy between y and $Y_m(x)$ is minimized and the amount of work required to determine the c_j substantially reduced by selecting the base points x_i as the roots of the Chebyshev polynomial of degree m + 1, i.e.,

$$x_i = \cos \frac{(2i - 1)}{2(m + 1)} \qquad (i = 1, 2, \ldots, m + 1) \qquad (3\text{-}325)$$

At these points, the polynomials have the following orthogonality property with respect to summation as well as integration:

$$\sum_{a=1}^{m+1} T_j(x_a)\, T_k(x_a) = 0 \qquad (j \neq k) \tag{3-326}$$

$$\sum_{a=1}^{m+1} T_j(x_a)\, T_k(x_a) = \frac{m+1}{2} \qquad [j = k;\ j, k < (m+1)] \tag{3-327}$$

This property is derived from the corresponding orthogonality property of the cosine functions and makes it possible to determine the c_j from

$$c_1 = \frac{1}{m+1} \sum_{i=1}^{m+1} y_i\, T_1(x_i) \tag{3-328}$$

$$c_j = \frac{2}{m+1} \sum_{i=1}^{m+1} y_i\, T_j(x_i) \qquad (j = 2, 3, \ldots, m+1) \tag{3-329}$$

Once the coefficients c_j of the linear combination of T_j have been determined, $Y_m(x)$ can be conveniently transformed into the equivalent Chebyshev interpolating polynomial in $[1, -1]$

$$Y_m(x) = \sum_{i=1}^{m+1} b_i\, x^{i-1} \tag{3-330}$$

as shown below.

Let

$$a_{1j} = (-1)^{j+1} c_{2j-1} \qquad [j = 1, 2, \ldots, (2j - 1) \leq m] \tag{3-331}$$

$$a_{i1} = 2^{i-2} c_i \qquad (i = 2, 3, \ldots, m + 1) \tag{3-332}$$

and

$$a_{ij} = c_{[i+2(j-1)]} [2a_{i-1,j} - a_{i,j-1}] \qquad \begin{matrix} \{i = 2, 3, \ldots, [i+2(j-1)] \leq m+1\} \\ \{j = 2, 3, \ldots, [i+2(j-1)] \leq m+1\} \end{matrix} \tag{3-333}$$

Then, the coefficients b_i of the interpolating polynomial can be determined from

$$b_i = \sum_j a_{ij} \qquad \begin{matrix} (i = 1, 2, \ldots, m + 1) \\ \{j = 1, 2, \ldots, [i+2(j-1)] \leq m+1\} \end{matrix} \tag{3-334}$$

Finally, the polynomial so determined can be used to interpolate in the interval $[t_1, t_{m+1}]$ by means of the transformation of variables defined by Equation (3-319).

The present version of GTDS can handle any of 10 bodies, one of which is the central body. A solar/lunar/planetary file by Chebyshev approximating the polynomials is generated covering the entire time interval of interest. The file contains polynomials for each component of position and velocity and for each element of the matrices that transform from the selenocentric true of date to the selenographic coordinate system and from the mean equator and equinox of date to the true of date coordinate system, as required by the application. The file also contains coefficients for the equation of the equinoxes, ΔH, used to correct the mean Greenwich sidereal time as given in Equation (3-38). Three SLP Ephemeris Files are created: one for mean of B1950.0 data, one for mean of J2000.0 data, and one for true of date data.

3.7 REFERENCES

1. Her Majesty's Stationery Office: 1961, *Explanatory Supplement*, Nautical Almanac Office, London.

2. U.S. Government Printing Office: (published yearly), *The Astronomical Almanac*, Nautical Almanac Office, Washington, D.C.

3. Melbourne, W. G., Mulholland, J. D., Sjogren, W. L., and Sturms, F. M.: 1968, *Constants and Related Information for Astrodynamic Calculations, 1968*, Jet Propulsion Laboratory Technical Report 32-1306, July 1968.

4. Lieske, J. H.: 1979, "Precession Matrix Based on IAU (1976) System of Astronomical Constants," *Astronomy and Astrophysics*, Vol. 73, pp. 282-284.

5. Kalensher, B. E.: 1961, *Selenographic Coordinates*, Jet Propulsion Laboratory Technical Report 32-41, February 1961.

6. Standish, E. M.: 1982, *JPL Export Ephemeris User's Guide*, March 1982.

7. Nautical Almanac Office and H. M. Nautical Almanac Office: 1983, *Supplement to the Astronomical Almanac 1984*, U.S. Naval Observatory, Washington, D.C., and the Royal Greenwich Observatory, U.K.

8. TRW Systems Group: 1970, *Houston Operations Predictor/Estimator (HOPE) Engineering Manual*, Report TRW 70-FMT-792A, June 1970.

9. Escobal, P. R.: 1965, *Methods of Orbit Determination*, New York, John Wiley and Sons, Inc.

10. Battin, R. H.: 1964, *Astronautical Guidance*, New York, McGraw Hill.

11. Cefola, P. J., Long, A. C., and Nimitz, K. S.: 1972, *The Next Generation of Orbit Prediction Formulations for Artificial Satellites*, Computer Sciences Corporation Report 9101-053000-01TR, September 1972.

12. Cefola, P. J.: 1972, *Equinoctial Orbit Elements—Application to Artificial Satellite Orbits*, AIAA Paper 72-937, presented at the AIAA/AAS Astrodynamics Conference, Palo Alto, California, September 11-12, 1972.

13. Baker, R. M. L., Jr.: 1961, *Astrodynamics, Applications, and Advanced Topics*, New York, Academic Press.

14. Dallas, S. S., and Rinderle, E. A.: 1972, *A Comparison of Cowell's Method and a Variation-of-Parameters Method for the Computation of Precision Satellite Orbits*, Jet Propulsion Laboratory Technical Memorandum 392-101, Final Report, September 1972.

15. Brodie, R. A., Newell, F. F., Ekelund, J. E., and Warner, M. R.: 1969, *Double Precision Orbit Determination Program*, Vol. III, Jet Propulsion Laboratory Technical Report JPL-900-56; also, NASA Report NASA-CR-105589, June 1969.

16. Goddard Space Flight Center: 1968, *Satellite Geodesy Theory and Applications*, Wolf Research and Development Corp.

17. Curtright, J.: 1972, *DSN Frequency and Time Scale Change from UTC to IAT or New UTC*, Jet Propulsion Laboratory Technical Report 32-1526, Vol. VIII.

18. Chi, A. R. and Fosque, H. S.: 1971, *Changes in Standard Frequency and Time-Signal Broadcast—January 1, 1972*, Goddard Space Flight Center Report X-810-71-489, November 1971.

19. Biemesderfer, C. D.: 1983, *Testing, Reporting, and Maintenance Program (TRAMP) Maintenance Operations Guide*, Computer Sciences Corporation Report CSC/TM-83/6119, October 1983.

CHAPTER 4—PERTURBATION MODELS AND VARIATIONAL EQUATIONS

For orbital prediction using the method of special perturbations, the equations of motion of the satellite are integrated numerically. The perturbing acceleration vector is required to construct these equations, which are presented in Chapter 5. The sources of these perturbations are identified and the appropriate perturbation models presented in this chapter. The total perturbation model and the variational equations are described in Section 4.1. The specific perturbations, discussed in Sections 4.2 through 4.8, include the following:

- Gravitational acceleration due to n point masses, $\ddot{\bar{R}}_{PM}$ (Section 4.2)
- Gravitational acceleration due to the nonsphericity of the gravitational potential, $\ddot{\bar{R}}_{NS}$ (Section 4.3)
- Acceleration due to the mutual nonspherical gravitational attraction of the Earth and Moon, $\ddot{\bar{R}}_{IO}$ (not currently available in GTDS) (Section 4.4)
- Acceleration due to aerodynamic forces, $\ddot{\bar{R}}_{D}$ (Section 4.5)
- Acceleration due to solar radiation pressure, $\ddot{\bar{R}}_{SR}$ (Section 4.6)
- Acceleration due to attitude control system corrections, $\ddot{\bar{R}}_{TAC}$ (not currently available in GTDS) (Section 4.7)
- Acceleration due to the thrusting of the spacecraft engines, $\ddot{\bar{R}}_{T}$ (Section 4.8)

All or any subset of these effects can be included in the perturbing acceleration vector, which is used in the construction of the equations of motion using either the Cowell or Variation of Parameters formulations.

The partial derivatives of the current state vector with respect to the initial state vector are required in the differential correction process. These partial derivatives, which constitute the state transition matrix, can be obtained by numerically integrating a system of variational equations in conjunction with the Cowell orbit generator. The construction of these variational equations is discussed in detail for each of the perturbing accelerations. Accelerations that are included in the equations of motion, but for which the estimation process is insensitive, can be omitted in the construction of the variational equations.

A method of computing the partial derivatives analytically is discussed in Section 4.9. This analytical approach is always used in the differential correction process in GTDS when the Variation of Parameters or Brouwer orbit generators are used and is optional in the Cowell differential correction process.

4.1 TOTAL PERTURBATION MODEL AND VARIATIONAL EQUATIONS

The total acceleration vector is the sum of the accelerations induced by each of the sources listed above (expressed in an inertial Cartesian coordinate system; i.e., mean equator and equinox of B1950.0, mean equator and equinox of J2000.0, or true of reference date)

$$\ddot{\bar{R}} = \ddot{\bar{R}}_{PM} + \ddot{\bar{R}}_{NS} + \ddot{\bar{R}}_{IO} + \ddot{\bar{R}}_{D} + \ddot{\bar{R}}_{SR} + \ddot{\bar{R}}_{TAC} + \ddot{\bar{R}}_{T} \tag{4-1}$$

The total perturbing acceleration vector is usually defined as the total acceleration excluding the point-mass gravitational acceleration caused by the central body.

The Cowell equations of motion of the satellite can be written in the form

$$\ddot{\bar{R}} = f(\bar{R}, \dot{\bar{R}}, t, \bar{p}) \tag{4-2}$$

where

$\bar{R}$ = column vector of the vehicle position coordinates
$\bar{p}$ = vector of the dynamic parameters of dimension ℓ

and

$$\bar{p} = [\bar{R}(t_0), \dot{\bar{R}}(t_0), \bar{p}^*]^T \tag{4-3}$$

where

$\bar{p}^*$ = constant model parameters pertaining to drag, gravitational harmonic coefficients, etc.

The model parameters $\bar{p}$, which may be included in the variational equations, are as follows:

- Position and velocity of the spacecraft at epoch in mean of B1950.0 coordinates, mean of J2000.0 coordinates, true of date coordinates, classical orbital elements, spherical coordinates, or Definitive Orbit Determination System (DODS) variables

- Gravitational parameter of the central body
- Harmonics of the central body
- Gravitational parameters of the perturbing bodies
- Aerodynamic drag parameter
- Solar radiation pressure parameter
- Powered flight parameters
- Attitude control parameters (not currently available in GTDS)

These parameters are determined in such a way as to reduce the differences between a computed and an observed orbit. This orbit determination process requires the computation of variations in the state variables, $\vec{R}(t)$ and $\dot{\vec{R}}(t)$, as functions of variables in this parameter set.

If Equation (4-2) is differentiated with respect to $\bar{p}$, the matrix equation

$$\frac{\partial \ddot{\vec{R}}}{\partial \bar{p}} = \frac{\partial \ddot{\vec{R}}}{\partial \vec{R}} \frac{\partial \vec{R}}{\partial \bar{p}} + \frac{\partial \ddot{\vec{R}}}{\partial \dot{\vec{R}}} \frac{\partial \dot{\vec{R}}}{\partial \bar{p}} + \left(\frac{\partial \ddot{\vec{R}}}{\partial \bar{p}}\right)_{\text{explicit}} \tag{4-4}$$

is obtained. If the time, t, and the parameter set, $\bar{p}$, are independent, the differentiation with respect to t and $\bar{p}$ can be interchanged to give

$$\frac{d^2}{dt^2}\left(\frac{\partial \vec{R}}{\partial \bar{p}}\right) = \frac{\partial \ddot{\vec{R}}}{\partial \vec{R}} \frac{\partial \vec{R}}{\partial \bar{p}} + \frac{\partial \ddot{\vec{R}}}{\partial \dot{\vec{R}}} \frac{d}{dt}\left(\frac{\partial \vec{R}}{\partial \bar{p}}\right) + \left(\frac{\partial \ddot{\vec{R}}}{\partial \bar{p}}\right)_{\text{explicit}} \tag{4-5}$$

Defining the matrices

$$A(t) = \left[\frac{\partial \ddot{\vec{R}}(t)}{\partial \vec{R}}\right]_{3x3} \tag{4-6a}$$

$$B(t) = \left[\frac{\partial \ddot{\vec{R}}(t)}{\partial \dot{\vec{R}}}\right]_{3x3} \tag{4-6b}$$

$$C(t) = \left[\left(\frac{\partial \ddot{\bar{R}}(t)}{\partial \bar{p}}\right)_{\text{explicit}}\right]_{3x\ell} \tag{4-6c}$$

$$Y(t) = \left[\frac{\partial \bar{R}(t)}{\partial \bar{p}}\right]_{3x\ell} \tag{4-6d}$$

Equation (4-5) takes the form of a system of linear differential equations, called the variational equations, as follows:

$$\dot{Y} = A(t)\, Y + B(t)\, \dot{Y} + C(t) \tag{4-7}$$

Just as the basic Equation (4-1) is numerically integrated to obtain the position, $\bar{R}(t)$, and velocity, $\dot{\bar{R}}(t)$, of the satellite, the variational equations are integrated to obtain the matrices $Y(t)$ and $\dot{Y}(t)$, which yield the required partial derivatives. These partial derivatives are used to form the observation partial derivatives required for differential correction of the orbit. This application is discussed in Chapter 7.

The matrices A, B, and C are formulated for the case where $\ddot{\bar{R}}$ is of the form given in Equation (4-1)

$$A = \frac{\partial \ddot{\bar{R}}_{PM}}{\partial \bar{R}} + \frac{\partial \ddot{\bar{R}}_{NS}}{\partial \bar{R}} + \frac{\partial \ddot{\bar{R}}_{D}}{\partial \bar{R}} + \frac{\partial \ddot{\bar{R}}_{SR}}{\partial \bar{R}} + \frac{\partial \ddot{\bar{R}}_{TAC}}{\partial \bar{R}} + \frac{\partial \ddot{\bar{R}}_{T}}{\partial \bar{R}} \tag{4-8a}$$

$$B = \frac{\partial \ddot{\bar{R}}_{D}}{\partial \dot{\bar{R}}} \tag{4-8b}$$

$$C = \left(\frac{\partial \ddot{\bar{R}}}{\partial \bar{p}}\right)_{\text{explicit}} = \left[\frac{\partial \ddot{\bar{R}}}{\partial \bar{R}_0}, \frac{\partial \ddot{\bar{R}}}{\partial \dot{\bar{R}}_0}, \frac{\partial \ddot{\bar{R}}}{\partial \bar{p}^*}\right]_{\text{explicit}} = \left[0_3, 0_3, \frac{\partial \ddot{\bar{R}}}{\partial \bar{p}^*}\right] \tag{4-8c}$$

where

0_3 = 3×3 null matrix

$\frac{\partial \ddot{\bar{R}}}{\partial \bar{p}^*}$ = columns of explicit partial derivatives of the acceleration with respect to the model parameters:

$$\frac{\partial \ddot{\bar{R}}_{PM}}{\partial \mu}, \quad \frac{\partial \ddot{\bar{R}}_{PM}}{\partial \mu_k}, \quad \frac{\partial \ddot{\bar{R}}_{NS}}{\partial C_n^m}, \quad \cdots \text{ etc.}$$

4.2 POINT-MASS EFFECTS

To first order, the gravitational attraction of a perturbing body of mass m can be approximated as that arising from a dimensionless particle of mass m located at the center of mass of the body. An expression for the perturbing acceleration arising from n point masses is developed in this section.

4.2.1 N POINT-MASS PERTURBATION MODEL

In the development of the perturbation model for the gravitational effect of n massive bodies, the starting point is Newton's second law of motion and law of gravitation (References 1, 2, and 3).

The second law of motion for a body of mass m, acted upon by a force $\bar{F}$, is given by

$$\bar{F} = \frac{d}{dt}\left(m \frac{d\bar{R}}{dt}\right) \tag{4-9}$$

which, when m is constant, reduces to

$$\bar{F} = m \frac{d^2\bar{R}}{dt^2} \tag{4-10}$$

Here $\bar{R}$ is a vector from the center of an inertial coordinate system to the satellite.

The gravitational force acting on a satellite of mass m due to the attraction of a body of mass m_k, which is assumed to act as a point mass, given by

$$\bar{F}_k = -\frac{G\, m\, m_k}{R_{kp}^3} \bar{R}_{kp} \tag{4-11}$$

where G is the universal gravitational constant and $\bar{R}_{kp}$ is the vector from the body k to the satellite (see Figure 4-1).

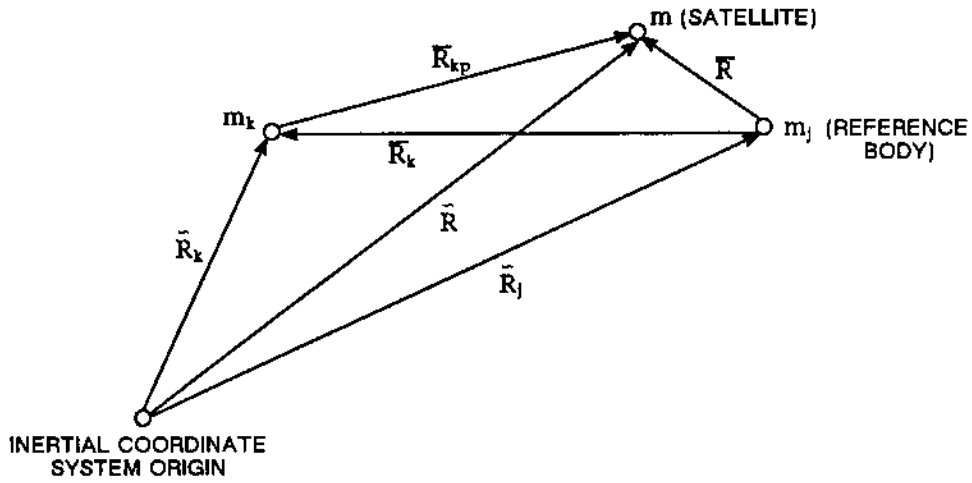

Figure 4-1. Schematic of Point-Mass Gravitational Bodies

To obtain the total contribution from all perturbing bodies, a summation over k is performed as follows:

$$\bar{F} = -\sum_{k=1}^{n} \frac{G\, m\, m_k}{R_{kp}^3}\, \bar{R}_{kp} \tag{4-12}$$

When this expression is substituted into Equation (4-10), the acceleration experienced by a satellite attracted by n point masses is obtained in an inertial coordinate system as

$$\frac{d^2 \bar{R}}{dt^2} = -\sum_{k=1}^{n} \frac{G\, m_k}{R_{kp}^3}\, \bar{R}_{kp} \tag{4-13}$$

For convenience and ease in the interpretation of results, it is advantageous to refer the motion of the satellite to one of the perturbing bodies. The force on body j, the reference or central body, is given by

$$\bar{F}_j = \sum_{\substack{k=1 \\ k \neq j}}^{n} \frac{G\, m_j\, m_k}{R_k^3}\, \bar{R}_k \tag{4-14}$$

where $\bar{R}_k$ is a vector from the reference jth body to the kth body. The acceleration of the reference body with respect to the inertial coordinate system is given by

$$\frac{d^2 \bar{R}_j}{dt^2} = \sum_{\substack{k=1 \\ k \neq j}}^{n} \frac{G\, m_k}{R_k^3}\, \bar{R}_k \tag{4-15}$$

Subtracting Equation (4-15) from Equation (4-13) yields

$$\frac{d^2 \bar{R}}{dt^2} - \frac{d^2 \bar{R}_j}{dt^2} = -\sum_{k=1}^{n} \frac{G\, m_k}{R_{kp}^3}\, \bar{R}_{kp} - \sum_{\substack{k=1 \\ k \neq j}}^{n} \frac{G\, m_k}{R_k^3}\, \bar{R}_k \tag{4-16}$$

Substituting $\bar{R} - \bar{R}_j = \bar{R} = \bar{R}_{jp}$ and $\bar{R}_{kp} = \bar{R} - \bar{R}_k$ into Equation (4-16) yields the acceleration due to n point masses

$$\ddot{\bar{R}}_{PM} = \frac{d^2 \bar{R}}{dt^2} = -\frac{\mu}{R^3}\, \bar{R} + \sum_{\substack{k=1 \\ k \neq j}}^{n} \mu_k \left[\frac{\bar{R}_k - \bar{R}}{|\bar{R}_k - \bar{R}|^3} - \frac{\bar{R}_k}{|\bar{R}_k|^3} \right] \tag{4-17}$$

where $\bar{R}_{PM}$, $\bar{R}$, and $\bar{R}_k$ are expressed in mean of B1950.0 coordinates, mean of J2000.0 coordinates, or true of reference date coordinates, whichever is the basic coordinate frame. The gravitational parameter, μ, is the product of the mass of a given body and

the universal gravitational constant. In particular, $\mu_k = G\,m_k$ for the kth body, and $\mu = G\,m_j$ for the central body.

When only the effects of the central body are included in Equation (4-17), an analytic solution can be obtained. This solution is the basis for construction of the Variation of Parameters methods, which are discussed in Chapter 5. Special perturbation methods are required for orbit propagation only when additional perturbation effects are considered. Consequently, the perturbing acceleration vector does not include the first term on the right-hand side of Equation (4-17).

When the satellite is in a close orbit around the reference body, significant round-off errors can occur in the computation of Equation (4-17) due to the differencing of nearly equal numbers. When the Earth is the central body, this error has not been found to be significant. However, it may be important in the computation of third-body effects due to the Earth when the Moon is the central body. This difficulty can be removed by rewriting the equations of motion in a different, but equivalent, form.

Designate $|\overline{R}_{kp}|$ by r_{kp}, $|\overline{R}_k|$ by r_k, $|\overline{R}|$ by r, and the included angle between R and R_k by θ ; then

$$r_{kp}^2 = r^2 + r_k^2 - 2r\,r_k\cos\theta \tag{4-18}$$

The ratio $1/r_{kp}$ can be expanded in terms of Legendre functions as

$$\frac{1}{r_{kp}} = \frac{1}{r_k}[P_0(\cos\theta) + P_1(\cos\theta)\,h + P_2(\cos\theta)\,h^2 + \ldots] = \frac{1+B}{r_k} \tag{4-19}$$

where

$$h = \frac{r}{r_k} \tag{4-20}$$

$$B = \sum_{j=1}^{\infty} P_j(\cos\theta)\,h^j \tag{4-21}$$

Substituting the expansion of the numerator

$$\frac{1}{|\bar{R}_k - \bar{R}|^3} = \frac{1}{r_{kp}^3} = \frac{(1 + B)^3}{r_k^3} \tag{4-22}$$

and the relationship $\bar{R}_k = \bar{R} - \bar{R}_{kp}$ into Equation (4-17) yields

$$\ddot{\bar{R}}_{PM} = \frac{d^2\bar{R}}{dt^2} = -\frac{\mu}{R^3}\bar{R} + \sum_{\substack{k=1 \\ k \neq j}}^{n} \mu_k \left[\frac{-\bar{R}_{kp}(3B + 3B^2 + B^3) - \bar{R}}{|\bar{R}_k|^3}\right] \tag{4-23}$$

This procedure eliminates the numerical difficulty. The series in h is truncated by terminating the series when $h^n \leq \epsilon_h$, where ϵ_h is a predetermined tolerance.

4.2.2 ASSOCIATED PARTIAL DERIVATIVES

The associated partial derivatives are given by

$$\begin{aligned}\frac{\partial \ddot{\bar{R}}_{PM}}{\partial \bar{R}} = &-\left(\frac{\mu}{R^3} + \sum_{k=1}^{n} \frac{\mu_k}{|\bar{R}_k - \bar{R}|^3}\right) I \\ &+ 3\left(\frac{\mu \bar{R}\bar{R}^T}{R^5} + \sum_{k=1}^{n}\left[\mu_k \frac{(\bar{R}_k - \bar{R})(\bar{R}_k - \bar{R}^T)}{|\bar{R}_k - \bar{R}|^5}\right]\right)\end{aligned} \tag{4-24}$$

$$\frac{\partial \ddot{\bar{R}}_{PM}}{\partial \dot{\bar{R}}} = 0_3 \tag{4-25}$$

where I is the identity matrix of dimension three.

The associated C-matrix columns for the model parameters μ and μ_k are given by

$$\frac{\partial \ddot{\bar{R}}_{PM}}{\partial \mu} = -\frac{\bar{R}}{R^3} \tag{4-26}$$

$$\frac{\partial \ddot{\bar{R}}_{PM}}{\partial \mu_k} = \frac{(\bar{R}_k - \bar{R})}{|\bar{R}_k - \bar{R}|^3} - \frac{\bar{R}_k}{R_k^3} \tag{4-27}$$

4.3 NONSPHERICAL GRAVITATIONAL EFFECTS

Most solar system bodies are known to have figures that depart from the point-mass, or spherical, model. The nonsphericity of the gravitational potential may give rise to a significant perturbation of the satellite trajectories. Therefore, accurate orbit determination may require the inclusion of nonspherical terms. The gravitational potentials of the Earth and Moon are the best known of all the solar system bodies because of extensive tracking and analysis of close Earth and lunar satellites. The figures of planets with natural satellites are known, although less accurately, through study of the motion of their natural satellites.

4.3.1 NONSPHERICAL GRAVITATIONAL PERTURBATION MODEL

The method of representing the gravitational potential due to the nonsphericity of a massive body can be found in numerous publications (References 3, 4, and 5). The gravitational field of the body is derived from a scalar potential ψ that satisfies Poisson's equation

$$\nabla^2 \psi(r, \phi, \lambda) = -4\pi \mu_k \varrho(r, \phi, \lambda) \tag{4-28}$$

where

- r = magnitude of the vector from the body's center of mass to the satellite
- ϕ = geocentric, selenocentric, or planetocentric latitude
- λ = geocentric, selenocentric, or planetocentric longitude (measured east from the prime meridian)

Above the surface of the perturbing body, the mass density, ϱ, is zero; consequently, Equation (4-28) reduces to the Laplacian, $\nabla^2\psi = 0$. Use of a standard separation of variables technique yields the solution

$$\psi(r,\phi,\lambda) = \frac{\mu}{r} + \frac{\mu}{r}\sum_{n=1}^{\infty} C_n^0\left(\frac{R_e}{r}\right)^n P_n^0(\sin\phi) + \frac{\mu}{r}\sum_{n=1}^{\infty}\sum_{m=1}^{n}\left(\frac{R_e}{r}\right)^n P_n^m(\sin\phi)[S_n^m \sin m\lambda + C_n^m \cos m\lambda] \tag{4-29}$$

where the first term is the point-mass potential for Keplerian motion; the second and third terms are the nonspherical potential due to the sum of the zonal and tesseral harmonics, respectively; and

μ = gravitational parameter of the central body

R_e = radius of the body (usually taken as the equatorial radius)

P_n^m = associated Legendre function

S_n^m, C_n^m = harmonic coefficients, i.e.,

- zonal harmonics for $m = 0$
- sectorial harmonics for $m = n$
- tesseral harmonics for $n > m \neq 0$

(Note: $J_n = -C_n^0$)

The term $n = 1$ is usually not present when the origin of the coordinate system is placed at the center of mass.

The total gravitational force is the gradient of ψ. Therefore, the noncentral force acting on the spacecraft due to the attracting body is the gradient of the nonspherical terms in the potential function ψ.

Expressing the gradient in body-fixed coordinates (Figure 4-2), the following form for the inertial acceleration vector is obtained (see the discussion following Equation (4-38)):

$$\bar{a}_b = \begin{bmatrix} a_{x_b} \\ a_{y_b} \\ a_{z_b} \end{bmatrix} = \frac{\partial\psi}{\partial r}\left(\frac{\partial r}{\partial \bar{r}_b}\right)^T + \frac{\partial\psi}{\partial\phi}\left(\frac{\partial\phi}{\partial \bar{r}_b}\right)^T + \frac{\partial\psi}{\partial\lambda}\left(\frac{\partial\lambda}{\partial \bar{r}_b}\right)^T \tag{4-30}$$

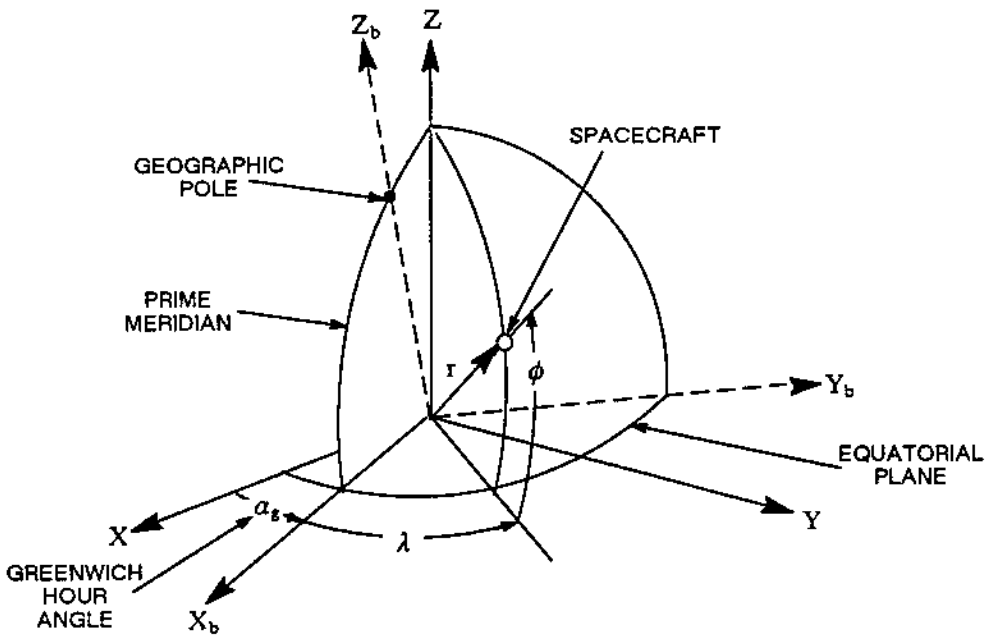

Figure 4-2. Body-Fixed System

The partial derivatives of the nonspherical portion of the potential with respect to r, ϕ, and λ are given by

$$\frac{\partial \psi}{\partial r} = -\frac{1}{r}\frac{\mu}{r}\sum_{n=2}^{\infty}\left(\frac{R_e}{r}\right)^n (n+1)\sum_{m=0}^{n}\left(C_n^m \cos m\lambda + S_n^m \sin m\lambda\right) P_n^m(\sin\phi) \quad (4\text{-}31a)$$

$$\frac{\partial \psi}{\partial \phi} = \frac{\mu}{r}\sum_{n=2}^{\infty}\left(\frac{R_e}{r}\right)^n \sum_{m=0}^{n}\left(C_n^m \cos m\lambda + S_n^m \sin m\lambda\right) \times \left[P_n^{m+1}(\sin\phi) - (m \tan\phi) P_n^m(\sin\phi)\right] \quad (4\text{-}31b)$$

$$\frac{\partial \psi}{\partial \lambda} = \frac{\mu}{r}\sum_{n=2}^{\infty}\left(\frac{R_e}{r}\right)^n \sum_{m=0}^{n} m\left(S_n^m \cos m\lambda - C_n^m \sin m\lambda\right) P_n^m(\sin\phi) \quad (4\text{-}31c)$$

The Legendre functions and the terms cos $m\lambda$, sin $m\lambda$, and (m tan ϕ) are computed via recursion formulas, as follows:

$$P_n^0(\sin\phi) = \frac{(2n-1)\sin\phi\, P_{n-1}^0(\sin\phi) - (n-1)\, P_{n-2}^0(\sin\phi)}{n} \qquad (4\text{-}32a)$$

$$P_n^m(\sin\phi) = P_{n-2}^m(\sin\phi) + (2n-1)\cos\phi\, P_{n-1}^{m-1}(\sin\phi) \qquad (m \neq 0,\ m < n) \quad (4\text{-}32b)$$

$$P_n^m(\sin\phi) = (2n-1)\cos\phi\, P_{n-1}^{n-1}(\sin\phi) \qquad (m \neq 0,\ m = n) \quad (4\text{-}32c)$$

where

$$P_0^0(\sin\phi) = 1 \qquad (4\text{-}33a)$$

$$P_1^0(\sin\phi) = \sin\phi \qquad (4\text{-}33b)$$

$$P_1^1(\sin\phi) = \cos\phi \qquad (4\text{-}33c)$$

and

$$\sin m\lambda = 2\cos\lambda \sin[(m-1)\lambda] - \sin[(m-2)\lambda] \qquad (4\text{-}34a)$$

$$\cos m\lambda = 2\cos\lambda \cos[(m-1)\lambda] - \cos[(m-2)\lambda] \qquad (4\text{-}34b)$$

$$m\tan\phi = [(m-1)\tan\phi)] + \tan\phi \qquad (4\text{-}34c)$$

The recursion relationships above are the most efficient method of computing the complete set of associated Legendre polynomials and spherical harmonics up to a certain order and degree. However, higher degree harmonic terms can cause satellites with repeating ground tracks to undergo large perturbations when the trajectory and the harmonic frequency are synchronized (resonant). The synchronization causes the satellite to sample the gravitational field in such a way that large cumulative perturbations result. Individual resonant harmonics can be computed in GTDS without using the recursive algorithm described above. Use of a low-order recursive harmonic model with

nonrecursive computation of high-order resonant terms is considerably more efficient than carrying out recursive computation of the total high-order harmonic model.

The partial derivatives of r, ϕ, and λ with respect to x_b, y_b, and z_b are computed from the expressions

$$\frac{\partial r}{\partial \bar{r}_b} = \frac{\bar{r}_b^T}{r} \tag{4-35}$$

$$\frac{\partial \phi}{\partial \bar{r}_b} = \frac{1}{\sqrt{x_b^2 + y_b^2}}\left[-\frac{z_b\,\bar{r}_b^T}{r^2} + \frac{\partial z_b}{\partial \bar{r}_b}\right] \tag{4-36}$$

$$\frac{\partial \lambda}{\partial \bar{r}_b} = \frac{1}{(x_b^2 + y_b^2)}\left[x_b \frac{\partial y_b}{\partial \bar{r}_b} - y_b \frac{\partial x_b}{\partial \bar{r}_b}\right] \tag{4-37}$$

where $\partial x_b/\partial \bar{r}_b$, $\partial y_b/\partial \bar{r}_b$, and $\partial z_b/\partial \bar{r}_b$ are the row vectors (1, 0, 0), (0, 1, 0), and (0, 0, 1), respectively.

Substituting Equations (4-35) through (4-37) into Equation (4-30) yields

$$a_{x_b} = \left(\frac{1}{r}\frac{\partial \psi}{\partial r} - \frac{z_b}{r^2\sqrt{x_b^2 + y_b^2}}\frac{\partial \psi}{\partial \phi}\right)x_b - \left(\frac{1}{(x_b^2 + y_b^2)}\frac{\partial \psi}{\partial \lambda}\right)y_b \tag{4-38a}$$

$$a_{y_b} = \left(\frac{1}{r}\frac{\partial \psi}{\partial r} - \frac{z_b}{r^2\sqrt{x_b^2 + y_b^2}}\frac{\partial \psi}{\partial \phi}\right)y_b + \left(\frac{1}{x_b^2 + y_b^2}\frac{\partial \psi}{\partial \lambda}\right)x_b \tag{4-38b}$$

$$a_{z_b} = \left(\frac{1}{r}\frac{\partial \psi}{\partial r}\right)z_b + \frac{\sqrt{x_b^2 + y_b^2}}{r^2}\frac{\partial \psi}{\partial \phi} \tag{4-38c}$$

where a_{x_b}, a_{y_b}, and a_{z_b} are the components of the inertial acceleration of the spacecraft expressed in the body-fixed coordinate system and not the acceleration with respect to the body-fixed coordinate system. Thus, it is necessary to transform these components into an inertial frame before integrating the equations of motion.

Since the numerical computations of the program are calculated in the inertial mean equator and equinox of B1950.0 or J2000.0 coordinate system, a series of transformations

is made to represent the acceleration vector in this system. For the case of the Earth, there are two options available to accomplish this. The first is the more accurate, whereas the second is computationally faster.

For the more accurate option, the inertial acceleration $\bar{a}_b$, expressed in body-fixed coordinates, is transformed to the inertial mean of B1950.0 or J2000.0 axes by means of the transformation

$$\ddot{\bar{R}}_{NS} = C^T B^T \bar{a}_b \tag{4-39}$$

where B^T transforms from body-fixed to true of date coordinates and C^T transforms from true of date to inertial mean of B1950.0 or J2000.0 coordinates, as discussed in Sections 3.3.1 and 3.3.2. The matrix B^T accounts for polar motion and Greenwich sidereal time.

The simpler option neglects polar motion by assuming the geographic pole z_b to be aligned with the spin axis z in the true of date system. This allows the nonspherical gravity components to be expressed directly in true of date coordinates. Thus, by replacing (r_b, x_b, y_b, z_b) in Equations (4-30) and (4-35) through (4-38) by (r, x, y, z), the true of date components are calculated directly. The longitude and latitude are calculated as follows:

$$\lambda = \alpha - \alpha_g \tag{4-40}$$

$$\phi = \sin^{-1}\left(\frac{z}{r}\right) \tag{4-41}$$

where

α = right ascension of the spacecraft, $\alpha = \tan^{-1}(y/x)$

α_g = right ascension of Greenwich

Computation of the acceleration due to the nonspherical Moon in B1950.0 or J2000.0 coordinates requires some different operations than those used for the Earth. Because the right ascension of the Greenwich meridian has no meaning, the step of going from body-fixed coordinates to the true of date system cannot be implemented.

The lunar body-fixed coordinates (also known as selenographic coordinates) are coincident with the principal axes of inertia and are defined in the following way:

- x′ axis lies along a direction nearly colinear with the Moon-to-Earth vector
- z′ axis lies along the axis of rotation, or polar axis, of the Moon
- y′ axis lies in the equatorial plane of the Moon and completes a right-handed coordinate system

Three rotations are necessary to transform the selenographic acceleration vector to a vector referred to the mean Earth equator and equinox of B1950.0 or J2000.0 system. The first rotation transforms the acceleration vector to the true Earth equator and equinox of date coordinate system centered at the Moon (selenocentric). The other two rotations involve the precession and nutation effects that are included to express the acceleration in the B1950.0 or J2000.0 system. These rotations are discussed in Sections 3.3.1 and 3.3.3.

4.3.2 ASSOCIATED PARTIAL DERIVATIVES

The partial derivatives of $\bar{a}_b$ with respect to $\bar{r}_b$ are obtained by differentiating Equation (4-30), yielding

$$\frac{\partial \bar{a}_b}{\partial \bar{r}_b} = \frac{\partial}{\partial \bar{r}_b}\left(\frac{\partial \psi}{\partial r}\right)\frac{\partial r}{\partial \bar{r}_b} + \frac{\partial}{\partial \bar{r}_b}\left(\frac{\partial \psi}{\partial \phi}\right)\frac{\partial \phi}{\partial \bar{r}_b} + \frac{\partial}{\partial \bar{r}_b}\left(\frac{\partial \psi}{\partial \lambda}\right)\frac{\partial \lambda}{\partial \bar{r}_b} + \frac{\partial \psi}{\partial r}\frac{\partial^2 r}{\partial \bar{r}_b^2} + \frac{\partial \psi}{\partial \phi}\frac{\partial^2 \phi}{\partial \bar{r}_b^2} + \frac{\partial \psi}{\partial \lambda}\frac{\partial^2 \lambda}{\partial \bar{r}_b^2} \tag{4-42}$$

The required partial derivatives of $\partial\psi/\partial r$, $\partial\psi/\partial\phi$, and $\partial\psi/\partial\lambda$ with respect to $\bar{r}_b$ are obtained by differentiating Equations (4-31) as follows:

$$\frac{\partial}{\partial \bar{r}_b}\begin{bmatrix} \frac{\partial \psi}{\partial r} \\ \frac{\partial \psi}{\partial \phi} \\ \frac{\partial \psi}{\partial \lambda} \end{bmatrix} = \begin{bmatrix} \frac{\partial^2 \psi}{\partial r^2} & \frac{\partial^2 \psi}{\partial r \partial \phi} & \frac{\partial^2 \psi}{\partial r \partial \lambda} \\ \frac{\partial^2 \psi}{\partial \phi \partial r} & \frac{\partial^2 \psi}{\partial \phi^2} & \frac{\partial^2 \psi}{\partial \phi \partial \lambda} \\ \frac{\partial^2 \psi}{\partial \lambda \partial r} & \frac{\partial^2 \psi}{\partial \lambda \partial \phi} & \frac{\partial^2 \psi}{\partial \lambda^2} \end{bmatrix} \begin{bmatrix} \frac{\partial r}{\partial \bar{r}_b} \\ \frac{\partial \phi}{\partial \bar{r}_b} \\ \frac{\partial \lambda}{\partial \bar{r}_b} \end{bmatrix} \tag{4-43}$$

To minimize computations, the symmetry property of the second partial derivatives of ψ is utilized as indicated below:

$$\frac{\partial^2\psi}{\partial r^2} = \frac{\mu}{r^3}\sum_{n=2}^{\infty}\left(\frac{R_e}{r}\right)^n (n+2)(n+1) \times \sum_{m=0}^{n}(C_n^m \cos m\lambda + S_n^m \sin m\lambda)\, P_n^m(\sin\phi) \tag{4-44a}$$

$$\frac{\partial^2\psi}{\partial r\partial\phi} = \frac{\partial^2\psi}{\partial\phi\partial r} = -\frac{\mu}{r^2}\sum_{n=2}^{\infty}\left(\frac{R_e}{r}\right)^n (n+1) \times \sum_{m=0}^{n}(C_n^m \cos m\lambda + S_n^m \sin m\lambda) \times [P_n^{m+1}(\sin\phi) - m\tan\phi\, P_n^m(\sin\phi)] \tag{4-44b}$$

$$\frac{\partial^2\psi}{\partial r\partial\lambda} = \frac{\partial^2\psi}{\partial\lambda\partial r} = -\frac{\mu}{r^3}\sum_{n=2}^{\infty}\left(\frac{R_e}{r}\right)^n (n+1) \times \sum_{m=0}^{n} m\,(S_n^m \cos m\lambda - C_n^m \sin m\lambda)\, P_n^m(\sin\phi) \tag{4-44c}$$

$$\frac{\partial^2\psi}{\partial\phi^2} = \frac{\mu}{r}\sum_{n=2}^{\infty}\left(\frac{R_e}{r}\right)^n \sum_{m=0}^{n}(C_n^m \cos m\lambda + S_n^m \sin m\lambda)\left\{\tan\phi\, P_n^{m+1}(\sin\phi) + [m^2\sec^2\phi - m\tan^2\phi - n(n+1)]\, P_n^m(\sin\phi)\right\} \tag{4-44d}$$

$$\frac{\partial^2\psi}{\partial\phi\partial\lambda} = \frac{\partial^2\psi}{\partial\lambda\partial\phi} = \frac{\mu}{r}\sum_{n=2}^{\infty}\left(\frac{R_e}{r}\right)^n \sum_{m=0}^{n} m(S_n^m \cos m\lambda - C_n^m \sin m\lambda) \times [P_n^{m+1}(\sin\phi) - m \tan\phi\, P_n^m(\sin\phi)] \tag{4-44e}$$

$$\frac{\partial^2\psi}{\partial\lambda^2} = -\frac{\mu}{r}\sum_{n=2}^{\infty}\left(\frac{R_e}{r}\right)^n \sum_{m=0}^{n} m^2(C_n^m \cos m\lambda + S_n^m \sin m\lambda)\, P_n^m(\sin\phi) \tag{4-44f}$$

The partial derivatives of r, ϕ, and λ with respect to $\bar{r}_b$ are given in Equations (4-35) through (4-37). The required second partial derivatives of r, ϕ, and λ with respect to $\bar{r}_b$ are obtained by differentiating Equations (4-35) through (4-37) with respect to $\bar{r}_b$, yielding

$$\frac{\partial^2 r}{\partial\bar{r}_b^2} = \frac{1}{r}\left[I - \frac{\bar{r}_b\,\bar{r}_b^T}{r^2}\right] \tag{4-45}$$

$$\frac{\partial^2\phi}{\partial\bar{r}_b^2} = -\frac{1}{(x_b^2 + y_b^2)^{3/2}}\left[\left(\frac{\partial z_b}{\partial\bar{r}_b}\right)^T - \frac{z_b\,\bar{r}_b}{r^2}\right]\left[x_b\left(\frac{\partial x_b}{\partial\bar{r}_b}\right) + y_b\left(\frac{\partial y_b}{\partial\bar{r}_b}\right)\right] - \frac{1}{r^2\sqrt{x_b^2 + y_b^2}}\left[\bar{r}_b\left(\frac{\partial z_b}{\partial\bar{r}_b}\right) + z_b I - \frac{2z_b}{r^2}\,\bar{r}_b\,\bar{r}_b^T\right] \tag{4-46}$$

$$\frac{\partial^2\lambda}{\partial\bar{r}_b^2} = -\frac{2}{(x_b^2 + y_b^2)}\begin{bmatrix}-y_b\\ x_b\\ 0\end{bmatrix}\left[x_b\left(\frac{\partial x_b}{\partial\bar{r}_b}\right) + y_b\left(\frac{\partial y_b}{\partial\bar{r}_b}\right)\right] + \frac{1}{(x_b^2 + y_b^2)}\begin{bmatrix}0 & -1 & 0\\ 1 & 0 & 0\\ 0 & 0 & 0\end{bmatrix} \tag{4-47}$$

where $\partial x_b/\partial\bar{r}_b$, $\partial y_b/\partial\bar{r}_b$, and $\partial z_b/\partial\bar{r}_b$ are (1, 0, 0), (0, 1, 0), and (0, 0, 1), respectively. The symmetry properties of the second partial derivatives of r, ϕ, and λ yield

$$\frac{\partial^2}{\partial x_b\,\partial y_b} = \frac{\partial^2}{\partial y_b\,\partial x_b} \tag{4-48a}$$

$$\frac{\partial^2}{\partial x_b \, \partial z_b} = \frac{\partial^2}{\partial z_b \, \partial x_b} \tag{4-48b}$$

$$\frac{\partial^2}{\partial y_b \, \partial z_b} = \frac{\partial^2}{\partial z_b \, \partial y_b} \tag{4-48c}$$

As noted previously, the potential function ψ satisfies Laplace's equation, $\nabla^2\psi = 0$. Therefore,

$$\frac{\partial^2\psi}{\partial x_b^2} = -\left(\frac{\partial^2\psi}{\partial y_b^2} + \frac{\partial^2\psi}{\partial z_b^2}\right) \tag{4-49}$$

In view of this and the symmetry of the matrix in Equation (4-43), it is necessary to compute only the three elements above the principal diagonal and the two elements on the principal diagonal.

The equations for computing the elements of the C-matrix appearing in the variational equations (Equation (4-7)) are obtained by differentiating Equation (4-30) with respect to C_n^m and S_n^m

$$\frac{\partial \bar{a}_b}{\partial C_n^m} = \frac{\partial}{\partial C_n^m}\left(\frac{\partial\psi}{\partial r}\right)\frac{\partial r}{\partial \bar{r}_b} + \frac{\partial}{\partial C_n^m}\left(\frac{\partial\psi}{\partial\phi}\right)\frac{\partial\phi}{\partial \bar{r}_b} + \frac{\partial}{\partial C_n^m}\left(\frac{\partial\psi}{\partial\lambda}\right)\frac{\partial\lambda}{\partial \bar{r}_b} \tag{4-50}$$

$$\frac{\partial \bar{a}_b}{\partial S_n^m} = \frac{\partial}{\partial S_n^m}\left(\frac{\partial\psi}{\partial r}\right)\frac{\partial r}{\partial \bar{r}_b} + \frac{\partial}{\partial S_n^m}\left(\frac{\partial\psi}{\partial\phi}\right)\frac{\partial\phi}{\partial \bar{r}_b} + \frac{\partial}{\partial S_n^m}\left(\frac{\partial\psi}{\partial\lambda}\right)\frac{\partial\lambda}{\partial \bar{r}_b} \tag{4-51}$$

where the second partial derivatives of ψ are obtained by differentiating Equations (4-31) with respect to C_n^m and S_n^m

$$\frac{\partial}{\partial C_n^m}\begin{bmatrix}\partial\psi/\partial r\\ \partial\psi/\partial\phi\\ \partial\psi/\partial\lambda\end{bmatrix} = \left(\frac{\mu}{r}\right)\left(\frac{R_e}{r}\right)^n\begin{bmatrix}-\frac{1}{r}(n+1)\cos m\lambda\, P_n^m(\sin\phi)\\ \cos m\lambda[P_n^{m+1}(\sin\phi) - m\tan\phi P_n^m(\sin\phi)]\\ -m\sin m\lambda\, P_n^m(\sin\phi)\end{bmatrix} \tag{4-52}$$

$$\frac{\partial}{\partial S_n^m}\begin{bmatrix}\partial\psi/\partial r\\ \partial\psi/\partial\phi\\ \partial\psi/\partial\lambda\end{bmatrix} = \left(\frac{\mu}{r}\right)\left(\frac{R_e}{r}\right)^n \begin{bmatrix} -\frac{1}{r}(n+1)\sin m\lambda\, P_n^m(\sin\phi)\\ \sin m\lambda[P_n^{m+1}(\sin\phi) - m\tan\phi\, P_n^m(\sin\phi)]\\ m\cos m\lambda\, P_n^m(\sin\phi)\end{bmatrix} \quad (4\text{-}53)$$

As in the case of the accelerations due to nonsphericity that were developed in Section 4.3.1, the partial derivatives for use in the variational equations must be transformed from the body-fixed axes to inertial mean of B1950.0 or J2000.0 coordinates. As discussed previously, these transformations can be determined to high precision or by a simpler and faster method in which polar motion is neglected.

In the more accurate option, where polar motion is accounted for, the transformations of the partial derivatives of $\ddot{\bar{R}}_{NS}$ with respect to $\bar{R}$ are determined by taking the partial derivatives of Equation (4-39) as follows:

$$\frac{\partial\ddot{\bar{R}}_{NS}}{\partial\bar{R}} = (B\,C)^T\frac{\partial\bar{a}_b}{\partial\bar{r}_b}\frac{\partial\bar{r}_b}{\partial\bar{R}} = (B\,C)^T\frac{\partial\bar{a}_b}{\partial\bar{r}_b}B\,C \quad (4\text{-}54)$$

The matrices C and B are presented in Section 3.3.1 and 3.3.2, respectively.

In the simpler option, polar motion is neglected and $\bar{a}_b$, as well as its partial derivatives, are calculated with respect to the true of date coordinates. This is accomplished by replacing (r_b, x_b, y_b, z_b) in Equations (4-39), (4-42), (4-43), and (4-45) through (4-49) by (r, x, y, z), the true of date coordinates, and by replacing the matrix B with the identity matrix I in Equations (4-39) and (4-54).

The partial derivatives of $\ddot{\bar{R}}_{NS}$ with respect to model parameters C_n^m and S_n^m are obtained for the more accurate option as follows:

$$\frac{\partial\ddot{\bar{R}}_{NS}}{\partial C_n^m} = (B\,C)^T\frac{\partial\bar{a}_b}{\partial C_n^m} \quad (4\text{-}55)$$

$$\frac{\partial\ddot{\bar{R}}_{NS}}{\partial S_n^m} = (B\,C)^T\frac{\partial\bar{a}_b}{\partial S_n^m} \quad (4\text{-}56)$$

For the simpler option, (r_b, x_b, y_b, z_b) is replaced by (r, x, y, z) in Equations (4-50) and (4-51), and the matrix B is replaced by the identity matrix I in Equations (4-55) and (4-56).

4.4 INDIRECT OBLATION PERTURBATION MODEL (NOT CURRENTLY AVAILABLE IN GTDS)

Up to this point, two types of gravitational accelerations acting on the spacecraft have been considered: the acceleration due to n point masses, measured relative to one of the point masses, called the reference body; and the acceleration arising from the nonspherical portion of the gravitational potentials of one or more of the n bodies, which directly influence the spacecraft motion. These nonspherical attractions also affect the inertial acceleration of the reference body, resulting in an indirect acceleration of the spacecraft relative to the reference body (Reference 6). The two bodies of most concern are the Earth and Moon.

Inspection of Equation (4-29) reveals the rapid attenuation of the gravitational attraction with increasing order of the spherical harmonics and increasing distance from the body. For the Earth, C_2^0 (or $-J_2$) is of order 10^{-3} of the Keplerian term, while all the other harmonic coefficients are of order 10^{-6} or less. In the Moon's gravitational potential, the size of the higher order terms relative to the central term is larger than in the case of the Earth, but the c_2^0 term is dominant. Consequently, the only nonspherical potential terms considered for the mutual interaction of the Earth and Moon are the second zonal harmonics of each, and the resulting effects are referred to as indirect oblation effects.

The complex motions of the Earth-Moon system, including lunisolar precession and nutation, physical libration of the Moon, and perturbations in the lunar orbit, are accounted for in GTDS. Thus, any significant indirect oblateness effects are due to the use of a relative coordinate system (Equation (4-16)) in place of an inertial coordinate system and not to errors in the lunar ephemeris.

Considering the Moon to be the spacecraft, the force acting on the point-mass Moon due to the nonsphericity of the Earth is (Section 4.3)

$$\mu_M \ddot{\bar{R}}_M(E) = f\left(C_i^j,\ S_i^j,\ \bar{r}_{EM},\ t\right) \tag{4-57}$$

where

C_i^j and S_i^j = harmonic coefficients of the Earth's nonspherical potential

$\bar{r}_{EM}$ = Moon's position vector in geocentric coordinates

t = time argument used to determine the orientation of the inertial and geocentric axes

Similarly, the force acting on the point-mass Earth due to the nonsphericity of the Moon is

$$\mu_E \ddot{\bar{R}}_E(M) = f\left(c_i^j,\ s_i^j,\ \bar{r}_{ME},\ t\right) \tag{4-58}$$

where

c_i^j and s_i^j = harmonic coefficients of the Moon's nonspherical potential
$\bar{r}_{ME}$ = Earth's position vector in selenocentric coordinates
t = time argument used to determine the orientation of the inertial and selenographic axes

The force acting on the point-mass Moon due to the Earth's oblateness, $\mu_M \ddot{\bar{R}}_M(E)$, produces an equal and opposite force acting on the Earth. Therefore, the inertial acceleration of the Earth due to the force of attraction between the Earth and Moon due to the oblateness of the Earth and the point-mass Moon is given by

$$\ddot{\bar{R}}_E(E) = -\frac{\mu_M}{\mu_E} \ddot{\bar{R}}_M(E) \tag{4-59}$$

Similarly, the force of attraction between the Earth and Moon due to the oblateness of the Moon and the point-mass Earth produces an inertial acceleration of the Moon given by

$$\ddot{\bar{R}}_M(M) = -\frac{\mu_E}{\mu_M} \ddot{\bar{R}}_E(M) \tag{4-60}$$

Therefore, the inertial acceleration of the Earth due to the oblateness of the Earth and Moon is

$$\ddot{\bar{R}}_E = \ddot{\bar{R}}_E(M) + \ddot{\bar{R}}_E(E) = -\mu_M \left[\frac{1}{\mu_E} \ddot{\bar{R}}_M(E) - \frac{1}{\mu_M} \ddot{\bar{R}}_E(M)\right] \tag{4-61}$$

and the inertial acceleration of the Moon due to the oblateness of the Earth and Moon is

$$\ddot{\bar{R}}_M = \ddot{\bar{R}}_M(E) + \ddot{\bar{R}}_M(M) = \mu_E \left[\frac{1}{\mu_E} \ddot{\bar{R}}_M(E) - \frac{1}{\mu_M} \ddot{\bar{R}}_E(M)\right] \tag{4-62}$$

The resulting indirect acceleration of the spacecraft is equal and opposite to the acceleration of the reference body; consequently,

$$\ddot{\bar{R}}_{IO} = \begin{cases} -\ddot{\bar{R}}_E = \mu_M \left[\frac{1}{\mu_E} \ddot{\bar{R}}_M(E) - \frac{1}{\mu_M} \ddot{\bar{R}}_E(M) \right] & \text{when the Earth is the reference body} \\ -\ddot{\bar{R}}_M = -\mu_E \left[\frac{1}{\mu_E} \ddot{\bar{R}}_M(E) - \frac{1}{\mu_M} \ddot{\bar{R}}_E(M) \right] & \text{when the Moon is the reference body} \end{cases} \tag{4-63}$$

The method for determining the inertial acceleration of the point-mass Moon due to an oblate Earth, $\ddot{\bar{R}}_M(E)$, and the inertial acceleration of the point-mass Earth due to an oblate Moon, $\ddot{\bar{R}}_E(M)$, are presented in Section 4.3. However, since the effects of the higher harmonic terms can be neglected for this application and only the second zonal harmonics considered, the gravitational potential in Equation (4-29) reduces to

$$\psi(r, \phi) = \frac{\mu}{2r} C_2^0 \left(\frac{R_e}{r} \right)^2 (3 \sin^2 \phi - 1) \tag{4-64}$$

The partial derivatives of ψ with respect to r and ϕ are

$$\frac{\partial \psi}{\partial r} = -\frac{3}{2} \frac{\mu}{r^4} + R_e C_2^0 (3 \sin^2 \phi - 1) \tag{4-65a}$$

$$\frac{\partial \psi}{\partial \phi} = \frac{\mu}{r_3} R_e C_2^0 (3 \sin \phi \cos \phi) \tag{4-65b}$$

and the partial derivatives of r and ϕ with respect to $\bar{r}$ are

$$\frac{\partial r}{\partial \bar{r}} = \frac{\bar{r}^T}{r} \tag{4-66a}$$

$$\frac{\partial \phi}{\partial \bar{r}} = \frac{1}{r \cos \phi} \begin{bmatrix} -\sin \phi \cos \lambda \\ -\sin \phi \sin \lambda \\ \cos^2 \phi \end{bmatrix} \tag{4-66b}$$

Since the oblate potential model is symmetric about the pole, and neglecting polar motion, the inertial acceleration of the point-mass Moon due to the Earth's oblateness can be expressed in geocentric true of date coordinates as follows:

$$\begin{aligned}\bar{a}_M(E) &= \frac{\partial \psi}{\partial r_M}\left(\frac{\partial r_M}{\partial \bar{r}_M}\right)^T + \frac{\partial \psi}{\partial \phi_M}\left(\frac{\partial \phi_M}{\partial \bar{r}_M}\right)^T \\ &= -\frac{3}{2}\frac{\mu_E}{r_M^4} R_e C_2^0 (3 \sin^2 \phi_M - 1)\frac{\bar{r}_M}{r_M} + \frac{3\mu_E R_e C_2^0}{r_M^4 \cos \phi_M}\begin{bmatrix} -\sin \phi_M \cos \lambda_M \\ -\sin \phi_M \sin \lambda_M \\ \cos^2 \phi_M \end{bmatrix}\end{aligned} \tag{4-67}$$

where

μ_E = gravitational constant of the Earth

R_e = equatorial radius of the Earth

C_2^0 = second zonal harmonic coefficient for the Earth

$\bar{r}_M$ = lunar position vector in true of date coordinates

ϕ_M = geocentric latitude of the Moon

λ_M = right ascension of the Moon in true of date coordinates

The acceleration vector $\bar{a}_M(E)$ is transformed to inertial mean of B1950.0 or J2000.0 coordinates via the transformation matrix C^T of Section 3.3.1.3, i.e.,

$$\ddot{\bar{R}}_M(E) = C^T \bar{a}_M(E) \tag{4-68}$$

The inertial acceleration of the point-mass Earth due to the Moon's oblateness is expressed in selenographic coordinates as

$$\bar{a}_E(M) = -\frac{3}{2}\frac{\mu_M}{r_E^4} R_m c_2^0 (3 \sin^2 \phi_E - 1)\frac{\bar{r}_E}{r_E} + \frac{3\mu_M}{r_E^4}\frac{R_m c_2^0}{\cos \phi_E}\begin{bmatrix} -\sin \phi_E \cos \lambda_E \\ -\sin \phi_E \sin \lambda_E \\ \cos^2 \phi_E \end{bmatrix} \tag{4-69}$$

where

μ_M = gravitational constant of the Moon

R_m = equatorial radius of the Moon

c_2^0 = second zonal harmonic coefficient for the Moon

$\bar{r}_E$ = position vector of the Earth in selenographic coordinates

ϕ_E = selenographic latitude of the Earth

λ_E = selenographic longitude of the Earth

Transformation of $\bar{a}_E(E)$ to inertial mean of B1950.0 or J2000.0 coordinates yields

$$\ddot{\bar{R}}_E(M) = C^T M^T \bar{a}_E(M) \tag{4-70}$$

where the M^T matrix transforms from selenographic to selenocentric true of date coordinates (Section 3.3.3), and the C^T matrix transforms from true of date to mean of B1950.0 or J2000.0 coordinates. If a true of reference date inertial system is being utilized, then the C^T matrix in Equations (4-68) and (4-70) is set equal to the identity matrix.

4.5 AERODYNAMIC FORCES AND ATMOSPHERIC MODELS

A general discussion of the aerodynamic forces acting on a spacecraft and the related atmospheric models is presented in Section 4.5.1. Descriptions of the GTDS aerodynamic force modeling and related partial derivatives are given in Sections 4.5.2 and 4.5.3, respectively. The Jacchia-Roberts atmospheric model is discussed in Section 4.5.4, with the related partial derivatives given in Section 4.5.5. The modified Harris-Priester atmospheric model is described in Section 4.5.6, with the related partial derivatives in Section 4.5.7. Section 4.5.8 describes the low-altitude model.

4.5.1 INTRODUCTION

The modeling of the aerodynamic force acting on a spacecraft in a near-Earth orbit is difficult from two standpoints. First, the characterization of the density at very high altitudes above the surface is extremely complex. Although the exact natures of the phenomena are not well understood, there is experimental evidence that diurnal and seasonal variations, as well as effects due to changes in solar flux and geomagnetic activity, can be modeled with some degree of success.

Atmospheric density models can be divided into two types. Models of the first type are characterized by their dependence on altitude and their independence of any other parameters. Those of the second type are characterized by their dependence not only on altitude, but also on the position of the Sun relative to the Earth and the amount of energy emitted from the Sun.

Several atmospheric models have been constructed over the past several years (References 7 through 14) to account for various geomagnetic and solar activities. There are three main types of solar radiation known to affect the atmospheric density. The first type, which is the most important in terms of the effect on the structure of the atmosphere, results from solar ultraviolet radiation impinging on the atmosphere. Its effect on temperature and density is at a maximum 2 to 3 hours after local noon. This radiation heats the atmosphere by conduction and thereby increases the density at higher altitudes. The process is known as the diurnal (or day-night) effect and causes a redistribution of density, resulting in a diurnal bulge in the atmosphere.

The second type of solar activity affecting the atmosphere results from extreme ultraviolet radiation. The atmospheric oscillations that are in phase with this solar flux are often referred to as the erratic or 27-day variations, since the oscillations sometimes exhibit a semiregular character for intervals of several months, during which a period of 27 days is easily recognizable. It has been found that the decimetric flux from the Sun apparently varies in the same manner as the extreme ultraviolet emission and can therefore be used as a fairly reliable index of short-term solar activity. The decimetric flux, specifically the 10.7-centimeter radiation, is expressed in units of 10^{-22} watts/meter2/hertz bandwidth and is denoted by the symbol $F_{10.7}$.

The third type of radiation is corpuscular in nature and is referred to as the solar wind. It is responsible for the changes in intensity and energy spectrum observed in the cosmic radiation and is the largest single factor affecting short-term fluctuations in the atmospheric density. Experiments onboard Pioneer V were the first to establish that the 11-year solar (Sun spot) cycle is a phenomenon that is not localized near the Earth or its immediate environment but rather affects large volumes of the inner solar system. The solar wind is modeled as an interplanetary plasma streaming radially and irregularly outward from the Sun, compressing the Earth's magnetic field on the sunward side and extending it on the night side.

Atmospheric oscillations connected with geomagnetic storms are of significant amplitude but of very short duration (1 or 2 days). Present-day studies indicate a correlation of the atmospheric density with the geomagnetic activity.

Apart from the difficulty of accurately representing the environment (density) at the spacecraft location, the second aspect of the problem lies in the complication of rigorously modeling the force itself as a function of the spacecraft configuration and attitude.

GTDS provides the user with the choice of two atmospheric density models and three types of force representation. The atmospheric density models available are the modified Harris-Priester and the Roberts analytic formulation of the Jacchia 1971 model (referred to as the Jacchia-Roberts model). The Harris-Priester model is the simpler of the two and permits the most rapid computation of the density. It does not include effects due to seasonal variations or to changes in the solar flux or geomagnetic activity, as does the Jacchia-Roberts model.

The aerodynamic force can be represented, at the specification of the user, as the following:

- A simple drag force acting along the relative wind velocity vector on a spherical spacecraft
- A force with components normal to and along the axis of a cylindrical spacecraft
- A force with components along each of the three spacecraft body axes for a configuration consisting of a cylinder with solar paddles oriented at some angle to the axis of the cylinder

These modeling options, and the related partial derivatives, are described in detail in the following subsections.

4.5.2 AERODYNAMIC FORCE MODELING

Rigorous treatment of the aerodynamics of free molecular flow involves the representation of the complex interaction of the atmospheric molecules with the surface molecules of the spacecraft. Under certain conditions, this interaction is characterized as a specular or perfectly elastic reflection of the impinging molecules. The reflection is termed diffuse when the impinging molecules penetrate the surface, experience multiple collisions with the body molecules, and are reemitted randomly with no memory of their prior history. In the case of specular reflection, there is no momentum transfer and, hence, no force tangential to a local surface element. Diffuse reflection does result in such a component of force, although it is small. In general, both types of phenomena are involved in varying degrees, depending upon the details of the surface reflectivity and emissivity, temperature, and free-stream constituents and their mean molecular motion. Conditions typical of most actual situations result in forces that can be adequately represented in terms of the specular reflection equations. Therefore, the force modeling in GTDS makes this simplifying assumption and computes the force acting on a local surface element as the momentum transfer normal to that element.

The forces on all elements of the spacecraft surfaces exposed to the free-stream must be resolved in some coordinate frame and summed to obtain the total aerodynamic force

acting on the spacecraft. This resolution has been performed for a number of elemental shapes at various orientations. GTDS makes use of the force coefficients defined in Table 4-1 for spheres, cylinders, and flat plates. A force coefficient, C_F, is defined as the nondimensional quantity

$$C_F = \frac{F}{\frac{1}{2}\varrho V^2 A} \tag{4-71}$$

where

- F = magnitude of the force acting on the object
- ϱ = density of the medium through which the object is moving
- V = magnitude of the velocity of the object with respect to the medium producing the force
- A = arbitrary reference area

The velocity of the spacecraft relative to the atmosphere is determined in the inertial coordinate system by subtracting the motion of the atmosphere, assumed to rotate with the Earth, from that of the spacecraft, as follows:

$$\bar{V}_{rel} = \dot{\bar{R}} - (\bar{\omega} \times \bar{R}) \tag{4-72}$$

The Earth rotation vector, $\bar{\omega}$, must be appropriately defined in the inertial frame (mean equator and equinox of B1950.0, mean equator and equinox of J2000.0, or true equator and equinox of reference date).

For the case of a spherical spacecraft, the drag acceleration is computed as follows, using the general form of Equation (4-71) and $C_D = 1.0$ from Table 4-1:

$$\ddot{\bar{R}}_D = -S_s \varrho \bar{V}_{rel} |\bar{V}_{rel}| \tag{4-73}$$

where

$$S_s = \frac{1}{2} C_D \left(\frac{A}{m}\right) = \frac{1}{2}\left(\frac{\pi d^2}{4m}\right) \tag{4-74}$$

Table 4-1. Aerodynamic Force Coefficients for Elementary Surfaces

SURFACE SHAPE	REFERENCE DIRECTION FOR MEASUREMENT OF ANGLE α TO RELATIVE VELOCITY VECTOR	REFERENCE AREA	FORCE COEFFICIENT(S) AS FUNCTIONS OF α	DIRECTION OF FORCE COMPONENT
Sphere	Relative wind velocity	Cross-sectional area of sphere	$C_D = 2.0$	Along relative wind vector
Circular Cylinder (exterior surface only)	Cylinder axis	Length times diameter of the cylinder	$C_{N_C} = \frac{8}{3} \sin^2 \alpha$	Normal to cylinder axis in the plane of the axis and the relative velocity
			$C_{A_C} = 0$	Along cylinder axis
Flat Plate	Normal to plate	Area of plate	$C_{N_P} = 4.0 \cos^2 \alpha$	Normal to the plate
			$C_{T_P} = 0$	Tangent to the plate

In the above equation, d is the spacecraft diameter and m is the spacecraft mass. If there is propulsive thrust acting on the spacecraft, the mass m is variable and is represented as a polynomial in the burn time. The polynomial coefficients are assumed to be known.

When the spacecraft configuration is more complicated than a sphere, it is necessary to know the attitude, in addition to the orbit, in order to model the aerodynamic force.

It is not necessary to compute the entire direction cosine matrix Q when the spacecraft is a cylinder (with enclosing end plates). Due to the axial symmetry, it is only necessary to know the direction cosines q_{11}, q_{21}, q_{31} of the cylinder axis. The unit vector

$$\hat{X}_B = q_{11}\,\hat{i} + q_{21}\,\hat{j} + q_{31}\,\hat{k} \tag{4-75}$$

then gives the axis orientation in the inertial coordinate frame. As indicated in Table 4-1, the force component along the axis is proportional to the square of the velocity component normal to the end plates. The normal force component is proportional to the square of the velocity component normal to the cylinder.* Therefore, the velocity relative to the atmosphere is resolved into normal and axial components to obtain the total acceleration for the cylindrical spacecraft as

$$\overline{N} = S_c\,\hat{X}_B \times (\hat{X}_B \times \overline{V}_{rel})\,|\hat{X}_B \times \overline{V}_{rel}| \tag{4-76a}$$

$$\overline{A} = -S_e\,\hat{X}_B\,(\hat{X}_B \cdot \overline{V}_{rel})\,|\hat{X}_B \cdot \overline{V}_{rel}| \tag{4-76b}$$

$$\ddot{\overline{R}}_D = \varrho(\overline{N} + \overline{A}) \tag{4-76c}$$

In these equations

$$S_c = \frac{1}{2}\left(\frac{C_{N_C}}{\sin^2 a}\right)\left(\frac{A}{m}\right) = \frac{1}{2}\left(\frac{4}{3}\right)\left(\frac{L\,D}{m}\right) = \frac{2L\,D}{3m} \tag{4-77a}$$

$$S_e = \frac{1}{2}\left(\frac{C_{N_P}}{\cos^2 a}\right)\left(\frac{A}{m}\right) = \frac{1}{2}(2)\left(\frac{\pi\,d^2}{4m}\right) = \frac{\pi\,d^2}{4m} \tag{4-77b}$$

* This is analogous to the solar radiation case, where the force is proportional to the effective area normal to the incident radiation (Section 4.6), and the determination of this effective area is directly analogous to the determination of the effective area normal to the relative velocity vector.

where L is the length of the cylinder and d is the diameter. As before, m is the spacecraft mass, which can be variable.

The third type of spacecraft configuration optionally available in GTDS is a cylinder with solar paddles, mounted on trunnion pivots which are orthogonal to the cylinder axis. The incidence angle, i_p, defines the angle between the axis and the paddle surface. The spacecraft axis system is chosen so the x axis corresponds with the cylinder axis, y is the trunnion axis, and z is orthogonal to x and y. The y axis is directed so that positive i_p corresponds with positive rotation about y, according to the right-hand rule.

This configuration is not axisymmetric and therefore requires the calculation of the complete transformation matrix Q (from body to inertial axes). It is most convenient to transform the relative wind velocity into spacecraft body axes, compute the force components in this frame, and then transform the result back into the inertial coordinate frame. This leads to the following equations for the aerodynamic acceleration:

$$\overline{V}_B = Q^{-1}\,\overline{V}_{rel} = \dot{x}_B\ \hat{i}_B + \dot{y}_B\ \hat{j}_B + \dot{z}_B\ \hat{k}_B \tag{4-78a}$$

$$V_N = \dot{x}_B \sin i_p + \dot{z}_B \cos i_p \tag{4-78b}$$

$$F_{x_B} = -S_e\,\dot{x}_B\,|\dot{x}_B| - S_p\,V_N\,|V_N| \sin i_p \tag{4-78c}$$

$$F_{y_B} = -S_c\,\dot{y}_B\,\sqrt{\dot{y}_B^2 + \dot{z}_B^2} \tag{4-78d}$$

$$F_{z_B} = -S_c\,\dot{z}_B\,\sqrt{\dot{y}_B^2 + \dot{z}_B^2} - S_P\,V_N\,|V_N| \cos i_p \tag{4-78e}$$

$$\ddot{\overline{R}}_D = -\varrho\,Q\,\overline{F}_B \tag{4-78f}$$

The definitions of S_c and S_e are the same as in Equations (4-77). The solar paddle contribution is

$$S_p = \frac{1}{2}\left(\frac{C_{N_P}}{\cos^2 a}\right)\left(\frac{A_p}{m}\right) = \frac{2A_p}{m} \tag{4-79}$$

where the paddle area, A_p, is an input constant.

The representation of the aerodynamic forces in Equations (4-79) does not consider the effect of mutual shadowing or shielding from the free-stream flow between the cylindrical and solar paddle surfaces.* Such effects are geometrically very complex, particularly if multiple interference reflections between cylinder and paddles are considered. The simplifications resulting from the neglect of this phenomenon in Equation (4-78) are thought to be consistent with the original assumption of purely specular reflection in the specification of the individual surface type coefficients.

The factor ϱ in the three expressions for $\ddot{\bar{R}}_D$ is not simply the atmospheric density, ϱ_a. It also includes the following scale factor to permit an adjustment of the $\varrho\, C_F$ product:

$$\varrho = \varrho_a (1 + \varrho_1) \tag{4-80}$$

A default value of $\varrho_1 = 0$ is set in the program. However, this value can be modified by user input, or it can be estimated in the differential correction process. Adjustment of ϱ_1 does not alter the instantaneous direction of $\ddot{\bar{R}}_D$; it simply changes the magnitude.

Optionally, the drag scale factor ϱ_1 can be modeled as a polynomial such that

$$\varrho_1 = \sum_{i=0}^{N} a_i t^i \quad (N \leq 5) \tag{4-81}$$

In addition, the trajectory propagation timespan can be partitioned into segments, and independent values for the drag scale parameter coefficients, a_i, can be specified/estimated for each segment.

4.5.3 ASSOCIATED PARTIAL DERIVATIVES FOR AERODYNAMIC FORCE MODELING

When the aerodynamic force option is exercised in GTDS, it is necessary to compute the partial derivatives of $\ddot{\bar{R}}_D$ with respect to variations in the spacecraft local inertial state for use in the variational equations. For all configurations, the portion of the partial derivative that accounts for the effects of density variation is

$$\frac{\partial \ddot{\bar{R}}_D}{\partial \bar{R}} = \frac{\ddot{\bar{R}}_D}{\varrho_a} \frac{\partial \varrho_a}{\partial \bar{R}} \tag{4-82}$$

* Shadowing of the cylinder end plates by the cylindrical surface itself is considered.

since density depends only upon the spacecraft local position and not upon the local velocity. The forms for $\partial \varrho_a / \partial \bar{R}$ are presented in Sections 4.5.5 and 4.5.7 for the Jacchia-Roberts and Harris-Priester models, respectively.

All three forms for $\ddot{\bar{R}}_D$ are expressed in terms of $\bar{V}_{rel}$, which can be written in a slightly different form from that in Equation (4-72), as follows:

$$\bar{V}_{rel} = \dot{\bar{R}} - \Omega \bar{R} \tag{4-83a}$$

where the matrix Ω is given by

$$\Omega = \begin{bmatrix} 0 & -\omega_3 & \omega_2 \\ \omega_3 & 0 & -\omega_1 \\ -\omega_2 & \omega_1 & 0 \end{bmatrix} \tag{4-83b}$$

Thus, the partial derivatives can be computed with respect to $\bar{V}_{rel}$, and these can then be used to compute

$$\frac{\partial \ddot{\bar{R}}_D}{\partial \dot{\bar{R}}} = \frac{\ddot{\bar{R}}_D}{\partial \bar{V}_{rel}} \tag{4-84a}$$

$$\frac{\partial \ddot{\bar{R}}_D}{\partial \bar{R}} = \left(\frac{\ddot{\bar{R}}_D}{\partial \bar{V}_{rel}} \right) \Omega \tag{4-84b}$$

The partial derivatives of the three configuration forms with respect to $\bar{V}_{rel}$ $(\dot{x}_1, \dot{x}_2, \dot{x}_3)$ are given below:

Sphere

$$\frac{\partial \ddot{\bar{R}}_D}{\partial \bar{V}_{rel}} = -S_s \varrho \left(\frac{\bar{V}_{rel} \bar{V}_{rel}^T}{|\bar{V}_{rel}|} + |\bar{V}_{rel}| I \right) \tag{4-85}$$

Cylinder

$$M = |\hat{X}_B \times \bar{V}_{rel}| \tag{4-86a}$$

$$M^2 = (\hat{X}_B \times \bar{V}_{rel}) \cdot (\hat{X}_B \times \bar{V}_{rel}) \tag{4-86b}$$

$$\sigma = \hat{X}_B \cdot \bar{V}_{rel} \tag{4-86c}$$

$$\bar{W}_1 = (q_{11}^2 - 1)\ \hat{i} + q_{11}\, q_{21}\ \hat{j} + q_{11}\, q_{31}\ \hat{k} \tag{4-86d}$$

$$\bar{W}_2 = q_{21}\, q_{11}\ \hat{i} + (q_{21}^2 - 1)\ \hat{j} + q_{21}\, q_{31}\ \hat{k} \tag{4-86e}$$

$$\bar{W}_3 = q_{31}\, q_{11}\ \hat{i} + q_{31}\, q_{21}\ \hat{j} + (q_{31}^2 - 1)\ \hat{k} \tag{4-86f}$$

$$\frac{\partial \ddot{\bar{R}}_D}{\partial \dot{x}_i} = \varrho \left[S_c\, M\, \bar{W}_i - \frac{\bar{N}}{M^2} (\bar{W}_i \cdot \bar{V}_{rel}) + \frac{2\bar{A}}{\sigma}\, q_{i1} \right] \qquad (i = 1, 2, 3) \tag{4-86g}$$

The partial derivatives of the atmospheric drag acceleration with respect to the drag scale factor, ϱ_1, and the drag scale factor polynomial coefficients, a_i, are the following:

$$\frac{\partial \ddot{\bar{R}}}{\partial \varrho_1} = \frac{\ddot{\bar{R}}_D}{(1 + \varrho_1)} \tag{4-87a}$$

$$\frac{\partial \ddot{\bar{R}}_D}{\partial a_j} = \frac{\partial \ddot{\bar{R}}_D}{\partial \varrho_1} \frac{\partial \varrho_1}{\partial a_i} = t^j \frac{\ddot{\bar{R}}_D}{(1 + \varrho_1)} \tag{4-87b}$$

Cylinder + Paddles

$$\frac{\partial F_{x_B}}{\partial \dot{x}_B} = -2[S_e\, |\dot{x}_B| + S_p\, |V_N|\, \sin^2 i_p] \tag{4-88a}$$

$$\frac{\partial F_{x_B}}{\partial \dot{y}_B} = 0 \tag{4-88b}$$

$$\frac{\partial F_{x_B}}{\partial \dot{z}_B} = -2S_p |V_N| \cos i_p \sin i_p \tag{4-88c}$$

$$\frac{\partial F_{y_B}}{\partial \dot{x}_B} = 0 \tag{4-88d}$$

$$\frac{\partial F_{y_B}}{\partial \dot{y}_B} = \frac{F_{y_B}}{\dot{y}_B} - \frac{S_c \dot{y}_B^2}{\sqrt{\dot{y}_B^2 + \dot{z}_B^2}} \tag{4-88e}$$

$$\frac{\partial F_{y_B}}{\partial \dot{z}_B} = -\frac{S_c \dot{y}_B \dot{z}_B}{\sqrt{\dot{y}_B^2 + \dot{z}_B^2}} \tag{4-88f}$$

$$\frac{\partial F_{z_B}}{\partial \dot{x}_B} = \frac{\partial F_{x_B}}{\partial \dot{z}_B} \tag{4-88g}$$

$$\frac{\partial F_{z_B}}{\partial \dot{y}_B} = \frac{\partial F_{y_B}}{\partial \dot{z}_B} \tag{4-89h}$$

$$\frac{\partial F_{z_B}}{\partial \dot{z}_B} = -S_c \left[\sqrt{\dot{y}_B^2 + \dot{z}_B^2} + \frac{\dot{z}_B^2}{\sqrt{\dot{y}_B^2 + \dot{z}_B^2}} \right] - 2S_p |V_N| \cos^2 i_p \tag{4-88i}$$

$$\frac{\partial \ddot{\bar{R}}_D}{\partial \bar{V}_{rel}} = \varrho \, Q \, \frac{\partial \bar{F}_B}{\partial \bar{V}_B} \, Q^{-1} \tag{4-88j}$$

4.5.4 JACCHIA-ROBERTS ATMOSPHERIC MODEL

In Reference 13, L. G. Jacchia defined two empirical profiles to represent the temperature as a function of the altitude and the exospheric temperature. One profile is defined

for the altitude range from 90 to 125 kilometers and the other for the region above 125 kilometers. Jacchia used these temperature functions in the appropriate thermodynamic differential equations to determine the density as a function of the altitude and the exospheric temperature. He assumed that mixing is predominant between 90 and 100 kilometers and substituted the low-altitude temperature profile into the barometric differential equation for this regime. Diffusive equilibrium was assumed above 100 kilometers, leading to the use of the low-altitude temperature profile in the diffusion differential equation for altitudes between 100 and 125 kilometers and the high-altitude temperature profile for altitudes above 125 kilometers.

Jacchia solved these differential equations by integrating them numerically over the altitude regions for various constant values of exospheric temperature, assuming fixed boundary conditions at the 90-kilometer lower altitude limit. He then tabulated these numerical results for use in the simulation of aerodynamic drag effects upon satellites. Most mechanizations of this atmosphere model in computer programs have involved some means for storing the tabular data and for interpolating values at altitudes computed by the trajectory integration and at exospheric temperatures calculated by the Jacchia formulas. Although the densities determined by this model are accurate, these mechanizations are generally slow running and/or require large blocks of core storage. In addition, the absence of explicit analytic expressions means that the drag partial derivatives must be calculated numerically.

C. E. Roberts, Jr., presented a method (Reference 14) for evaluating the Jacchia model analytically, and this formulation is used in the mechanization in GTDS. Roberts found that the barometric and diffusion differential equations could be integrated by partial fractions, using Jacchia's low-altitude temperature profile for the range from 90 to 125 kilometers. Above 125 kilometers, Roberts used a different assymptotic function than the one introduced empirically by Jacchia to obtain an integrable form. Apart from the difficulties of numerical computations with a finite number of digits, the Roberts analytic expressions match the Jacchia results exactly from 90 to 125 kilometers and to close approximation above 125 kilometers. The existence of these analytic expressions makes possible the computation of analytic forms for the drag partial derivatives. Since the Roberts formulas were derived for the Jacchia 1970 model, his constants have been adjusted for the later 1971 model. In addition, an error has been corrected in the function W(v) given by Roberts in Equations (12) of Reference 14.

The computations begin with equations given in the Jacchia report to determine the exospheric temperature and corrections to the standard density due to various effects.

Before execution of a trajectory generation, GTDS determines the total timespan of interest. Then, from a permanent data file, one set of values of geomagnetic activity data and two sets of solar flux data are retrieved. The geomagnetic data set is the 3-hour geomagnetic planetary index, K_p. One set of the solar flux data is the daily average

10.7-centimeter solar flux, $F_{10.7}$, as observed at the solar observatory at Ottawa, Canada; the other set is the 81-day running average (centered at the day of interest), $F^{avg}_{10.7}$, of $F_{10.7}$. The solar flux data are substituted into the equation

$$T_c = 379° + 3.°24\, F^{avg}_{10.7} + 1.°3\, [F_{10.7} - F^{avg}_{10.7}] \tag{4-89}$$

for determining the nighttime minimum global exospheric temperature for zero geomagnetic activity. The preprocessing computation of Equation (4-89) is done for each day of the timespan of interest, beginning 1 day prior to the start of the trajectory. The daily values of T_c and the 3-hourly values of K_p (beginning 6.7 hours prior to trajectory start) are stored in a working file for use in the computation of the trajectory.

At each trajectory integration time point, the value of T_c is retrieved from the working file for the day before the current time. This accounts for the fact that there is a 1-day lag in the temperature variation with respect to solar flux change. This value of T_c is used to compute the uncorrected exospheric temperature T_1 from the formula

$$T_1 = T_c \left\{1 + 0.3\left[\sin^{2.2}\theta + (\cos^{2.2}\eta - \sin^{2.2}\theta)\cos^{3.0}\left(\frac{\tau}{2}\right)\right]\right\} \tag{4-90}$$

where

$$\eta = \frac{1}{2}\,|\phi - \delta_s| \tag{4-91a}$$

$$\theta = \frac{1}{2}\,|\phi + \delta_s| \tag{4-91b}$$

$$\tau = H - 37.°0 + 6.°0 \sin (H + 43.°0) \qquad (-\pi < \tau < \pi) \tag{4-91c}$$

In the above equations, δ_s is the Sun's declination, and the geodetic latitude, ϕ, is given by

$$\phi = \tan^{-1}\left\{\frac{1}{(1 - f)^2}\left[\frac{X_3}{(X_1^2 + X_2^2)^{1/2}}\right]\right\} \tag{4-92}$$

The constant f is the geodetic flattening, and X_1, X_2, X_3 are the components of the unit position vector of the spacecraft in true of date coordinates. The parameter

$$H = 180^{\circ}.0 \left\{ \frac{(S_1 X_2 - S_2 X_1)}{\pi |S_1 X_2 - S_2 X_1|} \cos^{-1} \left[\frac{S_1 X_1 + S_2 X_2}{(S_1^2 + S_2^2)^{1/2} (X_1^2 + X_2^2)^{1/2}} \right] \right\} \quad (4\text{-}93)$$

is the local hour angle of the Sun (counted from upper culmination). The components S_1, S_2, S_3 comprise the unit vector to the Sun in true of date coordinates.

The effect of the geomagnetic activity upon the atmospheric temperature and density shows a lag behind the geomagnetic disturbance. Thus, the value of K_p is retrieved from the working file for a time 6.7 hours earlier than the current integration time point. The correction to the exospheric temperature is given by

$$\Delta T_\infty = 28^{\circ}.0 K_p + 0^{\circ}.03 e^{K_p} \qquad (Z \geq 200 \text{ kilometers}) \quad (4\text{-}94a)$$

$$\Delta T_\infty = 14^{\circ}.0 K_p + 0^{\circ}.02 e^{K_p} \qquad (Z < 200 \text{ kilometers}) \quad (4\text{-}94b)$$

The corrected exospheric temperature is

$$T_\infty = T_1 + \Delta T_\infty \quad (4\text{-}95)$$

and the inflection point temperature is

$$T_x = 371^{\circ}.6678 + 0.0518806 T_\infty - 294^{\circ}.3505 e^{-0.00216222 T_\infty} \quad (4\text{-}96)$$

These two temperatures, together with the spacecraft altitude, are used in the Roberts equations to compute the standard density value. However, a number of corrections must be applied to the standard density values to account for various physical effects. These corrections are given by formulas from Jacchia's paper (Reference 13) and are presented next, before the discussion proceeds to the Roberts equations.

In addition to the correction to the exospheric temperature, there is another direct geomagnetic effect on the standard density below 200 kilometers, as follows:

$$(\Delta \log_{10} \varrho)_G = 0.012 K_p + 1.2 \times 10^{-5} e^{K_p} \quad (4\text{-}97)$$

The semiannual density variation is given by the following relationships (for altitude Z in kilometers):

$$(\Delta \log_{10} \varrho)_{SA} = f(Z)\, g(t) \tag{4-98}$$

where

$$f(Z) = (5.876 \times 10^{-7} Z^{2.331} + 0.06328)\, e^{-0.002868Z} \tag{4-99a}$$

$$g(t) = 0.02835 + [0.3817 + 0.17829 \sin (2\pi \tau_{SA} + 4.137)] \times \sin (4\pi \tau_{SA} + 4.259) \tag{4-99b}$$

$$\tau_{SA} = \Phi + 0.09544 \left\{ \left[\frac{1}{2} + \frac{1}{2} \sin (2\pi \Phi + 6.035) \right]^{1.65} - \frac{1}{2} \right\} \tag{4-99c}$$

$$\Phi = \frac{JD_{1958}}{365.2422} \tag{4-99d}$$

In the last equation, JD_{1958} is the number of Julian days from January 1, 1958, and 365.2422 is the number of days in a tropical year.

The correction for the seasonal latitudinal variation of the lower thermosphere is given by

$$(\Delta \log_{10} \varrho)_{LT} = 0.014\,(Z - 90)\, e^{[-0.0013(Z-90)^2]} \times \sin (2\pi \Phi + 1.72) \sin \phi \,|\sin \phi| \tag{4-100}$$

Finally, the correction for the seasonal latitudinal variation of helium is

$$(\Delta \log_{10} \varrho)_{He} = 0.65 \left| \frac{\delta_s}{\epsilon} \right| \left[\sin^3 \left(\frac{\pi}{4} - \frac{\phi\, \delta_s}{2|\delta_s|} \right) - 0.35355 \right] \tag{4-101}$$

where ϵ is the obliquity of the ecliptic.

As mentioned earlier, for altitudes below 125 kilometers Roberts used the same temperature profile that Jacchia used, i.e.,

$$T(Z) = T_x + \frac{d_1}{35^4} \sum_{n=0}^{4} C_n Z^n \tag{4-102}$$

where

$$d_1 = T_x - T_0 \tag{4-103a}$$

$$T_0 = 183.0 \text{ K} \tag{4-103b}$$

$$C_0 = -89284375.0 \tag{4-103c}$$

$$C_1 = 3542400.0 \quad (\text{kilometers}^{-1}) \tag{4-103d}$$

$$C_2 = -52687.5 \quad (\text{kilometers}^{-2}) \tag{4-103e}$$

$$C_3 = 340.5 \quad (\text{kilometers}^{-3}) \tag{4-103f}$$

$$C_4 = -0.8 \quad (\text{kilometers}^{-4}) \tag{4-103g}$$

and where T_x is the inflection point temperature (at Z_x = 125 kilometers) given by Equation (4-96). Roberts substituted the temperature profile given by Equation (4-102) in the barometric differential equation and integrated by partial fractions to obtain

$$\varrho_s(Z) = \left(\frac{\varrho_0 T_0}{M_0}\right) \frac{M(Z)}{T(Z)} F_1^k \exp(k F_2) \tag{4-104}$$

as the expression for density for $90 < Z \leq 100$ kilometers, where the subscript 0 refers to conditions at 90 kilometers. The mean molecular weight is given as

$$M(Z) = \sum_{n=0}^{6} A_n Z^n \tag{4-105}$$

where

$$A_0 = -435093.363387 \tag{4-106a}$$

$$A_1 = 28275.5646391 \quad (\text{kilometers}^{-1}) \tag{4-106b}$$

$$A_2 = -765.33466108 \quad (\text{kilometers}^{-2}) \tag{4-106c}$$

$$A_3 = 11.043387545 \quad (\text{kilometers}^{-3}) \tag{4-106d}$$

$$A_4 = -0.08958790995 \quad (\text{kilometers}^{-4}) \tag{4-106e}$$

$$A_5 = 0.00038737586 \quad (\text{kilometers}^{-5}) \tag{4-106f}$$

$$A_6 = -0.000000697444 \quad (\text{kilometers}^{-6}) \tag{4-106g}$$

These constants give a value of $M(90) = M_0 = 28.82678$, which is not too different from the value of the sea level mean molecular mass, M_s, of 28.960.

The value of the density at the lower limit is assumed to be constant at $\varrho_0 = 3.46 \times 10^{-9}$ grams/centimeter^3. The constant k in Equation (4-104) is

$$k = -\frac{35^4 g_s R_a^2}{R d_1 C_4} \tag{4-107}$$

where

g_s = 9.80665 meters/second^2 = sea level acceleration due to gravity

R_a = 6356.766 kilometers

R = 8.31432 Joules/degrees Kelvin-mole (universal gas constant)

The functions F_1 and F_2 in Equation (4-104) are

$$F_1 = \left(\frac{Z + R_a}{90 + R_a}\right)^{p_1} \left(\frac{Z - r_1}{90 - r_1}\right)^{p_2} \left(\frac{Z - r_2}{90 - r_2}\right)^{p_3} \left(\frac{Z^2 - 2X\,Z + X^2 + Y^2}{8100 - 180X + X^2 + Y^2}\right)^{p_4} \tag{4-108a}$$

$$F_2 = (Z - 90)\left[A_6 + \frac{p_5}{(Z + R_a)(90 + R_a)}\right] + \frac{p_6}{Y} \tan^{-1}\left[\frac{Y(Z - 90)}{Y^2 + (Z - X)(90 - X)}\right] \tag{4-108b}$$

In these functions, r_1 and r_2 are the two real roots and X and Y are the real and imaginary parts $(Y > 0)$, respectively, of the complex conjugate roots of the quadratic

$$P(Z) = \sum_{n=0}^{4} C_n^* Z^n \tag{4-109}$$

with coefficients

$$C_0^* = \frac{35^4\, T_x}{C_4\, d_1} + \frac{C_0}{C_4} \tag{4-110a}$$

$$C_n^* = \frac{C_n}{C_4} \qquad (1 \le n \le 4) \tag{4-110b}$$

for values of C_n given by Equations (4-103). The parameters p_i in the functions F_i are given by

$$p_2 = \frac{S(r_1)}{U(r_1)} \tag{4-111a}$$

$$p_3 = \frac{-S(r_2)}{U(r_2)} \tag{4-111b}$$

$$p_5 = \frac{S(-R_a)}{V} \tag{4-111c}$$

$$\begin{aligned} p_4 = \{&B_0 - r_1 r_2 R_a^2 [B_4 + B_5(2X + r_1 + r_2 - R_a)] + W(r_1) p_2 \\ &- r_1 r_2 B_5 R_a (X^2 + Y^2) + W(r_2) p_3 \\ &+ r_1 r_2(R_a^2 - X^2 - Y^2) p_5\}/X^* \end{aligned} \tag{4-111d}$$

$$\begin{aligned} p_6 = {} & B_4 + B_5(2X + r_1 + r_2 - R_a) - p_5 - 2(X + R_a)p_4 \\ & - (r_2 + R_a)p_3 - (r_1 + R_a)p_2 \end{aligned} \tag{4-111e}$$

$$p_1 = B_5 - 2p_4 - p_3 - p_2 \tag{4-111f}$$

In these parameters,

$$X^* = -2r_1 r_2 R_a(R_a^2 + 2X R_a + X^2 + Y^2) \tag{4-112a}$$

$$V = (R_a + r_1)(R_a + r_2)(R_a^2 + 2X R_a + X^2 + Y^2) \tag{4-112b}$$

$$U(r_i) = (r_i + R_a)^2(r_i^2 - 2X r_i + X^2 + Y^2)(r_1 - r_2) \tag{4-112c}$$

$$W(r_i) = r_1 r_2 R_a(R_a + r_i)\left(R_a + \frac{X^2 + Y^2}{r_i}\right) \tag{4-112d}$$

The function $W(r_i)$ is corrected from an erroneous expression given in Reference 14. Finally, the coefficients B_n and the function $S(Z)$ are given by

$$B_n = \alpha_n + \beta_n \frac{T_x}{T_x - T_0} \tag{4-113a}$$

$$S(Z) = \sum_{n=0}^{5} B_n Z^n \qquad (4\text{-}113b)$$

where n = 0, 1, ..., 5, and

$$a_0 = 3144902516.672729 \qquad (4\text{-}114a)$$

$$a_1 = -123774885.4832917 \qquad (4\text{-}114b)$$

$$a_2 = 1816141.096520398 \qquad (4\text{-}114c)$$

$$a_3 = -11403.31079489267 \qquad (4\text{-}114d)$$

$$a_4 = 24.36498612105595 \qquad (4\text{-}114e)$$

$$a_5 = 0.008957502869707995 \qquad (4\text{-}114f)$$

$$\beta_0 = -52864482.17910969 \qquad (4\text{-}115a)$$

$$\beta_1 = -16632.50847336828 \qquad (4\text{-}115b)$$

$$\beta_2 = -1.308252378125 \qquad (4\text{-}115c)$$

$$\beta_3 = 0.0 \qquad (4\text{-}115d)$$

$$\beta_4 = 0.0 \qquad (4\text{-}115e)$$

$$\beta_5 = 0.0 \qquad (4\text{-}115f)$$

As noted above, Equation (4-104) is valid below Z = 100 kilometers, where mixing is assumed to be predominant. However, diffusive equilibrium is assumed above

Z = 100 kilometers; hence, the profile given by Equation (4-102) was substituted into the diffusion differential equations (one for each constituent of the atmosphere) and integrated by partial fractions by Roberts to yield, for $100 < Z \leq 125$ kilometers,

$$\varrho_s(Z) = \sum_{i=1}^{5} \varrho_i(Z) \tag{4-116}$$

Rigorously, the density at 100 kilometers, $\varrho(100)$, should be evaluated by means of Equation (4-104) for the particular exospheric temperature T_∞ of interest. However, since the evaluation of that equation is computationally expensive, it is preferable to avoid adding that expense to that already necessary to compute Equation (4-116). This is avoided in GTDS by precomputing values of $\varrho(100)$ using Equation (4-104) for a series of values of T_∞. These values have been least-squares curve fitted by the polynomial

$$\frac{\varrho(100)}{M_s} = \sum_{n=0}^{6} \zeta_n T_\infty^n \tag{4-117}$$

where

$$\zeta_0 = 0.1985549 \times 10^{-10} \tag{4-118a}$$

$$\zeta_1 = -0.183349 \times 10^{-14} \tag{4-118b}$$

$$\zeta_2 = 0.1711735 \times 10^{-17} \tag{4-118c}$$

$$\zeta_3 = -0.1021474 \times 10^{-20} \tag{4-118d}$$

$$\zeta_4 = 0.3727894 \times 10^{-24} \tag{4-118e}$$

$$\zeta_5 = -0.7734110 \times 10^{-28} \tag{4-118f}$$

$$\zeta_6 = 0.7026942 \times 10^{-32} \tag{4-118g}$$

and M_s is the sea level mean molecular mass = 28.96 grams/mole. This approximation is used in Equation (4-116).

The constituent mass densities for altitudes between 100 and 125 kilometers are given by

$$\varrho_i(Z) = \varrho(100) \frac{M_i}{M_s} \mu_i \left[\frac{T(100)}{T(Z)}\right]^{1+a_i} F_3^{M_i k} \exp(M_i k F_4) \qquad (4\text{-}119)$$

The identification of the constituents and the values of the corresponding constants in Equation (4-119) are given in Table 4-2.

Table 4-2. Atmospheric Constituents and Related Constants

INDEX i	CONSTITUENT	MOLECULAR MASS (M_i) (GRAMS/MOLE)	THERMAL DIFFUSION COEFFICIENT (a_i)	CONSTITUENT NUMBER DENSITY × $[M_s/\varrho(100)]$ DIVIDED BY AVOGADRO'S NUMBER (μ_i)
1	N	28.0134	0	0.78110
2	Ar	39.948	0	0.93432×10^{-2}
3	He	4.0026	-0.38	0.61471×10^{-5}
4	O_2	31.9988	0	0.161778
5	O	15.9994	0	0.95544×10^{-1}
6	H	1.00797	0	-

Hydrogen is an insignificant constituent at altitudes below 125 kilometers; hence, it is not included in Equations (4-116) and (4-119). The temperature at 100 kilometers is given by Equation (4-102) in the form

$$T(100) = T_x + \Omega d_1 \qquad (4\text{-}120)$$

where

$$\Omega = 35^{-4} \sum_{n=0}^{4} C_n(100)^n = -0.94585589 \tag{4-121}$$

is the precomputed value of the polynomial for 100 kilometers. The parameter k in Equation (4-119) is the same as defined previously, and the functions F_3 and F_4 are given by

$$F_3 = \left(\frac{Z + R_a}{R_a + 100}\right)^{q_1} \left(\frac{Z - r_1}{100 - r_1}\right)^{q_2} \left(\frac{Z - r_2}{100 - r_2}\right)^{q_3} \left(\frac{Z^2 - 2XZ + X^2 + Y^2}{100^2 - 200X + X^2 + Y^2}\right)^{q_4} \tag{4-122a}$$

$$F_4 = \frac{q_5(Z - 100)}{(Z + R_a)(R_a + 100)} + \frac{q_6}{Y} \tan^{-1}\left[\frac{Y(Z - 100)}{Y^2 + (Z - X)(100 - X)}\right] \tag{4-122b}$$

The parameters q_i are defined as

$$q_2 = \frac{1}{U(r_1)} \tag{4-123a}$$

$$q_3 = \frac{-1}{U(r_2)} \tag{4-123b}$$

$$q_5 = \frac{1}{V} \tag{4-123c}$$

$$q_4 = \frac{1 + r_1 r_2(R_a^2 - X^2 - Y^2) q_5 + W(r_1) q_2 + W(r_2) q_3}{X^*} \tag{4-123d}$$

$$q_6 = -q_5 - 2(X + R_a) q_4 - (r_2 + R_a) q_3 - (r_1 + R_a) q_2 \tag{4-123e}$$

$$q_1 = -2q_4 - q_3 - q_2 \tag{4-123f}$$

and X, Y, r_1, r_2, X^*, V, U(v), and W(v) are the same as defined previously.

Finally, diffusive equilibrium is still assumed for the region above 125 kilometers, but the temperature profile given by Equation (4-102) is no longer valid. Jacchia defined the temperature for the upper region by the empirical asymptotic function

$$T(Z) = T_x + \frac{2}{\pi}(T_\infty - T_x) \tan^{-1} \left\{ 0.95\pi \left(\frac{T_x - T_0}{T_\infty - T_x} \right) \left(\frac{Z - 125}{35} \right) \times \left[1 + 4.5 \times 10^{-6} (Z - 125)^{2.5} \right] \right\} \quad (4\text{-}124)$$

In order to be able to integrate the diffusion differential equations in closed form, Roberts replaced Jacchia's Equation (4-124) with the function

$$T(Z) = T_\infty - (T_\infty - T_x) \exp \left[- \left(\frac{T_x - T_0}{T_\infty - T_x} \right) \left(\frac{Z - 125}{35} \right) \left(\frac{\ell}{R_a + Z} \right) \right] \quad (4\text{-}125)$$

This temperature profile is continuous at $Z_x = 125$ kilometers regardless of the choice of the parameter ℓ. The slope is continuous at Z_x if

$$\ell = 1.9(R_a + Z_x) = 12315.3554 \text{ (kilometers)} \quad (4\text{-}126)$$

The value of ℓ is not set equal to this constant in GTDS but is computed by a procedure to be described later.

Integration of the diffusion differential equations for the temperature profile given by Equation (4-125) yields, for the first five constituents (i = 1, 2, ..., 5) in Table 4-2,

$$\rho_i(Z) = \rho_i(125) \left(\frac{T_x}{T} \right)^{1+\alpha_i+\gamma_i} \left(\frac{T_\infty - T}{T_\infty - T_x} \right)^{\gamma_i} \quad (4\text{-}127)$$

where

$$\gamma_i = \frac{M_i g_0 R_a^2}{R \ell T_\infty} \left(\frac{T_\infty - T_x}{T_x - T_0} \right) \left(\frac{35}{6481.766} \right) \quad (4\text{-}128)$$

The constituent mass densities at 125 kilometers can be obtained rigorously from Equation (4-119). However, as in the case of the density at 100 kilometers, GTDS makes a curve-fitting approximation to give (for i = 1, 2, ..., 5)

$$\log_{10} [d_i(125)] = \sum_{j=0}^{6} \delta_{ij} T_\infty^j \tag{4-129}$$

as a function of the exospheric temperature, where d_i is the constituent number density divided by Avogadro's number ($\varrho_i = M_i d_i$). The polynomial coefficients δ_{ij} in Equation (4-129) have been determined for best fits to the values corresponding to Equation (4-119) and are given in Table 4-3.

The value of the helium density computed by Equation (4-127) must be corrected for the seasonal latitudinal variation as given by Equation (4-101). The specific form is

$$[\varrho_3(Z)]_{\text{corrected}} = \varrho_3(Z)\ 10^{(\Delta \log_{10} \varrho)_{He}} \tag{4-130}$$

Above 500 kilometers, the concentration of hydrogen (i = 6 in Table 4-2) becomes sufficiently large that it also must be taken into account, as follows:

$$\varrho_6(Z) = \varrho_6(500)\left[\frac{T(500)}{T(Z)}\right]^{(1+\alpha_6+\gamma_6)} \left[\frac{T_\infty - T(Z)}{T_\infty - T(500)}\right]^{\gamma_6} \tag{4-131}$$

where the hydrogen density at 500 kilometers is

$$\varrho_6(500) = \frac{M_6}{A}\ 10^{\{73.13 - [39.4 - 5.5\log_{10}(T_{500})]\ \log_{10}(T_{500})\}} \tag{4-132}$$

For exospheric temperatures lower than approximately 600 degrees Kelvin, the relative concentration of hydrogen is significant. At altitudes lower than 500 kilometers, however, the resulting density error is partially compensated for by the least-squares fitting of Roberts' parameter ℓ (see Equation (4-136), given later).

Table 4-3. Polynomial Coefficients for Constituent Densities at 125 Kilometers

DEGREE OF POLYNOMIAL TERM (J)	CONSTITUENT (I)				
	(1) N_2	(2) Ar	(3) He	(4) O_2	(5) O
0	0.1093155×10^{2}	0.8049405×10^{1}	0.7646886×10^{1}	0.9924237×10^{1}	0.1097083×10^{2}
1	0.1186783×10^{-2}	0.2382822×10^{-2}	$-0.4383486 \times 10^{-3}$	0.1600311×10^{-2}	0.6118742×10^{-4}
2	$-0.1677341 \times 10^{-5}$	$-0.3391366 \times 10^{-5}$	0.4694319×10^{-6}	$-0.2274761 \times 10^{-5}$	$-0.1165003 \times 10^{-6}$
3	0.1420228×10^{-8}	0.2909714×10^{-8}	$-0.2894886 \times 10^{-9}$	0.1938454×10^{-8}	$0.9239354 \times 10^{-10}$
4	$-0.7139785 \times 10^{-12}$	$-0.1481702 \times 10^{-11}$	$0.9451989 \times 10^{-13}$	$-0.9782183 \times 10^{-12}$	$-0.3490739 \times 10^{-13}$
5	$0.1969715 \times 10^{-15}$	$0.4127600 \times 10^{-15}$	$-0.1270838 \times 10^{-16}$	$0.2698450 \times 10^{-15}$	$0.5116298 \times 10^{-17}$
6	$-0.2296182 \times 10^{-19}$	$-0.4837461 \times 10^{-19}$	0.0	$-0.3131808 \times 10^{-19}$	0.0

In Equation (4-131), γ_6 is computed by means of Equation (4-128). The quantity A in Equation (4-132) is Avogadro's number ($A = 6.02257 \times 10^{23}$). The temperature at 500 kilometers is computed in Equation (4-125). Finally, the constituents are summed to yield

$$\varrho_s(Z) = \sum_{i=1}^{6} \varrho_i(Z) \tag{4-133}$$

as the standard density for the region $Z > 125$ kilometers.

The standard density, as computed by Equations (4-104), (4-116), or (4-133) must be corrected for geomagnetic activity (by Equation (4-97)), the semiannual variation (by Equation (4-98)), and the seasonal latitudinal variation of the lower thermosphere (by Equation (4-100)). These effects are summed logarithmically to obtain

$$(\Delta \log_{10} \varrho)_{corr} = (\Delta \log_{10} \varrho)_G + (\Delta \log_{10} \varrho)_{SA} + (\Delta \log_{10} \varrho)_{LT} \tag{4-134}$$

Thus, the final corrected density is

$$\varrho(Z) = \varrho_s(Z)\, 10^{(\Delta \log_{10} \varrho)_{corr}} \tag{4-135}$$

The standard densities, as computed by Equations (4-104) and (4-116) for the region $90 < Z \leq 125$ kilometers, agree exactly with values published by Jacchia in Reference 13. Above 125 kilometers, however, the values given by Equation (4-133) do not agree exactly with the Jacchia data, due to Roberts' introduction of a different form (Equation (4-125)) for the temperature profile at the higher altitudes. Values of the parameter ℓ in Roberts' temperature profile were determined for a series of exospheric temperatures, such that the resulting density profiles versus altitude (from 125 kilometers to 2500 kilometers) gave the best least-squares fit to the Jacchia tabulated data. Three sample fits are shown in Figure 4-3 for low, medium, and high values of the exospheric temperature. Note that the maximum deviation from the Jacchia values is less than 6.7 percent. The best-fit values of ℓ are shown in Figure 4-4 as a function of the exospheric temperature T_∞. The curve in the figure is the polynomial

$$\ell = \sum_{j=0}^{4} \ell_j T_\infty^j \tag{4-136}$$

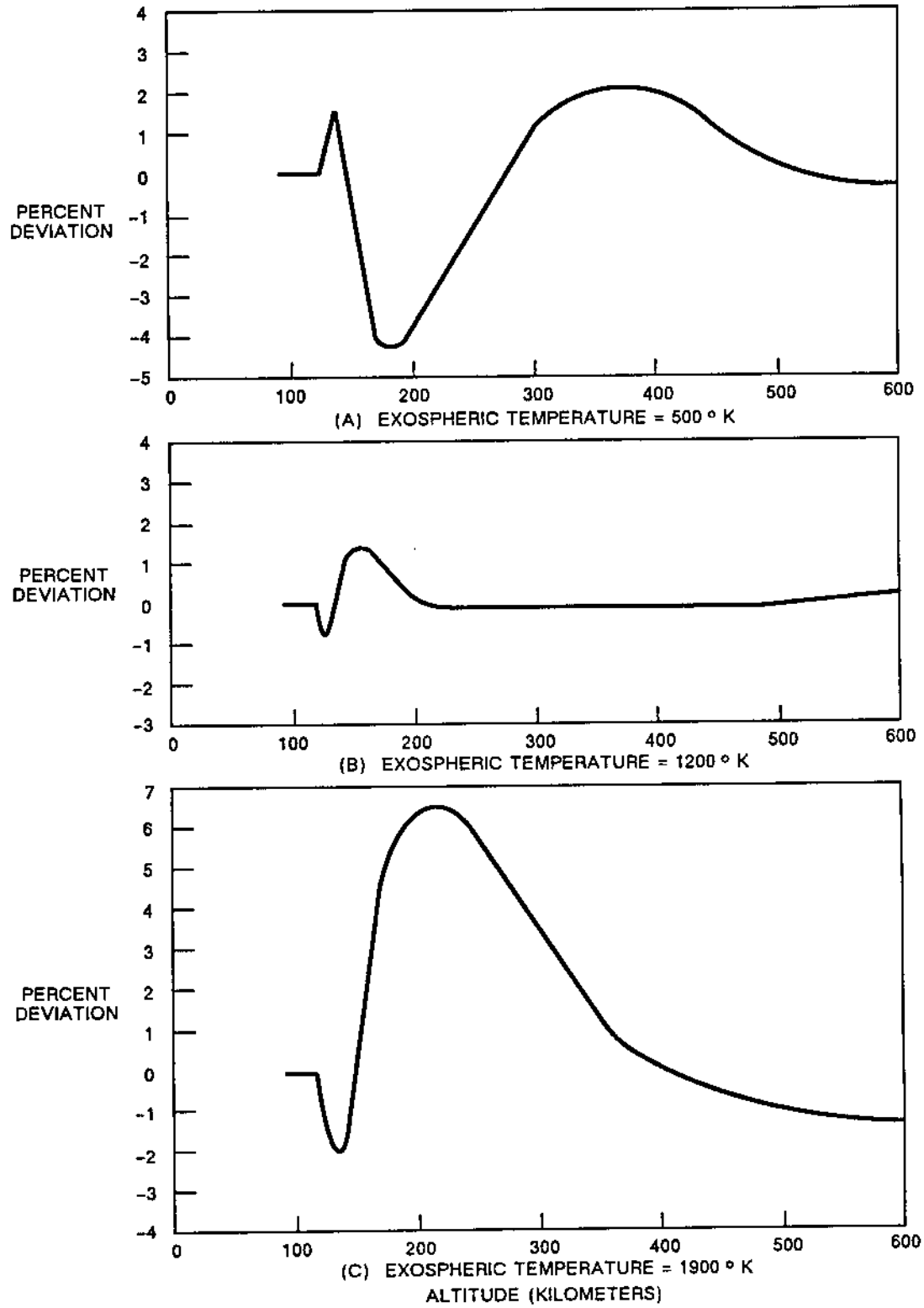

Figure 4-3. Sample Deviations of Jacchia-Roberts Densities From Jacchia 1971 Values

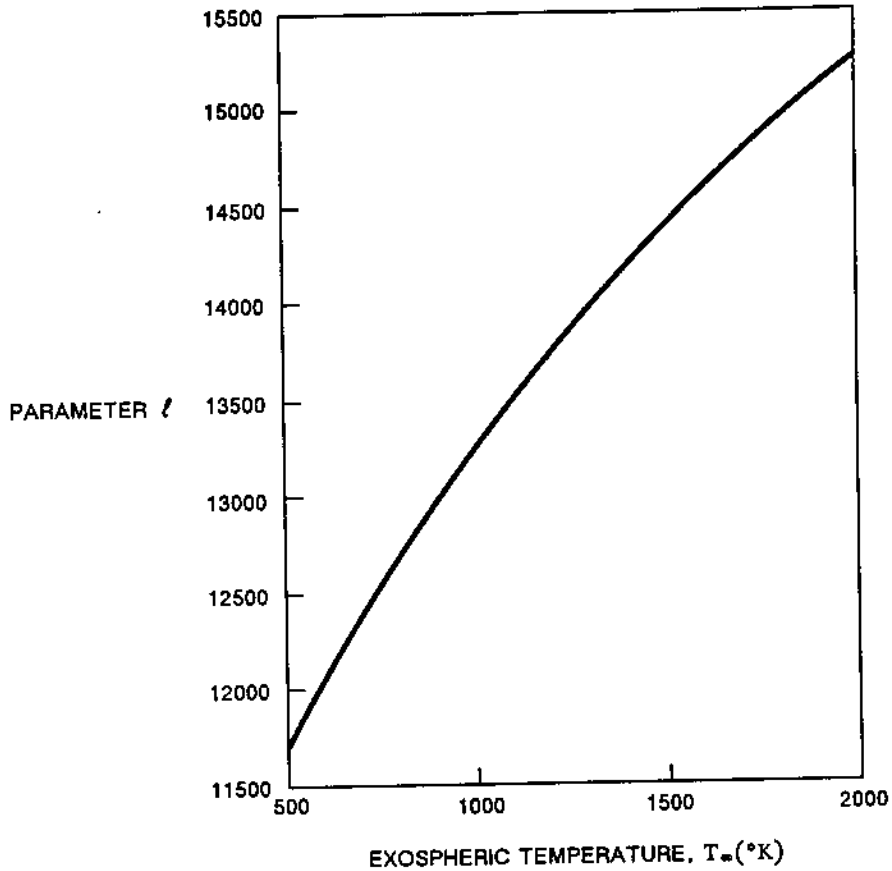

Figure 4-4. Best-Fit Values of ℓ as a Function of the Exospheric Temperature T_∞

with coefficients

$$\ell_0 = 0.1031445 \times 10^5 \tag{4-137a}$$

$$\ell_1 = 0.2341230 \times 10^1 \tag{4-137b}$$

$$\ell_2 = 0.1579202 \times 10^{-2} \tag{4-137c}$$

$$\ell_3 = -0.1252487 \times 10^{-5} \tag{4-137d}$$

$$\ell_4 = 0.2462708 \times 10^{-9} \tag{4-137e}$$

computed to best fit the optimum ℓ values. Equation (4-136) is programmed in GTDS to provide the means for selecting ℓ in Equation (4-125). In general, the values of ℓ are such that the slope of the temperature profile is discontinuous at Z_x = 125 kilometers, but this is not thought to be of any serious consequence.

4.5.5 ASSOCIATED PARTIAL DERIVATIVES FOR THE JACCHIA-ROBERTS MODEL

The equations for computing the partial derivative $\partial\varrho/\partial\bar{R}$, which appears in Equation (4-82), are presented in this section for the Jacchia-Roberts model. Equation (4-135) for the density is written in the form

$$\varrho(Z) = \varrho_s(Z)\,\Delta\varrho_c \tag{4-138}$$

and the desired partial derivative becomes

$$\frac{\partial\varrho}{\partial\bar{R}} = \varrho_s \frac{\partial(\Delta\varrho_c)}{\partial\bar{R}} + \Delta\varrho_c \frac{\partial\varrho_s}{\partial\bar{R}} \tag{4-139}$$

The variation of the correction factor is derived from Equations (4-134) and (4-97) through (4-100)

$$\begin{aligned}\frac{\partial(\Delta\varrho_c)}{\partial\bar{R}} = \frac{\Delta\varrho_c}{0.4342944819}\Bigg\{ & g(t)\, f'(Z) \frac{\partial Z}{\partial\bar{R}} \\ & + 0.014 \sin(2\pi\Phi + 1.72)\, e^{-0.0013(Z-90)^2} \\ & \times \Bigg([1 - 0.0026(Z-90)^2] \sin\phi\,|\sin\phi| \frac{\partial Z}{\partial\bar{R}} \\ & + 2(Z-90)\,|\sin\phi| \cos\phi \frac{\partial\phi}{\partial\bar{R}} \Bigg) \Bigg\}\end{aligned} \tag{4-140}$$

where

$$\begin{aligned}f'(Z) = & -0.002868\, f(Z) \\ & + 2.331(5.876 \times 10^{-7})\, Z^{1.331}\, e^{-0.002868Z}\end{aligned} \tag{4-141}$$

The variation of altitude with position, $\partial Z/\partial \bar{R}$, is equivalent to $\partial h/\partial \bar{R}$ computed in Equation (4-166) in Section 4.5.7. Differentiation of Equation (4-92) yields

$$\frac{\partial \phi}{\partial \bar{R}} = \frac{\sin 2\phi}{2} \begin{bmatrix} -\dfrac{X_1}{X_1^2 + X_2^2} \\ -\dfrac{X_2}{X_1^2 + X_2^2} \\ \dfrac{1}{X_3} \end{bmatrix} \tag{4-142}$$

The variation of the standard density is computed directly from the barometric differential equation (Reference 13) for altitudes below 100 kilometers

$$\frac{\partial \varrho_s}{\partial \bar{R}} = \varrho_s \left[\left(\frac{1}{M} \sum_{n=1}^{6} n A_n Z^{n-1} - \frac{M g}{R T} \right) \frac{\partial Z}{\partial \bar{R}} - \frac{1}{T} \frac{\partial T}{\partial \bar{R}} \right] \tag{4-143}$$

and from the diffusion differential equation (Reference 13) for altitudes above 100 kilometers

$$\frac{\partial \varrho_s}{\partial \bar{R}} = -\frac{1}{T} \left[\left(\frac{\varrho' g_0 R_a^2}{R(Z + R_a)^2} \right) \frac{\partial Z}{\partial \bar{R}} + (\varrho_s + a_3 \varrho_3) \frac{\partial T}{\partial \bar{R}} \right] \tag{4-144}$$

where

$$\varrho' = \sum_{i=1}^{6} \varrho_i M_i$$

The partial derivatives of the temperature are computed by differentiating Equation (4-102) for altitudes below 125 kilometers

$$\frac{\partial T}{\partial \bar{R}} = \frac{T - T_0}{d_1} \left(\frac{\partial T_x}{\partial T_\infty} \right) \frac{\partial T_\infty}{\partial \bar{R}} + \left(\frac{d_1}{35^4} \sum_{n=1}^{4} n C_n Z^{n-1} \frac{\partial Z}{\partial \bar{R}} \right) \tag{4-145}$$

or Equation (4-125) for altitudes above 125 kilometers

$$\frac{\partial T}{\partial \bar{R}} = \frac{\partial T_\infty}{\partial \bar{R}} + \left(\frac{T - T_\infty}{T_\infty - T_x}\right)\left\{\left(1 - \frac{\partial T_x}{\partial T_\infty}\right) - \left(\frac{Z - Z_x}{R_e + Z}\right)\left(\frac{\ell}{35}\right)\right.$$

$$\left. \times \left[\frac{\partial T_x}{\partial T_\infty} - \frac{T_x - T_0}{T_\infty - T_x}\left(1 - \frac{\partial T_x}{\partial T_\infty}\right) + \frac{T_x - T_0}{\ell}\sum_{j=1}^{4} j\,\ell_j\,T_\infty^{j-1}\right]\right\}\frac{\partial T_\infty}{\partial \bar{R}} \quad (4\text{-}146)$$

$$- \left(\frac{T - T_\infty}{T_\infty - T_x}\right)(T_x - T_0)\left[\frac{R_e + Z_x}{(R_e + Z)^2}\right]\left(\frac{\ell}{35}\right)\frac{\partial Z}{\partial \bar{R}}$$

Finally, the derivatives of T_x and T_∞ are computed by differentiating Equations (4-96) and (4-90), respectively, as follows:

$$\frac{\partial T_x}{\partial T} = 0.0518806 + (294.3505)(0.0021622)\,e^{-0.0021622 T_\infty} \quad (4\text{-}147)$$

$$\frac{\partial T_\infty}{\partial \bar{R}} = 0.3\,T_c\left\{2.2\,\sin^{1.2}\theta\,\cos\theta\left[1 - \cos^{3.0}\left(\frac{\pi}{2}\right)\right]\frac{\partial \theta}{\partial \bar{R}}\right.$$

$$- 2.2\,\cos^{1.2}\eta\,\sin\eta\,\cos^{3.0}\left(\frac{\tau}{2}\right)\frac{\partial \eta}{\partial \bar{R}} \quad (4\text{-}148)$$

$$\left. - \frac{3}{2}(\cos^{2.2}\eta - \sin^{2.2}\theta)\,\cos^2\left(\frac{\tau}{2}\right)\sin\left(\frac{\tau}{2}\right)\frac{\partial \tau}{\partial \bar{R}}\right\}$$

In the latter expression (from Equations (4-92) and (4-93)),

$$\frac{\partial \eta}{\partial \bar{R}} = \frac{1}{2}\,\frac{\phi - \delta_s}{|\phi - \delta_s|}\,\frac{\partial \phi}{\partial \bar{R}} \quad (4\text{-}149a)$$

$$\frac{\partial \theta}{\partial \bar{R}} = \frac{1}{2}\,\frac{\phi + \delta_s}{|\phi + \delta_s|}\,\frac{\partial \phi}{\partial \bar{R}} \quad (4\text{-}149b)$$

$$\frac{\partial \tau}{\partial X_i} = \frac{\pi}{180}\left\{1 + \frac{\pi}{30}\cos\left[\frac{\pi(H + 43.0)}{180}\right]\right\}\frac{\partial H}{\partial X_i} \tag{4-149c}$$

$$\frac{\partial H}{\partial X_i} = \frac{180}{\pi}\left(\frac{S_1 X_2 - S_2 X_1}{|S_1 X_2 - S_2 X_1|}\right) \times \left\{\frac{1}{[(X_1^2 + X_2^2)^{1/2}(S_1^2 + S_2^2) - (S_1 X_1 - S_2 X_2)^2]^{1/2}}\right\} \times \left[\frac{S_1 X_1 - S_2 X_2) X_i}{X_1^2 + X_2^2} - \frac{X_1 X_2}{S_i}\right]\left(\frac{1 - X_i}{R}\right) \tag{4-149d}$$

$$\frac{\partial \tau}{\partial X_3} = 0 \tag{4-149e}$$

In the above equations, the subscript i = 1, 2.

It might be argued that the term in Equation (4-146) involving the derivative $\partial \ell / \partial T_\infty$ should not be included, since Roberts considered ℓ as a constant in his integration. However, T_∞ and $T_x = F(T_\infty)$ were also held constant for the integration over altitude. Therefore, if variations in T_∞ are taken into account, and ℓ is a function of T_∞, then the derivative of ℓ should also be included and is computed by differentiating Equation (4-136), the best-fitting polynomial to the optimum values of ℓ.

4.5.6 MODIFIED HARRIS-PRIESTER ATMOSPHERIC MODEL

Harris and Priester determined the physical properties of the upper atmosphere theoretically by solving the heat conduction equation under quasi-hydrostatic conditions (References 10 through 12). Approximations for fluxes from the extreme ultraviolet and corpuscular heat sources were included, but the model averaged the semiannual and seasonal latitudinal variations and did not attempt to account for the extreme ultraviolet 27-day effect. The atmospheric model presently included in GTDS is a modification of the Harris-Priester concept. The modification attempts to account for the diurnal bulge by including a cosine variation between a maximum density profile at the apex of the diurnal bulge (which is located approximately 30 degrees east of the subsolar point) and a minimum density profile at the antapex of the diurnal bulge. Discrete values of the maximum and minimum density-altitude profiles, shown in Table 4-4, correspond to the mean solar activity and are stored in tabular form as $\varrho_M(h_i)$ and $\varrho_m(h_i)$, respectively. Different maximum and minimum profiles can be specified for different levels of solar activity.

Table 4-4. Density Altitude Tables

HEIGHT (KM)	MINIMUM DENSITY (GM/KM³)	MAXIMUM DENSITY (GM/KM³)
100	497400.	497400.
120	24900.	24900.
130	8377.	8710.
140	3899.	4059.
150	2122.	2215.
160	1263.	1344.
170	800.8	875.8
180	528.3	601.0
190	361.7	429.7
200	255.7	316.2
210	183.9	239.6
220	134.1	185.3
230	99.49	145.5
240	74.88	115.7
250	57.09	93.08
260	44.03	75.55
270	34.30	61.82
280	26.97	50.95
290	21.39	42.26
300	17.08	35.26
320	10.99	25.11
340	7.214	18.19
360	4.824	13.37
380	3.274	9.955
400	2.249	7.492

HEIGHT (KM)	MINIMUM DENSITY (GM/KM³)	MAXIMUM DENSITY (GM/KM³)
420	1.558	5.684
440	1.091	4.355
460	0.7701	3.362
480	0.5474	2.612
500	0.3916	2.042
520	0.2819	1.605
540	0.2042	1.267
560	0.1488	1.005
580	0.1092	0.7997
600	0.08070	0.6390
620	0.06012	0.5123
640	0.04519	0.4121
660	0.03430	0.3325
680	0.02632	0.2691
700	0.02043	0.2185
720	0.01607	0.1779
740	0.01281	0.1452
760	0.01036	0.1190
780	0.008496	0.09776
800	0.007069	0.08059
840	0.004680	0.05741
880	0.003200	0.04210
920	0.002210	0.03130
960	0.001560	0.02360
1000	0.001150	0.01810

Exponential interpolation is used between entries, i.e., the minimum and maximum densities, ϱ_m and ϱ_M, are given by

$$\varrho_m(h) = \varrho_m(h_i) \exp\left(\frac{h_i - h}{H_m}\right) \qquad (h_i \leq h \leq h_{i+1}) \tag{4-150a}$$

$$\varrho_M(h) = \varrho_M(h_i) \exp\left(\frac{h_i - h}{H_M}\right) \qquad (h_i \leq h \leq h_{i+1}) \tag{4-150b}$$

and the respective scale heights, H_m and H_M, are given by

$$H_m = \frac{h_i - h_{i+1}}{\ln\left[\frac{\varrho_m(h_{i+1})}{\varrho_m(h_i)}\right]} \tag{4-151a}$$

$$H_M = \frac{h_i - h_{i+1}}{\ln\left[\frac{\varrho_M(h_{i+1})}{\varrho_M(h_i)}\right]} \tag{4-151b}$$

A good approximation (neglecting polar motion) for the height, h, is

$$h = r - r_s \tag{4-152}$$

where r_s is the radius of the Earth given by Equations (3-116) and (3-128) as

$$r_s = \frac{R_e(1 - f)}{\sqrt{1 - (2f - f^2)\cos^2\delta}} \tag{4-153}$$

and

r = magnitude of the satellite position vector
R_e = equatorial radius of the Earth
f = Earth's flattening coefficient

δ = declination of the satellite; it is assumed that δ equals the geocentric latitude of the subsatellite point

If the density is assumed to be maximum at the apex of the bulge, then the cosine variation between the maximum and minimum density profiles is

$$\varrho_0(h) = \varrho_m(h) + [\varrho_M(h) - \varrho_m(h)] \cos^n\left(\frac{\psi}{2}\right) \tag{4-154}$$

where ψ is the angle between the satellite position vector and the apex of the diurnal bulge. The angle ψ is given by

$$\cos\psi = \sin\delta \sin\delta_s + \cos\delta \cos\delta_s \cos(\alpha - \alpha_s - \lambda_{lag}) \tag{4-155}$$

where

δ_s = declination of the Sun

α = right ascension of the satellite

α_s = right ascension of the Sun

λ_{lag} = lag angle between the Sun line and the apex of the diurnal bulge (approximately 30 degrees)

It can be calculated in vector notation as

$$\psi = \cos^{-1}\left(\frac{\bar{r} \cdot \hat{U}_B}{r}\right) \tag{4-156}$$

or the cosine function in Equation (4-154) can be determined directly as

$$\cos^n\left(\frac{\psi}{2}\right) = \left[\frac{1 + \cos\psi}{2}\right]^{n/2} = \left[\frac{1}{2} + \frac{\bar{r} \cdot \hat{U}_B}{2r}\right]^{n/2} \tag{4-157}$$

where

$\bar{r}$ = satellite position vector expressed in inertial geocentric coordinates

$\hat{U}_B$ = unit vector directed toward the apex of the diurnal bulge expressed in inertial geocentric coordinates

The vector $\hat{U}_B$ has the following components:

$$U_{B_x} = \cos \delta_s \cos (\alpha_s + \lambda_{lag}) \tag{4-158a}$$

$$U_{B_y} = \cos \delta_s \sin (\alpha_s + \lambda_{lag}) \tag{4-158b}$$

$$U_{B_z} = \sin \delta_s \tag{4-158c}$$

In the modeling of accelerations in GTDS, the drag coefficient, C_D, and atmospheric density, ϱ(h), always occur together as a product. The following error model is introduced to account for systematic errors in either C_D or ϱ:

$$C_D \varrho = C_{D_0}(1 + \varrho_1)[1 + \varrho_2(t - t_0)] \left[1 + \varrho_3 \cos^n \left(\frac{\psi}{2}\right)\right] \varrho_0(h) \tag{4-159}$$

where

C_{D_0} = a priori specified drag coefficient

ϱ_1 = scale factor error coefficient on $C_D \varrho$

ϱ_2 = error coefficient of time variation of $C_D \varrho$

ϱ_3 = error coefficient accounting for deviations in the diurnal variation of ϱ(h)

t = time of the instantaneous satellite position

t_0 = epoch time

The altitude density function, ϱ_0(h), is determined from Equation (4-154). The quantities ϱ_1, ϱ_2, ϱ_3, and n are adjustable parameters for the error model.

4.5.7 ASSOCIATED PARTIAL DERIVATIVES FOR THE MODIFIED HARRIS-PRIESTER MODEL

Equation (4-159) for the product of the drag coefficient and the density can be partitioned as follows:

$$C_D = C_{D_0}(1 + \varrho_1)[1 + \varrho_2(t - t_0)] \tag{4-160}$$

$$\varrho(h) = \left[1 + \varrho_3 \cos^n\left(\frac{\psi}{2}\right)\right]\left[\varrho_m + (\varrho_M - \varrho_m)\cos^n\left(\frac{\psi}{2}\right)\right] \tag{4-161}$$

Making use of Equations (4-150) and (4-151), the partial derivative of the density with respect to position is then given by

$$\frac{\partial \varrho}{\partial \bar{R}} = \left(\frac{\partial \varrho}{\partial \varrho_m}\frac{\partial \varrho_m}{\partial h} + \frac{\partial \varrho}{\partial \varrho_M}\frac{\partial \varrho_M}{\partial h}\right)\frac{\partial h}{\partial \bar{R}} + \frac{\partial \varrho}{\partial \psi}\frac{\partial \psi}{\partial R} \tag{4-162}$$

where

$$\frac{\partial \varrho}{\partial \varrho_m} = \left[1 - \cos^n\left(\frac{\psi}{2}\right)\right]\left[1 + \varrho_3 \cos^n\left(\frac{\psi}{2}\right)\right] \tag{4-163a}$$

$$\frac{\partial \varrho}{\partial \varrho_M} = \cos^n\left(\frac{\psi}{2}\right)\left[1 + \varrho_3 \cos^n\left(\frac{\psi}{2}\right)\right] \tag{4-163b}$$

$$\frac{\partial \varrho_m}{\partial h} = -\frac{\varrho_m}{H_m} \tag{4-163c}$$

$$\frac{\partial \varrho_M}{\partial h} = -\frac{\varrho_M}{H_M} \tag{4-163d}$$

The partial derivative of the density with respect to ψ and the partial derivative of ψ with respect to $\bar{R}$ are obtained from Equations (4-156) and (4-161) as follows:

$$\frac{\partial \varrho}{\partial \psi} = -\frac{n}{2} \cos^{n-1}\left(\frac{\psi}{2}\right) \sin\left(\frac{\psi}{2}\right)\left\{(\varrho_M - \varrho_m)\left[1 + \varrho_3 \cos^n\left(\frac{\psi}{2}\right)\right] + \varrho_3\left[\varrho_m + (\varrho_M - \varrho_m) \cos^n\left(\frac{\psi}{2}\right)\right]\right\} \tag{4-164}$$

$$\frac{\partial \psi}{\partial \bar{R}} = \frac{1}{\sin \psi}\left[\left(\frac{\bar{R} \cdot \hat{U}_B}{R^3}\right)\bar{R} - \frac{\hat{U}_B}{R}\right] \tag{4-165}$$

The partial derivative of the height with respect to $\bar{R}$ is obtained by differentiating Equation (4-152), yielding

$$\frac{\partial h}{\partial \bar{R}} = \frac{\bar{R}}{R} - R_e\left\{\frac{1 - f)(2f - f^2) \cos \delta}{[1 - (2f - f^2) \cos^2 \delta]^{3/2}}\right\} \frac{\partial(\cos \delta)}{\partial \bar{R}} \tag{4-166}$$

where

$$\frac{\partial(\cos \delta)}{\partial \bar{R}} = \frac{1}{R^4 \cos \delta}\begin{bmatrix} X Z^2 \\ Y Z^2 \\ -Z(X^2 + Y^2) \end{bmatrix} \tag{4-167}$$

Substitution of Equations (4-163) through (4-167) into Equation (4-162) determines the partial derivative of ϱ with respect to $\bar{R}$, as required in Equation (4-82).

The error coefficients ϱ_1, ϱ_2, and ϱ_3 contribute the following partial derivatives to the C-matrix appearing in the variational equations:

$$\frac{\partial \ddot{\bar{R}}_D}{\partial \varrho_1} = \frac{\ddot{\bar{R}}_D}{C_D} C_{D_0}[1 + \varrho_2(t - t_0)] = \frac{\ddot{\bar{R}}_D}{(1 + \varrho_1)} \tag{4-168a}$$

$$\frac{\partial \ddot{\bar{R}}_D}{\partial \varrho_2} = \frac{\ddot{\bar{R}}_D}{C_D} C_{D_0}(1 + \varrho_1)(t - t_0) = \frac{\ddot{\bar{R}}_D(t - t_0)}{[1 + \varrho_2(t - t_0)]} \tag{4-168b}$$

$$\frac{\partial \ddot{\bar{R}}_D}{\partial \varrho_3} = \frac{\ddot{\bar{R}}_D}{\varrho(h)}\left[\varrho_m + (\varrho_M - \varrho_m)\cos^n\left(\frac{\psi}{2}\right)\right]\cos^n\left(\frac{\psi}{2}\right)$$

$$= \frac{\ddot{\bar{R}}_D \cos^n\left(\frac{\psi}{2}\right)}{\left[1 + \varrho_3 \cos^n\left(\frac{\psi}{2}\right)\right]} \qquad (4\text{-}168c)$$

4.5.8 LOW-ALTITUDE MODEL

For orbit propagation at altitudes below approximately 100 kilometers, a low-altitude atmospheric density model is available. This model consists of a tabulation of the density, ϱ_a, versus the altitude extracted from the U.S. atmospheric model (Reference 15).

4.6 SOLAR RADIATION PRESSURE

The GTDS solar radiation pressure model and the associated partial derivatives are discussed in Sections 4.6.1 and 4.6.2, respectively.

4.6.1 SOLAR RADIATION PRESSURE PERTURBATION MODEL

The force due to solar radiation pressure on a vehicle's surface is proportional to the effective area A of the surface normal to the incident radiation, the surface reflectivity η, and the luminosity L_s of the Sun; and it is inversely proportional to the square of the distance R_{vs} from the Sun and the speed of light c.

The magnitude of the force due to direct solar radiation pressure on an area A is therefore given by*

$$F = \frac{L_s C_R A}{4\pi R_{vs}^2 c} \qquad (4\text{-}169)$$

where

$$C_R = 1 + \eta \qquad \text{(e.g., } C_R = 1.95 \text{ for aluminum)} \qquad (4\text{-}170)$$

* The determination of the effective area A of the surface normal to the incident radiation is directly analogous to the determination of the effective area normal to the relative velocity vector for modeling aerodynamic forces, which is discussed in detail in Section 4.5.2.

The magnitude of the acceleration acting on a spacecraft of mass m and area A, due to direct solar radiation pressure at one astronomical unit from the Sun, is

$$\frac{F}{m} = \frac{S}{c} \frac{C_R A}{m} \tag{4-171}$$

where S denotes the mean solar flux at one astronomical unit. The quantities C_R, A, and m are grouped together, since they are spacecraft properties and can be determined prior to flight. The magnitude of the acceleration on a spacecraft due to direct solar radiation at the actual distance R_{vs} from the Sun is given by

$$\frac{F}{m} = \frac{S}{c} \frac{R_{sun}^2}{R_{vs}^2} \frac{C_R A}{m} \tag{4-172}$$

where R_{sun} designates one astronomical unit, i.e., the semimajor axis of the Earth's orbit.

All of the above factors except R_{vs} are constant for a given spacecraft and mission. For computational convenience, P_s replaces $\frac{S}{c}$. The quantity P_s is defined as the force on a perfectly absorbing surface ($\eta = 0$) due to solar radiation pressure at one astronomical unit.

The acceleration due to direct solar radiation is away from the Sun, that is, in the direction of

$$\bar{R}_{vs} = \bar{R} - \bar{R}_s \tag{4-173}$$

where

$\bar{R}$ = position vector of the vehicle in inertial mean of B1950.0 or J2000.0 coordinates

$\bar{R}_s$ = position vector of the Sun in the inertial mean of B1950.0 or J2000.0 coordinates

The model for the acceleration $\ddot{\bar{R}}_{SR}$ due to direct solar radiation is

$$\ddot{\bar{R}}_{SR} = \nu P_s R_{sun}^2 \frac{C_R A}{m} \frac{\bar{R}_{vs}}{R_{vs}^3} \tag{4-174}$$

where ν is an eclipse factor such that

$\nu = 0$ if the satellite is in shadow (umbra)

$\nu = 1$ if the satellite is in sunlight

$0 < \nu < 1$ if the satellite is in penumbra

A simple cylindrical shadow model is used to determine the eclipse factor. From Figure 4-5, it is apparent that the satellite is in sunlight ($\nu = 1$) if

$$D = \bar{R}' \cdot \hat{U}_s > 0 \tag{4-175}$$

where

$\bar{R}'$ = satellite position vector relative to the shadowing body

$\hat{U}_s$ = solar position unit vector relative to the shadowing body

If $D < 0$ and the vector

$$\bar{S}_c = \bar{R}' - D\,\hat{U}_s \tag{4-176}$$

has a magnitude less than the body radius a_p, then the spacecraft is in shadow (i.e., $\nu = 0$); otherwise, it is assumed that the satellite is in sunlight and $\nu = 1$.

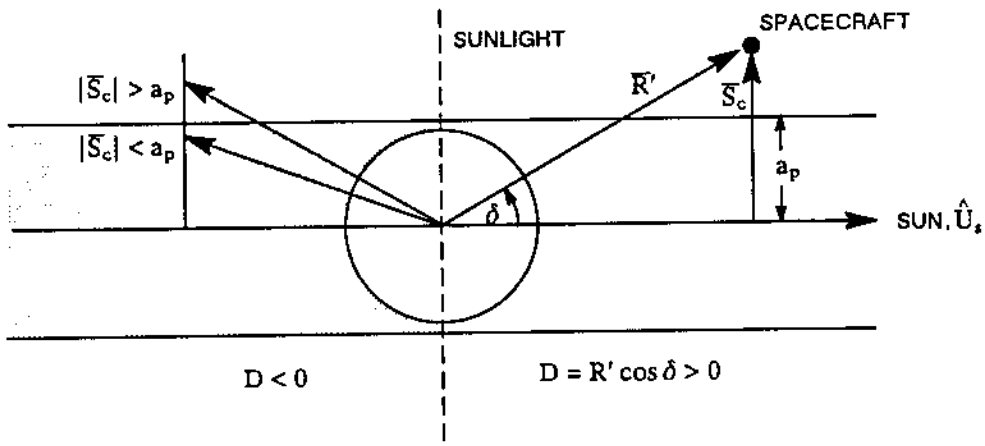

Figure 4-5. Cylindrical Shadow Model

4.6.2 ASSOCIATED PARTIAL DERIVATIVES

The partial derivatives of $\ddot{\bar{R}}_{SR}$ with respect to position are

$$\frac{\partial \ddot{\bar{R}}_{SR}}{\partial \bar{R}} = \nu \frac{P_S R_{sun}^2 C_R A}{m|\bar{R} - \bar{R}_s|^3}\left[I - \frac{3[\bar{R} - \bar{R}_s][\bar{R} - \bar{R}_s]^T}{|\bar{R} - \bar{R}_s|^2}\right] \tag{4-177}$$

$$\frac{\partial \ddot{\bar{R}}_{SR}}{\partial \dot{\bar{R}}} = 0_3 \tag{4-178}$$

and for the solar pressure model parameter

$$k = \frac{P_s A}{m} \tag{4-179}$$

$$\frac{\partial \ddot{\bar{R}}_{SR}}{\partial k} = \nu R_{sun}^2 C_R \frac{[\bar{R} - \bar{R}_s]}{|\bar{R} - \bar{R}_s|^3} \tag{4-180}$$

4.7 ATTITUDE CONTROL EFFECTS

The function of the attitude control system is related to two modes of operation. During the first mode, commonly known as the acquisition and cruise mode, the attitude control system is used to establish and maintain three-axis-stable orientation of the satellite. Such an orientation is obtained during an interplanetary flight, for example, by fixing two directions in space. One direction is always such that the sensitive surface of the solar panels faces the Sun and the other direction is determined by pointing an onboard sensor toward a predetermined star. Usually another requirement that must be satisfied during the latter portion of the flight is that the high-gain antenna used for communications should point toward the Earth.

In the second mode of operation, applicable during midcourse maneuvers, the attitude control system orients the satellite so that the thrust vector of the vehicle-fixed rocket motor is aligned along a predetermined direction in space. This orientation is maintained during the maneuver by controlling the thrust vector to pass through the center of mass of the satellite. After the maneuver, the attitude control system reestablishes the cruise orientation.

The low-thrust forces, generated by the normal functions of the attitude control system, can produce accelerations of 1×10^{-7} centimeters/second^2 to 3×10^{-7} centimeters/second^2. This can result in a target miss of 100 to 300 kilometers at Mars, for example. The translational forces producing the acceleration are the result of thrusters not acting in couples, thruster misalignment and unbalance, or gas leaks through the valves during times that the thrusters are not firing.

The attitude control perturbation model is described in Section 4.7.1, and the associated partial derivatives are given in Section 4.7.2.

4.7.1 ATTITUDE CONTROL PERTURBATION MODEL (NOT CURRENTLY AVAILABLE IN GTDS)

The model used to account for the attitude control accelerations has been constructed from the application of curve-fitting techniques to telemetered data and is defined as follows:

$$\ddot{\vec{r}}_{TAC} = \begin{Bmatrix} a_x + b_x(t - T_{ac1}) + c_x(t - T_{ac1})^2 \\ a_y + b_y(t - T_{ac1}) + c_y(t - T_{ac1})^2 \\ a_z + b_z(t - T_{ac1}) + c_z(t - T_{ac1})^2 \end{Bmatrix} [u(t - T_{ac1}) - u(t - T_{ac2})] \quad (4\text{-}181)$$

The coefficients (a_x, a_y, a_z, $\cdots$ c_x, c_y, c_z) are low-thrust polynomial coefficients to be determined. The terms T_{ac1} and T_{ac2} are input epochs at which the attitude control acceleration polynomials are turned on and off, respectively. The function u is defined by

$$u(t - T_{ac1}) = \begin{cases} 1 & (t \geq T_{ac1}) \\ 0 & (t < T_{ac1}) \end{cases} \quad (4\text{-}182)$$

$$u(t - T_{ac2}) = \begin{cases} 1 & (t \geq T_{ac2}) \\ 0 & (t < T_{ac2}) \end{cases} \quad (4\text{-}183)$$

The subscript x denotes the acceleration component along the spacecraft's x_v (roll) axis, the subscript y denotes the acceleration component along the spacecraft's y_v (pitch) axis, and the subscript z denotes the acceleration component along the spacecraft's z_v (yaw) axis.

Two transformations are necessary to represent this acceleration in the mean of B1950.0 or J2000.0 coordinate system: (1) a transformation from the vehicle-fixed coordinate

system (x_v, y_v, z_v) to the true of date coordinate system and (2) a transformation from the true of date coordinate system to the mean of B1950.0 or J2000.0 coordinate system.

The transformation from the vehicle-fixed coordinate system to the true of date coordinate system is described in Section 3.3.12 and is given by

$$\bar{r} = Q\,\bar{r}_V \tag{4-184}$$

where the transformation matrix Q is defined in Section 3.3.12. The matrix C^T, which transforms from the true of date system to the mean of B1950.0 or J2000.0 system, is described in Section 3.3.1. Thus, the total transformation is given by

$$\ddot{\bar{R}}_{TAC} = C^T Q\,\ddot{\bar{r}}_{TAC} \tag{4-185}$$

4.7.2 ASSOCIATED PARTIAL DERIVATIVES

Since C, Q, and $\ddot{\bar{r}}_{TAC}$ are functions of time only, and not of the satellite position or velocity, then

$$\frac{\partial \ddot{\bar{R}}_{TAC}}{\partial \bar{R}} = \frac{\partial \ddot{\bar{R}}_{TAC}}{\partial \dot{\bar{R}}} = 0_3 \tag{4-186}$$

The contributions to the variational equations (Equation (4-7)) of the control system acceleration parameters a_x, a_y, a_z, ..., c_z are

$$\frac{\partial \ddot{\bar{R}}_{TAC}}{\partial \bar{a}} = C^T Q\,[u(t - T_{ac1}) - u(t - T_{ac2})] \tag{4-187a}$$

$$\frac{\partial \ddot{\bar{R}}_{TAC}}{\partial \bar{b}} = (t - T_{ac1})\,\frac{\partial \ddot{\bar{R}}_{TAC}}{\partial \bar{a}} \tag{4-187b}$$

$$\frac{\partial \ddot{\bar{R}}_{TAC}}{\partial \bar{c}} = (t - T_{ac1})^2\,\frac{\partial \ddot{\bar{R}}_{TAC}}{\partial \bar{a}} \tag{4-187c}$$

where $\bar{a}$, $\bar{b}$, and $\bar{c}$ denote the vectors

$$\bar{a} = \begin{bmatrix} a_x \\ a_y \\ a_z \end{bmatrix} \tag{4-188a}$$

$$\bar{b} = \begin{bmatrix} b_x \\ b_y \\ b_z \end{bmatrix} \tag{4-188b}$$

$$\bar{c} = \begin{bmatrix} c_x \\ c_y \\ c_z \end{bmatrix} \tag{4-188c}$$

4.8 THRUST EFFECTS

There are many forces acting on a spacecraft during the transfer phase and orbiting phases of its trajectory. Even though such forces have been modeled, the state of the vehicle is still uncertain, primarily because of the imprecision associated with the injection conditions and the physical parameters appearing in the mathematical models. Very small errors in the thrust magnitude and/or thrust direction at injection magnify into very large errors in the position and velocity near the target body. To avoid such errors and attain preassigned terminal conditions, spacecraft are designed with the capability to perform multiple propulsive maneuvers during the interplanetary phase of a mission. Furthermore, if the spacecraft is to orbit a distant planet, maneuvering capability must be available to inject into orbit.

The GTDS polynomial thrust acceleration model is described in Section 4.8.1, and the associated partial derivatives are given in Section 4.8.2. The GTDS tabular thrust force model and high-thrust maneuver modeling are discussed in Sections 4.8.3 and 4.8.4, respectively.

4.8.1 POLYNOMIAL THRUST ACCELERATION MODEL

The model describing the acceleration during corrective maneuvers is based on the reduction of data taken during the motor burn testing procedures and is represented in an inertial true of date system by

$$\ddot{\bar{r}}_T = a[u(t - T_0) - u(t - T_f)]\ \hat{U}_T \tag{4-189}$$

where

a = magnitude of the thrust acceleration

$\hat{U}_T$ = unit vector in the direction of the thrust acceleration

T_0 = effective initiation time of the motor burn (ET)

T_f = effective termination time of the motor burn (ET)

and u is as defined in Equations (4-182) and (4-183).

The motor's effective burn time is

$$T_b = T_f - T_0 \tag{4-190}$$

The magnitude of the propulsive acceleration is modeled as follows:

$$a = a_0 + a_1 \tau + a_2 \tau^2 + a_3 \tau^3 + a_4 \tau^4 \tag{4-191}$$

where

$$\tau = t - T_0 \tag{4-192}$$

Equation (4-191) characterizes the thrust acceleration as a fourth-degree polynomial in τ, the time from effective thrust initiation. The polynomial coefficients a_0, a_1, a_2, a_3, and a_4 are dynamic model parameters, which can optionally be specified or estimated, and represent the effective thrust-mass ratio as a function of time.

The unit vector $\hat{U}_T$ is directed along the spacecraft's thrust axis (assumed to be coincident with the x_v axis). The true of date components of the vector $\bar{U}_T$ are

$$U_T = \begin{bmatrix} \cos \alpha_T \cos \delta_T \\ \sin \alpha_T \cos \delta_T \\ \sin \delta_T \end{bmatrix} \tag{4-193}$$

where

α_T = right ascension of the spacecraft's thrust axis relative to the true equator and equinox of date

δ_T = declination of the spacecraft's thrust axis relative to the true equator and equinox of date

The thrust axis orientation is represented by the fourth-degree polynomials in τ, as follows:

$$\alpha_T = \alpha_0 + \alpha_1 \tau + \alpha_2 \tau^2 + \alpha_3 \tau^3 + \alpha_4 \tau^4 \tag{4-194a}$$

$$\delta_T = \delta_0 + \delta_1 \tau + \delta_2 \tau^2 + \delta_3 \tau^3 + \delta_4 \tau^4 \tag{4-194b}$$

where α_0, α_1, ..., α_4, δ_0, ..., δ_4 are dynamic parameters, which can optionally be estimated.

The unit vector $\hat{U}_T$ can also be expressed in the orbital frame system, which is obtained from the orbit plane system (Section 3.2.5) by a translation of the origin to the center of mass of the spacecraft and a redesignation of axes such that

$$\bar{r}_{of} = E_1 \bar{r}_{op} \tag{4-195}$$

where

$$E_1 = \begin{bmatrix} 0 & 1 & 0 \\ 0 & 0 & 1 \\ 1 & 0 & 0 \end{bmatrix} \tag{4-196}$$

The thrust direction is defined by a rotation of Y_T (the yaw angle) about the z_{of} axis, followed by a rotation of P_T (the pitch angle) about the new x axis. The components of $\hat{U}_T$ in the orbital frame system are of the same form as Equation (4-193), with δ_T replaced by Y_T and a_T replaced by P_T. The true of date components of $\hat{U}_T$ are then given by

$$\hat{U}_T = (E_1 E)^T \hat{U}_{T_{of}} = E_{of}^T \hat{U}_{T_{of}} \tag{4-197}$$

where E is the transformation matrix from the inertial true of date system to the orbit plane system (see Section 3.3.5).

The thrust acceleration is expressed in the true equator and equinox of date coordinate system via the unit vector $\hat{U}_T$. The transformation to the mean equator and equinox of B1950.0 or J2000.0 coordinate system is accomplished as follows:

$$\ddot{\bar{R}}_T = C^T \ddot{\bar{r}}_T \tag{4-198}$$

where the transformation matrix C^T is described in Section 3.3.1.

4.8.2 ASSOCIATED PARTIAL DERIVATIVES

When the acceleration $\ddot{\bar{R}}_T$ is modeled in the direction $\hat{U}_T$ given by Equation (4-193), it is independent of both $\bar{R}$ and $\dot{\bar{R}}$; therefore,

$$\frac{\partial \ddot{\bar{R}}_T}{\partial \bar{R}} = \frac{\partial \ddot{\bar{R}}_T}{\partial \dot{\bar{R}}} = 0 \tag{4-199}$$

However, when the direction of the acceleration $\hat{U}_T$ is expressed as in Equation (4-197), the following partial derivatives are used.

Using Equations (4-189), (4-197), and (4-198), the thrust acceleration during a thrusting interval can be expressed as

$$\ddot{\bar{R}}_T = a\,(E_1 E C)^T \hat{U}_{T_{of}} \tag{4-200}$$

Since only the matrix E is a function of position and velocity,

$$\frac{\partial \ddot{\bar{R}}_T}{\partial \bar{R}} = a\, C^T \frac{\partial E^T}{\partial \bar{R}} E_I^T \hat{U}_{T_{of}} \tag{4-201}$$

and

$$\frac{\partial \ddot{\bar{R}}_T}{\partial \dot{\bar{R}}} = a\, C^T \frac{\partial E^T}{\partial \dot{\bar{R}}} E_I^T \hat{U}_{T_{of}} \tag{4-202}$$

The rows of the matrix E are defined in Section 3.3.5 to be the unit vectors $\hat{U}$, $\hat{V}$, and $\hat{W}$. The necessary partial derivatives then can be expressed, using subscript notation, as

$$\frac{\partial U_i}{\partial \dot{x}_j} = 0 \tag{4-203}$$

$$\frac{\partial U_i}{\partial x_j} = \frac{\delta_{ij}}{r} - \frac{x_i x_j}{r^3} \tag{4-204}$$

$$\frac{\partial W_i}{\partial x_j} = \frac{1}{L}\frac{\partial L_i}{\partial x_j} - \frac{L_i}{L^2}\frac{\partial L}{\partial x_j} \tag{4-205}$$

$$\frac{\partial W_i}{\partial \dot{x}_j} = \frac{1}{L}\frac{\partial L_i}{\partial \dot{x}_j} - \frac{L_i}{L^2}\frac{\partial L}{\partial \dot{x}_j} \tag{4-206}$$

$$\frac{\partial V_i}{\partial p} = \begin{bmatrix} 0 & -W_3 & W_2 \\ W_3 & 0 & -W_1 \\ -W_2 & W_1 & 0 \end{bmatrix} \begin{bmatrix} \frac{\partial U_1}{\partial p} \\ \frac{\partial U_2}{\partial p} \\ \frac{\partial U_3}{\partial p} \end{bmatrix} + \begin{bmatrix} 0 & U_3 & -U_2 \\ -U_3 & 0 & U_1 \\ U_2 & U_1 & 0 \end{bmatrix} \begin{bmatrix} \frac{\partial W_1}{\partial p} \\ \frac{\partial W_2}{\partial p} \\ \frac{\partial W_3}{\partial p} \end{bmatrix} \tag{4-207}$$

where

δ_{ij} = Kronecker delta operator

L_i = components of the angular momentum vector $(\bar{R} \times \dot{\bar{R}})$

L = magnitude of the angular momentum vector

p = any one of the parameters of $\bar{R}$ or $\dot{\bar{R}}$, x_1, x_2, x_3, $\dot{x}_1$, $\dot{x}_2$, $\dot{x}_3$

and

$$\frac{\partial L_i}{\partial x_j} = \begin{bmatrix} 0 & \dot{x}_3 & -\dot{x}_2 \\ -\dot{x}_3 & 0 & \dot{x}_1 \\ \dot{x}_2 & -\dot{x}_1 & 0 \end{bmatrix} \tag{4-208}$$

$$\frac{\partial L_i}{\partial \dot{x}_j} = \begin{bmatrix} 0 & -x_3 & x_2 \\ x_3 & 0 & -x_1 \\ -x_2 & x_1 & 0 \end{bmatrix} \tag{4-209}$$

$$\frac{\partial L}{\partial p} = \frac{1}{L} \sum_{i=1}^{3} L_i \frac{\partial L_i}{\partial p} \tag{4-210}$$

The C matrix components resulting from the acceleration model parameters a_0, ..., a_4 are given by

$$\frac{\partial \ddot{\bar{R}}_T}{\partial \bar{a}} = \frac{\ddot{\bar{R}}_T}{a} \bar{\Gamma}_4^T \tag{4-211}$$

$$\frac{\partial \ddot{\bar{R}}_T}{\partial \bar{\alpha}} = a[u(t - T_0) - u(t - T_f)]\, C^T\, \hat{U}_\alpha\, \bar{\Gamma}_3^T \tag{4-212}$$

$$\frac{\partial \ddot{\bar{R}}_T}{\partial \bar{\delta}} = a[u(t - T_0) - u(t - T_f)]\, C^T\, \hat{U}_\delta\, \bar{\Gamma}_3^T \tag{4-213}$$

where

$$\bar{a} = \begin{bmatrix} a_0 \\ a_1 \\ a_2 \\ a_3 \\ a_4 \end{bmatrix} \tag{4-214}$$

$$\bar{\alpha} = \begin{bmatrix} \alpha_0 \\ \alpha_1 \\ \alpha_2 \\ \alpha_3 \end{bmatrix} \tag{4-215}$$

$$\bar{\delta} = \begin{bmatrix} \delta_0 \\ \delta_1 \\ \delta_2 \\ \delta_3 \end{bmatrix} \tag{4-216}$$

$$\bar{\Gamma}_n^T = [1, \tau, \tau^2, \ldots, \tau^n] \tag{4-217}$$

$$\hat{U}_\alpha = \frac{\partial \hat{U}_T}{\partial \alpha_T} = \begin{bmatrix} -\sin \alpha_T \cos \delta_T \\ \cos \alpha_T \cos \delta_T \\ 0 \end{bmatrix} \tag{4-218}$$

$$\hat{U}_\delta = \frac{\partial \hat{U}_T}{\partial \delta_T} = \begin{bmatrix} -\cos \alpha_T \sin \delta_T \\ -\sin \alpha_T \sin \delta_T \\ \cos \delta_T \end{bmatrix} \tag{4-219}$$

4.8.3 TABULAR THRUST FORCE MODEL

The GTDS tabular thrust model is appropriate for long-burn, low-thrust maneuvers. This model provides a linearly varying thrust acceleration interpolated from values provided in

a table of mass and thrust as functions of time. The table can contain up to 101 values of thrust and mass, and up to 20 such tables can be included (with nonoverlapping times of applicability). Either the thrust can be applied as provided or a correction can be estimated.

The thrust acceleration vector, $\ddot{\bar{R}}(t_i)$, at a tabular point, t_i, is computed as follows:

$$\ddot{\bar{R}}_T(t_i) = (1 + a_\tau)\left[\frac{F(t_i)}{M(t_i)}\right]\hat{\bar{V}}(t_i) \tag{4-220}$$

where

i = 1, 2, ..., 101
a_τ = estimated thrust variation coefficient (set to zero when not estimating)
$M(t_i)$ = table entry for the mass (kilograms)
$\hat{\bar{V}}(t_i)$ = unit velocity vector

and the thrust magnitude, $F(t_i)$, in kilonewtons, is given by

$$F(t_i) = F'(t_i)\,C \tag{4-221}$$

where

$F'(t_i)$ = table entry for the thrust magnitude value (kilonewtons)
C = calibration factor (0 percent to 100 percent)

The value of the thrust acceleration at any given time between maneuver ignition and cutoff is computed by linear interpolation between two consecutive values of $\ddot{\bar{R}}_T$ that bracket the time in question.

If the application option is chosen for the thrust, then a_τ is set to zero; and the thrust table, mass table, and corresponding calibration factor of the thrust are the only items used in calculating $\ddot{\bar{R}}_T$ at any instant of time. If the thrust estimation option is chosen,

then the variational equations require the partial derivative of $\ddot{\bar{R}}_T$ with respect to a_τ, which is given by interpolating between two consecutive values of the following equation:

$$\frac{\partial \ddot{\bar{R}}_T(t_i)}{\partial a_\tau} = \frac{F(t_i)}{M(t_i)} \hat{V}(t_i) \qquad (4\text{-}222)$$

One thrust coefficient, a_τ, can be estimated for each thrust table included in the force model computations.

The limitation to this model is that thrust levels can be applied or estimated only in the spacecraft velocity direction.

4.8.4 HIGH-THRUST MANEUVER MODELING

For launch support, high-thrust maneuvers are modeled in the spacecraft orbit frame coordinate system, so that the nominal maneuver parameters determined prior to launch will be independent of the actual liftoff time. Section 4.8.4.1 describes maneuver modeling, and Section 4.8.4.2 discusses the estimation of maneuver parameters.

4.8.4.1 High-Thrust Maneuver Model

The maneuver is characterized by the following quantities:

t_{ig} = maneuver start (ignition) time

t_{bo} = maneuver end (burnout) time

m_{ig} = vehicle mass at ignition time

m_{bo} = vehicle mass at burnout time

P_{ig} = pitch angle at ignition

Y_{ig} = yaw angle at ignition

T_{ig} = thrust magnitude at ignition

$\dot{P}_{ig}$ = pitch angle rate (assumed constant during a maneuver)

$\dot{Y}_{ig}$ = yaw angle rate (assumed constant during a maneuver)

$\dot{T}_{ig}$ = thrust rate (assumed constant during a maneuver)

The coordinate system in which the pitch and yaw angles are measured is defined in terms of the position of the vehicle at a given time. The quantities $\hat{x}_p$, $\hat{y}_p$, and $\hat{z}_p$ are unit vectors describing this coordinate system, where

$$\hat{x}_p = \frac{\dot{\bar{r}} \times \bar{r}}{|\dot{\bar{r}} \times \bar{r}|} \tag{4-223}$$

$$\hat{y}_p = \frac{\bar{r} \times \hat{x}_p}{|\bar{r} \times \hat{x}_p|} \tag{4-224}$$

$$\hat{z}_p = \frac{\bar{r}}{|\bar{r}|} \tag{4-225}$$

where $\bar{r}$ and $\dot{\bar{r}}$ are the vehicle position and velocity vectors, respectively.

Two cases must be distinguished. The maneuver platform is said to be 'fixed' if the $(\hat{x}_p, \hat{y}_p, \hat{z}_p)$ coordinate system is evaluated at ignition and not reevaluated during the rest of the maneuver interval. The maneuver platform is said to be 'torqued' if the $(\hat{x}_p, \hat{y}_p, \hat{z}_p)$ coordinate system is evaluated each time the thrust acceleration is computed. The mass loss rate, $\dot{m}$, which is assumed to be constant, is given by

$$\dot{m} = \frac{m_{bo} - m_{ig}}{t_{bo} - t_{ig}} \tag{4-226}$$

If the platform is torqued, $\hat{x}_p$, $\hat{y}_p$, and $\hat{z}_p$ are computed from Equations (4-223) through (4-225) above. The mass, m(t), at the current time of integration (t) is then found as

$$\Delta t = t - t_{ig} \tag{4-227}$$

$$m(t) = m_{ig} - \dot{m}\,\Delta t \tag{4-228}$$

The pitch and yaw angles (P and Y) and the thrust magnitude (T) (see Figure 4-6) are found using

$$P = P_{ig} + \dot{P}\,\Delta t \tag{4-229}$$

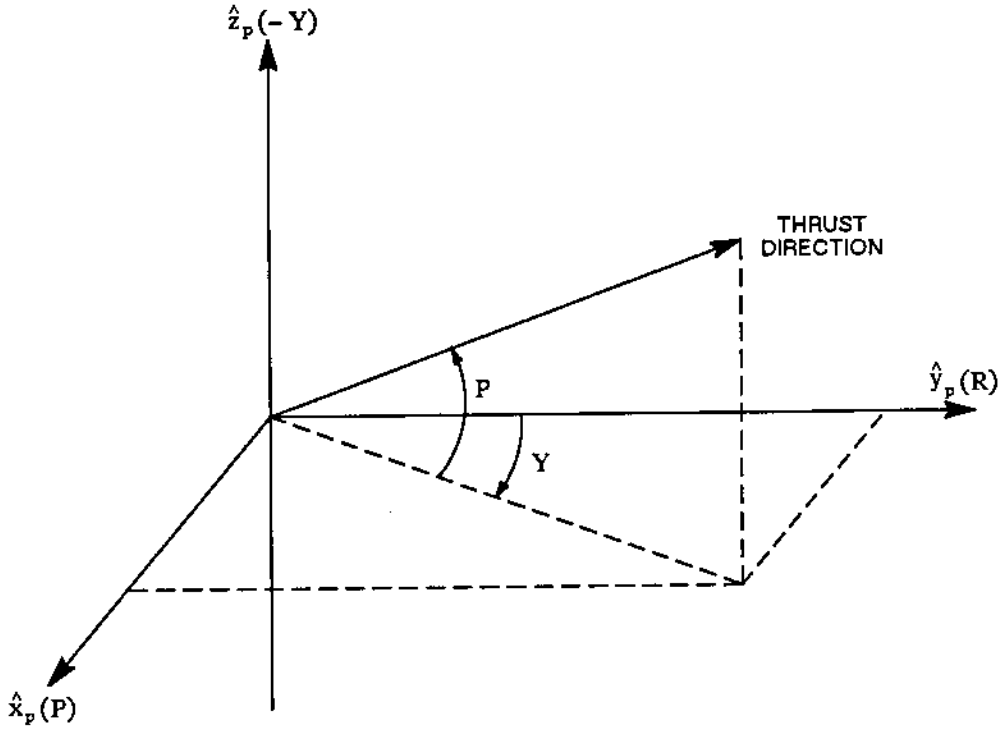

NOTE: THE ROTATIONS ARE FIRST ABOUT THE $\hat{x}_p$ AXIS BY AN ANGLE P AND THEN ABOUT THE $-\hat{z}_p$ AXIS BY AN ANGLE Y.

Figure 4-6. Yaw and Pitch Angle Coordinate System

$$Y = Y_{ig} + \dot{Y}\,\Delta t \tag{4-230}$$

$$T = T_{ig} + \dot{T}\Delta t \tag{4-231}$$

The vehicle's thrust acceleration vector, $\ddot{\bar{R}}_T$, in the coordinate system of integration, is then found using

$$\ddot{\bar{R}}_T = \frac{T[\cos(P)\,\sin(Y)\,\hat{x}_p + \cos(P)\,\cos(Y)\,\hat{y}_p + \sin(P)\,\hat{z}_p]}{m} \tag{4-232}$$

4.8.4.2 High-Thrust Maneuver Estimation

Accurate prediction of the trajectory of a spacecraft during a maneuver period requires estimation of the parameters pertinent to the thrust model (e.g., P, Y, and T and their rates in Section 4.8.4.1). The method of determining these parameters assumes that both the preignition and postburnout state vectors are known and that a maneuver is required that will allow the orbit predictor to generate the postburnout vector from the preignition vector via the normal orbit prediction processes.

4.8.4.2.1 Initialization

The initial configuration for maneuver computation is shown in Figure 4-7. From this configuration, the following parameters are defined:

t_i = time of preignition state vector

t_f = time of postburnout state vector

$\bar{S}_i$ = preignition state vector = $(\bar{r}_i, \dot{\bar{r}}_i)^T$

$\bar{S}_f$ = postburnout state vector = $(\bar{r}_f, \dot{\bar{r}}_f)^T$

r_{max} = maximum position tolerance

$\dot{r}_{max}$ = maximum velocity tolerance

Figure 4-7. Initial Configuration for Maneuver Computation

The following preparatory steps are then taken:

1. The vector $\bar{S}_i$ is integrated to t_{ig}, generating $\bar{S}_{ig} = (\bar{r}_{ig}, \dot{\bar{r}}_{ig})^T$
2. The vector $\bar{S}_f$ is integrated to t_{bo}, generating $\bar{S}_{bo} = (\bar{r}_{bo}, \dot{\bar{r}}_{bo})^T$
3. The vector $\bar{S}_i$ is integrated to t_f, assuming an entirely free-flight trajectory, generating $\bar{S}_f' = (\bar{r}_b, \dot{\bar{r}}_b)^T$

4. The unit vectors $\hat{x}_p$ and $\hat{y}_p$ are computed as

$$\hat{x}_p = \frac{\dot{\bar{r}}_b \times \bar{r}_b}{|\dot{\bar{r}}_b \times \bar{r}_b|} \tag{4-233}$$

$$\hat{y}_p = \frac{\bar{r}_b \times \hat{x}_p}{|\bar{r}_b \times \hat{x}_p|} \tag{4-234}$$

and the velocity difference at t_f is computed as

$$\Delta\dot{\bar{r}} = \dot{\bar{r}}_f - \dot{\bar{r}}_b \tag{4-235}$$

The initial estimate of the maneuver parameters is then

$$P_0 = \sin^{-1}\left[\frac{\bar{r}_b \cdot \Delta\dot{\bar{r}}}{|\bar{r}_b|\,|\Delta\dot{\bar{r}}|}\right] \tag{4-236}$$

$$Y_0 = \tan^{-1}\left[\frac{\hat{x}_p \cdot \Delta\dot{\bar{r}}}{\hat{y}_p \cdot \Delta\dot{\bar{r}}}\right] \tag{4-237}$$

$$T_0 = \frac{\dot{m}\,|\Delta\dot{\bar{r}}|}{\ln\left[\frac{m_{ig}}{m_{ig} - \dot{m}\,(t_{bo} - t_{ig})}\right]} \tag{4-238}$$

$$\dot{P}_0 = 0 \tag{4-239}$$

$$\dot{Y}_0 = 0 \tag{4-240}$$

$$\dot{T}_0 = 0 \tag{4-241}$$

4.8.4.2.2 Estimation

An iterative method is then invoked to successively refine the estimates of the maneuver parameters until either acceptable agreement between the initial and computed burnout vectors is obtained or a user-specified maximum number of iterations is reached. A description of the convergence test and differential correction process for this method is given below, followed by a discussion.

Convergence Test

A convergence test is applied after each iteration; this test proceeds in the following manner. First, $\bar{S}_{ig}$ is integrated to time t_{bo} using the current estimate of the maneuver parameters

$$\bar{M} = (P_0,\ Y_0,\ T_0,\ \dot{P}_0,\ \dot{Y}_0,\ \dot{T}_0) \tag{4-242}$$

thereby generating $\bar{S}'_{bo}$. The miss vector, $\Delta\bar{S}$, is computed as

$$\Delta\bar{S} = \bar{S}_{bo} - \bar{S}'_{bo} = (\Delta\bar{r},\ \Delta\dot{\bar{r}})^T \tag{4-243}$$

If $|\Delta\bar{r}| < r_{max}$ and $|\Delta\dot{\bar{r}}| < \dot{r}_{max}$, then the agreement is satisfactory, the current maneuver parameters are accepted, and processing terminates.

Differential Correction Process

If the convergence test fails, the first-order Taylor series expansion of the state vector is made using

$$\Delta\bar{S} = \left(\frac{\partial\bar{S}}{\partial\bar{M}}\right)\Delta\bar{M} \tag{4-244}$$

where $\Delta\bar{S}$ is the miss vector in Equation (4-243) above; and $\Delta\bar{M}$, the unknown correction to $\bar{M}$, is given by

$$\Delta\bar{M} = (\Delta P_0,\ \Delta Y_0,\ \Delta T_0,\ \Delta\dot{P}_0,\ \Delta\dot{Y}_0,\ \Delta\dot{T}_0) \tag{4-245}$$

The transformation matrix $\partial\overline{S}/\partial\overline{M}$ is computed using approximations to the various partial derivatives as follows:

$$\frac{\partial\overline{S}}{\partial P} = \frac{\overline{S}'_{bo}(P_0 + \delta P) - \overline{S}'_{bo}(P_0)}{\delta P} \tag{4-246a}$$

$$\frac{\partial\overline{S}}{\partial Y} = \frac{\overline{S}'_{bo}(Y_0 + \delta Y) - \overline{S}'_{bo}(Y_0)}{\delta Y} \tag{4-246b}$$

$$\frac{\partial\overline{S}}{\partial T} = \frac{\overline{S}'_{bo}(T_0 + \delta T) - \overline{S}'_{bo}(T_0)}{\delta T} \tag{4-246c}$$

$$\frac{\partial\overline{S}}{\partial \dot{P}} = \frac{\overline{S}'_{bo}(\dot{P}_0 + \delta \dot{P}) - \overline{S}'_{bo}(\dot{P}_0)}{\delta \dot{P}} \tag{4-246d}$$

$$\frac{\partial\overline{S}}{\partial \dot{Y}} = \frac{\overline{S}'_{bo}(\dot{Y}_0 + \delta \dot{Y}) - \overline{S}'_{bo}(\dot{Y}_0)}{\delta \dot{Y}} \tag{4-246e}$$

$$\frac{\partial\overline{S}}{\partial \dot{T}} = \frac{\overline{S}'_{bo}(\dot{T}_0 + \delta \dot{T}) - \overline{S}'_{bo}(\dot{T}_0)}{\delta \dot{T}} \tag{4-246f}$$

where the following abbreviations are made:

$$\overline{S}'_{bo}(P_0 + \delta P) = \overline{S}'_{bo}(P_0 + \delta P,\ Y_0,\ T_0,\ \dot{P}_0,\ \dot{Y}_0,\ \dot{T}_0) \tag{4-247a}$$

$$\overline{S}'_{bo}(Y_0 + \delta Y) = \overline{S}'_{bo}(P_0,\ Y_0 + \delta Y,\ T_0,\ \dot{P}_0,\ \dot{Y}_0,\ \dot{T}_0) \tag{4-247b}$$

$$\vdots \qquad\qquad \vdots$$

$$\overline{S}'_{bo}(\dot{T}_0 + \delta \dot{T}) = \overline{S}'_{bo}(P_0,\ Y_0,\ T_0,\ \dot{P}_0,\ \dot{Y}_0,\ \dot{T}_0 + \delta \dot{T}) \tag{4-247f}$$

The quantities $\overline{S}'_{bo}(P_0 + \delta P)$, etc., are found by incrementing the appropriate maneuver parameter (keeping the remaining five parameters at their nominal values) and using the orbit predictor to integrate $\overline{S}_{ig}$ to time t_{bo} with the new maneuver parameters. The variations (δP, δY, etc.) are differentials whose default values are the following:

- δP = 1 degree
- δY = 1 degree
- δT = 2200 newtons
- $\delta \dot{P}$ = 0.01 degree per second
- $\delta \dot{Y}$ = 0.01 degree per second
- $\delta \dot{T}$ = 4.4 newtons per second

Generation of the state vectors in Equations (4-246) requires six computation cycles by the orbit predictor, one for each variation in the nominal values of the maneuver parameters, $\overline{M}$.

The matrix $\partial\overline{S}/\partial\overline{M}$ is then found as

$$\frac{\partial \overline{S}}{\partial \overline{M}} = \left[\frac{\partial \overline{S}}{\partial P} \quad \frac{\partial \overline{S}}{\partial Y} \quad \frac{\partial \overline{S}}{\partial T} \quad \frac{\partial \overline{S}}{\partial \dot{P}} \quad \frac{\partial \overline{S}}{\partial \dot{Y}} \quad \frac{\partial \overline{S}}{\partial \dot{T}} \right]^T \tag{4-248}$$

and Equation (4-244) is solved as

$$\Delta\overline{M} = \left(\frac{\partial\overline{S}}{\partial\overline{M}}\right)^{-1} \Delta\overline{S} \tag{4-249}$$

The new maneuver parameters are then found using

$$\overline{M} \leftarrow \overline{M} + \Delta\overline{M} \tag{4-250}$$

Next, the convergence test described above is applied.

Discussion

In practice, reevaluating the transformation matrix in Equations (4-246) in every iteration can be very time consuming if the orbit predictor uses a Runge-Kutta integration method with a small step size for integrating over a maneuver period. A considerable savings can be obtained if the transformation matrix is evaluated in the first iteration and then not evaluated in the next N (user-specified number) iterations. Only when the corrections $\Delta\overline{M}$ (in Equation (4-249)) are small would the full transformation matrix in Equation (4-246) be reevaluated to reflect near convergence.

4.9 ANALYTIC PARTIAL DERIVATIVES

The differential correction process requires the development of a set of partial derivatives called the matrizant, or state transition matrix. These partial derivatives give the relationships between perturbations in the spacecraft state at observation times to perturbations in the state at the epoch. Analytic expressions for these partial derivatives, which were developed originally for the Brouwer-Lyddane method (References 16 and 17), are available for use with all of the orbit generators utilized in GTDS. The perturbation variables utilized in the analytic partial derivatives are defined in such a way as to couple the perturbation propagation process with the differential correction process. These variables are referred to as the DODS variables.

4.9.1 DEFINITION OF THE PERTURBATION VARIABLES

In the statistical estimation process, the spacecraft dynamic state variables in $\overline{x}$ are normally expressed in an inertial Cartesian coordinate system. As a result, the estimator algorithm solves for the differential correction, $\delta\overline{x}_{i+1}$, to be added to the epoch state on

the i^{th} iteration, $\bar{x}_i$, to yield an improved estimate, $\bar{x}_{i+1}$. Note that the unknowns that are solved for are corrections to the Cartesian state variables. The variables for the Brouwer-Lyddane theory are also state corrections, but are defined as follows:

$$x_1 = \frac{\delta a}{a} \qquad \text{(semimajor axis)} \qquad (4\text{-}251a)$$

$$x_2 = \delta e \qquad \text{(eccentricity)} \qquad (4\text{-}251b)$$

$$x_3 = e\,\delta f \qquad \text{(true anomaly)} \qquad (4\text{-}251c)$$

$$x_4 = \delta\alpha \qquad \text{(rotation about } \hat{\alpha}) \qquad (4\text{-}251d)$$

$$x_5 = \delta\beta \qquad \text{(rotation about } \hat{\beta}) \qquad (4\text{-}251e)$$

$$x_6 = \delta\gamma \qquad \text{(rotation about } \hat{\gamma}) \qquad (4\text{-}251f)$$

$$x_7 = \frac{a}{r^2}\,\delta r \qquad \text{(radial distance)} \qquad (4\text{-}251g)$$

$$x_8 = \frac{2}{n\,a\,\sqrt{1 - e^2\cos E}}\,\delta v \qquad \text{(velocity)} \qquad (4\text{-}251h)$$

$$x_9 = \delta\theta \qquad \text{(flight path angle)} \qquad (4\text{-}251i)$$

$$x_{19} = \delta\Omega + \delta\omega \qquad \text{(longitude of periapsis)} \qquad (4\text{-}251j)$$

The variables x_1, x_2, and x_3 account for in-plane perturbations of the orbit, i.e., perturbations in the semimajor axis, a, the eccentricity, e, and the true anomaly, f, respectively. The variable x_3 can also be related to a perturbation in the mean anomaly, M, as follows:

$$x_3 = \frac{e\sqrt{1 - e^2}}{(1 - e\cos E)^2}\,\delta M \qquad (4\text{-}252)$$

The variables x_4, x_5, and x_6 account for angular rotations of the orbit plane. Figure 4-8 illustrates an orbit around a planet. The unit vector $\hat{\alpha}$ is normal to the orbit plane; the unit vector $\hat{\beta}$ lies in the orbit plane and is displaced from the ascending node by the angle δ_a. The unit vector $\hat{\gamma}$ forms a right-hand system with $\hat{\alpha}$ and $\hat{\beta}$, i.e., $\hat{\gamma} = \hat{\alpha} \times \hat{\beta}$. Variable x_4 accounts for the rotational perturbation $\delta\alpha$ about $\hat{\alpha}$, x_5 accounts for the rotational perturbation $\delta\beta$ about $\hat{\beta}$, and x_6 accounts for the rotational perturbation $\delta\gamma$ about $\hat{\gamma}$. Variables x_4, x_5, and x_6 can be related to the orbit inclination, i, the right ascension of the ascending node, Ω, and the argument of periapsis, ω, as follows:

$$\delta i = x_5 \cos \delta_a - x_6 \sin \delta_a \tag{4-253}$$

$$\delta\Omega = \frac{x_5 \sin \delta_a + x_6 \cos \delta_a}{\sin i} \tag{4-254}$$

$$\delta\omega = x_4 - \frac{x_3}{e} - (x_5 \sin \delta_a + x_6 \cos \delta_a) \cot i \tag{4-255}$$

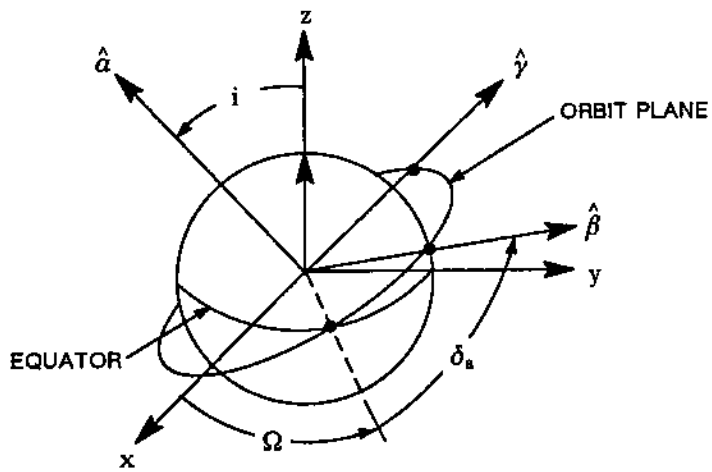

Figure 4-8. Orbital Geometry

The angle δ_a between the line of nodes and the $\hat{\beta}$ vector defines the $\hat{\beta}$ and $\hat{\gamma}$ directions. This angle can be ω_0, $\omega_0 + f_0$, $\omega + f$, or some other specified angle. In the equations that follow, δ_a is assumed to be $\omega + f$, i.e., $\hat{\beta}$ is directed towards the spacecraft.

Only six of the 10 variables in Equation (4-251) are independent. Therefore, any six can be selected to be solved for in any orbit determination problem. The selection criteria are dependent upon the sensitivity of the variables to pertinent characteristics of the orbit being determined. Experience has shown that variables x_1, x_2, x_3, x_4, x_5, x_6, and x_{19} are usually a reliable set of variables to use in a variety of Earth orbital missions. The dependence of the variables on orbital characteristics is shown in Table 4-5.

Table 4-5. DODS Variable Dependency

	a	e	I	Ω	ω	M	E	f	r	θ	δ_a	V
$\dot{x}_1$	✓											
x_2		✓										
x_3					✓	✓	✓	✓				
x_4					✓						✓	
x_5			✓	✓	✓						✓	
x_6			✓	✓	✓						✓	
x_7	✓	✓			✓	✓	✓	✓	✓			
x_8	✓	✓			✓	✓	✓	✓				✓
x_9		✓			✓	✓	✓	✓		✓		
x_{19}						✓	✓	✓			✓	

The Brouwer-Lyddane theory was developed for use with drag-free orbits. However, for high-altitude, small-eccentricity orbits, the primary effect of drag is a secular change in the mean anomaly. This effect is relatively small and is noticeable only over a long period

of time. Consequently, an optional first-order correction to the mean anomaly is included of the form

$$\Delta M_{DRAG} = \sum_{q=0}^{m} \sum_{p=2}^{3} N_{pq}(t - t_q)^p \qquad (m = 0, 1, 2, \ldots, 19) \qquad (4\text{-}256)$$

where

N_{pq} = Brouwer drag parameters

t_q = reference time associated with the Brouwer drag parameters

The correction is applied to the mean motion as follows:

$$M'' = n_0 \Delta t + \dot{M} \Delta t + M_0'' + \Delta M_{DRAG} \qquad (4\text{-}257)$$

Forty DODS variables, which account for the forty drag parameters N_{pq} in Equation (4-256), are defined as

$$x_{20+q} = \frac{N_{2q}}{n^2} \qquad (q = 0, 1, \ldots, 19) \qquad (4\text{-}258a)$$

$$x_{40+q} = \frac{N_{3q}}{n^2} \qquad (q = 0, 1, \ldots, 19) \qquad (4\text{-}258b)$$

These variables are estimated by means of the differential correction process to determine the secular corrections to the mean anomaly.

4.9.2 STATE TRANSITION MATRIX ELEMENTS

The statistical estimation algorithm requires the matrix of partial derivatives of the observations $f(t_i)$ at time t_i with respect to the solve-for state variables x_j at the epoch time t_0. These partial derivatives are computed as follows:

$$\frac{\partial f(t_i)}{\partial x_j} = \frac{\partial f(t_i)}{\partial \bar{r}(t_i)} \frac{\partial \bar{r}(t_i)}{\partial x_j} \qquad (j = 1, 2, \ldots, 19) \qquad (4\text{-}259)$$

The partial derivative of the observation model $f(t_i)$ with respect to the osculating Cartesian state vector $\bar{r}(t_i)$ is modeled as described in Chapter 7. However, the partial derivatives of the osculating Cartesian state with respect to the DODS variables must be determined. When the Brouwer or Brouwer-Lyddane theory is being utilized, $\partial\bar{r}(t_i)/\partial x_j$ is obtained analytically, where the solve-for variables x_j are the DODS variables. When one of the other GTDS orbit generators is used, requiring numerical integration of the orbital equations, two options are available: (1) the required partial derivatives can be obtained from numerical solution of the variational equations or (2) the above analytic partial derivatives can be used by replacing, via the chain rule, the required partial derivative in Equation (4-249) with

$$\frac{\partial\bar{r}(t_i)}{\partial x_j} = \frac{\partial\bar{r}(t_i)}{\partial x_k}\frac{\partial x_k}{\partial x_j} \tag{4-260}$$

where, in this case, the variables x_k are the DODS variables, the first term on the right represents the analytic partial derivatives of the osculating Cartesian state with respect to the DODS variables, and the second term represents the partial derivatives of the DODS variables with respect to the appropriate solve-for variables, depending on the orbit generator being used.

The analytic partial derivatives of the osculating Cartesian state with respect to the DODS variables are approximated by two-body Keplerian partial derivatives evaluated using the osculating Keplerian elements at t_i and t_0. This approach neglects the higher order effects of the Brouwer secular variation, as well as the partial derivatives of the osculating position and velocity with respect to the Brouwer mean position and velocity. These partial derivatives, which are developed in Reference 18, are presented below.

$$\frac{\partial\bar{r}}{\partial x_1} = \bar{r} - \frac{3}{2}(t - t_0)\,\dot{\bar{r}} \tag{4-261}$$

$$\frac{\partial\dot{\bar{r}}}{\partial x_1} = -\frac{\dot{\bar{r}}}{2} + \frac{3}{2}\frac{\mu\,\bar{r}(t - t_0)}{r^3} \tag{4-262}$$

$$\frac{\partial\bar{r}}{\partial x_2} = -\frac{1}{(1 - e^2)}\left[(\cos E_0 + e)\,\bar{r} - \frac{1}{n}(2 - e^2 - e\cos E)(\sin E)\,\dot{\bar{r}}\right] \tag{4-263}$$

$$\frac{\partial \dot{\bar{r}}}{\partial x_2} = \frac{1}{(1 - e^2)}\left[(\cos E)\,\dot{\bar{r}} - \frac{\mu \sin E}{n\,r^2}(1 + e\cos E - e^2 - e^2\cos^2 E)\,\bar{r}\right] \tag{4-264}$$

$$\begin{aligned}\frac{\partial \bar{r}}{\partial x_3} = \frac{a^2}{r}\Bigg\{&\frac{\sin E}{\sqrt{1 - e^2}}[2\cos E_0 + e\sin^2 E_0 - 2e - (1 - e^2)\cos E]\,\hat{p} \\ &+ [1 - (2\cos E_0 + e\sin^2 E_0 - \cos E)\cos E]\,\hat{q}\Bigg\}\end{aligned} \tag{4-265}$$

$$\begin{aligned}\frac{\partial \dot{\bar{r}}}{\partial x_3} = \frac{n\,a^4}{\sqrt{1 - e^2}\,r^3}\{&[1 + 2\cos E(\cos E_0 - \cos E) \\ &- e[\cos E(\sin^2 E + \cos^2 E_0) + 2\cos E_0] \\ &+ e^2(2\cos^2 E + \cos^2 E_0) - e^3\cos^3 E]\,\hat{p} \\ &- \sqrt{1 - e^2}\,\sin E\{(\cos E_0 - \cos E)[e(\cos E + \cos E_0) - 2]\}\,\hat{q}\end{aligned} \tag{4-266}$$

$$\frac{\partial \bar{r}}{\partial x_4} = \hat{\alpha} \times \bar{r} \tag{4-267}$$

$$\frac{\partial \dot{\bar{r}}}{\partial x_4} = \hat{\alpha} \times \dot{\bar{r}} \tag{4-268}$$

$$\frac{\partial \bar{r}}{\partial x_5} = \hat{\beta} \times \bar{r} \tag{4-269}$$

$$\frac{\partial \dot{\bar{r}}}{\partial x_5} = \hat{\beta} \times \dot{\bar{r}} \tag{4-270}$$

$$\frac{\partial \bar{r}}{\partial x_6} = \hat{\gamma} \times \bar{r} \tag{4-271}$$

$$\frac{\partial \dot{\bar{r}}}{\partial x_6} = \hat{\gamma} \times \dot{\bar{r}} \tag{4-272}$$

$$\frac{\partial \bar{r}}{\partial x_7} = 2\frac{\partial \bar{r}}{\partial x_1} + (1 - e^2)\cos E \frac{\partial \bar{r}}{\partial x_2} - \sqrt{1 - e^2}\sin E_0 \frac{\partial \bar{r}}{\partial x_3} \tag{4-273}$$

$$\frac{\partial \dot{\bar{r}}}{\partial x_7} = 2\frac{\partial \dot{\bar{r}}}{\partial x_1} + (1 - e^2)\cos E \frac{\partial \dot{\bar{r}}}{\partial x_2} - \sqrt{1 - e^2}\sin E_0 \frac{\partial \dot{\bar{r}}}{\partial x_3} \tag{4-274}$$

$$\frac{\partial \bar{r}}{\partial x_8} = (1 - e\cos E_0)\frac{\partial \bar{r}}{\partial x_1} + (1 - e^2)\cos E_0 \frac{\partial \bar{r}}{\partial x_2} - \sqrt{1 - e^2}\sin E_0 \frac{\partial \bar{r}}{\partial x_3} \tag{4-275}$$

$$\frac{\partial \dot{\bar{r}}}{\partial x_8} = (1 - e\cos E_0)\frac{\partial \dot{\bar{r}}}{\partial x_1} + (1 - e^2)\cos E_0 \frac{\partial \dot{\bar{r}}}{\partial x_2} - \sqrt{1 - e^2}\sin E_0 \frac{\partial \dot{\bar{r}}}{\partial x_3} \tag{4-276}$$

$$\frac{\partial \bar{r}}{\partial x_9} = -\sqrt{1 - e^2}\sin E_0 \frac{\partial \bar{r}}{\partial x_2} - (e + \cos E_0)\frac{\partial \bar{r}}{\partial x_3} \tag{4-277}$$

$$\frac{\partial \dot{\bar{r}}}{\partial x_9} = -\sqrt{1 - e^2}\sin E_0 \frac{\partial \dot{\bar{r}}}{\partial x_2} - (e + \cos E_0)\frac{\partial \dot{\bar{r}}}{\partial x_3} \tag{4-278}$$

$$\frac{\partial \bar{r}}{\partial x_{19}} = \frac{a(1 - e\cos E_0)^2}{(1 - e^2)(1 - e\cos E)}\left[-\sqrt{1 - e^2}(\sin E)\,\hat{p} + (1 - e^2)(\cos E)\,\hat{q}\right] \tag{4-279}$$

$$\frac{\partial \dot{\bar{r}}}{\partial x_{19}} = \frac{a^4 n(1 - e\cos E)^2}{r^3\sqrt{1 - e^2}}\left[(e - \cos E)\,\hat{p} - \sqrt{1 - e^2}(\sin E)\,\hat{q}\right] \tag{4-280}$$

where $\hat{p}$ and $\hat{q}$ are unit vectors in the orbit plane, with $\hat{p}$ directed toward perigee and $\hat{q}$ advanced 90 degrees in the direction of motion from perigee, i.e., $\hat{q} = \hat{a} \times \hat{p}$. The parameter n is the mean motion.

The Brouwer mean elements are utilized when the above equations are used for determining the partial derivatives at time t. Although the Brouwer mean elements at time t are

not determined from two-body relationships, the above equations still provide a good approximation for the state transition matrix elements for the mean motion.

The partial derivatives of the position and velocity with respect to the DODS drag parameters x_{20}, ..., x_{59} are

$$\frac{\partial \bar{r}}{\partial x_{20+q}} = n_0 \dot{\bar{r}}(t - t_q)^2 \tag{4-281a}$$

$$\frac{\partial \dot{\bar{r}}}{\partial x_{20+q}} = -\frac{(t - t_q)^2}{\sqrt{a_0 r^3}}\{(\csc E - e_0)\ \hat{p} + \sqrt{1 - e_0^2}\ (\sin E)\ \hat{q}\} \tag{4-281b}$$

$$\frac{\partial \bar{r}}{\partial x_{40+q}} = n_0(t - t_q)\frac{\partial \bar{r}}{\partial x_{20+q}} \tag{4-282a}$$

$$\frac{\partial \dot{\bar{r}}}{\partial x_{40+q}} = n_0(t - t_q)\frac{\partial \dot{\bar{r}}}{\partial x_{20+q}} \tag{4-282b}$$

In the above equations, q = 0, 1, ..., 19.

4.9.3 CONVERSION OF DIFFERENTIAL CORRECTIONS

Use of the preceding partial derivatives results in the expression of the state perturbations at epoch time in terms of DODS variables. Consequently, the weighted least-squares estimator algorithm yields the differential corrections in terms of DODS variables. These corrections must then be converted into more meaningful variables, such as Keplerian elements or Cartesian components. Specifically, GTDS converts the DODS corrections x_1, x_2, ..., x_{19} into corrections of the Brouwer mean elements, i.e., Keplerian elements. The reference mean elements at epoch are then updated to begin the next iteration.

As described in Section 4.9.2, when analytic partial derivatives are used in GTDS with orbit generators other than the Brouwer or Brouwer-Lyddane techniques, the statistical estimation algorithm is modified by introducing the partial derivatives of the DODS variables with respect to the solve-for state variables appropriate for the orbit generator in use. The estimation algorithm then yields the differential corrections in terms of these solve-for state variables.

Only six of the DODS variables described in Section 4.9.1 are independent. The user has the option of selecting which elements are to be corrected. The following conversion

equations show the dependency of the mean Keplerian element corrections on all the DODS variables. However, only the six independent variables selected for inclusion in the differential correction process should be included. All the other DODS variables should be set equal to zero. The following equations also include the conversion relationships for the related variables E, f, r, θ, δ_a, and V:

$$\Delta a = a\, x_1 + 2a\, x_7 + a^3\, \zeta_5\, x_8 \tag{4-283a}$$

$$\Delta e = x_2 + \zeta_1\, x_7 + \zeta_5\, \zeta_6\, x_8 + r\, \zeta_8\, x_9 \tag{4-283b}$$

$$\Delta i = x_5 \cos \delta_a - x_6 \sin \delta_a \tag{4-283c}$$

$$\Delta \Omega = \frac{1}{\sin i}(x_5 \sin \delta_a + x_6 \cos \delta_a) \tag{4-283d}$$

$$\Delta \omega = -\frac{1}{e}\, x_3 + x_4 - \zeta_{12}\, x_5 - \zeta_{13}\, x_6 - \zeta_3\, x_7 - \zeta_7\, x_8 - \zeta_9\, x_9 \tag{4-283e}$$

$$\Delta M = \frac{1}{e}\, \zeta_{11}\, x_3 + \zeta_3\, \zeta_{11}\, x_7 + \zeta_7\, \zeta_{11}\, x_8 + \zeta_9\, \zeta_{11}\, x_9 + \zeta_{11}\, x_{19} \tag{4-283f}$$

$$\Delta E = \frac{1}{e}\, \zeta_{10}\, x_3 + \zeta_3\, \zeta_{10}\, x_7 + \zeta_7\, \zeta_{10}\, x_8 + \zeta_9\, \zeta_{10}\, x_9 + \zeta_{10}\, x_{19} \tag{4-283g}$$

$$\Delta f = \frac{1}{e}\, x_3 + \zeta_3\, x_7 + \zeta_7\, x_8 + \zeta_9\, x_9 + x_{19} \tag{4-283h}$$

$$\Delta r = \zeta_2\, x_7 \tag{4-283i}$$

$$\Delta \theta = x_9 \tag{4-283j}$$

$$\Delta \delta_a = x_4 - \zeta_{12}\, x_5 - \zeta_{13}\, x_6 + x_{19} \tag{4-283k}$$

$$\Delta V = \frac{a}{2}\, \zeta_4\, x_8 \tag{4-283ℓ}$$

where

$$\zeta_1 = \frac{1 - e^2 - r^3 V^3 \cos\theta}{\mu a^2 e} \tag{4-284a}$$

$$\zeta_2 = \frac{r^2}{a} \tag{4-284b}$$

$$\zeta_3 = \frac{\zeta_1 (2a e + r \cos f) + \zeta_2 (1 + e \cos f) - 2a (1 - e^2)}{r e \sin f} \tag{4-284c}$$

$$\zeta_4 = n\sqrt{1 - e^2 \cos^2 E} \tag{4-284d}$$

$$\zeta_5 = \frac{V}{\mu} \zeta_4 \tag{4-284e}$$

$$\zeta_6 = \frac{(1 - e^2) a^2 - r^2 \cos^2\theta}{2e} \tag{4-284f}$$

$$\zeta_7 = \frac{\zeta_5 \zeta_6 (2a e + r e + r \cos f) - a^3 (1 - e^2)}{r e \sin f} \tag{4-284g}$$

$$\zeta_8 = \frac{r V^2}{\mu a e} \sin\theta \cos\theta \tag{4-284h}$$

$$\zeta_9 = \frac{\zeta_8 (2a e + r \cos f)}{e \sin f} \tag{4-284i}$$

$$\zeta_{10} = \frac{1 - e \cos E}{\sqrt{1 - e^2}} \tag{4-284j}$$

$$\zeta_{11} = \frac{(1 - e \cos E)^2}{\sqrt{1 - e^2}} \tag{4-284k}$$

$$\zeta_{12} = \frac{\cos i \sin \delta_a}{\sin i} \qquad (4\text{-}284\ell)$$

$$\zeta_{13} = \frac{\cos i \cos \delta_a}{\sin i} \qquad (4\text{-}284m)$$

4.10 REFERENCES

1. Brouwer, D. and Clemence, G. M.: 1961, *Methods of Celestial Mechanics*, Academic Press, New York.

2. Danby, J. M. A.: 1962, *Fundamentals of Celestial Mechanics*, Macmillan, New York.

3. Escobal, P. R.: 1965, *Methods of Orbit Determination*, John Wiley & Sons, New York.

4. Kaula, W. M.: 1966, *Theory of Satellite Geodesy*, Blaisdell Press, Los Angeles, California.

5. Sturms, F. M.: *Equations of Motion for a Double Precision Trajectory Program*, Volume IV, Jet Propulsion Laboratory Report SPS 37-29.

6. Moyer, T. D.: 1971, *Mathematical Formulation of the Double-Precision Orbit Determination Program (DPODP)*, Jet Propulsion Laboratory Technical Report 32-1527, May 1971.

7. Jacchia, L. G.: 1960, "A Variable Atmospheric-Density Model from Satellite Accelerations," *Journal of Geophysical Research*, 65(9), pp. 2775-82.

8. Jacchia, L. G.: 1963, "Variations in the Earth's Upper Atmosphere as Revealed by Satellite Drag," *Reviews of Modern Physics*, 35(4), October 1963, pp. 973-91.

9. Jacchia, L. G.: 1964, *The Temperature above the Thermopause*, Smithsonian Astrophysical Observatory Special Report No. 150, Cambridge, Massachusetts, April 1964.

10. Harris, I. and Priester, W.: 1952, "Time Dependent Structure of the Upper Atmosphere," *Journal of Atmospheric Sciences*, 19(4), July 1952, also NASA TN D-1443.

11. Harris, I. and Priester, W.: 1962, *Theoretical Models for the Solar Cycle Variation of the Upper Atmosphere*, Goddard Space Flight Center Report NASA-TN-D-144, August 1962.

12. Harris, I. and Priester, W.: 1965, "Atmospheric Structure and Its Variations in the Region from 120 to 80 KM," *COSPAR International Reference Atmosphere (CIRA) 1965*, Space Research IV, North Holland Publishing Company, Amsterdam.

13. Jacchia, L. G.: 1971, *Revised Static Models of the Thermosphere and Exosphere with Empirical Temperature Profiles*, Smithsonian Astrophysical Observatory Special Report No. 332, Cambridge, Massachusetts, May 1971.

14. Roberts, E. R., Jr.: 1971, "An Analytic Model for Upper Atmosphere Densities Based Upon Jacchia's 1970 Models," *Celestial Mechanics*, 4(3/4), December 1971, pp. 368-377.

15. Committee on Extension of the Standard Atmosphere: 1976, *U. S. Standard Atmosphere, 1976*, United States Government Printing Office, Washington, D.C., 1976.

16. Brouwer, D.: 1959, "Solution of the Problem of Artificial Satellite Theory Without Drag," *The Astronomical Journal*, 64(1274), October 1959, pp. 378-397.

17. Lyddane, R. H.: 1963, "Small Eccentricities or Inclinations in the Brouwer Theory of the Artificial Satellite," *The Astronomical Journal*, 68(8), October 1963, pp. 555-558.

18. Goddard Space Flight Center: 1971, *Definitive Orbit Determination Operating System Description*, Edition II, Goddard Space Flight Center Report X-544-71-35, January 1971.

CHAPTER 5—FORMULATION OF THE ORBITAL EQUATIONS OF MOTION

5.1 INTRODUCTION

Direct analytical solution of the differential equations describing the motion of a satellite perturbed by the total acceleration vector (Equation (4-1)) is not possible. Historically, solutions to this problem have been obtained using two principal approaches. In one approach, known as the General Perturbation Method, the perturbation model is limited such that an analytical solution is possible. Brouwer theory is a well known orbit generation technique that falls in this category. Brouwer formulated the problem of an Earth satellite, perturbed by point-mass and zonal gravitational effects, in terms of canonical variables and analytically solved the resulting Hamilton-Jacobi differential equations to first order in a small parameter, using the Von Zeipel method. The resulting orbit generation method is extremely efficient, but its accuracy is limited by the restricted perturbation model and the truncated small-parameter expansions (Reference 1).

In a second approach, known as the Special Perturbation Method, the entire perturbation model can be included in the differential equations (also known as the equations of motion). The differential equations are solved by the numerical integration techniques described in Chapter 6. The Cowell method is the best known orbit generation technique that falls into this category. In the Cowell approach, the equations of motion are expressed in terms of the total acceleration vector (i.e., point-mass central body effects plus perturbing accelerations) and solved directly for the position and velocity vectors.

Considerable research has been done that focused on improving the accuracy and efficiency of orbit generation methods. This research indicates that there is no best orbit generation procedure for all orbit types. For this reason, several orbit generation formulations are included in GTDS; taken together, these formulations are suited to a broad range of accuracy and efficiency requirements for the various classes of satellite orbits supported by GSFC.

In general, development of optimum methods for orbit prediction consists of reformulating the equations of motion in terms of a new set of variables such that the resulting equations are more amenable to solution. The principal guidelines used in these reformulations are given below.

1. Choose a dependent variable set that is appropriate for the numerical method of solution.

General Perturbation Methods usually require the use of canonical variables, which are amenable to the use of averaging transformation techniques such as the Von Zeipel

method. Similarly, in the Special Perturbation Methods, selection of appropriate variables may be dictated by the numerical method of solution. For example, the accuracy of numerical integration formulas increases with order. However, each integration formula has a numerical stability region, outside of which the error growth is exponential (see References 2 and 3 for a more complete discussion of numerical stability). For a given set of differential equations, this stability region dictates the allowable stepsizes. As a result, changing dependent variables can affect the stability characteristics of the process.

Reformulations of the Class II equations of motion* in terms of other dependent variables usually results in a set of Class I equations of motion,* e.g., the Variation of Parameters equations (Section 5.7). In general, Class I multistep numerical integration formulas (Equations (6-21) and (6-26)) have smaller regions of numerical stability than the Class II multistep methods (Equations (6-22) and (6-27)). Consequently, the numerical stability characteristics of the transformed equations of motion are a very important consideration.

Well-behaved equations of motion, i.e., those that change only slightly due to a small change in the elements, will yield large regions of numerical stability in terms of stepsize, thus allowing the use of the accurate high-order formulas. For example, element sets that are constants, or vary linearly with time in the unperturbed problem, yield equations of motion that are more numerically stable than the corresponding set of equations expressed in terms of the position and velocity coordinates.

2. Choose an independent variable so as to achieve a uniform local error over the entire orbit.

Efficient numerical integration can be achieved by adjusting the stepsize to achieve a uniform local error over the entire orbit. For near-circular orbits, fixed-step integration produces a uniform local error when time is the independent variable. To achieve a uniform error for eccentric orbits, a mechanism is required for using a small time step in the region of large perturbations and a large time step in the region of small perturbations. A variable stepsize integration algorithm is available in GTDS (see Section 6.9); however, frequent stepsize changes are costly and usually introduce error. For this reason, formulations have been developed that achieve a uniform error through analytic stepsize regularization, accomplished through the use of an independent variable other than time. A new independent variable s, related to the time t by

$$ds = \frac{\sqrt{\mu}}{r^n} dt \tag{5-1}$$

is available in GTDS, where r is the magnitude of the satellite's position vector and n is known as the uniformization constant. The effect of such a transformation is that fixed

* Class I differential equations are of the form $dy/dx = f(x,y)$; Class II differential equations are of the form $d^2y/dx^2 = f(x, y)$

steps in s yield smaller steps in time for small r (where the perturbations are usually larger) than for large r.

The appropriate choice for the uniformization constant depends on both the dependent variable set and the local error source. In the Cowell method, the primary source of local error is inaccurate integration of the point-mass and J_2 gravitational effects of the Earth. A uniformization constant of 3/2 is appropriate for these perturbations and is used in the Time Regularized Cowell orbit generator (Section 5.3). The Delaunay-Similar (DS) equations of motion (Section 5.5) are uniformized for the J_2 oblateness perturbation through the choice of a uniformization constant of 2. The Kustaanheimo-Stiefel (KS) formulation (Section 5.4) uses a uniformization constant of 1, which removes the singularity at collision from the equations of motion. In the Intermediate Orbit formulation (Section 5.11), the uniformization constant can be adjusted to produce uniformization with respect to the dominant source of local error. It should be noted that uniformization of local error cannot be achieved through analytic stepsize regulation alone for highly elliptic, long-period orbits, for which both the nonspherical effects of the Earth and lunar effects are equally important. In such cases, a variable stepsize algorithm is also needed.

3. Choose a dependent variable set in terms of which the solutions to the unperturbed problem are closed, explicit expressions in the independent variable.

In General Perturbation applications, the need for such dependent variable sets is clear. However, such variable sets also are advantageous for use in Special Perturbation Methods. Differential equations for quantities that vary slowly and smoothly with time are known to be more amenable to numerical integration methods (i.e., more numerically stable) than those for quantities that vary rapidly. In the case of satellite motion, the acceleration caused by the attraction of the primary body is usually much greater than the perturbing accelerations arising from other bodies, nonspherical effects, etc. Since dependent variable sets exist that yield closed, explicit solutions to the unperturbed problem, it is logical to remove the point-mass effects of the primary body from the differential equations by considering the relative elliptic orbit described about the primary as a first approximation to the motion. Thus, the equations of motion of such dependent variables include motion arising only from the perturbing acceleration vector. Methods that employ this approach are known as Variation of Parameters (VOP) methods (Section 5.7). GTDS includes VOP orbit generators that use Keplerian, equinoctial, rectangular, Delaunay–Similar (DS), and Kustaanheimo-Stiefel (KS) element sets. The resultant formulations vary with respect to the regularity of the dependent variables and the choice of independent variables. GTDS also includes the Intermediate Orbit formulation, in which the equations of motion represent the variation, arising from other perturbations, about the solution to the point-mass Earth plus J_2 problem.

4. Choose a completely regular dependent variable set.

It is desirable, from the standpoint of generality, to use a set of dependent variables that is well defined, or regular, for the full range of possible orbital conditions. For example, the Keplerian and Delaunay variables are not well defined for small eccentricities or for small or near 180-degree inclinations. Unfortunately, regularity and the requirement for tractable canonical formulations of General Perturbation Methods appear to be mutually exclusive. For this reason, the Brouwer-Lyddane formulation was developed in terms of Poincaré rather than Delaunay variables for use with small eccentricity and small inclination satellites. For Special Perturbation applications, the KS and rectangular variables are completely regular. The equinoctial elements consist of two variable sets which together yield a completely regular set except at collision.

5. Choose a dependent variable set for which the equations of motion are completely regular.

The practical effect of singularities in the equations of motion is to cause rapid oscillations in some of the orbital elements when the orbit is in a near-singular condition. This condition is not desirable from the standpoint of efficiency in numerical integration. Accurate integration of such equations requires extremely small stepsizes in the near-singular region. The rectangular variables and equinoctial elements yield completely regular equations of motion except at collision. The KS equations of motion are completely regular, while the VOP equations of motion are singular for the Kepler and Delaunay elements at small eccentricities and at small and near 180-degree inclinations.

6. Choose a dependent variable set such that the equations of motion have dynamically stable solutions for the unperturbed problem.

A solution is dynamically stable if small variations of the initial values produce a variation of the solution that remains small for any value of the independent variable greater than zero. Dynamic stability is one of the primary motivations for the KS transformation. This characteristic should be particularly advantageous when the solution is obtained via numerical integration.

7. Choose an element set for which the equations of motion do not contain short periodic effects.

As mentioned previously, the efficiency of numerical integration is optimal for the integration of variables that vary smoothly and slowly. Elimination of short periodic effects from the equations of motion significantly smooths the dependent variable motion, thus allowing the use of very large stepsizes. The Intermediate Orbit elements and the Method of Averages (Section 5.8) use this approach. The equations of motion of an averaged element set are integrated. The resulting orbit generation method is extremely efficient but is limited to average element accuracy rather than the osculating element accuracy achieved in high-precision methods.

It should be noted that several of the guidelines stated above are mutually exclusive. The requirements of the specific application dictate which of the guidelines are most important. The characteristics of the orbit generation methods available in GTDS are summarized in Tables 5-1 and 5-2.

The choice of an optimum orbit generation method is dependent on the orbit type, accuracy, and efficiency requirements. In general, the reformulated high-precision methods are more accurate than the Cowell method. However, the transformations required in these formulations increase computational time; therefore, these methods should be used only for orbits for which they yield improved accuracy at larger stepsizes as compared with the Cowell method, or where these methods have a more appropriate method of analytic stepsize control than does Time Regularized Cowell.

For circular orbits, analytic stepsize regularization is not necessary. In fact, integration of the time equation increases computational time and can introduce errors into the solution. For orbits with eccentricity greater than 0.1, analytic stepsize regulation is usually beneficial. The independent variable is therefore an important consideration in the choice of the orbit generation formulation. As the uniformization constant is increased, the size of the time step at perigee decreases and that at apogee increases. This constant should be chosen so that the local error is uniformized over the entire orbit.

For applications that require high efficiency, it is important to consider the number of output points required. Using analytic methods such as Brouwer theory, the computational cost is directly proportional to the number of output points. However, when numerical integration is used, the cost is mainly dependent on the arc length and not the number of intermediate output points. For DC applications, the computational cost of the averaged orbit generation methods is often competitive with that of Brouwer theory and offers considerably greater flexibility with respect to the perturbation model.

5.2 COWELL METHOD

The Cowell equations of motion of a satellite are expressed by the general formula

$$\frac{d^2\bar{r}}{dt^2} = -\frac{\mu\,\bar{r}}{|\,\bar{r}\,|^3} + \bar{P} \qquad (5\text{-}2)$$

where

$\bar{r}$ = position vector in an inertial Cartesian coordinate system

t = physical time

Table 5-1. Characteristics of High-Precision Orbit Generators

ORBIT GENERATOR	METHOD OF SOLUTION	COMPUTATIONAL SPEED	ANALYTIC STEPSIZE CONTROL	TIME REGULARIZATION CONSTANT	LIMITATIONS	COMMENTS
Cowell	Multistep numerical integration using Störmer-Cowell formulas	Medium	No		None	
Time Regularized Cowell	Multistep numerical integration using Störmer-Cowell formulas	Medium	Yes	3/2	None	
VOP—Keplerian	Multistep numerical integration using Adams formulas	Medium	No		Singularities for e=0; i=0, 180° Elliptic motion only	Provides closed-form solution to unperturbed problem
VOP—Equinoctial	Multistep numerical integration using Adams formulas	Medium	No		Elliptic motion only	Provides closed-form solution to unperturbed problem
VOP—Rectangular	Multistep numerical integration using Adams formulas	Medium	No		None	Provides closed-form solution to unperturbed problem
Intermediate Orbit	Multistep numerical integration using Adams formulas	Medium	Yes	2	Singularities for e=0; i=0, 63.4° Elliptic motion only	Provides closed-form solution to J_2 through J_6 problem
KS	Multistep numerical integration using Adams formulas	Medium	Yes	1	Elliptic motion only	Provides closed-form, stable oscillator solution to unperturbed problem
DS	Multistep numerical integration using Adams formulas	Medium	Yes	2	Singularities for e=0; i=0, 180° Elliptic motion only	Provides closed-form, dynamically stable solution to unperturbed problem
Chebyshev Series	Picard iteration	Low	N/A		None	

Table 5-2. Characteristics of Approximate Orbit Generators

ORBIT GENERATOR	METHOD OF SOLUTION	COMPUTATIONAL SPEED	ANALYTIC STEPSIZE CONTROL	TIME REGULARIZATION CONSTANT	LIMITATIONS	COMMENTS
Brouwer	Analytic	High	N/A		Singularities for e=0, I=0, 63.4° Elliptic motion only	Solution includes only J_2 through J_5 effects
Brouwer-Lyddane	Analytic	High	N/A		Singularities for I=63.4° Elliptic motion only	Solution includes only J_2 through J_5 effects
Vintl	Analytic	High	N/A		Elliptic motion only	Solution includes J_2 through J_4 effects
Averaged Kepler	Multistep numerical integration using Adams formulas	High	No		Singularities for e=0, I=0, 180° Elliptic motion only	Solution does not include short-period effects
Averaged Equinoctial	Multistep numerical integration using Adams formulas	High	No		Elliptic motion only	Solution does not include short-period effects

μ = gravitational constant of the central body
$\bar{P}$ = total perturbing acceleration

The acceleration $\bar{P}$ can include any of the perturbing accelerations discussed in Chapter 4.

This set of three Class II differential equations is solved directly for the position vector using the Störmer-Cowell numerical integration formulas (Equations (6-22) and (6-27)). The three Class I equations for the velocity vector $\dot{\bar{r}}$

$$\frac{d\dot{\bar{r}}}{dt} = -\frac{\mu \bar{r}}{|\bar{r}|^3} + \bar{P} \tag{5-3}$$

are integrated using the Adams numerical integration formulas (Equations (6-21) and (6-26)) in the case of velocity-dependent perturbations, such as atmospheric drag.

The Cartesian coordinates and the equations of motion are regular, except at collision. This method can be used for elliptic, parabolic, and hyperbolic orbits. The point-mass gravitational attraction of the primary body appears explicitly in the equations of motion and is usually the dominant acceleration that must be integrated.

For circular orbits, the choice of time as the independent variable produces a uniform local error with respect to the integration of the two-body acceleration at each integration step. The Time Regularized Cowell formulation (Section 5.3) was developed to achieve uniformization of local error in the case of noncircular orbits.

5.3 TIME REGULARIZED COWELL

Efficient numerical integration is aided by making the local error uniform at each integration step. With the Cowell method, the equations of motion (Equations (5-2) and (5-3)) must be uniform with respect to the dominant local error source, which is generally the point-mass and J_2 gravitational accelerations. These equations are already uniform for circular orbits. For noncircular orbits, however, the Cowell equations must be reformulated in terms of a new independent variable s, defined by the relationship

$$\frac{d}{dt} = \frac{\sqrt{\mu}}{r^n} \frac{d}{ds} \tag{5-4}$$

where n is the uniformization constant and r is the magnitude of the position vector. The resulting equations of motion are called the Time Regularized Cowell equations. The

choice of 3/2 for n uniformizes the local error with respect to the point-mass and J_2 gravitational effects.

Under this general transformation, the Time Regularized Cowell equations of motion become

$$\bar{r}'' = n\left(\frac{r'\,\bar{r}'}{r}\right)-r^{(2n-3)}\,\bar{r} + \frac{r^{2n}}{\mu}\bar{P}\left(t,\ \bar{r},\ \frac{\sqrt{\mu}}{r^n}\bar{r}'\right) \tag{5-5}$$

where the prime notation refers to differentiation with respect to the independent variable s. This equation involves derivatives with respect to the variable s only. The inertial position vector is obtained by integrating Equation (5-5) using the Class II Störmer-Cowell formulas (Equations (6-22) and (6-27)). The inertial velocity vector is obtained by integrating Equation (5-5) using the Class I Adams formulas (Equations (6-21) and (6-26)). Since the velocity appears explicitly in the equations of motion, the velocity equation must be integrated event in the case of velocity-free perturbations. In addition, the following Class II equation is integrated for the time:

$$t'' = \frac{n\,r^{2n-1}\,\dot{r}}{\mu} \tag{5-6}$$

Comparison of the Time Regularized Cowell and the Cowell integration schemes indicates that the favorable properties of simplicity, precision, and adaptability are shared by both methods, while for highly eccentric or drag-perturbed orbits, the analytic stepsize regularization afforded by the Time Regularized Cowell method is superior. It should be noted that uniform local error cannot be achieved through analytic stepsize control alone for highly elliptic, long-period orbits with equally important contributions from the nonspherical effects of both the Earth and Moon. For these cases, a variable stepsize algorithm, or regularization of both time and the separation from the Earth center of mass, should be used.

5.4 KUSTAANHEIMO-STEIFEL (KS) FORMULATION

By means of the KS transformation, the nonlinear equations of two-body motion are transformed to a set of linear, dynamically stable differential equations, similar to those of an unperturbed harmonic oscillator (see Reference 4 for a complete derivation). This transformation consists of choosing a set of regular dependent variables such that the resulting differential equations are regular, i.e., have no singularities. Regularization of the differential equations requires the extension of the position and velocity vectors from

three-dimensional to four-dimensional vectors. The singularity at collision is removed by choosing the generalized eccentric anomaly E as the independent variable, such that

$$\frac{dE}{dt} = \frac{2\omega}{r} \tag{5-7}$$

where the frequency ω is related to the negative of the total energy $\omega = \sqrt{h/2}$. In addition, this transformation produces analytic stepsize regulation with a uniformization constant of 1. Therefore, a time equation must also be integrated. A time element τ is introduced such that

$$t = \tau - \frac{1}{\omega}(\bar{u}, \bar{u}') \tag{5-8}$$

where $\bar{u}$ and $\bar{u}'$ are the transformed position and velocity vectors ($\bar{u}' = d\bar{u}/dE$), and the notation $(\bar{u}, \bar{u}')$ denotes the scalar product of the two vectors. This time element varies linearly with the independent variable for unperturbed motion and is therefore more amenable to numerical integration than the time equation. (See Appendix B for a more detailed discussion of the time elements.)

Regularized equations of motion behave considerably better with respect to numerical integration than the corresponding nonregularized equations. For unperturbed two-body motion, every solution to the regularized differential equations is dynamically stable. This means that small variations of the initial values produce a variation of the solution that remains small for any positive value of the independent variable. Dynamic stabilization of the KS equations of motion is accomplished by using a time element and by including as a dependent variable the frequency ω, which is related to the total energy, and taking advantage of the fact that it is a constant of the motion for conservative forces. Consequently, a total of 10 equations of motion are integrated.

The KS equations of motion are formulated as VOP equations in terms of regular elements: the frequency ω, the time element τ, and the two vectors of four components each, $\bar{\alpha}$ and $\bar{\beta}$. Elements are quantities which, during unperturbed two-body motion, are constants or linear functions of the independent variable. The advantage of introducing elements is that they vary almost linearly if the motion is subjected to weak perturbations.

5.4.1 THE KS VARIATION OF PARAMETERS (VOP) EQUATIONS OF MOTION

The KS equations of motion are VOP equations in Lagrangian form. The equations for $\bar{\alpha}$ and $\bar{\beta}$ are

$$\frac{d\bar{\alpha}}{dE} = \left\{\frac{1}{2\omega^2}\left[\frac{V}{2}\bar{u} + \frac{r}{4}\left(\frac{\partial V}{\partial \bar{u}} - 2L^T\bar{P}\right)\right] + \frac{2}{\omega}\frac{d\omega}{dE}\bar{u}'\right\}\sin\left(\frac{E}{2}\right) \qquad (5\text{-}9a)$$

$$\frac{d\bar{\beta}}{dE} = -\left\{\frac{1}{2\omega^2}\left[\frac{V}{2}\bar{u} + \frac{r}{4}\left(\frac{\partial V}{\partial \bar{u}} - 2L^T\bar{P}\right)\right] + \frac{2}{\omega}\frac{d\omega}{dE}\bar{u}'\right\}\cos\left(\frac{E}{2}\right) \qquad (5\text{-}9a)$$

while the equations of motion for the time element τ and the frequency ω are

$$\frac{d\tau}{dE} = \frac{1}{8\omega^3}(\mu - 2r\,V) - \frac{r}{16\omega^3}\left(\bar{u},\ \frac{\partial V}{\partial \bar{u}} - 2L^T\bar{P}\right) - \frac{2}{\omega^2}\frac{d\omega}{dE}(\bar{u},\ \bar{u}') \qquad (5\text{-}10a)$$

$$\frac{d\omega}{dE} = -\frac{r}{8\omega^2}\frac{\partial V}{\partial \bar{u}} - \frac{1}{2\omega}(\bar{u}',\ L^T\bar{P}) \qquad (5\text{-}10b)$$

In the above equations,

- V = perturbing potential function
- $\bar{P}$ = additional perturbing accelerations
- μ = gravitational constant of the central body
- L = KS transformation matrix defined by Equation (5-21)

In GTDS, the perturbing potential V which is used is the potential arising from the J_2 nonspherical effects given by

$$V = \frac{3}{2}\mu R_e^2 J_2\left[\frac{z^2}{r^5} - \frac{1}{3r^3}\right] \qquad (5\text{-}11)$$

where R_e is the radius of the central body. The quantity $\bar{P}$ represents the perturbing accelerations due to higher harmonics, drag, radiation pressure, etc.

The components of $\bar{u}$, the transformed position vector, and $\bar{u}'$, the transformed velocity vector, are obtained from the elements as follows:

$$\bar{u} = \bar{\alpha} \cos\left(\frac{E}{2}\right) + \bar{\beta} \sin\left(\frac{E}{2}\right) \tag{5-12}$$

$$\bar{u}' = -\frac{1}{2} \bar{\alpha} \sin\left(\frac{E}{2}\right) + \frac{1}{2} \bar{\beta} \cos\left(\frac{E}{2}\right) \tag{5-13}$$

The magnitude of the position vector is

$$r = u_1^2 + u_2^2 + u_3^2 + u_4^2 \tag{5-14}$$

The position vector $\bar{r}$ of the satellite is computed for use in the evaluation of the perturbing accelerations using Equations (5-37) through (5-39). The velocity $\dot{\bar{r}}$ is also computed in the case of velocity-dependent accelerations, using Equations (5-40) through (5-42). The physical time is computed from

$$t = \tau - \frac{1}{\omega}(\bar{u}, \bar{u}') \tag{5-15}$$

The notation $(\bar{u}, \bar{u}')$ denotes the scalar product of the two vectors.

The transformed components of the perturbing accelerations are computed as

$$(L^T P)_1 = u_1 P_1 + u_2 P_2 + u_3 P_3 \tag{5-16}$$

$$(L^T P)_2 = -u_2 P_1 + u_1 P_2 + u_4 P_3 \tag{5-17}$$

$$(L^T P)_3 = -u_3 P_1 - u_4 P_2 + u_1 P_3 \tag{5-18}$$

$$(L^T P)_4 = u_4 P_1 - u_3 P_2 + u_2 P_3 \tag{5-19}$$

5.4.2 TRANSFORMATION FROM CARTESIAN POSITION AND VELOCITY TO KS PARAMETRIC VALUES

The KS transformation is defined as

$$\bar{x} = L(u) \cdot \bar{u} \tag{5-20}$$

where $\bar{x}$ is a vector whose first three components are the Cartesian position coordinates and the fourth component x_4 is always zero, i.e., $\bar{x} = (x, y, z, 0)$.

The matrix L(u) is the KS matrix with components given by

$$L = \begin{bmatrix} u_1 & -u_2 & -u_3 & u_4 \\ u_2 & u_1 & -u_4 & -u_3 \\ u_3 & u_4 & u_1 & u_2 \\ u_4 & -u_3 & u_2 & -u_1 \end{bmatrix} \tag{5-21}$$

The elements of this matrix are computed as follows.

Assuming that $\bar{r}$ and $\dot{\bar{r}}$ are given at the instant $t = t_0$, the radial distance is computed from

$$r = \sqrt{x^2 + y^2 + z^2} \tag{5-22}$$

and the frequency from

$$2\omega^2 = \frac{\mu}{r} - \frac{1}{2}|\dot{r}|^2 - V \tag{5-23}$$

where V represents the perturbing potential, which is the J_2 potential in GTDS (see Equation (5-11).

If $x \geq 0$, the parametric state vector is found from

$$u_1^2 + u_4^2 = \frac{1}{2}(r + x) \tag{5-24}$$

$$u_2 = \frac{y\,u_1 + z\,u_4}{r + x} \tag{5-25}$$

$$u_3 = \frac{z\,u_1 - y\,u_4}{r + x} \tag{5-26}$$

or, if $x \leq 0$, from

$$u_2^2 + u_3^2 = \frac{1}{2}(r - x) \tag{5-27}$$

$$u_1 = \frac{y\,u_2 + z\,u_3}{r - x} \tag{5-28}$$

$$u_4 = \frac{z\,u_2 - y\,u_3}{r - x} \tag{5-29}$$

The derivatives of the transformed position vector with respect to E are

$$u_1' = \frac{1}{4\omega}\,(u_1\,\dot{x} + u_2\,\dot{y} + u_3\,\dot{z}) \tag{5-30}$$

$$u_2' = \frac{1}{4\omega}\,(-u_2\,\dot{x} + u_1\,\dot{y} + u_4\,\dot{z}) \tag{5-31}$$

$$u_3' = \frac{1}{4\omega}\,(-u_3\,\dot{x} - u_4\,\dot{y} + u_1\,\dot{z}) \tag{5-32}$$

$$u_4' = \frac{1}{4\omega}\,(u_4\,\dot{x} - u_3\,\dot{y} + u_2\,\dot{z}) \tag{5-33}$$

The initial value of the time element is

$$\tau = \frac{1}{\omega}\,(\bar{u},\ \bar{u}') \tag{5-34}$$

If E = 0 is adopted as the initial value of the eccentric anomaly, then

$$\overline{\alpha} = \overline{u} \tag{5-35}$$

and

$$\overline{\beta} = 2\overline{u}' \tag{5-36}$$

5.4.3 TRANSFORMATION FROM KS PARAMETRIC VARIABLES TO CARTESIAN POSITION AND VELOCITY

Using Equation (5-20), the Cartesian components of position are calculated from

$$x = u_1^2 - u_2^2 - u_3^2 + u_4^2 \tag{5-37}$$

$$y = 2(u_1 u_2 - u_3 u_4) \tag{5-38}$$

$$z = 2(u_1 u_3 + u_2 u_4) \tag{5-39}$$

and the Cartesian velocity components are determined from

$$\dot{x} = \frac{4\omega}{r}(u_1 u_1' - u_2 u_2' - u_3 u_3' + u_4 u_4') \tag{5-40}$$

$$\dot{y} = \frac{4\omega}{r}(u_2 u_1' + u_1 u_2' - u_4 u_3' - u_3 u_4') \tag{5-41}$$

$$\dot{z} = \frac{4\omega}{r}(u_3 u_1' + u_4 u_2' + u_1 u_3' + u_2 u_4') \tag{5-42}$$

5.5 DELAUNAY-SIMILAR (DS) ELEMENTS

The DS method is a VOP formulation that was developed using the generalized true anomaly as the independent variable, such that

$$\frac{dt}{ds} = \frac{r^2}{G - \frac{1}{2}\left[\Phi - \frac{\mu}{\sqrt{2L}}\right]} \tag{5-43}$$

where L, G, and Φ are defined later in this section (see References 5, 6, and 7 for a more complete discussion).

This choice for the independent variable is particularly appropriate for numerical integration of the oblateness perturbation. The dependent variables are a generalization of the classical Delaunay elements and are singular for e = 0, i = 0, and at collision. The transformation of the equations of motion is carried out in terms of canonical variables. This approach leads to the requirement for a canonical variable, conjugate to the physical time, which is the negative of the total energy. The resulting set of equations of motion is uniformized with respect to integration of the J_2 nonspherical perturbation.

The geometrical and physical interpretations of the eight DS elements for the unperturbed problem are as follows:

- ψ = true anomaly
- g = argument of pericenter
- h = longitude of the ascending node
- ℓ = "mean" mean anomaly
- Φ = measure of the perturbing energy, which vanishes in unperturbed motion
- G = total angular momentum
- H = z component of the angular momentum
- L = total energy

where L_0 is the initial value of the total energy.

This set of DS elements contains one fast variable, the generalized true anomaly ψ. The element ℓ has been defined such that it is a constant in the case of unperturbed motion.

For the two-body problem, the DS elements yield closed and explicit solutions in terms of the independent variable. Not all of the DS elements are osculating. The reason is that the orbits are situated on the energy surface

$$F = F_0 + r^2 V = 0 \tag{5-44}$$

where F_0 is the unperturbed Hamiltonian.

This energy manifold depends on the perturbing potential V. The compute the osculating elements at a certain time, the potential V must be set equal to zero since, by definition, osculating elements represent the Keplerian position and velocity with respect to the moving coordinate system inherent in the VOP equations of motion.

In the following sections, the DS elements vector is denoted by

$$(a_1, a_2, a_3, a_4, a_5, a_6, a_7, a_8) = (\psi, g, h, \ell, \Phi, G, H, L) \tag{5-45}$$

5.5.1 THE DS VARIATION OF PARAMETERS (VOP) EQUATIONS OF MOTION

The DS equations of motion, which are VOP equations in canonical form, are as follows:

$$\frac{da_i}{ds} = \frac{\partial F_0}{\partial a_{i+4}} + V \frac{\partial}{\partial a_{i+4}}\left(\frac{r^2}{q}\right) + \frac{r^2}{q} \sum_{j=1}^{4} (D_{i+4,j}) \left(\frac{\partial V}{\partial x_j} - P_j\right) \qquad (i = 1, \ldots, 4) \tag{5-46}$$

$$\frac{da_{i+4}}{ds} = - V \frac{\partial}{\partial a_i}\left(\frac{r^2}{q}\right) - \frac{r^2}{q} \sum_{j=1}^{4} D_{ij} \left(\frac{\partial V}{\partial x_j} - P_j\right) \qquad (i = 1, \ldots, 4) \tag{5-47}$$

where x_1, x_2, and x_3 are the three components of $\bar{r}$ and x_4 is the time. The quantity V is the perturbing potential given in Equation (5-11), and the scaling factor q, defining the time transformation in Equation (5-43), is given by

$$q = a_6 - \frac{1}{2}\left(a_5 - \frac{\mu}{\sqrt{2a_8}}\right) \tag{5-48}$$

The unperturbed Hamiltonian F_0 is given by

$$F_0 = a_5 - \frac{\mu}{\sqrt{2a_8}} \tag{5-49}$$

and its derivatives by

$$\frac{\partial F_0}{\partial a_5} = 1 \tag{5-50}$$

$$\frac{\partial F_0}{\partial a_6} = 0 \tag{5-51}$$

$$\frac{\partial F_0}{\partial a_7} = 0 \tag{5-52}$$

$$\frac{\partial F_0}{\partial a_8} = \frac{\mu}{(2a_8)^{3/2}} \tag{5-53}$$

The vector $\bar{P}$ is the additional perturbing acceleration vector expressed in rectangular coordinates. The extension of phase space by the inclusion of time and total energy as variables results in the introduction of an additional canonical force

$$P_4 = - \frac{\partial F_0}{\partial \dot{\bar{r}}} \cdot \bar{P} \tag{5-54}$$

The elements of the 8 x 4 matrix D

$$D = \frac{\partial(x_1, x_2, x_3, x_4)}{\partial(a_1, a_2, \ldots, a_8)} \tag{5-55}$$

are computed by the following relationship:

$$\frac{\partial x_i}{\partial a_j} = \frac{\partial r}{\partial a_j}\tau_i + r\frac{\partial \tau_i}{\partial a_j} \qquad \begin{matrix}(i = 1, \ldots, 3)\\ (j = 1, \ldots, 8)\end{matrix} \tag{5-56}$$

where

$$\tau_1 = \cos(a_1 + a_2)\cos a_3 - \sin(a_1 + a_2)\sin a_3 \cos I \tag{5-57}$$

$$\tau_2 = \cos(a_1 + a_2)\sin a_3 + \sin(a_1 + a_2)\cos a_3 \cos I \tag{5-58}$$

$$\tau_3 = \sin(a_1 + a_2)\sin I \tag{5-59}$$

and

$$\cos I = \frac{|a_7|}{a_6} \tag{5-60}$$

$$\sin I = \text{sign}\,(a_7)\sqrt{1 - \frac{a_7^2}{a_6^2}} \tag{5-61}$$

$$r = \frac{p}{1 + e\cos a_1} \tag{5-62}$$

$$p = \frac{1}{\mu}\left(a_6 - a_5 + \frac{\mu}{\sqrt{2a_8}}\right)^2 \tag{5-63}$$

$$e = \sqrt{1 - \frac{2a_8 p}{\mu}} \tag{5-64}$$

The partial derivatives of τ_1, τ_2, τ_3, and x_4 are given in Table 5-3; the partial derivatives of r, p, q, and e are given in Table 5-4. The vector $\partial(r^2/q)/\partial\alpha$ is evaluated using the relationship

$$\frac{\partial}{\partial a_i}\left(\frac{r^2}{q}\right) = \frac{2r}{q}\frac{\partial r}{\partial a_i} - \frac{r^2}{q^2}\frac{\partial q}{\partial a_i} \tag{5-65}$$

The conservative accelerations present in V give rise to a differential equation for L, the total energy of the orbit,

$$\frac{dL}{ds} = \frac{r^2}{q}\left(\frac{\partial V}{\partial x_4} - P_4\right) \tag{5-66}$$

where

$$\frac{\partial V}{\partial x_4} = P_4 = 0 \tag{5-67}$$

Therefore, L is a constant in this case. This fact is exploited in GTDS by not numerically integrating the equation for L when only conservative forces are present. This avoids cumulative magnified errors in other elements that are driven by small numerical errors in L.

5.5.2 TRANSFORMATION FROM CARTESIAN POSITION AND VELOCITY TO DS ELEMENTS

It is assumed that $\bar{r}$, $\dot{\bar{r}}$, and t are given. In order to numerically integrate the DS equations of motion, the initial values of the DS variables are computed. The total angular momentum G is computed from

$$G = \sqrt{G_1^2 + G_2^2 + G_3^2} \tag{5-68}$$

where

$$\bar{G} = \bar{r} \times \dot{\bar{r}} \tag{5-69}$$

Table 5-3. Partial Derivatives of the Auxiliary Parameters τ_1, τ_2, τ_3, x_4

	$/\partial\alpha_1$	$/\partial\alpha_2$	$/\partial\alpha_3$	$/\partial\alpha_4$
$\partial\tau_1/$	$-\sin(\alpha_1+\alpha_2)\cos\alpha_3$ $-\cos(\alpha_1+\alpha_2)\sin\alpha_3\cos I$	$\frac{\partial\tau_1}{\partial\alpha_1}$	$-\cos(\alpha_1+\alpha_2)\sin\alpha_3$ $-\sin(\alpha_1+\alpha_2)\cos\alpha_3\cos I$	0
$\partial\tau_2/$	$-\sin(\alpha_1+\alpha_2)\sin\alpha_3$ $+\cos(\alpha_1+\alpha_2)\cos\alpha_3\cos I$	$\frac{\partial\tau_2}{\partial\alpha_1}$	$\cos(\alpha_1+\alpha_2)\cos\alpha_3$ $-\sin(\alpha_1+\alpha_2)\sin\alpha_3\cos I$	0
$\partial\tau_3/$	$\cos(\alpha_1+\alpha_2)\sin I$	$\frac{\partial\tau_3}{\partial\alpha_1}$	0	0
$\partial x_4/$	$\frac{\mu}{(2\alpha_8)^{3/2}}\left[\frac{r^2}{p_2}(1-e^2)^{3/2}-1\right]$	0	0	0

	$/\partial\alpha_5$	$/\partial\alpha_6$	$/\partial\alpha_7$	$/\partial\alpha_8$
$\partial\tau_1/$	0	$\frac{1}{\alpha_6}\sin(\alpha_1+\alpha_2)\sin\alpha_3\cos I$	$-\frac{1}{\alpha_6}\sin(\alpha_1+\alpha_2)\sin\alpha_3$	0
$\partial\tau_2/$	0	$-\frac{1}{\alpha_6}\sin(\alpha_1+\alpha_2)\cos\alpha_3\cos I$	$\frac{1}{\alpha_6}\sin(\alpha_1+\alpha_2)\cos\alpha_3$	0
$\partial\tau_3/$	0	$\frac{1}{\alpha_6}\frac{\cos^2 I}{\sin I}\sin(\alpha_1+\alpha_2)$	$-\frac{1}{\alpha_6}\frac{\cos I}{\sin I}\sin(\alpha_1+\alpha_2)$	0
$\partial x_4/$	$-\frac{\mu}{(2\alpha_8)^{3/2}}\sqrt{1-e^2}\frac{r}{p}$ $\times\sin\alpha_1\left(\frac{r}{p}+1\right)\frac{\partial e}{\partial\alpha_5}$	$-\frac{\partial x_4}{\partial\alpha_5}$	0	$\frac{3}{2\alpha_8}(\alpha_4-x_4)-\frac{\mu}{(2\alpha_8)^{3/2}}\frac{r}{p}$ $\times\sqrt{1-e^2}\sin\alpha_1\left(\frac{r}{p}+1\right)\frac{\partial e}{\partial\alpha_8}$

Table 5-4. Partial Derivatives of the Auxiliary Parameters q, p, e, r

	$/\partial\alpha_1$	$/\partial\alpha_2$	$/\partial\alpha_3$	$/\partial\alpha_4$
$\partial q/$	0	0	0	0
$\partial p/$	0	0	0	0
$\partial e/$	0	0	0	0
$\partial r/$	$\frac{e\, r_2}{p} \sin \alpha_1$	0	0	0

	$/\partial\alpha_5$	$/\partial\alpha_6$	$/\partial\alpha_7$	$/\partial\alpha_8$
$\partial q/$	$-\frac{1}{2}$	1	0	$\frac{-\mu}{2(2\alpha_8)^{3/2}}$
$\partial p/$	$-2\sqrt{\frac{p}{\mu}}$	$-\frac{\partial p}{\partial \alpha_5}$	0	$\frac{\mu}{(2\alpha_8)^{3/2}} \frac{\partial p}{\partial \alpha_5}$
$\partial e/$	$\frac{-\alpha_8}{e\,\mu} \frac{\partial p}{\partial \alpha_5}$	$-\frac{\alpha_8}{e\,\mu} \frac{\partial p}{\partial \alpha_6}$	0	$\frac{-1}{\mu\, e}\left[p + \alpha_8 \frac{\partial p}{\partial \alpha_8}\right]$
$\partial r/$	$\frac{r}{p}\left[\frac{\partial p}{\partial \alpha_5} - r \frac{\partial e}{\partial \alpha_5} \cos \alpha_1\right]$	$\frac{r}{p}\left[\frac{\partial p}{\partial \alpha_6} - r \frac{\partial e}{\partial \alpha_6} \cos \alpha_1\right]$	0	$\frac{r}{p}\left[\frac{\partial p}{\partial \alpha_5} - r \frac{\partial e}{\partial \alpha_5} \cos \alpha_1\right]$

The z component of the angular momentum $\overline{G}$ is given by

$$H = G_3 \tag{5-70}$$

The total energy L is computed as

$$L = -\frac{1}{2} v^2 + \frac{\mu}{r} - V \tag{5-71}$$

where

$$r = \sqrt{x^2 + y^2 + z^2} \tag{5-72}$$

$$v = \sqrt{\dot{x}^2 + \dot{y}^2 + \dot{z}^2} \tag{5-73}$$

and V is given by Equation (5-11).

The perturbing energy Φ is

$$\Phi = G - \sqrt{G^2 + 2r^2 V} + \frac{\mu}{\sqrt{2L}} \tag{5-74}$$

The generalized true anomaly is computed as

$$\psi = \tan^{-1}\left(\frac{\sin \psi}{\cos \psi}\right) \tag{5-75}$$

where

$$\cos \psi = \frac{1}{e}\left(\frac{p}{r} - 1\right) \tag{5-76}$$

$$\sin \psi = \frac{p \dot{r}}{e r^2}\left[\dot{\psi} + \frac{4r V}{\sqrt{\mu p}}\left(\frac{1}{r} + \frac{L \cos \psi}{\mu e}\right)\right]^{-1} \tag{5-77}$$

$$\dot{r} = \frac{(\bar{r} \cdot \dot{\bar{r}})}{r} \tag{5-78}$$

$$p = \frac{1}{\mu}\left(G + \frac{\mu}{\sqrt{2L}} - \Phi\right)^2 \tag{5-79}$$

$$e = \sqrt{1 - \frac{2L}{\mu} p} \tag{5-80}$$

and

$$\dot{\psi} = \frac{q}{r^2}\left[1 + V \frac{\partial(r^2/q)}{\partial \Phi}\right] \tag{5-81}$$

This last derivative, given by Equations (5-48) and (5-65), depends only on L, G, and Φ given above.

The longitude of the ascending node h is given by

$$h = \tan^{-1}\left(\frac{G_1}{-G_2}\right) \tag{5-82}$$

and the argument of pericenter g by

$$g = u - \psi \qquad (-\pi \leq g \leq \pi) \tag{5-83}$$

where

$$u = \tan^{-1}\left[\frac{z\,(G_1^2 + G_2^2) - G_3\,(x\,G_1 + y\,G_2)}{G\,(y\,G_1 - x\,G_2)}\right] \tag{5-84}$$

The eccentric anomaly E is computed as

$$E = 2 \tan^{-1}\left[\sqrt{\frac{1-e}{1+e}} \tan\left(\frac{\psi}{2}\right)\right] \qquad (-\pi \leq E \leq \pi) \tag{5-85}$$

and the variable ℓ is given by

$$\ell = t - \frac{\mu}{(2L)^{3/2}} \left[E - \psi - e\sqrt{1 - e^2}\ \frac{r}{p}\ \sin\psi \right] \tag{5-86}$$

5.5.3 TRANSFORMATION FROM DS ELEMENTS TO CARTESIAN POSITION AND VELOCITY

Predicted values of the DS variables (ψ, g, h, ℓ, Φ, G, H, and L) obtained from the numerical integration must be transformed to physical Cartesian position, velocity, and time to evaluate the perturbing forces and for computation of observations. The following equations yield the Cartesian state:

$$\bar{r} = \bar{c}\, x_1 + \bar{d}\, x_2 \tag{5-87}$$

$$\dot{\bar{r}} = \bar{c}\, \dot{x}_1 + \bar{d}\, \dot{x}_2 + \dot{\bar{c}}\, x_1 + \dot{\bar{d}}\, x_2 \tag{5-88}$$

where $\bar{c}$ and $\bar{d}$ are the vectors

$$\bar{c} = \begin{bmatrix} \cos g \cos h - \sin g \sin h \cos I \\ \cos g \sin h + \sin g \cos h \cos I \\ \sin g \sin I \end{bmatrix} \tag{5-89}$$

$$\bar{d} = \begin{bmatrix} -\sin g \cos h - \cos g \sin h \cos I \\ -\sin g \sin h + \cos g \cos h \cos I \\ \cos g \sin I \end{bmatrix} \tag{5-90}$$

and

$$x_1 = r \cos\psi \tag{5-91}$$

$$x_2 = r \sin\psi \tag{5-92}$$

and cos I, sin I, and r are computed using Equations (5-60) through (5-64).

The required derivatives for the velocities are given by

$$\dot{\bar{c}} = \bar{d}\,\dot{g} \tag{5-93a}$$

$$\dot{\bar{d}} = \bar{c}\,\dot{g} \tag{5-93b}$$

$$\dot{x}_1 = \dot{r}\cos\psi - r\,\dot{\psi}\sin\psi \tag{5-94a}$$

$$\dot{x}_2 = \dot{r}\sin\psi + r\,\dot{\psi}\cos\psi \tag{5-94b}$$

The quantity $\dot{r}$ can be expressed directly in terms of DS elements as

$$\dot{r} = \frac{e\,r^2\sin\psi}{p}\left[\dot{\psi} + \frac{4r\,V}{\sqrt{\mu\,p}}\left(\frac{1}{r} + \frac{L\cos\psi}{\mu\,e}\right)\right] \tag{5-95}$$

and $\dot{\psi}$ is given by Equation (5-81).

The physical time is computed from

$$t = \ell + \frac{\mu}{(2L)^{3/2}}\left(E - \psi - r\,\frac{e}{p}\sqrt{1 - e^2}\,\sin\psi\right) \tag{5-96}$$

where E is computed from Equation (5-85) and ℓ is computed from Equation (5-86).

5.6 PICARD ITERATION USING CHEBYSHEV SERIES

The Picard iteration method used in GTDS (derived in Reference 8) can be used to integrate the Class I Cowell equations of motion

$$\frac{d\dot{\bar{r}}}{dt} = \frac{-\mu\,\bar{r}}{r^3} + \bar{P} \tag{5-97}$$

$$\frac{d\bar{r}}{dt} = \dot{\bar{r}} \tag{5-98}$$

using the following iterative process (Reference 9):

$$\dot{\bar{r}}_{n+1}(t) = \dot{\bar{r}}(t_0) + \int_{t_0}^{t} \ddot{\bar{r}}(t', \bar{r}_n, \dot{\bar{r}}_n)\, dt' \tag{5-99}$$

$$\bar{r}_{n+1}(t) = \bar{r}(t_0) + \int_{t_0}^{t} \dot{\bar{r}}_{n+1}\, dt' \tag{5-100}$$

The starting values $\bar{r}_0(t)$, $\dot{\bar{r}}_0(t)$ are arbitrary continuous vector functions on the interval $[t_0, t]$, which satisfy the given initial conditions

$$\bar{r}_0(t_0) = \bar{r}(t_0) \tag{5-101}$$

$$\dot{\bar{r}}_0(t_0) = \dot{\bar{r}}(t_0) \tag{5-102}$$

In the present version of GTDS, $\bar{r}_0(t)$, $\dot{\bar{r}}_0(t)$ are solutions to the unperturbed problem ($\bar{P} = 0$ in Equation (5-97)). Since the sequence converges to a close approximation of the exact solution, the method can be used to generate very accurate solutions. Except at collision, the Cartesian coordinates and equations of motion are regular, which means that the method can be used for elliptic, parabolic, and hyperbolic orbits.

In order to solve Equations (5-97) and (5-98) for a given value of n (i.e., to accomplish one iteration), the Chebyshev series is used as follows. The position and velocity vectors available from the $(n-1)^{st}$ iteration, $\bar{r}_{n-1}$ and $\dot{\bar{r}}_{n-1}$, are evaluated at the Chebyshev points in time. (The precise locations of the Chebyshev points are given in the next section.) The forces (per unit mass) are then evaluated at each of these points in time (using the values of $\bar{r}_{n-1}$ and $\dot{\bar{r}}_{n-1}$). These special values of the acceleration vector are then used to determine the interpolating polynomial in time in the form of a Chebyshev series. The coefficients of the Chebyshev series are determined directly from the special values in a rather simple way due to the orthogonality of the Chebyshev polynomials (as described later in this section). The Chebyshev series representation of the acceleration is then integrated to obtain the Chebyshev series representation of the velocity to within an arbitrary constant of integration. The constant of integration is determined by requiring that the initial velocity $\dot{\bar{r}}(t_0)$ agree with the series for the velocity evaluated at t_0. The result is an approximation to $\bar{r}_n$. Similarly, the series representation of the velocity is then integrated to obtain the series representation of the position, where now the initial position $\bar{r}(t_0)$ is used to determine the constant of integration. The result is an approximation to $\bar{r}_n$, thus completing one step of the Picard Iteration procedure.

The preceding set of operations is repeated until two successive approximate solutions agree to within a tolerance that can be specified by the user. This completes one step of the integration, and the process is continued stepwise until the final time is attained.

A finite Chebyshev series fitted to a function has the significant property of making the least possible maximum error of all the common interpolating orthogonal polynomial series. The maximum error committed, as well as the overall truncation error, diminishes as the number of points used in the fitting increases. Since the error in the fitting of the accelerations oscillates with an amplitude less than or equal to the maximum error, the errors partially cancel each other during integration.

The Chebyshev series solution is derived in the following manner. The interval of time (t_0, t_f) is mapped linearly onto the interval (–1, 1) by means of the expression

$$\xi = 1 - 2\left(\frac{t - t_0}{t_f - t_0}\right) \tag{5-103}$$

where

ξ = normalized time
t_0 = initial time
t_f = final time
$t_f - t_0$ = interval of time for which the orbit is to be integrated by Chebyshev series

The normalized time $\xi = 1$ corresponds to $t = t_0$. The time points for which the Chebyshev series is to be fitted are the zeroes of the $(N+1)^{st}$ Chebyshev polynomial. At these points, the Chebyshev polynomials have an orthogonality property with respect to summation. The Chebyshev polynomials T_j are defined as

$$T_j(\xi) = \cos j(\cos^{-1}\xi) \qquad (-1 \leq \xi \leq 1) \tag{5-104}$$

and the N + 1 Chebyshev points are given by

$$\xi_k = \cos\left(\frac{k\pi}{N}\right) \qquad [k = 0, 1, \ldots, N;\ (N \leq 48)] \tag{5-105}$$

An interpolating polynomial $p_M(\xi)$, representing the ith component of acceleration as a function of the normalized time ξ, is expressed as a finite series in Chebyshev polynomials

$$p_M(\xi) = \sum_{j=0}^{M}{}' c_j T_j(\xi) \tag{5-106}$$

where M is the degree of the polynomial ($M \leq N$) and the prime denotes that the first term is factored by one-half (if M = N, the last term should also be factored by one-half). The quantities c_j are numerical coefficients which are determined from the ith acceleration components $\ddot{r}_i(\xi_k)$ at the Chebyshev points by means of the relationship

$$c_j = \frac{2}{N} \sum_{k=0}^{N}{}'' \ddot{r}_i(\xi_k) T_j(\xi_k) \tag{5-107}$$

where the double prime indicates that the first and last terms (for j = 0 and j = M) are factored by one-half.

The integration with respect to time is carried out using the following formula:

$$\int T_j(\xi)\, d\xi = \frac{1}{2}\left[\left(\frac{1}{j+1}\right) T_{j+1}(\xi) - \left(\frac{1}{j-1}\right) T_{j-1}(\xi)\right] \quad (j > 1) \tag{5-108}$$

Special cases hold for j = 0 and j = 1, i.e.,

$$\int T_0(\xi)\, d\xi = T_1(\xi) \tag{5-109}$$

$$\int T_1(\xi)\, d\xi = \frac{1}{4}\left[T_0(\xi) + T_2(\xi)\right] \tag{5-110}$$

The coefficients for the integral of the series for $p_M(\xi)$ are represented by b_j, i.e.,

$$\int_{-1}^{\xi} p_M(x)\, dx = \sum_{j=0}^{M+1} b_j T_j(\xi) \tag{5-111}$$

At $\xi = 1$, this expression for the ith velocity component is set equal to the initial value of that component of velocity by adjusting the constant b_0 to satisfy this condition. A similar adjustment is made after the integration of the velocity components to match the series evaluated at $\xi = 1$ with the initial component of position.

The integration formulas lead to a simple relationship between the quantities b_j and c_j, given by

$$b_j = \frac{1}{2j}(c_{j-1} - c_{j+1}) \qquad [1 \leq j \leq (M+1)] \tag{5-112}$$

where $c_{M+1} = c_{M+2} = 0$ by definition, and b_0 is obtained as described above.

Once the values of c_j are known, the summations required to evaluate $p_M(\xi)$ for any value of time can be done more efficiently by use of a backward recurrence relationship. Intermediate quantities d_j are computed using the algorithm

$$d_j(\xi) = 2\xi\, d_{j+1}(\xi) - d_{j+2}(\xi) + c_j \tag{5-113}$$

for $j = M, M-1, \ldots 0$, starting with $d_{M+1}(\xi) = d_{M+2}(\xi) = 0$. The value $p_M(\xi)$ is then computed from

$$p_M(\xi) = \frac{1}{2}[d_0(\xi) - d_2(\xi)] \tag{5-114}$$

5.7 GAUSSIAN VARIATION OF PARAMETERS FORMULATIONS

In real space, the unperturbed satellite orbit is a conic section lying in a plane that has a constant orientation, shape, and size relative to an inertial frame. For a perturbing acceleration that is small compared with the central attraction, the characteristics of the conic section (e.g., semimajor axis, eccentricity) vary slowly with time. To a lesser extent, the attitude of the orbital plane with respect to the inertial frame is a continuous function of time. However, the satellite's position along its orbit changes rapidly with time.

The numerical integration process is improved by introducing state variables that take advantage of this disparity of effect. The introduction of such variables allows comparison of the motion within the plane to a reference orbit and treatment of the motion of the plane as a slight correction. The VOP method uses this approach.

In this section, three orbit generators are discussed that are based on the Gaussian form of the VOP equations

$$\frac{\partial a}{\partial t} = \frac{\partial a}{\partial \dot{\bar{r}}} \bar{P} \tag{5-115}$$

where

a = slow element
$\dot{\bar{r}}$ = velocity vector
$\bar{P}$ = perturbing acceleration vector

and

$$\frac{\partial \beta}{\partial t} = \beta' + \frac{\partial \beta}{\partial \dot{r}} \bar{P} \tag{5-116}$$

where

β = fast element
β' = derivative of β for unperturbed two-body motion

These three orbit generators differ in the choice of dependent variables, i.e., either Keplerian, equinoctial, or rectangular elements. Some of the Keplerian elements become undefined when the inclination is zero or near 180 degrees, when the eccentricity is zero, and at collision. The equinoctial elements (discussed in Section 3.2.6) and rectangular elements are selected to eliminate all singularities except for collision. All three generators use time as the independent variable and are therefore well suited to the accurate integration of circular orbits. The Keplerian, equinoctial, and rectangular VOP formulations are discussed in Section 5.7.1, 5.7.2, and 5.7.3, respectively.

5.7.1 KEPLERIAN ELEMENTS

The input initial conditions for an orbit in GTDS can be expressed as rectangular components of the position and velocity at a given time t. The equations used in GTDS for the

conversion of rectangular position and velocity components to Keplerian elements are discussed in Section 3.3.8.3. For calculation of disturbing forces and for printout, GTDS converts instantaneous values of the Keplerian elements to rectangular components of position and velocity. The formulation used for these conversions is discussed in Section 3.3.8.1. Although all three classes of Keplerian orbits (elliptic, parabolic, and hyperbolic) are treated in the conversions, the VOP methods of GTDS apply only to the elliptic case.

The VOP equations of motion for Keplerian elements are taken in the form of the Gaussian planetary equations

$$\frac{da}{dt} = \frac{2\dot{\bar{r}}}{n^2 a} \cdot \bar{P} \tag{5-117a}$$

$$\frac{de}{dt} = \frac{\sqrt{1 - e^2}}{n a^2 e}\left[y_p \hat{x}_p - x_p \hat{y}_p + \frac{\sqrt{1 - e^2}}{n}\dot{\bar{r}}\right] \cdot \bar{P} \tag{5-117b}$$

$$\frac{di}{dt} = \frac{-\left[(y_p \hat{x}_p - x_p \hat{y}_p)\cos i + \frac{\partial \bar{r}}{\partial \Omega}\right] \cdot \bar{P}}{n a^2 \sqrt{1 - e^2}\sin i} \tag{5-117c}$$

$$\frac{d\Omega}{dt} = \frac{1}{n a^2 \sqrt{1 - e^2}\sin i}\frac{\partial \bar{r}}{\partial i} \cdot \bar{P} \tag{5-117d}$$

$$\frac{d\omega}{dt} = \frac{1}{n a^2}\left[\frac{-\sqrt{1 - e^2}}{e}(L \hat{x}_p + N \hat{y}_p) + \frac{\cot i}{\sqrt{1 - e^2}}\frac{\partial \bar{r}}{\partial i}\right] \cdot \bar{P} \tag{5-117e}$$

$$\frac{dM}{dt} = n + \frac{1}{n a^2}\left[-2\bar{r} - \frac{1 - e^2}{e}(L \hat{x}_p + N \hat{y}_p)\right] \cdot \bar{P} \tag{5-117f}$$

where x_p and y_p are the orbit plane coordinates given in Equation (3-176), $\hat{x}_p$ and $\hat{y}_p$ are Keplerian unit vectors defined in Section 3.2.5 and given by the inverse of

Equation (3-190), and $\bar{P}$ is the perturbing acceleration vector. The following auxiliary quantities are also defined:

$$n = \sqrt{\frac{\mu}{a^3}} \tag{5-118a}$$

$$\frac{\partial \bar{r}}{\partial \Omega} = \begin{bmatrix} -y \\ x \\ 0 \end{bmatrix} \tag{5-118b}$$

$$\frac{\partial \bar{r}}{\partial i} = \begin{bmatrix} z \sin \Omega \\ -z \cos \Omega \\ (x_p \sin \omega + y_p \cos \omega) \cos i \end{bmatrix} \tag{5-118c}$$

$$L = \frac{a^2}{r} [e \cos E - 1 - \sin^2 E] \tag{5-118d}$$

$$N = \frac{a^2 \sin E}{r\sqrt{1 - e^2}} (\cos E - e) \tag{5-118e}$$

The eccentric anomaly is obtained by solving Kepler's equation according to the method described in Section 3.3.8.1.

5.7.2 EQUINOCTIAL ELEMENTS

Since disturbing forces are calculated as rectangular components, and initial values can be rectangular components of position and velocity, GTDS has a capacity for converting Cartesian coordinates to equinoctial elements (see Section 3.3.9.2). The transformation from equinoctial elements to Cartesian coordinates is discussed in Section 3.3.9.1. The Gaussian equations in equinoctial elements are given by the following expressions (References 10 and 11):

$$\frac{da}{dt} = \frac{2\dot{\bar{r}}}{n^2 a} \cdot \bar{P} \tag{5-119a}$$

$$\frac{dh}{dt} = \left[\frac{1}{\mu} [(2\dot{X}_1 Y_1 - X_1 \dot{Y}_1) \hat{f} - X_1 \dot{X}_1 \hat{g}] + \frac{k}{G} (q I Y_1 - p X_1) \hat{w}\right] \cdot \bar{P} \tag{5-119b}$$

$$\frac{dk}{dt} = \left[-\frac{1}{\mu} \left[Y_1 \dot{Y}_1 \hat{f} - (2X_1 \dot{Y}_1 - \dot{X}_1 Y_1) \hat{g} \right] - \frac{h}{G} (q I Y_1 - p X_1) \hat{w} \right] \cdot \bar{P} \quad (5\text{-}119c)$$

$$\frac{d\lambda}{dt} = \left[n - \frac{2}{n a^2} \bar{r} + \beta \left(k \frac{\partial h}{\partial \dot{\bar{r}}} - h \frac{\partial k}{\partial \dot{\bar{r}}} \right) + \frac{1}{n a^2} (q I Y_1 - p X_1) \hat{w} \right] \cdot \bar{P} \quad (5\text{-}119d)$$

$$\frac{dp}{dt} = \left[\frac{1 + p^2 + q^2}{2G} Y_1 \hat{w} \right] \cdot \bar{P} \quad (5\text{-}119e)$$

$$\frac{dq}{dt} = \left[\frac{(1 + p^2 + q^2) I}{2G} X_1 \hat{w} \right] \cdot \bar{P} \quad (5\text{-}119f)$$

where

$$G = n a^2 \sqrt{1 - h^2 - k^2} \quad (5\text{-}119g)$$

The $\hat{f}$, $\hat{g}$, and $\hat{w}$ unit vectors are defined in Sections 3.2.5 and 3.3.9.1, while the components of the position and velocity vectors in the orbit plane X_1, Y_1, $\dot{X}_1$, $\dot{Y}_1$, and β are defined in Section 3.3.9.1.

5.7.3 RECTANGULAR FORMULATION (Not Currently Implemented in GTDS)

The initial Cartesian components of position and velocity completely define any orbit whether it be elliptic, parabolic, hyperbolic, or any degenerate rectilinear orbit. From the initial position and velocity, a completely general closed-form solution of the two-body problem is available for determining coordinates and velocities at any other time (Reference 12). The closed-form solution avoids the singularities associated with different types of two-body motion. In the rectangular VOP formulation, the dependent variables $\bar{r}_0$ and $\dot{\bar{r}}_0$ are the initial conditions at the time t_0 on an osculating two-body trajectory that yields the same state $\bar{r}_0$ and $\dot{\bar{r}}_0$ at time t as that of the perturbed trajectory. The dependent variable is the time. The osculating position and velocity at time t are obtained by inserting the perturbed initial conditions for the time of interest in the standard closed formulas for two-body motion.

The dependent variables, or perturbed initial conditions, are all slow variables, i.e., their time derivatives are all zero when the perturbing accelerations are set to zero. (A

perturbed initial condition is indicated by an asterisk in the following equations.) Therefore, all the equations of motion are in the form given in Equation (5-115). Then,

$$\frac{d\vec{r}_0^*}{dt} = \frac{\partial \vec{r}_0^*}{d\dot{\vec{r}}} \bar{P} \tag{5-120a}$$

$$\frac{d\dot{\vec{r}}_0^*}{dt} = \frac{\partial \dot{\vec{r}}_0^*}{d\dot{\vec{r}}} \bar{P} \tag{5-120b}$$

where the partial derivative matrices are as follows:

$$\begin{bmatrix} \partial x_0^*/\partial \dot{x} & \partial x_0^*/\partial \dot{y} & \partial x_0^*/\partial \dot{z} \\ \partial y_0^*/\partial \dot{x} & \partial y_0^*/\partial \dot{y} & \partial y_0^*/\partial \dot{z} \\ \partial z_0^*/\partial \dot{x} & \partial z_0^*/\partial \dot{y} & \partial z_0^*/\partial \dot{z} \end{bmatrix} = -\begin{bmatrix} g & 0 & 0 \\ 0 & g & 0 \\ 0 & 0 & g \end{bmatrix} + U \begin{bmatrix} \dot{x}_0^* \\ \dot{y}_0^* \\ \dot{z}_0^* \end{bmatrix} [\dot{x}\ \dot{y}\ \dot{z}]$$
$$+ \begin{bmatrix} x_0^* & \dot{x}_0^* \\ y_0^* & \dot{y}_0^* \\ z_0^* & \dot{z}_0^* \end{bmatrix} \begin{bmatrix} f s_2 & -(f-1) s_2 \\ (\dot{g} - 1) s_2 & -g s_2 \end{bmatrix} \begin{bmatrix} x & y & z \\ \dot{x} & \dot{y} & \dot{z} \end{bmatrix} \tag{5-121a}$$

$$\begin{bmatrix} \partial \dot{x}_0^*/\partial \dot{x} & \partial \dot{x}_0^*/\partial \dot{y} & \partial \dot{x}_0^*/\partial \dot{z} \\ \partial \dot{y}_0^*/\partial \dot{x} & \partial \dot{y}_0^*/\partial \dot{y} & \partial \dot{y}_0^*/\partial \dot{z} \\ \partial \dot{z}_0^*/\partial \dot{x} & \partial \dot{z}_0^*/\partial \dot{y} & \partial \dot{z}_0^*/\partial \dot{z} \end{bmatrix} = \begin{bmatrix} f & 0 & 0 \\ 0 & f & 0 \\ 0 & 0 & f \end{bmatrix} + U \begin{bmatrix} \ddot{x}_0^* \\ \ddot{y}_0^* \\ \ddot{z}_0^* \end{bmatrix} [\dot{x}\ \dot{y}\ \dot{z}]$$
$$+ \begin{bmatrix} x_0^* & \dot{x}_0^* \\ y_0^* & \dot{y}_0^* \\ z_0^* & \dot{z}_0^* \end{bmatrix} \begin{bmatrix} -\dfrac{\dot{f} s_1 + (f-1)/r_0^*}{r_0^*} & \dfrac{(f-1) s_1}{r_0^*} \\ -\dot{f} s_1 & (f-1) s_2 \end{bmatrix} \begin{bmatrix} x & y & z \\ \dot{x} & \dot{y} & \dot{z} \end{bmatrix} \tag{5-121b}$$

The position and velocity are computed as follows:

$$\vec{r} = f\,\vec{r}_0^{\,*} + g\,\dot{\vec{r}}_0^{\,*} \tag{5-122a}$$

$$\dot{\vec{r}} = \dot{f}\,\vec{r}_0^{\,*} + \dot{g}\,\dot{\vec{r}}_0^{\,*} \tag{5-122b}$$

where

$$f = 1 - \frac{\mu\, s_2}{r_0^*} \tag{5-123a}$$

$$g = (t - t_0) - \mu\, s_3 \tag{5-123b}$$

$$\dot{f} = -\frac{\mu\, s_1}{r\, r_0^*} \tag{5-123c}$$

$$\dot{g} = 1 - \frac{\mu\, s_2}{r} \tag{5-123d}$$

In the above formulas, μ is the gravitational constant and

$$r_0^* = [(x_0^*)^2 + (y_0^*)^2 + (z_0^*)^2]^{1/2} \tag{5-124a}$$

$$r = r_0^*\, s_0 + \sigma_0^*\, s_1 + \mu\, s_2 \tag{5-124b}$$

$$s_0 = 1 + \frac{a^*\,\psi^2}{2\,!} + \frac{(a^*)^2\,\psi^4}{4\,!} + \frac{(a^*)^3\,\psi^6}{6\,!} + \cdots \tag{5-124c}$$

$$s_1 = \psi + \frac{a^*\,\psi^3}{3\,!} + \frac{(a^*)^2\,\psi^5}{5\,!} + \frac{(a^*)^3\,\psi^7}{7\,!} + \cdots \tag{5-124d}$$

$$s_2 = \frac{\psi^2}{2!} + \frac{a^* \psi^4}{4!} + \frac{(a^*)^2 \psi^6}{6!} + \frac{(a^*)^3 \psi^8}{8!} + \ldots \qquad (5\text{-}124e)$$

$$s_3 = \frac{\psi^3}{3!} + \frac{a^* \psi^5}{5!} + \frac{(a^*)^2 \psi^7}{7!} + \frac{(a^*)^3 \psi^9}{9!} + \ldots \qquad (5\text{-}124f)$$

where the parameter ψ satisfies the following modified form of Kepler's equation:

$$t = t_0 + r_0^* s_1 + \sigma_0^* s_2 + \mu s_3 \qquad (5\text{-}125)$$

The equation is solved for ψ using a Newton-Raphson iteration process. In this equation,

$$\sigma_0^* = x_0^* \dot{x}_0^* + y_0^* \dot{y}_0^* + z_0^* \dot{z}_0^* \qquad (5\text{-}126a)$$

$$a^* = \left(\dot{x}_0^*\right)^2 + \left(\dot{y}_0^*\right)^2 + \left(\dot{z}_0^*\right)^2 - \frac{2\mu}{r} \qquad (5\text{-}126b)$$

The parameter U is evaluated as follows:

$$U = \mu(\psi s_4 - 3s_5) \qquad (5\text{-}127)$$

where

$$s_4 = \frac{\psi^4}{4!} + \frac{a^* \psi^6}{6!} + \frac{(a^*)^2 \psi^8}{8!} + \frac{(a^*)^3 \psi^{10}}{10!} + \ldots \qquad (5\text{-}128a)$$

$$s_5 = \frac{\psi^5}{5!} + \frac{a^* \psi^7}{7!} + \frac{(a^*)^2 \psi^9}{9!} + \frac{(a^*)^3 \psi^{11}}{11!} + \ldots \qquad (5\text{-}128b)$$

The following accelerations at time t_0 on the osculating trajectory are also used:

$$\ddot{x}_0^* = -\frac{\mu x_0^*}{(r_0^*)^3} \qquad (5\text{-}129a)$$

$$\ddot{y}_0^* = -\frac{\mu\, y_0^*}{(r_0^*)^3} \tag{5-129b}$$

$$\ddot{z}_0^* = -\frac{\mu\, z_0^*}{(r_0^*)^3} \tag{5-129c}$$

Initial conditions are specified by the values x_0, y_0, z_0, $\dot{x}_0$, $\dot{y}_0$, $\dot{z}_0$ of the coordinates at a given reference time t_0. At time t_0,

$$\begin{bmatrix} x_0^* \\ y_0^* \\ z_0^* \\ \dot{x}_0^* \\ \dot{y}_0^* \\ \dot{z}_0^* \end{bmatrix} = \begin{bmatrix} x_0 \\ y_0 \\ z_0 \\ \dot{x}_0 \\ \dot{y}_0 \\ \dot{z}_0 \end{bmatrix} \tag{5-130}$$

5.8 NUMERICAL AVERAGING FORMULATIONS

The efficiency of numerical integration methods can be increased by eliminating short-period effects (i.e., those with a period less than or equal to the satellite's period) from the equations of motion. The Method of Averages uses this approach, wherein the equations of motion for an average element set are integrated. The resulting orbit generation method is extremely efficient but is limited to average element accuracy rather than the osculating element accuracy achieved in high-precision methods.

The averaging methods are particularly useful for orbit determination problems for which the cost of precision orbit calculations is prohibitively expensive or where high accuracy is not essential. Mission design, for example, is based on the consideration of both the scientific objectives of the mission and the engineering constraints. Optimum mission design usually requires a large number of orbit calculations to determine the characteristics of the proposed orbits. An averaging orbit prediction process is well suited to the preliminary stages of mission planning where long-term trends, not local fluctuations, are of primary interest. The averaging methods can also be useful for differential correction problems involving large quantities of data. The only assumption required for application

of the averaging method is that the orbital elements remain reasonably constant throughout one period.

The averaging process can be handled either analytically or numerically (Reference 13). The analytic method averages the effect of each perturbation (drag, oblateness, third-body effects, etc.) separately. The resulting closed-form expressions for the averaged rates can be used to construct a very efficient orbit generator. The numerical averaging technique combines many of the advantages of analytic averaging with the ability to simulate the effect of any small perturbations that can be deterministically modeled. These effects are included by averaging out the short-period oscillations in the perturbations by means of a mechanical quadrature technique. By using the Gaussian form of the Variation of Parameters equations in conjunction with the GTDS force model, the long-term effect of any combination of perturbations can be computed. Consequently, the numerical technique is more flexible than the analytic method.

5.8.1 THE AVERAGED EQUATIONS OF MOTION

The averaging methods in GTDS use either the equinoctial or the Keplerian formulation (Section 5.7) of the Variation of Parameters equations of motion. The precision Variation of Parameters equations can be written in the form

$$\dot{\bar{x}} = \epsilon\, f(\bar{x},\, y) \tag{5-131a}$$

$$\dot{y} = h(\bar{x}) + \epsilon\, g(\bar{x}, y) \tag{5-131b}$$

where

- $\bar{x}$ = vector of slow osculating or orbital elements
- y = fast osculating orbital element (e.g., mean or eccentric anomaly)
- ϵ = a small parameter that is proportional to the perturbing acceleration

and f, g, and h are sufficiently smooth functions that are periodic in y with period 2π. The averaged solution to these equations is defined by (Reference 14)

$$\bar{x}_A(t) = \frac{1}{2\pi} \int_{y_A(t)-\pi}^{y_A(t)+\pi} \bar{x}(t')\, dy_A(t') \tag{5-132a}$$

$$y_A(t) = \frac{1}{2\pi} \int_{y_A(t)-\pi}^{y_A(t)+\pi} y(t')\, dy_A(t') \tag{5-132b}$$

Differentiating Equations (5-132) and substituting the results into Equations (5-131) yields the averaged equations of motion

$$\dot{\bar{x}}_A(t) = \frac{\epsilon}{2\pi} \int_{y_A(t)-\pi}^{y_A(t)+\pi} f\,[\bar{x}(t'),\ y(t')]\, dy_A(t') \tag{5-133a}$$

$$\dot{\bar{y}}_A(t) = \frac{1}{2\pi} \int_{y_A(t)-\pi}^{y_A(t)+\pi} \{h[\bar{x}(t')] + \epsilon\, g[\bar{x}(t'),\ y(t')]\}\, dy_A(t') \tag{5-133b}$$

When $\bar{x}_A(t')$ and $\bar{y}_A(t')$ are used in the evaluation of the arguments of the f, g, and h functions, the standard first-order averaged equations of motion are obtained (Reference 15). In GTDS, the integrals in Equations (5-133) are evaluated numerically using a Gaussian quadrature method.

5.8.2 NUMERICAL EVALUATION OF THE AVERAGED EQUATIONS OF MOTION

Four different approximations are currently available for evaluation of the arguments of the f, g, and h functions in Equations (5-133):

1. Traditional mean element behavior

$$\bar{x}(t') = \bar{x}_A(t) \tag{5-134a}$$

$$\bar{y}(t') = y_A(t') \tag{5-134b}$$

2. Traditional mean element behavior plus mean long-period effects

$$\bar{x}(t') = \bar{x}_A(t) + \dot{\bar{x}}_A(t)\ [t' - t] \tag{5-135a}$$

$$y(t') = y_A(t') \tag{5-135b}$$

where $\dot{\bar{x}}_A$ is the averaged rate computed in the previous evaluation.

3. Traditional mean element behavior plus short-period effects arising from J_2

$$\bar{x}(t') = \bar{x}_A(t) + \Delta\bar{x}_{J_2} \tag{5-136a}$$

$$y(t') = y_A(t') + \Delta y_{J_2} \tag{5-136b}$$

The short-period corrections are obtained using Brouwer theory.

4. Traditional mean element, mean long-period and short-period effects

$$\bar{x}(t') = \bar{x}_A(t) + \dot{\bar{x}}_A(t)\,[t' - t] + \Delta\bar{x}_{J_2} \tag{5-137a}$$

$$y(t') = y_A(t') + \Delta y_{J_2} \tag{5-137b}$$

Currently, only Equations (5-134) are available for evaluation of the argument in Equations (5-137).

5.8.3 AVERAGED EQUINOCTIAL VARIATION OF PARAMETERS FORMULATION

The averaged equinoctial formulation (Section 5.7.2) uses a slow element vector $\bar{x}$ = (a, h, k, p, q) and a fast variable equal to the mean longitude, λ. To uniformize the integrand in Equations (5-133) and to reduce computational time, the integration variable is transformed from the mean longitude to the eccentric longitude, F, using the relationship

$$\frac{dF_A}{d\lambda_A} = (1 - k_A \cos F_A - h_A \sin F_A)^{-1} \tag{5-138}$$

5.8.4 AVERAGED KEPLERIAN VARIATION OF PARAMETERS FORMULATION

The averaged Keplerian formulation uses a slow element vector $\bar{x}$ = (a, e, i, Ω, ω) and a fast variable equal to the mean anomaly, M. All four methods outlined in Section 5.8.2 are available for evaluation of the equations of motion. When methods 3 and 4 are used, the integration variable is transformed to the true anomaly, f, using the relationship

$$\frac{df_A}{dM_A} = \frac{a_A^2\sqrt{1 - e_A^2}}{r_A^2} \tag{5-139}$$

where r_A is the magnitude of the position vector computed using the averaged elements.

5.8.5 TRANSFORMATION FROM OSCULATING ORBITAL ELEMENTS TO AVERAGED ELEMENTS

The accuracy of predictions obtained using the averaged orbit generator are improved if initial average elements are used instead of osculating elements. In GTDS, this transformation is accomplished by solving the integral equation for the average semimajor axis

$$a_A(t) = \frac{1}{T_A}\int_{t-T_A/2}^{t+T_A/2} a(t')\,dt' \tag{5-140}$$

using the following Newton-Raphson iterative procedure:

$$F_n = [a_A(t)]_n - \frac{1}{(T_A)_n}\int_{t-(T_A/2)_n}^{t+(T_A/2)_n} a(t')\,dt' \tag{5-141a}$$

$$D_n = \frac{dF_n}{d[a_A(t)]_n} \tag{5-141b}$$

$$[a_A(t)]_{n+1} = [a_A(t)]_n - \frac{F_n}{D_n} \tag{5-141c}$$

where

$[a_A(t)]_0 = a \approx$ osculating semimajor axis

and where T_A, the average period, is

$$T_A = 2\pi\sqrt{\frac{a_A^3}{\mu}} \tag{5-142}$$

The average equinoctial element set is then computed by averaging the osculating elements over the average period, i.e.,

$$\bar{x}_A(t) = \frac{1}{T_A}\int_{t-T_A/2}^{t+T_A/2} \bar{x}(t')\,dt' \tag{5-143a}$$

$$y_A(t) = \frac{1}{T_A}\int_{t-T_A/2}^{t+T_A/2} y(t')\,dt' \qquad (5\text{-}143b)$$

The average equinoctial elements are transformed to average position and velocity vectors, Keplerian elements, and spherical coordinates.

5.9 BROUWER THEORY

GTDS includes two analytical solutions of satellite motion for a simplified disturbing potential field limited to zonal harmonic coefficients for J_2 through J_5 (see Section 4.3). Brouwer's first-order solution of this problem is obtained by applying the Von Zeipel method in Delaunay canonical variables (Reference 1). The resulting solution contains singularities for small inclinations and eccentricities and at a critical inclination of 63 degrees, 26 minutes.

It was shown in Reference 15 that the first-order Brouwer solution for secular and long-period effects is identical to that obtained using first-order numerical averaging (Section 5.8) with the same perturbing force model. Thus, Brouwer theory is equivalent to the first-order averaging solution plus short-period effects for the J_2 through J_5 perturbing acceleration. For applications that require more complete perturbation models, averaging methods are more accurate than Brouwer theory.

Brouwer theory provides a rapid means of determining a satellite ephemeris. Its precision is related to the error committed in omitting all perturbations except the low-order zonal harmonics. The orbit from the Brouwer theory can also be used as an intermediate orbit in the semianalytic techniques discussed in Section 5.11.

For applications that require high efficiency, it is important to consider the number of output points required. For Brouwer theory, the computational cost is directly proportional to the number of output points. However, when averaged numerical integration is used, the cost is mainly dependent on the arc length instead of the number of intermediate output points. For differential correction applications, the computational cost of the averaged orbit generation methods is often competitive with that of Brouwer theory and offers considerably greater flexibility with respect to the perturbation model.

Computationally, the Brouwer solution is divided into secular, long-period, and short-period terms. The solution consists of a secular motion, upon which is superimposed a number of long-period terms. Superimposed on the sum of the secular and long-period terms are a number of more rapid oscillations, or short-period terms. The periodic terms of both long and short period are developed to order J_2, while secular terms are developed to order $(J_2)^2$. The harmonic coefficients J_3, J_4, and J_5 are considered to be of order $(J_2)^2$ in the derivations.

The Delaunay elements are related to the classical elements in the following way:

$$
\begin{aligned}
L &= (\mu\, a)^{1/2} \\
G &= L\,(1 - e^2)^{1/2} \\
H &= G \cos i \\
\ell &= \text{mean anomaly} = M \\
g &= \text{argument of pericenter} = \omega \\
h &= \text{longitude of the ascending node} = \Omega
\end{aligned}
$$

However, the solution is written here in terms of classical elements (a, e, i, ℓ, g, h) = (a, e, i, M, ω, Ω). In the formulas that follow, double-primed variables refer to secular or mean motion, single-primed variables refer to secular plus long-period terms, and unprimed variables refer to secular plus long- and short-period terms. The unprimed variables are osculating elements.

Only the elements ℓ, g, and h undergo secular motions. Mean elements at epoch are denoted by a subscript 0 and the time elapsed from epoch by Δt. Mean elements are usually obtained from osculating elements by the procedure outlined in Section 5.9.1. The first-order solutions to the mean element equations of motion are

$$a'' = a_0'' + \Delta a \tag{5-144a}$$

$$e'' = e_0'' + \Delta e \tag{5-144b}$$

$$i'' = i_0'' + \Delta i \tag{5-144c}$$

$$\ell'' = n_0\,\Delta t + \dot{\ell}\,\Delta t + \ell_0'' + \Delta\ell + \Delta\ell_{DRAG} \qquad (0 \le \ell'' < 2\pi) \tag{5-144d}$$

$$g'' = \dot{g}\,\Delta t + g_0'' + \Delta g \qquad (0 \le g'' < 2\pi) \tag{5-144e}$$

$$h'' = \dot{h}\,\Delta t + h_0'' + \Delta h \qquad (0 \le h'' < 2\pi) \tag{5-144f}$$

where Δa, Δe, Δi, $\Delta \ell$, Δg, and Δh are user-provided perturbations not accounted for in the Brouwer-Lyddane model, and

$$\Delta \ell_{DRAG} = \sum_{q=0}^{19} \sum_{p=2}^{3} N_{p,q} (t - t_q)^p \tag{5-145}$$

where $N_{p,q}$ are the Brouwer drag coefficients and t_q is the reference time of the q^{th} $N_{p,q}$. This model is based on the premise that drag is a minor component of the total perturbation force.

The restricted perturbation model and first-order approximation, which are used in the derivation of these equations, can lead to errors that increase with time. The element rates of change are given by

$$\dot{\ell} = n_0 \eta \left(\gamma_2' \left\{ \frac{3}{2} (3\theta^2 - 1) + \frac{3}{32} \gamma_2' [25\eta^2 + 16\eta - 15 + (30 - 96\eta - 90\eta^2) \theta^2 + (105 + 144\eta + 25\eta^2) \theta^4] \right\} + \frac{15}{16} \gamma_4' (e'')^2 (3 - 30\theta^2 + 35\theta^4) \right) \tag{5-146}$$

$$\dot{g} = n_0 \left(\gamma_2' \left\{ \frac{3}{2} (5\theta^2 - 1) + \frac{3}{32} \gamma_2' [25\eta^2 + 24\eta - 35 + (90 - 192\eta - 126\eta^2) \theta^2 + (385 + 360\eta + 45\eta^2) \theta^4] \right\} + \frac{5}{16} \gamma_4' [21 - 9\eta^2 + (126\eta^2 - 270) \theta^2 + (385 - 189\eta^2) \theta^4] \right) \tag{5-147}$$

$$\dot{h} = n_0 \left(\gamma_2' \left\{ \frac{3}{8} \gamma_2' [(9\eta^2 + 12\eta - 5) \theta - (35 + 36\eta + 5\eta^2) \theta^3] - 3\theta \right\} + \frac{5}{4} \gamma_4' \theta (5 - 3\eta^2) (3 - 7\theta^2) \right) \tag{5-148}$$

The following substitutions have been made to abbreviate the preceding expressions:

$$n_0 = \sqrt{\frac{\mu}{(a'')^3}} \tag{5-149a}$$

$$\eta = \sqrt{1 - (e'')^2} \tag{5-149b}$$

$$\theta = \cos i'' \tag{5-149c}$$

$$k_2 = \frac{J_2 R_e^2}{2} \tag{5-149d}$$

$$k_3 = - J_3 R_e^3 \tag{5-149e}$$

$$k_4 = - \frac{3J_4 R_e^4}{8} \tag{5-149f}$$

$$k_5 = - J_5 R_e^5 \tag{5-149g}$$

$$\gamma_2 = \frac{k_2}{(a'')^2} \tag{5-149h}$$

$$\gamma_3 = \frac{k_3}{(a'')^3} \tag{5-149i}$$

$$\gamma_4 = \frac{k_4}{(a'')^4} \tag{5-149j}$$

$$\gamma_5 = \frac{k_5}{(a'')^5} \tag{5-149k}$$

$$\gamma_2' = \frac{\gamma_2}{\eta^4} \tag{5-149ℓ}$$

$$\gamma_3' = \frac{\gamma_3}{\eta^6} \tag{5-149m}$$

$$\gamma_4' = \frac{\gamma_4}{\eta^8} \tag{5-149n}$$

$$\gamma_5' = \frac{\gamma_5}{\eta^{10}} \tag{5-149o}$$

The secular terms depend only on the even zonal harmonic coefficients J_2 and J_4.

The mean value of the eccentric anomaly E'' is obtained iteratively from Kepler's equation

$$E'' - e'' \sin E'' = \ell'' \tag{5-150}$$

The mean true anomaly f'' and mean radial distance r'' are given by

$$f'' = \tan^{-1}\left[\frac{\sqrt{1 - (e'')^2}\ \sin E''}{\cos E'' - e''}\right] \tag{5-151a}$$

$$r'' = a''(1 - e'' \cos E'') \tag{5-151b}$$

5.9.1 TRANSFORMATION FROM OSCULATING ORBITAL ELEMENTS TO BROUWER MEAN ELEMENTS

The iterative algorithm used for converting osculating Keplerian elements to Brouwer mean elements is described here (see References 16 and 17). This algorithm is useful in two situations. Since Brouwer or Brouwer-Lyddane theories require Brouwer mean elements as an initial state, the first application consists of converting osculating elements to mean elements for use with the Brouwer and Brouwer-Lyddane orbit generators. Secondly, osculating elements can be converted to Brouwer mean elements for reporting purposes. Such mean elements are also useful as initial data for the integration of orbits by the Method of Averaging and for other purposes.

Singular points for zero eccentricity, zero inclination, and at inclination 63 degrees, 26 minutes, do not permit calculation of mean elements there. Only Keplerian elliptic motion can be treated, which requires $0 \leq e \leq 1$.

The iterative process is executed according to the equation

$$x_i''^{(s+1)} = x_i''^{(s)} + [y_i - y_i^{(s)}] \quad (i = 1, 2, \ldots, 6) \tag{5-152}$$

where

$x_i''^{(s)}$ = i^{th} mean classical Keplerian element obtained from the s^{th} iteration

y_i = initial osculating Keplerian element

$y_i^{(s)}$ = osculating Keplerian element estimated from the s^{th} iteration

Double primes denote mean elements at the time of conversion. This algorithm ignores correlations between the elements of the order of 10^{-3}, which are of no practical importance in the calculations.

A convergence criteria limits the number of iterations. The sum of the squares of the differences between the estimated and the initially given osculating elements are compared with a prescribed tolerance. When the sum is less than the tolerance, the calculation is terminated.

The following method for obtaining the mean elements at a given time is more exact than those methods that propagate the mean elements from some previous time using Equations (5-144) and (5-145), since the propagated mean elements deteriorate with time due to perturbations not included in the solution. The values of the mean elements on the s^{th} iteration are used to compute estimates of the osculating elements. As shown by Equation (5-152), the difference between the s^{th} estimated value and the initial known value of the osculating elements is used to correct the s^{th} estimate of the mean elements. The starting approximation for the mean elements is the set of initially known osculating elements.

5.9.2 TRANSFORMATION FROM BROUWER MEAN ELEMENTS TO OSCULATING KEPLERIAN ELEMENTS

The osculating elements include the secular, long-period, and short-period terms. The osculating elements are expressed by

$$a = a'' \left\{ 1 + \gamma_2 \left[(-1 + 3\theta^2) \left(\frac{(a'')^3}{r'^3} - \eta^{-3} \right) + 3(1 - \theta^2) \frac{(a'')^3}{(r')^3} \cos(2g' + 2f') \right] \right\} \tag{5-153}$$

$$e = e'' + \delta_1 e + \frac{\eta^2}{2e''} \left(\gamma_2 \left\{ (-1 + 3\theta^2) \left[\frac{(a'')^3}{(r')^3} - \eta^{-3} \right] + 3(1 - \theta^2) \left[\frac{(a'')^3}{(r')^3} - \eta^{-4} \right] \cos(2g' + 2f') \right\} - \gamma_2'(1 - \theta^2) [3e'' \cos(2g' + f') + e'' \cos(2g' + 3f')] \right) \tag{5-154}$$

$$i = i'' + \delta_1 i + \frac{1}{2} \gamma_2' \theta (1 - \theta^2)^{1/2} [3 \cos(2g' + 2f') + 3e'' \cos(2g' + f') + e'' \cos(2g' + 3f')] \tag{5-155}$$

$$\ell = \ell'' + \delta_1 \ell - \frac{\eta^3}{4e''} \gamma_2' \left(2(-1 + 3\theta^2) \left[\frac{(a'')^2}{(r')^2} \eta^2 + \frac{a''}{r'} + 1 \right] \sin f' \right.$$
$$+ 3(1 - \theta^2) \left\{ \left[- \frac{(a'')^2}{(r'')^2} \eta^2 - \frac{a''}{r'} + 1 \right] \sin(2g' + f') \right. \qquad (5\text{-}156)$$
$$\left. \left. + \left[\frac{(a'')^2}{(r')^2} \eta^2 + \frac{a''}{r'} + \frac{1}{3} \right] \sin(2g' + 3f') \right\} \right)$$

$$g = g'' + \delta_1 g + \frac{\eta^2}{4e''} \gamma_2' \left(2(-1 + 3\theta^2) \left[\frac{(a'')^2}{(r')^2} \eta^2 + \frac{a''}{r'} + 1 \right] \sin f' \right.$$
$$+ 3(1 - \theta^2) \left\{ \left[- \frac{(a'')^2}{(r')^2} \eta^2 - \frac{a''}{r'} + 1 \right] \sin(2g' + f') \right.$$
$$\left. \left. + \left[\frac{(a'')^2}{(r')^2} \eta^2 + \frac{a''}{r'} + \frac{1}{3} \right] \sin(2g' + 3f') \right\} \right)$$
$$+ \frac{1}{4} \gamma_2' \{ 6(-1 + 5\theta^2) (f' - \ell' + e'' \sin f') \qquad (5\text{-}157)$$
$$+ (3 - 5\theta^2) [3 \sin(2g' + 2f') + 3e'' \sin(2g' + f')$$
$$+ e'' \sin(2g' + 3f')]\}$$

$$h = h'' + \delta_1 h - \frac{1}{2} \gamma_2' \theta [6(f' - \ell' + e'' \sin f') - 3 \sin(2g' + 2f') \qquad (5\text{-}158)$$
$$- 3e'' \sin(2g' + f') - e'' \sin(2g' + 3f')]$$

where the long-period effects (denoted by δ_1) affect the elements e, i, ℓ, g, and h, but not the semimajor axis a, and are given by the following equations:

$$\begin{aligned}
\delta_1 e = & \left\{ \frac{1}{8} \gamma_2' e'' \eta^2 [1 - 11\theta^2 - 40\theta^4 (1 - 5\theta^2)^{-1}] \right. \\
& \left. - \frac{5}{12} \frac{\gamma_4'}{\gamma_2'} e'' \eta^2 [1 - 3\theta^2 - 8\theta^4 (1 - 5\theta^2)^{-1}] \right\} \cos 2g'' \\
& + \left\{ \frac{1}{4} \frac{\gamma_3'}{\gamma_2'} \eta^2 \sin i'' + \frac{5}{64} \frac{\gamma_5'}{\gamma_2'} \eta^2 \sin i'' [4 + 3(e'')^2] \right. \\
& \left. \times [1 - 9\theta^2 - 24\theta^4 (1 - 5\theta^2)^{-1}] \right\} \sin g'' \\
& - \frac{35}{384} \frac{\gamma_5'}{\gamma_2'} (e'')^2 \eta^2 \sin i'' [1 - 5\theta^2 - 16\theta^4 (1 - 5\theta^2)^{-1}] \sin 3g''
\end{aligned} \tag{5-159}$$

$$\delta_1 i = - \frac{e'' \delta_1 e}{\eta^2 \tan i''} \tag{5-160}$$

$$\begin{aligned}
\delta_1 \ell = & \left\{ \frac{1}{8} \gamma_2' \eta^3 [1 - 11\theta^2 - 40\theta^4 (1 - 5\theta^2)^{-1}] \right. \\
& \left. - \frac{5}{12} \frac{\gamma_4'}{\gamma_2'} \eta^3 [1 - 3\theta^2 - 8\theta^4 (1 - 5\theta^2)^{-1}] \right\} \sin 2g'' \\
& + \left\{ - \frac{1}{4} \frac{\gamma_3'}{\gamma_2'} \frac{\eta^3}{e''} \sin i'' - \frac{5}{64} \frac{\gamma_5'}{\gamma_2'} \frac{\eta^3}{e''} \sin i'' [4 + 9(e'')^2] \right. \\
& \left. \times [1 - 9\theta^2 - 24\theta^4 (1 - 5\theta^2)^{-1}] \right\} \cos g'' \\
& + \frac{35}{384} \frac{\gamma_5'}{\gamma_2'} \eta^3 e'' \sin i'' [1 - 5\theta^2 - 16\theta^4 (1 - 5\theta^2)^{-1}] \cos 3g''
\end{aligned} \tag{5-161}$$

$$\delta_1 g = \left(-\frac{1}{16}\gamma_2'\{[2 + (e'')^2] - 11[2 + 3(e'')^2]\,\theta^2 - 40[2 + 5(e'')^2]\,\theta^4(1 - 5\theta^2)^{-1}\right.$$

$$- 400\,(e'')^2\,\theta^6(1 - 5\theta^2)^{-2}\} + \frac{5}{24}\frac{\gamma_4'}{\gamma_2'}\{2 + (e'')^2 - 3[2 + 3(e'')^2]\,\theta^2$$

$$\left. - 8\,[2 + 5(e'')^2]\,\theta^4(1 - 5\theta^2)^{-1} - 80\,(e'')^2\,\theta^6(1 - 5\theta^2)^{-2}\}\right) \sin 2g''$$

$$+ \left(\frac{1}{4}\frac{\gamma_3'}{\gamma_2'}\left(\frac{\sin i''}{e''} - \frac{e''\,\theta^2}{\sin i''}\right) + \frac{5}{64}\frac{\gamma_5'}{\gamma_2'}\right.$$

$$\times \left\{\left(\frac{\eta^2 \sin i''}{e''} - \frac{e''\,\theta^2}{\sin i''}\right)[4 + 3(e'')^2] + e''\sin i''[26 + 9(e'')^2]\right\}$$

$$\times [1 - 9\theta^2 - 24\theta^4(1 - 5\theta^2)^{-1}] \qquad (5\text{-}162)$$

$$- \frac{15}{32}\frac{\gamma_5'}{\gamma_2'}\,e''\,\theta^2 \sin i''[4 + 3(e'')^2][3 + 16\theta^2(1 - 5\theta^2)^{-1}$$

$$\left. + 40\,\theta^4(1 - 5\theta^2)^{-2}]\right) \cos g'' + \left(-\frac{35}{1152}\frac{\gamma_5'}{\gamma_2'}\{e'' \sin i''[3 + 2(e'')^2]\right.$$

$$\left. - \frac{(e'')^3\,\theta^2}{\sin i''}\right\}[1 - 5\theta^2 - 16\theta^4(1 - 5\theta^2)^{-1}]$$

$$+ \frac{35}{576}\frac{\gamma_5'}{\gamma_2'}\,(e'')^2\,\theta^2 \sin i''[5 + 32\theta^2(1 - 5\theta^2)^{-1} + 80\,\theta^4(1 - 5\theta^2)^{-2}]\Big) \cos 3g''$$

$$\delta_1 h = \left\{ -\frac{1}{8}\gamma_2' (e'')^2 \theta \left[11 + 80\theta^2(1 - 5\theta^2)^{-1} + 200\theta^4(1 - 5\theta^2)^{-2}\right] \right.$$

$$\left. + \frac{5}{12}\frac{\gamma_4'}{\gamma_2'} (e'')^2 \theta \left[3 + 16\theta^2(1 - 5\theta^2)^{-1} + 40\theta^4(1 - 5\theta^2)^{-2}\right] \right\} \sin 2g''$$

$$+ \left\{ \frac{1}{4}\frac{\gamma_3'}{\gamma_2'}\frac{e'' \theta}{\sin i''} + \frac{5}{64}\frac{\gamma_5'}{\gamma_2'}\frac{e'' \theta}{\sin i''} \left[4 + 3(e'')^2\right] \left[1 - 9\theta^2 - 24\theta^4(1 - 5\theta^2)^{-1}\right] \right.$$

$$+ \frac{15}{32}\frac{\gamma_5'}{\gamma_2'} e'' \theta \sin i'' \left[4 + 3(e'')^2\right] \left[3 + 16\theta^2(1 - 5\theta^2)^{-1} \right. \qquad (5\text{-}163)$$

$$\left. \left. + 40\theta^4(1 - 5\theta^2)^{-2}\right] \right\} \cos g''$$

$$+ \left\{ -\frac{35}{1152}\frac{\gamma_5'}{\gamma_2'}\frac{(e'')^3 \theta}{\sin i''} \left[1 - 5\theta^2 - 16\theta^4(1 - 5\theta^2)^{-1}\right] \right.$$

$$\left. - \frac{35}{576}\frac{\gamma_5'}{\gamma_2'} (e'')^3 \theta \sin i'' \left[5 + 32\theta^2(1 - 5\theta^2)^{-1} + 80\theta^4(1 - 5\theta^2)^{-2}\right] \right\} \cos 3g''$$

In these formulas, f′ and r′ are computed from

$$E' - e'' \sin E' = \ell' \qquad (5\text{-}164)$$

and

$$\tan\left(\frac{f'}{2}\right) = \left(\frac{1 + e''}{1 - e''}\right)^{1/2} \tan\left(\frac{E'}{2}\right) \qquad (5\text{-}165a)$$

$$\frac{a''}{r'} = \frac{1 + e'' \cos f'}{1 - (e'')^2} \qquad (5\text{-}165b)$$

or

$$\frac{r'}{a''} \sin f' = [1 - (e'')^2]^{1/2} \sin E' \qquad (5\text{-}166a)$$

$$\frac{r'}{a''} \cos f' = \cos E' - e'' \qquad (5\text{-}166b)$$

$$\frac{r'}{a''} = 1 - e'' \cos E' \tag{5-166c}$$

For the calculation of the coordinates at any time, the complete values of e and ℓ should be used for the solution of Kepler's equation

$$E - e \sin E = \ell \tag{5-167}$$

The conversion of osculating Keplerian elements to rectangular components of position and velocity is discussed in Section 3.3.8.

5.10 BROUWER-LYDDANE THEORY

Lyddane modified Brouwer's formulation to obtain algorithms applicable for zero eccentricity and zero inclination (Reference 18). He reformulated the orbital equations in terms of Poincaré variables rather than the Delaunay variables used by Brouwer. The solution, carried out by the Von Zeipel method, accounts for up to fifth-order zonal harmonics of the gravitational potential. The results are written here in classical elements rather than Poincaré elements.

The Brouwer formulas are suitable for the computation of the classical elements with one exception. In computing short-period terms, Lyddane uses ℓ'' and g'' instead of ℓ' and g'. Brouwer remarked that either is satisfactory, but in the Lyddane theory, ℓ' and g' may be ill defined. In addition, the relationships

$$(1/e'')\left[\left(\frac{a''}{r''}\right)^3 - \eta^{-3}\right] = \eta^{-6}\left[e''\eta + e''(1+\eta)^{-1} + 3\cos f'' + 3e''\cos^2 f'' + (e'')^2\cos^3 f''\right] \tag{5-168a}$$

and

$$(1/e'')\left[\left(\frac{a''}{r''}\right)^3 - \eta^{-4}\right] = \eta^{-6}\left[e'' + 3\cos f'' + 3e''\cos^2 f'' + (e'')^2\cos^3 f''\right] \tag{5-168b}$$

are used in the computation of δe to avoid roundoff problems, where η is defined in Equation (5-149b).

5.10.1 TRANSFORMATION FROM OSCULATING ORBITAL ELEMENTS TO BROUWER MEAN ELEMENTS

The mean motions due to secular terms are calculated by Equations (5-144) through (5-148) of Section 5.9.

5.10.2 TRANSFORMATION FROM BROUWER MEAN ELEMENTS TO OSCULATING KEPLERIAN ELEMENTS

The osculating elements are computed using Equations (5-169) through (5-185) (Reference 19). Since the periodic terms are somewhat lengthy, a number of substitutions have been made in these equations.

Semimajor Axis

$$a = a'' \left(1 + \gamma_2 \left\{ (3\theta^2 - 1) \frac{e''}{\eta^6} \left[e'' \eta + \frac{e''}{1+\eta} + \cos f''(3 + 3e'' \cos f'' + (e'')^2 \cos^2 f'') \right] + 3(1 - \theta^2) \left(\frac{a''}{r''}\right)^3 \cos(2f'' + 2g'') \right\} \right) \tag{5-169}$$

Eccentricity

$$e = \sqrt{(e'' + \delta e)^2 + (e'' \delta \ell)^2} \tag{5-170}$$

where

$$\begin{aligned} \delta e = \delta_1 e - \frac{\eta^2}{2} \Bigg\{ & \gamma_2'(1 - \theta^2) [3 \cos(2g'' + f'') + \cos(3f'' + 2g'')] \\ & - 3\gamma_2 \frac{1}{\eta_6}(1 - \theta^2) \cos(2g'' + 2f'') [3e'' \cos^2 f'' \\ & + 3 \cos f'' + (e'')^2 \cos^3 f'' + e''] \\ & - \gamma_2 \frac{1}{\eta^6} (3\theta^2 - 1) \left[e'' \eta + \frac{e''}{1+\eta} + 3e'' \cos^2 f'' + 3 \cos f'' + (e'')^2 \cos^3 f'' \right] \Bigg\} \end{aligned} \tag{5-171}$$

$$
\begin{aligned}
e'' \delta\ell = {} & B_4 \sin 2g'' - B_5 \cos g'' + B_6 \cos 3g'' \\
& - \frac{1}{4}\eta^3 \gamma_2' \left(2(3\theta^2 - 1)\left[\eta^2 \left(\frac{a''}{r''}\right)^2 + \frac{a''}{r''} + 1\right] \sin f'' \right. \\
& + 3(1 - \theta^2)\left\{\left[-\eta^2 \left(\frac{a''}{r''}\right)^2 - \frac{a''}{r''} + 1\right] \sin(2g'' + f'') \right. \\
& \left. \left. + \left[\eta^2 \left(\frac{a''}{r''}\right)^2 + \frac{a''}{r''} + \frac{1}{3}\right] \sin(3f'' + 2g'')\right\}\right)
\end{aligned}
\tag{5-172}
$$

and

$$
\delta_1 e = B_{13} \cos 2g'' + B_{14} \sin g'' - B_{15} \sin 3g'' \tag{5-173}
$$

Inclination

$$
i = 2 \sin^{-1} \left\{ \left[\sin\left(\frac{i''}{2}\right) \delta h\right]^2 + \left[\frac{1}{2}\delta i \cos\left(\frac{i''}{2}\right) + \sin\left(\frac{i''}{2}\right)^2\right\}^{1/2} \right. \tag{5-174}
$$

where

$$
\begin{aligned}
\delta i = {} & \frac{1}{2}\theta \gamma_2' \sin i''\{e'' \cos(3f'' + 2g'') \\
& + 3[e'' \cos(2g'' + f'') + \cos(2f'' + 2g'')]\} \\
& - \frac{A_{20}}{\eta^2}(B_7 \cos 2g'' + B_8 \sin g'' - B_9 \sin 3g'')
\end{aligned}
\tag{5-175}
$$

and

$$\sin\left(\frac{i''}{2}\right)\delta h = \frac{1}{2\cos\left(\frac{i''}{2}\right)}\Bigg(B_{10}\sin 2g'' + B_{11}\cos g'' + B_{12}\cos 3g''$$
$$- \frac{1}{2}\gamma_2'\theta\sin i''\{6(e''\sin f'' - \ell'' + f'')$$
$$- 3[\sin(2g'' + 2f'') + e''\sin(2g'' + f'')]$$
$$- e''\sin(3f'' + 2g'')\}\Bigg) \qquad (5\text{-}176)$$

Mean Anomaly ℓ, Argument of Perigee g, and Right Ascension of Ascending Node h

$$\ell = \tan^{-1}\left[\frac{e''\,\delta\ell\cos\ell'' + (e'' + \delta e)\sin\ell''}{(e'' + \delta e)\cos\ell'' - e''\,\delta\ell\sin\ell''}\right] \quad (\text{if } e \neq 0) \qquad (5\text{-}177)$$

$$\ell = 0 \quad (\text{if } e = 0) \qquad (5\text{-}178)$$

$$h = \tan^{-1}\left\{\frac{\sin\left(\frac{i''}{2}\right)\delta h\cos h'' + \sin h''\left[\frac{1}{2}\delta i\cos\left(\frac{i''}{2}\right) + \sin\left(\frac{i''}{2}\right)\right]}{\cos h''\left[\frac{1}{2}\delta i\cos\left(\frac{i''}{2}\right) + \sin\left(\frac{i''}{2}\right)\right] - \sin\left(\frac{i''}{2}\right)\delta h\sin h''}\right\} \quad (\text{if } i \neq 0) \qquad (5\text{-}179)$$

$$h = 0 \quad (\text{if } i = 0) \qquad (5\text{-}180)$$

$$g = (\ell + g + h) - \ell - h \qquad (5\text{-}181)$$

where

$$\ell + g + h = (\ell' + g' + h') + \left\{\frac{1}{4}\left[\frac{\eta^2}{\eta + 1}\right] e'' \gamma_2' \left[3(1 - \theta^2)\left\{\sin(3f'' + 2g'')\right.\right.\right.$$
$$\times \left[\frac{1}{3} + \left(\frac{a''}{r''}\right)^2 \eta^2 + \frac{a''}{r''}\right] + \sin(2g'' + f'')\left[1 - \left(\frac{a''}{r''}\right)^2 \eta^2 - \frac{a''}{r''}\right]\Bigg\}$$
$$\left.\left.+ 2 \sin f''(3\theta^2 - 1)\left[1 + \left(\frac{a''}{r''}\right)^2 \eta^2 + \frac{a''}{r''}\right]\right]\right\} \qquad (5\text{-}182)$$
$$+ \frac{3}{2} \gamma_2'[(5\theta^2 - 2\theta - 1)(e'' \sin f'' + f'' - \ell'')] + (3 + 2\theta - 5\theta^2)$$
$$\times \left(\frac{1}{4} \gamma_2' \{e'' \sin(3f'' + 2g'') + 3[\sin(2g'' + 2f'') + e'' \sin(2g'' + f'')]\}\right)$$

where

$$(\ell' + g' + h') = (\ell'' + g'' + h'') + B_3 \cos 3g'' + B_1 \sin 2g'' + B_2 \cos g'' \qquad (5\text{-}183)$$

The quantity θ is defined in Equation (5-149c). The following abbreviations are introduced to shorten the written formulas:

$$A_1' = \frac{1}{(1 - 5\theta^2)} \qquad (5\text{-}184a)$$

$$A_1 = \frac{1}{8} \gamma_2' \eta^2 (1 - 11\theta^2 - 40\theta^4 A_1') \qquad (5\text{-}184b)$$

$$A_2' = 3\theta^2 + 8\theta^4 A_1' \qquad (5\text{-}184c)$$

$$A_2 = \frac{5}{12}\,\frac{\gamma_4'}{\gamma_2'}\,\eta^2(1 - A_2') \tag{5-184d}$$

$$A_3 = \frac{\gamma_5'}{\gamma_2'}\,[3(e'')^2 + 4] \tag{5-184e}$$

$$A_4 = \frac{\gamma_5'}{\gamma_2'}\,(1 - 3A_2') \tag{5-184f}$$

$$A_5 = A_3(1 - 3A_2') \tag{5-184g}$$

$$A_6 = \frac{1}{4}\,\frac{\gamma_3'}{\gamma_2'} \tag{5-184h}$$

$$A_7 = A_6\,\eta^2 \sin i'' \tag{5-184i}$$

$$A_8 = \frac{\gamma_5'}{\gamma_2'}\,(e'')^2\,(1 - 5\theta^2 - 16\theta^4\,A_1') \tag{5-184j}$$

$$A_9 = \eta^2 \sin i'' \tag{5-184k}$$

$$A_{10} = 2 + (e'')^2 \tag{5-184ℓ}$$

$$A_{11} = 3(e'')^2 + 2 \tag{5-184m}$$

$$A_{12} = A_{11}\,\theta^2 \tag{5-184n}$$

$$A_{13} = [5(e'')^2 + 2]\,\theta^4\,A_1' \tag{5-184o}$$

$$A_{14} = (e'')^2 \theta^6 (A_1')^2 \tag{5-184p}$$

$$A_{15} = \theta^2 A_1' \tag{5-184q}$$

$$A_{16} = A_{15}^2 \tag{5-184r}$$

$$A_{17} = e'' \sin i'' \tag{5-184s}$$

$$A_{18} = \frac{A_{17}}{1 + \eta} \tag{5-184t}$$

$$A_{19} = (1 + \theta) \sin i'' \tag{5-184u}$$

$$A_{20} = e''\theta \tag{5-184v}$$

$$A_{21} = e'' A_{20} \tag{5-184w}$$

$$A_{22} = A_{20} \tan\left(\frac{i''}{2}\right) \tag{5-184x}$$

$$A_{23} = \eta^2 A_{17} \tag{5-184y}$$

$$A_{24} = A_{11} + 2 \tag{5-184z}$$

$$A_{25} = 16A_{15} + 40A_{16} + 3 \tag{5-184aa}$$

$$A_{26} = \frac{1}{8} A_{21}(11 + 200A_{16} + 80A_{15}) \tag{5-184bb}$$

and

$$B_1 = \eta(A_1 - A_2) - \left[\frac{1}{16}(A_{10} - 400A_{14} - 40A_{13} - 11A_{12}) + \frac{1}{8}A_{21}(11 + 200A_{16} + 80A_{15})\right]\gamma_2' + \frac{5}{24}[-80A_{14} - 8A_{13} - 3A_{12} + 2A_{25}A_{21} + A_{10}]\frac{\gamma_4'}{\gamma_2'} \quad (5\text{-}185a)$$

$$B_2 = A_6 A_{18}[2 + \eta - (e'')^2] + \frac{5}{64}A_5 A_{18}\eta^2 - \frac{15}{32}A_4 A_{17}\eta^3 + A_{20}\tan\left(\frac{i''}{2}\right)\left[\frac{5}{64}A_5 + A_6\right] + \frac{5}{64}A_4 A_{17}[9(e'')^2 + 26] + \frac{15}{32}A_3 A_{20} A_{25}\sin i''(1 - \theta) \quad (5\text{-}185b)$$

$$B_3 = \frac{35}{576}\frac{\gamma_5'}{\gamma_2'}e''\sin i''(\theta - 1)A_{21}[80A_{16} + 5 + 32A_{15}] - \frac{35}{1152}\frac{A_8}{e''}\left\{A_{21}\tan\left(\frac{i''}{2}\right) + [2(e'')^2 + 3(1 - \eta^3)]\sin i''\right\} \quad (5\text{-}185c)$$

$$B_4 = \eta e''(A_1 - A_2) \quad (5\text{-}185d)$$

$$B_5 = \eta\left\{\frac{5}{64}A_4 A_9[9(e'')^2 + 4)] + A_7\right\} \quad (5\text{-}185e)$$

$$B_6 = \frac{35}{384}\eta^3 A_8 \sin i'' \quad (5\text{-}185f)$$

$$B_7 = \eta^2 A_{17} A_1'\left[\frac{1}{8}\gamma_2'(1 - 15\theta^2) - \frac{5}{12}\frac{\gamma_4'}{\gamma_2'}(1 - 7\theta^2)\right] \quad (5\text{-}185g)$$

$$B_8 = \frac{5}{64} A_3 \eta^2 (1 - 9\theta^2 - 24\theta^4 A_1') + \eta^2 A_6 \tag{5-185h}$$

$$B_9 = \frac{35}{384} \eta^2 A_8 \tag{5-185i}$$

$$B_{10} = \sin i'' \left[\frac{5}{12} \frac{\gamma_4'}{\gamma_2'} A_{21} A_{25} - A_{26} \gamma_2' \right] \tag{5-185j}$$

$$B_{11} = A_{21} \left[\frac{5}{64} A_5 + A_6 + \frac{15}{32} A_3 A_{25} \sin^2 i'' \right] \tag{5-185k}$$

$$B_{12} = - \left[(80A_{16} + 32A_{15} + 5) \left(\frac{35}{576} \frac{\gamma_5'}{\gamma_2'} e'' \sin^2 i'' A_{21} \right) + \frac{35}{1152} A_8 A_{20} \right] \tag{5-185ℓ}$$

$$B_{13} = e'' (A_1 - A_2) \tag{5-185m}$$

$$B_{14} = \frac{5}{64} A_5 \eta^2 \sin i'' + A_7 \tag{5-185n}$$

$$B_{15} = \frac{35}{384} A_8 \eta^2 \sin i'' \tag{5-185o}$$

The mean value of the eccentric anomaly E'' is obtained iteratively from Kepler's equation

$$E'' - e'' \sin E'' = \ell'' \tag{5-186}$$

The mean true anomaly f'', the mean radial distance r'', and the ratio of the mean semi-major axis and the mean radial distance are given by

$$f'' = \tan^{-1} \left[\frac{\sqrt{1 - (e'')^2} \sin E''}{\cos E'' - e''} \right] \tag{5-187}$$

$$r'' = a''(1 - e'' \cos E'') \tag{5-188}$$

$$\frac{a''}{r''} = \frac{1}{(1 - e'' \cos E'')} \tag{5-189}$$

5.11 INTERMEDIATE ORBIT

The Intermediate Orbit methods used in GTDS (Reference 20) are semianalytic methods which combine analytic theory and numerical integration. The solution to a simpler problem obtained by means of an analytic theory is used as a reference solution, and the difference is the time rate of change between the true solution and this reference solution is integrated to obtain the true solution. Either a Variation of Parameters or an Encke approach can be used in the development of these methods. Using Intermediate Orbit methods causes the quantities on the right-hand side of the resulting differential equations to vary slowly and smoothly with time, making them more amenable to numerical integration methods (i.e., more numerically stable) than the original differential equations.

Intermediate Orbit methods can be developed for any analytical theory; however, only two intermediate orbits have been considered for implementation in GTDS. The first is an orbit in which short-period effects due to J_2 have been eliminated using the Brouwer theory. The second is the orbit resulting from J_2 perturbations using the complete Brouwer theory for secular, long-period, and short-period perturbations. The equations of motion are better conditioned for numerical integration when they are smoothed by removal of fast varying short-period J_2 effects or when made slower and smoother varying by using the complete Brouwer theory to remove secular, long-period, and short-period perturbations arising from J_2. Orbits of small eccentricity and low inclination can be considered by an option that uses the same intermediate orbits as above but which are expressed in Poincaré rather than Delaunay variables.

Efficient numerical integration is achieved through minimizing local error by an appropriate choice of a uniformization constant, n. This involves selection of a new independent variable, s, related to the time t by

$$ds = \frac{\sqrt{\mu}}{r^n} dt \tag{5-190}$$

where

r = magnitude of the satellite's position vector

μ = gravitational constant

n = uniformization constant

To a considerable extent, the optimum choice of n depends on the dominant perturbation affecting the orbit under consideration. Thus, for the Intermediate Orbit method based on short-period J_2 perturbations, the main portion of J_2 must be modeled, leading to a choice of n = 2. However, the Intermediate Orbit method using the full Brouwer theory may still require a selection of n = 2 (or higher for an elliptic orbit) if the orbit is significantly perturbed by drag. If the intermediate orbit is out of the high-drag region, then the choice of n depends upon the ellipticity of the orbit and whether or not third-body perturbations are significant.

GTDS's full Brouwer intermediary is an osculating Keplerian orbit that changes due to J_2, the coefficient of the second zonal harmonic. Perturbations due to J_2 dominate those caused by other gravitational harmonics, third bodies, drag, etc., for many close-Earth satellites. While other secular perturbations eventually cause the intermediate and true orbit to become widely separated, the GTDS intermediary stays near the true orbit much longer than the two-body solution.

5.12 VINTI THEORY

Vinti theory is a General Perturbation Method. In an approach similar to that of Brouwer, the dependent variable set is chosen such that the Hamilton-Jacobi equations of motion are separable. Of the 11 coordinate systems that have this property, oblate spheroidal coordinates ϱ, η, θ are chosen since they are most appropriate for describing motion about an oblate Earth. These coordinates are related to the rectangular position coordinates as follows:

$$x + iy = (\varrho^2 + c^2)(1 - \eta^2)^{1/2} e^{i\phi} \tag{5-191a}$$

$$z = \varrho \eta \tag{5-191b}$$

where

$$c^2 = R_3^2 J_2 \left(1 - \frac{1}{4} J_3^2 J_2^{-3}\right) \tag{5-192a}$$

$$i = \sqrt{-1} \tag{5-192b}$$

and

R_e = mean equatorial radius of the Earth

J_2, J_3 = coefficients of the zonal harmonics (see Section 4.3.1)

On the other hand, Brouwer theory was developed in terms of elliptic coordinates, which are most appropriate for describing motion about a point-mass body.

Vinti obtains an analytic solution for perturbed satellite motion arising from a potential of the form

$$V = -\mu(\varrho^2 + c^2 \eta^2)^{-1} (\varrho + \eta \delta) \tag{5-193}$$

where

$$\delta = -\frac{1}{2} R_e J_2^{-1} J_3 \tag{5-194}$$

The above potential leads to a fit of the gravitational potential

$$V = -\frac{\mu}{r}\left\{1 - \sum_{n=2}^{\infty}\left[\left(\frac{R_e}{r}\right)^n J_n P_n(\sin \theta)\right]\right\} \tag{5-195}$$

exactly for the second zonal harmonic and about two-thirds of the fourth zonal harmonic.

The resulting solution gives the periodic terms correctly to order J_2^2 and the secular terms for the intermediate orbit to arbitrarily high order. The mathematical details are given in

Reference 21. This method for treating the effects of J_3 eliminates singularities for small eccentricities and for small or 180-degree inclinations, which usually occur in perturbation theories. Thus, Vinti theory is particularly appropriate for computation of polar and circular equatorial orbits.

5.13 REFERENCES

1. Brouwer, D.: 1959, "Solution of the Problem of Artificial Satellite Theory Without Drag," *Astronomical Journal*, 64(1274), November 1959, pp. 378-397.

2. Henrici, P.: 1962, *Discrete Variable Methods in Ordinary Differential Equations*, John Wiley & Sons, Inc., New York.

3. Lapidus, L. and Sunfeld, J.: 1971, *Numerical Solution of Ordinary Differential Equations*, Academic Press, Inc., New York.

4. Stiefel, E. L. and Scheifele, G.: 1971, *Linear and Regular Celestial Mechanics*, Springer-Verlag, New York.

5. Scheifele, G. and Stiefel, E.: 1972, *Canonical Satellite Theory*, Report to ESRO, prepared under ESOC Contract No. 219/70/AR, February 1972.

6. Scheifele, G.: 1973, *Numerical Orbit Computation Based on a Canonical Intermediate Orbit*, Report to ESRO, prepared under ESOC Contract No. 490/72/AR, September 1973, with Appendix by S. Samway.

7. Samway, R. C.: 1973, *A Special Perturbation Method Based on Canonical Delaunay-Similar Elements with the True Anomaly as the Independent Variable*, Applied Mechanics Research Laboratory Report 1054, July 1973.

8. Petrovski, I. G.: 1973, *Ordinary Differential Equations*, (R. A. Silverman, editor and translator), Dover Publications, Inc., New York.

9. Feagin, T.: 1973, *Description of the Numerical Integration of the Equations of Motion of a Space Vehicle Using Chebyshev Series*, Goddard Space Flight Center Report X582-73-176, June 1973.

10. Long, A. C., Nimitz, K. S., and Cefola, P. J.: 1973, *The Next Generation of Orbit Prediction Formulations for Artificial Satellites II*, Computer Sciences Corporation Report 9101-14600-01TR, March 1973.

11. Broucke, R. A.: 1970, "On the Matrizant of the Two-Body Problem," *Astronomy and Astrophysics*, 6(2), pp. 173-182.

12. Goodyear, W. H.: 1965, "Completely General Closed-Form Solution for Coordinates and Partial Derivatives of the Two-Body Problem," *Astronomical Journal*, 70(3), April 1965, pp. 189-192.

13. Cefola, P. J., Long, A. C., and Holloway, G., Jr.: 1974, "The Long-Term Prediction of Artificial Satellite Orbits," AIAA Paper No. 74-170, presented at the AIAA 12th Aerospace Sciences Meeting, Washington, D. C., January 30–February 1, 1974.

14. Velez, C. E. and Fuchs, A. J.: 1974, "A Review of Averaging Techniques and Their Application to Orbit Determination Systems," AIAA Paper No. 74-171, presented at AIAA 12th Aerospace Sciences Meeting, Washington, D. C., January 30–February 1, 1974.

15. Morrison, J. A.: 1966, "Generalized Method of Averaging and the Von Zeipel Method," in *Progress in Astronautics and Aeronautics, Vol. 17: Methods in Astrodynamics and Celestial Mechanics*, (R. L. Duncombe and V. G. Szebehely, editors), Academic Press, New York, pp. 117-138.

16. Cain, B. J.: 1967, "Determination of Mean Elements for Brouwer's Satellite Theory," *Astronomical Journal*, 67(6), August 1962, pp. 391-392.

17. Walter, H. G.: 1967, "Conversion of Osculating Orbital Elements into Mean Elements," *Astronomical Journal*, 72(8), October 1967, pp. 994-997.

18. Lyddane, R. H.: 1963, "Small Eccentricities or Inclinations in the Brouwer Theory of the Artificial Satellite," *Astronomical Journal*, 68(8), October 1963, pp. 555-558.

19. Leech, H. W.: 1974, *Evaluation of Brouwer Differential Correction and Complementary Perturbation Capability in the Definitive Orbit Determination System*, Computer Sciences Corporation Report 3000-07000-01TM, April 1974.

20. Alfriend, K. T. and Velez, C. E.: 1975, "The Application of General Perturbation Theories to the Artificial Satellite Problem," *Acta Astronautica*, Vol. 2, pp. 577-591.

21. Vinti, J. P.: 1969, "Improvement of the Spheroidal Method for Artificial Satellites," *Astronomical Journal*, 74(1), February 1969, pp. 25-34.

CHAPTER 6—NUMERICAL INTEGRATION OF THE EQUATIONS OF MOTION AND VARIATIONAL EQUATIONS

This chapter describes the Störmer-Cowell/Adams integration processes available in GTDS for the integration of the Cowell and various VOP (Chapter 5) formulations of the equations of motion. These processes were selected on the basis of several efficiency studies (References 1 and 2) comparing various classes of popular integration algorithms as applied to special perturbation techniques. This chapter also describes several single-step Runge-Kutta integration methods, which are used in GTDS for reentry predictions and as a starter for certain multistep processes.

6.1 MULTISTEP NUMERICAL INTEGRATION METHODS

Multistep methods of the type described below were found to minimize the number of derivative evaluations required to produce a given accuracy at the end of the requested interval of integration. Since, in general, the major cost in computing an orbit is the evaluation of the complex force function (Chapter 4), this implies that multistep algorithms are most efficient.

Within the class of multistep methods, options such as the following must still be selected:

1. **Type of Formulation**—Methods can be used that solve second-order systems directly (Class II), such as Störmer's method; or that normalize the second-order system into a higher dimensional first-order system and use a Class I formula, such as Adams-Bashforth.

2. **Type of Algorithm**—Several algorithms can be selected within the multistep predictor-corrector schemes, ranging from PE (prediction only) to $P(EC)^n$, $PE(CE)^n$, and $PECE^*$, where P = predict, E = evaluate derivative, C = correct, and E^* = pseudoevaluate, i.e., correct or recorrect only part of the total derivative.

3. **Order or Process**—Various order formulas can be selected to use in the algorithm, recognizing the fact that higher order formulas are more accurate but less stable.

4. **Stepsize Control**—Since the orbit dynamics can undergo large variations during a revolution (e.g., high-eccentricity orbits), an algorithm must be selected to allow stepsize variations. This can be done either by numerical monitoring of local errors or by analytic transformations of the independent variable (time regularization).

Most of the above-mentioned degrees of freedom are available in GTDS and have been studied for various problems (References 3 and 4). Some general conclusions reached are as follows:

1. For formulations involving second-order equations, Class II integrators should be used to solve the system directly, utilizing a Class I method to obtain first derivatives if required.

2. The highest possible order formula, subject only to the constraints of numerical stability, should be used.

3. Pseudoevaluate algorithms significantly increase the stability regions of predictor-corrector schemes at little or no cost in efficiency.

4. Efficiency dictates the use of stepsize control for moderate- and high-eccentricity orbits. Analytic stepsize control is more efficient and reliable than numerical stepsize control.

5. The choice of the best integrator and independent variable is highly dependent on the choice of formulation of the equations of motion. Formulation characteristics such as the regularity, or smoothness, of the dependent variables and dynamic stability influence parameters such as the numerical stability regions, choice of order, etc. As new formulations are introduced, careful matching of appropriate numerical schemes is required.

In the following sections, the multistep methods based on Newton's interpolating polynomial are derived and the basic algorithms for iteration, starting, interpolation, and stepsize control are discussed.

6.1.1 ADAMS-COWELL ORDINATE SECOND SUM FORMULAS

The formulas for the integration and interpolation of the equations of motion and the variational equations are basically of the Newtonian type derivable from standard difference operator techniques. For the integration, these formulas define the well-known predictor-corrector Adams method for first-order equations and the Cowell method for second-order systems. Formulas of the same class can be used to perform the required interpolations to determine values not given in the integration process and to form the starting set of solution values required by the predictor-corrector process.

In the following discussion, an outline of the derivations of the required formulas is given. In addition, a detailed description of the computational algorithms necessary to perform the integration is presented.

The quantities s and h denote real numbers, and the linear operators ∇, E^s, D, and I are defined as

$$\nabla f(t) = f(t) - f(t - h) \qquad \left\{\begin{matrix}\text{Backward}\\ \text{Difference}\\ \text{Operator}\end{matrix}\right\} \tag{6-1}$$

$$E^s f(t) = f(t + sh) \qquad \left\{\begin{matrix}\text{Shifting}\\ \text{Operator}\end{matrix}\right\} \tag{6-2}$$

$$D f(t) = \frac{d}{dt} f(t) = \dot{f}(t) \qquad \left\{\begin{matrix}\text{Differentiation}\\ \text{Operator}\end{matrix}\right\} \tag{6-3}$$

$$I f(t) = f(t) \qquad \left\{\begin{matrix}\text{Identity}\\ \text{Operator}\end{matrix}\right\} \tag{6-4}$$

Two well-known relations among these operators are

$$E^s = (I - \nabla)^{-s} \tag{6-5a}$$

and

$$h D = -\ln(I - \nabla) \tag{6-5b}$$

Utilizing Equations (6-5), the following operator identities can be derived:

$$E^s = h\left[\frac{(I - \nabla)^{-s}}{-\ln(I - \nabla)}\right] D \tag{6-6a}$$

$$E^s = h^2\left[\frac{(I - \nabla)^{-s}}{\{\ln(I - \nabla)\}^2}\right] D^2 \tag{6-6b}$$

Expanding the bracketed terms in a ∇ series yields

$$E^s = h\left[\nabla^{-1} + \sum_{i=0}^{\infty} \gamma'_{i+1}(s)\, \nabla^i\right] D \tag{6-7}$$

$$E^s = h^2\left[\nabla^{-2} + (s-1)\, \nabla^{-1} + \sum_{i=0}^{\infty} \gamma''_{i+2}(s)\, \nabla^i\right] D^2 \tag{6-8}$$

where $\gamma'_i(s)$ and $\gamma''_i(s)$ are given by the following recursive formulas in s (see Reference 5):

$$\gamma_0(s) = \gamma'_0(s) = \gamma''_0(s) = 1 \tag{6-9}$$

$$\gamma'_i(s) = \sum_{j=0}^{i} \gamma'_j(0)\, \gamma_{i-j}(s) \qquad (i = 0, 1, 2, \ldots, k) \tag{6-10}$$

$$\gamma''_i(s) = \sum_{j=0}^{i} \gamma''_j(0)\, \gamma_{i-j}(s) \qquad (i = 0, 1, 2, \ldots k) \tag{6-11}$$

where

$$\gamma_i(s) = \frac{s + i - 1}{i}\, \gamma_{i-1}(s) \tag{6-12}$$

and

$$\gamma'_i(0) = -\sum_{j=0}^{i-1} \frac{1}{i - j + 1}\, \gamma'_j(0) \tag{6-13}$$

$$\gamma_i''(0) = \sum_{j=0}^{i} \gamma_j'(0)\, \gamma_{i-j}'(0) \tag{6-14}$$

Applying the operators in Equations (6-7) and (6-8) to the functions $\dot{x}(t)$ and $x(t)$, respectively, and truncating after k terms, gives

$$\dot{x}(t + sh) = h\left[\nabla^{-1} \ddot{x}(t) + \sum_{i=0}^{k} \gamma_{i+1}'(s)\, \nabla^i \ddot{x}(t)\right] \tag{6-15}$$

$$x(t + sh) = h^2\left[\nabla^{-2} \ddot{x}(t) + (s - 1)\, \nabla^{-1} \ddot{x}(t) + \sum_{i=0}^{k} \gamma_{i+2}''(s)\, \nabla^i \ddot{x}(t)\right] \tag{6-16}$$

The quantities $\nabla^{-1} \ddot{x}(t)$ and $\nabla^{-2} \ddot{x}(t)$ are called the first and second sums of $\ddot{x}(t)$ and satisfy the relationships

$$\nabla^{-1} \ddot{x}(t) - \nabla^{-1} \ddot{x}(t - h) = \ddot{x}(t) \tag{6-17}$$

and

$$\nabla^{-2} \ddot{x}(t) - \nabla^{-2} \ddot{x}(t - h) = \nabla^{-1} \ddot{x}(t) \tag{6-18}$$

By varying the value for s, Equations (6-15) and (6-16) define the Adams-Cowell predictor-corrector formulas, as well as the Newtonian interpolation and starting formulas. For example, the Adams-Cowell predictor formulas are obtained by setting $s = 1$ and $x_n = x(t_n) = x(t_0 + n\,h)$ to give

$$\dot{x}_{n+1} = h\left[\nabla^{-1} \ddot{x}_n + \sum_{i=0}^{k} \gamma_{i+1}'(1)\, \nabla^i \ddot{x}_n\right] \tag{6-19}$$

and

$$x_{n+1} = h^2\left[\nabla^{-2}\,\ddot{x}_n + \sum_{i=0}^{k} \gamma''_{i+2}(1)\,\nabla^i\,\ddot{x}_n\right] \tag{6-20}$$

The preceding equations can be expressed in ordinate form as

$$\dot{x}_{n+1} = h\left[{}^{I}S_n + \sum_{i=0}^{k} \beta_i\,\ddot{x}_{n-i}\right] \tag{6-21}$$

$$x_{n+1} = h^2\left[{}^{II}S_n + \sum_{i=0}^{k} \alpha_i\,\ddot{x}_{n-i}\right] \tag{6-22}$$

where

$${}^{I}S_n = \nabla^{-1}\,\ddot{x}_n \tag{6-23}$$

$${}^{II}S_n = \nabla^{-2}\,\ddot{x}_n \tag{6-24}$$

The coefficients α_i and β_i can be expressed as functions of γ'_i and γ''_i from the recursive relations given by Equations (6-9) through (6-14); for example,

$$\alpha_i = (-1)^i \sum_{m=i}^{k} \binom{m}{i} \gamma''_{m+2}(1) \qquad (i = 0,\ 1,\ 2,\ \ldots\ k) \tag{6-25}$$

The Adams-Cowell corrector formulas are obtained from Equations (6-15) and (6-16) by setting $s = 0$ and $t = t_{n+1}$, yielding

$$\dot{x}_{n+1} = h\left[{}^{I}S_n + \sum_{i=0}^{k} \beta_i^{*}\,\ddot{x}_{n+1-i}\right] \tag{6-26}$$

and

$$x_{n+1} = h^2 \left[{}^{II}S_n + \sum_{i=0}^{k} a_i^* \ddot{x}_{n+1-i} \right] \tag{6-27}$$

where a_i^* and β_i^* are computed analogously to a_i and β_i but using $\gamma_i''(0)$ and $\gamma_i'(0)$. The quantities β_i and β_i^* are called the summed ordinate Adams-Moulton predictor-corrector coefficients, and a_i and a_i^* are the corresponding Störmer-Cowell coefficients. These coefficients are tabulated in rational form in Reference 5 for formulas of order 4 through 15.

6.1.2 PREDICT-PSEUDOCORRECT ALGORITHM FOR THE EQUATIONS OF MOTION

The concept of pseudoevaluation is introduced as a device that helps stabilize the numerical integration at little or no cost in computation. In a predictor-corrector scheme, the numerical stability region is proportional to the number of derivative evaluations within a given step (Reference 6). For systems of the form

$$\dot{x} = f(x) + \epsilon\, g(x) \tag{6-28}$$

where ϵ is a small parameter, the stability region is mainly influenced by the f(x) term.

The idea, then, is to introduce into a predictor-corrector algorithm designed to solve the above system a pseudoevaluation, i.e., a partial evaluation of $\dot{x}$, where f(x) is recomputed using the latest corrected value of x and g(x) is reused based on a previous value of x. For example, if the equations to be integrated have the form

$$\ddot{\bar{R}} = \frac{-\mu \bar{R}}{R^3} + \bar{P}(t, \bar{R}, \dot{\bar{R}}) \tag{6-29}$$

where the first term represents the primary attracting body acting on the satellite, the perturbing acceleration $\bar{P}(t, \bar{R}, \dot{\bar{R}})$ is comparatively small, and given the accelerations $\ddot{\bar{R}}(t_{n-i})$ and the sums

$${}^{I}S_n = \nabla^{-1} \ddot{\bar{R}}_n \qquad (i = 0, 1, 2, \ldots k) \tag{6-30a}$$

$${}^{II}S_n = \nabla^{-2} \ddot{\bar{R}}_n \qquad (i = 0, 1, 2, \ldots k) \tag{6-30b}$$

then the iterative algorithm to advance to time t_{n+1} is as follows:

1. **Predict**. Using Equations (6-21) and (6-22), predict values (denoted by superscript p)

$$\bar{R}^{(p)}(t_{n+1}) = \left[X_{n+1}^{(p)},\ Y_{n+1}^{(p)},\ Z_{n+1}^{(p)}\right] \tag{6-31a}$$

$$\dot{\bar{R}}^{(p)}(t_{n+1}) = \left[\dot{X}_{n+1}^{(p)},\ \dot{Y}_{n+1}^{(p)},\ \dot{Z}_{n+1}^{(p)}\right] \tag{6-31b}$$

2. **Evaluate**. Using Equation (6-29), evaluate

$$\ddot{\bar{R}}(t_{n+1}) = \frac{-\mu\,\bar{R}_{n+1}^{(p)}}{R_{n+1}^{(p)3}} + P\left[t_{n+1},\ \bar{R}_{n+1}^{(p)},\ \dot{\bar{R}}_{n+1}^{(p)}\right] \tag{6-32}$$

3. **Correct**. Using Equations (6-26) and (6-27) obtain the improved values (denoted by the superscript c) $\bar{R}_{n+1}^{(c)}$ and $\dot{\bar{R}}_{n+1}^{(c)}$.

4. **Test**. Compare the magnitude of the vector $[\bar{R}^{(p)}(t_{n+1}) - \bar{R}^{(c)}(t_{n+1})]$ against a prescribed tolerance. If this quantity is sufficiently small, proceed to step 5; otherwise, replace the values $\bar{R}^{(p)}$ and $\dot{\bar{R}}^{(p)}$ with $\bar{R}^{(c)}$ and $\dot{\bar{R}}^{(c)}$ and repeat steps 2 through 4.

5. **Pseudocorrect**. Compute the acceleration

$$\ddot{\bar{R}}(t_{n+1}) = \frac{-\mu\,\bar{R}_{n+1}^{(c)}}{R_{n+1}^{(c)3}} + P\left[t_{n+1},\ \bar{R}_{n+1}^{(p)},\ \dot{\bar{R}}_{n+1}^{(p)}\right] \tag{6-33}$$

   where the P term is obtained from step 2.

6. **Update Sums**. Compute the updated sums

$${}^{I}S_{n+1} = {}^{I}S_n + \ddot{\bar{R}}(t_{n+1}) \tag{6-34}$$

$${}^{II}S_{n+1} = {}^{II}S_n + {}^{I}S_{n+1} \tag{6-35}$$

The computational cycle (steps 1 through 6) can then be repeated with n = n + 1.

In n-body or Earth-Moon trajectory computations, the equations of motion will frequently be independent of the velocity term, $\dot{\bar{R}}$; i.e., the acceleration is of the form

$$\ddot{\bar{R}} = \frac{-\mu \bar{R}}{R^3} + P(t, \bar{R}) \tag{6-36}$$

For trajectory segments possessing this characteristic, the preceding computational cycle can be simplified: in step 1, the predicted $\dot{\bar{R}}^{(p)}$ need not be computed; and in step 3, the provisional corrected values $\dot{\bar{R}}^{(c)}$ are not required. After the test in step 4 is satisfied, $\dot{\bar{R}}^{(c)}$ can be obtained by one application of the corrector formula in Equation (6-26).

For the case of the integration of VOP type formulations, the concept of pseudoevaluation should be extended to include the major perturbation beyond the central force, in particular, J_2 for near-Earth satellites. This is due to the fact that in these formulations the stability is governed by the principal perturbations. The central force contribution is analytically integrated and, hence, does not influence numerical stability.

6.1.3 CORRECTOR-ONLY COWELL INTEGRATION FOR LINEAR SYSTEMS

From the Adams-Cowell corrector equations, the following closed-form equations can be derived when the equation being integrated is linear:

$$y_{n+1} = h^2 \left[{}^{II}S_n + \sum_{i=0}^{k} a_i^* \ddot{y}_{n+1-i} \right] \tag{6-37}$$

$$\dot{y}_{n+1} = h \left[{}^{I}S_n + \sum_{i=0}^{k} \beta_i^* \ddot{y}_{n+1-i} \right] \tag{6-38}$$

Such a linear equation is

$$\ddot{y} = a(t)\, y + b(t)\, \dot{y} + f(t) \tag{6-39}$$

where a(t), b(t), and f(t) are known time-varying functions.

Equations (6-37) and (6-38) can be written as

$$y_{n+1} = h^2\left[{}^{II}S_n + \alpha_0^* \ddot{y}_{n+1} + \sum_{i=1}^{k} \alpha_i^* \ddot{y}_{n+1-i}\right] \tag{6-40}$$

and

$$\dot{y}_{n+1} = h\left[{}^{I}S_n + \beta_0^* \ddot{y}_{n+1} + \sum_{i=1}^{k} \beta_i^* \ddot{y}_{n+1-i}\right] \tag{6-41}$$

By expanding the derivative $\ddot{y}_{n+1}$, the following are obtained:

$$y_{n+1} = h^2\left[{}^{II}S_n + \alpha_0^* a_{n+1} y_{n+1} + \alpha_0^* b_{n+1} \dot{y}_{n+1} + \alpha_0^* f_{n+1} + \sum_{i=1}^{k} \alpha_i^* \ddot{y}_{n+1-i}\right] \tag{6-42}$$

$$\dot{y}_{n+1} = h\left[{}^{I}S_n + \beta_0^* a_{n+1} y_{n+1} + \beta_0^* b_{n+1} \dot{y}_{n+1} + \beta_0^* f_{n+1} + \sum_{i=1}^{k} \beta_i^* \ddot{y}_{n+1-i}\right] \tag{6-43}$$

Defining the known quantities

$$x_n = h^2\left[{}^{II}S_n + \alpha_0^* f_{n+1} + \sum_{i=1}^{k} \alpha_i^* \ddot{y}_{n+1-i}\right] \tag{6-44}$$

$$v_n = h\left[{}^{I}S_n + \beta_0^* f_{n+1} + \sum_{i=1}^{k} \beta_i^* \ddot{y}_{n+1-i}\right] \tag{6-45}$$

and the matrix

$$H = \begin{bmatrix} h^2 \alpha_0^* a_{n+1} & h^2 \alpha_0^* b_{n+1} \\ h \beta_0^* a_{n+1} & h \beta_0^* b_{n+1} \end{bmatrix} \tag{6-46}$$

then Equations (6-42) and (6-43) can be written as

$$\begin{bmatrix} y_{n+1} \\ \dot{y}_{n+1} \end{bmatrix} = H \begin{bmatrix} y_{n+1} \\ \dot{y}_{n+1} \end{bmatrix} + \begin{bmatrix} x_n \\ v_n \end{bmatrix} \tag{6-47}$$

The solution to Equation (6-47) is

$$\begin{bmatrix} y_{n+1} \\ \dot{y}_{n+1} \end{bmatrix} = [I - H]^{-1} \begin{bmatrix} x_n \\ v_n \end{bmatrix} \tag{6-48}$$

It should be noted that the inverse in the preceding equation will always exist if h is sufficiently small. The inverse depends only on the coefficients a and b and need be computed only once when solving equations of the form of Equation (6-39) with different nonhomogeneous terms f(t).

6.1.4 CORRECTOR-ONLY ALGORITHM FOR VARIATIONAL EQUATIONS

In the Cowell formulation, the position and velocity partial derivatives of the satellite motion with respect to any parameter appearing in the acceleration model in Equation (6-29) or state (dynamic parameters) can be obtained by the numerical integration of the variational equations

$$\ddot{Y} = A(t)\, Y + B(t)\, \dot{Y} + C(t) \tag{6-49}$$

from initial conditions at t_0 given by

$$Y(t_0) = \frac{\partial \bar{R}(t_0)}{\partial \bar{p}} \tag{6-50a}$$

$$\dot{Y}(t_0) = \frac{\partial \dot{\bar{R}}(t_0)}{\partial \bar{p}} \tag{6-50b}$$

where

$$A(t) = \left[\frac{\partial \ddot{\bar{R}}(t)}{\partial \bar{R}}\right]_{3x3} \tag{6-51}$$

$$B(t) = \left[\frac{\partial \ddot{\bar{R}}(t)}{\partial \dot{\bar{R}}}\right]_{3x3} \tag{6-52}$$

$$C(t) = \left[\frac{\partial \ddot{\bar{R}}(t)}{\partial \bar{p}}\right] \quad \begin{pmatrix} 3 \times \ell \text{ matrix of} \\ \text{acceleration partial derivatives} \end{pmatrix} \tag{6-53}$$

$$Y(t) = \left[\frac{\partial \bar{R}(t)}{\partial \bar{p}}\right] \quad \begin{pmatrix} 3 \times \ell \text{ matrix of} \\ \text{position partial derivatives} \end{pmatrix} \tag{6-54}$$

and

$$\dot{Y}(t) = \left[\frac{\partial \dot{\bar{R}}(t)}{\partial \bar{p}}\right] \quad \begin{pmatrix} 3 \times \ell \text{ matrix of} \\ \text{velocity partial derivatives} \end{pmatrix} \tag{6-55}$$

The vector $\bar{p}$ contains the parameters in the acceleration model that are being estimated. The components of the matrices A, B, and C were developed in Chapter 4.

Optionally, the components of $\bar{p}$ correspond to the spacecraft's position and velocity at epoch and can be expressed in mean of B1950.0 or J2000.0 Cartesian coordinates, true of date Cartesian coordinates, classical Keplerian orbital elements, spherical coordinates, or DODS variables. The initial conditions for the variational equations, Equation (6-49), are

dependent upon the coordinate systems selected. The partial derivatives of $\bar{R}$ and $\dot{\bar{R}}$ with respect to Keplerian elements and spherical coordinates can be obtained from Sections 3.3.8 and 3.3.4, respectively. Since the first six elements of $\bar{p}$ are the state vector, the first six columns of C are zero. Most model parameters such as thrust, drag, harmonic coefficients, etc., enter into $P(t, \bar{R}, \dot{\bar{R}})$ of Equation (6-29) linearly, so that the computation of C(t) can be simplified by retaining many of the quantities used in the computation of $\ddot{\bar{R}}(t)$.

The integration of system Equation (6-49) can be performed by the utilization of the corrector-only formula Equation (6-48) as described below.

Assuming that the satellite position and velocity, $\bar{R}(t_{n-i})$ and $\dot{\bar{R}}(t_{n-i})$, the matrices $\ddot{Y}_{n+1-i}$ ($i = 1, 2, \ldots k$), and the summation matrices ${}^{I}P_n$ and ${}^{II}P_n$ ($3 \times \ell$) are known, then the algorithm to advance Y to time t_{n+1} is as follows:

1. Compute the matrices $A(t_{n+1})$, $B(t_{n+1})$, and $C(t_{n+1})$, which depend only on t_{n+1}, $\bar{R}_{n+1}$, and $\dot{\bar{R}}_{n+1}$.

2. Compute the 6×6 matrix $[I - H]^{-1}$, where

$$H = \begin{bmatrix} h^2 \alpha_0^* A_{n+1} & h^2 \alpha_0^* B_{n+1} \\ h \beta_0^* A_{n+1} & h \beta_0^* B_{n+1} \end{bmatrix} \tag{6-56}$$

   and α_i^* and β_i^* are the corrector coefficients of Equations (6-26) and (6-27) and h is the stepsize.

3. Form the $3 \times \ell$ matrices, X_n and V_n, as

$$X_n = h^2 \left[{}^{II}P_n + \sum_{i=1}^{k} \alpha_i^* \ddot{Y}_{n+1-i} + \alpha_0^* C_{n+1} \right] \tag{6-57}$$

$$V_n = h \left[{}^{I}P_n + \sum_{i=1}^{k} \beta_i^* \ddot{Y}_{n+1-i} + \beta_0^* C_{n+1} \right] \tag{6-58}$$

4. Compute the required position and velocity partial derivatives, Y_{n+1} and $\dot{Y}_{n+1}$, by the matrix equation

$$\begin{bmatrix} Y_{n+1} \\ \dot{Y}_{n+1} \end{bmatrix}_{6\times\ell} = [I - H]^{-1}_{6\times 6} \begin{bmatrix} X_n \\ V_n \end{bmatrix}_{6\times\ell} \tag{6-59}$$

5. Complete the cycle by updating the acceleration partial derivatives and sums by

$$\ddot{Y}_{n+1} = A_{n+1}\, Y_{n+1} + B_{n+1}\, \dot{Y}_{n+1} + C_{n+1} \tag{6-60}$$

$${}^{I}P_{n+1} = {}^{I}P_n + \ddot{Y}_{n+1} \tag{6-61}$$

$${}^{II}P_{n+1} = {}^{II}P_n + {}^{I}P_{n+1} \tag{6-62}$$

After $\bar{R}_{n+2}$ and $\dot{\bar{R}}_{n+2}$ are computed, steps 1 through 5 can be repeated with $n = n + 1$.

For cases where the perturbing acceleration $\bar{P}$ in Equation (6-29) is independent of the velocity, the matrix B in Equation (6-49) is zero, so that the variational equations reduce to

$$\ddot{Y} = A(t)\, Y + C(t) \tag{6-63}$$

As in the case of the equations of motion, the computational algorithm can then be simplified. Specifically, in step 1 only the matrices A and C are required, and in step 2 the matrix H becomes the 3×3 matrix

$$H = h^2 a_0^* A_{n+1} \tag{6-64}$$

The required partial derivatives are then given by

$$Y_{n+1} = [I - H]^{-1} X_n \tag{6-65}$$

$$\dot{Y}_{n+1} = h \beta_0^* A_{n+1} Y_{n+1} + V_n \tag{6-66}$$

The order and stepsize used in the integration of the variational equations can differ from that used in the integration of the equations of motion without any significant difficulty.

6.1.5 MULTISTEP INTERPOLATION

The multistep interpolator uses the first and second ordinate sums and the backpoints (accelerations) computed during multistep integration to compute the spacecraft position and velocity and the associated partial derivatives (if desired) at a request time.

For the most efficient use of the multistep integration techniques, the values at the request time, t, of the integrated position and velocity of the variational equations are produced by interpolation from the stored accelerations (backpoints) and the first and second ordinate sums. When the time-regularized equations of motion (Section 5.3) are integrated, an additional interpolation is required to determine the time-regularized independent variable, s, at the request time.

6.1.5.1 Multistep Interpolation With Fixed-Step Integration

The general summed form of the Adams predictor/corrector equation at a point (t + sh) is

$$\dot{x}(t + sh) = h\left[{}^{I}S_n + \sum_{j=0}^{k} (-1)^j \sum_{i=j}^{k} \gamma'_{i+1}(s) \binom{i}{j} \ddot{x}(t - jh)\right] \qquad (6\text{-}67)$$

and the Cowell predictor/corrector at (t + sh) is

$$x(t + sh) = h^2\left[{}^{II}S_n + (s - 1)\,{}^{I}S_n + \sum_{j=0}^{k} (-1)^j \sum_{i=j}^{k} \gamma''_{i+2}(s) \binom{i}{j} \ddot{x}(t - jh)\right] \qquad (6\text{-}68)$$

where

- $s = 1$ and $t = t_n$ for the Adams-Bashforth and Störmer-Cowell predictor equations (Equations (6-21) and (6-22))
- $s = 0$ and $t = t_{n+1}$ for the Adams-Moulton and Cowell corrector equations (Equations (6-26) and (6-27))
- $-1 < s < 0$ and $t = t_n$ for interpolation

The quantities $\gamma'(s)$ and $\gamma''(s)$ are parameters used in computing the coefficients of $\ddot{x}$.

When s is equal to 0 or 1 and the order of the integration method has been chosen, then the coefficients of the accelerations ($\ddot{x}$) can be precomputed. When interpolation is being performed, however, the coefficients must be recomputed for each requested time, t_r, where

$$t_r = \frac{s - t_n}{h} \tag{6-69}$$

The multistep interpolation algorithm is as follows:

1. Compute constants $\gamma_i'(0)$ and $\gamma_i''(0)$, to be utilized in later calculations, using Equations (6-13) and (6-14) with

$$\gamma_0'(0) = 1 \tag{6-70}$$

for i = 1, 2, ..., k, where

k+1 = order of Adams Class I integrator
k+2 = order of Cowell Class II integrator

2. Let $s = \frac{t - t_n}{h}$ in the following steps, where

t_n = time associated with the most recent entry in the backpoints table, $\ddot{x}_n$
t = request time
h = step size

3. Compute $\gamma_i(s)$ (where i = 0, 1, ..., k+2) using Equations (6-9) and (6-12).
4. Compute $\gamma'(s)$ (where i = 0, 1, ..., k+1) using Equations (6-9) and (6-10).
5. Compute $\delta'(s)$ (where i = 0, 1, ..., k)

$$\delta_0'(s) = \sum_{j=1}^{k+1} \gamma_i'(s) \tag{6-71}$$

$$\delta_i'(s) = (-1)^i \left[\gamma_{i+1}'(s) + \sum_{j=i+2}^{k+1} \binom{j-1}{i} \gamma_j'(s) \right] \tag{6-72}$$

The quantity $\binom{m}{i}$ is computed as $\frac{m!}{(m-i)!\, i!}$, and

$$\delta_k'(s) = \gamma_{k+1}'(s) \tag{6-73}$$

In the above expressions, i = 1, 2, ..., k–1.

6. Compute the velocity as follows:

$$\dot{x}(t) = \dot{x}(t_n + sh) = h \left[{}^{I}S_n + \sum_{i=0}^{k} \delta_i'(s)\, \ddot{x}_{n-i} \right] \tag{6-74}$$

where

$^{I}S_n$ = first ordinate sums
$\ddot{x}$ = accelerations in the backpoints table
n = number of accelerations in the backpoints table

and s, h, and $\delta_i'(s)$ have been defined previously.

7. Compute $\gamma''(s)$ (where i = 0, 1, ..., k+2) using Equations (6-9) and (6-11).

8. Compute $\delta_i''(s)$ (where i = 0, 1, ..., k)

$$\delta_0''(s) = \sum_{i=2}^{12} \gamma_j''(s) \tag{6-75}$$

$$\delta_i''(s) = (-1)^i \left[\gamma_{i+1}''(s) + \sum_{j=i+3}^{k+2} \binom{j-2}{i} \gamma_j''(s) \right] \tag{6-76}$$

where i = 1, 2, ..., k–1, and

$$\delta_k''(s) = \gamma_{k+2}''(s) \tag{6-77}$$

9. Compute the position

$$x(t) = x(t_n + sh) = h^2 \left[{}^{II}S_n + (s-1)\,{}^{I}S_n + \sum_{i=0}^{k} \delta_i''(s)\,\ddot{x}_{n-1} \right] \tag{6-78}$$

where

${}^{I}S_n$ and ${}^{II}S_n$	=	first and second ordinate sums
$\ddot{x}$	=	accelerations in the backpoints table
n	=	number of accelerations in the backpoints table

and s, h, and $\delta_i''(s)$ have been defined previously.

6.1.5.2 Multistep Interpolation With Time-Regularized Integration

When the integration is performed with regularized time as the independent variable, an additional interpolation is required to determine the value of the independent variable, s_r, that corresponds to the requested time, t_r. Reference 7 discusses the precision of the interpolation when precomputed files of the accelerations and first and second sums are used.

When first and second sums are available for each backpoint (i.e., during the integration), a technique similar to that described for the fixed-step integration, but requiring additional steps for convergence of s_r, is used. If the sums are not available at each step (such as when accelerations are retrieved from precomputed data files), then this technique is not sufficiently precise (see Reference 7).

6.1.6 THE STARTING PROCEDURE

Two starting procedures are available in GTDS, an iterative method and a Runge-Kutta method. The iterative starter is generally used; however, the Runge-Kutta method can optionally be used as a starter for multistep integration methods.

6.1.6.1 Iterative Starter

The starting arrays $\ddot{\bar{R}}_{n-i}$, $\ddot{Y}_{n-i}$ (i = 0, 1, 2, ... k) and the associated first and second sums required by the integration process can be computed by an iterative procedure based on Equations (6-15) and (6-16) using varying values for s. If m = [(k + 1)/2], where the brackets indicate the greatest integer function, and $\bar{R}_0$, $\dot{\bar{R}}_0$, and $\ddot{\bar{R}}_0$ are the given initial values at t = t_0 of Equation (6-29) (the process is analogous for Equation (6-49)), then the values $\bar{R}_i$, $\dot{\bar{R}}_i$, and $\ddot{\bar{R}}_i$ (i = ± 1, ± 2, · · · ± m) can be computed by successive approximations, yielding the required starting values.

Let $\delta_i'(s)$ and $\delta_i''(s)$ be the coefficients of the ordinate forms of Equations (6-15) and (6-16), with k = 2m; then,

$$\dot{x}(t_n + sh) = h\left[{}^{I}S_n + \sum_{i=0}^{2m} \delta_i'(s)\, \ddot{x}_{n-i}\right] \tag{6-79}$$

$$x(t_n + sh) = h^2\left[{}^{II}S_n + (s - 1)\,{}^{I}S_n + \sum_{i=0}^{2m} \delta_i''(s)\, \ddot{x}_{n-i}\right] \tag{6-80}$$

If $\ddot{\bar{R}}^{(j)}$ denotes the jth approximation, the $(j + 1)^{st}$ approximation is given by the following procedure:

1. Compute the sums ${}^{I}S_n$ and ${}^{II}S_n$ using

$${}^{I}S_m = \frac{\dot{\bar{R}}_0}{h} - \sum_{i=0}^{2m} \delta_i'(-m)\, \ddot{\bar{R}}^{(j)}_{m-1} \tag{6-81}$$

$${}^{II}S_m = \frac{\bar{R}_0}{h^2} + (m + 1)\,{}^{I}S_m - \sum_{i=0}^{2m} \delta_i''(-m)\, \ddot{\bar{R}}^{(j)}_{m-1} \tag{6-82}$$

2. Compute the corrected position and velocity vectors using Equations (6-80) and (6-79), with n = m and s = (i - m), as follows:

$$\bar{R}_i^{(j+1)} = h^2\left[{}^{II}S_m + (i - m - 1)\,{}^{I}S_m + \sum_{\ell=0}^{2m} \delta_\ell''(i - m)\,\ddot{\bar{R}}_{m-\ell}^{(j)}\right] \qquad (6\text{-}83)$$

$$\dot{\bar{R}}_i^{(j+1)} = h\left[{}^{I}S_m + \sum_{\ell=0}^{2m} \delta_\ell'(i - m)\,\ddot{\bar{R}}_{m-\ell}^{(j)}\right] \qquad (6\text{-}84)$$

where $i = \pm 1, \pm 2, \ldots \pm m$

3. Compute the acceleration, $\ddot{\bar{R}}_j^{(j+1)}$, using the force model. This completes the iteration.

Steps 1 through 3 are repeated until the successive values of $\bar{R}_i$ and $\dot{\bar{R}}_i$ converge.

As in the process described in Section 6.2, if the accelerations are velocity free, simplifications in the computational algorithm can be made. Specifically, in step 2 the computation of $\dot{\bar{R}}_j^{(j+1)}$ can be omitted until convergence on the positions $\bar{R}_i$.

The first approximation (j = 1) can be obtained by a variety of methods. Near a primary, two-body analysis can be used effectively, either in the form of orbital elements or f and g series. Between two primaries, either a single-step, low-order method or a prestored ephemeris should be used.

6.1.6.2 Runge-Kutta Starter

The multistep methods avoid the multiple function evaluations at each integration step that are characteristic of the Runge-Kutta method, but they are not self-starting. Starting from an initial position and velocity, the Runge-Kutta method presented in Section 6.2.1 can be used to build the required starting array for the Cowell and Time Regularized Cowell equations of motion and variational equations.

6.1.7 LOCAL ERROR CONTROL

Local error control for the multistep integrator can be performed by changing the integration stepsize to minimize the local truncation error. The stepsizes can be set by distance

from the central body or can be changed on a step-by-step basis to minimize a function approximating the local error. Since each change of the stepsize requires rebuilding the difference tables, a variation is to change the step only by halving or doubling. For highly eccentric orbits, these controls may not be sufficient. In those cases, use of time regularization (described in Section 6.4) is more satisfactory.

For automatic control of the error, stepsizes are selected based on the magnitude of the local error, ϵ_n, computed on a step-by-step basis by the Milne formula

$$\epsilon_n = \frac{C\,|\bar{R}_n^{(p)} - \bar{R}_n^{(c)}|}{|R_n^{(c)}|} \tag{6-85}$$

where C is a constant depending on the order of Equations (6-22) and (6-27). The vectors $\bar{R}_n^{(p)}$ and $\bar{R}_n^{(c)}$ are the predicted and finally accepted position vectors, respectively, computed at time $t = t_n$. The stepsizes are selected so that ϵ_n at each step satisfies the constraint equation

$$T_2 \leq \epsilon_n \leq T_1 \tag{6-86}$$

where T_1 and T_2 are specified upper and lower bounds on the local error.

The variable stepsize integration algorithm is as follows. At each step n, the test in Equation (6-86) is performed. Depending on the result of this test, one of the three following cases applies:

1. $\epsilon_n > T_1$

   The stepsize is decreased, and the nth computed point is rejected and recomputed with the new stepsize, where the required back values are obtained by interpolation.

2. $\epsilon_n > T_2$

   The stepsize is increased, the nth computed point is accepted, and the integration proceeds with the new stepsize, where the required back values are obtained by using every other point from a saved array of points if $h_{new} = 2h$ or by interpolation if $h < h_{new} < 2h$. A maximum increase of 2h is allowed.

3. ϵ_n satisfies Equation (6-95) (given in Section 6.2)

   The integration proceeds uninterrupted.

In either case 1 or 2, h_{new} is computed by the formula

$$h_{new} = h\left[\frac{T_3}{\epsilon_n}\right]^{1/k} \tag{6-87}$$

where T_3 is a specified allowable local error satisfying $T_2 \leq T_3 \leq T_1$.

When stepsizes are specified as a function of radial distances from the primary, the required stepsizes and radial distances can be determined by an integration calibration process, computing the stepsize based on the local truncation error. Since the stepsize distribution over the orbit generally depends on the orbital elements, particularly the semimajor axis and the eccentricity, such a calibration would be repeated only if these elements changed considerably. This model of integration is generally less sensitive to the numerical difficulties associated with variable stepsize integration.

The same stepsizes are used for integration of the variational equations and the equations of motion.

6.2 THE RUNGE-KUTTA INTEGRATION METHOD

The Runge-Kutta method is a numerical integration technique by which the value of the dependent variable at some future time can be calculated from a weighted summation formula, similar to a numerical quadrature. This method is equivalent to a Taylor series solution of the equations of motion up to a certain power of the integration stepsize in the independent variable. Taylor series solutions require differentiation of a given function a number of times, followed by evaluation of these derivatives at the point of interest. The Runge-Kutta method requires evaluation of the derivative at a number of selected points within the integration time step. For example, in the spacecraft equations of motion the acceleration is evaluated a number of times within each integration step to obtain the position and velocity at the end of the integration step.

Runge-Kutta methods have the advantage that the interval of integration can be readily changed. The formulas are single step; thus, they do not require any past history of values. In common with other special perturbation methods, the Runge-Kutta method is extremely flexible.

The three Runge-Kutta methods available in GTDS are the Shanks eighth-order Runge-Kutta formulation, the Hull Runge-Kutta 3(4+) integrator, and the fourth-order Runge-Kutta integrator with Gill's coefficients. These are described in the following subsections.

6.2.1 SHANKS EIGHTH-ORDER RUNGE-KUTTA FORMULAS

The Shanks Runge-Kutta formula used in GTDS is an eighth-order formulation requiring 10 function evaluations (Reference 8). The expression f(x, y) is the derivative on the right-hand side of the first-order differential equation dx/dy = f(x, y) that is to be evaluated. This function arises from the equations of motion or from the variational equations. The Shanks eighth-order Runge-Kutta algorithm is computed as described below.

The following formulas apply to a single component of the vector of the quantities being integrated, where the vector of dependent variables is denoted by $\bar{x}$ and the independent variable is denoted by y:

$$f_0 = f(\bar{x}_0, y_0) \tag{6-88a}$$

$$f_i = f(\bar{x}_0 + k_i, \; y_0 + a_i h) \qquad (i = 2, \ldots, 9) \tag{6-88b}$$

where

$$k_1 = a_1 h \, b_{1,0} \, f_0 \tag{6-89a}$$

$$k_i = a_i h \sum_{j=0}^{i} b_{2,j} \, f_j \qquad (i = 2, \ldots, 9) \tag{6-89b}$$

The next value of the component x is computed from the present value x_0 and the Shanks coefficients a_i, b_{ij}, c_i, as follows:

$$x = \bar{x}_0 + \sum_{i=0}^{9} c_i \, f_i \tag{6-90}$$

In these formulas, the Runge-Kutta stepsize in the independent variable is denoted by h and the subscript 0 designates current values. Table 6-1 contains the coefficients for the eighth-order Runge-Kutta scheme. The coefficients are presented in a form convenient for calculating the summations required to determine the k_i values.

Table 6-1. Coefficients for the Eighth-Order Runge-Kutta Scheme

INDEX I	VALUE OF THE a_I COEFFICIENT	VALUE OF $a_I \sum_{j=0}^{I-1} b_{I,j}$
1	4/27	4/27
2	2/9	1/18 (1 + 3)
3	1/3	1/12 (1 + 0 + 3)
4	1/2	1/8 (1 + 0 + 0 + 3)
5	2/3	1/54 (13 + 0 - 27 + 42 + 8)
6	1/6	1/4320 (389 + 0 - 54 + 966 - 824 + 243)
7	1	1/20 (-234 + 0 + 81 - 1164 + 656 - 122 + 800)
8	5/6	1/288 (-127 + 0 + 18 - 678 + 456 - 9 + 576 + 4)
9	1	1/820 (1481 + 0 - 81 + 7104 - 3376 + 72 - 5040 - 60+ 720)
$(c_0 + c_1 + c_2 + c_3 + c_4 + c_5 + c_6 + c_7 + c_8 + c_9) = 1/840 (41 + 0 + 0 + 27 + 272 + 27 + 216 + 0 + 216 + 41)$		

6.2.2 HULL RUNGE-KUTTA FORMULAS

The Hull Runge-Kutta 3(4+) integrator (Reference 9) is used in GTDS to perform impact computations. This Runge-Kutta method is a self-starting, single-step integration scheme that computes the value $\bar{x}(t_2)$ for some $t_2 = t_1 + \tau$ (where τ is the Runge-Kutta stepsize, $\tau > 0$), given a first-order differential equation

$$\frac{d\bar{x}}{dt} = f(t, \bar{x}) \tag{6-91}$$

with initial condition

$$\bar{x}(t_1) = \bar{x}_1 \tag{6-92}$$

where

- f = function arising from the equations of motion or the variational equations
- t = independent variable (usually time)
- $\bar{x}$ = vector of the dependent variables
- $\bar{x}_1$ = value of $\bar{x}$ at time t_1

This is accomplished by evaluating the function f at N values of t ($t_1 \leq t \leq t_2$) and using the weighted averages of these values to compute the correction to the initial value, x_1.

If

$$f_1 = f(t_1, x_1) \tag{6-93a}$$

$$f_j = f(t_1 + a_j\tau, \; x_1 + k_j) \tag{6-93b}$$

where

$$k_j = \tau \sum_{\ell=1}^{M_j} b_{j\ell} f_\ell \qquad [\text{for all } j \; (2 \leq j \leq N)] \tag{6-94}$$

then the dependent variable $x(t_2)$ is as follows:

$$x(t_2) = x(t_1 + \tau) = x_1 + \tau \sum_{j=1}^{N} c_j f_j \tag{6-95}$$

Table 6-2 gives the coefficients a_j, $b_{j\ell}$, c_j for the Hull Runge-Kutta 3(4+) method (N = 5, $M_j = j - 1$) for integration of first-order differential equations. This method is of order p, where $4 < p < 5$. An estimate of the truncation error, computed by differencing the values

of $x(t_1 + \tau)$ obtained using this integration method and a similar method of order 3, is given by

$$E(t_1 + \tau) = \tau \sum_{j=1}^{5} \delta_j f_j \tag{6-96}$$

where the values of δ_j are error coefficients given in Table 6-2 and f_j is evaluated according to the Runge-Kutta 3(4+) method. If E_{max} is a predetermined maximum that the relative truncation error

$$E_{rel} = \frac{E(t_1 + \tau)}{|x(t_1 + \tau)|} \tag{6-97}$$

is allowed to reach, then the optimum stepsize, given the initial Runge-Kutta stepsize τ, is

$$\tau_{opt} = \tau \left(\frac{E_{max}}{E_{rel}} \right)^{1/4} \tag{6-98}$$

The optimum stepsize (τ_{opt}) can be used in the Hull Runge-Kutta 3(4+) method to vary the stepsizes.

6.2.3 FOURTH-ORDER RUNGE-KUTTA FORMULAS WITH GILL'S COEFFICIENTS

The fourth-order Runge-Kutta integrator with Gill's coefficients (RKG) (Reference 10) is provided for propagation of the spacecraft state vector and the state partial derivatives. The RKG method computes the integration stepsize as a function of the eccentricity.

The equations of motion or variational equations are expressed as a set of first-order differential equations

$$\frac{d\bar{x}}{dt} = f(\bar{x}, t) \tag{6-99}$$

with the initial condition

$$\bar{x}(t_0) = \bar{x}_0 \tag{6-100}$$

Table 6-2. Coefficients for the Runge-Kutta 3(4+) Integrator (N = 5)

INDEX j	COEFFICIENTS		
	a_j	c_j	δ_j
1	0	0.10888304916410344	$-0.49939143641338931 \times 10^{-2}$
2	2/7	0.24547988976401333	$0.68461187539313607 \times 10^{-1}$
3	7/15	0.33907286031851855	-0.10922264375986756
4	35/38	0.44251397222216452	0.18170514205348768
5	1	-0.13594977146879983	-0.13594977146879983

INDEX	COEFFICIENTS $b_{j\ell}$ (M_j = j - 1)			
j \ ℓ	1	2	3	4
1	-	-		-
2	0.28571428571428571			-
3	$-0.93777509730408418 \times 10^{-1}$	0.56044417639707508	-	-
4	0.60836163032387864	-1.2040651669594905	1.5167561682145592	-
5	1.4613130509525770	-3.8111651289355121	3.6068242907277299	-0.25697221274479485

where

f = function arising from the equations of motion or variational equations

t = independent variable

$\bar{X}$ = vector of dependent variables

The procedure to advance $\bar{X}$ from t_0 to time t_R is as follows. The Runge-Kutta stepsize hour, h_r, is computed from

$$h_r = q \frac{R^2}{\sqrt{GM}} \tag{6-101}$$

where

$$q = \begin{cases} 0.01 & (\text{for } e \geq 0.2) \\ 0.5 & (\text{for } e < 0.2) \end{cases} \tag{6-102}$$

and

R = magnitude of the position vector
GM = gravitational constant of the central body

If

$$h_r > t_R - t_0 \tag{6-103}$$

then

$$h_r = t_R - t_0 \tag{6-104}$$

where t_R is the desired output time.

The parameters $\bar{x}$ are then advanced to time $t_4 = t_0 + h_r$ as follows:

$$\bar{K}_1 = h_r f(\bar{x}_0, t_0) \tag{6-105}$$

$$\bar{x}_1 = \bar{x}_0 + \frac{1}{2} \bar{K}_1 \tag{6-106}$$

$$\bar{q}_1 = \bar{K}_1 \tag{6-107}$$

$$\bar{K}_2 = h_r f(\bar{x}_1, t_0 + \frac{1}{2} h_r) \tag{6-108}$$

$$\bar{x}_2 = \bar{x}_1 + \left(1 - \sqrt{\frac{1}{2}}\right)(\bar{K}_2 - \bar{q}_1) \tag{6-109}$$

$$\bar{q}_2 = (2 - \sqrt{2})\,\bar{K}_2 + \left(3\sqrt{\frac{1}{2}} - 2\right)\bar{K}_1 \tag{6-110}$$

$$\bar{K}_3 = h_r\, f(\bar{x}_2,\ t_0 + \frac{1}{2} h_r) \tag{6-111}$$

$$\bar{x}_3 = \bar{x}_2 + \left(1 + \sqrt{\frac{1}{2}}\right)(\bar{K}_3 - \bar{q}_2) \tag{6-112}$$

$$\bar{q}_3 = (2 + \sqrt{2})\,\bar{K}_3 - \left(3\sqrt{\frac{1}{2}} + 2\right)\bar{q}_2 \tag{6-113}$$

$$\bar{K}_4 = h_r\, f(\bar{x}_3,\ t_0 + h_r) \tag{6-114}$$

$$\bar{x}_4 = \bar{x}_3 + \frac{1}{6}\bar{K}_4 - \frac{1}{3}\bar{q}_3 \tag{6-115}$$

6.3 MAPPING OF POSITION PARTIAL DERIVATIVES

It is well known from the theory of linear differential equations that the solution of the n-dimensional linear system

$$\dot{\bar{x}} = D(t)\,\bar{x} \tag{6-116}$$

satisfying the initial condition

$$\bar{x}(t_0) = \bar{x}_0 \tag{6-117}$$

is given by

$$\bar{x}(t) = \Phi(t,\ t_0)\,\bar{x}_0 \tag{6-118}$$

where Φ is a fundamental matrix solution of Equation (6-67), i.e., an n × n matrix satisfying

$$\dot{\Phi} = D(t)\,\Phi \tag{6-119}$$

with initial condition

$$\Phi(t_0, t_0) = I \tag{6-120}$$

In this context, $\Phi(t, t_0)$ is called the state transition matrix. The properties of Φ can be used to enhance the computational algorithm for position and velocity partial derivatives as follows. During the integration of a trajectory, a column of C(t) corresponding to a dynamic parameter can become zero. For example, when leaving the sphere of influence of the Earth, the acceleration partial derivative with respect to a geopotential coefficient of the Earth becomes effectively zero. If this time is denoted by T, then the position partial derivative with respect to this parameter, denoted by $x_j(t)$, satisfies an equation of the form of Equation (6-67) for t > T, where

$$D(t) = \begin{bmatrix} 0 & I \\ A(t) & B(t) \end{bmatrix}_{6\times 6} \tag{6-121}$$

with an initial condition $\bar{x}(T)$.

If $\Phi(t, T)$ denotes the state transition matrix satisfying $\Phi(T, T) = I$, then the required position partial derivative can be obtained for any t > T by

$$\bar{x}(t) = \Phi(t, T)\,\bar{x}(T) \tag{6-122}$$

The overall state transition matrix, $\Phi(t, t_0)$ for t > T can be computed by

$$\Phi(t, t_0) = \Phi(t, T)\,\Phi(T, t_0) \tag{6-123}$$

where the elements of the matrix $\Phi(T, t_0)$ are given by

$$\Phi(T, t_0) = \begin{bmatrix} \frac{\partial \bar{R}(T)}{\partial \bar{R}_0} & \frac{\partial \bar{R}(T)}{\partial \dot{\bar{R}}_0} \\ \frac{\partial \dot{\bar{R}}(T)}{\partial \bar{R}_0} & \frac{\partial \dot{\bar{R}}(T)}{\partial \dot{\bar{R}}_0} \end{bmatrix} \tag{6-124}$$

The components of $\Phi(T, t_0)$ are contained in the Y and $\dot{Y}$ matrices defined in Equations (6-54) and (6-55) when $t = T$ (assuming $\bar{p}$ contains the state).

The computational strategy for computing the partial derivative of $\bar{x}(t)$ is to integrate the variational equations up to $t = T$ using the method described in Section 6.1.4 or the method described in Section 6.2. At that point, the matrix $\Phi(T, t_0)$ is stored; $\Phi(T, T)$ is initialized; and, for any $t > T$, $\bar{x}(t)$ is computed using Equation (6-73) and $\Phi(t, t_0)$ is computed using Equation (6-123). A similar process can be used for multiple event times $(T_1, T_2, \ldots T_r)$ at which various columns of C(t) become zero. Assuming $T_1 \leq T_2 \leq \ldots \leq T_r \leq t$, Equation (6-123) becomes

$$\Phi(t, t_0) = \Phi(t, T_r)\, \Phi(T_r, T_{r-1}) \ldots \Phi(T_1, T_0) \tag{6-125}$$

6.4 TIME REGULARIZATION

For orbits that are highly eccentric or that connect regions with significantly different gravitational force magnitudes, accurate direct integration of Equation (6-29) or (6-49), with time as the independent variable, usually requires either a very small fixed stepsize or many stepsize changes in a variable stepsize scheme. Frequent stepsize changes are costly and result in errors propagating due to the interpolation procedure used to restart.

To improve this situation, the classical approach is to transform the independent variable to a new variable, denoted by s, defined by the relation (Reference 11)

$$\frac{dt}{ds} = \frac{R^n}{\sqrt{\mu}} \quad (1 \leq n \leq 2) \tag{6-126}$$

For $n = 1$ or 2, this variable corresponds to the use of eccentric anomaly or true anomaly as the independent variable in the integration of elliptic motion. The use of regularization in the computation of free-flight Earth-Moon trajectories is investigated in Reference 12.

This study indicates increased computational accuracy and a significant reduction in computation time due to regularization.

To express Equation (6-29) or (6-49) in terms of the new independent variable s, the following notation is employed:

$$D\,g = \frac{dg}{ds} = \frac{R^n}{\sqrt{\mu}}\,\dot{g} \tag{6-127}$$

$$D^2\,g = \frac{d^2\,g}{ds^2} = \frac{R^n}{\mu}\left[n\,R^{n-1}\,\dot{R}\,\dot{g} + R^n\,\ddot{g}\right] \tag{6-128}$$

where

$$\dot{R} = \frac{\overline{R}\cdot\dot{\overline{R}}}{R} \tag{6-129}$$

and g(t) is any arbitrary vector-valued function in the t system. Similarly,

$$D^{-1}\,g = \dot{g} = \frac{\sqrt{\mu}}{R^n}\,g' \tag{6-130}$$

$$D^{-2}\,g = \ddot{g} = \frac{\mu}{R^n}\left[R^{-n}\,g'' - \frac{n\,R'}{R^{n+1}}\,g'\right] \tag{6-131}$$

where the prime indicates differentiation with respect to s, and

$$R' = \frac{R^{n-1}}{\sqrt{\mu}}\,(\overline{R}\cdot\dot{\overline{R}}) \tag{6-132}$$

The transformed Equation (6-29) can then be expressed as

$$\overline{R}'' = D^2\,\overline{R}(t) \tag{6-133}$$

$$t'' = \frac{n R^{2n-1} \dot{R}}{\mu} \tag{6-134}$$

The integration of Equation (6-134) is required to compute the time, t, as a function of the new independent variable, s.

The integration of Equations (6-133) and (6-134) can be carried out with essentially the same procedures outlined in the previous sections. The additional remarks required are as follows:

1. Given t(s), $\bar{R}(s)$, and $\bar{R}'(s)$, a corresponding $\bar{R}''(s)$ is determined by first computing the time derivatives

$$\dot{\bar{R}}(s) = D^{-1} \bar{R}' = \frac{\sqrt{\mu}}{R^n(s)} \bar{R}'(s) \tag{6-135}$$

and

$$\ddot{\bar{R}}(s) = \frac{-\mu \bar{R}(s)}{R^3(s)} + P[t(s), \bar{R}(s), \dot{\bar{R}}(s)] \tag{6-136}$$

yielding

$$\bar{R}''(s) = \frac{n R' \bar{R}'}{R} - R^{2n-3} \bar{R} + \frac{R^{2n}}{\mu} P\left(t, \bar{R}, \frac{\sqrt{\mu}}{R^n} \bar{R}'\right) \tag{6-137}$$

2. The value of the independent variable, s, corresponding to an output request time or measurement time, t_r, can be obtained by inverse interpolation in the t_i array obtained by the integration of Equation (6-134). This value of s can then be used to compute the required $\bar{R}$ and $\dot{\bar{R}}$ by the interpolation procedure indicated in Section 6.1.5.

Analogous regularization procedures can be used for Equation (6-49). The regularized variational equations are of the form

$$Y'' = \left[\frac{R^{2n}}{\mu} A(t)\right] Y + \frac{R^n}{\sqrt{\mu}}\left[B(t) + \frac{n \dot{R} I}{R}\right] Y' + \frac{R^{2n}}{\mu} C(t) \tag{6-138}$$

An additional advantage of using regularized time is that the initial (fixed) stepsize can be conveniently selected as a fraction of the regularized period S, where, if T is the satellite period,

$$S = \int_0^T \frac{\sqrt{\mu}}{R^n} \, dt \tag{6-139}$$

The integral can be evaluated by quadrature for the two-body problem by a change of variable from t to true anomaly, f, resulting in the formula

$$S = \frac{1}{p^{(n-2+1/2)}} \int_0^{2\pi} (1 + e \cos f)^{n-2} \, df \tag{6-140}$$

where p is the semilatus rectum of the ellipse. Frequently, a fraction of this period (of the order 1/100) will serve as an adequate stepsize for the integration of Equations (6-131) and (6-132).

A drawback of the method is that the equations of motion in the τ system (Equation (6-133)) always contain explicit first derivatives, regardless of the situation in the t system, (see Equation (6-131)). Thus, the computational simplifications possible for velocity-free accelerations do not apply. Hence, the trade-off between the advantages and disadvantages of the regularized time integration depend upon the stepsize, length of arc, efficiency requirements, and eccentricity magnitude.

Experience has shown that regularized time integration considerably improves the efficiency of variable stepsize integration for moderate to high eccentricities ($e \geq 0.2$). For the Cowell formulation, the value $n = 3/2$ seems to give best results, whereas, for orbital element formulations, the optimum value of n appears to be 2 (Reference 13). Improvements in the accuracy of the integration of the time equation (Equation (6-134)) can also be obtained through use of a time element (see Appendix B).

6.5 REFERENCES

1. Moore, W. and Beaudet, P.: 1973, "The Testing of Fixed-Step Numerical Integration Processes for the Cowell Method of Special Perturbations," Proceedings of the Conference on the Numerical Solution of Ordinary Differential Equations, Springer Lecture Notes in Mathematics, Vol. 362.

2. Velez, C. E., Cefola, P., et al.: 1973, "Calculation of Precision Satellite Orbits with Non-Singular Elements," Proceedings of the Conference on the Numerical Solution of Ordinary Differential Equations, Springer Lecture Notes in Mathematics, Vol. 362.

3. Long, A., and Wei, S.: 1973, "Evaluation of GTDS Orbit Generators for the AE-C Mission," Computer Sciences Corporation Report No. 3000-07400-01TM, November 1973.

4. Beaudet, P.: 1974, "The Testing and Comparison of Various Methods of Special Perturbations," Computer Sciences Corporation Report No. 3000-08600-01TM, March 1974.

5. Maury, J. L., and Brodsky, G. P.: 1969, "Cowell Type Numerical Integration as Applied to Satellite Orbit Computation," Goddard Space Flight Center Report X-553-69-46, also NASA Report NASA-TM-X-63542, December 1969.

6. Velez, C. E., and Dixon, B.: 1974, "On the Choice of Numerical Integration Methods in the Computation of Orbits," Goddard Space Flight Center Report X-582-74-97, April 1974.

7. Gau, J. N.: 1980, *Precision of Interpolating the Orbit Files Generated by Cowell Methods*, Computer Sciences Corporation Report CSC/SD-80/6098, December 1980.

8. Shanks, E. B.: 1966, "Solution of Differential Equations by Evaluation of Functions," *Mathematics of Computation*, Vol. 20, pp. 21-38.

9. Hull, D. G. and Bettis, D. G.: "Optimal Runge-Kutta Methods," presented at the AAS/AIAA Astrodynamics Specialist Conference, Nassau, Bahamas, July 28-30, 1975.

10. Battin, R. H.: 1987, *An Introduction to the Mathematics and Methods of Astrodynamics*, AIAA Education Series, American Institute of Aeronautics and Astronautics, Inc., New York, New York, 1987.

11. Tapley, B. D., Szebehely, V., and Lewallen, J. M.: 1969, "Trajectory Optimization Using Regularized Variables," *AIAA Journal*, Vol. 7, No. 6, September 1969, pp. 1010-1017.

12. Szebehely, V., Pierce, D. A., and Standish, E. M.: 1964, "A Group of Earth-to-Moon Trajectories with Consecutive Collisions," in *Celestial Mechanics and Astrodynamics*, (V. G. Szebehely, editor), New York, Academic Press, p. 35.

13. Peñas, A.: 1973, "Accurate Integration of Orbits Using Delaunay-Similar Elements," Goddard Space Flight Center Report X-582-73-375, December 1973.

CHAPTER 7—MEASUREMENT MODELS

Spacecraft tracking measurement modeling involves the measurement of some physical property of electromagnetic wave propagation between the tracking station and the spacecraft and analytically relating the measured quantities to the spacecraft state vector. This chapter presents the models and associated equations for measurement modeling in GTDS. The models consist of kinematic equations that yield the ideal values of the measurements in trajectory-related units (e.g., range, range rate, azimuth, and elevation). Therefore, the modeled measurements are functions of the spacecraft's best estimated position and velocity, as well as specified model parameters (e.g., tracking station location and timing errors). Preprocessing of the actual data, which is usually done separately, includes calibration, time-correction, smoothing, and compacting and converting the raw tracking data into units compatible with the calculated measurements. However, the preprocessor program does not correct for the effects of atmospheric refraction and may not correct for propagation times, transponder delays, or antenna mount errors. As a result, corrections for these systematic errors are computed in GTDS and applied to the actual data. Systematic errors may still be present.

The procedures and formulations presented in this chapter describe all data types that are implemented in GTDS. Section 7.1 presents a general description of the forms of the computed measurements and their partial derivatives. Section 7.2 gives the equations and transformations for modeling ideal measurements and their partial derivatives for ground-based tracking systems. Sections 7.3, 7.4, and 7.5 discuss TDRSS tracking, radar altimeter tracking, and very long baseline interferometer tracking, respectively. Atmospheric effects are discussed in Section 7.6, and other corrections (light-time delay, transponder delay, and antenna mount errors) are presented in Section 7.7. Finally, the interrelationship between the measurement models and the estimation process is summarized in Section 7.8.

7.1 GENERAL DESCRIPTION

The basic orbit determination process consists of differentially correcting estimates for a set of parameters to minimize the sum of squares of the weighted differences between the actual measurements and the corresponding quantities computed from the measurement model. In GTDS, this model is assumed to be of the form

$$O_c = f_0[\bar{R}(t + \delta t, \bar{p}), \dot{\bar{R}}(t + \delta t, \bar{p}), \bar{r}_s] + b + RF_c \qquad (7\text{-}1)$$

where

t = time tag of the measurement

δt = timing bias

O_c = computed measurement at the corrected time $t + \delta t$

$\bar{R}, \dot{\bar{R}}$ = vehicle position and velocity at an appropriate time related to $t = t + \delta t$ (For many measurements modeled in GTDS, the position and velocity are expressed in local tangent coordinates with respect to a station position, $\bar{r}_s$. Other measurements are modeled in terms of the vehicle inertial state vector. In either case, the state vector is dependent on the dynamic parameter vector, $\bar{p}$. For TDRSS tracking, the TDRS position and velocity are also included in the measurement model.)

b = measurement bias or offset

f_0 = geometric relationship defined by the measurement type at time $t + \delta t$

RF_c = correction to the measurement due to atmospheric refraction, light-time delay, transponder delay, antenna mount errors, etc.

The measurement model parameters that can be estimated are the following:

$\bar{p}$ = dynamic parameters in the equations of motion that can be estimated; these include variables related to the position and velocity, gravitational harmonic coefficients, drag parameters, etc.

$\bar{r}_s$ = location in Earth-fixed coordinates of the transmitting and receiving stations, as well as the Bilateration Ranging Transponder (BRT) locations in the case of TDRSS Bilateration Ranging Transponder System (BRTS) tracking

b = measurement bias, which depends on the measurement type and the tracking station

δt = timing bias, which is both station and pass dependent

The measurement models simulate the following tracking system data types, for the data types listed:

- Goddard Range and Range-Rate (GRARR) System, Applications Technology Satellites Ranging (ATSR) System, STDN Ranging Equipment (SRE) Very High Frequency (VHF) System, SRE Unified S-band (USB) System, and Space Ground Link System (SGLS)
  - Range or propagation time delay
  - Range rate, range difference, or Doppler shift

  - X gimbal angle or azimuth
  - Y gimbal angle or elevation
- C-band Radar System and Smithsonian Astrophysical Observatory (SAO) Laser Systems
  - Range
  - Azimuth
  - Elevation
- Minitrack Interferometer System
  - Direction cosine ℓ
  - Direction cosine m
- Tracking and Data Relay Satellite System (TDRSS)
  - Range
  - Doppler shift
  - Azimuth
  - Elevation
- Radar Altimeter (RA) System (not currently available)
  - Altitude
- Very Long Baseline Interferometer (VLBI) System (not currently available)
  - Time difference
  - Time-rate difference

After preprocessing, some measurements are converted to metric form while others are in the form of time intervals. In general, the time tag on each measurement is converted to coordinated universal time (UTC), which is derived from Atomic Time (A.1) so as to be a close approximation to UT2 (see Chapter 3).

The differential correction process requires the calculation of the computed measurements and the systematic error corrections that are applied to the actual measurement data. The process also requires computation of the partial derivatives of the measurements with respect to the model parameters $\bar{p}$, $\bar{r}_s$, b, and δt. These partial derivatives can be expressed as follows:

$$\frac{\partial O_c}{\partial \bar{p}} = \frac{\partial f_0}{\partial \bar{p}} \tag{7-2a}$$

$$\frac{\partial O_c}{\partial \bar{r}_s} = \frac{\partial f_0}{\partial \bar{r}_s} \tag{7-2b}$$

$$\frac{\partial O_c}{\partial b} = 1 \tag{7-2c}$$

$$\frac{\partial O_c}{\partial(\delta t)} = \frac{\partial f_0}{\partial(\delta t)} = \dot{f}_0 \tag{7-2d}$$

It is assumed that the partial derivatives of the systematic error correction terms, RF_c, with respect to $\bar{p}$, $\bar{r}_s$, b, and δt, are either zero or negligible.

7.2 GROUND-BASED TRACKER MODELS

This section presents the transformations and equations for computing the ideal measurements (i.e., no systematic errors b, RF_c, or δt present). The measurements correspond to those from the GRARR, ATSR, USB, SRE, SGLS, C-band, laser, and Minitrack systems. The tracking process is described in Section 7.2.1, with a discussion of the local tangent plane coordinates given in Section 7.2.2. The measurement equations and partial derivatives are given in Section 7.2.3. Since many of the measurements are common to more than one of these systems (e.g., the range rate, $\dot{\varrho}$, is common to GRARR, ATSR, and USB), the discussion is organized by measurement type rather than by measurement system.

7.2.1 TRACKING PROCESS

For all systems except the Minitrack System, the electromagnetic signal is transmitted from the ground station at time t_T and is received at the satellite at time t_v. The signal is retransmitted by the satellite transponder (except for the laser systems, where a retroreflector is used) at time $t_v + \Delta\tau$, where $\Delta\tau$ is the transponder delay. The return signal is received at the ground station at time t_R. Thus, precise modeling requires that the tracking system be treated as a dynamic process, since both the satellite and the tracking station are moving relative to inertial space during the time it takes the signal to traverse the round trip from the ground station to the satellite and back.

The tracking instruments measure three basic quantities: the time interval required for the signal to traverse the path from the ground transmitter to the satellite and back to the ground receiver, the direction of the received signal at the ground station as measured by the receiver antenna gimbal angles, and the Doppler frequency shift of the received signal compared with the transmitted signal. Preprocessor programs multiply the round-trip time interval by the signal propagation speed, thereby converting it to the geometric distance. The GTDS measurement model then relates the station-to-spacecraft range vector to the geometric distance and its direction angles at the receiver. The Doppler frequency shift

data are related to the station-to-spacecraft range rate as described in Appendix A (Sections A.1.2.3 and A.3.2) and in Appendix C.

7.2.2 LOCAL TANGENT PLANE COORDINATES

The ground-based tracking measurement models are most conveniently expressed in station-centered local tangent plane coordinates, except for the USB and ATSR range and range-rate measurements. At the time of the measurement computation, the spacecraft state vector is available in either B1950.0, J2000.0, or true of reference date inertial coordinates. The inertial state vector must first be transformed to body-fixed coordinates using the appropriate transformation matrices from Section 3.3. The transformation from mean of B1950.0 or J2000.0 coordinates to body-fixed coordinates is expressed as

$$\bar{r}_b(t) = B(t)\, C(t)\, \bar{R}(t) \tag{7-3a}$$

$$\dot{\bar{r}}_b(t) = \dot{B}(t)\, C(t)\, \bar{R}(t) + B(t)\, C(t)\, \dot{\bar{R}}(t) \tag{7-3b}$$

where C and B are the transformation matrices from B1950.0 or J2000.0 coordinates to true of date coordinates (Section 3.3.1) and from true of date to body-fixed coordinates (Section 3.3.2), respectively; $\bar{R}$ and $\bar{r}_b$ are the spacecraft position vectors in B1950.0 or J2000.0 coordinates and body-fixed coordinates, respectively; and $\dot{\bar{R}}$ and $\dot{\bar{r}}_b$ are the spacecraft velocity vectors in B1950.0 or J2000.0 coordinates and body-fixed coordinates, respectively. The tracking station position vector, $\bar{r}_s$, expressed in body-fixed coordinates, is given in Section 3.3.7 as

$$\bar{r}_s = \begin{bmatrix} (N_s + h_s) \cos \phi_s \cos \lambda_s \\ (N_s + h_s) \cos \phi_s \sin \lambda_s \\ [N_s(1 - e^2) + h_s] \sin \phi_s \end{bmatrix} \tag{7-4}$$

where $e^2 = 2f - f^2$, f is the flattening coefficient of the Earth, and

$$N_s = \frac{R_e}{\sqrt{1 - (2f - f^2) \sin^2 \phi_s}} \tag{7-5}$$

The spacecraft position and velocity vectors, expressed in local tangent plane coordinates, are given in Section 3.3.7 as

$$\bar{r}_{lt}(t) = M_{lt}[\bar{r}_b(t) - \bar{r}_s] \tag{7-6a}$$

$$\dot{\bar{r}}_{lt}(t) = M_{lt}\,\dot{\bar{r}}_b(t) \tag{7-6b}$$

Substituting Equations (7-3) into Equations (7-6) relates the local tangent coordinates to the inertial coordinates

$$\bar{r}_{lt} = M_{lt}[B(t)\,C(t)\,\bar{R}(t) - \bar{r}_s] \tag{7-7a}$$

$$\dot{\bar{r}}_{lt} = M_{lt}[\dot{B}(t)\,C(t)\,\bar{R}(t) + B(t)\,C(t)\,\dot{\bar{R}}(t)] \tag{7-7b}$$

The vectors $\bar{r}_{lt}$ and $\dot{\bar{r}}_{lt}$ are used to model the tracking measurements.

The partial derivatives of the computed measurement are calculated using local tangent coordinates as the intermediate system (except for the USB and ATSR ranges and range rates) as follows:

$$\frac{\partial O_c}{\partial \bar{p}} \cong \frac{\partial f_0}{\partial \bar{p}} = \frac{\partial f_0}{\partial \bar{r}_{lt}}\,\frac{\partial \bar{r}_{lt}}{\partial \bar{R}}\,\frac{\partial \bar{R}}{\partial \bar{p}} + \frac{\partial f_0}{\partial \dot{\bar{r}}_{lt}}\left[\frac{\partial \dot{\bar{r}}_{lt}}{\partial \bar{R}}\,\frac{\partial \bar{R}}{\partial \bar{p}} + \frac{\partial \dot{\bar{r}}_{lt}}{\partial \dot{\bar{R}}}\,\frac{\partial \dot{\bar{R}}}{\partial \bar{p}}\right] \tag{7-8}$$

From Equations (7-7),

$$\frac{\partial \bar{r}_{lt}}{\partial \bar{R}} = M_{lt}\,B(t)\,C(t) \tag{7-9a}$$

$$\frac{\partial \dot{\bar{r}}_{lt}}{\partial \bar{R}} = M_{lt}\,\dot{B}(t)\,C(t) \tag{7-9b}$$

$$\frac{\partial \dot{\bar{r}}_{lt}}{\partial \dot{\bar{R}}} = M_{lt}\,B(t)\,C(t) \tag{7-9c}$$

Substituting Equations (7-9) into Equation (7-8) yields

$$\frac{\partial O_c}{\partial \bar{p}} \cong \frac{\partial f_0}{\partial \bar{r}_{It}} M_{It} B(t) C(t) \frac{\partial \bar{R}}{\partial \bar{p}} + \frac{\partial f_0}{\partial \dot{\bar{r}}_{It}} \left[M_{It} \dot{B}(t) C(t) \frac{\partial \bar{R}}{\partial \bar{p}} + M_{It} B(t) C(t) \frac{\partial \dot{\bar{R}}}{\partial \bar{p}} \right] \quad (7\text{-}10)$$

The matrices $\partial \bar{R}/\partial \bar{p}$ and $\partial \dot{\bar{R}}/\partial \bar{p}$ are obtained from the variational equations described in Chapter 4. The partial derivatives of the vacuum measurements, $\partial f_0/\partial \bar{r}_{It}$ and $\partial f_0/\partial \dot{\bar{r}}_{It}$, are presented in Section 7.2.3.

7.2.3 MEASUREMENT EQUATIONS AND PARTIAL DERIVATIVES

In the absence of an atmosphere, electromagnetic signals follow a straight line path between the station and the spacecraft, traveling at the vacuum speed of light. Equations describing vacuum signal propagation are presented below, along with the pertinent partial derivatives required for the orbit determination and error analysis processes. Corrections for atmospheric effects are given in Section 7.6. A functional description of each trajectory sensor system, as well as a description of the data preprocessing, can be found in Appendix A.

7.2.3.1 Gimbal Angles

The gimbal angles provide the direction of the received downlink signal at the ground station. For rotatable dish antennas, the direction angles are measured from the antenna gimbaling system. For the fixed antennas in the Minitrack System, however, the signal direction is determined from principles of interferometry.

Assuming no atmospheric refraction, the signal direction at the ground receiver is determined from the straight-line propagation path from the spacecraft at time t_v to the receiving station antenna at time t_R. GTDS approximates this direction by the instantaneous straight-line path from the spacecraft to the station at time t_v. This approximation introduces negligible error in the signal direction angles because of the relatively small distance (relative to inertial space) traversed by the station during the downlink propagation time interval.

The following subsections describe the various gimbal angle models included in GTDS.

7.2.3.1.1 Gimbal Angles X_{30} and Y_{30} (GRARR, ATSR, USB, and Laser Systems)

The gimbal angles for the 30-foot antennas in the GRARR, ATSR, USB, and laser systems are denoted X_{30} and Y_{30}. The X_{30}-axis is aligned north-south in the local horizon

(tangent) plane at the tracking station. The reference plane for the angular measurements is the vertical plane, which is aligned east-west and includes the tracking station zenith. The angle X_{30} is measured from the vertical axis (zenith) to the projection of the station-to-spacecraft vector onto the reference plane. This angle is positive when the spacecraft is east of the station, i.e.,

$$X_{30} = \tan^{-1}\left(\frac{x_{lt}}{z_{lt}}\right) \qquad \left(-\frac{\pi}{2} \leq X_{30} \leq \frac{\pi}{2}\right) \tag{7-11}$$

The angle Y_{30} is measured from the projection of the station-to-spacecraft vector onto the reference plane to the vector itself. This angle is positive when the spacecraft is north of the station, i.e.,

$$Y_{30} = \tan^{-1}\left(\frac{y_{lt}}{\sqrt{x_{lt}^2 + z_{lt}^2}}\right) \qquad \left(-\frac{\pi}{2} \leq Y_{30} \leq \frac{\pi}{2}\right) \tag{7-12}$$

The partial derivatives of X_{30} and Y_{30} with respect to the local tangent plane coordinates are

$$\frac{\partial X_{30}}{\partial \bar{r}_{lt}} = \frac{1}{(x_{lt}^2 + z_{lt}^2)}\left[z_{lt},\ 0,\ -x_{lt}\right] \tag{7-13a}$$

$$\frac{\partial X_{30}}{\partial \dot{\bar{r}}_{lt}} = 0 \tag{7-13b}$$

and

$$\frac{\partial Y_{30}}{\partial \bar{r}_{lt}} = \frac{1}{\rho^2}\left[\frac{-x_{lt}\, y_{lt}}{\sqrt{x_{lt}^2 + z_{lt}^2}},\ \sqrt{x_{lt}^2 + z_{lt}^2},\ \frac{-y_{lt}\, z_{lt}}{\sqrt{x_{lt}^2 + z_{lt}^2}}\right] \tag{7-13c}$$

$$\frac{\partial Y_{30}}{\partial \dot{\bar{r}}_{lt}} = 0 \tag{7-13d}$$

where

$$\varrho = \sqrt{x_{lt}^2 + y_{lt}^2 + z_{lt}^2} \tag{7-14}$$

7.2.3.1.2 Gimbal Angles X_{85} and Y_{85} (USB System)

The gimbal angles associated with the USB 85-foot antennas are denoted X_{85} and Y_{85}. The X_{85}-axis is aligned east-west in the local horizon (tangent) plane at the tracking station. The reference plane for the angular measurements is the vertical plane, which is aligned north-south and includes the tracking station zenith. The angle X_{85} is measured from the vertical axis (zenith) to the projection of the station-to-spacecraft vector onto the reference plane. This angle is positive when the spacecraft is south of the station, i.e.,

$$X_{85} = \tan^{-1}\left(-\frac{y_{lt}}{z_{lt}}\right) \qquad \left(-\frac{\pi}{2} \leq X_{85} \leq \frac{\pi}{2}\right) \tag{7-15}$$

The angle Y_{85} is measured from the projection of the station-to-spacecraft vector onto the reference plane to the vector itself. This angle is positive when the spacecraft is east of the station, i.e.,

$$Y_{85} = \tan^{-1}\left(\frac{x_{lt}}{\sqrt{y_{lt}^2 + z_{lt}^2}}\right) \qquad \left(-\frac{\pi}{2} \leq Y_{85} \leq \frac{\pi}{2}\right) \tag{7-16}$$

The partial derivatives of X_{85} and Y_{85} with respect to the local tangent plane coordinates are

$$\frac{\partial X_{85}}{\partial \bar{r}_{lt}} = \frac{1}{(y_{lt}^2 + z_{lt}^2)}[0, \; -z_{lt}, \; y_{lt}] \tag{7-17a}$$

$$\frac{\partial X_{85}}{\partial \dot{\bar{r}}_{lt}} = 0 \tag{7-17b}$$

and

$$\frac{\partial Y_{85}}{\partial \bar{r}_{lt}} = \frac{1}{\varrho^2}\left[\sqrt{y_{lt}^2 + z_{lt}^2}, \; \frac{-x_{lt}\, y_{lt}}{\sqrt{y_{lt}^2 + z_{lt}^2}}, \; \frac{-x_{lt}\, z_{lt}}{\sqrt{y_{lt}^2 + z_{lt}^2}}\right] \tag{7-18a}$$

$$\frac{\partial Y_{85}}{\partial \dot{\bar{r}}_{lt}} = 0 \qquad (7\text{-}18b)$$

7.2.3.1.3 Gimbal Angles A and E (ATSR, C-Band, and Laser Systems)

The azimuth angle, A, is measured in the local tangent (horizon) plane, clockwise from north to the projection of the station-to-spacecraft vector onto the local tangent plane. This angle is positive when measured eastward (clockwise) from north, i.e.,

$$A = \sin^{-1}\left(\frac{x_{lt}}{\sqrt{x_{lt}^2 + y_{lt}^2}}\right) \qquad (0 \leq A \leq 2\pi) \qquad (7\text{-}19a)$$

$$A = \cos^{-1}\left(\frac{y_{lt}}{\sqrt{x_{lt}^2 + y_{lt}^2}}\right) \qquad (0 \leq A \leq 2\pi) \qquad (7\text{-}19b)$$

The elevation angle, E, is measured from the projection of the station-to-spacecraft vector onto the local tangent plane to the vector itself. This angle is positive whenever the spacecraft is above the horizon, i.e.,

$$E = \tan^{-1}\left(\frac{z_{lt}}{\sqrt{x_{lt}^2 + y_{lt}^2}}\right) \qquad (7\text{-}20)$$

The partial derivatives of A and E with respect to the local tangent plane coordinates are

$$\frac{\partial A}{\partial \bar{r}_{lt}} = \frac{1}{(x_{lt}^2 + y_{lt}^2)}\left[\, y_{lt},\ -x_{lt},\ 0\right] \qquad (7\text{-}21a)$$

$$\frac{\partial A}{\partial \dot{\bar{r}}_{lt}} = 0 \qquad (7\text{-}21b)$$

and

$$\frac{\partial E}{\partial \bar{r}_{lt}} = \frac{1}{\varrho^2}\left[\frac{-x_{lt}\, z_{lt}}{\sqrt{x_{lt}^2 + y_{lt}^2}},\ \frac{-y_{lt}\, z_{lt}}{\sqrt{x_{lt}^2 + y_{lt}^2}},\ \sqrt{x_{lt}^2 + y_{lt}^2}\right] \qquad (7\text{-}22a)$$

$$\frac{\partial E}{\partial \dot{\bar{r}}_{lt}} = 0 \tag{7-22b}$$

7.2.3.1.4 Direction Cosines ℓ and m (Minitrack System)

The direction cosine ℓ is the cosine of the angle between the station-to-spacecraft vector and the axis pointing toward the east in the local tangent system (the $\hat{x}_{lt}$ axis). This direction cosine is positive when the spacecraft is east of the station, i.e.,

$$\ell = \frac{x_{lt}}{\varrho} \tag{7-23}$$

The direction cosine m is the cosine of the angle between the station-to-spacecraft vector and the axis pointing toward the north in the local tangent system (the $\hat{y}_{lt}$ axis). This direction cosine is positive when the spacecraft is north of the station, i.e.,

$$m = \frac{y_{lt}}{\varrho} \tag{7-24}$$

The partial derivatives of ℓ and m with respect to the local tangent plane coordinates are

$$\frac{\partial \ell}{\partial \bar{r}_{lt}} = \frac{1}{\varrho^3}\left[(y_{lt}^2 + z_{lt}^2), \quad -x_{lt}\, y_{lt}, \quad -x_{lt}\, z_{lt}\right] \tag{7-25a}$$

$$\frac{\partial \ell}{\partial \dot{\bar{r}}_{lt}} = 0 \tag{7-25b}$$

and

$$\frac{\partial m}{\partial \bar{r}_{lt}} = \frac{1}{\varrho^3}\left[-x_{lt}\, y_{lt}, \quad (x_{lt}^2 + z_{lt}^2), \quad -y_{lt}\, z_{lt}\right] \tag{7-26a}$$

$$\frac{\partial m}{\partial \dot{\bar{r}}_{lt}} = 0 \tag{7-26b}$$

7.2.3.2 Range (GRARR, ATSR, USB, SRE VHF, Laser, SGLS, and C-Band Systems)

From the description of the tracking process in Section 7.2.1, it is seen that all trackers provide the user with the round-trip light-time delay from the transmitter through the spacecraft to the ground receiver, along with an associated time tag. The round-trip range is seen to be

$$\varrho_{RT} = |\bar{r}_v(t_v) - \bar{r}_T(t_T)| + |\bar{r}_R(t_R) - \bar{r}_v(t_v + \Delta\tau)| \qquad (7\text{-}27)$$

where

ϱ_{RT} = round-trip range
$\bar{r}_v$ = spacecraft position vector in inertial Cartesian coordinates
$\bar{r}_T$ = ground transmitter position vector in inertial Cartesian coordinates
$\bar{r}_R$ = ground receiver position vector in inertial Cartesian coordinates
$\Delta\tau$ = spacecraft transponder delay
t_T = time the signal is transmitted from the ground station
t_v = time the signal is received at the satellite
t_R = time the signal is received at the ground station

In the case of the USB and C-band systems, the time tag on the raw data corresponds to the time t_R at which the measured signal arrives at the ground receiver; for the GRARR and ATSR systems, the time tag on the raw data corresponds to the ground receive time, t_R, less the measured value of the round-trip light-time delay. For all systems, the preprocessor provides GTDS with $\varrho(t_R)$, the average of the uplink and downlink propagation distances $(\varrho_{RT}/2)$. The value $\varrho(t_R)$ is generated by multiplying the measured round-trip propagation delay by c/2. The preprocessor also provides t_R by making the appropriate modifications to the raw time tag for the GRARR and ATSR data.

For the greatest accuracy, the expected value of the range should be calculated by determining the uplink and downlink path of the signal as defined in Equation (7-27). This method requires an iterative process to determine the uplink and downlink light-time delays. A second, less accurate, method is to approximate the range by calculating the instantaneous range at the spacecraft turnaround time. The iterative method is used to calculate the expected range for the USB, SRE VHF, laser, SGLS, C-band, and ATSR systems, while the instantaneous method is used for the GRARR VHF system.

7.2.3.2.1 Iterative Method for the Expected Range

The expected value of the range $\varrho(t_R)$ is computed from ephemeris information and station coordinates using the following equation:

$$\varrho(t_R) = \frac{1}{2}\left[\,|\bar{r}_v(t_v) - \bar{r}_T(t_T)| + |\bar{r}_v(t_v) - \bar{r}_R(t_R)|\,\right] \tag{7-28}$$

For simplicity, this equation is presented in an inertial reference frame, where

- $\bar{r}_v$ = spacecraft inertial position vector
- $\bar{r}_T$ = transmitting site inertial position vector
- $\bar{r}_R$ = receiving site inertial position vector
- t_T = time at which the measured signal left the ground transmitter
- t_v = time at which the measured signal was received and retransmitted by the spacecraft (The assumption of instantaneous turnaround is used; the constant bias in the measured range caused by the spacecraft electronic delay is accounted for as a measurement error elsewhere in GTDS.)
- t_R = time tag of the reduced measured range (i.e., the time at which the measured signal arrived at the ground receiver)

The algorithm used in GTDS to compute $\varrho(t_R)$ proceeds as follows:

1. Calculate $\bar{r}_R(t_R)$
2. Calculate iteratively the downlink propagation distance, $\varrho_d(t_R)$, using the following equations:

$$\varrho_d(t_R) = |\bar{r}_v(t_v) - \bar{r}_R(t_R)| \tag{7-29a}$$

$$\delta_d(t_R) = \frac{\varrho_d(t_R)}{c} \tag{7-29b}$$

$$t_v = t_R - \delta_d(t_R) \tag{7-29c}$$

The iteration process is initiated by assuming that $t_v = t_R$ and is terminated when successive values of $\delta_d(t_R)$ agree to within 10^{-8} second.

3. Calculate iteratively the uplink propagation distance, $\varrho_u(t_R)$, using the following equations:

$$\varrho_u(t_R) = |\bar{r}_v(t_v) - \bar{r}_T(t_T)| \tag{7-30a}$$

$$\delta_u(t_R) = \frac{\varrho_u(t_R)}{c} \tag{7-30b}$$

$$t_T = t_v - \delta_u(t_R) \tag{7-30c}$$

The iteration is initiated by assuming that $\delta_u(t_R) = \delta_d(t_R)$ and is terminated when successive values of $\delta_u(t_R)$ agree to within 10^{-8} second.

4. The following geometrically exact equation is used to compute the expected value of the range, $\varrho(t_R)$, for the USB, SRE VHF, C-band, ATSR, laser, and SGLS systems:

$$\varrho(t_R) = \frac{\varrho_u(t_R) + \varrho_d(t_R)}{2} \tag{7-31}$$

7.2.3.2.2 Instantaneous Method for the Expected Range

Range data produced by the GRARR VHF system is less accurate than that produced by the other tracking systems; therefore, it does not warrant the application of the iterative solution described above. Instead, the following more efficient algorithm is used to determine an instantaneous approximation for $\varrho(t_R)$ using GRARR range data:

$$\begin{aligned} \varrho(t_R) &= |\bar{r}_v(t_v) - \bar{r}_T(t_v)| = |\bar{r}_{lt}(t_v)| \\ &= \sqrt{x_{lt}^2 + y_{lt}^2 + z_{lt}^2} \end{aligned} \tag{7-32}$$

where

$$t_v = t_R - \frac{\varrho(t_R)}{c} \tag{7-33}$$

and $\bar{r}_{lt}$ is the spacecraft position vector in local tangent plane coordinates.

7.2.3.2.3 Range Partial Derivatives

The partial derivatives of the expected range (Equation (7-28)) in inertial coordinates (USB System) are

$$\frac{\partial \varrho(t_R)}{\partial \bar{r}_v(t_v)} = \frac{1}{2\varrho_u \varrho_d} \{\varrho_d[\bar{r}_v^T(t_v) - \bar{r}_T^T(t_T)] + \varrho_u[\bar{r}_v^T(t_v) - \bar{r}_R^T(t_R)]\} \tag{7-34a}$$

$$\frac{\partial \varrho(t_R)}{\partial \dot{\bar{r}}_v(t_v)} = 0 \tag{7-34b}$$

If it is assumed that $\varrho_u = \varrho_d = \varrho(t_R)$, Equation (7-34a) reduces to

$$\frac{\partial \varrho(t_R)}{\partial \bar{r}_v(t_v)} = \frac{1}{2\varrho(t_R)} \{2\bar{r}_v^T(t_v) - [\bar{r}_T^T(t_T) + \bar{r}_R^T(t_R)]\} \tag{7-35}$$

The partial derivatives of the expected range in local tangent plane coordinates (for the remaining systems) are

$$\frac{\partial \varrho(t_R)}{\partial \bar{r}_{lt}(t_v)} = \frac{\bar{r}_{lt}^T(t_v)}{\varrho(t_R)} \tag{7-36}$$

$$\frac{\partial \varrho(t_R)}{\partial \dot{\bar{r}}_{lt}(t_v)} = 0 \tag{7-37}$$

7.2.3.3 Range Rate (GRARR, ATSR, USB, VHF, and SGLS Systems)

The range rate of a spacecraft is determined by measuring the Doppler shift of a signal resulting from the relative motion between the station and the spacecraft. This can be done either by measuring the time required to count a fixed number of Doppler-plus-bias cycles, as with GRARR, ATSR, and SGLS, or by counting the Doppler-plus-bias cycles over a fixed time interval, as with USB and VHF. For all tracking systems, the preprocessor converts the raw Doppler information transmitted from the stations to range rate and a time tag.

There are three modes of calculating the expected value of the range rate for each of these tracking systems. In the first method, the range rate is obtained by computing the

time difference quotient of ranges calculated at the beginning and at the end of the Doppler count interval, iteratively correcting for the light-time delays. The second method uses the instantaneous ranges at the beginning and at the end of the count interval, with no corrections for the light-time delays. The third, and least accurate, method is to calculate an instantaneous range rate at the midpoint of the Doppler count interval as seen at the spacecraft. The first method is used to compute the expected value of the range rate for the USB and VHF systems, while the other two methods are used (optionally) for the GRARR, ATSR, and SGLS systems.

7.2.3.3.1 Iterative Range Difference Method

The modeling of the expected value of the range rate that is most precise is to difference the average range at the beginning and end of the count interval as shown below (Reference 1):

$$\dot{\varrho}\,(t_R) = \frac{[\varrho_u(t_R) + \varrho_d(t_R)] - [\varrho_u(t_R - \Delta t_{RR}) + \varrho_d(t_R - \Delta t_{RR})]}{2\Delta t_{RR}} \qquad (7\text{-}38)$$

where

$\varrho_u(t_R)$ = uplink propagation path of a signal arriving at the receiver at t_R

$\varrho_d(t_R)$ = downlink propagation path of a signal arriving at the receiver at t_R

Δt_{RR} = Doppler count time interval

The calculations for these uplink and downlink ranges are iteratively corrected for the light-time delay in exactly the same manner as the expected ranges modeled in Section 7.2.3.2.1. This method is used for USB and SRE VHF measurements where the time tag on the measured data is t_R (corresponding to the end of the count interval) and the count interval, Δt_{RR}, corresponds to the sample interval. This method is accurate for both two-way and three-way Doppler measurements. Two-way Doppler measurements are obtained when the transmitting and receiving antennas are the same, while three-way Doppler measurements are obtained when the transmitting and receiving antennas are different.

The range-rate partial derivatives with respect to the epoch state elements, $\bar{R}$ and $\dot{\bar{R}}$, are computed most efficiently by using the following algorithms for the range partial derivatives:

$$\frac{\partial \dot{\varrho}(t_R)}{\partial \bar{R}} = \frac{\frac{\partial \varrho(t_R)}{\partial \bar{R}} - \frac{\partial \varrho(t_R - \Delta t_{RR})}{\partial \bar{R}}}{\Delta t_{RR}} \tag{7-39}$$

$$\frac{\partial \dot{\varrho}(t_R)}{\partial \dot{\bar{R}}} = \frac{\frac{\partial \varrho(t_R)}{\partial \dot{\bar{R}}} - \frac{\partial \varrho(t_R - \Delta t_{RR})}{\partial \dot{\bar{R}}}}{\Delta t_{RR}} \tag{7-40}$$

7.2.3.3.2 Instantaneous Range Difference

A less accurate but more efficient range difference formulation is available in GTDS for GRARR, ATSR, and SGLS. It is assumed in this model that propagation delays are negligible compared with the Doppler count time interval. The resulting equation is

$$\dot{\varrho} = \frac{\varrho(t_v + \Delta t_{RR}) - \varrho(t_v)}{\Delta t_{RR}} = \frac{|\bar{r}_{It}(t_v + \Delta t_{RR})| - |\bar{r}_{It}(t_v)|}{\Delta t_{RR}} \tag{7-41}$$

The two range vectors $\bar{r}_{It}(t_v + \Delta t_{RR})$ and $\bar{r}_{It}(t_v)$ are computed in the same manner as those for the range computations (Section 7.2.3.2.2). In order to use this method in GTDS, the preprocessor must provide t_R, the time of the received signal at the beginning of the Doppler count interval, and Δt_{RR}, the count interval. In the case of the SGLS range-rate measurement, the preprocessor provides $t_R + 1$ second. The partial derivatives of $\dot{\varrho}$ with respect to local tangent coordinates are

$$\frac{\partial \dot{\varrho}}{\partial \bar{r}_{It}} = \frac{1}{\Delta t_{RR}} \left\{ \frac{\bar{r}_{It}^T(t_v + \Delta t_{RR})}{|\bar{r}_{It}(t_v + \Delta t_{RR})|} - \frac{\bar{r}_{It}^T(t_v)}{|\bar{r}_{It}(t_v)|} \right\} \tag{7-42}$$

$$\frac{\partial \dot{\varrho}}{\partial \dot{\bar{r}}_{It}} = 0 \tag{7-43}$$

7.2.3.3.3 Average Range Rate

A third method, which is the least accurate but most efficient, calculates the instantaneous range rate at the midpoint of the Doppler count interval as seen at the spacecraft.

This value is used to approximate the average range rate over the uplink and downlink paths and is therefore denoted $\dot{\varrho}_{avg}$. It is computed as

$$\dot{\varrho}_{avg} = \frac{\bar{r}_{lt}(t_v) \cdot \dot{\bar{r}}_{lt}(t_v)}{|\bar{r}_{lt}(t_v)|} \tag{7-44}$$

The position and velocity vectors are expressed in station-centered local tangent plane coordinates evaluated at the vehicle turnaround time, t_v.

This method is used for the GRARR and ATSR range-rate models. When this method is used, the preprocessor modifies the time tag on the GRARR data according to the relationship

$$t_v = t_R + \frac{\Delta t_{RR}}{2} - \frac{|\bar{r}_{lt}(t_v)|}{c} \tag{7-45}$$

The partial derivatives of $\dot{\varrho}_{avg}$ with respect to local tangent plane coordinates are

$$\frac{\partial \dot{\varrho}_{avg}}{\partial \bar{r}_{lt}} = \frac{1}{\varrho}\left[\dot{\bar{r}}_{lt}^T - \frac{\dot{\varrho}}{\varrho}\bar{r}_{lt}^T\right] \tag{7-46}$$

$$\frac{\partial \dot{\varrho}_{avg}}{\partial \dot{\bar{r}}_{lt}} = \frac{\bar{r}_{lt}^T}{\varrho} \tag{7-47}$$

7.3 TRACKING AND DATA RELAY SATELLITE SYSTEM (TDRSS) MODELS

In this section, the modeling of measurements from TDRSS is discussed (Reference 2). Following an overview of the different types of tracking configurations, the details of the modeling of range and Doppler measurements and their partial derivatives with respect to solve-for parameters are given. Models for the TDRS beam angles are also presented.

7.3.1 TARGET TRACKING CONFIGURATION OF TDRSS

The three basic tracking-configuration categories in TDRSS are as follows:

- Hybrid tracking
- Two-way tracking
- One-way tracking

For descriptive purposes, the path of the tracking signal is defined as a chain of nodes and legs. A node is either a station or a spacecraft that can transmit and/or receive the tracking signal. A leg is the signal path between two nodes. The measurements related to these configurations are discussed below. Although the two-way tracking configuration is the one that will be most frequently used, the hybrid tracking configuration measurements are discussed first because of the generality of this configuration. The two-way and one-way configuration measurements are described next, followed by a discussion of differenced one-way relay Doppler measurements.

7.3.1.1 Hybrid Relay Range and Doppler Measurements

Using the definitions for nodes and legs, the signal path of a hybrid relay range measurement is depicted schematically in Figure 7-1. The tracking signal originates and is transmitted from a transmitting antenna at the White Sands station (node 1), propagates through the forward-link TDRS (node 2), arrives at the receiver on the target (node 3), is relayed to the return-link TDRS (node 4), and is finally received at a receiving antenna at the White Sands, New Mexico, station (node 5). The target tracked by TDRSS can be either an orbiting user spacecraft or a ground transponder.

For a hybrid relay Doppler measurement, the signal path is similar to that of a range measurement, except that there is an extra node and an extra leg. The coherent Doppler signal is transmitted from the receiving antenna (node 6) and is mixed at the return-link TDRS (node 4) to maintain the phase coherency with the Doppler signal transmitted from the transmitting antenna (node 1). The mixed Doppler signal is finally received at the receiving antenna (node 5). The coherent Doppler signal propagation (leg 5) is shown as a dashed line in Figure 7-1. Node 6 and node 5 are physically the same antenna but are located at different positions in the inertial coordinate system because of the Earth's rotation.

7.3.1.2 Two-Way Relay Range and Doppler Measurements

For a two-way relay range or Doppler measurement, the tracking signal also originates from a transmitting antenna, propagates via a TDRS to a target, is retransmitted by the target back to the same TDRS, and is received by the same ground antenna. Figure 7-2 shows the two-way tracking configuration in which nodes 1, 5, and 6 are physically associated with the same antenna but are located at different positions in the inertial coordinate system because of the Earth's rotation. Nodes 2 and 4 are associated with the same TDRS but are located at different positions in the inertial coordinate system because of the orbital motion of the TDRS.

7.3.1.3 One-Way Relay Doppler Measurements

For a one-way relay Doppler measurement, a wide-beam tracking signal originates from the target (node 3), proceeds to the return-link TDRS (node 4), mixes with the coherent

Doppler signal transmitted from the ground receiving antenna (node 6), and is finally received by the ground receiving antenna (node 5). Figure 7-3 shows a schematic diagram of the one-way tracking configuration. There is no one-way relay range measurement.

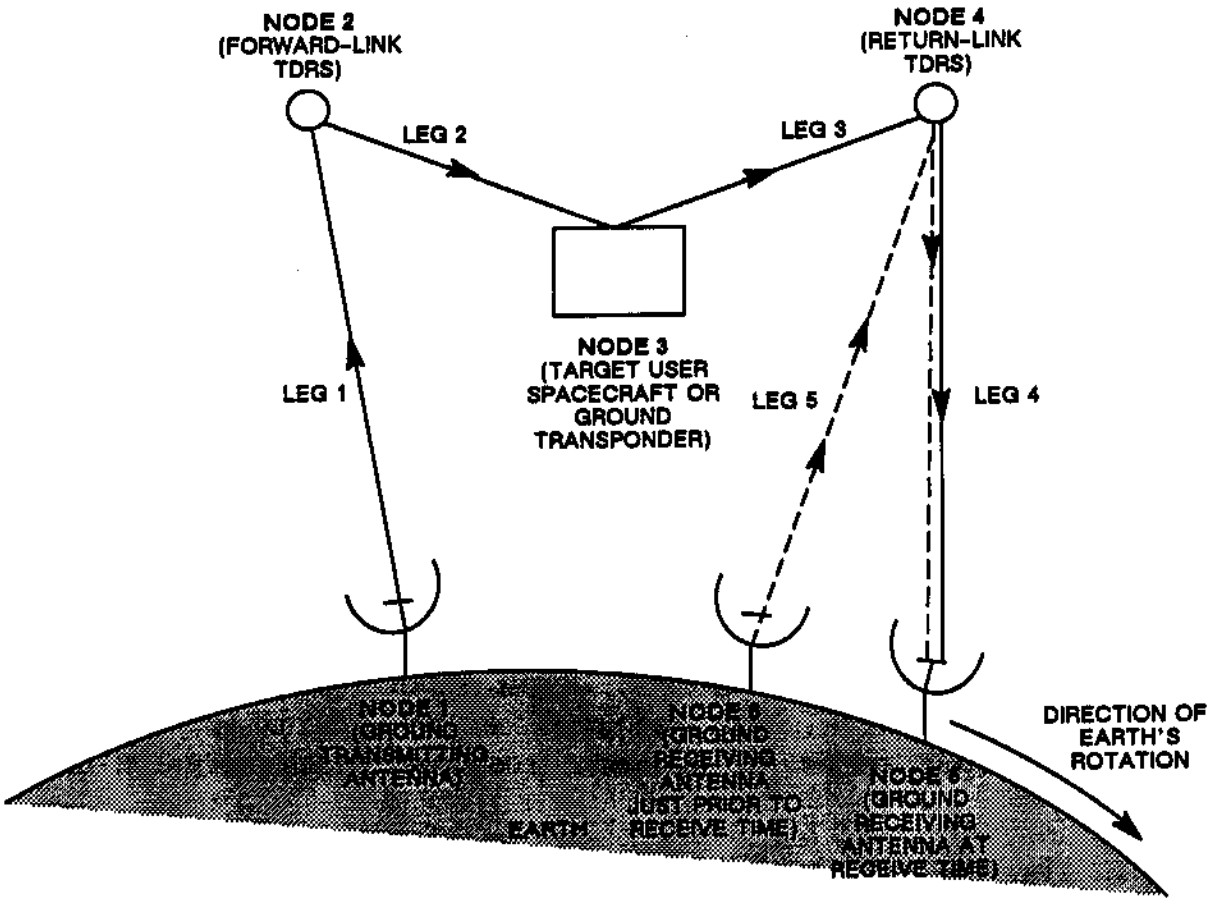

NOTE: NODE 5 AND NODE 6 REPRESENT THE SAME PHYSICAL ANTENNA AT DIFFERENT TIMES.

Figure 7-1. Hybrid Relay Range and Doppler Tracking Configuration Using Two TDRSs as Relays

7.3.1.4 Differenced One-Way Relay Doppler Measurements

Another type of measurement is feasible with the one-way tracking configuration. With a wide-beam antenna system, the one-way tracking signal generated from the user spacecraft can be received by all three TDRSs. By differencing two streams of one-way Doppler

measurements, most of the oscillator frequency bias is cancelled. This is called a differenced one-way relay Doppler measurement. With the multiple-access (MA) antenna system on TDRS, this type of measurement allows near-simultaneous tracking of up to five user spacecraft (see Reference 3).

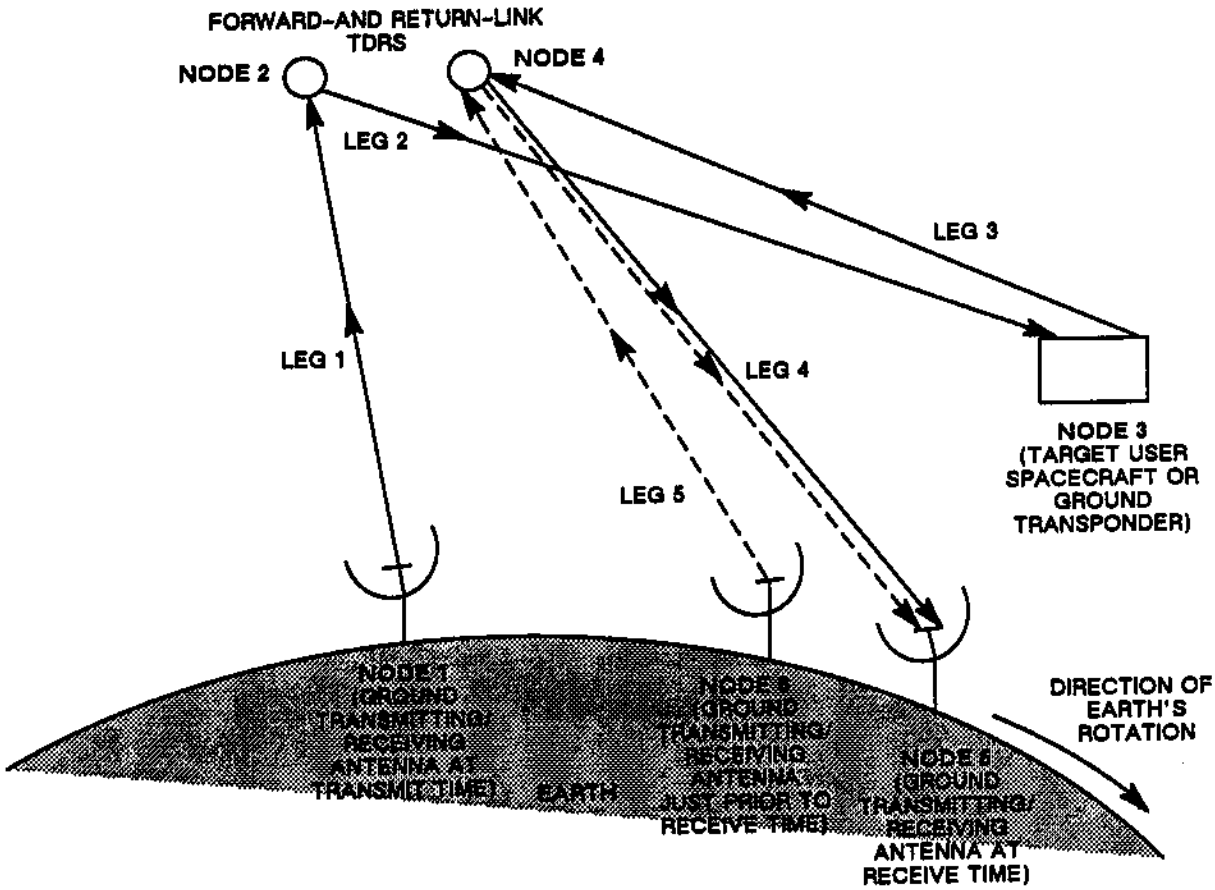

NOTES: NODE 2 AND NODE 4 REPRESENT THE SAME TDRS AT DIFFERENT TIMES.

NODE 1, NODE 5, AND NODE 6 REPRESENT THE SAME PHYSICAL ANTENNA AT DIFFERENT TIMES.

Figure 7-2. Two-Way Relay Range and Doppler Tracking Configuration Using One TDRS as the Relay

7.3.2 MODELING OF TDRSS RANGE MEASUREMENTS

The time tag associated with a measurement is the receive time of the tracking signal at the receiving station. Therefore, the backward signal-trace method is used in determining

when the signal was transmitted at each node and the position of the node at the moment of transmittal. During the course of signal tracing, the signal travel time is iteratively corrected for each leg. After the actual transmit time at node 1 is determined (see Figure 7-4), the distances (legs) between nodes are summed, and the result is halved to give the computed range measurement, which is compared with the measured ambiguous range to resolve the range ambiguity. In the modeling, transponder delay, atmospheric refraction (Section 7.6), measurement bias, timing bias, and user spacecraft antenna offset (Section 7.7.4) can be optionally invoked.

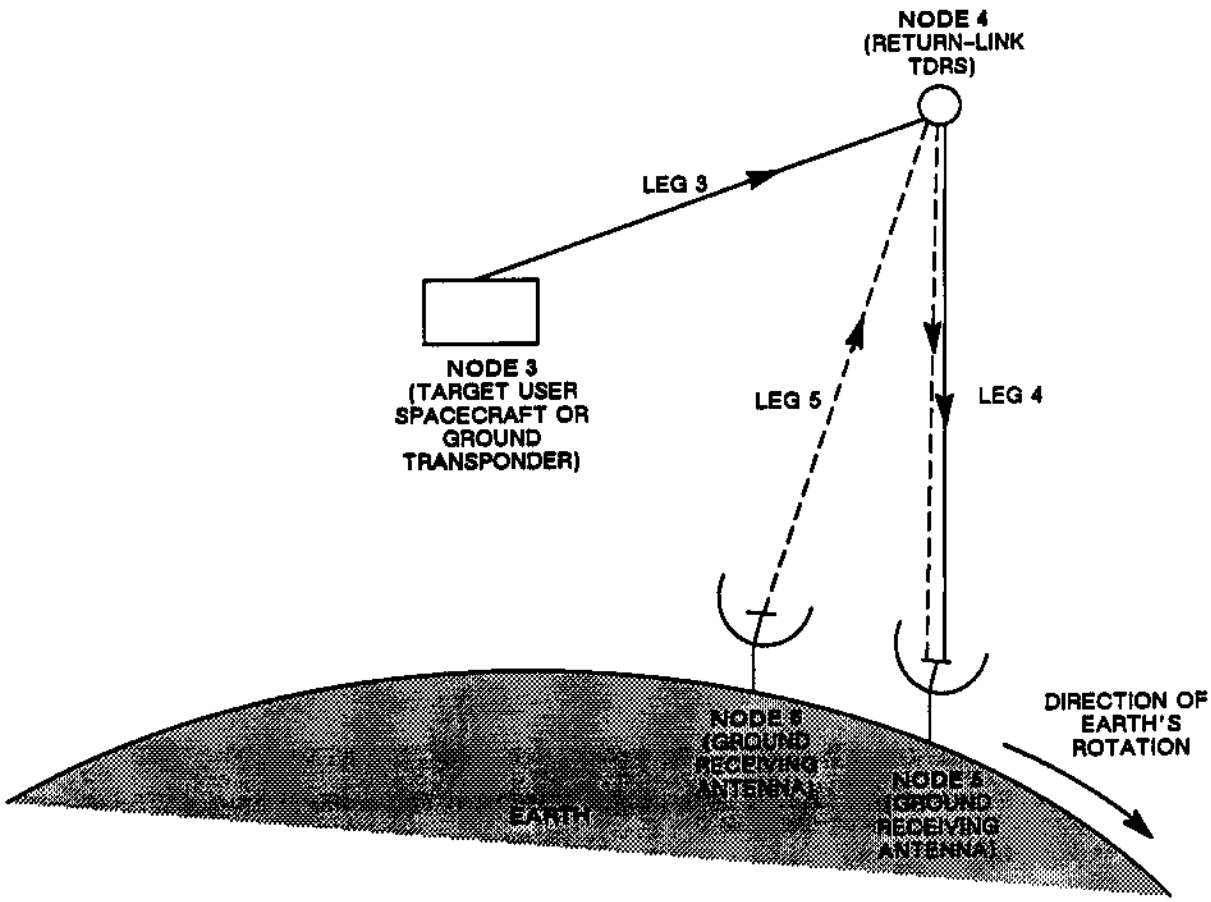

NOTE: NODE 5 AND NODE 6 REPRESENT THE SAME PHYSICAL ANTENNA AT DIFFERENT TIMES.

Figure 7-3. One-Way Relay Doppler Tracking Configuration Using One TDRS as the Relay

The iterative method for range computation, the transponder delay correction computations, and the range ambiguity computations specific to TDRSS are described below in Sections 7.3.2.1, 7.3.2.2, and 7.3.2.3, respectively.

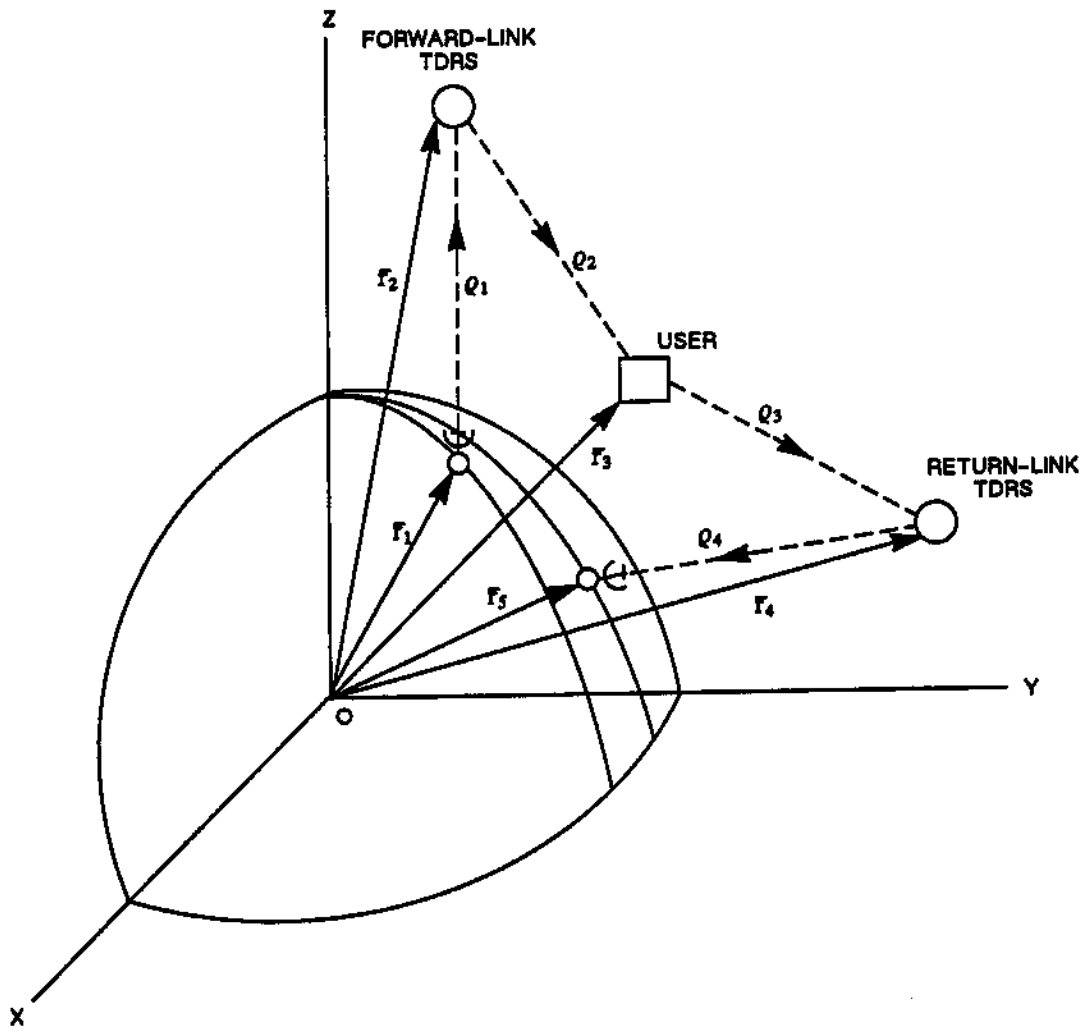

Figure 7-4. Position Vectors for All TDRSS Nodes in Inertial Coordinates

7.3.2.1 Iterative Method for Range Computation

If the tracking signal is transmitted from node j at time t_j and received at node j + 1 at time t_{j+1} (see Figure 7-4), then the distance ϱ_j traversed by the signal between these two nodes is

$$\varrho_j = c \cdot (t_{j+1} - t_j) = |\bar{r}_{j+1}(t_{j+1}) - \bar{r}_j(t_j)| \tag{7-48}$$

where

c = speed of light
$\bar{r}_j(t_j)$ = position of node j at time t_j
$\bar{r}_{j+1}(t_{j+1})$ = position of node j + 1 at time t_{j+1}

The tracking node positions, $\bar{r}_j(t_j)$, correspond exactly to the position of the phase center of the associated TDRSS tracking antenna. In general, for spacelinks the difference between this position and that of the center of mass of the TDRS or user spacecraft is neglected. The option is available in GTDS (see Section 7.7.4) to account for this antenna offset for the user spacecraft.

The Newton-Raphson iterative scheme (Reference 4) is adopted to solve the actual signal transmit time, t_j, so that

$$t_j^{n+1} = t_j^n + \frac{c \cdot (t_{j+1}^n - t_j^n) - |\bar{r}_{j+1}(t_{j+1}) - \bar{r}_j(t_j^n)|}{c - \left[\hat{u}_{j,j+1}^n \cdot \bar{v}_j(t_j^n)\right]} \tag{7-49}$$

where

t_j^{n+1} = $(n+1)^{th}$ approximation for t_j
t_j^n = n^{th} approximation for t_j
$\hat{u}_{j,j+1}^n$ = n^{th} approximation for the unit vector along the vector $[\bar{r}_{j+1}(t_{j+1}) - \bar{r}_j(t_j^n)]$
$\bar{v}_j(t_j^n)$ = velocity of node j at t_j^n

This iterative scheme is continued until the condition $\left|t_j^{p+1} - t_j^p\right| \leq \epsilon$ is satisfied, where ϵ is a small tolerance (e.g., $\epsilon = 10^{-8}$ second). Once the signal transmit time, t_j, at node j is found, the distance between the two nodes can then be calculated.

The process is repeated progressively backward for the leg between nodes j – 1 and j. Without any transponder delay at node j, the signal reception time, t_j, is the same as the retransmission time, t_j, which was just computed. With transponder delay, the signal reception time at node j must be corrected by subtracting the transponder delay to give the actual reception time, t_j',

$$t_j' = t_j - D_j \tag{7-50}$$

where D_j is the transponder delay at node j. This correction is discussed further in Section 7.3.2.2.

After the signal reception time at node j is determined, the distance between node j – 1 and node j can be computed. This process is continued until the node where the signal originated is reached. For two-way and hybrid data, this backward signal tracing starts at node 5 and ends at node 1. For one-way data, it starts at node 5 but ends at node 3.

Finally, the range, summed over all the legs, is computed as

$$\varrho(T) = \frac{1}{2} \sum_{j=1}^{4} \varrho_j \qquad \text{(for two-way and hybrid data)} \tag{7-51}$$

$$\varrho(T) = \sum_{j=3}^{4} \varrho_j \qquad \text{(for one-way data)} \tag{7-52}$$

where $\varrho(T)$ is the computed range measurement in kilometers at time tag T. The atmospheric refraction corrections discussed in Section 7.6 are applied to this computed range.

The sum in Equation (7-51) is multiplied by a factor of one-half to be consistent with the definition of the measured range discussed in Appendix A.

In solving Equation (7-49), the number of iterations can be reduced by proper selection of $\bar{r}_j(t_j^0)$. The process could be started by setting $\bar{r}_j(t_j^0) = \bar{r}_j(t_{j+1})$. In the case of TDRSS, the magnitude of the radius vector for all the relay spacecraft is about 36,000 kilometers, which corresponds to a light time of about 0.12 second.

The iterative process is started in one of two ways. If the measurement is the same type as another recent measurement, the results of the light-time solution of the previous measurement (plus an offset) are used to start the iteration procedure for the new measurement. In the absence of prior information, the iterative process can be started by setting $\bar{r}_j(t_j^0) = \bar{r}_j(t_{j+1} - 0.12 \text{ second})$.

Using this simplification, the total number of iterations can be reduced from three or four for each leg to one or two. Considerable computer resources can be saved in a typical computer run of a few thousand measurements of two-way data, for instance, that have four legs to be iteratively computed.

Further computer resource savings can be gained by evaluating $\bar{v}_j(t_j)$ only once at t_j^1 for the first iteration and keeping it as a constant in later iterations for light time. This is justified by looking at the denominator of Equation (7-49), since the velocity of any Earth spacecraft is on the order of 10 kilometers per second, which is much less than the speed of light. In addition, the difference in $\bar{v}_j(t_j)$ from iteration to iteration is inherently very small and is even more insignificant when compared with the speed of light.

7.3.2.2 TDRSS Transponder Delay Correction

A transponder does not retransmit a received signal instantaneously but does so after a delay of a fraction of a second. The relationship between the reception time and the retransmission time is

$$t_j' = t_j - D_j \tag{7-53}$$

where

t_j' = signal reception time at node j

t_j = signal retransmission time from node j

D_j = transponder delay at node j

This transponder delay has two profound effects on range modeling. One is a range correction due to the spacecraft displacement during this small period of time. The other, which is predominant, is the distance that would have been traversed by the tracking signal that is held by the transponder. These effects will be discussed separately.

In the discussion of the range computation in Section 7.3.2.1, the backward signal tracing follows nodes 5-4-3-2-1, as shown in Figures 7-4 and 7-5, when there is no transponder

delay associated with any of the spacecraft. The computed range is simply the sum of the distances between all the nodes, i.e., $\varrho_4 + \varrho_3 + \varrho_2 + \varrho_1$.

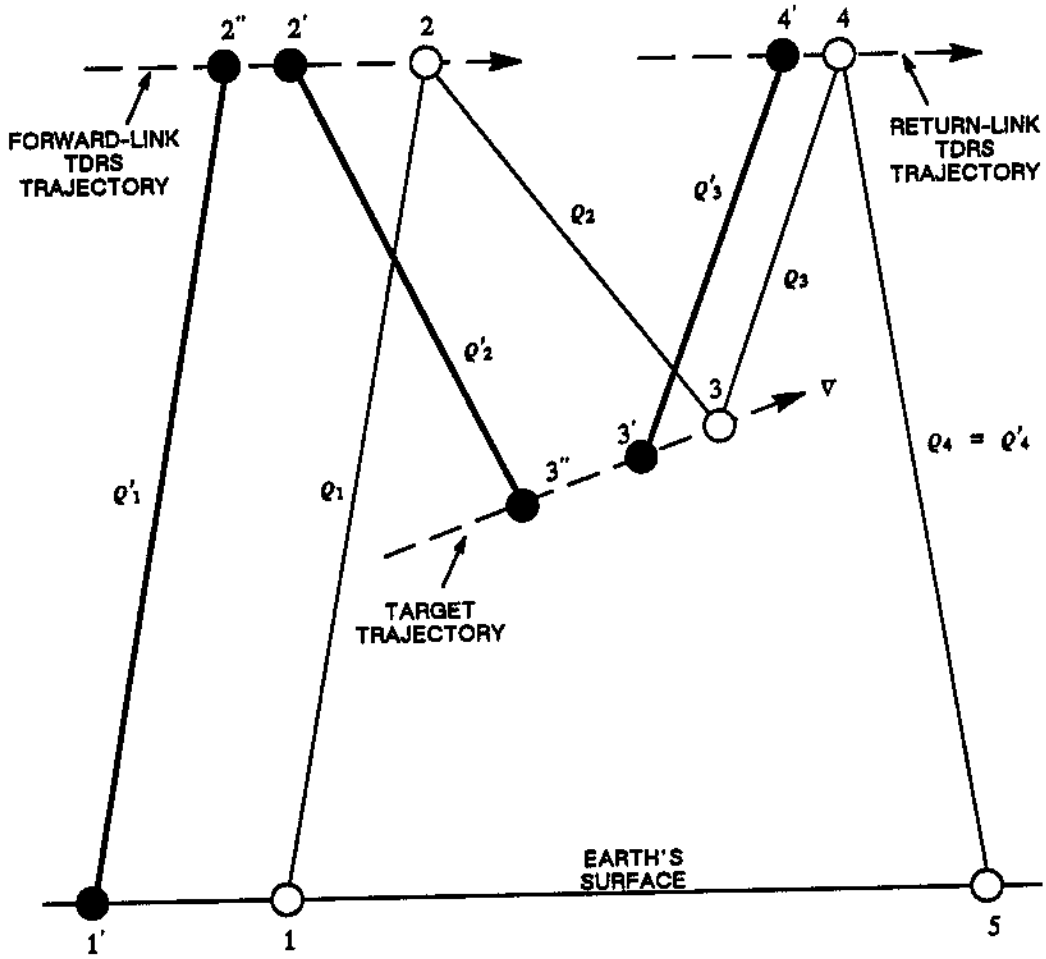

Figure 7-5. Configuration of All Nodes Because of Transponder Delays

If both the TDRS transponder and the target transponder have delays, the backward signal tracing follows the nodes 5-4-4′-3′-3″-2′-2″-1′, as shown in Figure 7-5. In this case, the distance between the receive station and the return-link TDRS, ϱ'_4, is evaluated, as before, by using their positions at nodes 5 and 4, respectively. However, the distance between the return-link TDRS and the target, ϱ'_3, is computed when they are at locations 4′ and 3′, respectively; the distance between the target and the forward-link TDRS, ϱ'_2, is computed when they are at locations 3″ and 2′, respectively; and the distance between the forward-link TDRS and the transmit station, ϱ'_1, is calculated when they are located at 2″

and $1'$, respectively. Location $4'$ of the return-link TDRS is determined using $t_{4'} = t_4 - D_4$, where D_4 is the transponder delay of the return-link TDRS. Likewise, target position $3'$ is computed by the iterative light-time procedure, and position $3''$ is determined by using $t_{3''} = (t_{3'} - D_3)$.

Since all the transponder delays are very small (on the order of 10^{-7} seconds), a target spacecraft with a velocity of 10 kilometers per second would move 10^{-6} kilometer along its trajectory. This movement will make ϱ_1, ϱ_2, ϱ_3, and ϱ_4 different from ϱ_1', ϱ_2', ϱ_3', and ϱ_4', respectively, but only by a small amount. If the target is a ground transponder, the difference between the sums of ϱ_s and ϱ_s' is even smaller. However, the bias incurred because of transponder delay (equal to the delay multiplied by the speed of light) can be much more significant. Therefore, the computed range measurement, after considering transponder delays and light-time corrections, can be rewritten in terms of the position vectors of all the nodes

$$\varrho(T) = \frac{1}{2}\left(\sum_{j=1}^{4} |\bar{r}_{j+1} - \bar{r}_j| + \sum_{k=2}^{4} c\, D_k\right) \tag{7-54}$$

where $\bar{r}_j$ is the position vector of node j shown in Figure 7-4.

7.3.2.3 Range Ambiguity

As discussed in Appendix A, the range measurement is ambiguous by a multiple of PN code periods. This ambiguity must be resolved before evaluating the (observed-minus-computed (O-C)) residual between the measured range and the computed range in the estimation process.

In general, the PN code period is a function of frequency. For TDRSS range data, the PN code period is computed as follows (References 5 and 6):

$$P = \frac{L}{R} \tag{7-55a}$$

$$L = (2^{10} - 1) \times 2^8 \text{ chips} \tag{7-55b}$$

$$R = F_{rec} \times \frac{31}{96 \times S} \text{ chips per second} \tag{7-55c}$$

where

P = PN code period (seconds)

L = length of pseudorandom code (chips)

R = rate of pseudorandom code (chips per second)

F_{rec} = frequency received at the return-link TDRS from a target (hertz)

S = 1600 for single-access return-link service at K-band frequency; otherwise, $S = 240$

Although the PN code period is a function of the receive frequency, which may drift, it is treated as a constant for a continuous pass of tracking data. Once the PN code period is evaluated, the range ambiguity interval is computed as follows:

$$\varrho_A = \frac{c\,P}{2} \tag{7-56}$$

where

ϱ_A = range ambiguity interval (kilometers) (the range measurement in Appendix A is one-half the round-trip range)

c = speed of light

P = PN code period (seconds)

The number of ambiguity intervals for a measured range at time tag T is then determined by satisfying the following test:

$$|n(T)\,\varrho_A + \varrho_0(T) - \varrho(T)| \leq \frac{1}{2}\,\varrho_A \tag{7-57}$$

where

$n(T)$ = integer number of ambiguity intervals for a measured range at time tag T

$\varrho(T)$ = computed range at time tag T (kilometers)

$\varrho_0(T)$ = measured range at time tag T (kilometers)

ϱ_A = range ambiguity interval (kilometers)

The measured range is then restored, i.e.,

$$\varrho_0'(T) = n(T)\,\varrho_A + \varrho_0(T) \tag{7-58}$$

and the residual between the measured and computed ranges is evaluated by

$$(O - C) = \varrho_0'(T) - \varrho(T) \tag{7-59}$$

When estimation is done by differential correction, the number of ambiguity intervals, n, needs to be computed only once in a computer run for each range measurement and can be used in every differential correction iteration.

7.3.3 PARTIAL DERIVATIVES FOR RANGE MEASUREMENTS WITH RESPECT TO SOLVE-FOR PARAMETERS

Table 7-1 lists the available solve-for parameters when TDRSS tracking measurements are processed. When a parameter is chosen to be a solve-for parameter, the partial derivative of the measurements with respect to this solve-for parameter is required for the estimation process.

7.3.3.1 Range Measurement Partial Derivatives With Respect to the Position Vectors

The partial derivatives of the range with respect to the position vectors depend on the identity of each node and on the type of range measurement. The position vectors can include the spacecraft state vector, TDRS state vectors, and tracking station and ground transponder locations.

Generally, the partial derivative of a range measurement with respect to the epoch state of a node can be expressed as

$$\frac{\partial \varrho(T)}{\partial \bar{X}_j(t_0)} = \frac{\partial \varrho(T)}{\partial \bar{X}_j(t_j)} \cdot \frac{\partial \bar{X}_j(t_j)}{\partial \bar{X}_j(t_0)} \tag{7-60a}$$

or

$$\frac{\partial \varrho(T)}{\partial \bar{X}_j(t_0)} = \frac{\partial \varrho(T)}{\partial \bar{X}_j(t_j)}\,\phi_j(t_j,\, t_0) \tag{7-60b}$$

Table 7-1. TDRSS Solve-For Parameters

TYPE	SOLVE-FOR PARAMETERS
Dynamic solve-for parameters for user spacecraft	State vector Aerodynamic drag parameter Solar radiation reflectivity coefficient Gravitational model parameters Powered flight parameters (thrust)
Dynamic solve-for parameters for TDRS spacecraft	State vector of the first TDRS Solar radiation reflectivity coefficient of the first TDRS State vector of the second TDRS Solar radiation reflectivity coefficient of the second TDRS State vector of the third TDRS Solar radiation reflectivity coefficient of the third TDRS
Static solve-for parameters	Transponder delays Measurement biases Timing biases Tracking station and ground transponder geodetics

where

$\varrho(T)$ = computed range measurements at time tag T

$\bar{X}_j(t_0)$ = state vector (position and velocity) of node j at epoch, t_0

$\bar{X}_j(t_j)$ = instantaneous state vector of node j at time t_j

$\phi_j(t_j, t_0)$ = $\partial\bar{X}_j(t_j)/\partial\bar{X}_j(t_0)$, the state transition matrix of node j from time t_j to t_0

The time t_0 is the epoch of the estimated solution. For a differential correction estimator, t_0 can be set equal to any time that is in or near the timespan covered by the data.

7.3.3.2 Partial Derivatives of Hybrid Relay Range Measurement With Respect to the Position Vectors

For a hybrid relay range measurement, all five associated nodes are different. Using Equations (7-54) and (7-60), the partial derivatives with respect to the instantaneous position, $\bar{r}$, and velocity, $\dot{\bar{r}}$, of each node are computed as follows:

$$\frac{\partial \varrho(T)}{\partial \bar{r}_5(t_5 = T)} = \frac{1}{2}\,\hat{u}_4 \qquad \text{(for receive station)} \qquad (7\text{-}61a)$$

$$\frac{\partial \varrho(T)}{\partial \bar{r}_4(t_4)} = \frac{1}{2}\,(\hat{u}_3 - \hat{u}_4) \qquad \text{(for return-link TDRS)} \qquad (7\text{-}61b)$$

$$\frac{\partial \varrho(T)}{\partial \bar{r}_3(t_3)} = \frac{1}{2}\,(\hat{u}_2 - \hat{u}_3) \qquad \text{(for target, either user spacecraft or ground transponder)} \qquad (7\text{-}61c)$$

$$\frac{\partial \varrho(T)}{\partial \bar{r}_2(t_2)} = \frac{1}{2}\,(\hat{u}_1 - \hat{u}_2) \qquad \text{(for forward-link TDRS)} \qquad (7\text{-}61d)$$

$$\frac{\partial \varrho(T)}{\partial \bar{r}_1(t_1)} = \frac{1}{2}\,\hat{u}_1 \qquad \text{(for transmit station)} \qquad (7\text{-}61e)$$

$$\frac{\partial \varrho(T)}{\partial \dot{\bar{r}}_j(t_j)} = 0 \qquad (j = 1, 2, 3, 4, 5)\ \text{(for all nodes)} \qquad (7\text{-}61f)$$

where $\hat{u}_j$, the unit vector along the leg between nodes j and j + 1, is given by

$$\hat{u}_j = \frac{\bar{r}_{j+1} - \bar{r}_j}{|\bar{r}_{j+1} - \bar{r}_j|} \qquad (7\text{-}62)$$

7.3.3.3 Partial Derivatives of Two-Way Relay Range Measurement With Respect to the Position Vectors

Essentially, Equations (7-61) can be used to evaluate the partial derivatives of two-way relay range measurements with respect to the position vectors. However, certain

simplifications can be made because nodes 1 and 5 (transmit and receive stations) are identical and nodes 2 and 4 (forward-link and return-link TDRS) are the same. In calculating partial derivatives, r_1 is replaced by r_5, whose variations closely approximate those of r_1. Similarly, r_2 is replaced by r_4. The velocity vectors $\dot{r}_1$ and $\dot{r}_2$ are similarly replaced by $\dot{r}_5$ and $\dot{r}_4$, respectively.

Equations (7-61) can be simplified to evaluate the derivatives of a two-way relay range measurement with respect to the instantaneous position, $\bar{r}$, and velocity, $\dot{\bar{r}}$, of each node as follows:

$$\frac{\partial \varrho(T)}{\partial \bar{r}_5(t_5)} = \frac{1}{2}(\hat{u}_4 - \hat{u}_1) \qquad \text{(for station)} \qquad (7\text{-}63a)$$

$$\frac{\partial \varrho(T)}{\partial \bar{r}_4(t_4)} = \frac{1}{2}(\hat{u}_1 - \hat{u}_2 + \hat{u}_3 - \hat{u}_4) \qquad \text{(for TDRS)} \qquad (7\text{-}63b)$$

$$\frac{\partial \varrho(T)}{\partial \bar{r}_3(t_3)} = \frac{1}{2}(\hat{u}_2 - \hat{u}_3) \qquad \text{(for target)} \qquad (7\text{-}63c)$$

$$\frac{\partial \varrho(T)}{\partial \dot{\bar{r}}_j(t_j)} = 0 \qquad (j = 1, 2, 3, 4, 5) \text{ (for all nodes)} \qquad (7\text{-}63d)$$

7.3.3.4 Partial Derivatives of One-Way Relay Range Measurement With Respect to the Position Vectors

A one-way relay range measurement actually does not exist in TDRSS. It is included here mainly to lay a foundation for modeling the one-way relay Doppler measurement and the differenced one-way relay Doppler measurement (described in Section 7.3.4). For a one-way relay measurement, there is no node 1 or node 2. The computed range will be

$$\varrho(T) = \frac{1}{2}\left(\sum_{j=3}^{4} |\bar{r}_{j+1} - \bar{r}_j| + c \cdot D_4\right) \qquad (7\text{-}64)$$

The transponder delay of node 3 is not relevant. The partial derivatives of one-way relay range with respect to the instantaneous position and velocity of each node are

$$\frac{\partial \varrho(T)}{\partial \bar{r}_5(t_5)} = \frac{1}{2}\,\hat{u}_4 \qquad \text{(for receive station)} \qquad (7\text{-}65a)$$

$$\frac{\partial \varrho(T)}{\partial \bar{r}_4(t_4)} = \frac{1}{2}\,(\hat{u}_3 - \hat{u}_4) \qquad \text{(for return-link TDRS)} \qquad (7\text{-}65b)$$

$$\frac{\partial \varrho(T)}{\partial \bar{r}_3(t_3)} = -\frac{1}{2}\,\hat{u}_3 \qquad \text{(for target)} \qquad (7\text{-}65c)$$

$$\frac{\partial \varrho(T)}{\partial \dot{\bar{r}}_j(t_j)} = 0 \qquad (j = 1, 2, 3, 4, 5)\ \text{(for all nodes)} \qquad (7\text{-}65d)$$

7.3.3.5 Partial Derivatives of Short Range (Coherent Range) Measurement With Respect to the Position Vectors

As described in Section 7.3.1.1, the phase relationship of all the Doppler measurements in TDRSS is maintained by transmitting a coherent Doppler signal from the receive station to the return-link TDRS and mixing it with the Doppler signal retransmitted by the target. Modeling of the Doppler measurement will be described in Section 7.3.4. The computation of the partial derivatives of the short range (coherent range) that will be used later in modeling the Doppler measurement is included here for completeness, although the short-range measurement does not exist in TDRSS. The computed short range is

$$\varrho(T) = \frac{1}{2}(|\bar{r}_5 - \bar{r}_4| + |\bar{r}_4 - \bar{r}_6| + c \cdot D_4) \qquad (7\text{-}66)$$

Since node 6 is identical to node 5, the partial derivatives of the short range with respect to the instantaneous position and velocity of each node are

$$\frac{\partial \varrho(T)}{\partial \bar{r}_5(t_5)} = \frac{1}{2}\,(\hat{u}_4 - \hat{u}_5) \qquad \text{(for receive station)} \qquad (7\text{-}67a)$$

$$\frac{\partial \varrho(T)}{\partial \bar{r}_4(t_4)} = \frac{1}{2}(\hat{u}_5 - \hat{u}_4) \qquad \text{(for return-link TDRS)} \tag{7-67b}$$

$$\frac{\partial \varrho(T)}{\partial \bar{r}_j(t_j)} = 0 \qquad \begin{array}{l}(j = 1, 2, 3)\\ \text{(for target, forward-link}\\ \text{TDRS, and transmit station)}\end{array} \tag{7-67c}$$

$$\frac{\partial \varrho(T)}{\partial \dot{\bar{r}}_j(t_j)} = 0 \qquad \begin{array}{l}(j = 1, 2, 3, 4, 5)\\ \text{(for all nodes)}\end{array} \tag{7-67d}$$

where the unit vector, $\hat{u}_5$, of the fifth leg (see Figure 7-1) is given by

$$\hat{u}_5 = \frac{\bar{r}_4 - \bar{r}_6}{|\bar{r}_4 - \bar{r}_6|} \tag{7-68}$$

7.3.3.6 Range Measurement Partial Derivatives With Respect to Transponder Delay

From Equations (7-53) and (7-54), the partial derivative of the range measurement with respect to transponder delay is

$$\begin{aligned}\frac{\partial \varrho(T)}{\partial D_k} &= \frac{1}{2}\left(c + \sum_{j=1}^{k-1} \frac{\partial \varrho_j}{\partial D_k}\right)\\ &= \frac{1}{2}\left(c + \sum_{j=1}^{k-1} \frac{\partial \varrho_j}{\partial t_k} \cdot \frac{\partial t_k}{\partial D_k}\right)\end{aligned} \tag{7-69a}$$

or

$$\frac{\partial \varrho(T)}{\partial D_k} = \frac{1}{2}\left(c - \sum_{j=1}^{k-1} \frac{\partial \varrho_j}{\partial t_k}\right) \tag{7-69b}$$

where

$$\frac{\partial \varrho_j}{\partial t_{j+1}} = c\left(1 - \frac{\partial t_j}{\partial t_{j+1}}\right) \tag{7-70a}$$

$$\frac{\partial t_j}{\partial t_{j+1}} = \frac{c - (\hat{u}_j \cdot \dot{\bar{r}}_{j+1})}{c - (\hat{u}_j \cdot \dot{\bar{r}}_j)} \tag{7-70b}$$

7.3.3.6.1 Partial Derivative for Transponder Delay at the Forward-Link TDRS

Since this delay only affects the positions of node 2 and node 1 from a backward tracing (see Figure 7-5), using Equations (7-69b) and (7-54) gives the partial derivative of the half-range measurement with respect to the transponder delay at the forward-link TDRS, as follows:

$$\frac{\partial \varrho(T)}{\partial D_2} = \frac{1}{2}\left(c - \frac{\partial \varrho_1}{\partial t_2}\right) \tag{7-71a}$$

where

$$\frac{\partial \varrho_1}{\partial t_2} = \frac{\partial}{\partial t_2}|\bar{r}_2 - \bar{r}_1| = \frac{\hat{u}_1 \cdot (\dot{\bar{r}}_2 - \dot{\bar{r}}_1)}{1 - \frac{1}{c}(\hat{u}_1 \cdot \dot{\bar{r}}_1)} \tag{7-71b}$$

and $\hat{u}_1$ is the unit vector of $\bar{\varrho}_1$.

7.3.3.6.2 Partial Derivative for Transponder Delay at the Target (User Spacecraft or Ground Transponder)

Transponder delay at the target is associated with node 3, thereby affecting the positions of node 3, node 2, and node 1 by backward tracing. Using Equations (7-69b) and (7-54), the partial derivative of the range measurement with respect to the target transponder delay is given by

$$\frac{\partial \varrho(T)}{\partial D_3} = \frac{1}{2}\left[c - \left(\frac{\partial \varrho_2}{\partial t_3} + \frac{\partial \varrho_1}{\partial t_3}\right)\right] \tag{7-72}$$

where

$$\frac{\partial \rho_2}{\partial t_3} = \frac{\partial}{\partial t_3} |\bar{r}_3 - \bar{r}_2| = \frac{\hat{u}_2 \cdot (\dot{\bar{r}}_3 - \dot{\bar{r}}_2)}{1 - \frac{1}{c}(\hat{u}_2 \cdot \dot{\bar{r}}_2)} \tag{7-73a}$$

$$\frac{\partial \rho_1}{\partial t_3} = \frac{\partial}{\partial t_3} |\bar{r}_2 - \bar{r}_1| = \frac{\hat{u}_1 \cdot (\dot{\bar{r}}_2 - \dot{\bar{r}}_1)}{1 - \frac{1}{c}(\hat{u}_1 \cdot \dot{\bar{r}}_1)} \left(1 - \frac{1}{c} \frac{\partial \rho_2}{\partial t_3}\right) \tag{7-73b}$$

The last equation was derived using the chain rule and the identity

$$\frac{\partial t_2}{\partial t_3} = 1 - \frac{1}{c} \frac{\partial \rho_2}{\partial t_3} \tag{7-74}$$

which is deduced from the range equation (Equation (7-48)).

7.3.3.6.3 Partial Derivatives for Transponder Delay at the Return-Link TDRS

Since this delay is associated with node 4, it will affect the position of nodes 4, 3, 2, and 1. The partial derivative of the range measurement with respect to the transponder delay of the return-link TDRS is

$$\frac{\partial \rho(T)}{\partial D_4} = \frac{1}{2}\left[c - \left(\frac{\partial \rho_3}{\partial t_4} + \frac{\partial \rho_2}{\partial t_4} + \frac{\partial \rho_1}{\partial t_4}\right)\right] \tag{7-75}$$

where

$$\frac{\partial \rho_3}{\partial t_4} = \frac{\hat{u}_3 \cdot (\dot{\bar{r}}_4 - \dot{\bar{r}}_3)}{1 - \frac{1}{c}(\hat{u}_3 \cdot \dot{\bar{r}}_3)} \tag{7-76a}$$

$$\frac{\partial \rho_2}{\partial t_4} = \frac{\hat{u}_2 \cdot (\dot{\bar{r}}_3 - \dot{\bar{r}}_2)}{1 - \frac{1}{c}(\hat{u}_2 \cdot \dot{\bar{r}}_2)} \left(1 - \frac{1}{c} \frac{\partial \rho_3}{\partial t_4}\right) \tag{7-76b}$$

$$\frac{\partial \varrho_1}{\partial t_4} = \frac{\hat{u}_1 \cdot (\dot{\bar{r}}_2 - \dot{\bar{r}}_1)}{1 - \frac{1}{c}(\hat{u}_1 \cdot \dot{\bar{r}}_1)}\left(1 - \frac{1}{c}\frac{\partial \varrho_3}{\partial t_4} - \frac{1}{c}\frac{\partial \varrho_2}{\partial t_4}\right) \tag{7-76c}$$

For all practical cases, $\partial \varrho_j / \partial t_k$ is negligible when compared with the speed of light in Equations (7-71a), (7-72), and (7-75). Therefore, the following formula is used for each node:

$$\frac{\partial \varrho(T)}{\partial D_k} = \frac{c}{2} \tag{7-77}$$

7.3.3.7 Range Measurement Partial Derivatives With Respect to Other Systematic Biases and Uncertainties

The partial derivatives of range measurements with respect to measurement biases, timing biases, and nonstate dynamic solve-for parameters are discussed in this section.

7.3.3.7.1 Measurement Biases

Measurement biases, B, that are specific to a given type of measurement, O_c, and to a given receive station, can be applied and solved for. As is true for all these biases, the partial derivative with respect to a TDRSS measurement bias is unity:

$$\frac{\partial O_c(T)}{\partial B} = 1 \tag{7-78}$$

7.3.3.7.2 Timing Bias (Time Tag Error)

The actual receive time, t_5, of a signal at the receive station (node 5) can differ from the measured receive time (i.e., the time tag T of the measurement) due to a clock bias, t_B, as follows:

$$t_5 = T + t_B \tag{7-79}$$

The partial derivative of the measurement with respect to the timing bias (time tag error) is

$$\frac{\partial O_c}{\partial t_B} = \frac{\partial O_c}{\partial t_5} \tag{7-80}$$

For a range measurement,

$$O_c = \varrho(T) = \frac{1}{2}\left(\sum_{j=1}^{4} \varrho_j + \sum_{k=2}^{4} c\,D_k\right) \tag{7-81}$$

Since

$$\varrho_j = c(t_{j+1} - t_j) = |\bar{r}_{j+1} - \bar{r}_j| \tag{7-82}$$

then

$$\frac{\partial \varrho_j}{\partial t_{j+1}} = c\left(1 - \frac{\partial t_j}{\partial t_{j+1}}\right) \tag{7-83}$$

where

$$\frac{\partial t_j}{\partial t_{j+1}} = \frac{c - (\hat{u}_j \cdot \dot{\bar{r}}_{j+1})}{c - (\hat{u}_j \cdot \dot{\bar{r}}_j)} \tag{7-84}$$

Therefore, the partial derivative of a range measurement with respect to the timing bias is

$$\begin{aligned} \frac{\partial \varrho(T)}{\partial t_B} &= \frac{\partial \varrho(T)}{\partial t_5} = \frac{1}{2}\sum_{j=1}^{4} \frac{\partial \varrho_j}{\partial t_5} \\ &= \frac{1}{2}\sum_{j=1}^{4}\left[c\left(1 - \frac{\partial t_j}{\partial t_{j+1}}\right)\left(\frac{\partial t_{j+1}}{\partial t_5}\right)\right] \\ &= \frac{c}{2}\left(1 - \frac{\partial t_i}{\partial t_5}\right) \end{aligned} \tag{7-85}$$

where the subscript i indicates the initial node of the measurement (i = 3 for one-way and i = 1 for two-way or hybrid).

7.3.3.7.3 Nonstate Dynamic Solve-For Parameters

The partial derivative of the measurement O_c with respect to a dynamic solve-for parameter, s, is calculated by the equation

$$\frac{\partial O_c}{\partial s} = \sum_j \frac{\partial O_c}{\partial x_j} \cdot \frac{\partial x_j}{\partial s} \tag{7-86}$$

where the sum is over all spacecraft involved in the measurement, in principle. Because a solve-for parameter, such as the coefficient of solar reflectivity, may be specific to an individual spacecraft, only one term of the sum may be nonvanishing, and only one dot product needs to be calculated.

Some of the solve-for parameters listed in Table 7-1, such as the coefficients of solar reflectivity for the TDRSs, do not involve the target spacecraft. Other solve-for parameters are treated as being specific to the target spacecraft. That is, in updating the estimate of such solve-for parameters, only the effect of these parameters on the target spacecraft is considered, and the partial derivative calculated is simply

$$\frac{\partial O_c}{\partial s} = \frac{\partial O_c}{\partial \bar{x}_{target}} \cdot \frac{\partial \bar{x}_{target}}{\partial s} \tag{7-87}$$

Thus, only one term of the sum is calculated for any of the nonstate dynamic solve-for parameters.

7.3.4 MODELING OF DOPPLER AND DIFFERENCED DOPPLER MEASUREMENTS

In this section, TDRSS Doppler measurement modeling in the nondestruct mode is discussed. The basic derivation and its application to two-way Doppler measurement modeling can be found in Reference 7.

The Doppler-shifted carrier frequency via the long-trip path (i.e., from node 1 though nodes 2, 3, and 4 to node 5) is

$$\begin{aligned} \nu_\ell &= (\nu_0)_\ell \left(1 - \frac{\dot{\varrho}_1}{c}\right)\left(1 - \frac{\dot{\varrho}_2}{c}\right)\left(1 - \frac{\dot{\varrho}_3}{c}\right)\left(1 - \frac{\dot{\varrho}_4}{c}\right) \\ &\cong (\nu_0)_\ell \left[1 - \frac{(\dot{\varrho}_1 + \dot{\varrho}_2 + \dot{\varrho}_3 + \dot{\varrho}_4)}{c}\right] \\ &\cong (\nu_0)_\ell \left(1 - \frac{\dot{\varrho}_\ell}{c}\right) \end{aligned} \tag{7-88}$$

where

ν_ℓ = Doppler-shifted carrier frequency via the long-trip path
$(\nu_0)_\ell$ = unshifted radiated carrier frequency via the long-trip path
$\dot{\varrho}_\ell$ = time rate of change of long-trip full range

Equation (7-88) is also valid for one-way Doppler measurements, except that in this case,

$$\varrho_\ell = \varrho_3 + \varrho_4 \tag{7-89}$$

The phase of the Doppler signal is maintained by transmitting a coherent pilot-tone frequency to the return-link TDRS. The frequency is also Doppler-shifted, as follows:

$$\begin{aligned} \nu_s &= (\nu_0)_s \left(1 - \frac{\dot{\varrho}_5}{c}\right)\left(1 - \frac{\dot{\varrho}_4}{c}\right) \\ &\cong (\nu_0)_s \left[1 - \frac{(\dot{\varrho}_5 + \dot{\varrho}_4)}{c}\right] \\ &\cong (\nu_0)_s \left(1 - \frac{\dot{\varrho}_s}{c}\right) \end{aligned} \tag{7-90}$$

where

ν_s = Doppler-shifted pilot-tone frequency for the short-trip path (i.e., from node 6, through node 4, to node 5)

$(\nu_0)_s$ = unshifted pilot-tone frequency

$\dot{\varrho}_s$ = time rate of change of the short-trip full range

These two Doppler-shifted frequencies are mixed according to a certain ratio in the transponder of the return-link TDRS to produce the observed Doppler shift

$$\nu_d = [a\,\nu_\ell + b\,\nu_s] - [a\,(\nu_0)_\ell + b\,(\nu_0)_s] \tag{7-91}$$

where a and b are hardware-related constants.

Substituting Equations (7-88) and (7-90) into Equation (7-91) and rewriting in terms of range differences, $\Delta\varrho_\ell$ and $\Delta\varrho_s$, over the Doppler counting interval, ΔT, the measured Doppler shift can be expressed as

$$\nu_{d_c}(T) = -\frac{1}{c}(A\,\dot{\varrho}_\ell + B\,\dot{\varrho}_s) = -\frac{1}{c\,\Delta t}[A\,\Delta\varrho_\ell(T) + B\,\Delta\varrho_s(T)] \tag{7-92}$$

where

$\nu_{d_c}(T)$ = computed average Doppler shift tagged at time T

A = $a\,(\nu_0)_\ell$
= effective transmit frequency from the user

B = $b\,(\nu_0)_\ell$
= pilot-tone frequency translation from the return-link TDRS

$\Delta\varrho_\ell(T)$ = $\varrho_\ell(T) - \varrho_\ell(T - \Delta T)$
= difference between the full long-path range at times T and $T - \Delta T$

$\Delta\varrho_s(T)$ = $\varrho_s(T) - \varrho_s(T - \Delta T)$
= difference between the full short-path range at times T and $T - \Delta T$

The effective transmit frequency from the user must be retrieved from the tracking data. The values of the pilot-tone frequency translation, which are listed in Table 7-2, depend on both the return-link access-service type and the frequency band of the link.

The previously calculated long- and short-path ranges for a configuration can be saved. This provides substantial savings in computation time whenever the Doppler counting interval is equal to the time between measurements, in which case the previously saved ranges at T – ΔT and the currently computed ranges at T are used directly to model a Doppler measurement according to Equation (7-92).

Table 7-2. Value of Pilot Tone Frequency Translation, B, Applicable to Determination of TDRSS Average Doppler Shift

RETURN-LINK SERVICE ID	FREQUENCY BAND	B (MHz) [1, 2, 3]
SA1 (single access)	K-band (14 GHz)	-1475.0
SA2	K-band	-1075.0
SA1	S-band (1.6 GHz)	13677.5 - INT[2A + 0.5]/2.0
SA2	S-band	13697.5 - INT[2A + 0.5]/2.0
MA (multiple access)	S-band	-2127.5

NOTES:

1. Values of B may be subject to change
2. The parameter A is the effective transmit frequency from the target spacecraft
3. INT [ ] means truncate to closest integer

Units: GHz = gigahertz
MHz = megahertz

7.3.5 PARTIAL DERIVATIVES OF DOPPLER MEASUREMENTS WITH RESPECT TO SOLVE-FOR PARAMETERS

If the Doppler measurements are to be used for the estimation of any solve-for parameter, the partial derivatives of the Doppler measurements with respect to the solve-for parameters must be computed.

7.3.5.1 Doppler Measurement Partial Derivatives With Respect to the Position Vectors

Although the partial derivatives of Doppler measurements with respect to the position vectors depend on the identity of each node and on the type of Doppler measurement, they can be expressed in the general form

$$\frac{\partial \nu_d(T)}{\partial \bar{X}_j(t_0)} = \frac{\partial \nu_d(T)}{\partial \bar{X}_j(t_j)} \Phi_j(t_j, t_0) \tag{7-93}$$

where

$\nu_d(T)$ = computed full Doppler measurement at time tag T
$\bar{X}_j(t_0)$ = state vector (position and velocity) of node j at epoch, t_0
$\bar{X}_j(t_j)$ = instantaneous state vectors of node j at time tag t_j
$\Phi_j(t_j, t_0)$ = state transition matrix of node j from t_j to t_0

where t_0 is equal to any time that is in or near the data span for a batch differential corrector.

Substituting Equation (7-92) into Equation (7-93) produces

$$\frac{\partial \nu_d(T)}{\partial \bar{X}_j(t_0)} = -\frac{1}{c\,\Delta T}\left[A\,\frac{\partial \varrho_\ell(T)}{\partial \bar{X}_j(t_j)} + B\,\frac{\partial \varrho_s(T)}{\partial \bar{X}_j(t_j)}\right]\Phi_j(t_j, t_0)$$
$$+ \frac{1}{c\,\Delta T}\left[A\,\frac{\partial \varrho(T - \Delta T)}{\partial \bar{X}_j(t_j - \Delta T)} + B\,\frac{\partial \varrho_s(T - \Delta T)}{\partial \bar{X}_j(t_j - \Delta T)}\right]\Phi_j(t_j - \Delta T, t_0) \tag{7-94}$$

All the range partial derivatives in brackets are described in Section 7.3.3 for all nodes, except that they should be multiplied by a factor of 2 because ϱ_ℓ and ϱ_s are the full round-trip ranges (not the half-trip ranges used in the range measurement modeling). These derivatives are evaluated at the current time tag, T, and at the time $T - \Delta T$, where ΔT is the counting interval for the nondestruct Doppler frequency.

The range partial derivatives at the previous time tag can be saved and then used in the computation of the Doppler partial derivatives if the previous time tag is equal to $T - \Delta T$, which is the start time of a Doppler count. Otherwise, all the partial derivatives must be evaluated at both T and $T - \Delta T$.

7.3.5.2 Doppler Measurement Partial Derivatives With Respect to Transponder Delay

Using Equation (7-92), the partial derivative of the Doppler measurement with respect to the transponder delay can be expressed as

$$\begin{aligned}
\frac{\partial \nu_d(T)}{\partial D_j} &= -\frac{1}{c\,\Delta T}\left[A\,\frac{\partial \Delta\rho_\ell(T)}{\partial D_j} + B\,\frac{\partial \Delta\rho_s(T)}{\partial D_j}\right] \\
&= -\frac{1}{c\,\Delta T}\left\{\left[A\,\frac{\partial \rho_\ell(T)}{\partial D_j} + B\,\frac{\partial \rho_s(T)}{\partial D_j}\right]\right. \\
&\quad \left. -\left[A\,\frac{\partial \rho_\ell(T-\Delta T)}{\partial D_j} + B\,\frac{\partial \rho_s(T-\Delta T)}{\partial D_j}\right]\right\} \qquad (7\text{-}95) \\
&= -\frac{1}{c\,\Delta T}\left\{(-1)\left[A\,\frac{\partial \rho_\ell(T)}{\partial t_j} + B\,\frac{\partial \rho_s(T)}{\partial t_j}\right]\right. \\
&\quad \left. +\left[A\,\frac{\partial \rho_\ell(T-\Delta T)}{\partial t_j} + B\,\frac{\partial \rho_s(T-\Delta T)}{\partial t_j}\right]\right\}
\end{aligned}$$

where $(\partial\rho_\ell/\partial t_j)$ and $(\partial\rho_s/\partial t_j)$ can be evaluated for both the current time tag, T, and the previous time tag, $T - \Delta T$, by Equations (7-71b), (7-73), and (7-76) for transponder delays associated with the forward-link TDRS, the target, and the return-link TDRS, respectively. If the transponder delay is associated with the forward-link TDRS or the target, $\partial\rho_s/\partial t_j$ will be zero because the short-path full range is only associated with the return-link TDRS.

7.3.5.3 Doppler Measurement Partial Derivatives With Respect to Other Solve-For Parameters

The partial derivatives of Doppler measurements with respect to a measurement bias are unity, as shown in Equation (7-78). For a timing bias, the partial derivatives of both the

long-path and the short-path (coherent mode) ranges must be evaluated at two points in time, as follows:

$$\frac{\partial \nu_d(T)}{\partial t_B} = \frac{-\left[A \frac{\partial \Delta \rho_\ell(T)}{\partial t_B} + B \frac{\partial \Delta \rho_s(T)}{\partial t_B}\right]}{c\,\Delta T}$$

$$= -\frac{1}{c\,\Delta T}\left\{A\left[\frac{\partial \rho_\ell(T)}{\partial t_B} - \frac{\partial \rho_\ell(T - \Delta T)}{\partial t_B}\right]\right. \qquad (7\text{-}96)$$

$$\left. + B\left[\frac{\partial \rho_s(T)}{\partial t_B} - \frac{\partial \rho_s(T - \Delta T)}{\partial t_B}\right]\right\}$$

where $\partial \rho_\ell / \partial t_B$ and $\partial \rho_s / \partial t_B$ can be evaluated by Equations (7-83) and (7-85) with a multiplication factor of 2, since ρ_ℓ and ρ_s are full ranges.

For other nonstate dynamic solve-for parameters, the general form of the partial derivatives of the Doppler measurements is similar to Equation (7-86).

7.3.6 FORMULATION OF DIFFERENCED ONE-WAY DOPPLER MEASUREMENT AND ITS PARTIAL DERIVATIVES

The differenced one-way Doppler measurement is defined as

$$\Delta \nu_d(T) = \nu_d(T)\Big|_{\substack{\text{comparison}\\ \text{TDRS}}} - \nu_d(T)\Big|_{\substack{\text{reference}\\ \text{TDRS}}} \qquad (7\text{-}97)$$

The partial derivative of a differenced one-way Doppler measurement with respect to any solve-for parameter, s, can be generalized and written as

$$\frac{\partial \Delta \nu_d(T)}{\partial s} = \frac{\partial \nu_d(T)}{\partial s}\Bigg|_{\substack{\text{comparison}\\ \text{TDRS}}} - \frac{\partial \nu_d(T)}{\partial s}\Bigg|_{\substack{\text{reference}\\ \text{TDRS}}} \qquad (7\text{-}98)$$

where the values of $\partial \nu_d(T)/\partial s$ for both comparison and reference TDRSs can be evaluated by utilizing Equations (7-94) through (7-96).

7.3.7 TDRS RADIO FREQUENCY (RF) BEAM ANGLES MEASUREMENT MODEL

The TDRS radio frequency (RF) beam angles are the azimuth and elevation of the TDRS return link to either the multiple-access (MA) antenna or a single-access (SA) antenna,

measured in a TDRS vehicle-fixed coordinate system. The TDRS spacecraft vehicle-fixed coordinate system is a right-handed, orthogonal coordinate system centered at the TDRS center of mass, such that the position components are the following:

X_b = along the north-south slew axis of the SA antennas, positive east when the TDRS is on station

Y_b = along the solar array panel rotation axis, positive south when on station

Z_b = perpendicular to X_b and Y_b, positive towards the Earth subsatellite point

The beam angles are the following:

AZ = azimuth, measured in the $X_b - Z_b$ plane, from the Z_b axis to the projection of the P unit vector (defined below) in the $X_b - Z_b$ plane

EL = elevation, measured as the elevation of the TDRS return link above (positive in the $-Y_b$ direction) the $X_b - Z_b$ plane

In addition, the unit vector along the TDRS return link, $\hat{P}$, is known as the spatial beam vector when rotated to TDRS track-oriented coordinate frame.

The TDRS vehicle-fixed coordinate system and the beam angles are illustrated in Figure 7-6.

To obtain the measured spatial beam vector, the computational steps described below are followed.

1. The unit vector (X_b, Y_b, Z_b) for RF beam pointing in TDRS vehicle-fixed coordinates is computed as follows:

$$X_b = \cos(EL) \sin(AZ) \tag{7-99a}$$

$$Y_b = -\sin(EL) \tag{7-99b}$$

$$Z_b = \cos(EL) \cos(AZ) \tag{7-99c}$$

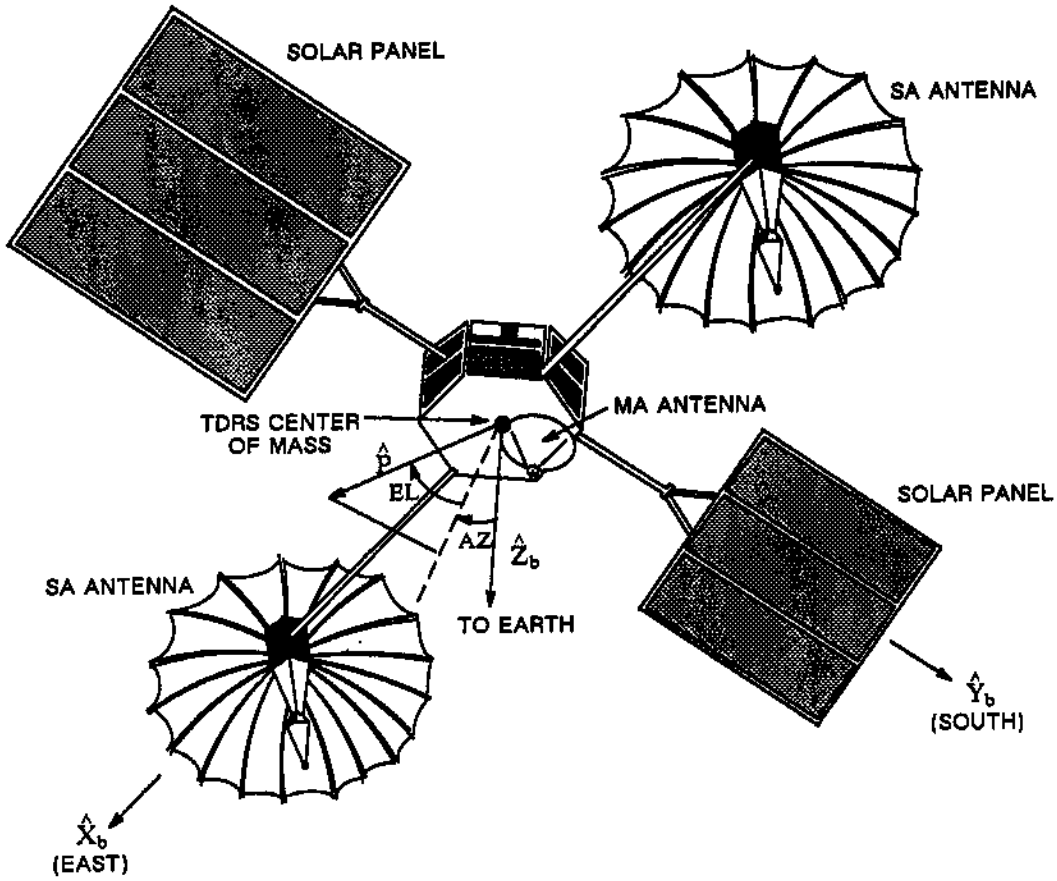

Figure 7-6. Definition of the TDRS Vehicle-Fixed Coordinates and RF Beam Angles

2. The measured spatial beam vector, $\hat{P}_o$, is computed in the track-oriented frame by rotating the unit vector for the RF beam pointing through the roll, pitch, and yaw angles (ϕ, θ, ψ) to the TDRS track-oriented system as follows:

$$\hat{P}_o = \begin{bmatrix} r_{11} & r_{12} & r_{13} \\ r_{21} & r_{22} & r_{23} \\ r_{31} & r_{32} & r_{33} \end{bmatrix} \begin{bmatrix} X_b \\ Y_b \\ Z_b \end{bmatrix} \tag{7-100}$$

where

$$r_{11} = \cos\theta \cos\psi - \sin\theta \sin\phi \sin\psi \quad (7\text{-}101a)$$

$$r_{12} = -\cos\phi \sin\psi \quad (7\text{-}101b)$$

$$r_{13} = \sin\theta \cos\psi + \cos\theta \sin\phi \sin\psi \quad (7\text{-}101c)$$

$$r_{21} = \cos\theta \sin\psi + \sin\theta \sin\phi \cos\psi \quad (7\text{-}101d)$$

$$r_{22} = \cos\phi \cos\psi \quad (7\text{-}101e)$$

$$r_{23} = \sin\theta \sin\psi - \cos\theta \sin\phi \cos\psi \quad (7\text{-}101f)$$

$$r_{31} = -\sin\theta \cos\phi \quad (7\text{-}101g)$$

$$r_{32} = \sin\phi \quad (7\text{-}101h)$$

$$r_{33} = \cos\theta \cos\phi \quad (7\text{-}101i)$$

The computed spatial beam vector, $\hat{P}_c$, and the computed AZ and EL angles, are obtained using the computation steps described below.

1. The unit vector from the return-link TDRS to the user spacecraft or transponder is computed in inertial coordinates as

$$\hat{P}_c' = \frac{\bar{r}_S - \bar{r}_T}{|\bar{r}_S - \bar{r}_T|} \quad (7\text{-}102)$$

where

$\bar{r}_T$ = position vector of the return-link TDRS at the measurement time

$\bar{r}_S$ = position vector of the user spacecraft or transponder at the measurement time

2. The unit vector $\hat{P}_c'$ is rotated to the TDRS track-oriented coordinates to obtain the computed spatial beam vector, $\hat{P}_c$.

The TDRS track-oriented coordinate axes ($\hat{x}_T$, $\hat{y}_T$, $\hat{z}_T$) are defined as follows:

$$\hat{z}_T = -\frac{\bar{r}_T}{|\bar{r}_T|} \tag{7-103a}$$

$$\hat{y}_T = -\frac{\bar{r}_T \times \bar{v}_T}{|\bar{r}_T \times \bar{v}_T|} \tag{7-103b}$$

$$\hat{x}_T = \hat{y}_T \times \hat{z}_T \tag{7-103c}$$

The transformation of the unit vector $\hat{P}_c'$, expressed in inertial coordinates, to the TDRS track-oriented frame is then given by

$$\hat{P}_c = R_T \hat{P}_c' \tag{7-104}$$

where

$$R_T = \begin{bmatrix} \hat{x}_T \cdot \hat{X} & \hat{x}_T \cdot \hat{Y} & \hat{x}_T \cdot \hat{Z} \\ \hat{y}_T \cdot \hat{X} & \hat{y}_T \cdot \hat{Y} & \hat{y}_T \cdot \hat{Z} \\ \hat{z}_T \cdot \hat{X} & \hat{z}_T \cdot \hat{Y} & \hat{z}_T \cdot \hat{Z} \end{bmatrix} \tag{7-105}$$

where $\hat{X}$, $\hat{Y}$, and $\hat{Z}$ are unit vectors along the inertial coordinate axes.

3. The (X_b, Y_b, Z_b) components of the unit vector for RF beam pointing are computed by rotating $\hat{P}_c$ through the measured yaw, pitch, and roll angles. This is the inverse of the rotation given in Equation (7-100).

4. The measured AZ and EL angles are computed by inverting Equations (7-99) using the values of $(\hat{X}_b, \hat{Y}_b, \hat{Z}_b)$ from step 3.

   The spatial beam angle observed-minus-computed (O-C) value, [O – C], is determined from

$$[O - C] = \arccos (\hat{P}_o \cdot \hat{P}_c) \tag{7-106}$$

where

$\hat{P}_o$ = measured spatial beam vector
$\hat{P}_c$ = computed spatial beam vector

7.4 RADAR ALTIMETER MODEL (Not Currently Available in GTDS)

GTDS models the satellite's orbital state vector in inertial coordinates. However, the radar altimeter measures the height of the satellite relative to the actual sea surface at the subsatellite point. Thus, the measurement modeling must relate the inertial coordinates to the actual sea surface height. This is accomplished by expressing both the satellite's position and the sea surface in body-fixed coordinates, x_b, y_b, and z_b. The following subsections discuss the surface model, the measurement equation, and the associated partial derivatives.

7.4.1 SURFACE MODEL

The sea surface is primarily determined by the Earth's gravity potential, which is the sum of the gravitational potential and the potential of the centrifugal force resulting from the Earth's rotation. A particular equipotential surface of the Earth's geopotential field, called a geoid, passes through the mean sea level surface and is nearly spherical, with flattening at the poles and a pear-shaped bulge in the southern hemisphere. The geoid approximates very closely (within a meter or two) the real sea surface in ocean areas. Small static and dynamic differences between the instantaneous sea surface and the geoid are caused by currents, tides, and weather phenomena. Typical magnitudes of these deviations (References 8 and 9) are presented in Table 7-3. Since complete information is unavailable for modeling these small effects, they are neglected in the radar altimeter model.

A reference surface is utilized that is conveniently chosen to be a rotationally symmetric ellipsoid that best fits the geoid in a least-squares sense. The maximum distance between this ellipsoid and the geoid is approximately 100 meters. This ellipsoidal surface also represents an equipotential surface of the normal geopotential, which includes (in addition to the point-mass term) even zonal harmonic coefficients, of which only C_2^0 and C_4^0 are significant. As a result, the sum of the additional terms needed to fully describe the geopotential (i.e., the disturbing potential) is small (Reference 10).

Table 7-3. Sea Surface—Geoid Deviation Sources

SOURCE	TYPICAL MAGNITUDE
Sea swell	1 meter
Wind waves	1 meter
Storm surges	10 centimeters
Barotropic depressions	10 centimeters
Currents	1 meter
Tides	1 meter

Figure 7-7 shows an exaggerated cross section of the geoid and the reference ellipsoid. The distance measured along the normal to the reference ellipsoid from point Q to the point P on the geoid is called the geoidal undulation and is designated by U. The vector $\hat{n}$ is the unit vector perpendicular to the reference ellipsoid, and $\hat{n}'$ is the unit vector perpendicular to the geoid.

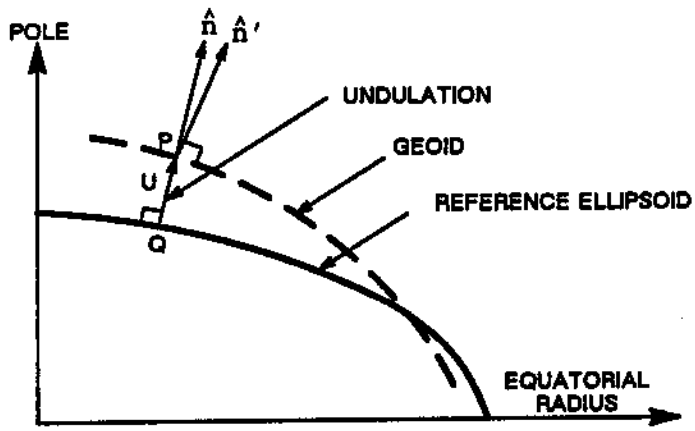

Figure 7-7. Geoid Undulation

Expressing the geopotential function, ψ, as the sum of the normal geopotential, ψ_N, and the disturbing potential, ψ_D, yields

$$\psi(r, \phi', \lambda) = \psi_N(r, \phi', \lambda) + \psi_D(r, \phi', \lambda) \tag{7-107}$$

where, from Section 4.3,

$$\psi_N(r, \phi', \lambda) = \frac{\mu}{r} + \frac{\mu}{r}\left[C_2^0\left(\frac{R_e}{r}\right)^2 P_2^0(\sin\phi') + C_4^0\left(\frac{R_e}{r}\right)^4 P_4^0(\sin\phi')\right] \quad (7\text{-}108)$$

and

$$\psi_D(r, \phi', \lambda) = \frac{\mu}{r}\left[\Delta C_2^0\left(\frac{R_e}{r}\right)^2 P_2^0(\sin\phi') + \Delta C_4^0\left(\frac{R_e}{r}\right)^4 P_4^0(\sin\phi')\right]$$

$$+ \frac{\mu}{r}\sum_{\substack{n=2\\ n\neq 2,4}}^{\infty} C_n^0\left(\frac{R_e}{r}\right)^n P_n^0(\sin\phi') \quad (7\text{-}109)$$

$$+ \frac{\mu}{r}\sum_{n=2}^{\infty}\sum_{m=1}^{n}\left(\frac{R_e}{r}\right)^n P_n^m(\sin\phi')\,[S_n^m \sin m\lambda + C_n^m \cos m\lambda]$$

In these equations,

- r = geocentric radius
- ϕ' = geocentric latitude
- λ = longitude
- R_e = Earth's equatorial radius

The geopotential function (the sum of the normal geopotential and the disturbing potential) differs from the gravitational potential in that it includes a term that represents the centrifugal potential due to the Earth's rotation. This term is included in the second zonal harmonic coefficient. Furthermore, the C_4^0 term in the normal geopotential is a function of C_2^0, whereas C_2^0 and C_4^0 are not functionally related in the gravitational potential. Consequently, ΔC_2^0 and ΔC_4^0 are included in Equation (7-109) to account for these differences.

To evaluate the magnitude of the geoidal undulations, the geoid of potential ψ_0 is compared with the reference ellipsoid of the same potential $\psi_N(Q) = \psi_0$. The normal potential $\psi_N(P)$ at P can be approximated by the linear relationship

$$\psi_N(P) = \psi_N(Q) + \left(\frac{\partial \psi_N}{\partial \hat{n}}\right)_Q U = \psi_N(Q) - \gamma(Q)\, U \qquad (7\text{-}110)$$

where $\gamma(Q)$ is normal gravity, i.e., the magnitude of the gradient of the normal geopotential on the reference ellipsoid at the point Q, where the algebraic sign is consistent with geodetic convention.

By definition,

$$\psi(P) = \psi_N(P) + \psi_D(P) \qquad (7\text{-}111)$$

and

$$\psi(P) = \psi_0 = \psi_N(Q) \qquad (7\text{-}112)$$

Substituting Equations (7-111) and (7-112) into Equation (7-110) yields Brun's Formula (Reference 10) for the geoidal undulation

$$U = \frac{\psi_D(P)}{\gamma(Q)} \qquad (7\text{-}113)$$

The geoidal undulation U is a function of the disturbing potential at the point P and normal gravity γ at the point Q. However, frequently the coordinates of the point Q are known but not those of point P. In this case, evaluation of the disturbing potential ψ_D at Q instead of P will cause only a small error in the calculation of U.

A better approximation for the disturbing potential, $\psi_D(P)$, can be obtained by correcting the geocentric radius, r, by the undulation U, calculated as described above. This value can then be used in Equation (7-113) to obtain a better value of U. Standard (normal)

gravity, which is the gradient of the normal potential ψ_N, is derived as a function of geodetic latitude and equatorial gravity in Reference 8, yielding

$$\gamma = \gamma_e(1 - f_2 \sin \phi + f_4 \sin^4 \phi) \tag{7-114}$$

where

$$f_2 = -f + \frac{5}{2}m + \frac{1}{2}f^2 - \frac{26}{7}f\,m + \frac{15}{4}m^2 \tag{7-115a}$$

$$f_4 = -\frac{1}{2}f^2 + \frac{5}{2}f\,m \tag{7-115b}$$

$$m + \frac{3}{2}m^2 = \frac{\omega^2 R_e}{\gamma_e} \tag{7-115c}$$

and

γ_e = normal equatorial gravity, which is 978.049 centimeters/second^2 for the International Ellipsoid

ω = Earth's rotation rate = $0.72921151 \times 10^{-4}$ radians/second

ϕ = geodetic latitude

f = flattening of the reference ellipsoid; f = (a – b)/c, where a and b are the semimajor and semiminor axes, respectively, of the reference ellipsoid

The value of m is obtained iteratively from the expression

$$m_n = \frac{\Omega^2 R_e}{\gamma_e} - \frac{3}{2}m_{n-1}^2 \tag{7-116}$$

starting from $m_0 = 0.00344986$.

The normal geopotential field and the normal gravity field of the reference ellipsoid are determined by four constants, usually chosen to be the following:

- a = semimajor axis of the reference ellipsoid
- f = flattening of the reference ellipsoid
- γ_e = equatorial gravity
- ω = Earth's angular speed of rotation

The flattening f of the reference ellipsoid of revolution and the values of C_2^0 for the spherical harmonic expansion of the normal potential are directly related. Thus, C_2^0 can be used instead of f as one of the four constants.

7.4.2 MEASUREMENT EQUATION

Ideally, the radar altimeter measures the minimum distance from the spacecraft to the sea surface, which is equivalent to the distance from the sea surface to the spacecraft measured normal to the sea surface. Since the sea surface is closely approximated by the geoid, the geoid is a convenient reference surface for altimetry. However, the present global mathematical models of the geoid are not accurate in fine detail. In the remainder of this section, the term geoid will denote the mathematical model of the geoid represented by means of a spherical harmonic expansion.

The minimum distance from the geoid to the spacecraft is indicated by the line segment OP in Figure 7-8. Solving for this distance is difficult because of the complicated form of the equations for the geopotential. Therefore, an approximation to the distance H is made by using the length H' of the line segment OP' along the normal to the reference ellipsoid passing through the spacecraft.

The spacecraft position is assumed to be known in Earth-fixed Cartesian coordinates, x_b, y_b, and z_b, by transforming from inertial to body-fixed coordinates using the methods of Section 3.3.1. The geocentric latitude, ϕ', the longitude, λ, and the magnitude, r_b, of the position vector to the spacecraft are given by

$$\phi' = \tan^{-1}\left[\frac{z_b}{\sqrt{x_b^2 + y_b^2}}\right] \tag{7-117}$$

$$\lambda = \tan^{-1}\left[\frac{y_b}{x_b}\right] \tag{7-118}$$

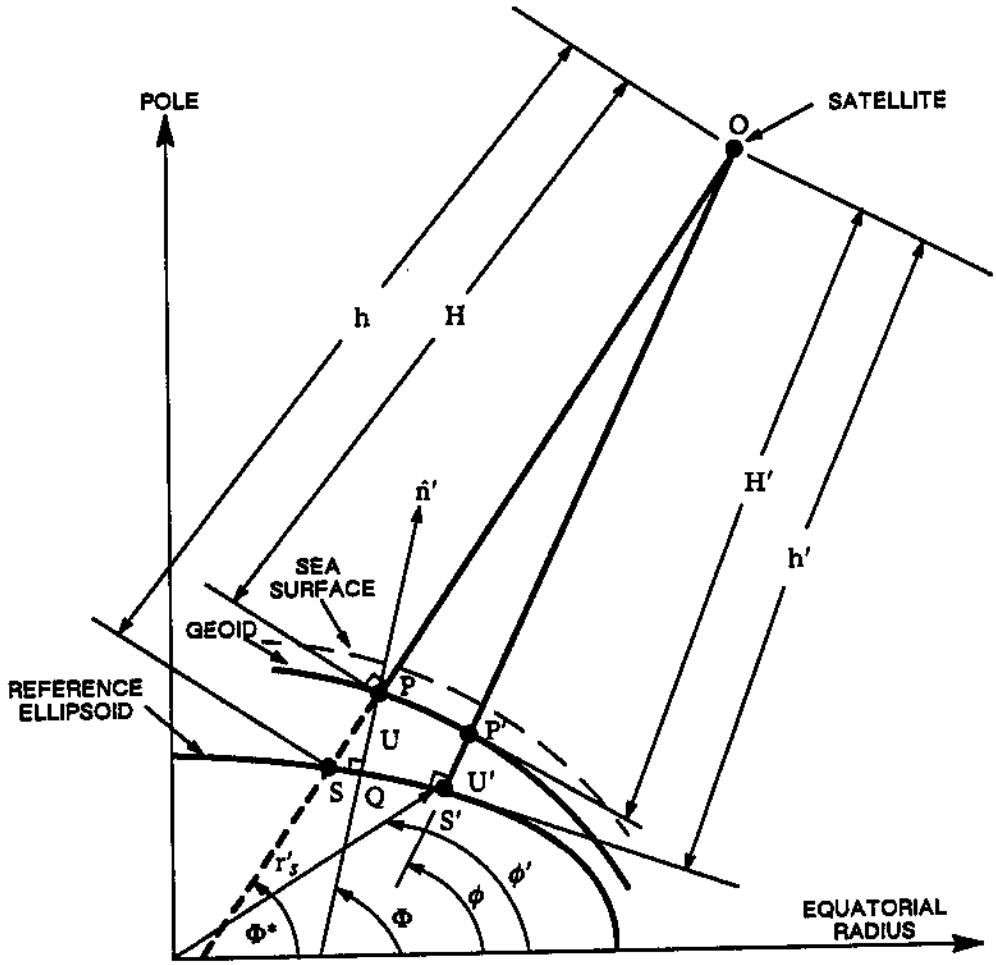

Figure 7-8. Geoid Geometry

and

$$r_b = \sqrt{x_b^2 + y_b^2 + z_b^2} \tag{7-119}$$

The geodetic latitude, ϕ, and the altitude h' to the subsatellite point S' on the reference ellipsoid are obtained from Section 3.3.6 as

$$\tan \phi = \frac{z_b}{\sqrt{x_b^2 + y_b^2}} \left[1 - \frac{N}{(N + h')} (2f - f^2) \right]^{-1} \tag{7-120}$$

where

$$N = \frac{R_e}{\sqrt{1 - (2f - f^2)\sin^2\phi}} \tag{7-121}$$

and

$$h' = \frac{\sqrt{x_b^2 + y_b^2}}{\cos\phi} - N \tag{7-122}$$

Equations (7-120), (7-121), and (7-122) must be solved iteratively.

The geoidal undulation U' at S' is obtained from Brun's Equation, Equation (7-113), (where $\psi_D(P)$ is given in Equation (7-109) and $\gamma(S')$ is given in Equation (7-114)) and, if necessary, using the procedure described in Section 7.4.1 to obtain the required precision.

Then, the resulting approximation for H is

$$H \cong H' = h' - U' \tag{7-123}$$

7.4.3 PARTIAL DERIVATIVES

Partial derivatives of the measurement are determined by transforming the measurement partial derivatives with respect to body-fixed coordinates to partial derivatives with respect to inertial Cartesian coordinates as described in Section 7.2.2. The partial derivative of H with respect to $\bar{r}_b$ is transformed to a partial derivative with respect to $\bar{R}$ as follows:

$$\frac{\partial H}{\partial \bar{R}} = \frac{\partial H}{\partial \bar{r}_b}\frac{\partial \bar{r}_b}{\partial \bar{R}} = \frac{\partial H}{\partial \bar{r}_b} \tag{7-124}$$

The partial derivative of H in Equation (7-124) involves numerous higher order terms because of the dependence of the location of P' (Figure 7-8) on the undulation U' and the

coordinates x_b, y_b, and z_b. However, these effects can be neglected to first order. The partial derivative of H with respect to $\bar{r}_b$ is therefore approximated as

$$\frac{\partial H}{\partial \bar{r}_b} = \frac{\partial h'}{\partial \bar{r}_b} = \frac{\bar{h}'^T}{h'} \tag{7-125}$$

where

$$\bar{h}' = \begin{bmatrix} x_b - x' \\ y_b - y' \\ z_b - z' \end{bmatrix} \tag{7-126}$$

Equation (7-125) is exact for a spherical geoid.

7.5 VERY LONG BASELINE INTERFEROMETER (VLBI) MODEL (Not Currently Available in GTDS)

The Very Long Baseline Interferometer (VLBI) System records signals transmitted by a satellite, along with timing signals from a local atomic clock, at two or more ground stations. The presence at each station of accurate atomic clocks, which can be coordinated by comparison with portable clocks dispatched between stations, means that the signals from the satellite recorded at each station can be time correlated with great precision. The ground stations measure phase differences between simultaneously received signals transmitted by the spacecraft. The measurable data are a phase difference time interval, τ, and its time derivative, $\dot{\tau}$. The time difference, τ, is the difference in the spacecraft range as measured from each of the ground stations on a given baseline, divided by the speed of light, c. Neglecting atmospheric effects, the time difference between reception of the same wavefront or phase at the first and second stations is

$$\tau = \frac{1}{c}(\varrho_1 - \varrho_2) = \frac{1}{c}\left[|\bar{r}_{1t_1}(t)| - |\bar{r}_{1t_2}(t + \tau)| \right] \tag{7-127}$$

where ϱ_1 and ϱ_2 are the ranges from the first and second stations to the satellite, respectively. The range vectors $\bar{r}_{1t_1}$ and $\bar{r}_{1t_2}$ are evaluated in the local tangent plane system centered at the first and second stations, respectively. An iterative procedure is required to determine τ, since the actual light time between the satellite and the station is not known initially. The iteration is initiated by assuming that τ is zero on the right-hand side of Equation (7-127).

The time-rate (Doppler) difference, $\dot{\tau}$, is the difference in the spacecraft range rate as measured from each station, divided by c, i.e.,

$$\dot{\tau} = \frac{1}{c}(\dot{\varrho}_1 - \dot{\varrho}_2) = \frac{1}{c}\left\{\left[\frac{\bar{r}_{1t_1}(t) \cdot \dot{\bar{r}}_{1t_1}(t)}{\varrho_1}\right] - \left[\frac{\bar{r}_{1t_2}(t+\tau) \cdot \dot{\bar{r}}_{1t_2}(t+\tau)}{\varrho_2}\right]\right\} \quad (7\text{-}128)$$

The partial derivatives of τ and $\dot{\tau}$ with respect to the epoch state vector components and dynamic model parameters are given by

$$\frac{\partial \tau}{\partial \bar{p}} = \frac{1}{c}\left\{\frac{\partial \varrho_1(t)}{\partial \bar{r}_{1t}(t)} \frac{\partial \bar{r}_{1t}(t)}{\partial \bar{R}(t)} \frac{\partial \bar{R}(t)}{\partial \bar{p}} + \frac{\partial \varrho_2(t')}{\partial \bar{r}_{1t}(t')} \frac{\partial \bar{r}_{1t}(t')}{\partial \bar{R}(t')} \frac{\partial \bar{R}(t')}{\partial \bar{p}}\right\} \quad (7\text{-}129)$$

$$\begin{aligned}\frac{\partial \dot{\tau}}{\partial \bar{p}} = \frac{1}{c}\Bigg\{&\frac{\partial \dot{\varrho}_1(t)}{\partial \bar{r}_{1t}(t)} \frac{\partial \bar{r}_{1t}(t)}{\partial \bar{R}(t)} \frac{\partial \bar{R}(t)}{\partial \bar{p}} \\ &+ \frac{\partial \dot{\varrho}_1(t)}{\partial \dot{\bar{r}}_{1t}(t)}\left[\frac{\partial \dot{\bar{r}}_{1t_1}(t)}{\partial \bar{R}(t)} \frac{\partial \bar{R}(t)}{\partial \bar{p}} + \frac{\partial \dot{\bar{r}}_{1t_1}(t)}{\partial \dot{\bar{R}}(t)} \frac{\partial \dot{\bar{R}}(t)}{\partial \bar{p}}\right] \\ &- \frac{\partial \dot{\varrho}_2(t')}{\partial \bar{r}_{1t_2}(t')} \frac{\partial \bar{r}_{1t}(t')}{\partial \bar{R}(t')} \frac{\partial \bar{R}(t')}{\partial \bar{p}} \\ &+ \frac{\partial \dot{\varrho}_2(t')}{\partial \dot{\bar{r}}_{1t_2}(t')}\left[\frac{\partial \dot{\bar{r}}_{1t_2}(t')}{\partial \bar{R}(t')} \frac{\partial \bar{R}(t')}{\partial \bar{p}} + \frac{\partial \dot{\bar{r}}_{1t_2}(t')}{\partial \dot{\bar{R}}(t')} \frac{\partial \dot{\bar{R}}(t')}{\partial \bar{p}}\right]\Bigg\}\end{aligned} \quad (7\text{-}130)$$

where $t' = t + \tau$

The partial derivatives $\partial \bar{R}(t)/\partial \bar{p}$ and $\partial \dot{\bar{R}}(t)/\partial \bar{p}$ are obtained from solutions to the variational equations; the partial derivatives $\partial \bar{r}_{1t}(t)/\partial \bar{R}(t)$, $\partial \dot{\bar{r}}_{1t}(t)/\partial \bar{R}(t)$, and $\partial \dot{\bar{r}}_{1t}(t)/\partial \dot{\bar{R}}(t)$ are presented in Section 7.2.2; and the partial derivatives of ϱ and $\dot{\varrho}$ with respect to their respective station-centered local tangent plane coordinates are given in Sections 7.2.3.2 and 7.2.3.3.

7.6 ATMOSPHERIC EFFECTS

All satellite radar tracking measurements from ground tracking stations are affected by the propagation characteristics of electromagnetic radiation through the Earth's

atmosphere. The bending, or refraction, of the rays means that a measurement of the direction of the signal propagation at the ground does not correspond to the direction of the relative position vector between the spacecraft and the tracking station. This ray bending also requires that the interpretation of the Doppler-shift measurement must be based on the projection of the appropriate velocity along the local propagation path direction, not along the relative position vector. Since the local propagation speed in the atmosphere is different from the vacuum speed, the interpretation of time-delay measurements must account for this effect.

In principle, the refraction effects can be characterized in terms of the variable local index of refraction, n, of the medium through which the signal is propagated. It is assumed in the correction algorithms that locally the atmosphere is spherically symmetric with respect to the center of the Earth; therefore, n varies only with the altitude, h (measured radially), at each tracking station. However, the n-versus-h profile is determined as a function of the station location and the variations in solar flux. The nature of these dependencies is discussed in the following sections, which present the mathematical algorithms characterizing the three basic refraction effects considered.

7.6.1 TROPOSPHERE MODEL (References 11 and 12)

The troposphere is the familiar gaseous atmosphere, which extends from the Earth's surface upward to a sensible limit of about 30 kilometers. For the microwave frequencies of interest in spacecraft tracking, the troposphere is essentially a nondispersive medium, i.e., the index of refraction, n, is independent of the frequency of the signal transmitted through it. Within this region, n is expressed as

$$n = 1 + N_T \tag{7-131}$$

where the tropospheric refractivity, N_T, depends only on the thermodynamic properties of the air. Since temperature and pressure data are not readily available at altitude, surface data are used to compute the surface refractivity, N_s, and an exponential decay with altitude is assumed, as follows:

$$N_T = N_s\, e^{-(h-h_s)/H_T} \tag{7-132}$$

where h_s and N_s are the altitude and refractivity at the tracking site, respectively, and H_T is the tropospheric scale height, i.e.,

$$H_T = \frac{1}{N_s} \int_{h_s}^{\infty} N_T(h)\, dh \tag{7-133}$$

The National Bureau of Standards Central Radio Propagation Laboratory (NBS CRPL) gives values of the scale height for different values of the surface refractivity. Reference 11 stresses the importance of using corresponding values of H_T and N_s. (Some formulations have fixed H_T at a standard value, allowing only N_s to vary.) Computation of the tropospheric corrections is discussed in detail in Sections 7.6.3 and 7.6.4.

7.6.2 IONOSPHERE MODELS (References 13 through 17)

Above the troposphere is another atmospheric region called the ionosphere, consisting of ionized particles and extending from about 80 kilometers to beyond 1000 kilometers. The index of refraction, n, is less than 1 in this dispersive medium, and it is expressed rigorously in terms of the ionospheric refractivity, N_I. For the sign convention chosen, the ionospheric refractivity N_I is greater than 0 and

$$n^2 = 1 - 2N_I \tag{7-134}$$

The difference from unity is small; and to first order in the refractivity N_I, n can be written in a form analogous to that for the troposphere as follows:

$$n = 1 - N_I \tag{7-135}$$

The refractivity depends on the electron density, N_e (in electrons/meter^3), and the signal frequency, ν (in hertz), according to

$$N_I = \frac{40.3N_e}{\nu^2} \tag{7-136}$$

The electron density profile for the ionosphere reaches a maximum value, N_m, at altitude h_m, decaying to zero very rapidly below and very slowly above this altitude (Figure 7-9). The exact shape of the profile and the values of N_m and h_m are highly variable functions of geographical location, time of day, season, and sunspot activity. If sufficient ionospheric sounding data are measured (with an ionosonde or a backscattering radar) at a given location and time, a reasonably accurate construction can be made of the electron density profile. From these data, interpolated to the time and geographic location of interest, the values of N_m and h_m can be estimated.

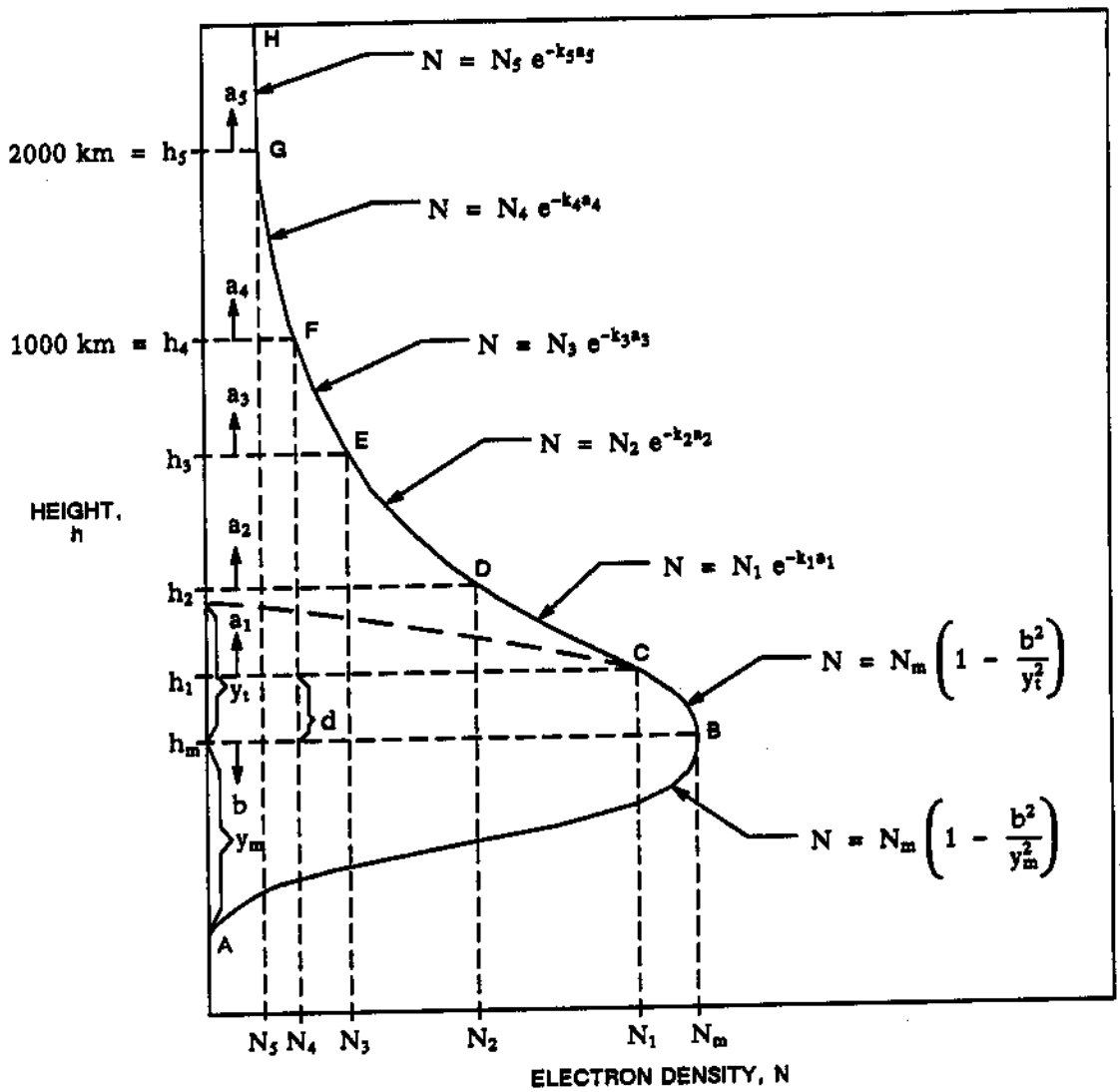

Figure 7-9. Empirical Worldwide Electron Density Profile

7.6.2.1 Modified Chapman Profile

The quantities N_m and h_m define only one point on the electron-density-versus-altitude profile. The other points can be assumed to lie on a modified Chapman profile in the form (Reference 13)

$$N_e = N_m e^{(1-z-e^{-z})} \tag{7-137}$$

$$z = \frac{h - h_m}{H_I} \tag{7-138}$$

where h is the altitude and H_I is the ionospheric scale height.

Substituting the modified Chapman profile (Equation (7-137)) into Equation (7-136) gives

$$N_I = \frac{40.3N_m}{\nu^2} e^{(1-z-e^{-z})} \tag{7-139}$$

as the altitude variation of the ionospheric refractivity.

It is generally conceded that the modified Chapman profile does not represent the best possible normalized profile. The fixed ratio of the total electron content above the maximum point to that below tends to be too large, on the average, compared with the observed diurnal variation. However, the theoretical foundation upon which Chapman based the derivation (Reference 14) and the susceptibility of the function to treatment of refraction effects in a closed analytical form argue for its continued use.

In GTDS, the maximum electron density, N_m, and its associated altitude, h_m, are determined as functions of the tracking station location and the variations in solar flux. The method of characterizing and determining these variables is described in Section 7.6.2.3. The ionospheric scale height is given in Reference 13 as

$$H_I = \frac{5}{3}[30 + 0.2(h_m - 200)] \quad \text{(kilometers)} \tag{7-140}$$

7.6.2.2 Empirical Worldwide Profile

The electron density profile is modeled as consisting of a biparabolic bottomside layer, a parabolic topside layer, and a five-sectioned topside exponential layer, as shown in Figure 7-9. This profile is defined by the following equations:

Bottomside:

$$N_I = N_m\left(1 - \frac{b_2}{y_m^2}\right)^2 \quad \text{(Segment A–B)} \tag{7-141}$$

Topside:

$$N_I = N_m \left(1 - \frac{b^2}{y_t^2}\right) \quad \text{(Segment B–C)} \tag{7-142a}$$

$$N_I = N_1 e^{-k_1 a_1} \quad \text{(Segment C–D)} \tag{7-142b}$$

$$N_I = N_2 e^{-k_2 a_2} \quad \text{(Segment D–E)} \tag{7-142c}$$

$$N_I = N_3 e^{-k_3 a_3} \quad \text{(Segment E–F)} \tag{7-142d}$$

$$N_I = N_4 e^{-k_4 a_4} \quad \text{(Segment F–G)} \tag{7-142e}$$

$$N_I = N_5 e^{-k_5 a_5} \quad \text{(Segment G–H)} \tag{7-142f}$$

where

$$y_t = a\, y_m \tag{7-143a}$$

$$a = \begin{cases} 1 & \text{(for } f_0 F_2 \leq 10.5 \text{ megahertz)} \\ 1 + 0.1333\,(f_0 F_2 - 10.5) & \text{(for } f_0 F_2 > 10.5 \text{ megahertz)} \end{cases} \tag{7-143b}$$

$$b = h - h_m \tag{7-143c}$$

$$a_1 = h - h_1 \tag{7-143d}$$

$$a_2 = h - h_2 \tag{7-143e}$$

$$a_3 = h - h_3 \tag{7-143f}$$

$$a_4 = h - h_4 \tag{7-143g}$$

$$a_5 = h - h_5 \tag{7-143h}$$

The empirical profile is completely defined by the parameters h_m, N_m, and y_m for the bottomside segment and N_1, N_2, N_3, N_4, N_5, k_1, k_2, k_3, k_4, k_5, h_1, h_2, h_3, h_4, and h_5 for the topside segment. The maximum electron density point (h_m, N_m) is determined as

a function of the location and the variations of the solar flux, as described in Section 7.6.2.3. The parameters h_1 through h_5 are defined as follows:

$$h_1 = h_m + d \tag{7-144a}$$

$$h_2 = h_1 + \frac{1}{3}(1.0 \times 10^3 - h_1) \tag{7-144b}$$

$$h_3 = h_1 + \frac{2}{3}(1.0 \times 10^3 - h_1) \tag{7-144c}$$

$$h_4 = 1000 \quad \text{(kilometers)} \tag{7-144d}$$

$$h_5 = 2000 \quad \text{(kilometers)} \tag{7-144e}$$

and d can be determined from

$$d = \frac{\sqrt{1 + k_1^2 y_t^2} - 1}{k_1} \tag{7-145}$$

The values of N_1 through N_5 are determined sequentially for the adjacent lower profile segments so as to maintain continuity of N_I at the segment interfaces, i.e.,

$$N_1 = \left(1 - \frac{d^2}{y_t^2}\right) N_m \tag{7-146a}$$

$$N_2 = N_1 e^{-k_1(h_2 - h_1)} \tag{7-146b}$$

$$N_3 = N_2 e^{-k_2(h_3 - h_2)} \tag{7-146c}$$

$$N_4 = N_3 e^{-k_3(h_4 - h_3)} \tag{7-146d}$$

$$N_5 = N_4 e^{-k_4(h_5 - h_4)} \tag{7-146e}$$

The final independent variables for the segmented N_I-versus-h profile are the maximum electron density, N_m, its associated altitude, h_m, the half-thickness of the bottomside layer, y_m, and the decay constants, k_1 through k_5, for the five topside exponential layers, respectively. The method for determining these variables in GTDS is described in Section 7.6.2.3.

7.6.2.3 Electron Density Profile Parameters

Both the Chapman and the empirical profiles require the maximum electron density, N_m, and its associated altitude, h_m. These variables are determined (References 15 and 17) as functions of the critical frequency of the F_2 layer, f_0F_2, and the M-factor, which is the ratio of MUF(3000)F_2 (the highest frequency usable for a 3000-kilometer single-hop propagation via the F_2 layer) to the critical frequency, f_0F_2, i.e.,

$$h_m = [1346.92 - 526.40 \times (\text{M-factor}) + 59.825 \times (\text{M-factor})^2] \qquad (7\text{-}147a)$$

$$N_m = 1.24 \times 10^{-2} \times (f_0F_2)^2 \qquad (7\text{-}147b)$$

where N_m is in electrons per meter^3, h_m is in kilometers, and f_0F_2 is in hertz. The critical frequency and the M-factor are functions of the location and the solar flux variations.

The critical frequency, f_0F_2, and the M-factor (also denoted $M(3000)F_2$), required for the profile calculation, are computed from monthly $U_{s,k}$ coefficient sets using equations based on Fourier series expansions and spherical harmonic analysis, which were developed by the Institute for Telecommunication Sciences (ITS) in Boulder, Colorado (now National Oceanic and Atmospheric Administration - Boulder).

The values of f_0F_2 and $M(3000)F_2$ are functions $\Omega(\phi, \lambda, T)$ of the geodetic latitude, ϕ, longitude, λ, and time, T. The function $\Omega(\phi, \lambda, T)$ can be expressed by a series of products of time-dependent functions D(T) and position-dependent geodetic functions $G(\phi, \lambda)$ as follows:

$$\Omega(\phi, \lambda, T) = \Omega[D(T), G(\phi, \lambda)] = \sum_{k=0}^{K} D_k(T)\, G_k(\phi, \lambda) \qquad (7\text{-}148)$$

where K is the cutoff point for the approximate representation of Ω (K = 75 when $\Omega = f_0F_2$ and K = 48 when $\Omega = M(3000)F_2$). These cutoff points were originally determined using a Student's t test.

The time-dependent functions can be expanded in their Fourier series representation with the coefficients $A_j^{(k)}$ and $B_j^{(k)}$ as follows:

$$D_k(T) = A_0^{(k)} + \sum_{j=1}^{H} [A_j^{(k)} \cos jT + B_j^{(k)} \sin jT] \qquad (7\text{-}149)$$

The number of harmonics retained in the series is H. Higher harmonics are not considered since they are produced more by noise than by real physical variation. It is sufficient to use H = 6 for the f_0F_2 computation and H = 4 for the $M(3000)F_2$ computation.

The Fourier coefficients $A_j^{(k)}$ and $B_j^{(k)}$ are numerically mapped as predicted, or final, coefficients $U_{s,k}$, which are the f_0F_2 or $M(3000)F_2$ coefficient sets used for the f_0F_2 and $M(3000)F_2$ computations, respectively, i.e.,

$$A_j^{(k)} = U_{2j,k} \qquad (j = 0, 1, \ldots H) \tag{7-150a}$$

$$B_j^{(k)} = U_{2j-1,k} \qquad (j = 1, 2, \ldots H) \tag{7-150b}$$

Thus,

$$\Omega(\phi, \lambda, T) = \sum_{k=0}^{K} U_{0,k}\, G_k(\phi, \lambda) + \sum_{j=1}^{H} \left[\cos jT \cdot \sum_{k=0}^{K} U_{2j,k}\, G_k(\phi, \lambda) + \sin jT \cdot \sum_{k=0}^{K} U_{2j-1,k}\, G_k(\phi, \lambda) \right] \tag{7-151}$$

The geodetic functions $G_k(\phi, \lambda)$ are linear combinations of the surface spherical harmonics. Extensive investigations to find the best arguments for the harmonic functions resulted in the use of the modified magnetic dip, $x = x(\phi, \lambda)$, since smaller residuals between the measured and computed test data values for f_0F_2 were obtained for this case than for any other case. Thus, $G_k(\phi, \lambda)$ is both an explicit and an implicit function of latitude, ϕ, and longitude, λ, i.e.,

$$G_0(\phi, \lambda) = \sin^{q_0} x \tag{7-152a}$$

$$G_k(\phi, \lambda) = \sin^{q_k} x \cdot \cos^k \phi \cdot \sin k\lambda \qquad (k = 1, 2, \ldots K) \tag{7-152b}$$

where q_k denotes the highest power of sin x for the k^{th}-order harmonic in longitude.

The modified magnetic dip, x, is an explicit function of the latitude and the magnetic dip, ℓ, where ℓ is computed from the magnetic field components $X(\phi, \lambda)$, $Y(\phi, \lambda)$, $Z(\phi, \lambda)$, i.e.,

$$\sin x = \frac{1}{\sqrt{\ell^2 + \cos \phi}} \tag{7-153}$$

$$\ell = \tan^{-1}\left[\frac{-Z}{\sqrt{X^2 + Y^2}}\right] \tag{7-154}$$

where X, Y, and Z are the north, east, and vertical components of the magnetic field vector. They are computed following the spherical harmonic analysis of the magnetic field by Chapman and Bartels, as discussed in detail in Reference 16.

Defining

$$\theta = 90° - \phi \tag{7-155a}$$

and

$$R = \frac{R_e}{R_e + h_m} \tag{7-155b}$$

where

R_e = equatorial radius of the Earth

h_m = height of the F_2 layer

the following expressions for X, Y, and Z result:

$$X = \sum_{n=1}^{6} \sum_{m=0}^{n} \frac{d}{d\theta} P_{n,m}(\cos \theta) \left[g_n^m \cos m\lambda + h_n^m \sin m\lambda\right] R^{n+2} \tag{7-156a}$$

$$Y = \sum_{n=1}^{6} \sum_{m=0}^{n} \frac{m\, P_{n,m}(\cos\theta)}{\sin\theta} [g_n^m \sin m\lambda - h_n^m \cos m\lambda] R^{n+2} \qquad (7\text{-}156b)$$

$$Z = \sum_{n=1}^{6} \sum_{m=0}^{n} -(n+1)\, P_{n,m}(\cos\theta) [g_n^m \cos m\lambda + h_n^m \sin m\lambda] R^{n+2} \qquad (7\text{-}156c)$$

Values tabulated from the analysis of the magnetic field for epoch 1960 are used for the coefficients g_n^m and h_n^m. The quantity $P_{n,m}(\cos\theta)$ is a multiple of the associated Legendre function.

In addition to the maximum electron density, the empirical electron density profile also requires the half-thickness of the bottomside layer, y_m, and the five topside decay constants, k_1 through k_5. The bottomside layer half-thickness is interpolated from tables in which y_m is modeled as a function of f_0F_2 and the local time. The five topside decay constants are interpolated from tables as functions of f_0F_2, the magnetic latitude, and the daily solar flux. Adjustments for seasonal effects are then made for y_m and the lower three exponential decay constants. The magnetic latitude is given by

$$\phi_m = \sin^{-1} [\sin\phi \sin\phi_p + \cos\phi \cos\phi_p \cos(\lambda - \lambda_p)] \qquad (7\text{-}157)$$

where (ϕ_p, λ_p) are the geodetic latitude and longitude of the magnetic north pole.

7.6.3 CHAPMAN PROFILE REFRACTION CORRECTIONS

The refraction correction formulas described in this section assume a spherically symmetric atmosphere. The tropospheric correction terms utilize an exponential refractivity profile, and the ionospheric correction terms utilize a modified Chapman electron density profile. Approximations in the derivation limit the application at very small elevation angles. The values for N_m and h_m used in the following equations are determined as functions of the location of the tracking station and the time as described in Section 7.6.2.3. The scale height, H_I, is calculated from Equation (7-140).

7.6.3.1 Range Correction

There are two speeds associated with electromagnetic signal propagation through a medium of index of refraction n, as follows:

$$c_p = \text{phase speed} = \frac{c}{n} \qquad (7\text{-}158a)$$

$$c_g = \text{group speed} = \frac{c}{n + \nu \dfrac{dn}{d\nu}} \qquad (7\text{-}158b)$$

where c is the vacuum speed of light.

The phase speed, c_p, is the speed associated with a phenomenon sensed by a phase measurement. The group speed, c_g, is the speed associated with a measurement of the transmission time of an energy pulse. In a nondispersive medium, such as the troposphere, $dn/d\nu = 0$ by definition. Therefore, the phase and group speeds are the same, in terms of the refractivity given by Equation (7-131), i.e.,

$$c_p = c_g = \frac{c}{n} = \frac{c}{1 + N_T} \qquad (7\text{-}159)$$

The ionosphere, however, is dispersive and the two speeds are different. Appropriate differentiations and substitutions of Equations (7-134), (7-135), and (7-136) into Equations (7-158) show that, to first order in N_I,

$$c_p = \frac{c}{n} \cong \frac{c}{1 - N_I} \qquad (7\text{-}160a)$$

$$c_g = n\,c \cong (1 - N_I)\,c \cong \frac{c}{1 + N_I} \qquad (7\text{-}160b)$$

The phase speed is greater than the vacuum speed of light. The time associated with the transmission of a signal over a path from the tracking station to the spacecraft is written as

$$\Delta t_p = \int_{\text{total path}} ds/c_p = \frac{1}{c} \int_{\text{troposphere}} (1 + N_T)\, ds + \frac{1}{c} \int_{\text{ionosphere}} (1 - N_I)\, ds \qquad (7\text{-}161a)$$

$$\Delta t_g = \int_{\text{total path}} ds/c_g = \frac{1}{c} \int_{\text{troposphere}} (1 + N_T)\, ds + \frac{1}{c} \int_{\text{ionosphere}} (1 + N_I)\, ds \qquad (7\text{-}161b)$$

depending on whether or not the measurement is of a phase or a group transmission property. In these expressions, ds is the increment of length along the signal propagation path.

The first terms in Equations (7-161) (unity in the integrands) represent the vacuum transmission times, and the second terms (the refractivities) represent the time corrections, Δt_c, caused by the atmosphere. The evaluation of Equations (7-161), by substituting for the refractivities from Equations (7-132) and (7-139), yields the total atmospheric range correction in the form

$$\Delta\rho = c\,\Delta t_c = \csc E\,[Q + U - (P + V)\cot^2 E] \tag{7-162}$$

The ionospheric terms are

$$Q = \pm \frac{40.3\,N_m\,e\,H_I}{\nu^2}\left[e^{-e^{-z}} - e^{-e\,\{(h_m - h_L)/H_I\}}\right] \tag{7-163a}$$

$$P = \pm \frac{40.3\,N_m\,e\,H_I}{\nu^2\,r_s}\left\{h\left[e^{-e^{-z}} - e^{-e\,\{(h_m - h_L)/H_I\}}\right] - (h - h_L) - H_I\,[S(Z) - S_L]\right\} \tag{7-163b}$$

where the positive sign denotes the range increment due to a group delay and the negative sign corresponds to the phase range decrement. The tropospheric delay terms are

$$U = H_T\,N_s \tag{7-164a}$$

$$V = \frac{H_T^2\,N_s}{r_s} \tag{7-164b}$$

In Equations (7-162) through (7-164),

- E = elevation of the straight line relative position vector from the tracking station to the spacecraft
- h = spacecraft altitude
- r_s = tracking station radius from the center of the Earth
- ν = frequency of the signal transmission
- h_L = lower altitude limit for the ionosphere (set at 80 kilometers in GTDS)

and

$$S(z) = e^{-z} - \frac{e^{-2z}}{2 \cdot 2!} + \frac{e^{-3z}}{3 \cdot 3!} - \frac{e^{-4z}}{4 \cdot 4!} + \cdots \tag{7-165}$$

$$S_L = 0.5772156649 + \left(\frac{h_m - h_L}{H_I}\right) \tag{7-166}$$

where

$$z = \frac{h - h_m}{H_I} \tag{7-167}$$

The expression S_L is used as the evaluation of the series S(z) at the lower limit because of convergence difficulties with the expression given by Equation (7-165).

The approximations made in the evaluation of the integrals in Equations (7-161) limit the validity of the form of the solution given by Equation (7-162). In particular, the error increases as the elevation angle decreases. Hence, the algorithm that is implemented in GTDS modifies this basic form (Equation (7-162)) to minimize the erroneous excursions at low elevation angles.

Typically, the true range refraction correction increases monotonically as the elevation angle decreases. Equation (7-162), however, can exhibit a maximum value at some angle and then decrease (even to negative values) for smaller angles. The maximum value is found by setting the following derivative to zero

$$\frac{d\Delta\varrho}{dE} = -(\cot E)\,\Delta\varrho + 2(P + V)\cot E \csc^3 E \tag{7-168}$$

and solving for $E = E_M$

$$\cot^2 E_M = \frac{Q + U - 2(P + V)}{3(P + V)} \tag{7-169}$$

In an example computed for typical troposphere and ionosphere profiles and for a VHF frequency of 136 megahertz, the maximum value given by Equation (7-169) occurred at

roughly $E_M = 22$ degrees. Thus, it would not be a good approximation to truncate the range corrections to this same maximum value for all elevations E less than 22 degrees. Accordingly, the algorithm in GTDS simply replaces the true $\cot^2 E$ term in Equation (7-162) with the limiting value given by Equation (7-169) when $\cot^2 E$ is greater than $\cot^2 E_M$. The (csc E) factor in Equation (7-162) causes the range correction to continue to increase as E decreases below E_M. In fact, it is necessary to truncate this factor (and hence the range correction) at a small elevation angle to prevent the values from becoming unrealistically large. On the basis of comparisons with ray traces computed through a typical ionospheric profile, it was determined that the (csc E) cutoff should be made for sin E less than 0.225. The comparison of the ray trace results with the GTDS algorithm is shown in Figure 7-10. The ionosphere was represented as a modified Chapman profile given by Equation (7-137), with

$$N_m = 1.0 \times 10^{12} \text{ electrons/meter}^3$$

$$h_m = 300 \text{ kilometers}$$

$$H_I = 65 \text{ kilometers}$$

$$\nu = 136 \text{ megahertz}$$

For $E \geq 35$ degrees, the corrections given by Equation (7-162) are essentially the same as the exact ray trace results. Below this angle the errors are less than 20 percent. Since uncertainties in the knowledge of the ionospheric characteristics can exceed 50 percent, it is not worthwhile from a practical standpoint to insist on greater accuracy in the algorithm at lower elevation angles.

7.6.3.2 Elevation-Angle-Dependent Corrections

Bouguer's Formula, the analogue to Snell's Law for a spherically stratified medium, gives

$$n\, r \sin i = \text{constant} \tag{7-170}$$

along any ray through the medium. Here i is the local incidence angle between the ray and the radius vector of magnitude r. Substituting $r_s + h$ for r in this formula and evaluating at two points on a ray yields the following relationship for the two incidence angles as functions of the altitudes and indices of refraction:

$$\frac{\sin i_0}{\sin i} = \frac{n}{n_0}\left(\frac{r_s + h}{r_s + h_0}\right) \tag{7-171}$$

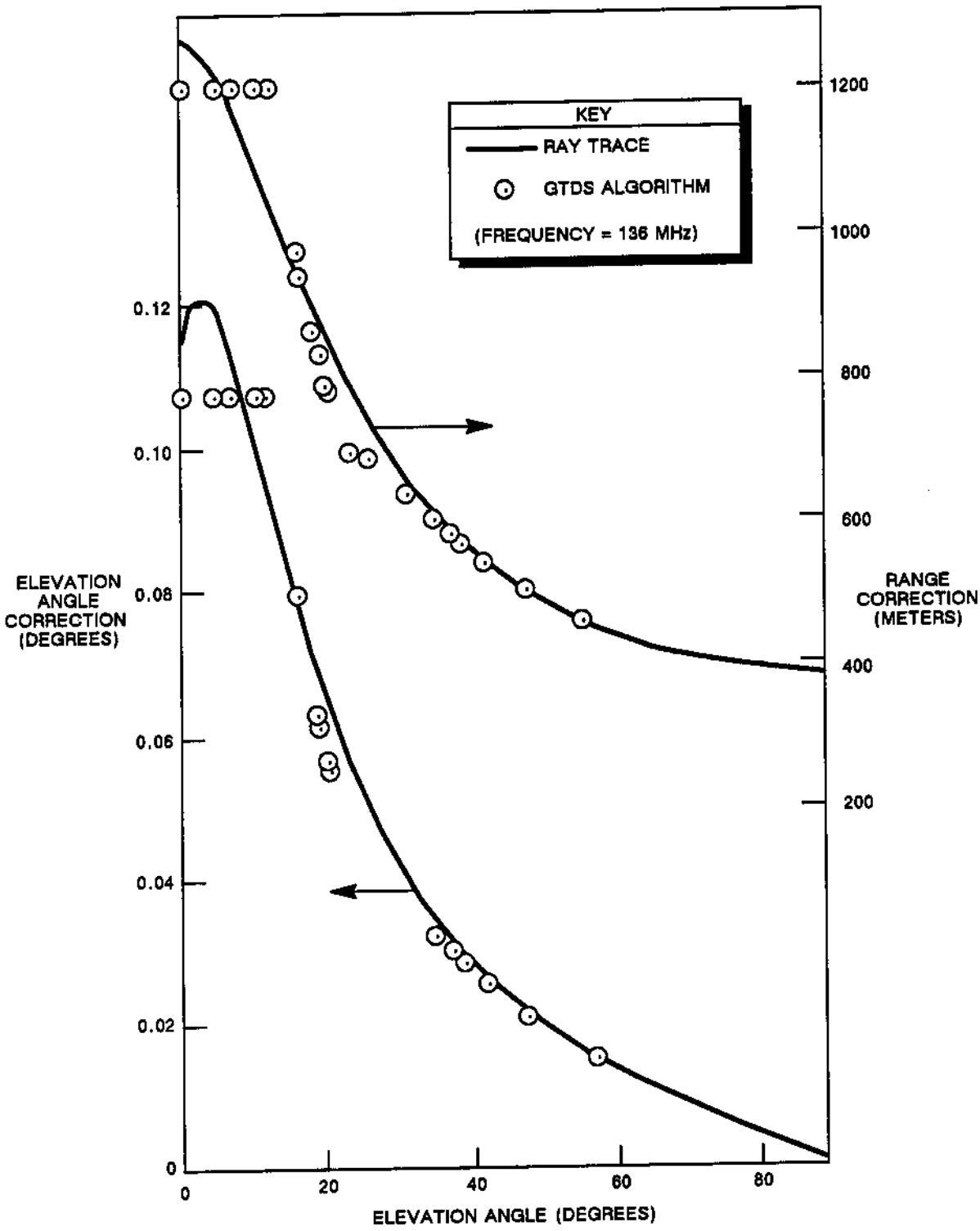

Figure 7-10. Refraction Correction Comparison of the Ray Trace Versus the GTDS Algorithm

If the initial point is taken at the tracking station, the apparent elevation angle of the ray is E_a. The initial point yields

$$h_0 = 0 \tag{7-172a}$$

$$n_0 = 1 + N_s \tag{7-172b}$$

$$\sin i_0 = \cos E_a \tag{7-172c}$$

Substituting Equations (7-172) into Equation (7-171) yields

$$\cos E_a = \frac{n(r_s + h)}{(1 + N_s) r_s} \sin i \tag{7-173}$$

If i were known a priori at the spacecraft position, Equation (7-173) could be used to compute the apparent elevation angle at the ground station. However, i is not known and Equation (7-173) must be modified to reformulate the desired solution in terms of quantities that are known. An approximation is made to an integration along the ray, resulting in

$$\cos E_a = \frac{\cos E}{(1 + N_s)(1 + I)} \tag{7-174}$$

where

$$I = \frac{\cot E}{r_s \delta} [Q - U - (P - V)(2 + \cot^2 E)] \tag{7-175}$$

$$\delta = \cos^{-1}\left(\frac{r_s \cos E}{r_s + h}\right) - E \tag{7-176}$$

Equation (7-174) is used as given for the correction of Minitrack data, since the direction cosines with respect to the station horizontal baseline both involve the factor E_a. The

correction for the elevation angle is determined (via the tangent of the difference of two angles) to give

$$E_a - E = \tan^{-1}\left\{\frac{\cos E\left[\sqrt{(1 + N_s)^2 (1 + I)^2 - \cos^2 E} - \sin E\right]}{\cos^2 E + \sin E\sqrt{(1 + N_s)^2 (1 + I)^2 - \cos^2 E}}\right\} \quad (7\text{-}177)$$

The refraction corrections to the X and Y gimbal angles (for both the 30-foot and 85-foot antennas) enter through the dependence of these angles on the elevation angle of the propagation path. The appropriate corrections are

$$(X_A - X)_{30} = \tan^{-1}\left\{\frac{\sin A \cos E\left[\sin E - \sqrt{(1 + N_s)^2 (1 + I)^2 - \cos^2 E}\right]}{\sin E\sqrt{(1 + N_s)^2 (1 + I)^2 - \cos^2 E + \sin^2 A \cos^2 E}}\right\} \quad (7\text{-}178a)$$

$$(Y_A - Y)_{30} = \sin^{-1}\left\{\frac{\cos A \cos E}{(1 + N_s)(1 + I)}\left[\sqrt{1 - \cos^2 A \cos^2 E} - \sqrt{(1 + N_s)^2 (1 + I)^2 - \cos^2 A \cos^2 E}\right]\right\} \quad (7\text{-}178b)$$

$$(X_A - X)_{85} = \tan^{-1}\left\{\frac{\cos A \cos E\sqrt{(1 + N_s)^2 (1 + I)^2 \cos^2 E} - \sin E}{\sin E\sqrt{(1 + N_s)^2 (1 + I)^2 - \cos^2 E + \cos^2 A \cos^2 E}}\right\} \quad (7\text{-}178c)$$

$$(Y_A - Y)_{85} = \sin^{-1}\left\{\frac{\sin A \cos E}{(1 + N_s)(1 + I)}\left[\sqrt{1 - \sin^2 A \cos^2 E} - \sqrt{(1 + N_s)^2 (1 + I)^2 - \sin^2 A \cos^2 E}\right]\right\} \quad (7\text{-}178d)$$

where A is the azimuth angle.

7.6.3.3 Doppler Corrections

The effects of atmospheric refraction on USB Doppler measurements are expressed in Appendix C in terms of difference vectors $\Delta\hat{u}$ and $\Delta\hat{d}$ between unit vectors along the actual (uplink and downlink) propagation paths and the straight lines characterizing the hypothetical vacuum propagation paths. Figure C-1 depicts the geometry of the two- or three-way Doppler signal transmission. From this figure, the four equations that define

the conditions at each end of the uplink and downlink paths are (Equations (C-12) and (C-14))

$$\hat{u}_T = \hat{u} + \Delta\hat{u}_T \tag{7-179a}$$

$$\hat{u}_v = \hat{u} + \Delta\hat{u}_v \tag{7-179b}$$

$$\hat{d}_v = \hat{d} + \Delta\hat{d}_v \tag{7-179c}$$

$$\hat{d}_R = \hat{d} + \Delta\hat{d}_R \tag{7-179d}$$

where

$$\hat{u} = \frac{\bar{r}_v - \bar{r}_T}{|\bar{r}_v - \bar{r}_T|} \tag{7-180a}$$

and

$$\hat{d} = \frac{\bar{r}_R - \bar{r}_v}{|\bar{r}_R - \bar{r}_v|} \tag{7-180b}$$

are unit vectors pointing up along the uplink path and down along the downlink path (both paths are characterized as straight line relative position vectors), and

$\bar{r}_v$ = satellite position vector

$\bar{r}_T$ = ground transmitter position vector

$\bar{r}_R$ = ground receiver position vector

An equation was derived in Appendix C for the Doppler-plus-bias cycle count N for the two-way or three-way measurement made by the USB system. The atmospheric refraction effect is the term $\Delta\dot{\varrho}_{avg}/2$ (Equation (C-34)).

The quantity

$$\Delta\dot{\varrho}_{avg} = \frac{\Delta\dot{\varrho}(t + \Delta t_{RR}) + \Delta\dot{\varrho}(t)}{2} \tag{7-181}$$

is the average of the quantities obtained by evaluating

$$\Delta\dot{\varrho} = \Delta\hat{u}_T \cdot \dot{\bar{r}}_T + \Delta\hat{d}_v \cdot \dot{\bar{r}}_v - \Delta\hat{u}_v \cdot \Delta\hat{d}_R \cdot \dot{\bar{r}}_R \tag{7-182}$$

at the beginning and at the end of the Doppler-plus-bias counting interval.

The computation of the USB Doppler refraction effect, therefore, requires a means for computing the correction vectors $\Delta\hat{u}_T$, $\Delta\hat{u}_v$, $\Delta\hat{d}_v$, and $\Delta\hat{d}_R$ at the appropriate times. The correction vector $\Delta\hat{u}_T$ for the uplink path at an instant when the ground station transmits a signal to the spacecraft is the difference between the unit vectors $\hat{u}_T$ and $\hat{u}$ along the actual and the hypothetical vacuum propagation paths. It must lie in the plane defined by $\hat{u}$ and the local vertical $\hat{v}_T$ at the station, *if it is assumed that the refractive medium is a spherically layered atmosphere*. Therefore, $\Delta\hat{u}_T$ is expressed as a linear combination* of $\hat{u}$ and $\hat{v}_T$

$$\Delta\hat{u}_T = A\,\hat{u} + B\,\hat{v}_T \tag{7-183}$$

In terms of the apparent elevation angle, E_a, of the actual propagation path and the straight-line relative position vector elevation angle, E,

$$\hat{u}_T \cdot \hat{u} = \cos(E_a - E) \tag{7-184a}$$

$$\hat{u}_T \cdot \hat{v}_T = \sin E_a \tag{7-184b}$$

Substituting from Equations (7-179) and (7-183) into Equations (7-184) and solving explicitly for A and B yields

$$A = \frac{\cos E_a}{\cos E} - 1 \tag{7-185a}$$

$$B = \sin E_a - \tan E \cos E_a \tag{7-185b}$$

*The vectors $\hat{u}$ and $\hat{v}_T$ coincide in the exceptional case of a direct overhead alignment. However, this case works out correctly, since A = –B, giving $\Delta\hat{u}_T = 0$.

Equation (7-174) can then be used to eliminate E_a, giving finally

$$A = \frac{1}{(1 + N_s)(1 + I)} - 1 \tag{7-186a}$$

$$B = \frac{1}{(1 + N_s)(1 + I)} \left[\sqrt{(1 + N_s)^2 (1 + I)^2 - \cos^2 E} - \sin E \right] \tag{7-186b}$$

where I is as defined in Equation (7-175) and N_s is the tropospheric surface refractivity at the transmitter.

Similar considerations apply in the determination of the correction vector $\Delta\hat{u}_v$ for the uplink path at the instant when the signal is received at the spacecraft. The geometry and notation are presented in Figure 7-11. Here again, the correction vector is expressed as a linear combination

$$\Delta\hat{u}_v = C\,\hat{u} + D\,\hat{v}_v \tag{7-187}$$

The following relationships are obtained from Figure 7-11:

$$\hat{u} \cdot \hat{v}_v = \cos \sigma \tag{7-188a}$$

$$\hat{u}_v \cdot \hat{u} = \cos a \tag{7-188b}$$

$$\hat{u}_v \cdot \hat{v}_v = \cos i \tag{7-188c}$$

$$\cos a = \cos \sigma \cos i + \sin \sigma \sin i \tag{7-188d}$$

Straightforward manipulation of these relationships, using Equations (7-187) and (7-179), yields a system of two simultaneous equations in the unknown coefficients C and D. The solutions for C and D in terms of i and σ are

$$C = \frac{\sin i}{\sin \sigma} - 1 \tag{7-189a}$$

$$D = \cos i - \cot \sigma \sin i \tag{7-189b}$$

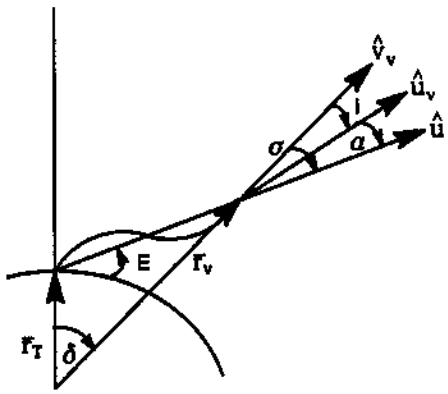

Figure 7-11. Uplink Path Geometry at Spacecraft Signal Reception

Equating the right-hand sides of Equations (7-173) and (7-174), making use of Equation (7-118), and solving explicitly for sin i yields

$$\sin i = \frac{r_T}{r_v} \frac{\cos E}{(1 - N_I)(1 + I)} \tag{7-190}$$

Examination of the triangle in Figure 7-11 shows that

$$E + \frac{\pi}{2} + \delta + \sigma = \pi \tag{7-191a}$$

or

$$E + \delta = \frac{\pi}{2} - \sigma \tag{7-191b}$$

Therefore,

$$\sin \sigma = \cos (E + \delta) \tag{7-192}$$

From Equation (7-176), this can be reduced to

$$\sin \sigma = \cos (E + \delta) = \frac{r_T}{r_v} \cos E \tag{7-193}$$

Substituting Equations (7-190) and (7-192) into Equations (7-189) finally yields

$$C = \frac{1}{(1 - N_I)(1 + I)} - 1 \tag{7-194a}$$

$$D = \frac{1}{(1 - N_I)(1 + I)} \left[\sqrt{(1 - N_I)^2 (1 + I)^2 - \frac{r_T^2 \cos^2 E}{r_v^2}} - \sqrt{1 - \frac{r_T^2 \cos^2 E}{r_v^2}} \right] \tag{7-194b}$$

If the same procedure is repeated for the downlink path to solve for the correction vectors $\Delta\hat{d}_v$ and $\Delta\hat{d}_R$, the result is

$$\Delta\hat{d}_v = C' \hat{d} + D' \hat{v}_v \tag{7-195a}$$

$$\Delta\hat{d}_R = A' \hat{d} + B' \hat{v}_R \tag{7-195b}$$

The solutions for C′ and A′ are identical with those for C and A, whereas the solutions for D′ and B′ are the negatives of those for D and B (Equations (7-194) and (7-186)).

The quantities I and N_I appear in the expressions for the primed and unprimed values of A, B, C, and D. Equations (7-139), (7-163), and (7-175) show the dependence of these quantities on the signal transmission frequency. The uplink carrier frequency should be used to compute the unprimed quantities, while the downlink carrier frequency should be used for the primed quantities.

The Doppler refraction correction for GRARR VHF and for sidetone ATSR data is shown in Appendix C (Equation (C-42)) to be of the form $(-\Delta\hat{u}_v \cdot \dot{r}_v)$, where the spacecraft

velocity, $\dot{\bar{r}}_v$, is taken at the signal turnaround time corresponding to the midpoint of the Doppler count interval. This time is the measurement time tag (the preprocessor-determined midpoint of the Doppler count interval) corrected in the orbit determination processing for the light time from the spacecraft to the station. The light-path bending term, $\Delta\hat{u}_v$, is computed according to Equations (7-187), (7-189), and (7-194). The vector $\hat{u}$ is defined (Equation (C-12)) as the unit vector directed along the instantaneous relative position vector from the station to the spacecraft. All other parameters in Equations (7-189) and (7-194) are defined in terms of this instantaneous relative geometry.

7.6.4 SEGMENTED PROFILE REFRACTION CORRECTIONS

The refraction correction formulas, described in Reference 15, assume that the total refraction correction is the sum of the tropospheric and ionospheric corrections as follows:

$$\Delta\varrho = \Delta\varrho_T + \Delta\varrho_I \tag{7-196a}$$

$$\Delta E = \Delta E_T + \Delta E_I \tag{7-196b}$$

$$\Delta\dot{\varrho} = \Delta\dot{\varrho}_T + \Delta\dot{\varrho}_I \tag{7-196c}$$

where $\Delta\varrho_T$, ΔE_T, and $\Delta\dot{\varrho}_T$ are due to the troposphere, and $\Delta\varrho_I$, ΔE_I, and $\Delta\dot{\varrho}_I$ are due to the ionosphere. These individual corrections are presented below.

7.6.4.1 Tropospheric Correction

The tropospheric corrections are obtained from Reference 12 and assume that the atmosphere has spherical symmetry and an exponential refractivity function as described by Equation (7-132). The equations are applicable over the entire range of elevation angles (0 degrees to 90 degrees).

Using monthly mean values of the refractivity, N_s, and the scale height, H_T, the following parameters are calculated:

$$p = \sqrt{\frac{2H_T}{r_s}} \tag{7-197a}$$

$$q = \frac{10^{-6} N_s r_s}{H_T} \tag{7-197b}$$

where $r_s = 6369.96$

The range and elevation angle corrections are

$$\Delta\varrho_T = 10^{-6} N_s H_T \left(m - \frac{1}{2} \frac{10^{-6} N_s r_s^2 L^2 \cos^2 E_a}{\varrho H_T} \right) \quad \text{(kilometers)} \tag{7-198a}$$

$$\Delta E_T = 10^{-6} N_s \cos E_a \left(i - \frac{r_s L}{\varrho} \right) \quad \text{(radians)} \tag{7-198b}$$

where

E_a = apparent elevation angle of the received signal
ϱ = slant range to the satellite

The quantity L is given by

$$L = 1 - i \sin E_a + \frac{1}{2} 10^{-6} N_s i^2 \tag{7-199}$$

and the quantities i (bending integral) and m are complex integral functions of the refractivity function and the elevation angle. Reference 12 presents the following approximations for i and m which are accurate over the entire range of elevation angles:

$$i = F(\sin E_a,\ I_1,\ I_2,\ i_0,\ i_1,\ p) \tag{7-200a}$$

$$m = F(\sin E_a,\ M,\ M_2,\ m_0,\ m_1,\ p) \tag{7-200b}$$

where the function F is given by

$$F(a, F_1, F_2, f_0, f_1, p) = \cfrac{1}{a + \cfrac{g_1}{a + \cfrac{g_2 \times 1.08885}{a + \cfrac{g_3 \times 1.320903}{a + g_4 \times 1.21313}}}} \tag{7-201}$$

with

$$g_1 = p^2 F_1 \tag{7-202a}$$

$$g_2 = \left(\frac{p^2 F_2}{g_1}\right) - g_1 \tag{7-202b}$$

$$g_3 = \frac{g_2}{f_0^2 F_1 \left(1 + \frac{g_1}{g_2}\right) - (1 + f_1 F_1)} \tag{7-202c}$$

$$g_4 = \frac{f_0 g_1}{p_3} \tag{7-202d}$$

The variables I_1, I_2, i_0, and i_1 are

$$I_1 = \frac{1}{2}\left(1 - \frac{1}{2} q\right) \tag{7-203a}$$

$$I_2 = \frac{3}{4}\left(1 - \frac{3}{4} q\right) + \frac{1}{8} q^2 \tag{7-203b}$$

$$i_0 = \sqrt{\pi}\,(1 - 0.9206\, q)^{-0.4468} \tag{7-203c}$$

$$i_1 = \frac{2}{1 - q} \tag{7-203d}$$

and the variables M_1, M_2, m_0, and m_1 are

$$M_1 = \frac{1}{2}\left(1 - \frac{3}{4}\,q\right) \tag{7-204a}$$

$$M_2 = \frac{3}{4}\left(1 - \frac{25}{24}\,q + \frac{11}{36}\,q^2\right) \tag{7-204b}$$

$$m_0 = i_0\left(1 + q + \frac{1}{12}\,q^2\,i_0^2\right) - \frac{1}{2}\,q\,k_0 \tag{7-204c}$$

$$m_1 = \frac{2\left(1 + \frac{1}{4}\,q\,i_0^2\right)}{1 - q} \tag{7-204d}$$

with

$$k_0 = \sqrt{2\pi}\,(1 - 0.9408\,q)^{-0.4759} \tag{7-205}$$

The range-rate correction is given by

$$\Delta\dot{\varrho}_T = -10^{-6}\,\dot{E}_a\,N_s\,H_T\cos E_a\left[n^2 - \frac{r_s}{\varrho}\,q\,L\cos^2 E_a \times (i + 10^{-6}\,N_s\,i\,j - j\sin E_a)\right] \tag{7-206}$$

where

$$j = F(\sin E_a,\ J_1,\ J_2,\ j_0,\ j_1,\ p) \tag{7-207a}$$

$$n = F(\sin E_a,\ N_1,\ N_2,\ n_0,\ n_1,\ p) \tag{7-207b}$$

The variables J_1, J_2, j_0, and j_1 are

$$J_1 = \frac{3}{2} I_1 \tag{7-208a}$$

$$J_2 = \frac{1}{2}(5I_2 - J_1^2) \tag{7-208b}$$

$$j_0 = \sqrt{i_1} \tag{7-208c}$$

$$j_1 = \frac{i_2}{j_0} \tag{7-208d}$$

where

$$i_2 = \frac{\sqrt{\pi}}{(1 - 1.023\,q)^{1.8}} \tag{7-209}$$

The variables N_1, N_2, n_0, and n_1 are

$$N_1 = \frac{3}{2} M_1 \tag{7-210a}$$

$$N_2 = \frac{1}{2}(5M_2 - N_1^2) \tag{7-210b}$$

$$n_0 = \sqrt{m_1} \tag{7-210c}$$

$$n_1 = \frac{\dfrac{i_0}{(1 - q)^2} + i_2\,q + \dfrac{1}{4}\,i_2\,(i_0\,q)^2}{n_0} \tag{7-210d}$$

7.6.4.2 Ionospheric Correction

Ionospheric refraction corrections are computed from the empirical electron density profile, described in Section 7.6.2.2, and its integrated electron content. The profile is computed for the latitude, ϕ, and longitude, λ, where the radio wave from the measuring station to the satellite penetrates the ionosphere. This is called the subionospheric point and is computed as a function of the station latitude, ϕ_s, and longitude, λ_s, and the elevation angle, E, and azimuth angle, A, from the station to the satellite, as follows:

$$\phi = \sin^{-1} (\sin \phi_s \cos a + \cos \phi_s \sin a \cos A) \tag{7-211}$$

$$\lambda = \lambda_s + \sin^{-1} \left(\frac{\sin A \sin a}{\cos \phi} \right) \tag{7-212}$$

where a is the geocentric angle between the station and the subionospheric point, given by

$$a = \frac{\pi}{2} - E - \sin^{-1} \left(\frac{R_e \cos E}{R_e + h_m} \right) \tag{7-213}$$

and h_m is the height of the ionosphere at the maximum electron density above the surface of the Earth. On the first iteration, h_m is estimated to be 300 kilometers. After computing h_m via Equation (7-147), the difference between the computed and estimated values of h_m is determined. If this difference is less than 1 kilometer, its effect is negligible; if it is greater than or equal to 1 kilometer, iterative computations of Equations (7-211) through (7-213) are made to obtain a new value of h_m.

The total vertical electron content, N_I, required by the correction algorithm is obtained by integrating the electron density profile in Equations (7-141) and (7-142) from zero to the height of the satellite, h. For a satellite below the biparabolic layer of the ionosphere,

$$\bar{N}_I = 0 \tag{7-214}$$

For the satellite in the bottomside biparabolic layer,

$$\bar{N}_I = \int_0^h N_I \, dh = N_m \left[\frac{8}{15} y_m - (h_m - h) + \frac{2}{3} \frac{(h_m - h)^3}{y_m^2} - \frac{1}{5} \frac{(h_m - h)^5}{y_m^4} \right] \tag{7-215}$$

where y_m is the half-thickness of the bottomside layer of the segmented electron density profile.

For the satellite in the topside parabolic layer,

$$N_I = N_m \left[\frac{8}{15} y_m - (h_m - h) + \frac{(h_m - h)^3}{3y_t^2} \right] \tag{7-216}$$

where y_t is the thickness of the topside parabolic layer (see Figure 7-9) and is given by

$$y_t = a\, y_m \tag{7-217}$$

where

$$a = \begin{cases} 1 & (\text{for } f_0F_2 \leq 10.5 \text{ megahertz}) \\ 1 + 0.1333\,(f_0F_2 - 10.5) & (\text{for } f_0F_2 > 10.5 \text{ megahertz}) \end{cases} \tag{7-218}$$

For a satellite in the first exponential layer,

$$\overline{N}_I = N_m \left(\frac{8}{15} y_m + d - \frac{d_3}{3y_t^2} \right) + N_m \left(1 - \frac{d^2}{y_t^2} \right) \left(\frac{1 - e^{-k_1(h-h_1)}}{k_1} \right) \tag{7-219}$$

where

$$d = \frac{\sqrt{1 + k_1^2 y_t^2} - 1}{k_1} \tag{7-220}$$

For a satellite in the second exponential layer,

$$\overline{N}_I = N_m\left(\frac{8}{15}\,y_m + d - \frac{d_3}{3y_t^2}\right) + N_m\left(1 - \frac{d^2}{y_t^2}\right) \times \left(\frac{1 - e^{-k_1(h_2-h_1)}}{k_1} + \frac{e^{-k_1(h_2-h_1)} - e^{-[k_1(h_2-h_1)+k_2(h-h_2)]}}{k_2}\right) \tag{7-221}$$

For a satellite in the third exponential layer,

$$\overline{N}_I = N_m\left(\frac{8}{15}\,y_m + d - \frac{d_3}{3y_t^2}\right) + N_m\left(1 - \frac{d^2}{y_t^2}\right) \times \left\{\frac{1 - e^{-k_1(h_2-h_1)}}{k_1} + \frac{e^{-k_1(h_2-h_1)}\left[1 - e^{-k_2(h_3-h_2)}\right]}{k_2} + \frac{e^{-[k_1(h_2-h_1)+k_2(h_3-h_2)]}\left[1 - e^{-k_3(h-h_3)}\right]}{k_3}\right\} \tag{7-222}$$

For a satellite in the fourth exponential layer,

$$\overline{N}_I = N_m\left(\frac{8}{15}\,y_m + d - \frac{d^3}{3y_t^2}\right) + N_m\left(1 - \frac{d^2}{y_t^2}\right) \times \left\{\frac{1 - e^{-k_1(h_2-h_1)}}{k_1} + \frac{e^{-k_1(h_2-h_1)}\left[1 - e^{-k_2(h_3-h_2)}\right]}{k_2} + \frac{e^{-[k_1(h_2-h_1)+k_2(h_3-h_2)]}\left[1 - e^{-k_3(h_4-h_3)}\right]}{k_3} + \frac{e^{-[k_1(h_2-h_1)+k_2(h_3-h_2)+k_3(h_4-h_3)]}\left[1 - e^{-k_4(h-h_4)}\right]}{k_4}\right\} \tag{7-223}$$

Finally, for a satellite in or above the fifth exponential layer,

$$\bar{N}_I = N_m\left(\frac{8}{15}\,y_m + d - \frac{d^3}{3y_i^2}\right) + N_m\left(1 - \frac{d^2}{y_i^2}\right)$$
$$\times\left\{\frac{1 - e^{-k_1(h_2-h_1)}}{k_1} + \frac{e^{-k_1(h_2-h_1)}\left[1 - e^{-k_2(h_3-h_2)}\right]}{k_2}\right.$$
$$+ \frac{e^{-[k_1(h_2-h_1)+k_2(h_3-h_2)]}\left[1 - e^{-k_3(h_4-h_3)}\right]}{k_3} \qquad (7\text{-}224)$$
$$+ \frac{e^{-[k_1(h_2-h_1)+k_2(h_3-h_2)+k_3(h_4-h_3)]}\left[1 - e^{-k_4(h_5-h_4)}\right]}{k_4}$$
$$\left. + \frac{e^{-[k_1(h_2-h_1)+k_2(h_3-h_2)+k_3(h_4-h_3)+k_4(h_5-h_4)]}\left[1 - e^{-k_5(h-h_5)}\right]}{k_5}\right\}$$

The range correction, $\Delta\varrho_I$, is computed from the vertical electron content and the elevation angle at which the radiowave passes through the ionosphere, as follows:

$$\Delta\varrho_I = \frac{40.3\,\bar{N}_I}{f^2\sqrt{1 - \left(\frac{R_e}{R_e + h_{mean}}\right)^2 \cos^2 E_a}} \qquad (7\text{-}225)$$

where the quantity f is the transmission frequency, the height of the mean of the electron distribution, h_{mean}, is given by

$$h_{mean} = h_m + \frac{1}{2}\,\frac{N_I}{N_m} - \frac{8}{15}\,y_m \qquad (7\text{-}226)$$

and

$$\frac{1}{f} = \left(\frac{1}{2f_u^2} + \frac{1}{2f_d^2}\right)^{1/2} \qquad (7\text{-}227)$$

where f_u and f_d are the uplink and downlink frequencies, respectively.

The range-rate correction, $\Delta\dot{\varrho}_I$, is obtained by differencing two successive range corrections in the following form:

$$\Delta\dot{\varrho}_I = - \frac{\Delta\varrho_I(t) - \Delta\varrho_I(t - \Delta t)}{\Delta t} \tag{7-228}$$

At the start of a data span for which no previous range correction exists, $\Delta\dot{\varrho}_I$ assumes one of the forms described below.

Satellites Below the Lower Biparabolic Layer

$$\Delta\dot{\varrho}_I = 0 \tag{7-229}$$

Satellites Within the Lower Biparabolic Layer

$$\Delta\dot{\varrho}_I = -\frac{d\Delta\varrho_I}{dt} = -\left(\frac{f_0F_2}{f}\right)^2 \times \frac{(40.3 \times 1.24 \times 10^{-2})\left[1 - \left(\frac{h_m - h}{y_m}\right)^2\right]^2}{\left[1 - \left(\frac{R_e}{R_e + h_{mean}} \cos E_a\right)^2\right]^{1/2}} \times \dot{h}$$

$$+ \frac{\Delta\varrho_I \left(\frac{R_e}{R_e + h_{mean}}\right)^2 \sin E_a \cos E_a}{1 - \left(\frac{R_e}{R_e + h_{mean}} \cos E_a\right)^2} \times \dot{E} \tag{7-230}$$

where

$\dot{h}$ = altitude rate of the satellite

$\dot{E}$ = elevation rate of the satellite

Satellites in the Topside Parabolic Layer

$$\Delta\dot{\varrho}_I = -\frac{d\Delta\varrho_I}{dt} = -\left(\frac{f_0F_2}{f}\right)^2 \times \frac{(40.3 \times 1.24 \times 10^{-2})\left[1 - \frac{(h_m - h)^2}{y_t^2}\right]}{\left[1 - \left(\frac{R_e}{R_e + h_{mean}} \cos E_a\right)^2\right]^{1/2}} \times \dot{h}$$

$$+ \frac{\Delta\varrho_I \left(\frac{R_e}{R_e + h_{mean}}\right)^2 \sin E_a \cos E_a}{1 - \left(\frac{R_e}{R_e + h_{mean}} \cos E_a\right)^2} \times \dot{E} \qquad (7\text{-}231)$$

Satellites in the Exponential Layers

$$\Delta\dot{\varrho}_I = -\frac{d\Delta\varrho_I}{dt} = -\left(\frac{f_0F_2}{f}\right)^2 \times \frac{(40.3 \times 1.24 \times 10^{-2})\left[1 - \frac{d^2}{y_t^2}\right]}{\left[1 - \left(\frac{R_e}{R_e + h_{mean}} \cos E_a\right)^2\right]^{1/2}} \times \dot{h} \times em$$

$$+ \frac{\Delta\varrho_I \left(\frac{R_e}{R_e + h_{mean}}\right)^2 \sin E_a \cos E_a}{1 - \left(\frac{R_e}{R_e + h_{mean}} \cos E_a\right)^2} \times \dot{E} \qquad (7\text{-}232)$$

The exponential multiplier, em, of the $\dot{h}$ term can take on five different forms, as defined below.

For a satellite in the first exponential layer,

$$em = e^{-k_1(h-h_1)} \qquad (7\text{-}233)$$

For a satellite in the second exponential layer,

$$em = e^{-k_1(h_2-h_1)}\, e^{-k_2(h-h_2)} \qquad (7\text{-}234)$$

For a satellite in the third exponential layer,

$$em = e^{-k_1(h_2-h_1)}\, e^{-k_2(h_3-h_2)}\, e^{-k_3(h-h_3)} \tag{7-235}$$

For a satellite in the fourth exponential layer,

$$em = e^{-k_1(h_2-h_1)}\, e^{-k_2(h_3-h_2)}\, e^{-k_3(h_4-h_3)}\, e^{-k_4(h-h_4)} \tag{7-236}$$

Finally, for a satellite in or above the fifth exponential layer,

$$em = e^{-k_1(h_2-h_1)}\, e^{-k_2(h_3-h_2)}\, e^{-k_3(h_4-h_3)}\, e^{-k_4(h_5-h_4)}\, e^{-k_5(h-h_5)} \tag{7-237}$$

The elevation angle correction, ΔE_a, is given by

$$\cos\,(\Delta E_a) = \frac{X_1 \cos a - X_2}{(X_1^2 + X_2^2 - 2X_1 X_2 \cos a)^{1/2}} \tag{7-238}$$

where

$$X_1 = [(R_e + h)^2 - R_e^2 \cos^2 E_a]^{1/2} + R_e \cos E_a \tan\left(\frac{a}{2}\right) \tag{7-239}$$

$$X_2 = R_e \sin E_a - R_e \cos E_a \tan\left(\frac{a}{2}\right) \tag{7-240}$$

$$a = \frac{1}{2}\left(\frac{f_0F_2}{f}\right)^2 \xi \frac{\tan \phi_0 \sec^2 \phi_0}{r_0} \frac{\overline{N}_I}{N_m} \quad \text{(deviation angle)} \tag{7-241}$$

$$r_0 = R_e + h_{mean} \tag{7-242}$$

$$h_{mean} = h_m + \frac{1}{2}\frac{\bar{N}_I}{N_m} - \frac{8}{15} y_m \tag{7-243}$$

$$\sin \phi_0 = \frac{R_e}{r_0} \cos E_a \tag{7-244}$$

The variable ξ is tabulated as a function of

$$\left(\frac{f_0 F_2}{f}\right) \sec^2 \phi_m \tag{7-245}$$

where

$$\sin \phi_m = \frac{R_e}{r_m} \cos E_a \tag{7-246}$$

and

$$r_m = R_e + h_m \tag{7-247}$$

7.7 ADDITIONAL CORRECTIONS

This section discusses the modeling in GTDS of the light-time, ground antenna mount, transponder delay, and spacecraft antenna offset corrections.

7.7.1 LIGHT-TIME CORRECTION

GTDS provides for a light-time correction which can be applied to GRARR, C-band, and Minitrack measurements for greater accuracy of modeling. All of these measurement types are modeled (Section 7.2.3) in terms of the instantaneous relative position vector from the tracking station to the spacecraft, computed in the local tangent coordinate system (Section 7.2.2). Since the spacecraft is the only object that is moving in this coordinate system, the appropriate time for calculating the instantaneous relative position vector is the time t_v, when the vehicle transponder turns the tracking signal around. (For the one-way Minitrack signal, t_v corresponds to the time when the signal was transmitted by

the spacecraft.) The actual measurement is time-tagged at the time t_R, when the signal is received at the ground station. The light-time correction consists of making an approximation to t_v by changing the measurement time tag to

$$t_v = t_R - \frac{\Delta\varrho}{c} \tag{7-248}$$

where $\Delta\varrho$ is the one-way relative range from the spacecraft to the tracking station. A first approximation to $\Delta\varrho$ is determined in GTDS by computing the relative range vector at the actual measurement time, t_R, utilizing the spacecraft position vector at t_R. The difference between this relative range and the correct relative range corresponding to t_v could be corrected by means of an iterative estimation algorithm. However, this is not done in GTDS, since the very small improvement in accuracy is insignificant compared with the degree of the approximation implicit in the basic measurement model. Thus, the first estimate for $\Delta\varrho$ is used in computing the light-time correction to the measurement time tag.

7.7.2 GROUND ANTENNA MOUNT CORRECTIONS

For X and Y antennas, a correction is performed on range and range-rate measurements, since the electrical phase center of the antenna moves with the antenna and is displaced from the geodetic point of reference which is the center of the fixed axis. The correction ΔR applied for range is

$$\Delta R = D \cos (Y) \tag{7-249}$$

which, by differentiation with respect to time, gives the correction for the range rate

$$\Delta\dot{R} = -D \sin (Y)\, \dot{Y} \tag{7-250}$$

In these expressions, Y is the measured Y angle and D is the nominal distance from the electrical phase center to the center of the fixed axis. The correction to ΔR and $\Delta\dot{R}$ due to the X angle and the corrections to the X and Y angles due to the displacement of the electrical phase center are ignored.

7.7.3 TRANSPONDER DELAY CORRECTION

For those tracking systems that use a transponder onboard the satellite to receive and then retransmit a signal, the transponder delay, i.e., the time interval between reception and

transmission of a given signal, must be taken into consideration. These satellite transponder time delays are functions of the frequency of the signal received by the transponder, i.e.,

$$\Delta\tau = f(\nu_R) \tag{7-251}$$

The characteristics of the function f for a specific transponder must be determined experimentally by calibration of the transponder on the ground before launch.

For tracking systems other than TDRSS, the function obtained in this manner can then be entered in GTDS as a table of transponder delay times versus the frequency, from which the delay for any intermediate value of the frequency can be obtained by interpolation. As an alternative, provision is made in GTDS to use nominal (default) tables or constant delay times. See Section 7.3.2.2 for a description of the method used for TDRSS.

7.7.4 SPACECRAFT ANTENNA OFFSET CORRECTIONS

In general, when computing the range to a spacecraft, it is assumed that the tracking antenna is located at the center-of-mass of the spacecraft. However, in cases where the tracking antenna is located at a significant distance (e.g., more than 5 meters) from the center-of-mass, this offset can be accounted for in modeling the tracking measurements using the model described in this section. Currently, this capability is only available for the user spacecraft in computing TDRSS and/or SGLS tracking measurements.

The antenna offset vector, $\Delta\bar{r}_a$, is assumed to have constant components in the orbit plane coordinate frame (described in Section 3.2.5), i.e.,

$$\Delta\bar{r}_a = \Delta H\ \hat{x}_{op} + \Delta L\ \hat{y}_{op} + \Delta C\ \hat{z}_{op} \tag{7-252}$$

where

$$\hat{x}_{op} = \frac{\bar{r}}{|\bar{r}|} \tag{7-253a}$$

$$\hat{y}_{op} = \hat{z}_{op} \times \hat{x}_{op} \tag{7-253b}$$

$$\hat{z}_{op} = \frac{\bar{r} \times \dot{\bar{r}}}{|\bar{r} \times \dot{\bar{r}}|} \tag{7-253c}$$

and $\bar{r}$ is the radius vector of the spacecraft center-of-mass.

The true antenna location to be used in the computation of the spacecraft tracking measurements is then given by

$$\bar{r}_a = \bar{r} + \Delta\bar{r}_a \tag{7-254}$$

7.8 ESTIMATION MODEL

The deviation between the actual measurement and the computed measurement is modeled as a first-order Taylor series expansion around the predicted measurement. This expansion relates deviations in the measurement residuals to deviations in dynamic parameters, station locations, measurement biases, and time biases, and it establishes the required set of linear regression equations. The estimation model for any measured quantity can then be written as

$$O_0 - O_c = \frac{\partial O_c}{\partial \bar{q}} \overline{\Delta q} + n \tag{7-255}$$

where

O_0 = actual measurement with time tag t

O_c = computed measurement based on a previous estimate of the parameter vector $\bar{q}$

$\overline{\Delta q}$ = correction to the parameter vector $\bar{q}$

n = measurement noise

The parameter vector $\bar{q}$ can consist of dynamic parameters, $\bar{p}$ (those parameters involved in the equations of motion); station locations, $\bar{r}_s$; measurement biases, b; and measurement time biases, δt. The total parameter vector can then be written as

$$\bar{q} = \begin{bmatrix} \bar{p} \\ \bar{r}_s \\ b \\ \delta t \end{bmatrix} \tag{7-256}$$

The modeled measurement can be written functionally as

$$O_c = f(\bar{q}, t) = f(\bar{p}, \bar{r}_s, b, \delta t, t) \tag{7-257}$$

Substituting the appropriate partial derivatives of Equation (7-257) into Equation (7-255) yields

$$O_0 - O_c = \left(\frac{\partial O_c}{\partial \overline{p}}\right)\overline{\Delta p} + \left(\frac{\partial O_c}{\partial \overline{r}_s}\right)\overline{\Delta r}_s + \left(\frac{\partial O_c}{\partial b}\right)\Delta b + \left(\frac{\partial O_c}{\partial(\delta t)}\right)\Delta(\delta t) + n \quad (7\text{-}258)$$

which can be written in a more compact form as

$$O_0 - O_c = \left[\frac{\partial O_c}{\partial \overline{p}} \mid \frac{\partial O_c}{\partial \overline{r}_s} \mid \frac{\partial O_c}{\partial b} \mid \frac{\partial O_c}{\partial(\delta t)}\right]\begin{bmatrix}\overline{\Delta p}\\ \overline{\Delta r}_s\\ \Delta b\\ \Delta(\delta t)\end{bmatrix} + n \quad (7\text{-}259)$$

or

$$O_0 - O_c = F\,\overline{\Delta q} + n \quad (7\text{-}260)$$

Equation (7-260) defines the linear regression equations that are solved by the iterative classical or sequential weighted least-squares methods described in Chapter 8. The formulation, as shown in Equation (7-260), describes m equations (for m measurements) in p unknowns (the number of q parameters). The matrix F in Equation (7-260) is of dimension ($m \times p$). Chapter 8 derives the required solution to the normal equations in terms of F and the weighting matrix, W, under the assumption that W is a diagonal matrix, that is, that the measurements are uncorrelated. Under this assumption, the terms in the normal equations requiring F can be developed on a measurement-by-measurement basis, yielding the solution of the normal equations without explicitly forming the full ($m \times p$) F matrix. This is a standard method for all existing least-squares orbit determination programs and is discussed in more detail in Chapter 8.

7.9 REFERENCES

1. Ryan, J.: 1968, *Apollo Unified S-Band Range Rate Data Utilization Techniques*, Goddard Space Flight Center Report X-830-68-431, November 1968.

2. Liu, S. Y.: 1980, *Mathematical Specification for the Tracking and Data Relay Satellite System (TDRSS)*, Computer Sciences Corporation Report CSC/SD-80/6007, February 1980.

3. Teles, J., and Ayers, C.: 1977, "Advanced Spacecraft Tracking Techniques Using the Tracking and Data Relay Satellite System (TDRSS)," paper presented at the AAS/AIAA Astrodynamics Conference, Jackson, Wyoming, September 7–9, 1977.

4. Carnaham, B., Luther, H. A., and Wilkes, J. O.: 1969, *Applied Numerical Methods*, John Wiley and Sons, New York, 1969.

5. Teles, J., and Guedeney, V. S.: 1978, *TDRSS Observed and Computed Measurement Algorithms*, Goddard Space Flight Center Report TDO 78-43, April 1978.

6. Cowan, D. J.: 1978, *Computed TDRS Doppler Measurements and Range Ambiguity Interval Applicable to TDRS Range Data* (Preliminary), Goddard Space Flight Center, Code 572, Memorandum, February 1978.

7. Ayres, C. L., Stull, H. E., and Teles, J.: 1975, *Tracking Data Relay Range and Range-Rate Observation Modeling via the Applications Technology Satellite-6 (ATS-6)*, Goddard Space Flight Center Report X-570-75-53, March 1975.

8. Greenwood, J. A., et al.: 1967, *Radar Altimetry from a Spacecraft and Its Potential Application to Geodesy and Oceanography*, New York University School of Engineering and Science, Department of Meteorology and Oceanography, Report on Contract N62306-1589, U. S. Naval Oceanographic Office, May 1967.

9. Brown, R. D., and Fury, R. J.: 1972, *Determination of the Geoid from Satellite Altimeter Data*, Computer Sciences Corporation Report 5035-21000-01TM, April 1972.

10. Heiskanen, W. A., and Moritz, H.: 1967, *Physical Geodesy*, W. H. Freeman and Company, 1967.

11. Berbert, J. H., and Parker, H. C.: 1970, *GEOS Satellite Tracking Corrections for Refraction in the Troposphere*, Goddard Space Flight Center Report X-514-70-55, February 1970.

12. Marini, J. W.: 1971, *Closed Form Satellite Tracking Data Corrections for an Arbitrary Tropospheric Profile*, Goddard Space Flight Center Report X-551-71-122 (Preprint), March 1971.

13. Freeman, J. J.: 1965, *Final Report on Ionospheric Correction to Tracking Parameters*, Goddard Space Flight Center Report NAS 5-9782, November 3, 1965.

14. Davies, K.: 1965, *Ionospheric Radio Propagation*, National Bureau of Standards Monograph 80, April 1, 1965.

15. DBA Systems, Inc.: 1972, *Ionospheric and Tropospheric Refraction Corrections in GTDS*, DBA Systems, Inc. Final Report, prepared for Goddard Space Flight Center under Contract No. NAS 5-11730, September 1972.

16. Jones, W. B., Graham, R. P., and Leftin, M.: 1969, *Advances in Ionospheric Mapping by Numerical Methods*, ESSA Research Laboratories Technical Report ERL 107-ITS-75, Boulder, Colorado, May 1969.

17. Schmid, P. E., et al.: 1973, *NASA-GSFC Ionospheric Corrections to Satellite Tracking Data*, Goddard Space Flight Center Report X-591-73-281, December 1973.

CHAPTER 8—ESTIMATION

The basic orbit estimation problem involves solving for values of a set of parameters from a measurement model (described in Chapter 7) so as to minimize, in the sense of weighted least squares, the differences between a computed and a measured trajectory. The model parameters include the trajectory of the vehicle (initial conditions and differential equation parameters), the locations of the ground stations and relay spacecraft, and the bias errors in their instruments or clocks (these errors may vary as a function of the pass over a station). In practice, values are determined for only a selected subset of the model parameters.

Since the measurements made by a tracking system are imperfect, no trajectory fits them exactly. At best, only an estimate of the actual trajectory can be obtained from the data. GTDS uses a classical weighted least-squares estimator (derived in Section 8.2). For a theoretical discussion of estimation, see References 1 through 6.

8.1 DESCRIPTION OF THE PROBLEM

Let a set of m measurements, denoted by an m-dimensional vector $\bar{y}$, be given. These measurements are assumed to be equal to a known vector function $\bar{f}$ of a set of p parameters, denoted by a p-dimensional vector $\bar{x}$, plus additive random noise, denoted by a vector $\bar{n}$, i.e.,

$$\bar{y} = \bar{f}(\bar{x}) + \bar{n} \tag{8-1}$$

The above equation is called a nonlinear regression equation. The trajectory determination problem is to estimate $\bar{x}$ given $\bar{y}$, the functional form of $\bar{f}$, and the statistical properties of $\bar{n}$.

The estimation process attempts to deduce a value for $\bar{x}$ that minimizes the weighted sum of the squares of the measurement residuals $[\bar{y} - \bar{f}(\bar{x})]$ between the actual measurements and the measurements computed using the mathematical model. More precisely, the following is minimized:

$$Q(\bar{x}) = [\bar{y} - \bar{f}(\bar{x})]^T W[\bar{y} - \bar{f}(\bar{x})] \tag{8-2}$$

where W is the m × m weighting matrix. The scalar quantity, Q, is called the loss function. An a priori estimate of the state, $\bar{x}_0$, is assumed to be available for use in the minimization. The deviation of $\bar{x}_0$ from the true value of the state is assumed to have zero mean and covariance, $P_{\Delta x_0}$.

A necessary condition for the loss function to be minimum with respect to $\bar{x}$ is that $\partial Q/\partial \bar{x} = 0$. Therefore, the value of $\bar{x}$ that minimizes Q is a root of the equation.

$$\frac{\partial Q}{\partial \bar{x}} = -2\,[\bar{y} - \bar{f}(\bar{x})]^T\, W \left(\frac{\partial \bar{f}}{\partial \bar{x}}\right) = 0 \tag{8-3}$$

The method of solving this nonlinear minimization is to linearize Equation (8-3) and then apply a standard Newton-Raphson procedure to iteratively solve the nonlinear problem. Expanding $\bar{f}(\bar{x})$ in a truncated Taylor series about the a priori estimate, $\bar{x}_0$, yields

$$\bar{f}(\bar{x}) = \bar{f}(\bar{x}_0) + F\,\overline{\Delta x} \tag{8-4}$$

where

$$\overline{\Delta x} = \bar{x} - \bar{x}_0 \tag{8-5}$$

and

$$F = \left(\frac{\partial \bar{f}}{\partial \bar{x}}\right)_{\bar{x}=\bar{x}_0} \qquad \left\{\begin{array}{l}\text{m} \times \text{p matrix of}\\ \text{partial derivatives of}\\ \bar{f}(\bar{x}) \text{ with respect to } \bar{x},\\ \text{evaluated at } \bar{x} = \bar{x}_0\end{array}\right\} \tag{8-6}$$

The linearized measurement vector becomes

$$\overline{\Delta y} = F\,\overline{\Delta x} + \bar{n} \tag{8-7}$$

where

$$\overline{\Delta y} = \bar{y} - \bar{f}(\bar{x}_0) \tag{8-8}$$

Substituting Equations (8-4) and (8-7) into Equation (8-3) yields the linearized partial derivative of the loss function in Equation (8-3)

$$-2\,(\overline{\Delta y} - F\,\overline{\Delta x})^T\, W\, F = 0 \tag{8-9}$$

which can immediately be solved for $\overline{\Delta x}$, yielding the classic equation for the best estimate, $\hat{\Delta x}$,

$$\hat{\Delta x} = (F^T W F)^{-1} F^T W \overline{\Delta y} \tag{8-10}$$

The value of $\hat{x}$, the estimate derived from the linearized system, is

$$\hat{x} = \bar{x}_0 + \hat{\Delta x} \tag{8-11}$$

The symmetric matrix $(F^T W F)$ is called the normal matrix. The inverse of this $p \times p$ matrix is the covariance matrix of the error in the weighted least-squares estimate, $\hat{x}$.

As a result of the linearization performed in Equation (8-4), the correction $\hat{\Delta x}$ must be small so as not to violate linearity. This means that the a priori estimate, $\bar{x}_0$, must be reasonably close to the true external solution of Equation (8-2). If such is not the case, the process is iteratively repeated in a standard Newton-Raphson procedure, each time using the last best estimate $\hat{x}$ as a reference for the linearization. The iterations continue until the differential correction vector $\hat{\Delta x}$ is truly small (i.e., approaching zero), which is equivalent to minimizing the original nonlinear loss function, Q(x).

In the following sections the specific estimator algorithms implemented in GTDS and their associated covariance matrices are derived and discussed, and details concerning the application of the estimation process are described. Much of the material is taken from References 4, 5, and 6.

8.2 BATCH ESTIMATOR ALGORITHM

To facilitate the derivation of an iterative weighted least-squares solution, the various quantities that are iteration dependent will be subscripted with an i. Thus, $\overline{\Delta x}$ in Equation (8-5) is written $\overline{\Delta x_i} = \bar{x} - \hat{x}_i$, where $\hat{x}_i$ is the best estimate of $\bar{x}$, the extended state, obtained from the i^{th} iteration. At the beginning of the process (0^{th} iteration), $\hat{x}_0 = \bar{x}_0$ is the a priori value of these solve-for variables. The objective is to determine $\hat{x}_{i+1}$ from $\hat{x}_i$ so as to minimize the loss function.

The discussion that follows uses the expectation operator $\mathcal{E}\{\}$. If u denotes a random, unbiased variable, the expectation of u, $\mathcal{E}\{u\}$, equals zero. The expectation of a variable x is the mean value of x or the first moment of x

$$\mathcal{E}\{x\} = \bar{x} \tag{8-12}$$

The covariance is the expectation of the product of the deviations of two random variables from their mean

$$\text{cov}\{x, y\} = \mathcal{E}\{(x - \mathcal{E}\{x\})(y - \mathcal{E}\{y\})\} \tag{8-13}$$

The initial assumption that the measurement vector $\bar{y}$ can be related to the state and model parameters at epoch time, t_0, is given as

$$\bar{y} = \bar{f}(\bar{x}, \bar{z}) + \bar{n} \tag{8-14}$$

where two classes of variables are included. The p-dimensional vector $\bar{x}$, designated the solve-for vector, contains as components the state and model parameters whose values are known with limited certainty and are to be estimated. The q-dimensional vector $\bar{z}$, designated the consider vector, contains as components all model parameters whose values are known with limited certainty but are not to be estimated. Nevertheless, the uncertainty of $\bar{z}$, is to be considered. A priori values of $\bar{x}$ and $\bar{z}$ are specified as $\bar{x}_0$ and $\bar{z}_0$, with respective covariance matrices $P_{\Delta x_0}$ and $P_{\Delta z_0}$, i.e., .

$$\mathcal{E}\{\bar{x}_0\} \equiv \bar{x} \tag{8-15a}$$

$$\text{cov}\{\bar{x}_0 - \bar{x}\} \equiv P_{\Delta x_0} \tag{8-15b}$$

$$\mathcal{E}\{\bar{z}_0\} \equiv \bar{z} \tag{8-15c}$$

$$\text{cov}\{\bar{z}_0 - \bar{z}\} \equiv P_{\Delta z_0} \tag{8-15d}$$

On the i^{th} iteration, the loss function is defined to be

$$Q(\bar{x}) = [\bar{y} - \bar{f}(\bar{x}, \bar{z}_0)]^T W [\bar{y} - \bar{f}(\bar{x}, \bar{z}_0)] + (\bar{x} - \bar{x}_0)^T P^{-1}_{\Delta x_0}(\bar{x} - \bar{x}_0) \tag{8-16}$$

The second term on the right has been added to the loss function to constrain the best estimate to the a priori specified $\bar{x}_0$, with the degree of constraint dependent upon the uncertainty $P_{\Delta x_0}$. This term accounts for the fact that $\bar{x}_0$ is known to be accurate to a confidence level given by $P_{\Delta x_0}$. Therefore, any solution is constrained to satisfy the a priori realization $\bar{x}_0$ to within the limits of its uncertainty.

To obtain the weighted least-squares solution that minimizes $Q(\bar{x})$ in Equation (8-16), the same procedure is followed as is used in Section 8.1. First $\partial Q/\partial \bar{x}$ is linearized; then, a Newton-Raphson procedure is iteratively applied to solve the nonlinear minimization problem. For convenience, the value of $\hat{\bar{x}}_i$ for the i^{th} iteration is considered first, and the nonlinear regression equation is linearized as follows:

$$\bar{f}(\bar{x}, \bar{z}) = \bar{f}(\hat{\bar{x}}_i, \bar{z}_0) + F_i \overline{\Delta x_i} + E_i \overline{\Delta z_i} \tag{8-17}$$

where

$$\overline{\Delta x_i} = \bar{x} - \hat{\bar{x}}_i \tag{8-18a}$$

$$\overline{\Delta z_i} = \bar{z} - \bar{z}_0 \tag{8-18b}$$

and

$$F_i = \left(\frac{\partial \bar{f}}{\partial \bar{x}}\right)_{(\bar{x},\ \bar{z} = \hat{\bar{x}}_i,\ \bar{z}_0)} \tag{8-19a}$$

$$E_i = \left(\frac{\partial \bar{f}}{\partial \bar{z}}\right)_{(\bar{x},\ \bar{z} = \hat{\bar{x}}_i,\ \bar{z}_0)} \tag{8-19b}$$

Since the consider variables $\bar{z}$ are not being estimated, their values remain equal to $\bar{z}_0$.

Substituting terms with nonzero mean from Equation (8-17) into Equation (8-16) yields the linearized loss function

$$\begin{aligned} Q'(\overline{\Delta x_i}) = {} & [\overline{\Delta y_i} - F_i \overline{\Delta x_i}]^T W [\overline{\Delta y_i} - F_i \overline{\Delta x_i}] \\ & + (\overline{\Delta x_i} - \tilde{\overline{\Delta x_i}})^T P_{\Delta x_0}^{-1} (\overline{\Delta x_i} - \tilde{\overline{\Delta x_i}}) \end{aligned} \tag{8-20}$$

where the measurement residuals are

$$\overline{\Delta y_i} = \bar{y} - \bar{f}(\hat{\bar{x}}_i, \bar{z}_0) \tag{8-21}$$

and the deviation of the a priori estimate from the i^{th} iterative estimate is

$$\bar{\Delta x}_i = \bar{x}_0 - \hat{x}_i \tag{8-22}$$

The value of $\bar{\Delta x}_i$ that minimizes Q', denoted by $\hat{\Delta x}_{i+1}$, is therefore

$$\hat{\Delta x}_{i+1} = (F_i^T W F_i + P_{\Delta x_0}^{-1})^{-1} [F_i^T W \bar{\Delta y}_i + P_{\Delta x_0}^{-1} \bar{\Delta x}_i] \tag{8-23}$$

and the best estimate of the solve-for variables is

$$\hat{x}_{i+1} = \bar{x}_0 + \sum_{k=1}^{i+1} \hat{\Delta x}_k = \hat{x}_i + \hat{\Delta x}_{i+1} \tag{8-24}$$

This estimation process is iteratively applied until the convergence criteria (discussed in Section 8.6.3) are satisfied.

Equation (8-23) is the estimation algorithm used in GTDS. It requires the inversion of a $p \times p$ matrix, the same dimension as the vector of solve-for variables. Insofar as the estimation algorithm is concerned, it makes no difference whether consider variables are included. Equation (8-23) depends only on the values $\bar{z}_0$, not on the uncertainty, $P_{\Delta z_0}$. This might be expected, since the uncertainty resulting from the inclusion of consider variables affects only the second-order statistics or covariances (i.e., the ensemble properties). The last term on the right in Equation (8-23) can only be included subsequent to the initial iteration, since on the initial iteration $\bar{\Delta x} = 0$.

The estimation algorithm in Equation (8-23) differs slightly from the classical weighted least-squares algorithm (Equation (8-10)). This difference results from the addition of the second term on the right in the loss function (Equation (8-16)).

8.2.1 MEAN AND COVARIANCE OF ESTIMATE

The best estimate $\hat{x}$ which results from convergence of the estimation algorithm will next be examined to determine its statistical properties. Two quantities are of concern, the expected (mean) value and the covariance of the estimate. The expected value of the deviation $\hat{\Delta x}$ yields the amount of bias in the estimate, while the covariance indicates the

amount of dispersion or uncertainty. Obviously, zero bias and minimum dispersion are the qualities sought.

In the following discussion, it is assumed that the iterations have converged and that the unsubscripted variables $\bar{x}$, $\overline{\Delta x}$, $\overline{\Delta y}$, etc., correspond to the converged solution and perturbations about it.

The expected value and covariance of the measurement noise vector, $\bar{n}$, are assumed to be

$$\mathcal{E}\{\bar{n}\} = 0 \tag{8-25a}$$

$$\text{cov}\{\bar{n}\} = W^{-1} \tag{8-25b}$$

and the linearized vector of measurement residuals can be written as

$$\overline{\Delta y} = F\,\overline{\Delta x} + E\,\overline{\Delta z} + \bar{n} \tag{8-26}$$

Therefore, the expected value of $\overline{\Delta y}$ is

$$\mathcal{E}\{\overline{\Delta y}\} = \mathcal{E}\{F\,\overline{\Delta x}\} \tag{8-27a}$$

since

$$\mathcal{E}\{\bar{n}\} = \mathcal{E}\{\overline{\Delta z}\} = 0 \tag{8-27b}$$

The covariance of $\overline{\Delta y}$ is

$$\begin{aligned} \text{cov}\{\overline{\Delta y}\} &= \mathcal{E}\{[\overline{\Delta y} - \mathcal{E}(\overline{\Delta y})]\,[\overline{\Delta y} - \mathcal{E}(\overline{\Delta y})]^T\} \\ &= E\,\mathcal{E}\{\overline{\Delta z}\,\overline{\Delta z}^T\}\,E^T + E\,\mathcal{E}\{\overline{\Delta z}\,\bar{n}^T\} + \mathcal{E}\{\bar{n}\,\overline{\Delta z}^T\}\,E^T + \mathcal{E}\{\bar{n}\,\bar{n}^T\} \\ &= E\,P_{\Delta z_0}\,E^T + W^{-1} \end{aligned} \tag{8-28}$$

where the correlation between the consider variable errors and the measurement noise is assumed zero, i.e.,

$$\mathcal{E}\{\overline{\Delta z}\,\bar{n}^T\} = 0 \tag{8-29}$$

The mean of the best estimate $\hat{\bar{x}}_{i+1}$ is

$$\begin{aligned}\mathcal{E}\{\hat{\bar{x}}_{i+1} - \bar{x}\} &= \mathcal{E}\{\hat{\Delta x}_{i+1} - \overline{\Delta x_i}\} \\ &= (F^T W F + P_{\Delta x_0}^{-1})^{-1} [F^T W \mathcal{E}\{\overline{\Delta y}\} + P_{\Delta x_0}^{-1} \mathcal{E}\{\bar{\Delta x}\} \\ &\quad - (F^T W F + P_{\Delta x_0}^{-1}) \mathcal{E}\{\overline{\Delta x}\}] \\ &= (F^T W F + P_{\Delta x_0}^{-1})^{-1} P_{\Delta x_0}^{-1} \mathcal{E}\{\bar{x}_0 - \bar{x}\}\end{aligned} \tag{8-30}$$

However, $\bar{x}_0$ was defined to have an expected value equal to $\bar{x}$ (see Equation (8-15a)). Therefore,

$$\mathcal{E}\{\hat{\bar{x}} - \bar{x}\} = 0 \tag{8-31a}$$

and

$$\mathcal{E}\{\hat{\bar{x}}\} = \bar{x} \tag{8-31b}$$

Equations (8-31) show that the best estimate is unbiased. The covariance of the error in the estimate is

$$\begin{aligned}P_{\Delta x} &= \mathcal{E}\{[\hat{\bar{x}}_{i+1} - \bar{x}][\hat{\bar{x}}_{i+1} - \bar{x}]^T\} = \mathcal{E}\{[\hat{\Delta x}_{i+1} - \overline{\Delta x_i}][\Delta x_{i+1} - \overline{\Delta x_i}]^T\} \\ &= \psi \{F^T W E P_{\Delta z_0} E^T W F + F^T W F + P_{\Delta x_0}^{-1} \\ &\quad + F^T W [E \mathcal{E}\{\overline{\Delta z} (\overline{\Delta x} - \bar{\Delta x})^T\} P_{\Delta x_0}^{-1} + E \mathcal{E}\{\overline{\Delta z}\, \bar{n}^T\} W F] \\ &\quad + [P_{\Delta x_0}^{-1} \mathcal{E}\{\overline{\Delta x} - \bar{\Delta x}) \overline{\Delta z}^T\} E^T + F^T W \mathcal{E}\{\bar{n}\, \overline{\Delta z}^T\} E] W F \\ &\quad + P_{\Delta x_0}^{-1} \mathcal{E}\{(\overline{\Delta x} - \bar{\Delta x})\, \bar{n}^T\} W F + F^T W \mathcal{E}\{\bar{n} (\overline{\Delta x} - \bar{\Delta x})^T\} P_{\Delta x_0}\} \psi^T\end{aligned} \tag{8-32}$$

where

$$\psi = \left(F^T W F + P_{\Delta x_0}^{-1}\right)^{-1} \tag{8-33}$$

To simplify Equation (8-32), the following definitions are made:

$$C_{\Delta x_0 \Delta z} = \mathcal{E}\{(\overline{\Delta x} - \tilde{\Delta x})\,\overline{\Delta z}^T\} = \mathcal{E}\{(\bar{x} - \bar{x}_0)(\bar{z} - \bar{z}_0)^T\} = \mathcal{E}\{(\bar{x}_0 - \bar{x})(\bar{z}_0 - \bar{z})^T\} \tag{8-34a}$$

$$C^T_{\Delta x_0 \Delta z} = \mathcal{E}\{\overline{\Delta z}\,(\overline{\Delta x} - \tilde{\Delta x})^T\} = \mathcal{E}\{(\bar{z} - \bar{z}_0)(\bar{x} - \bar{x}_0)^T\} = \mathcal{E}\{(\bar{z}_0 - \bar{z})(\bar{x}_0 - \bar{x})^T\} \tag{8-34b}$$

$$C_{\Delta z n} = \mathcal{E}\{\overline{\Delta z}\,\bar{n}^T\} = \mathcal{E}\{(\bar{z} - \bar{z}_0)\,\bar{n}^T\} = 0 \tag{8-35a}$$

$$C^T_{\Delta z n} = \mathcal{E}\{\bar{n}\,\overline{\Delta z}^T\} = \mathcal{E}\{\bar{n}\,(\bar{z} - \bar{z}_0)^T\} = 0 \tag{8-35b}$$

$$C_{\Delta x_0 n} = \mathcal{E}\{(\overline{\Delta x} - \tilde{\Delta x})\,\bar{n}^T\} = \mathcal{E}\{(\bar{x} - \bar{x}_0)\,\bar{n}^T\} = 0 \tag{8-36a}$$

$$C^T_{\Delta x_0 n} = \mathcal{E}\{\bar{n}\,(\overline{\Delta x} - \tilde{\Delta x})^T\} = \mathcal{E}\{\bar{n}\,(\bar{x} - \bar{x}_0)^T\} = 0 \tag{8-36b}$$

Therefore, Equation (8-32) becomes

$$P_{\Delta x} = \psi\,\{F^T W E P_{\Delta z_0} E^T W F + \psi^{-1} + F^T W E C^T_{\Delta x_0 \Delta z} P^{-1}_{\Delta x_0} + P^{-1}_{\Delta x_0} C_{\Delta x_0 \Delta z} E^T W F\}\,\psi^T \tag{8-37}$$

In Equations (8-35) and (8-36), it is assumed that no statistical correlation exists between the measurement noise and the error in the solve-for or consider variables. The correlation between errors in the a priori solve-for and consider variables, $C_{\Delta x_0 \Delta z}$, is neglected in GTDS, primarily because a priori values of this correlation matrix are usually unavailable. The terms are maintained in Equation (8-37) for completeness and for possible use in the error analysis application discussed later. In the event that no consider variables are included, Equation (8-37) reduces to

$$P_{\Delta x} = \psi = (F^T W F + P^{-1}_{\Delta x_0})^{-1} \tag{8-38}$$

which is the gain matrix in the estimation algorithm (Equation (8-33)).

It was stated previously that a desirable quality of an estimate is small dispersions. It is evident from Equation (8-38) that the covariance matrix of error in the estimate, $P_{\Delta x}$, varies with the measurement uncertainty, W^{-1}, and the a priori covariance matrix of the solve-for variable uncertainty, $P_{\Delta x_0}$. Equation (8-37) shows that $P_{\Delta x}$ also varies with the covariance matrix of uncertainty in the consider variables, $P_{\Delta z_0}$. Therefore, minimizing the measurement noise, as well as the a priori uncertainty in the solve-for and consider variables, will result in reducing the dispersion or uncertainty in the estimated variables.

The correlation between errors in the solve-for and consider variables, which results from the processing, is

$$\begin{aligned} C_{\Delta x \Delta z} &= \mathcal{E}\{(\hat{\bar{x}} - \bar{x})\,(\bar{z}_0 - \bar{z})^T\} \\ &= \psi\,\{P_{\Delta x_0}^{-1}\, C_{\Delta x_0 \Delta z} - F^T\, W\, E\, P_{\Delta z_0}\} \end{aligned} \tag{8-39}$$

Even if the a priori correlation, $C_{\Delta x_0 \Delta z}$, is assumed to be zero, a correlation between errors in the solve-for and consider variables will result because of their dependency in the processing model.

8.2.2 MEASUREMENT PARTIAL DERIVATIVES

Throughout Sections 8.2 and 8.2.1, the components of the solve-for and consider vectors $\bar{x}$ and $\bar{z}$ have been ignored along with the way the components and their error covariances, $P_{\Delta x}$ and $P_{\Delta z}$, are associated with a specific time or epoch. Furthermore, it has been assumed in Equation (8-14) that the calculated measurements at various times ($t_1, t_2, \ldots, t_m$) can be related to the solve-for and consider variables at the epoch time, t_0. In Equation (8-17) it is assumed that the time varying matrices F_i and E_i can be calculated, which linearly relate the calculated measurements to variables at the epoch time. In the following section, attention is focused upon the solve-for and consider vector components, the manner in which the time dependency is accomplished, and the properties of the normal matrix which are utilized in its formation.

The general estimation (solve-for) vector $\bar{x}$ in the regression equation (Equation (8-14)) and the estimator equation (Equation (8-23)) contains the following types of variables:

$$\bar{x} = \begin{bmatrix} \bar{p} \\ \bar{r}_s \\ b \\ \delta t \end{bmatrix} = \{\text{solve-for vector}\} \tag{8-40}$$

where

$\bar{p}$ = dynamic parameters, consisting of the spacecraft state components at epoch and model parameters in the acceleration model (Equation (4-1)) for one user spacecraft and up to three TDRSs; the model parameters include gravity constants, the drag parameter, the solar radiation constant, and thrust

$\bar{r}_s$ = tracking station locations or Bilateration Ranging Transponder sites in Earth-fixed coordinates

b = measurement biases

δt = measurement timing bias

The mean of B1950.0 or J2000.0 Cartesian coordinates, $\bar{R}_0$ and $\dot{\bar{R}}_0$, are used for the purpose of describing the method.

Each row of the F(t) matrix in Equation (8-19a) contains partial derivatives of the computed measurement with respect to $\bar{R}_0$, $\dot{\bar{R}}_0$, and the other specified components of $\bar{p}$, $\bar{r}_s$, b, and δt. The dynamic variables $\bar{p}$ must be related to the epoch time through the state transition matrix, $\Phi(t_i, t_0)$, as discussed in Chapters 4 and 6. Partial derivatives with respect to $\bar{r}_s$, b, and δt are not dependent upon an epoch and can be obtained by differentiating the measurement equation explicitly.

The nonlinear measurement equation is written in Equation (7-1) as

$$O_c = f_0 [\bar{R}(t + \delta t, \bar{p}), \dot{\bar{R}}(t + \delta t, \bar{p}), \bar{r}_s)] + b + RF_c \qquad (8\text{-}41)$$

where

$\bar{R}$, $\dot{\bar{R}}$ = position and velocity vectors for user spacecraft; for TDRSS tracking, this also includes the position and velocity vectors for the TDRS

RF_c = systematic error correction to the measurement due to atmospheric refraction, light-time correction, transponder delay, antenna mount errors, etc.

The partial derivatives of a measurement, O_c, at time t_j, with respect to the solve-for variables $\bar{x}$ are at time t_0, are given by

$$\bar{a}_j = \frac{\partial O_c}{\partial \bar{x}} = \left[\frac{\partial O_c(t_j)}{\partial \bar{x}(t_j)}\right]\left[\frac{\partial \bar{x}(t_j)}{\partial \bar{x}(t_0)}\right] \tag{8-42}$$

The first matrix on the right-hand side is explicitly determined from the measurement equations in Chapter 7. The second term on the right-hand side, the state transition matrix, must be obtained by integrating the variational equations (or approximations of these equations), as described in Chapter 6 and in Section 8.2.3. Equation (8-42) constitutes a single row $\bar{a}$ of the F matrix.

On each iteration, the m measurements are sequentially processed to form the normal matrix $F^T W F$. Since the weighting matrix W is diagonal, the recursive relation for accumulating the normal matrix is

$$F^T W F = \sum_{j=1}^{m} \frac{\bar{a}_j^T \bar{a}_j}{\sigma_j^2} \tag{8-43}$$

where

$\bar{a}_j$ = j^{th} row of the F matrix given by Equation (8-42)

σ_j = standard deviation of the j^{th} measurement

By forming $F^T W F$ row-by-row instead of manipulating the full $(m \times p)$ F matrix, a saving in storage and computation time is realized. Since the matrix $F^T W F$ is symmetric, elements below the main diagonal need not be computed or stored.

The general consider vector $\bar{z}$ in the regression equation (Equation (8-14)) can have as components any model parameters in $\bar{p}$, $\bar{r}_s$, b, or δt.

Each row of the E(t) matrix in Equation (8-19b) contains partial derivatives of the computed measurements with respect to the specified components of $\bar{z}$. The partial derivatives with respect to the dynamic variables $\bar{p}$, specified in $\bar{z}$, can be calculated simultaneously with the dynamic partial derivatives in F(t) as described in Chapter 6. However, the partial derivatives in E(t) need only be computed on the final converged iteration, since the estimator equation (Equation (8-23)) is not dependent upon E(t).

In GTDS the components of the vectors $\bar{x}$ and $\bar{z}$ are merged on the final iteration to an expanded state vector $\bar{u}$. The elements of $\bar{u}$ are ordered as described above. The measurement partial derivatives are then calculated with respect to $\bar{u}$, and a $(p + q) \times (p + q)$ expanded state normal matrix $\bar{F}^T W \bar{F}$ is sequentially accumulated as described above. When all m measurements have been processed, selected elements of $\bar{F}^T W \bar{F}$ are extracted to form $F^T W F$, and $E^T W E$, and $E^T W F$, which are required to compute the covariance and correlation matrices in Equations (8-37) through (8-39). It should be noted that only elements on and above the main diagonal of $\bar{F}^T W \bar{F}$ need be calculated and stored.

8.2.3 COVARIANCE MATRIX TRANSFORMATIONS

The converged estimate, $\hat{\bar{x}}$, covariance matrix, $P_{\Delta x}$, and correlation matrix, $C_{\Delta x \Delta z}$, resulting from the differential correction process correspond to the epoch time, t_0. The spacecraft state vector components of $\hat{\bar{x}}$ can correspond to Cartesian coordinates in mean of B1950.0, mean of J2000.0, or true of date axes; classical Keplerian orbital elements; spherical coordinates; or DODS variables. For discussion purposes, the case where $\bar{x}$ contains one spacecraft state vector is addressed and the first six components (the state components) of $\hat{\bar{x}}$ are denoted by $\bar{s}$. The vector $\bar{s}$ can optionally be

$$\bar{s} = \underbrace{\begin{bmatrix} X \\ Y \\ Z \\ \dot{X} \\ \dot{Y} \\ \dot{Z} \end{bmatrix}}_{\substack{\text{Mean of} \\ \text{B1950.0 or} \\ \text{J2000.0}}} = \underbrace{\begin{bmatrix} x \\ y \\ z \\ \dot{x} \\ \dot{y} \\ \dot{z} \end{bmatrix}}_{\substack{\text{True of} \\ \text{Epoch}}} = \underbrace{\begin{bmatrix} a \\ e \\ i \\ \Omega \\ \omega \\ M \end{bmatrix}}_{\substack{\text{Keplerian} \\ \text{Elements}}} = \underbrace{\begin{bmatrix} r \\ \alpha \\ \delta \\ V \\ A \\ \beta \end{bmatrix}}_{\substack{\text{Spherical} \\ \text{Elements}}} = \underbrace{\begin{bmatrix} x_1 \\ x_2 \\ x_3 \\ x_4 \\ x_5 \\ x_6 \end{bmatrix}}_{\substack{\text{DODS} \\ \text{Variables}}} \qquad (8\text{-}44)$$

depending on the variable set used in the differential correction process. The upper left 6×6 submatrix of $P_{\Delta x}$, denoted $P_{\Delta s}$, also corresponds to the variables used in the differential correction process.

GTDS transforms the estimated state, $\bar{s}$, and its covariance matrix, $P_{\Delta s}$, to any of the other variable sets shown above. The constant solve-for parameters and consider parameters in $\hat{\bar{x}}$ and $\bar{z}$ of the original differential correction problem are not coordinate dependent. Only the state (position and velocity) depends upon the coordinate system utilized. Therefore, only the subset $\bar{s}$ of $\hat{\bar{x}}$ and submatrix $P_{\Delta s}$ of $P_{\Delta x}$ need to be considered in the coordinate transformation.

If the sets to which $\bar{s}$ and $P_{\Delta s}$ are being transformed are denoted by $\bar{s}'$ and $P_{\Delta s'}$, the nonlinear transformation can be written as

$$\bar{s}'(t_0) = h[\bar{s}(t_0)] \tag{8-45}$$

Transformations of this type between Cartesian and spherical coordinates are presented in Section 3.3.4 and between Cartesian and Keplerian elements are presented in Section 3.3.8.

To transform the covariance matrix, $P_{\Delta s}$, Equation (8-45) is linearized, yielding

$$\overline{\Delta s}'(t_0) = H(t_0)\,\overline{\Delta s}(t_0) \tag{8-46a}$$

where the transformation matrix from the unprimed to the primed system is given by

$$H(t_0) = \left(\frac{\partial \bar{s}'}{\partial \bar{s}}\right)_{t=t_0} \tag{8-46b}$$

These partial derivatives between Cartesian and spherical coordinates and Cartesian and Keplerian elements are presented in Sections 3.3.4 and 3.3.8, respectively. The covariance matrix, $P_{\Delta s}$, is defined as

$$P_{\Delta s}(t_0) = \mathcal{E}\{[\hat{\Delta s}(t_0) - \overline{\Delta s}(t_0)]\,[\hat{\Delta s}(t_0) - \overline{\Delta s}(t_0)]^T\} \tag{8-47}$$

where $\hat{\Delta s}$ and $\overline{\Delta s}$ correspond to the position and velocity components of $\hat{\Delta x}$ and $\overline{\Delta x}$ defined previously. The covariance matrix of transformed variables, $P_{\Delta s'}$, is defined as

$$P_{\Delta s'}(t_0) = \mathcal{E}\{[\hat{\Delta s}'(t_0) - \overline{\Delta s}'(t_0)]\,[\hat{\Delta s}'(t_0) - \overline{\Delta s}'(t_0)]^T\} \tag{8-48}$$

Substituting Equation (8-46a) into Equation (8-48) yields

$$P_{\Delta s'}(t_0) = H(t_0)\,P_{\Delta s}(t_0)\,H^T(t_0) \tag{8-49}$$

A second type of transformation is the propagation of the estimate, $\hat{x}$, and the covariance matrix, $P_{\Delta x}$. The estimate, $\hat{x}(t_0)$, is propagated by integrating the equations of motion from initial conditions, $\hat{x}(t_0)$, to other times of interest.

The propagation of the covariance matrix is performed using the state transition matrix from time t_0 to the time of interest. In deriving the state transition matrix, model parameters other than those estimated (solved for) can be considered as uncertain in the propagation process. The a priori values of the uncertain state and model parameters (whether solved for or considered) at epoch time t_0 are denoted by $\hat{u}(t_0)$ and their covariance matrix by $P_{\Delta u}(t_0)$. At any later time t, they are given by

$$\hat{u} = \begin{bmatrix} \hat{x} \\ \bar{z}_0 \end{bmatrix} \tag{8-50a}$$

and

$$P_{\Delta u} = \left[\begin{array}{c|c} P_{\Delta x} & C_{\Delta x \Delta z} \\ \hline C^T_{\Delta x \Delta z} & P_{\Delta z_0} \end{array}\right] \tag{8-50b}$$

It is assumed that $\hat{u}$ and $P_{\Delta u}$ are composed of state components $\bar{s}$ and uncertain model parameters $\bar{u}^*$. Perturbations about $\bar{u}(t)$ are related to perturbations about the a priori values as follows:

$$\overline{\Delta u}(t) = \phi(t, t_0)\, \overline{\Delta u}(t_0) \tag{8-51}$$

where the transition matrix ϕ is given by

$$\phi(t, t_0) = \left[\begin{array}{c|c} \Phi(t, t_0) & \theta(t, t_0) \\ \hline 0 & I \end{array}\right] \tag{8-52}$$

with

$$\Phi(t, t_0) = \left(\frac{\partial \bar{s}(t)}{\partial \bar{s}(t_0)}\right) \tag{8-53a}$$

and

$$\theta(t, t_0) = \left(\frac{\partial \bar{s}(t)}{\partial \bar{u}^*(t_0)}\right) \tag{8-53b}$$

By definition, the covariance matrix of $\hat{u}$ at time t is

$$P_{\Delta u}(t) = \mathcal{E}\{[\hat{\Delta u}(t) - \overline{\Delta u}(t)]\,[\hat{\Delta u}(t) - \overline{\Delta u}(t)]^T\} \tag{8-54a}$$

Substituting Equation (8-51) into Equation (81–54a) yields

$$P_{\Delta u}(t) = \phi(t, t_0)\, P_{\Delta u}(t_0)\, \phi^T(t, t_0) \tag{8-54b}$$

The covariance matrix of state (upper left 6 × 6 submatrix of $P_{\Delta u}$) is obtained by partitioning ϕ and $P_{\Delta u}$ into their $\bar{s}$ and $\bar{u}^*$ subparts as follows:

$$\begin{aligned} P_{\Delta s}(t) = {} & \Phi(t, t_0)\, P_{\Delta s}(t_0)\, \Phi^T(t, t_0) + \theta(t, t_0)\, C^T_{\Delta s \Delta u^*}\, \Phi^T(t, t_0) \\ & + \Phi(t, t_0)\, C_{\Delta s \Delta u^*}\, \theta^T(t, t_0) + \theta(t, t_0)\, P_{\Delta u^*}\, \theta^T(t, t_0) \end{aligned} \tag{8-55a}$$

If no uncertain model parameters are included in the propagation, Equation (8-55a) reduces to

$$P_{\Delta s}(t) = \Phi(t, t_0)\, P_{\Delta s}(t_0)\, \Phi^T(t, t_0) \tag{8-55b}$$

From the same partitioning, the correlation between the state $\bar{s}$ and $\bar{u}^*$ is given by

$$C_{\Delta s \Delta u^*}(t) = \Phi(t, t_0)\, C_{\Delta s \Delta u^*} + \theta(t, t_0)\, P_{\Delta u^*} \tag{8-56}$$

8.2.4 COMPUTATIONAL PROCEDURE FOR THE DIFFERENTIAL CORRECTION PROGRAM

This section describes conceptually how the estimation and covariance equations are solved in GTDS. Figure 8-1 shows a computational flow schematic, which aids in the

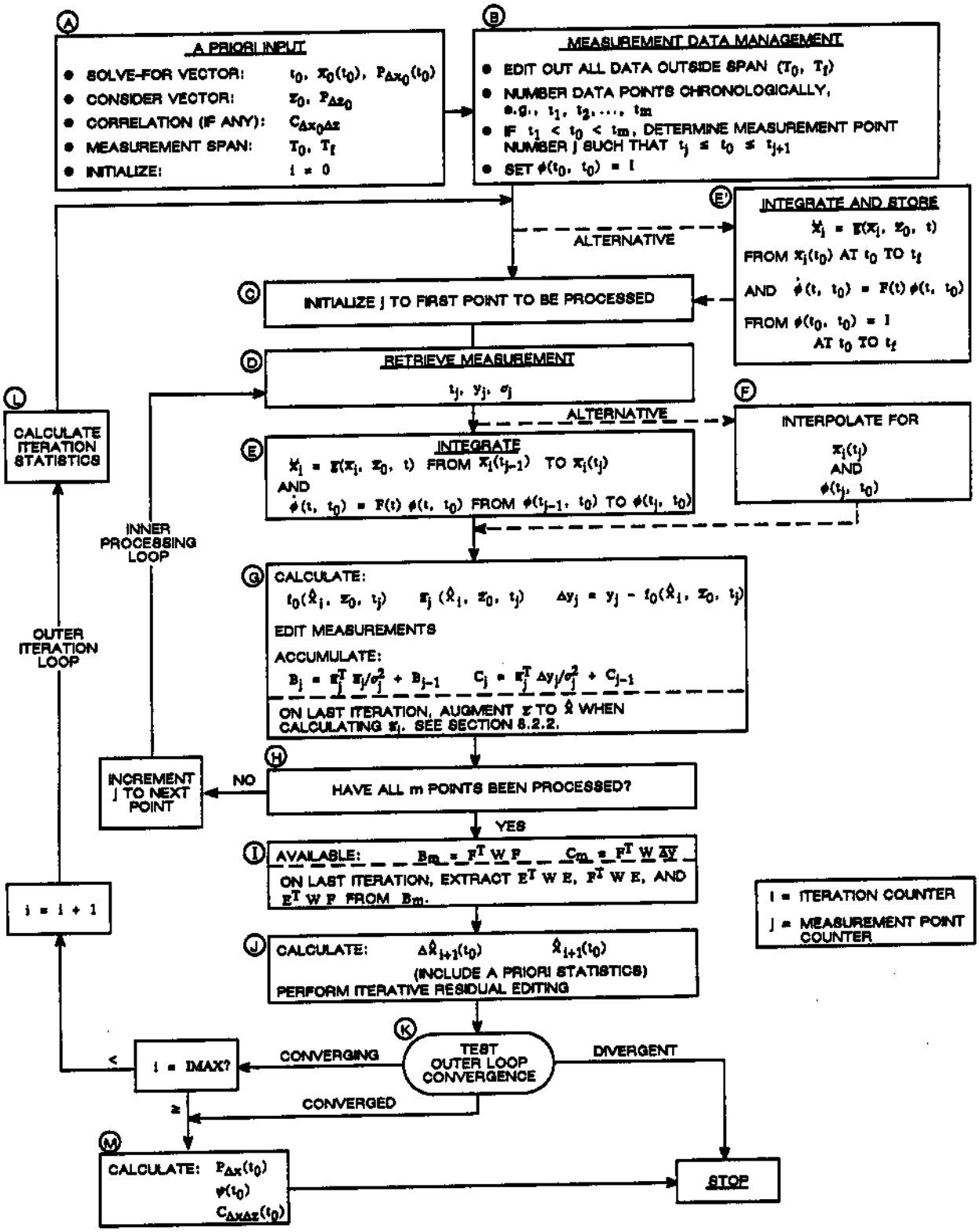

Figure 8-1. Computational Sequence for the Differential Correction Program

discussion. The figure is divided into functional blocks, and the discussion is similarly organized. The logic shown in Figure 8-1 is not the same as the specific source logic in GTDS but is presented to characterize the concepts. The circled letters in the following discussion refer to specific locations in the computational sequence illustrated in Figure 8-1.

8.2.4.1 A Priori Input

The process is initialized by specifying all necessary input data at Ⓐ. This includes the estimated and considered variables and their covariances, as well as measurement timespans and times to which the best estimates of the state and covariances are to be propagated. The state input is optionally expressed in any of several convenient coordinate systems. It is transformed to the basic coordinate system used in GTDS (i.e., mean equator and equinox of B1950.0, mean equator and equinox of J2000.0, or true equator and equinox of a given epoch) for subsequent processing. These transformations are described in Chapter 3.

8.2.4.2 Measurement Data Management

The next step is the preparation of the measurement data for processing at Ⓑ. This encompasses relocating the data within the specified measurement span from the original input device (single or multiple tapes, disk, or keyboard) to a working file convenient for subsequent retrieval during processing. During this relocation function, the data sequence can optionally be edited considering the type of measurement, the source of the data, the tracking station, and the timespan between adjacent points. The data on the working file are chronologically numbered, and the number of the data point that bounds the initial epoch time, t_0, from below is recorded. The data management function also includes determining whether the initial epoch time is less than the first data time, between the first and last data time, or larger than the last data time. For the first case, the data are processed sequentially from the first point at t_1 to the last point at t_m. For the second case, the processing starts backward in time from the initial epoch to the first data point. It then switches back to the initial epoch and proceeds forward in time to the last data point. In the third case, the data are processed backward in time from the last (chronological) data point to the first data point.

8.2.4.3 Outer Iteration Loop

The outer iteration loop begins at Ⓔ or Ⓒ. Normal GTDS operation starts at Ⓒ with initialization of the inner processing loop point counter, j, and subsequent integration of the ephemeris from measurement point to measurement point within the inner loop (at

Ⓔ). An alternative scheme begins the outer loop at Ⓔ' by calculating and storing the ephemeris and state transition matrix over the entire differential correction timespan (T_0 to T_f).

8.2.4.4 Inner Processing Loop

The inner processing loop starts by retrieving the first data point to be processed from the working file at Ⓓ. Under normal operation, the nonlinear equations of motion (see Chapter 5) and associated variational equations (see Chapter 4) are numerically integrated (see Chapter 6) to the data time at Ⓔ. Alternatively, if the ephemeris and state transition matrix are generated and stored at Ⓔ', their values are interpolated to the measurement time at Ⓕ. The best estimate of the measurement and its related residual $\overline{\Delta y_j}$ are calculated (see Chapter 7). Editing is performed based on the magnitude of this residual (see Section 8.6.2.1). If the measurement passes the editing test, the single row $\bar{a}_j$ of the F matrix corresponding to the measurement is computed at Ⓖ. To minimize core storage, the matrix products $F^T W \overline{\Delta y}$ and $F^T W F$ are accumulated as each row of F is calculated, as described in Section 8.2.2. It is apparent from Equation (8-23) that only these matrix products are required for determinating the estimate. All symmetric matrices (e.g., $F^T W F$) are stored in upper triangular form. On the last iteration, the matrix products $F^T W F$, $E^T W E$, $F^T W E$, and $E^T W F$ are accumulated for subsequent use in computing the covariance and correlation matrices. At Ⓗ tests are performed to determine if all m data points have been processed. If they have not, the measurement point counter j is incremented or decremented, depending on whether the data are being processed forward or backward in time. The procedure then returns to the beginning of the processing loop to retrieve the next point to be processed.

8.2.4.5 Estimation Computation

When all m data points have been processed, the complete matrix products $F^T W$ and $F^T W F$ are available at Ⓘ as is the measurement residual vector $\overline{\Delta y}$. On the last iteration, $F^T W E$, $E^T W F$, and $E^T W E$ are also available. The best estimate of the perturbations $\hat{\Delta x}_{i+1}$ and variables $\hat{x}_{i+1}$ are then calculated via Equations (8-23) and (8-24) at Ⓙ. The iterated residual editing procedure (see Section 8.6.2.2) is then used to refine this estimate.

8.2.4.6 Termination of Outer Iteration Loop

After determining an estimate at Ⓙ, the iteration is complete and convergence tests are performed at Ⓚ. The convergence criteria are described in Section 8.6.3. If the iterations are converging, the iteration counter i is tested against the maximum number of

iterations allowable. If the maximum has not been reached, the iteration counter is incremented and processing proceeds through (L) to begin the next iteration at (D). At (L) the measurement residual vector can be used to edit the data as discussed in Section 8.6.2, as well as to determine iteration statistics as discussed in Section 8.6.4. If the convergence test at (K) determines that divergence is occurring, processing can be terminated. If the iteration has converged, or the maximum number of iterations has been reached, then the covariance and correlation matrices at epoch t_0 are calculated at (M). Finally, the state vector, the covariance matrix, and the correlation matrix can be transformed to other space and time sets as described in Section 8.2.3.

8.3 ERROR ANALYSIS APPLICATION

The weighted least-squares estimation algorithm and the associated covariance and correlation matrices, derived in Sections 8.2 and 8.2.1, are summarized below.

Estimation Equation

$$\hat{\Delta x}_{i+1} = \left[F_i^T W F_i + P_{\Delta x_0}^{-1}\right]^{-1} \left(F_i^T W \overline{\Delta y_i} + P_{\Delta x_0}^{-1} \tilde{\Delta x}_i\right) \tag{8-57}$$

Covariance of Estimate

$$\begin{aligned} P_{\Delta x} = \psi \big[&F^T W E P_{\Delta z_0} E^T W F + F^T W E C_{\Delta x_0 \Delta z}^T P_{\Delta x_0}^{-1} \\ &+ P_{\Delta x_0}^{-1} C_{\Delta x_0 \Delta z} E^T W F + F^T W F + P_{\Delta x_0}^{-1}\big] \psi^T \end{aligned} \tag{8-58}$$

Correlation of Estimate and Consider Variables

$$C_{\Delta x \Delta z} = \psi \left[P_{\Delta x_0}^{-1} C_{\Delta x_0 \Delta z} - F^T W E P_{\Delta z_0}\right] \tag{8-59}$$

where

$$\psi = \left[F^T W F + P_{\Delta x_0}^{-1}\right]^{-1} \tag{8-60a}$$

$$P_{\Delta x_0} = \mathcal{E}\{(\bar{X}_0 - \bar{X})(\bar{X}_0 - \bar{X})^T\} \tag{8-60b}$$

$$P_{\Delta x} = \mathcal{E}\{(\hat{\bar{X}} - \bar{X})(\hat{\bar{X}} - \bar{X})^T\} \tag{8-60c}$$

$$P_{\Delta z_0} = \mathcal{E}\{(\bar{z}_0 - \bar{z})(\bar{z}_0 - \bar{z})^T\} \tag{8-60d}$$

$$C_{\Delta x_0 \Delta z} = \mathcal{E}\{(\bar{x}_0 - \bar{x})(\bar{z}_0 - \bar{z})^T\} \tag{8-60e}$$

$$C_{\Delta x \Delta z} = \mathcal{E}\{(\hat{\bar{x}} - \bar{x})(\bar{z}_0 - \bar{z})^T\} \tag{8-60f}$$

and $\hat{\bar{x}}$ is the converged $\hat{\bar{x}}_1$.

In Equations (8-57) through (8-59), only the estimator requires measurement data. The equations for the covariance and correlation matrices require only the statistics W of the measurements, which are usually known for specific classes of trackers and sensors. Therefore, if it is assumed that the a priori reference trajectory, $\bar{x}_0$, is the best estimate, the estimation equation can be omitted and the covariance and correlation matrices can be determined for specific mission sensors and measurement profiles. It must also be assumed that the mathematical models in the program accurately characterize the physical situation. Since actual measurements are not required, these operations can be performed during preflight studies to determine the following:

- The effect of measurement data errors (random and systematic), measurement timespans, and sampling rates on the accuracy of the estimated state and model parameters
- The effect of the trajectory dynamics and the trajectory/sensor relative geometry on the accuracy of the estimated state and model parameters
- The relative effects of different types of measurements on the accuracy of the estimated state and model parameters

Such problems are referred to as error analysis problems, since they are solely concerned with the influence that errors in problem variables have on the accuracy of the estimate. This type of analysis can strongly influence the design and enhancement of spacecraft missions, as well as establish requirements for measurement sensor accuracies, sampling rates, tracking times, and sensor locations. Currently this error analysis capability is only available for ground tracking measurement data.

The method for evaluating Equations (8-58) and (8-59) in GTDS is nearly identical to that for estimation applications. An a priori estimate of the solve-for and consider variables, $\bar{x}_0$ and $\bar{z}_0$, along with their covariance and correlation matrices, $P_{\Delta x_0}$, $P_{\Delta z_0}$ and $C_{\Delta x_0 \Delta z_0}$, is specified. The measurement schedule and measurement uncertainty W is also specified a priori. The program then proceeds to integrate the nonlinear differential equations of motion and their corresponding variational equations to the measurement times and

computes the measurement partial derivatives. The rows of the matrices F and E in Equations (8-58) and (8-59) are accumulated as the measurement statistics are processed. Ultimately, the covariance and correlation matrices, $P_{\Delta x}$ and $C_{\Delta x \Delta z}$, are calculated at the epoch time. The covariance and correlation matrices are then propagated to specified times T_1, T_2, ..., T_s by means of Equations (8-51), (8-52), (8-53), and (8-55). Analogously to the transformations presented in Equations (8-45) through (8-49), the time-transformed covariance matrix, $P_{\Delta s}(T_i)$, which is a submatrix of $P_{\Delta x}(T_i)$, is itself transformed to the $\bar{s}'$ system. From the nonlinear transformation

$$\bar{s}'(T_i) = h[\bar{s}(T_i)] \tag{8-61}$$

a linearization yields

$$\Delta s'(T_i) = H(T_i)\, \overline{\Delta s}(T_i) \tag{8-62}$$

where

$$H(T_i) = \left(\frac{\partial \bar{s}'}{\partial \bar{s}}\right)_{t=T_i} \tag{8-63}$$

The covariance matrix of $\hat{\bar{s}}'(T_i)$ is thus formed by appropriate substitution as

$$\begin{aligned} P_{\Delta s'}(T_i) &= \mathcal{E}\{[\hat{\Delta s}'(T_i) - \overline{\Delta s}'(T_i)][\hat{\Delta s}'(T_i) - \overline{\Delta s}'(T_i)]^T\} \\ &= H(T_i)\, P_{\Delta s}(T_i)\, H^T(T_i) \end{aligned} \tag{8-64}$$

The correlation $C_{\Delta s \Delta z}(T_i)$ is transformed to $C_{\Delta s' \Delta z}(T_i)$ as follows:

$$\begin{aligned} C_{\Delta s' \Delta z}(T_i) &= \mathcal{E}\{[\hat{\bar{s}}'(T_i) - \bar{s}'(T_i)]\, [\bar{z}_0 - \bar{z}]^T\} \\ &= \mathcal{E}\{[\hat{\Delta s}'(T_i) - \overline{\Delta s}'(T_i)]\, [\bar{z}_0 - \bar{z}]^T\} \\ &= \mathcal{E}\{H(T_i)\, [\hat{\Delta s}(T_i) - \overline{\Delta s}(T_i)]\, [\bar{z}_0 - \bar{z}]^T\} \\ &= H(T_i)\, C_{\Delta s \Delta z}(T_i) \end{aligned} \tag{8-65}$$

Since the estimation equation is not being solved, iteration is unnecessary.

Differentiating Equation (8-23) with respect to $\bar{z}$ and ignoring both the iteration notation and the $\bar{z}$ dependence on the matrix of measurement partial derivatives, the variation of the least-squares estimator with respect to the consider parameters is

$$\frac{\partial \hat{\Delta x}}{\partial \bar{z}} = -\left(F^T W F + P_{\Delta x_0}^{-1}\right)^{-1} F^T W E \tag{8-66}$$

Within the bounds of linearity, the responsiveness of the components of $\hat{\Delta x}$ to perturbations in the components of $\bar{z}$ are given in the epoch sensitivity matrix

$$S = \left(\frac{\partial \hat{\Delta x}_i}{\partial z_j} \Delta z_j\right) \tag{8-67}$$

From Equations (8-51) through (8-53) for the state vector $\bar{s}$, the perturbation about a given value of s is

$$\hat{\Delta s}(t) = \Phi(t, t_0)\ \hat{\Delta s}(t_0) + \theta(t, t_0)\ \overline{\Delta u^*} \tag{8-68}$$

Differentiating $\hat{\Delta s}(t)$ with respect to $\bar{u}^*$, the variation of the state components with respect to the consider dynamic parameters is obtained as follows:

$$\frac{\partial \hat{\Delta s}(t)}{\partial \bar{u}^*} = \Phi(t, t_0)\left[\frac{\partial \hat{\Delta s}}{\partial \bar{u}^*}\right] + \theta(t, t_0) \tag{8-69}$$

Then the time propagation of the matrix of functional sensitivities is

$$S(t) = \left(\frac{\partial \hat{\Delta s}(t)}{\partial u_j^*} \Delta u_j^*\right) \tag{8-70}$$

As in the transformation of the covariance matrix from $P_{\Delta s}$ to $P_{\Delta s'}$, a simple chain rule calculation yields the variation of the transformed state with respect to the consider variables

$$\left(\frac{\partial \hat{\Delta s}'(t)}{\partial \bar{z}}\right) = \left(\frac{\partial \hat{\Delta s}'(t)}{\partial \bar{s}(t)}\right)\left(\frac{\partial \bar{s}(t)}{\partial \bar{z}}\right) \tag{8-71}$$

To give more insight into the applicability of the sensitivity quantities, the i^{th} component of the least-squares estimator $\hat{\Delta s}$ is written in nonlinear functional form as

$$\hat{\Delta s}_i = \bar{g}_i(\bar{z}) \tag{8-72}$$

By expanding $\bar{g}_i(\bar{z})$ in a Taylor series about $\bar{z} = \bar{z}_0$, the following first-order approximation is obtained:

$$\hat{\Delta s}_i = \bar{g}_i(\bar{z}) = \bar{g}_i(\bar{z}_0) + \sum_j \left(\frac{\partial \hat{\Delta s}_i}{\partial z_j}\right) \Delta z_j \tag{8-73}$$

If the errors in the $\bar{z}$ parameters are uncorrelated in a Bayesian sense (as they are assumed to be in GTDS), and if the linearity assumption is valid, an estimate of the variance of $\hat{\Delta s}_i$ due solely to the variability in $\bar{z}$ is obtained. In particular, this variance estimate is given by invoking the variance operator on both sides of the above expression for $\hat{\Delta s}_i$ and noting that $\bar{g}_i(\bar{z}_0)$ is a constant and that the Δz_j values are uncorrelated. Therefore,

$$\sigma^2_{\hat{\Delta s}_i}(\bar{z}) = \sum_j \left(\frac{\partial \hat{\Delta s}_i}{\partial z_j}\right)^2 \sigma^2_{\Delta z_j} \tag{8-74}$$

Assuming the linearization is valid, it is easily seen that $\Delta z_j = \sigma_{\Delta z_j}$ in the sensitivity analysis. Hence, the sum of squares of the sensitivities for a given state component over all consider parameters plus the excess of the (i, i) element of the consider covariance of $\hat{\Delta s}$ over $\sigma^2_{\hat{\Delta s}_i}(\bar{z})$ yields the total variation observed in $\hat{\Delta s}_i$. This excess quantity is the (i,i) element of the normal matrix (measurement noise variance component) since the covariance equations were derived under the assumption that $\bar{n}$ and $\bar{z}_0$ are uncorrelated, thus uncoupling their effects on variance estimation.

It would appear that since an estimate is not actually being determined, it should make little difference whether model parameters are associated with the solve-for vector, $\bar{x}$, or the consider vector, $\bar{z}$. A subtle difference does exist, however. Components of the consider vector, $\bar{z}$, are maintained at their a priori specified values throughout the processing and therefore have no possibility for modification through estimation. As a result, their covariances never differ from those initially specified, i.e., $P_{\Delta z_0}$ in Equation (8-58). The solve-for variables, $\bar{x}$, have their values continually modified through the estimation

process, which is reflected through the changes in the variance elements in $P_{\Delta x}$. Because of the coupling, the uncertainty of the state components is affected differently if the same model parameter is associated with $\bar{x}$ rather than with $\bar{z}$.

8.4 SEQUENTIAL ESTIMATION (Not Currently Available in GTDS)

In the approach taken to the basic orbit estimation problem in the preceding sections of this chapter, the measurements are processed by classical least-squares methods, i.e., by processing the data in batches. The solution to the problem is the state vector (the system parameters or unknown constants) which is estimated from a set of measured data. Since the problem is nonlinear, the solution is linearized about the a priori state estimate and then iterated to minimize the loss function. This approach requires considerable computation time and cannot be applied to realtime situations.

An alternative approach is to perform the data reduction and parameter estimation in a sequential or recursive manner. The process is begun by making an initial estimate of the state vector from a minimum data set or from a judicious guess. Each new data point is combined with the previous parameter estimate by appropriately weighting the data point to give an improved estimate of the state. This process is repeated as each new data point is reduced. Hence, the procedure can be interrupted at any time and the best estimates of the system parameters and their uncertainties based on all accumulated data to that time are known. Other advantages of sequential weighted least-squares estimators are that at each step the calculations are fixed in size and format and that the need for storing previous data points is eliminated. Under certain assumptions, the sequential weighted least-squares estimator is identical to the Kalman minimum variance estimator. Additional discussion of sequential weighted least-squares and minimum variance estimation can be found in Reference 2.

The derivation of the Extended Kalman Filter from recursive weighted least-squares estimation is discussed in Section 8.4.1. Because of the sensitivity of Kalman filters to dynamic model errors associated with orbit generation, filters have been designed to adaptively estimate the true value of the unmodeled acceleration along with the state. This approach, dynamic model compensation, is discussed in Section 8.4.2. In Section 8.4.3, statistical adaptive filtering, which eliminates the need to specify a priori noise statistics, is discussed.

8.4.1 DERIVATION AND APPLICATIONS OF THE EXTENDED KALMAN FILTER

In reconsidering the weighted least-squares problem described in Section 8.1, an m-component measurement vector $\bar{y}$ is assumed. The nonlinear regression equation

(Equation (8-1)) is linearized about a reference state, $\bar{x}_0$, as shown in Equation (8-7). The best estimate, $\hat{x}$, in the classical weighted least-squares sense, is given by Equations (8-10) and (8-11) as

$$\hat{x}_m = \bar{x}_0 + \hat{\Delta x}_m \tag{8-75a}$$

where

$$\hat{\Delta x}_m = (F^T W F)^{-1} F^T W \overline{\Delta y} \tag{8-75b}$$

The subscript m indicates that the solution is based on an m-component measurement vector, and the quantities F, W, and $\overline{\Delta y}$ are defined by Equations (8-6), (8-12), and (8-8), respectively. If one more measurement is included, the correction has exactly the same form, i.e.,

$$\hat{\Delta x}_{m+1} = (F'^T W' F')^{-1} F'^T W' \overline{\Delta y'} \tag{8-76}$$

where F', W', and $\overline{\Delta y'}$ are related to F, W, and $\overline{\Delta y}$ as follows:

$$F' = \begin{bmatrix} F \\ --- \\ F_{m+1} \end{bmatrix} \tag{8-77a}$$

$$W' = \left[\begin{array}{c|c} W & 0 \\ \hline 0 & w_{m+1} \end{array}\right] \tag{8-77b}$$

$$\overline{\Delta y'} = \begin{bmatrix} \overline{\Delta y} \\ --- \\ \Delta y_{m+1} \end{bmatrix} \tag{8-77c}$$

and F_{m+1}, w_{m+1}, and Δy_{m+1} correspond to the $(m+1)^{st}$ measurement. In other words, the original matrices and vectors are augmented to include the next measurement.

Substituting Equations (8-77) into Equation (8-76) gives

$$\hat{\Delta x}_{m+1} = \left([F^T \mid F_{m+1}^T] \left[\begin{array}{c|c} W & 0 \\ \hline 0 & w_{m+1} \end{array}\right] \left[\begin{array}{c} F \\ \hline F_{m+1} \end{array}\right] \right)^{-1} [F^T \quad F_{m+1}^T] \left[\begin{array}{c|c} W & 0 \\ \hline 0 & w_{m+1} \end{array}\right] \left[\begin{array}{c} \overline{\Delta y} \\ \hline \Delta y_{m+1} \end{array}\right] \tag{8-78}$$

The quantity in parentheses in Equation (8-78) is the inverse of the covariance matrix of error, $P_{\Delta x_{m+1}}$, for the weighted least-squares estimate, $\hat{\Delta x}_{m+1}$, i.e.,

$$P_{\Delta x_{m+1}} = (F^T W F + F_{m+1}^T w_{m+1} F_{m+1})^{-1} \tag{8-79a}$$

However, $F^T W F$ is the inverse of the covariance matrix, $P_{\Delta x_m}$, which is based on m measurements. Therefore,

$$P_{\Delta x_{m+1}} = (P_{\Delta x_m}^{-1} + F_{m+1}^T w_{m+1} F_{m+1})^{-1} \tag{8-79b}$$

Equations (8-78) and (8-79a) are expressions for the state correction estimate and the covariance of the error in the estimate obtained by processing (m+1) measurements. These expressions can be written more conveniently in the following recursive form:

$$\hat{\Delta x}_{m+1} = \hat{\Delta x}_m + \overline{\Delta x} \tag{8-80a}$$

$$P_{\Delta x_{m+1}} = P_{\Delta x_m} + \Delta P \tag{8-80b}$$

where $\overline{\Delta x}$ and ΔP represent the changes in $\hat{\Delta x}_m$ and $P_{\Delta x_m}$ caused by the $(m+1)^{st}$ measurement. This form allows the state vector and covariance matrix to be determined as each measurement is sequentially processed.

As shown in Appendix E, Equation (8-80b) can be written as

$$P_{\Delta x_{m+1}} = P_{\Delta x_m} - P_{\Delta x_m} F_{m+1}^T [w_{m+1}^{-1} + F_{m+1} P_{\Delta x_m} F_{m+1}^T]^{-1} F_{m+1} P_{\Delta x_m} \tag{8-81a}$$

or

$$P_{\Delta x_{m+1}} = P_{\Delta x_m} - K F_{m+1} P_{\Delta x_m} = (I - K F_{m+1}) P_{\Delta x_m} \tag{8-81b}$$

where

$$K \equiv P_{\Delta x_m} F_{m+1}^T [w_{m+1}^{-1} + F_{m+1} P_{\Delta x_m} F_{m+1}^T]^{-1} \tag{8-82}$$

Substituting $P_{\Delta x_{m+1}}$ from Equation (8-81b) into the first term on the right-hand side of Equation (8-78) yields

$$\hat{\Delta x}_{m+1} = (I - K F_{m+1}) P_{\Delta x_m} [F^T W \overline{\Delta y} + F_{m+1}^T w_{m+1} \Delta y_{m+1}] \tag{8-83a}$$

Substituting Equations (8-75b) and (8-81b) into Equation (8-83a) yields

$$\hat{\Delta x}_{m+1} = (I - K F_{m+1}) \hat{\Delta x}_m + P_{\Delta x_{m+1}} F_{m+1}^T w_{m+1} \Delta y_{m+1} \tag{8-83b}$$

In Appendix E it is shown that

$$K = P_{\Delta x_{m+1}} F_{m+1}^T w_{m+1} \tag{8-84}$$

Therefore, Equation (8-83b) can be written as

$$\hat{\Delta x}_{m+1} = \hat{\Delta x}_m + K [\Delta y_{m+1} - F_{m+1} \hat{\Delta x}_m] \tag{8-85}$$

Summarizing the above results,

$$\hat{x}_{m+1} = \bar{x}_0 + \hat{\Delta x}_{m+1} \tag{8-86a}$$

$$\hat{\Delta x}_{m+1} = \hat{\Delta x}_m + K [\Delta y_{m+1} - F_{m+1} \hat{\Delta x}_m] \tag{8-86b}$$

$$P_{\Delta x_{m+1}} = P_{\Delta x_m} - K F_{m+1} P_{\Delta x_m} = (I - K F_{m+1}) P_{\Delta x_m} \tag{8-86c}$$

$$K = P_{\Delta x_m} F_{m+1}^T [w_{m+1}^{-1} + F_{m+1} P_{\Delta x_m} F_{m+1}^T]^{-1} \tag{8-86d}$$

where

$$F_{m+1} = \left(\frac{\partial \bar{f}_{m+1}}{\partial \bar{x}}\right)_{\bar{x}=\bar{x}_0}$$

and

Δy_{m+1} = linearized $(m+1)^{st}$ measurement (see Equation (8-8))

w_{m+1}^{-1} = variance of the $(m+1)^{st}$ measurement, e.g., σ_{m+1}^2

The preceding recursive form of the weighted least-squares estimate yields the update equations for the Extended Kalman Filter. The weighted least-squares estimate is a minimum variance estimate because the measurements are weighted with $W = 1/\sigma^2$. This is the condition necessary for Equation (8-79a) to be the covariance matrix of error. The matrix K is defined as the Kalman gain. For additional discussion of Kalman filter theory, see References 6, 7, and 8.

Assuming that F_{m+1}^T in Equation (8-84) is a matrix whose elements are all unity, then each element of the gain matrix, K, is a ratio between the statistical measure of uncertainty in the state estimate, $P_{\Delta x_{m+1}}$, and the uncertainty in the measurement, σ_{m+1}^2.

From the fundamental definition of the covariance matrix given in Equation (8-32), a more convenient form for $P_{\Delta x_{m+1}}$ can be derived using Equation (8-86b), as follows:

$$\begin{aligned}
P_{\Delta x_{m+1}} &= \mathcal{E}\{\hat{\Delta x}_{m+1}\ \hat{\Delta x}_{m+1}^T\} \\
&= \mathcal{E}\{[(I - K F_{m+1})\ \hat{\Delta x}_m + K \Delta y_{m+1}]\ [(I - K F_{m+1})\ \hat{\Delta x}_m + K \Delta y_{m+1}]^T\} \\
&= \mathcal{E}\{[(I - K F_{m+1})\ \hat{\Delta x}_m + K \Delta y_{m+1}]\ \hat{\Delta x}_m^T\ (I - K F_{m+1})^T \\
&\quad + [(I - K F_{m+1})\ \hat{\Delta x}_m + K \Delta y_{m+1}]\ \Delta y_{m+1}^T K^T\} \\
&= (I - K F_{m+1})\ \mathcal{E}\{\hat{\Delta x}_m\ \hat{\Delta x}_m^T\}\ (I - K F_{m+1})^T \\
&\quad + K\ \mathcal{E}\{\Delta y_{m+1}\ \hat{\Delta x}_m^T\}\ (I - K F_{m+1})^T \\
&\quad + (I - K F_{m+1})\ \mathcal{E}\{\hat{\Delta x}_m\ \Delta y_{m+1}^T\}\ K^T + K\ \mathcal{E}\{\Delta y_{m+1}\ \Delta y_{m+1}^T\}\ K^T
\end{aligned} \tag{8-87}$$

Assuming uncorrelated measurement errors, then

$$\mathcal{E}\{\Delta y_{m+1}\ \hat{\Delta x}_m^T\} = \mathcal{E}\{\hat{\Delta x}_m\ \Delta y_{m+1}^T\} = 0 \tag{8-88}$$

By definition

$$\mathcal{E}\{\hat{\Delta x}_m\ \hat{\Delta x}_m^T\} = P_{\Delta x_m} \tag{8-89a}$$

and

$$\mathcal{E}\{\Delta y_{m+1}\ \Delta y_{m+1}^T\} = w_{m+1}^{-1} \tag{8-89b}$$

Substituting Equations (8-88) and (8-89) into Equation (8-87) yields

$$P_{\Delta x_{m+1}} = (I - K F_{m+1})\, P_{\Delta x_m}\, (I - K F_{m+1})^T + K\, w_{m+1}^{-1}\, K^T \tag{8-90}$$

Equation (8-90) is preferred over Equation (8-86c) because, to first order, it is insensitive to errors in the filter gain, and it is better conditioned for numerical computations, since it is the sum of two symmetric nonnegative definite matrices.

Up to this point, the effect of adding one more measurement to a set of m measurements has been considered. These results will next be generalized to indicate sequential estimates without dependence on the size of the measurement vector, that is, j will represent the measurement counter, replacing m in the subscripts.

The prediction formulas for the Extended Kalman Filter follow from the discussion in Section 8.2.3 concerning the timewise propagation of state perturbations (Equations (8-51) through (8-53)). Including the state noise, $\overline{\omega}$, with zero mean and covariance, Q, the prediction equation can be written as

$$\hat{\Delta x}(t_{j+1} \mid t_j) = \Phi(t_{j+1} \mid t_j)\ \hat{\Delta x}(t_j \mid t_j) + \overline{\omega}_{j+1} \tag{8-91}$$

where $\hat{\Delta x}(t_{j+1} \mid t_j)$ denotes the best estimate of the correction at time t_{j+1} based on processing data through time t_j, and $\Phi(t_{j+1} \mid t_j)$ is the state transition matrix. For prediction

purposes, the state noise, $\bar{w}_{j+1}$, in Equation (8-91) is set equal to zero. The predicted covariance matrix at time t_{j+1} is obtained from Equation (8-91) as follows:

$$\begin{aligned} P_{\Delta x}(t_{j+1} \mid t_j) &= \mathcal{E}\{\hat{\Delta x}(t_{j+1} \mid t_j)\ \hat{\Delta x}^T(t_{j+1} \mid t_j)\} \\ &= \mathcal{E}\{[\Phi\ \hat{\Delta x}(t_j \mid t_j) + \bar{w}_{j+1}]\ [\Phi\ \hat{\Delta x}(t_j \mid t_j) + \bar{w}_{j+1}]^T\} \\ &= \mathcal{E}\{[\Phi\ \hat{\Delta x}(t_j \mid t_j) + \bar{w}_{j+1}]\ \hat{\Delta x}^T(t_j \mid t_j)\ \Phi^T + [\Phi\ \hat{\Delta x}(t_j \mid t_j) + \bar{w}_{j+1}]\ \bar{w}_{j+1}^T\} \\ &= \Phi\ \mathcal{E}\{\hat{\Delta x}(t_j \mid t_j)\ \hat{\Delta x}^T(t_j \mid t_j)\}\ \Phi^T + \mathcal{E}\{\bar{w}_{j+1}\ \hat{\Delta x}^T(t_j \mid t_j)\}\ \Phi^T \\ &\quad + \Phi\ \mathcal{E}\{\hat{\Delta x}(t_j \mid t_j)\ \bar{w}_{j+1}^T\} + \mathcal{E}\{\bar{w}_{j+1}\ \bar{w}_{j+1}^T\} \end{aligned} \tag{8-92a}$$

Assuming that the noise, $\bar{w}$, and the state, $\hat{\Delta x}$, are uncorrelated, Equation (8-92a) becomes

$$P_{\Delta x}(t_{j+1} \mid t_j) = \Phi\ P_{\Delta x}(t_j \mid t_j)\ \Phi^T + Q_{j+1} \tag{8-92b}$$

where Q_{j+1} is the covariance of the state noise, i.e.,

$$Q_{j+1} = \mathcal{E}\{\bar{w}_{j+1}\ \bar{w}_{j+1}^T\} \tag{8-93}$$

To use this formulation of the Extended Kalman Filter, a reference trajectory must be generated. This is done by numerically integrating a nonlinear second-order differential equation (see Equation (5-2)) of the form

$$\ddot{\bar{x}}_{ref}(t) = \bar{g}(\bar{x},\ t) \tag{8-94}$$

where $\bar{g}$ is a known function of the state variables, $\bar{x}$ is an n-dimensional state vector, $\bar{x}(t_0) = \bar{x}_0$, and $t \geq t_0$.

The predicted measurement residual error, $r(t_{j+1} \mid t_j)$, is

$$r(t_{j+1} \mid t_j) = y(t_{j+1}) - F_{j+1}\ \hat{\bar{x}}(t_{j+1} \mid t_j) \tag{8-95}$$

where $\hat{x}(t_{j+1} \mid t_j)$ is obtained from the integration of Equation (8-94) with the initial state for the integration obtained from the previous state updated by Equation (8-91), and the predicted measurement residual uncertainty, $Y(t_{j+1} \mid t_j)$, is given by

$$Y(t_{j+1} \mid t_j) = \mathcal{E}\{r(t_{j+1} \mid t_j)\, r^T(t_{j+1} \mid t_j)\} = F_{j+1}\, P_{\Delta x}(t_{j+1} \mid t_j)\, F_{j+1}^T + w_{j+1}^{-1} \qquad (8\text{-}96)$$

A comparison of these residuals with their theoretical statistical properties provides a means of judging the performance of the filter (see Section 8.6.4).

Equations (8-91) and (8-92b) are used to predict the state correction and covariance matrices at a future time t_{j+1}, based on the best estimate at the last measurement at time t_j. The next measurement, y_{j+1}, is then used to update the state correction and covariance matrices (Equation (8-85)). These steps are repeated until all the measurements have been processed. The advantage of this recursive estimator is that the estimate of the state and covariance based on processing m + 1 measurements uses the information contained in the $(m+1)^{st}$ measurement plus the state and covariance based on m measurements. The entire process of accumulating sums and inverting matrices does not have to be repeated when a new measurement is processed. The error covariance of the filter is inversely proportional to the measurement noise from Equation (8-79b). Large measurement noise implies that w_{m+1} is small, and hence P_{m+1} decreases by only a small amount. Small measurement noise implies a large w_{m+1}, and consequently a relatively large decrease in P_{m+1}.

The recursive equations can be applied from the first point on. In that case, the reference trajectory is chosen as $\hat{x}(t_0) = \bar{x}_0$, the a priori state; hence, $\hat{\Delta x}(t_0 \mid t_0) = 0$. There are two ways in which the Extended Kalman Filter can be used, with an updated reference trajectory or with a nonupdated reference trajectory. In the nonupdated reference approach, the corrections Δx are accumulated, and the a priori reference state, $\bar{x}_0$, is corrected only once, at the final time after all data are processed.

The updated state vector at the final time, based on processing all the data, is then smoothed back to the initial time to obtain the best estimate of the state at all intervening times. The covariance matrix can also be propagated backward in time via Equation (8-92b) to obtain the timewise variation of the uncertainty of the state based on processing all data.

If the batch of measurements is sufficiently large, a new initial reference state can be determined from the following equation:

$$\bar{x}'(t_0) = \bar{x}(t_0) + \hat{\Delta x}(t_0 \mid t_f) \qquad (8\text{-}97)$$

where

$\hat{\Delta x}(t_0 \mid t_f)$ = new best estimate of the state at t_0 based on processing all measurements

t_f = time of the final measurement

This reference state will be closer to the true initial state than will $\bar{x}(t_0)$. Using the new state, the data are reprocessed, i.e., the solution is linearized about $\bar{x}'(t_0)$, and the filtering process is repeated over the same batch of measurements. This process is repetitively applied until there is no change in the initial reference state. At that time, convergence to the best estimate of the state has been achieved, i.e., a solution has been found that is as close to the true solution as the neglected nonlinear effects will allow. These global iterations involve the same procedure as that which is followed in the batch processor (iterated weighted least squares). This mode is used when the signal-to-noise ratio is small, and a good initial estimate of the state is available.

Another approach (used primarily when the signal-to-noise ratio is large or when a good estimate of the state is unavailable) is to update the reference trajectory after processing each subset of the data vector $\bar{y}$. This allows large errors in the a priori state, $\bar{x}_0$, to be corrected early in the process, thereby assuring that the processing of later data satisfies linearity. This, in turn, improves the outer loop (global iteration) convergence. Linearization about $\hat{\bar{x}}(t_0)$ results in $\hat{\Delta x}(t_0 \mid t_0) = 0$. Hence, using Equation (8-91) and relinearizing about each point yields

$$\hat{\Delta x}(t \mid t_j) = 0 \qquad [t_j \leq t \leq t_{j+1} \text{ (for all j)}] \tag{8-98a}$$

Since, due to the relinearization,

$$\hat{\Delta x}(t_{j+1} \mid t_{j+1}) = \hat{\bar{x}}(t_{j+1} \mid t_{j+1}) - \hat{\bar{x}}(t_{j+1} \mid t_j) \tag{8-98b}$$

substitution of Equations (8-8), (8-98), and (8-99) into Equation (8-86b) gives

$$\hat{\bar{x}}(t_{j+1} \mid t_{j+1}) = \hat{\bar{x}}(t_{j+1} \mid t_j) + K(t_{j+1}) \{y(t_{j+1}) - f[\hat{\bar{x}}(t_{j+1} \mid t_j), t_{j+1}]\} \tag{8-99}$$

The preceding result is used for updating the state vector. The updated reference mode is ideally suited to realtime applications.

The Extended Kalman Filter for continuous-discrete systems as described above is the result of the application of the linear Kalman filter to a linearized nonlinear system, which

is relinearized after each measurement. The procedure for the updated reference mode is summarized below.

1. Store the reference state, $\hat{\bar{x}}(t_j \mid t_j)$, and the covariance matrix, $P_{\Delta x}(t_j \mid t_j)$.

2. Compute the predicted state at time t_{j+1} by numerically integrating Equation (8-94), i.e., obtain $\hat{\bar{x}}(t_{j+1} \mid t_j)$ given $\hat{\bar{x}}(t_j \mid t_j)$.

3. Calculate the state transition matrix from time t_j to time t_{j+1}, either analytically or numerically, as discussed in Section 4.10.2,

$$\Phi[(t_{j+1}, t_j; \hat{\bar{x}}(t_j \mid t_j)] = \left[\frac{\partial \bar{x}(t_{j+1})}{\partial \bar{x}(t_j)}\right]_{\bar{x}(t_j)=\hat{\bar{x}}(t_j \mid t_j)} \tag{8-100a}$$

4. Compute the predicted error covariance matrix at time t_{j+1} via Equation (8-92b)

$$P_{\Delta x}(t_{j+1} \mid t_j) = \Phi(t_{j+1}, t_j)\, P_{\Delta x}(t_j \mid t_j)\, \Phi^T(t_{j+1}, t_j) + Q_{j+1} \tag{8-100b}$$

5. Compute the measurement via Equation (8-1), assuming no noise,

$$y(t_{j+1}) = \bar{f}[\hat{\bar{x}}(t_{j+1} \mid t_j),\ t_{j+1}] \tag{8-100c}$$

6. Compute the partial derivative of the measurement via Equation (8-6)

$$F_{j+1} = \left(\frac{\partial \bar{f}}{\partial \bar{x}}\right)_{\bar{x}=\hat{\bar{x}}(t_{j+1} \mid t_j)} \tag{8-100d}$$

7. Test whether this is an acceptable measurement, i.e., determine whether the absolute value of the residual (observed-minus-computed value) is less than the root-mean-square (RMS) multiplier times the square root of the predicted measurement residual uncertainty $Y(t_{j+1} \mid t_j)$ in Equation (8-96). If it is not, reject the measurement, increment j, and return to step 1.

8. Calculate the filter gain matrix via Equation (8-86d)

$$K(t_{j+1}) = P_{\Delta x}(t_{j+1} \mid t_j)\, F_{j+1}^T\, [F_{j+1}\, P_{\Delta x}(t_{j+1} \mid t_j)\, F_{j+1}^T + w_{j+1}^{-1}]^{-1} \tag{8-100e}$$

9. Process the measurement $y(t_{j+1})$ to obtain the updated state via Equation (8-99)

$$\hat{x}(t_{j+1} \mid t_{j+1}) = \hat{x}(t_{j+1} \mid t_j) + K(t_{j+1}) \{y(t_{j+1}) - \bar{f}[\hat{x}(t_{j+1} \mid t_j), t_{j+1}]\} \quad (8\text{-}100f)$$

10. Compute the updated error covariance matrix at time t_{j+1} via Equation (8-90)

$$P_{\Delta x}(t_{j+1} \mid t_{j+1}) = [I - K(t_{j+1}) F_{j+1}] P_{\Delta x}(t_{j+1} \mid t_j) [I - K(t_{j+1}) F_{j+1}]^T + K(t_{j+1}) w_{j+1}^{-1} K^T(t_{j+1}) \quad (8\text{-}100g)$$

11. Increment j and return to step 1 to repeat the cycle for the next measurement.

12. Continue the cycle between step 1 and step 12 until a specified set of measurement data is processed.

13. Integrate back to epoch and output the results utilizing the data to time t_f, e.g., $\hat{x}(t_0 \mid t_f)$ and $P_{\Delta x}(t_0 \mid t_f)$, where t_f represents the time of the final data point in the set of measurements processed.

14. Continue the cycle between step 1 and step 14 until all the data are processed.

15. Make a final pass through the measurement data to compute the residual statistics and print the final reports.

One of the main difficulties associated with the filtering approach to orbit determination is filter divergence, i.e., the estimated (filtered) state diverges from the actual state. It can occur when estimates of the state become more accurate and, hence, the covariance becomes smaller. As a result, the Kalman gain decreases and new measurements exert less influence on the solution. The measurements, which are a realization of the true state, have a smaller effect than the "learned" dynamical model. Therefore, successive estimates of the state tend to follow the erroneous "learned" dynamical model and to diverge from the true state, which is reflected in the measurements. Consequently, the estimated covariance fails to represent the true estimation error.

Divergence can arise from the following sources:

- Linearization errors (e.g., measurement linearization)
- Computational errors (e.g., $P_{\Delta x}$ loses its positive semidefiniteness)
- Modeling errors
- Unknown noise statistics

Generally, the first source can be minimized by iterating the solution (updated reference trajectory). Computational errors can be minimized by square-root filtering algorithms (Reference 9) and program coding techniques (Reference 10). Modeling errors can be handled in either a nonadaptive or an adaptive manner. The nonadaptive methods modify the filter structure to maintain the Kalman gain at some suitable level for sustained filter operation. The Modified Extended Kalman Filter (MEKF) by Torroglosa (Reference 11) is a filter of this type. The adaptive techniques can be divided into structural and statistical methods. The structural or dynamic model compensation methods are designed to adaptively estimate the true value of the unmodeled acceleration along with the state. Tapley and his associates (References 12, 13, and 14) have followed this approach, which will be discussed in Section 8.4.2. The statistical methods are designed to correct the basic filter to accommodate the combined effects of all error sources, e.g., the neglected nonlinearities, unknown noise statistics, and computational error effects, in addition to the model errors. The Jazwinski Filter (Reference 15) is a filter of this type. Statistical adaptive filtering is discussed in Section 8.4.3.

8.4.2 DYNAMIC MODEL COMPENSATION FILTERING

The dynamic model compensation (DMC) techniques are designed to adaptively estimate the true value of the unmodeled acceleration along with the state. A sequential estimation method has been developed (References 12, 13, and 14) that compensates for the unmodeled effects in the differential equations that define the dynamical process. The advantages of this method are as follows:

- It can be used to obtain an improved estimate of the state vector in realtime applications.
- It yields information that can be used in postflight analysis to improve the basic dynamical model.

The unmodeled accelerations are assumed to be a first-order Gauss-Markov process, i.e., they consist of the superposition of a time-correlated component and a purely random component. The discussion of the mathematical model for this type of filter follows that given in Reference 12. There the technique is applied to estimate the state of a lunar orbiting spacecraft acted upon by unmodeled forces due to venting, water dumps, or translational forces due to unbalanced attitude control reactions.

The equations of motion of the nonlinear dynamical system are given by

$$\dot{\bar{r}} = \bar{v} \tag{8-101a}$$

$$\dot{\bar{v}} = \bar{a}_m(\bar{r}, \bar{v}, t) + \bar{a}_u(t) \tag{8-101b}$$

where $\bar{r}$ and $\bar{v}$ are the position and velocity components, $\bar{a}_m$ is the three-component acceleration vector used in the filter-world or nominal dynamical model, and $\bar{a}_u$ is the three-component vector of all unknown and/or unmodeled accelerations.

The unmodeled acceleration, $\bar{a}_u(t)$, is represented as a first-order Gauss-Markov process, $\bar{\epsilon}(t)$, which satisfies the differential equation

$$\dot{\bar{\epsilon}}(t) = A(t)\,\bar{\epsilon}(t) + B(t)\,\bar{u}(t) \tag{8-102}$$

where A(t) and B(t) are coefficient matrices, $\bar{\epsilon}(t)$ is a three-component vector, and $\bar{u}$ is a three-component vector of Gaussian noise whose components satisfy the a priori statistics

$$\mathcal{E}\{\bar{u}(t)\} = 0 \tag{8-103a}$$

$$\mathcal{E}\{\bar{u}(t)\,\bar{u}^T(t)\} = I\,\delta(t - \tau) \tag{8-103b}$$

The matrix I is a 3×3 identity matrix and $\delta(t - \tau)$ is the Dirac delta function. The quantity A(t) is a 3×3 diagonal matrix of the time correlation coefficients

$$A(t) = \begin{bmatrix} -1/T_1 & 0 & 0 \\ 0 & -1/T_2 & 0 \\ 0 & 0 & -1/T_3 \end{bmatrix} \tag{8-104}$$

where T_1, T_2, and T_3 are the correlation times, which are unknown parameters to be estimated by including the vector $\bar{T}$

$$\bar{T}^T = [T_1 \;\; T_2 \;\; T_3] \tag{8-105}$$

in the set of parameters to be estimated.

The quantity B(t) is a 3×3 diagonal matrix

$$B(t) = \begin{bmatrix} b_1 & 0 & 0 \\ 0 & b_2 & 0 \\ 0 & 0 & b_3 \end{bmatrix} \tag{8-106}$$

where the b_j are treated as specified constants.

When Equations (8-101) and (8-102) are combined with $\dot{T} = 0$, the dynamical system is described by the following set of first-order differential equations:

$$\dot{\bar{r}} = \bar{v} \tag{8-107a}$$

$$\dot{\bar{v}} = \bar{a}_m(\bar{r}, \bar{v}, t) + \bar{\epsilon}(t) \tag{8-107b}$$

$$\dot{\bar{\epsilon}} = A\,\bar{\epsilon} + B\,\bar{u}(t) \tag{8-107c}$$

$$\dot{T} = 0 \tag{8-107d}$$

If the state vector $\bar{x}$ is augmented as

$$\bar{x}^T = [\bar{r}^T \mid \bar{v}^T \mid \bar{\epsilon}^T \mid T^T] \tag{8-108}$$

the dynamical system in Equation (8-107) can be written as

$$\dot{\bar{x}} = \bar{g}(\bar{x}, \bar{u}, t) \tag{8-109a}$$

$$\bar{x}(t_0) = \bar{x}_0 \tag{8-109b}$$

where

$$\bar{g}^T = [\bar{v}^T \mid (\bar{a}_m + \bar{\epsilon})^T \mid (A\,\bar{\epsilon} + B\,\bar{u})^T \mid 0] \tag{8-109c}$$

and the initial conditions $\bar{x}_0$ are unknown.

For $t > t_j$, where t_j is a reference epoch, the solutions to Equation (8-107) in integral form are

$$\bar{r}(t) = \bar{r}(t_j) + \bar{v}(t_j)\,\Delta t + \int_{t_j}^{t} \bar{a}(\bar{r}, \bar{v}, \bar{\epsilon}, t)\,[t - \tau]\,d\tau \tag{8-110a}$$

$$\bar{v}(t) = \bar{v}(t_j) + \int_{t_j}^{t} \bar{a}(\bar{r}, \bar{v}, \bar{\epsilon}, t)\, d\tau \tag{8-110b}$$

$$\bar{\epsilon}(t) = E(t)\, \bar{\epsilon}(t_j) + \bar{\ell}(t_j) \tag{8-110c}$$

$$\bar{T}(t) = \bar{T}(t_j) \tag{8-110d}$$

where

$$\Delta t = t - t_j \tag{8-110e}$$

and

$$\bar{a}(\bar{r}, \bar{v}, \bar{\epsilon}, t) = \bar{a}_m(\bar{r}, \bar{v}, t) + \bar{\epsilon}(t) \tag{8-110f}$$

The matrices $E(t)$ and $\bar{\ell}(t_j)$ are defined as

$$E(t) = \begin{bmatrix} a_1 & 0 & 0 \\ 0 & a_2 & 0 \\ 0 & 0 & a_3 \end{bmatrix} \tag{8-111a}$$

$$\ell^T(t_j) = \left[\sigma_1(1 - a_1^2)^{1/2}\, u_1 \;\vdots\; \sigma_2(1 - a_2^2)^{1/2}\, u_2 \;\vdots\; \sigma_3(1 - a_3^2)^{1/2}\, u_3\right] \tag{8-111b}$$

where

$$a_k = \exp[-(t - t_j)/T_k] \qquad (k = 1, 2, 3) \tag{8-112a}$$

and

$$\sigma_k = b_k(2/T_k)^{1/2} \qquad (k = 1, 2, 3) \tag{8-112b}$$

Equation (8-110) can also be written as

$$\bar{x}(t, t_j) = \bar{G}[\bar{x}(t_j), t_j, t] + \bar{\omega}_j \quad (t \geq t_j) \tag{8-113a}$$

where

$$\bar{\omega}^T = [\omega_r^T \mid \omega_v^T \mid \omega_\epsilon^T \mid 0] \tag{8-113b}$$

is the state noise matrix which is due to the purely random components of the unmodeled accelerations

$$\bar{\omega}_j = \begin{bmatrix} \int_{t_j}^{t} \bar{\ell}(t_j)\,[t - \tau]\,d\tau \\ \int_{t_j}^{t} \bar{\ell}(t_j)\,d\tau \\ \bar{\ell}(t_j) \\ 0 \end{bmatrix} \tag{8-114}$$

The statistics of $\bar{\omega}$ are

$$\mathcal{E}[\bar{\omega}] = 0 \tag{8-115a}$$

$$\mathcal{E}[\bar{\omega}\,\bar{\omega}^T] = Q_j\,\delta_{ij} = \begin{bmatrix} Q_{rr} & Q_{rv} & Q_{r\epsilon} & 0 \\ Q_{rv} & Q_{vv} & Q_{v\epsilon} & 0 \\ Q_{r\epsilon} & Q_{\epsilon v} & Q_{\epsilon\epsilon} & 0 \\ 0 & 0 & 0 & 0 \end{bmatrix} \delta_{ij} \tag{8-115b}$$

where δ_{ij} is the Kronecker delta function and

$$Q_{rr} = \frac{S_j\,(\Delta t)^4}{4} \tag{8-116a}$$

$$Q_{rv} = Q_{vr} = \frac{S_j (\Delta t)^3}{2} \tag{8-116b}$$

$$Q_{r\epsilon} = Q_{\epsilon r} = \frac{S_j (\Delta t)^2}{2} \tag{8-116c}$$

$$Q_{vv} = S_j (\Delta t)^2 \tag{8-116d}$$

$$Q_{v\epsilon} = Q_{\epsilon v} = S_j \Delta t \tag{8-116e}$$

$$Q_{\epsilon\epsilon} = S_j \tag{8-116f}$$

and

$$S_j = \begin{bmatrix} \sigma_1^2(1 - a_1^2) & 0 & 0 \\ 0 & \sigma_2^2(1 - a_2^2) & 0 \\ 0 & 0 & \sigma_3^2(1 - a_3^2) \end{bmatrix} \tag{8-117}$$

The measurement equation for the j^{th} measurement is

$$\bar{y}_j = \bar{f}[\bar{x}(t_j), t_j] + \bar{n}_j \tag{8-118a}$$

where $\bar{n}_j$ is the measurement noise that satisfies the following conditions:

$$\mathcal{E}[\bar{n}] = 0 \tag{8-118b}$$

$$\mathcal{E}[\bar{n}\,\bar{n}^T] = R_j \delta_{ij} \tag{8-118c}$$

and R is the covariance matrix of the measurement noise.

The procedure then follows that of the Extended Kalman Filter described in Section 8.4.1, with the following modifications:

1. The state is predicted via Equation (8-113) with $\bar{\omega} \equiv 0$.
2. Equation (8-115) is used for Q_{j+1} in the predicted covariance matrix of error.
3. In the filter gain matrix K, the matrix R from Equation (8-118c) replaces w^{-1}.
4. The updated covariance matrix is computed via Equation (8-86c) rather than Equation (8-90).

The algorithm requires a priori values for the augmented state, $\bar{x}_0$, along with the a priori covariance matrices, $P_{\Delta x_0}$, Q_j, and R_j.

When applied to the Apollo 10 and 11 missions, the DMC method gave the following results:

1. Its accuracy was limited by the measurement noise rather than by the model inaccuracies.
2. The unmodeled accelerations were primarily due to neglected effects in the lunar potential, and the magnitude of the unmodeled accelerations was dominated by the radial component.
3. The estimated values of unmodeled accelerations were repeatable from orbit to orbit and from mission to mission.
4. The magnitude of the radial component of the unmodeled acceleration was highly correlated with the location of lunar surface mascons.

The obvious drawback of the preceding filtering theories is that the noise statistics must be supplied a priori. A remedy for this difficulty is discussed in the following section.

8.4.3 STATISTICAL ADAPTIVE FILTERING

Statistical adaptive filtering techniques are designed to correct the basic filter to account for the combined effects of all error sources, e.g., neglected nonlinearities, unknown noise statistics, computational errors, and model errors. One of the difficulties with filtering is the determination of the proper value of Q, the state noise covariance. Additional problems arise in determining the statistics associated with the measurement noise. Effects such as atmospheric refraction variation and random disturbances in the radar instrumentation are unpredictable. The assumptions that have been made are that $\bar{n}$, the measurement noise (Equation (8-1)), and $\bar{\omega}$, the state noise (Equation (8-91)), have zero mean. However, due to model errors and nonlinearities, this is rarely true. The goal of

statistical adaptive filtering is to determine the actual mean and covariance of both the state and measurement noise so that better estimates of the state can be obtained.

Numerous investigators have developed adaptive sequential estimation techniques based on the recursive Kalman filter equations (References 15 and 16). The J-adaptive filter is discussed as an example of statistical adaptive filters. Jazwinski developed a sequential adaptive estimator having the capability to track system state and model errors in the presence of large and unpredictable system or environmental variations. The approach is to add a low frequency random forcing function, representing the model errors, to the differential equation representing the system model. The filter then estimates this function as well as the state. The model chosen for this random forcing function is a polynomial with time-varying coefficients. This particular approach is especially useful in parameter identification problems.

It is assumed that the estimator system model is

$$\dot{\bar{x}} = \bar{g}_1(\bar{x}, t) + \bar{g}_2\, \bar{u}(t) \tag{8-119}$$

where $\bar{g}_1$ includes the accelerations that are well known, $\bar{g}_2$ includes possible unknown accelerations and model errors in $\bar{g}_1$, and $\bar{u}(t)$ is a random forcing function.

If $\bar{u}(t)$ is a linear polynomial in time, the discrete form of the system model over the time interval $[t_j, t_{j+1}]$ is

$$\bar{x}(t_{j+1}) = \bar{G}[\bar{x}(t_j), \bar{u}(t)] \tag{8-120a}$$

$$\bar{u}(t) = \bar{u}(t_j) + \dot{\bar{u}}(t_j)\,[t - t_j] \tag{8-120b}$$

where $\dot{u}$ is modeled as a random constant to be estimated.

The measurement model is the same as in previous sections, i.e.,

$$\bar{y}(t_j) = \bar{f}[\bar{x}(t_j),\ t_j] + \bar{n} \tag{8-121a}$$

where $\bar{n}$ is measurement noise with

$$\mathcal{E}\{\bar{n}\,\bar{n}^T\} = R \tag{8-121b}$$

Hence, the complete dynamical system model is

$$\hat{\bar{x}}(t_{j+1} \mid t_j) = \bar{G}[\hat{\bar{x}}(t_j \mid t_j),\ \bar{u}(t_{j+1} \mid t_j)] + \bar{w} \tag{8-122a}$$

$$\bar{u}(t_{j+1} \mid t_j) = \bar{u}(t_j \mid t_j) + \dot{\bar{u}}(t_{j+1} \mid t_j)\,\tau \tag{8-122b}$$

$$\dot{\bar{u}}(t_{j+1} \mid t_j) = \dot{\bar{u}}(t_j \mid t_j) \tag{8-122c}$$

where

$$\tau = t_{j+1} - t_j \tag{8-122d}$$

To describe the system, the covariance and correlation matrices are defined as follows:

$$\mathcal{E}\{\hat{\Delta x}(t_j)\ \hat{\Delta x}^T(t_j)\} = P(t_j \mid t_j) \tag{8-123a}$$

$$\mathcal{E}\{\hat{\Delta x}(t_j)\ \hat{\Delta u}^T(t_j)\} = C_{ux}(t_j \mid t_j) \tag{8-123b}$$

$$\mathcal{E}\{\hat{\Delta x}(t_j)\ \hat{\Delta \dot{u}}^T(t_j)\} = C_{\dot{u}x}(t_j \mid t_j) \tag{8-123c}$$

$$\mathcal{E}\{\hat{\Delta u}(t_j)\ \hat{\Delta u}^T(t_j)\} = U_{uu}(t_j \mid t_j) \tag{8-123d}$$

$$\mathcal{E}\{\hat{\Delta u}(t_j)\ \hat{\Delta \dot{u}}^T(t_j)\} = U_{u\dot{u}}(t_j \mid t_j) \tag{8-123e}$$

$$\mathcal{E}\{\hat{\Delta u}(t_j)\ \hat{\Delta \dot{u}}^T(t_j)\} = U_{\dot{u}\dot{u}}(t_j \mid t_j) \tag{8-123f}$$

where

$$\hat{\Delta x}(t_j) = \bar{x}(t_j) - \hat{\bar{x}}(t_j) \tag{8-124a}$$

$$\hat{\Delta u}(t_j) = \bar{u}(t_j) - \hat{\bar{u}}(t_j) \tag{8-124b}$$

$$\hat{\Delta u}(t_j) = \dot{\bar{u}}(t_j) - \hat{\dot{\bar{u}}}(t_j) \tag{8-124c}$$

Let

$$\bar{x}(t_{j+1} \mid t_j) = \phi\, \bar{x}(t_j) + \psi\, \bar{u}(t_j) + \psi_d\, \dot{\bar{u}}(t_j) \tag{8-125}$$

where

$$\phi(t_{j+1} \mid t_j) = \frac{\partial \bar{x}(t_{j+1})}{\partial \bar{x}(t_j)} \tag{8-126a}$$

$$\psi(t_{j+1} \mid t_j) = \frac{\partial \bar{x}(t_{j+1})}{\partial \bar{u}(t_j)} \tag{8-126b}$$

$$\psi_d(t_{j+1} \mid t_j) = \frac{\partial \bar{x}(t_{j+1})}{\partial \dot{\bar{u}}(t_j)} \tag{8-126c}$$

The Jazwinski Filter is derived by augmenting the state $\bar{x}$ with the vectors $\bar{u}$ and $\dot{\bar{u}}$ and using the Extended Kalman Filter in augmented form.

Equations (8-122b), (8-122c), and (8-125) can be combined to yield an augmented transition matrix

$$\phi = \begin{bmatrix} \phi & \psi & \psi_d \\ 0 & I & \tau \\ 0 & 0 & I \end{bmatrix} \tag{8-127}$$

The augmented form of the error covariance matrix is

$$P(t_j \mid t_j) = \begin{bmatrix} P & C_{ux} & C_{\dot{u}x} \\ C_{ux}^T & U_{uu} & U_{u\dot{u}} \\ C_{\dot{u}x}^T & U_{u\dot{u}}^T & U_{\dot{u}\dot{u}} \end{bmatrix} \tag{8-128}$$

The augmented state, gain, and measurement matrices are

$$X = \begin{bmatrix} x \\ u \\ \dot{u} \end{bmatrix} \tag{8-129a}$$

$$K = \begin{bmatrix} K_x \\ K_u \\ K_{\dot{u}} \end{bmatrix} \tag{8-129b}$$

$$F = [F \mid 0 \mid 0] \tag{8-129c}$$

Substituting Equations (8-127) and (8-128) into Equation (8-92b) and ignoring the state noise yields

$$P(t_{j+1} \mid t_j) = \begin{bmatrix} \phi & \psi & \psi_d \\ 0 & I & \tau \\ 0 & 0 & I \end{bmatrix} \begin{bmatrix} P & C_{ux} & C_{\dot{u}x} \\ C_{ux}^T & U_{uu} & U_{u\dot{u}} \\ C_{\dot{u}x}^T & U_{u\dot{u}}^T & U_{\dot{u}\dot{u}} \end{bmatrix} \begin{bmatrix} \phi^T & 0 & 0 \\ \psi^T & I & 0 \\ \psi_d^T & \tau & I \end{bmatrix} \tag{8-130}$$

Expanding the right-hand side, the upper triangular elements of $P(t_{j+1} \mid t_j)$ are

$$P(t_{j+1} \mid t_j) = \phi P \phi^T + \psi C_{ux}^T \phi^T + \psi_d C_{ux}^T \phi^T + \phi C_{ux} \psi^T + \psi U_{uu} \psi^T + \psi_d U_{uu}^T \psi^T + \phi C_{\dot{u}x} \psi_d^T + \psi U_{u\dot{u}} \psi_d^T + \psi_d U_{\dot{u}\dot{u}} \psi_d^T \quad (8\text{-}131a)$$

$$C_{ux}(t_{j+1} \mid t_j) = \phi C_{ux} + \psi U_{uu} + \psi_d U_{u\dot{u}}^T + \tau (\phi C_{\dot{u}x} + \psi U_{u\dot{u}} + \psi_d U_{\dot{u}\dot{u}}) \quad (8\text{-}131b)$$

$$C_{\dot{u}x}(t_{j+1} \mid t_j) = \phi C_{\dot{u}x} + \psi U_{u\dot{u}} + \psi_d U_{\dot{u}\dot{u}} \quad (8\text{-}131c)$$

$$U_{uu}(t_{j+1} \mid t_j) = U_{uu} + \tau U_{u\dot{u}}^T + \tau (U_{u\dot{u}} + \tau U_{\dot{u}\dot{u}}) \quad (8\text{-}131d)$$

$$U_{u\dot{u}}(t_{j+1} \mid t_j) = U_{u\dot{u}} + \tau U_{\dot{u}\dot{u}} \quad (8\text{-}131e)$$

$$U_{\dot{u}\dot{u}}(t_{j+1} \mid t_j) = U_{\dot{u}\dot{u}} \quad (8\text{-}131f)$$

where all the terms on the right-hand sides of Equations (8-131a) through (8-131f) are evaluated at $(t_j \mid t_j)$.

Substituting Equations (8-128) and (8-129) into Equation (8-86d) yields

$$\begin{bmatrix} K_x \\ K_u \\ K_{\dot{u}} \end{bmatrix} = \begin{bmatrix} P & C_{ux} & C_{\dot{u}x} \\ C_{ux}^T & U_{uu} & U_{u\dot{u}} \\ C_{\dot{u}x}^T & U_{u\dot{u}}^T & U_{\dot{u}\dot{u}} \end{bmatrix} \begin{bmatrix} F^T \\ 0 \\ 0 \end{bmatrix} \times \left\{ W_{j+1}^{-1} + [F \mid 0 \mid 0] \begin{bmatrix} P & C_{ux} & C_{\dot{u}x} \\ C_{ux}^T & U_{uu} & U_{u\dot{u}} \\ C_{\dot{u}x}^T & U_{u\dot{u}}^T & U_{\dot{u}\dot{u}} \end{bmatrix} \begin{bmatrix} F^T \\ 0 \\ 0 \end{bmatrix} \right\}^{-1} \quad (8\text{-}132)$$

Carrying out the indicated matrix multiplications,

$$\begin{bmatrix} K_x \\ K_u \\ K_{\dot{u}} \end{bmatrix} = \begin{bmatrix} P F^T (F P F^T + w_{j+1}^{-1})^{-1} \\ C_{ux}^T F^T (F P F^T + w_{j+1}^{-1})^{-1} \\ C_{\dot{u}x}^T F^T (F P F^T + w_{j+1}^{-1})^{-1} \end{bmatrix} \tag{8-133}$$

Substituting Equations (8-128) and (8-129) into Equation (8-86c) yields

$$\begin{aligned} P(t_{j+1} \mid t_{j+1}) &= \left(I - \begin{bmatrix} K_x \\ K_u \\ K_{\dot{u}} \end{bmatrix} [F \mid 0 \mid 0] \right) \begin{bmatrix} P & C_{ux} & C_{\dot{u}x} \\ C_{ux}^T & U_{uu} & U_{u\dot{u}} \\ C_{\dot{u}x}^T & U_{u\dot{u}}^T & U_{\dot{u}\dot{u}} \end{bmatrix} \\ &= \begin{bmatrix} I - K_x F & 0 & 0 \\ -K_u F & I & 0 \\ -K_{\dot{u}} F & 0 & I \end{bmatrix} \begin{bmatrix} P & C_{ux} & C_{\dot{u}x} \\ C_{ux}^T & U_{uu} & U_{u\dot{u}} \\ C_{\dot{u}x}^T & U_{u\dot{u}}^T & U_{\dot{u}\dot{u}} \end{bmatrix} \end{aligned} \tag{8-134}$$

Hence, the upper triangular elements of $P(t_{j+1} \mid t_{j+1})$ are

$$P(t_{j+1} \mid t_{j+1}) = (I - K_x F)\, P(t_{j+1} \mid t_j) \tag{8-135a}$$

$$C_{ux}(t_{j+1} \mid t_{j+1}) = (I - K_x F)\, C_{ux}(t_{j+1} \mid t_j) \tag{8-135b}$$

$$C_{\dot{u}x}(t_{j+1} \mid t_{j+1}) = (I - K_x F)\, C_{\dot{u}x}(t_{j+1} \mid t_j) \tag{8-135c}$$

$$U_{uu}(t_{j+1} \mid t_{j+1}) = U_{uu}(t_{j+1} \mid t_j) - K_u F\, C_{ux}(t_{j+1} \mid t_j) \tag{8-135d}$$

$$U_{u\dot{u}}(t_{j+1} \mid t_{j+1}) = U_{u\dot{u}}(t_{j+1} \mid t_j) - K_u F C_{\dot{u}x}(t_{j+1} \mid t_j) \tag{8-135e}$$

$$U_{\dot{u}\dot{u}}(t_{j+1} \mid t_{j+1}) = U_{\dot{u}\dot{u}}(t_{j+1} \mid t_j) - K_{\dot{u}} F C_{\dot{u}x}(t_{j+1} \mid t_j) \tag{8-135f}$$

Substituting Equation (8-129) into Equation (8-100) gives the update equation for the augmented state

$$\begin{bmatrix} \bar{x} \\ \bar{u} \\ \dot{\bar{u}} \end{bmatrix}_{(t_{j+1} \mid t_{j+1})} = \begin{bmatrix} \bar{x} \\ \bar{u} \\ \dot{\bar{u}} \end{bmatrix}_{(t_{j+1} \mid t_{j+1})} + \begin{bmatrix} K_x \\ K_u \\ K_{\dot{u}} \end{bmatrix} \{\bar{y}(t_{j+1}) - \bar{f}[\hat{\bar{x}}(t_{j+1} \mid t_j),\ t_{j+1}]\} \tag{8-136}$$

or

$$\bar{x}(t_{j+1} \mid t_{j+1}) = \bar{x}(t_{j+1} \mid t_j) + K_x \{\bar{y}(t_{j+1}) - \bar{f}[\hat{\bar{x}}(t_{j+1} \mid t_j),\ t_{j+1}]\} \tag{8-137a}$$

$$\bar{u}(t_{j+1} \mid t_{j+1}) = \bar{u}(t_{j+1} \mid t_j) + K_u \{\bar{y}(t_{j+1}) - \bar{f}[\hat{\bar{x}}(t_{j+1} \mid t_j),\ t_{j+1}]\} \tag{8-137b}$$

$$\dot{\bar{u}}(t_{j+1} \mid t_{j+1}) = \dot{\bar{u}}(t_{j+1} \mid t_j) + K_{\dot{u}} \{\bar{y}(t_{j+1}) - \bar{f}[\hat{\bar{x}}(t_{j+1} \mid t_j),\ t_{j+1}]\} \tag{8-137c}$$

Equations (8-125) and (8-130) are the prediction equations for the Jazwinski Filter, and Equations (8-133), (8-134), and (8-137) are the update equations. The inclusion of Equation (8-135f) is a modification by Torroglosa which keeps the covariance matrix of the state from becoming nonpositive definite. In the original Jazwinski Filter, the uncertainty in $\dot{u}$ was maintained constant and, hence, $U_{\dot{u}\dot{u}}(t_{j+1} \mid t_j) = \bar{U}_{\dot{u}\dot{u}}$. The initial conditions $\hat{\bar{x}}(0 \mid 0)$, $P_{\Delta x}(0 \mid 0)$, $U_{uu}(0 \mid 0)$, and $U_{\dot{u}\dot{u}}(0 \mid 0)$ must be specified. The correlation terms $C_{ux}(0 \mid 0)$, $C_{\dot{u}x}(0 \mid 0)$, $U_{u\dot{u}}(0 \mid 0)$, and the initial values of $\hat{\bar{u}}(0 \mid 0)$ and $\hat{\dot{\bar{u}}}(0 \mid 0)$ are set equal to zero externally.

8.4.4 COMPUTATIONAL PROCEDURE FOR THE FILTER PROGRAM

The computational sequence for the Filter Program is similar to that for the Differential Correction Program (see Section 8.2.4). The computational flow schematic is shown in

Figure 8-2. Both the figure and the accompanying discussion are divided into functional blocks. The computational sequence is described below. The circled letters in this discussion refer to specific locations in Figure 8-2.

8.4.4.1 A Priori Input

All necessary input data are specified at Ⓐ. This includes the estimated variables and their covariances, the measurement timespans, and the number of measurements per set. The state input can be expressed optionally in any of several convenient coordinate systems as in the Differential Correction Program. For subsequent processing, the state is transformed into the mean equator and equinox of B1950.0 or J2000.0 system or into the true equator and equinox of a given epoch system. The transformations are given in Chapter 3.

8.4.4.2 Data Management

The measurement data are prepared for processing at Ⓑ and Ⓒ. This encompasses relocating the data for the specified measurement span from the original input device (single or multiple tapes, disk, or keyboard) to a working file convenient for subsequent retrieval during processing. During this relocation function, the data sequence can optionally be edited considering the type of measurement, the source of the data, the tracking station, and the timespan between adjacent points. The data on the working file are chronologically numbered, and the number of the data point that bounds the initial epoch time, t_0, from below is recorded. The data management function also includes determining whether the initial epoch time is less than the first data time, between the first and last data time, or larger than the last data time. For the first case, the data are processed sequentially from the first point at t_1 to the last point at t_m. For the second case, the processing starts backward in time from the initial epoch to the first data point, and it then switches back to the initial epoch and proceeds forward in time to the last data point. In the third case, the data are processed backwards in time from the last (chronological) data point to the first.

8.4.4.3 Processing Loop

The processing loop begins by retrieving the first data point to be processed from the working file at Ⓓ. A test is made to determine the optimal integrator to be used considering the timespan between measurements at t_j and t_{j-1}. A predicted covariance for the measurement is calculated. The measurement, its residual, and the partial derivatives of the measurements with respect to parameters being estimated are computed at Ⓔ, determining whether to accept or reject the measurement at Ⓕ. If the measurement is

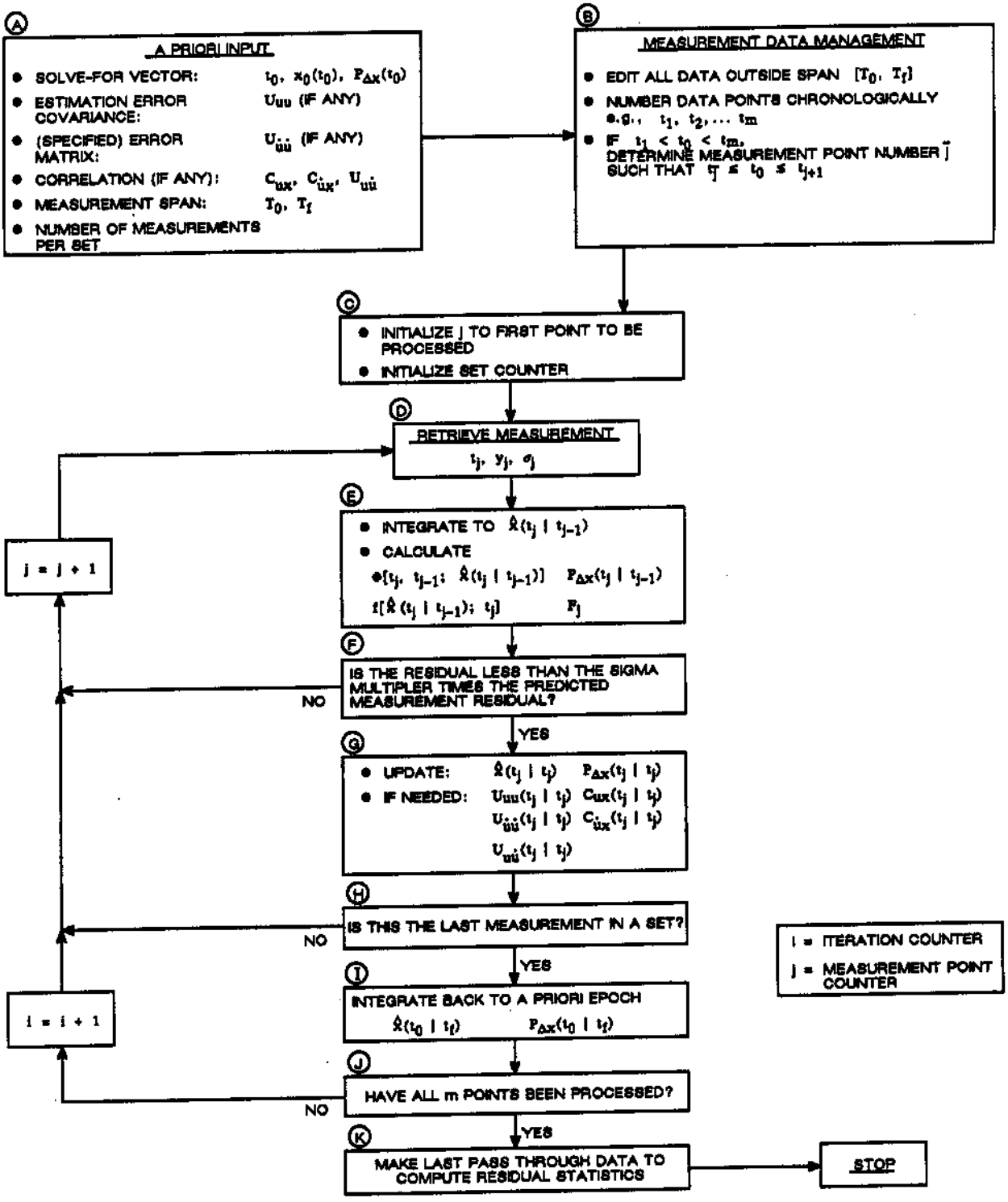

Figure 8-2. Computational Sequence for the Extended Kalman Filter

accepted, the Kalman gain is calculated; the state, state covariance matrix, and correlation matrices are updated; and the processed measurement is output at Ⓖ.

8.4.4.4 Data Set Loop

If it has been determined at Ⓗ that the last measurement of a set has been processed, the updated state at the last measurement time and its covariance matrix are printed. The updated state is then integrated backwards to the a priori epoch time and intermediate output reports are printed. (See Ⓘ.) After it has been determined at Ⓙ that all the measurements have been processed, a last pass is made through the measurement data to compute the residual statistics and print the final reports at Ⓚ.

8.5 COVARIANCE MATRIX INTERPRETATION

In the previous sections, equations have been presented for calculating the mean, $\hat{x}$, and the covariance matrix, $P_{\Delta x}$, of the errors in the estimated state and model parameters. There is little difficulty in recognizing the value of the mean (or estimated) value, but interpretation of the covariance and correlation matrices in terms of the uncertainty of the variables is not as clear. Yet, the covariance matrix yields a great deal of information on the statistical character of the variables. Some of these characteristics are described in the following subsections.

8.5.1 AUGMENTED VECTOR AND COVARIANCE

The estimation process yields the mean, $\hat{x}$, and covariance of errors, $P_{\Delta x}$, of the solve-for variables and the matrix $C_{\Delta x \Delta z}$ relating errors in the solve-for and consider variables. The mean, z_0, and covariance, $P_{\Delta z_0}$, of the consider variables are known a priori. As an aid in understanding the role of each of the matrices, the augmented (or expanded) state vector, $\bar{u}$, is defined as $(\bar{x} \mid \bar{z})^T$. The best estimate (or expected value) of u is $(\hat{x} \mid z_0)^T$. The covariance matrix of errors of $\bar{u}$ is $P_{\Delta u}$, which can be partitioned into the following components:

$$P_{\Delta u} = \left[\begin{array}{c|c} P_{\Delta x} & C_{\Delta x \Delta z} \\ \hline C_{\Delta z \Delta x} & P_{\Delta z_0} \end{array}\right] \tag{8-138}$$

where $P_{\Delta u}$ is a positive definite symmetric matrix. Therefore,

$$C_{\Delta z \Delta x} = C_{\Delta x \Delta z}^T \tag{8-139}$$

The submatrix $P_{\Delta z_0}$ remains constant throughout the processing, since the consider variable uncertainty cannot be improved through estimation.

The following subsections present a geometric heuristic interpretation of the covariance matrices $P_{\Delta u}$, $P_{\Delta x}$, and/or $P_{\Delta z_0}$ in terms of hyperdimensional volumes of constant probability in the (p + q)-, p-, and/or q-dimensional Euclidean space of the vector components.

8.5.2 HYPERELLIPSE PROBABILITIES

In the following discussion, the random vector $\mathbf{x}$ with uncertainty $P_{\Delta x}$ is considered. The discussion is equally applicable to the random variables $\mathbf{u}$ and $\mathbf{z}$. Assuming that the random vector $\mathbf{x}(t)$ is normally distributed, it can be completely described by its mean and covariance. The assumption that $\mathbf{x}(t)$ is normally distributed is partially justified as a result of an analogue of the Central Limit Theorem which states as follows: "If a large number of random variables are combined in a reasonably complicated fashion to form a single multivariate random variable, then this random variable will have a nearly normal distribution."

For the following discussion, it is assumed that the random vector of errors, $\overline{\Delta x}$, about the mean, $\hat{\mathbf{x}}$, is composed of six components. It is normally distributed with zero mean and covariance $P_{\Delta x}$. Its probability density function can be written as

$$p_x(\overline{\Delta x}) = \frac{1}{(2\pi)^3 \, |P_{\Delta x}|^{1/2}} \exp\left[-\frac{1}{2} \, \overline{\Delta x}^T P_{\Delta x}^{-1} \, \overline{\Delta x}\right] \tag{8-140}$$

If $P_{\Delta x}$ is a diagonal matrix, $\mathbf{x}$ has components that are statistically independent (uncorrelated), and $p_x(\overline{\Delta x})$ can then be factored into a product of six univariate functions of x_1, x_2, ..., x_6 (the one-dimensional marginal probability density functions of the six components of the state). This constitutes a sufficient condition for independence of the marginal random variables x_1, ..., x_6.

By virtue of its definition, $P_{\Delta x}$ is a nonnegative definite matrix so that it has nonnegative eigenvalues. Hence, a similarity transformation

$$\overline{\Delta y} = S \, \overline{\Delta x} \tag{8-141}$$

which diagonalizes $P_{\Delta x}$ is always possible, since the hypersurface of constant likelihood (constant value of probability density) in six-dimensional space is a hyperellipsoid, and by a rotation of axes it is possible to use the principal axes of the hyperellipsoid as

coordinate axes (i.e., to transform to another random variable space having uncorrelated or independent components). The $\overline{\Delta y}$ in Equation (8-141) represents space coordinates and is unrelated to the measurements.

Of interest is the probability that x_1 , x_2 , ..., x_6 lie within the hyperellipsoid

$$\overline{\Delta x}^T P_{\Delta x}^{-1} \overline{\Delta x} = \ell^2 \tag{8-142}$$

where ℓ is constant. By transforming to principal axes, this expression becomes

$$\frac{\Delta y_1^2}{\sigma_1^2} + \frac{\Delta y_2^2}{\sigma_2^2} + \cdots + \frac{\Delta y_6^2}{\sigma_6^2} = \ell^2 \tag{8-143}$$

where σ_1, σ_2, ..., σ_6 are the eigenvalues of $P_{\Delta x}$. The transformation matrix from $\overline{\Delta x}$ to $\overline{\Delta y}$ space is accomplished by the matrix of eigenvectors, S. By a second transformation, $\Delta z_i = \Delta y_i/\sigma_i$, the expression in Equation (8-143) becomes the equation for a hypersphere in six dimensions

$$\Delta z_1^2 + \Delta z_2^2 + \cdots + \Delta z_6^2 = \ell^2 \tag{8-144}$$

The probability of finding $\overline{\Delta z}$ inside this hypersphere is

$$\int\int \cdots \int_{\text{volume}} \frac{1}{(2\pi)^3} \exp\left\{-\frac{1}{2}(\Delta z_1^2 + \cdots + \Delta z_6^2)\right\} d\Delta z_1\, d\Delta z_2 \cdots d\Delta z_6 \tag{8-145}$$

where the integration is carried out over the volume of the hypersphere of radius Δr, where

$$\Delta r^2 = \Delta z_1^2 + \Delta z_2^2 + \cdots + \Delta z_6^2 \tag{8-146}$$

Thus, the probability of finding Δx_1, Δx_2, ..., Δx_6 inside the hyperellipsoid $\overline{\Delta x}^T P_{\Delta x}^{-1} \overline{\Delta x} = \ell^2$ is

$$P_r = \frac{1}{(2\pi)^3} \int_0^{\ell} e^{-1/2\Delta r^2} f(\Delta r)\, d\Delta r \tag{8-147}$$

where $f(\Delta r)$ is the spherically symmetric differential volume element.

In six-dimensional space, Equation (8-147) is

$$P_r = \frac{1}{(2\pi)^3} \int_0^{\ell} e^{-1/2\Delta r^2} (\pi^3 \Delta r^5)\, d\Delta r = \left[1 - \frac{1}{2} e^{-1/2\ell^2} \left(\frac{\ell^4}{4} + \ell^2 + 2\right)\right] \quad (8\text{-}148)$$

For ℓ = 1, 2, and 3, the probability is 0.014, 0.332, and 0.826, respectively. Also of interest are hyperellipsoids of other dimensions. Considering an m-dimensional random vector, where m = 1 through 7, the probabilities corresponding to ℓ = 1 through 4 (often called 1σ, 2σ, 3σ, and 4σ probabilities) are as shown in Table 8-1.

Table 8-1. Hyperellipse Probabilities

m \ ℓ	1	2	3	4
1	0.683	0.955	0.997	1.00
2	0.394	0.865	0.989	1.00
3	0.200	0.739	0.971	0.999
4	0.090	0.594	0.939	0.997
5	0.037	0.460	0.891	0.993
6	0.014	0.323	0.826	0.986
7	0.005	0.220	0.747	0.975

The problem of evaluating the hyperellipsoid, however, remains very difficult since it cannot be visualized. The equation for the ellipsoid can be transformed to its principal axes by means of the eigenvector transformation. The resulting diagonal matrix of eigenvalues yields the maximum excursions of the state variables. However, these excursions are in the transformed (principal) axes and therefore are maximum excursions for combinations of Δx_1, Δx_2, ..., Δx_6 and are still difficult to visualize.

8.5.3 HYPERRECTANGLE PROBABILITIES

Another method of interpreting the confidence regions of state variable uncertainty is by means of hyperrectangles instead of hyperellipses. Consider a two-dimensional case where $P_{\Delta x}$ is the covariance matrix

$$P_{\Delta x} = \begin{bmatrix} \sigma^2_{\Delta x_1} & \sigma_{\Delta x_1 \Delta x_2} \\ \sigma_{\Delta x_1 \Delta x_2} & \sigma^2_{\Delta x_2} \end{bmatrix} \quad (8\text{-}149)$$

The quadratic form $\overline{\Delta x}^T P_{\Delta x}^{-1} \overline{\Delta x} = \ell^2$ is

$$\sigma^2_{\Delta x_2} \Delta x_1^2 - 2\sigma_{\Delta x_1 \Delta x_2} \Delta x_1 \Delta x_2 + \sigma^2_{\Delta x_1} \Delta x_2^2 = \ell^2 |P_{\Delta x}| \tag{8-150}$$

This quadratic equation represents an ellipse such as that shown in Figure 8-3.

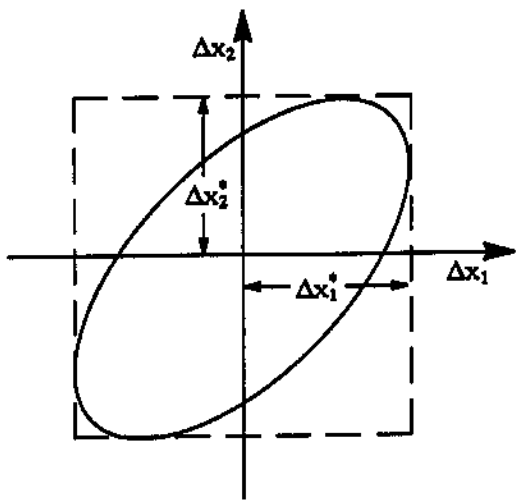

Figure 8-3. Error Ellipse and Rectangle

The width Δx_1^* and height Δx_2^* of the rectangle enclosing the ellipse are determined from Equation (8-150) for the condition that $d\Delta x_2/d\Delta x_1 = 0$ and $d\Delta x_1/d\Delta x_2 = 0$, respectively, yielding

$$\Delta x_2^* = \ell \sigma_{\Delta x_2} \tag{8-151a}$$

$$\Delta x_1^* = \ell \sigma_{\Delta x_1} \tag{8-151b}$$

Thus, the probability that Δx_1 lies within the region $-3\sigma_{\Delta x_1} \leq \Delta x_1 \leq 3\sigma_{\Delta x_1}$ is 0.997, Δx_2 falling wherever it may. The probability that Δx_2 lies within the region $-3\sigma_{\Delta x_2} \leq \Delta x_2 \leq 3\sigma_{\Delta x_2}$ is also 0.997, Δx_1 falling wherever it may. Assuming no significant correlations, the probability that Δx_1 and Δx_2 simultaneously lie within the respective regions $-3\sigma_{\Delta x_1} \leq \Delta x_1 \leq 3\sigma_{\Delta x_1}$ and $-3\sigma_{\Delta x_2} \leq \Delta x_2 \leq 3\sigma_{\Delta x_2}$ is therefore $(0.997)^2$ or 0.994. The probability that Δx_1 and Δx_2 lie within the 3σ ellipse is 0.989, slightly less than that for the rectangle due to the lesser area.

Extending this interpretation to six dimensions, the probability that Δx_1, Δx_2, ..., Δx_6 simultaneously lie within their 3σ hyperrectangles is $(0.997)^6$ or 0.982. The probability that they lie within the six-dimensional hyperellipsoid is 0.826, significantly lower because of the smaller volume. The hyperrectangle probabilities corresponding to ℓ = 1, 2, 3, and 4 and m = 1 through 7 are presented in Table 8-2.

Table 8-2. Hyperrectangle Probabilities

m \ ℓ	1	2	3	4
1	0.683	0.955	0.997	1.00
2	0.466	0.912	0.994	1.00
3	0.319	0.872	0.991	1.00
4	0.218	0.832	0.988	1.00
5	0.149	0.794	0.985	1.00
6	0.102	0.759	0.982	1.00
7	0.069	0.724	0.979	1.00

The hyperrectangle probabilities are much easier to analyze since the various sides of the hyperrectangles are multiples of the square root of the variances. However, it is important to be aware of the fact that the boundary of the hyperrectangle merely encloses a volume of space and in no way can be regarded as a boundary of constant probability as is the case with hyperellipses.

The hyperrectangle probabilities are particularly convenient during program checkout. By processing simulated data having Gaussian random error with zero mean and known variances, the residuals of the estimated vector can be compared with the calculated standard deviations. The distribution of residuals should satisfy the 1σ, 2σ, 3σ, and 4σ probabilities in Table 8-2.

8.5.4 CORRELATION COEFFICIENT

It has been shown that the off-diagonal covariance elements of a covariance matrix determine the deviation between the random vector coordinate axes and the principal axes of the hyperellipse of constant probability. When the covariance elements are zero, the principal axes are aligned with the coordinate axes and the components are independent of each other. Furthermore, the normal density function (Equation (8-140)) can then be factored into a product of n univariate functions of Δx_1, Δx_2, ..., Δx_n.

Another measure of the dependence of two random vectors $\overline{\Delta x}$ and $\overline{\Delta z}$ having a (p × q) correlation matrix

$$C_{\Delta x \Delta z} = \begin{bmatrix} \text{cov}(\Delta x_1, \Delta z_1) & \text{cov}(\Delta x_1, \Delta z_2) & \cdots & \text{cov}(\Delta x_1, \Delta z_q) \\ \text{cov}(\Delta x_2, \Delta z_1) & \cdot & & \cdot \\ \cdot & \cdot & & \cdot \\ \cdot & \cdot & & \cdot \\ \cdot & \cdot & & \cdot \\ \text{cov}(\Delta x_p, \Delta z_1) & \text{cov}(\Delta x_p, \Delta z_2) & \cdots & \text{cov}(\Delta x_p, \Delta z_q) \end{bmatrix} \tag{8-152}$$

is the correlation coefficient, defined as

$$\varrho_{ij} = \varrho(\Delta x_i, \Delta z_j) = \frac{\text{cov}(\Delta x_i, \Delta z_j)}{\sqrt{\text{var}(\Delta x_i)\ \text{var}(\Delta z_j)}} \tag{8-153}$$

The variance elements are the squares of the standard deviations for Δx_i and Δz_j, respectively, and lie along the main diagonal of $P_{\Delta x}$ and $P_{\Delta z}$, respectively. The correlation coefficient satisfies the following conditions:

- $\varrho = 0$ if and only if Δx_i and Δz_j (and therefore x_i and z_j) are uncorrelated
- $|\varrho| \leq 1$
- $\varrho = \pm 1$, if and only if

$$\left\{\frac{\Delta x_i}{\sigma_{\Delta x_i}}\right\} = \pm \left\{\frac{\Delta z_j}{\sigma_{\Delta z_j}}\right\} \tag{8-154}$$

where $\sigma_{\Delta x_i}$, $\sigma_{\Delta z_j}$ are the standard deviations of the errors x_i and z_j, respectively.

8.6 ESTIMATION-RELATED TECHNIQUES

Specific techniques required in the estimation process include matrix inversion, editing of residuals, iteration control, residual statistics, and hypothesis tests. These are discussed in the following subsections.

8.6.1 MATRIX INVERSION

The normal matrix is inverted by recursively inverting smaller matrices and by the use of the Schur identity. The symmetrical properties of the normal matrix are utilized during the inversion process. The Schur identity method is developed by assuming that the matrix to be inverted is of the form

$$[M] = \left[\begin{array}{c|c} [M_{11}] & [M_{12}] \\ \hline [M_{21}] & -[M_{22}] \end{array}\right] \tag{8-155}$$

with the inverse given by

$$[M]^{-1} = \left[\begin{array}{c|c} [H_{11}] & [H_{12}] \\ \hline [H_{21}] & [H_{22}] \end{array}\right] \tag{8-156}$$

Since

$$[M]\,[M]^{-1} = \left[\begin{array}{c|c} [I] & [0] \\ \hline [0] & [I] \end{array}\right] \tag{8-157}$$

then

$$[M_{11}]\,[H_{11}] + [M_{12}]\,[H_{21}] = [I] \tag{8-158a}$$

$$[M_{21}]\,[H_{11}] - [M_{22}]\,[H_{21}] = [0] \tag{8-158b}$$

Eliminating $[H_{21}]$ from Equations (8-158) and solving for $[H_{11}]$ gives

$$[M_{11}]\,[H_{11}] + [M_{12}]\,[M_{22}]^{-1}\,[M_{21}]\,[H_{11}] = [I] \tag{8-159a}$$

or

$$[H_{11}] = [M_{11}]^{-1} - [M_{11}]^{-1}\,[M_{12}]\,[M_{22}]^{-1}\,\{[M_{21}]\,[H_{11}]\} \tag{8-159b}$$

Premultiplying Equation (8-159) by $[M_{21}]\,[M_{11}]^{-1}$ gives

$$[M_{21}]\,[H_{11}] + [M_{21}]\,[M_{11}]^{-1}\,[M_{12}]\,[M_{22}]^{-1}\,[M_{21}]\,[H_{11}] = [M_{21}]\,[M_{11}]^{-1} \tag{8-160a}$$

or

$$[M_{21}]\,[H_{11}] = \Big[\,[I] + [M_{21}]\,[M_{11}]^{-1}\,[M_{12}]\,[M_{22}]^{-1}\Big]^{-1}\,[M_{21}]\,[M_{11}]^{-1} \tag{8-160b}$$

Substituting Equation (8-160b) into Equation (8-159b) gives

$$\begin{aligned}[H_{11}] = {} & [M_{11}]^{-1} - [M_{11}]^{-1}\,[M_{12}]\,[M_{22}]^{-1} \\ & \times \Big[\,[I] + [M_{21}]\,[M_{11}]^{-1}\,[M_{12}]\,[M_{22}]^{-1}\Big]^{-1}\,[M_{21}]\,[M_{11}]^{-1}\end{aligned} \tag{8-161}$$

The matrices $[H_{22}]$, $[H_{12}]$, and $[H_{21}]$ can be derived in a similar manner, yielding

$$[H_{22}] = -\Big[\,[M_{21}]\,[M_{11}]^{-1}\,[M_{12}] + [M_{22}]\Big]^{-1} \tag{8-162a}$$

$$[H_{12}] = -\,[M_{11}]^{-1}\,[M_{12}]\,[H_{22}] \tag{8-162b}$$

$$[H_{21}] = \;\;[M_{22}]^{-1}\,[M_{21}]\,[H_{11}] \tag{8-162c}$$

It is assumed that the inverse of $[M_{11}]$ is known and that $[M_{22}]$ is in all cases a (1×1) matrix. The matrix inversions required in Equations (8-161) and (8-162) are simply the

reciprocals of the elements of the respective matrices. The inversion begins by setting $[M_{11}]$ as

$$[M_{11}]^{-1} = \frac{1}{m_{11}} \tag{8-163}$$

and

$$-[M_{22}]^{-1} = -\frac{1}{m_{22}} \tag{8-164}$$

Equations (8-161) and (8-162) are then employed to determine the inverse of

$$\begin{bmatrix} m_{11} & m_{12} \\ m_{21} & m_{22} \end{bmatrix} \tag{8-165}$$

The result is called $[M_{11}]$ and the diagonal element following (in this case m_{33}) is used to form a new $[M_{22}]$. The process is continued along the diagonal until the required matrix is inverted. GTDS takes full advantage of the symmetry of the normal matrix by computing and storing only the upper triangle of the matrix. The inversion process is designed to invert a matrix in upper triangular form and store the result in the same manner.

8.6.2 EDITING OF MEASUREMENT RESIDUALS

The measurement residual, as computed by GTDS, is defined as the actual measurement minus the computed measurement that is based on the trajectory specified by the current state vector solution. Deletion of a measurement from the differential correction or filter computation can be accomplished by one or more of the following tests that are made on each iteration or filter set for each measurement:

- **By Time.** The measurement is rejected if it falls outside a specified timespan.
- **By Type.** The measurement type is among those to be rejected.
- **By Station.** The identifier of the station making the measurement is among those to be rejected.

- **By n^{th} Measurement.** Every n^{th} measurement of this type is to be processed; all other measurements are rejected.

- **By Deviation.** The measurement is rejected when the deviation from the orbit established by the previous iteration is greater than a specified value, or, in a filter run, when the residual differs from the predicted measurement residual, by more than a specified amount. The residual editing algorithms used in the Differential Correction Program are discussed in Sections 8.6.2.1 and 8.6.2.2.

- **By Geometry.** The measurement is rejected when the elevation angle of the line of sight from the tracking station is below a specified minimum value.

If a residual is deleted by any test, then the row of the augmented matrix F (the matrix of partial derivatives of the measurements with respect to the estimated parameters) corresponding to the measurement is not computed.

Preliminary measurement editing and the iterated residual editing procedure in GTDS are described below.

8.6.2.1 Preliminary Residual Editing

For the first outer loop iteration, the measurement fails the preliminary residual editing test if

$$\sqrt{w_{jj}} \; | \Delta y(t_j) | > R \tag{8-166}$$

where

$\Delta y(t_j)$ = measurement residual for the j^{th} measurement

R = maximum residual multiplier (this is a constant, with a default value of 10)

w_{jj} = component of the measurement weight matrix W corresponding to the j^{th} measurement

For subsequent outer loop iterations, the measurement is edited if

$$\sqrt{w_{jj}} \; | \Delta y(t_j) | > k \, RMSP_{i-1} + K \tag{8-167}$$

where

k = constant multiplier (default = 3)

K = additive constant (default = 0)

$RMSP_{i-1}$ = predicted root-mean-square (determined at the end of the previous least-squares iteration) for the current iteration (see Section 8.6.3)

The subscript i indexes the outer loop least-squares iterations.

8.6.2.2 Iterated Residual Editing Procedure

After the state estimate, $\hat{\bar{x}}_1$, is computed in each outer loop iteration, it can be refined using the iterated residual editing procedure. The three major steps followed in this procedure are as follows:

1. For each measurement, the predicted weighted measurement residual, $\Delta y^*(t_j)$, is computed by keeping only the linear term in the Taylor series expansion, as follows:

$$\Delta y^*(t_j) = \sqrt{w_{jj}}\, \Delta y(t_j) - \bar{a}_j\, \Delta\hat{\bar{x}}_{i+1,n-1} \tag{8-168}$$

where

w_{jj} = component of the measurement weighting matrix corresponding to j^{th} the measurement

$\Delta y(t_j)$ = j^{th} measurement residual computed in the outer loop

$\bar{a}_j$ = j^{th} row of the matrix F computed in the preliminary outer loop (defined in Equation (8-42))

$\Delta\hat{\bar{x}}_{i+1,n}$ = state correction computed in the n^{th} residual editing iteration, $\Delta\hat{\bar{x}}_{i+1,0}$, equals the correction computed in the i^{th} outer loop, $\Delta\hat{\bar{x}}_{i+1}$, given in Equation (8-23)

Next, an n-sigma editing test is applied by using the previous predicted root-mean-square (RMSP) to edit the predicted residual. The first residual editing iteration is initialized with $RMSP_0$ = RMSP from Equation (8-185). (Note that the root-mean-square (RMS) and the RMSP of the measurement residuals are defined further in Section 8.6.3.) If the predicted residual exceeds the tolerance

$$|\, \Delta y^*(t_j)\, | > kk \cdot RMSP_{n-1} \tag{8-169}$$

where kk is a multiplier that may or may not be the same as the quantity defined for preliminary residual editing), then the contribution of the measurement is removed from the normal equations. This is done by first eliminating the contribution of the measurement from Equation (8-23), as follows:

$$N_{i,n} \Leftarrow N_{i,n} - \bar{a}_j^T w_{jj}^* \bar{a}_j \tag{8-170}$$

$$S_{i,n} \Leftarrow S_{i,n} - \bar{a}_j^T w_{jj} \Delta y(t_j) \tag{8-171}$$

where

$$N_{i,0} = F_i^T W F_i + P_{\Delta x_0}^{-1} \tag{8-172}$$

$$S_{i,0} = F_i^T W \Delta \bar{y}_i + P_{\Delta x_0}^{-1} \Delta \bar{x}_i \tag{8-173}$$

Then the measurement residual $\Delta y(t_j)$ is removed from the vector of measurement residuals, i.e.,

$$\Delta \bar{y}_{i,n} \Leftarrow \Delta \bar{y}_{i,n} - [\Delta y(t_j) \text{ element}] \tag{8-174}$$

where

$$\Delta \bar{y}_{i,0} = \Delta \bar{y}_i \tag{8-175}$$

Next, the total number of measurements is reduced by one, i.e.,

$$m_{i,n} \Leftarrow m_{i,n} - 1 \tag{8-176}$$

where

$$m_{i,0} = m_i \tag{8-177}$$

This process is repeated until all the measurement data are examined.

2. The state correction vector, $\Delta\hat{\mathbf{x}}_{l+1,n}$; the estimation state vector, $\hat{\mathbf{x}}_{l+1,n}$; and the RMS and RMSP are recalculated as follows:

$$\Delta\hat{\mathbf{x}}_{l+1,n} = \mathbf{N}_{l,n}^{-1} \cdot \mathbf{S}_{l,n} \tag{8-178}$$

$$\hat{\mathbf{x}}_{l+1,n} = \hat{\mathbf{x}}_{l+1,n-1} + \Delta\hat{\mathbf{x}}_{l+1,n} \tag{8-179}$$

$$\mathrm{RMS}_n = \left\{\frac{1}{m_{l,n}} \left(\Delta\mathbf{y}_{l,n}^T \mathbf{W} \Delta\mathbf{y}_{l,n} + \Delta\bar{\mathbf{x}}_{l,n}^T \mathbf{P}_{\Delta\mathbf{x}_0}^{-1} \Delta\bar{\mathbf{x}}_{l,n}\right)\right\}^{1/2} \tag{8-180}$$

where

$$\Delta\bar{\mathbf{x}}_{l,n} = \bar{\mathbf{x}}_0 - \hat{\mathbf{x}}_{l+1,n-1} \tag{8-181}$$

and

$$\mathrm{RMSP}_n = \left\{\mathrm{RMS}_n^2 - \frac{2\Delta\hat{\mathbf{x}}_{l,n}^T \mathbf{S}_{l,n}}{m_{l,n}}\right\}^{1/2} \tag{8-182}$$

The quantities $\mathbf{N}_{l,n}$ and $\mathbf{S}_{l,n}$ are given in Equations (8-170) and (8-171), respectively, and $\Delta\mathbf{y}_{l,n}$ includes only those residuals that survived the residual editing. (Inclusion of the term in RMS_n that includes the a priori covariance is optional.)

3. Tests for convergence (or termination) of the inner loop residual editor are then performed. The process is terminated if any of the following criteria are satisfied:

a. The difference between the state update produced by the current recursive iteration and that produced by the preceding iteration is less than a specified tolerance.

b. The maximum allowable number of recursive iterations (default = 10) has been reached.

c. The relative difference of two successive values for RMSP is within a specified tolerance, i.e.,

$$\left|\frac{\mathrm{RMSP}_{n-1} - \mathrm{RMSP}_n}{\mathrm{RMSP}_n}\right| < \epsilon \tag{8-183}$$

where

$RMSP_{n-1}$ = predicted RMS for the $(n-1)^{th}$ residual editing loop

$RMSP_n$ = predicted RMS for the n^{th} residual editing loop

ϵ = specified tolerance

The final values obtained in Equations (8-178) through (8-182), by definition, are the $\Delta\hat{x}_{i+1}$, $\hat{x}_{i+1}$, RMS, and RMSP, respectively, of the entire outer loop, replacing those given in Equations (8-23), (8-24), (8-184), and (8-185). The final RMSP can also be used in the preliminary editing test for the next outer loop iteration.

8.6.3 ITERATION CONTROL FOR THE DIFFERENTIAL CORRECTION PROGRAM

Conditions that can cause termination of the differential correction process are as follows:

- Convergence of the solution
- Maximum number of consecutive iterations reached
- Maximum number of iterations reached

The convergence criteria in GTDS are based on iterative reduction of the square root of the mean square of the measurement residuals. This quantity, denoted by RMS, is calculated as follows on the i^{th} iteration:

$$RMS = \left\{\frac{1}{m}\left(\overline{\Delta y_i}^T W \overline{\Delta y_i} + \bar{\Delta x_i}^T P_{\Delta x_0}^{-1} \bar{\Delta x_i}\right)\right\}^{1/2} \tag{8-184}$$

where $\overline{\Delta y_i}$ and $\bar{\Delta x_i}$ are defined in Equations (8-21) and (8-22), and m is the number of measurements. If the value of RMS decreases during two consecutive iterations, the solution is converging. After a prespecified number of consecutive divergent iterations, the problem is terminated. After testing for convergence or divergence, a predicted RMS is calculated through first order in $\hat{\Delta x}_{i+1}$ for the next iteration as follows:

$$RMSP = \left\{\frac{1}{m}\left[(\overline{\Delta y_i} - F_i \hat{\Delta x}_{i+1})^T W (\overline{\Delta y_i} - F_i \hat{\Delta x}_{i+1}) + (\hat{\Delta x}_{i+1} - \bar{\Delta x_i})^T P_{\Delta x_0}^{-1} (\hat{\Delta x}_{i+1} - \bar{\Delta x_i})\right]\right\}^{1/2} \tag{8-185}$$

where $\hat{\Delta x}_{i+1}$, $\bar{\Delta x}_i$, and F_i are defined in Equations (8-23), (8-24), and (8-19a), respectively. The second term on the right is exactly correct for the $(i+1)^{st}$ iteration. The first term on the right linearly corrects the measurement residuals to account for the iteration. The first term on the right linearly corrects the measurement residuals to account for the differential correction $\hat{\Delta x}_{i+1}$. If the regression equation (Equation (8-14)) were linear, the predicted RMS (RMSP) would be exactly correct. The iterations are considered converged and the problem terminated when the following criterion is met:

$$\left| \frac{\text{RMSB} - \text{RMSP}}{\text{RMSB}} \right| < \epsilon \qquad (8\text{-}186)$$

where

RMSB = smallest RMS achieved compared with all previous iterations

ϵ = improvement ratio criterion specified by input

8.6.4 WEIGHTED LEAST-SQUARES AND FILTER STATISTICS

Upon completion of each iteration of the weighted least-squares fit or after a specified set of measurements has been filtered, a summary of the measurement residual statistics is calculated and printed. The statistical quantities that comprise the summary are computed for data types and residual groups that contain data from specific tracking stations. The following abbreviations are used in the statistical relationships:

where

$\overline{\Delta y_j}$ = j^{th} residual, $y_j - f[\hat{x}_1(t_j), \bar{z}_0]$

n_s = total number of residuals for a station and data type (group)

The measurement residual statistics are defined below.

<u>Root Mean Square Error</u>

The total weighted RMS, the predicted total RMSP, and the RMS for each station and data type are calculated from Equations (8-184) and (8-185). It is normally desirable that RMS be small, preferably zero.

Group Mean

The mean value of each residual group is a measure of the bias in the measurement and is calculated as follows:

$$\overline{m} = \frac{1}{n_s} \sum_{j=1}^{n_s} \overline{\Delta y_j} \tag{8-187}$$

It is desirable that $\overline{m}$ for each group be zero to be consistent with the assumption in Equation (8-25a) that the measurement noise has zero mean.

Sum of Squares About the Mean

The sum of the squares of the residuals about the mean of each residual group is

$$S = \sum_{j=1}^{n_s} (\overline{\Delta y_j} - \overline{m})^2 \tag{8-188}$$

Sample Standard Deviation

The sample standard deviation of each residual group is a measure of the dispersion of the measurement data and is calculated as follows;

$$\sigma = \left[\frac{1}{n_s - 1} \sum (\overline{\Delta y_j} - \overline{m})^2 \right]^{1/2} = \left(\frac{S}{n_s - 1} \right)^{1/2} \tag{8-189}$$

In GTDS, the approximation is made that n_s is large. Hence, $n_s - 1$ is replaced by n_s in the denominator of Equation (8-189). The standard deviation should be consistent with the values used in the priori weighting matrix, W.

Confidence Interval for the Group Mean

If the measurement residual group population is normally distributed with zero mean, then the variable

$$t = \frac{\overline{m}}{\sqrt{\sigma^2/n_s}} \tag{8-190}$$

has a t-distribution (Student's) with $(n_s - 1)$ degrees of freedom. Therefore, confidence intervals for the mean can be constructed from tables of the t-distribution. As n_s becomes large, the t-distribution approaches the normal distribution.

Measurement Residual Groups

For each iteration of the weighted least-squares fit, or after a specified set of measurements has been filtered, the following data are printed for each residual group:

- Number of measurements, n_s
- Number of rejected and accepted measurements
- Histograms of the measurements by the true anomaly

8.7 STATISTICAL OUTPUT REPORT MODELING

The Statistical Output Report (SOR) is designed for validating the tracking data and for calibrating trackers. The SOR groups the measurement residuals computed during the differential correction process in a number of different ways and computes the mean and standard deviation of each group of residuals. The basic groupings used in the SOR consist of SOR categories and SOR batches. Mean and standard deviation values based on SOR categories form the validation statistics, while the values based on SOR batches form the calibration statistics. Statistics for the first differential correction iteration residuals, the last differential correction iteration residuals, or both can be computed.

The SOR batches and categories are discussed in Section 8.7.1. Section 8.7.2 describes the SOR validation statistics, and the SOR calibration statistics are defined in Section 8.7.3. A noise estimate, based on the calibration statistics, is also computed in the SOR; this is discussed in Section 8.7.4.

8.7.1 SOR BATCHES AND CATEGORIES

An SOR batch corresponds roughly to the set of all measurements and residuals obtained from a particular tracking station during one tracking pass. The criteria used to form an SOR batch are the following:

- Tracking station
- Time difference between measurements
- Timespan of the batch
- Number of measurements in the batch
- Equipment mode (Reference 17, Table 4-3) (depending on the tracker type)
- Data rate (Reference 17, Table 4-4) (depending on the tracker type)
- Vehicle identification code (depending on the tracker type)
- Object number (depending on the tracker type)
- Range ambiguity (depending on the tracker type)
- Multifunction receiver number (depending on the tracker type)
- Frequency band (can be overridden) (TDRSS data only)

- Carrier frequency identification (can be overridden) (TDRSS data only)
- User bit rate (can be overridden) (TDRSS data only)
- Multiple-access antenna identification (TDRSS data only)
- Forward-link TDRS identification (TDRSS data only)
- Return-link TDRS identification (TDRSS data only)
- Ground transponder identification (TDRSS data only)

The mean and standard deviation statistics are computed separately for each measurement type within the batch.

An SOR category corresponds roughly to the set of all batches obtained from stations using the same tracker type. The criteria used to form an SOR category are the following:

- Measurement type (Reference 17, Table 4-2)
- Tracker type (Reference 17, Table 4-1)
- Equipment mode (depending on the tracker type)
- Data rate (depending on the tracker type)
- Frequency band (TDRSS data only)

8.7.2 SOR VALIDATION STATISTICS

The SOR validation mean and standard deviation statistics are based on SOR categories. The SOR category validation statistics are described in Section 8.7.2.1. Validation statistics are also computed for each batch and for each station, using some of the results from the category validation statistics. Section 8.7.2.2 defines the batch validation statistics, and the station validation statistics are given in Section 8.7.2.3.

8.7.2.1 Category Validation Statistics

The following three types of data are included in the category validation statistics:

- Data that are accepted by the differential correction process
- Data that are residually edited in the differential correction process
- Data that are edited by user-supplied specifications (preedited; see Section 8.6.2)

The data residuals in each category are first subjected to a maximum O-C residual test, in which each residual that exceeds a specified value is marked as "SOR O-C max" edited.

The mean, M_0, and variance, S_0^2, of the remaining unedited residuals are then computed as

$$M_0 = \frac{\sum_{j=1}^{n_0} \Delta y(t_j)}{n_0} \tag{8-191}$$

and

$$S_0^2 = \frac{\sum_{j=1}^{n_0} [\Delta y(t_j)]^2}{n_0} - M_0^2 \tag{8-192}$$

where

$\Delta y(t_j)$ = j^{th} unedited residual

n_0 = number of remaining unedited residuals

The remaining unedited residuals in each category are then subjected to an iterative n-sigma edit, i.e., they are edited if

$$|\Delta y(t_j) - M_{k-1}| > n\, S_{k-1} \tag{8-193}$$

where

M_{k-1} = mean of the unedited residuals from the previous edit loop

n = sigma multiplier

S_{k-1} = standard deviation of the unedited residuals from the previous edit loop

k = edit loop counter

The mean, M_k, and variance, S_k^2, of the residuals that are unedited on successive edit loops are computed using Equations (8-191) and (8-192), with n_k rather than n_0, where n_k is the number of unedited residuals on the k^{th} edit loop.

If the maximum number of iterative edit loops has not been reached and no additional residuals are edited, the iterative n-sigma edit is terminated. All residuals edited during the iterative n-sigma loop are marked as "SOR validation edited." The mean values and standard deviations of the final sets of unedited and edited residuals are computed separately as described above.

8.7.2.2 Batch Validation Statistics

For the batch validation statistics, no O-C maximum or n-sigma editing is performed. Instead, the final edit status from the category validation statistics is used in determining the edit status of the residuals in the batch. The mean values and standard deviations of both the validation-edited and the unedited residuals are computed separately for each batch. The batch and category validation statistics are the same only if the data from each category are obtained from exactly one batch.

8.7.2.3 Station Validation Statistics

Each SOR category is also partitioned into one or more groups, based on the tracking station. The mean values and standard deviations of the unedited and validation-edited residuals are computed for each station included in each category. The station and category validation statistics are identical if the category contains data obtained from only one station.

8.7.3 SOR CALIBRATION STATISTICS

The SOR mean and standard deviation calibration statistics are based on SOR batches and are described in Section 8.7.3.1. Ground transponder calibration statistics, based on the batch calibration statistics, are also computed and are described in Section 8.7.3.2.

8.7.3.1 Batch Calibration Statistics

The following types of data are included in the batch calibration statistics:

- Data that are accepted in the differential correction process
- Data that are edited in the differential correction process
- Data that are edited by user-supplied specification (preedited)

The validation edit status of the data is ignored. The data residuals in each batch are first subjected to a maximum O-C test in which each residual that exceeds a specified value is marked as calibration edited. The mean and standard deviation of the remaining unedited residuals are then computed as in the validation statistics.

Next, residuals in each batch are subjected to an iterative n-sigma calibration edit, as in the category validation statistics, and the mean and standard deviation values of the final sets of unedited and calibration-edited residuals are computed.

Although the maximum O-C value, the number of iterative loops, and the sigma multiplier are the same for both the category validation and batch calibration editing, the batch validation and batch calibration statistics are not the same. These statistics will only be the same if each category contains data from only one batch.

An additional validity indicator is computed whenever batch calibration statistics are computed. The indicator is set when the number of edited points from the batch validation statistics is not equal to the number of edited points from the batch calibration statistics and when

$$|M_e - M_u| > 3\,(S_e + S_u) \tag{8-194}$$

where

M_u = final unedited batch validation residual mean

M_e = final edited batch validation residual mean

S_u = final unedited batch validation residual standard deviation

S_e = final edited batch validation residual standard deviation

8.7.3.2 Ground Transponder Calibration Statistics

Additional calibration statistics are computed for TDRSS ground transponder tracking data. The batch calibration statistics for two-way and hybrid range data taken from each ground transponder user are used to compute the additional statistics, as follows:

$$M_M = \frac{\sum_{i=1}^{n_b} M_{C_i}}{n_b} \tag{8-195}$$

$$M_S = \frac{\sum_{i=1}^{n_b} S_{C_i}}{n_b} \tag{8-196}$$

$$S_M^2 = \frac{\sum_{i=1}^{n_b} M_{C_i}^2}{n_b} - M_M^2 \tag{8-197}$$

$$S_S^2 = \frac{\sum_{i=1}^{n_b} S_{C_i}^2}{n_b} - M_S^2 \tag{8-198}$$

where

M_{C_i} = final unedited batch calibration residual mean from the i^{th} batch

S_{C_i} = final unedited batch calibration standard deviation from the i^{th} batch

M_M = mean of the unedited batch calibration residual mean values

S_M = standard deviation of the unedited batch calibration residual mean values

M_S = mean of the unedited batch calibration residual standard deviations

S_S = standard deviation of the unedited batch calibration residual standard deviations

n_b = number of batches of either two-way or hybrid range data for each ground transponder user

8.7.4 BATCH CALIBRATION NOISE STATISTICS

A noise estimate for the residuals in the batch is computed whenever batch calibration statistics are computed. Both the Variate Difference Noise Analysis (VDNA) and Divided Difference Noise Analysis (DDNA) techniques are used (Reference 18). Data that are

unedited in the calibration statistics or n-sigma edited in the calibration statistics are included in the noise estimate. Due to the manner in which raw nondestruct Doppler and range-rate measurements are constructed during preprocessing, these types of data are treated somewhat differently than other types of data when the noise analysis techniques are applied (Reference 19).

8.7.4.1 VDNA Noise Estimation

The VDNA technique requires that the data be evenly spaced, which might not occur in practice because of frame dropout or the presence of invalid data. Thus, the most frequently occurring time-tag difference in the batch is computed, and those residuals that fall at other times are marked as data-gap edited and are not included in the VDNA noise estimate. The P^{th}-order VDNA noise estimate, σ_{P_v}, is computed as follows:

$$\Delta^0 V_i = \Delta y(t_i) \qquad (i = 1, 2, \ldots, N) \tag{8-199}$$

$$\Delta^P V_i = \Delta^{P-1} V_{i+1} - \Delta^{P-1} V_i \qquad [i = 1, 2, \ldots, (N - P)]\ (P > 0) \tag{8-200}$$

$$\sigma^2_{P_V} = \frac{\sum_{i=1}^{N-P} (\Delta^P V_i)^2}{f_q\,(N - P)} \tag{8-201}$$

where

$\Delta y(t_i)$ = i^{th} unedited residual

$\Delta^P V_i$ = i^{th} variate difference of order P

N = number of unedited residuals available for noise estimation

P = order of the variate differences

q = (P + 1) for nondestruct Doppler and range-rate data for which the majority (more than 50 percent) of the Doppler count intervals are equal to the most frequently occurring time-tag difference; for this case, the resultant $\sigma^2_{P_V}$ is also multiplied by two

= P for all other cases

and

$$f_q = \begin{bmatrix} 2q \\ q \end{bmatrix} = \frac{(2q)!}{q!\,q!} \tag{8-202}$$

For nondestruct range-rate data, the Doppler counter VDNA noise estimate, N_{CNTR}, is computed as

$$N_{CNTR} = M\left(\frac{2F_R}{c}\right) DCI\left(\frac{N_{\dot{R}}}{\sqrt{2}}\right) \tag{8-203}$$

where

F_R = receive frequency (hertz)

c = vacuum speed of light (meters per second)

M = 1000 (if $F_R < 3000$ megahertz)
= 100 (if $F_R \geq 3000$ megahertz)

$N_{\dot{R}}$ = averaged range-rate VDNA noise estimate (computed as in Equation (8-201))

DCI = Doppler count interval (seconds) (average Doppler count interval if it is not constant throughout the batch)

For nondestruct Doppler data, the Doppler counter VDNA noise estimate, N_{CNTR}, is computed as

$$N_{CNTR} = M\left(\frac{N_D}{\sqrt{2}}\right) \tag{8-204}$$

where N_D is the averaged Doppler VDNA noise estimate (computed as in Equation (8-201)).

8.7.4.2 DDNA Noise Estimation

The DDNA noise estimate, σ_{P_D}, is computed as follows:

$$\delta^0 V_i = y_i \qquad (i = 1, 2, \ldots, N) \tag{8-205}$$

$$\delta^P V_i = \frac{\delta^{P-1} V_{i+1} - \delta^{P-1} V_i}{t_{i+P} - t_i} \qquad [i = 1, 2, \ldots, (N - P)] \quad (P > 0) \tag{8-206}$$

$$W_{ij}^P = \frac{1}{\prod_{\substack{k=1 \\ k \neq j}}^{P+1} (t_{i+j+1} - t_{i+k-1})} \tag{8-207}$$

$$\sigma_{P_D}^2 = \frac{1}{N - P} \sum_{i=1}^{N-P} \frac{(\delta^P V_i)^2}{\sum_{j=1}^{P+1} (W_{ij}^P)^2} \tag{8-208}$$

where

t_i = time tag associated with V_i (seconds)

W_{ij}^P = weighting factor for the P^{th}-order divided differences

$\delta^P V_i$ = i^{th} divided difference of order P

For nondestruct range-rate or Doppler data, the DDNA noise estimate is computed only if the Doppler count interval associated with each data point is equal to the corresponding time-tag difference. In this case, the number of residuals (data points) available for noise estimation is incremented by one (i.e., N is set to N + 1), and the formation of the first-order (P = 1) averaged differences is bypassed.

For nondestruct range-rate data, the Doppler counter DDNA noise estimate, N_{CNTR}, is computed as

$$N_{CNTR} = M \frac{2F_R}{c} N_R' \tag{8-209}$$

where N'_R is the intermediate range-rate DDNA noise estimate (computed as in Equation (8-208)).

For nondestruct Doppler data, the Doppler counter DDNA noise estimate, N_{CNTR}, is computed as

$$N_{CNTR} = M N'_D \tag{8-210}$$

where N'_D is the Doppler DDNA noise estimate (computed as in Equation (8-208)).

8.7.4.3 Noise Analysis Editing and Convergence

Prior to formation of the noise estimate, the individual variate or divided differences are subjected to an iterative n-sigma edit. The edit criteria are basically variances to be tested directly against the squares of the differences. These criteria are as described below.

VDNA

1. Initial loop of the initial order:

   a. Unsampled range-rate and Doppler data

$$\left(\frac{3}{2}\,m\right)^2 \left(S_c^2 + M_c^2\right)\left(\frac{f_q}{2}\right) \tag{8-211}$$

   b. General

$$\left(\frac{3}{2}\,m\right)^2 \left(S_c^2 + M_c^2\right) f_q \tag{8-212}$$

2. Initial loop of other orders:

   a. Unsampled range-rate and Doppler data

$$\left(\frac{3}{2}\,m\right)^2 \sigma_{P-1}^2 \left(\frac{f_q}{2}\right) \tag{8-213}$$

   b. General

$$\left(\frac{3}{2}\,m\right)^2 \sigma_{P-1}^2 f_q \tag{8-214}$$

3. Other than the initial loop, all orders:

$$m^2 \sigma^2_{E-1} f_q \tag{8-215}$$

DDNA

1. Initial loop of the initial order:

$$\left(\frac{3}{2} m\right)^2 \left(S_c^2 + M_c^2\right) \tag{8-216}$$

2. Initial loop of other orders:

$$\left(\frac{3}{2} m\right)^2 \sigma^2_{P-1} \tag{8-217}$$

3. Other than the initial loop, all orders:

$$m^2 \sigma^2_{E-1} \tag{8-218}$$

In all of the above equations, the following symbol definitions are made:

m = sigma multiplier for the noise analysis "m-sigma" edit

σ^2_{P-1} = final variance for the P^{th}-order noise estimate computed as in Equation (8-201) (VDNA) or as in Equation (8-208) (DDNA)

σ^2_{E-1} = variance estimate for unedited differences on the $(E-1)^{st}$ edit loop of the same order

S_c = final unedited batch calibration standard deviation

M_c = final unedited batch calibration mean value

Each squared difference that exceeds the applicable edit criterion is marked as edited and is not included in either the variance estimate for that edit loop or the noise estimate for that order. All differences of a particular order are considered unedited prior to the initial edit loop of the order, regardless of the edit status of the differences from the previous order. If the maximum number of edit loops has not been reached and no additional editing has been performed, the iterative edit "m-sigma" loop is terminated.

The noise estimate itself is considered converged at the order level if either

(1)

$$\sigma_{P-2}\,(1 - C) \leq \sigma_{P-1} \leq \sigma_{P-2}\,(1 + C) \tag{8-219a}$$

and

$$\sigma_{P-1}\,(1 - C) \leq \sigma_{P} \leq \sigma_{P-1}\,(1 + C) \tag{8-219b}$$

or

(2)

$$\sigma_{P-2}\,(1 - C) \leq \sigma_{P} \leq \sigma_{P-2}\,(1 + C) \tag{8-220}$$

where

σ_i = i^{th}-order final noise estimate, computed as in Equation (8-201) (VDNA) or as in Equation (8-208) (DDNA)

C = noise estimation convergence criterion (default: C = 0.1)

For nondestruct Doppler or range-rate data, the intermediate noise estimates for Equations (8-201) and (8-208) are used to test for convergence, rather than the Doppler counter noise estimates.

8.8 REFERENCES

1. Schmidt, S. F.: 1966, "The Application of State Space Methods to Navigation Problems," *Advances in Control Systems*, Vol. 3 (C. T. Leondes, editor), Academic Press, New York, New York.

2. Deutsch, R.: 1965, *Estimation Theory*, Prentice-Hall, Englewood Cliffs, New Jersey.

3. Doob, J. L.: 1963, *Stochastic Processes*, John Wiley and Sons, New York, New York.

4. Gelb, A. (editor): 1974, *Applied Optimal Estimation*, The MIT Press, Cambridge, Massachusetts.

5. Escobal, P. R.: 1975, *Methods of Orbit Determination*, John Wiley and Sons, New York, New York.

6. Jazwinski, A. H.: 1970, *Stochastic Processes and Filtering Theory*, Academic Press, New York, New York.

7. Analytic Sciences Corporation: 1971, *A Short Course on Kalman Filter Theory and Application*, Reading, Massachusetts.

8. Kalman, R. E.: 1960, "New Methods and Results in Linear Prediction and Filtering Theory," Symposium on Engineering Applications of Random Function Theory and Probability, Purdue University, West Lafayette, Indiana, November 1960.

9. Andrews, A.: 1968, "A Square Root Formulation of the Kalman Covariance Equations," *AIAA Journal*, Vol. 6, June 1968, pp. 1165-1166.

10. Fitzgerald, R. J.: 1971, "Divergence of the Kalman Filter," *IEEE Transactions on Automatic Control*, Vol. 16, No. 6, December 1971, pp. 736-747.

11. Torroglosa, V.: 1973, *Filtering Theory Applied to Orbit Determination*, Goddard Space Flight Center Report X-582-73-379, December 1973.

12. Ingram, D. S. and Tapley, B. D.: 1974, "Lunar Orbit Determination in the Presence of Unmodeled Accelerations," *Celestial Mechanics*, Vol. 9, pp. 191-211.

13. Tapley, B. D. and Ingram, D. S.: 1973, "Orbit Determination in the Presence of Unmodeled Accelerations," *IEEE Transactions on Automatic Control*, Vol. 18, No. 4, August 1973, pp. 369-373.

14. Tapley, B. D. and Schutz, B. E.: 1974, *Estimation of Unmodeled Forces on a Lunar Satellite*, Department of Aerospace Engineering and Engineering Mechanics, University of Texas, Austin, Texas.

15. Jazwinski, A. H.: 1973, "Adaptive Sequential Estimation with Applications," Fifth IFAC Symposium on Automatic Control in Space, Genoa, Italy, June 1973; work done under NASA contracts NAS 8-26973 and NAS 5-22011.

16. Sage, A. P. and Husa, G.W.: 1969, "Algorithms for Sequential Adaptive Estimation of Prior Statistics," Information and Control Sciences Center, Southern Methodist University, Dallas, Texas; work done under Air Force Contract F44620-68-C-0023.

17. Nakai, Y. and Morse, B.: 1983, *Goddard Trajectory Determination System (GTDS) User's Guide*, Computer Sciences Corporation Report CSC/TM-82/6002UD1, March 1983.

18. Cowan, D.: 1980, *Implementation of Variate Difference Noise Analysis and Divided Difference Noise Analysis in GTDS*, Goddard Space Flight Center Memorandum, From D. Cowan to P. Chambers (GSFC Code 870), August 25, 1980.

19. Cowan, D.: 1981, *Additional Items for Processing Nondestruct Doppler Data Utilizing VDNA and DDNA in GTDS*, Goddard Space Flight Center Memorandum, From D. Cowan to P. Chambers (GSFC Code 870), February 11, 1981.

CHAPTER 9—LAUNCH AND EARLY ORBIT METHODS

The estimator algorithm in GTDS requires an a priori estimate of the spacecraft position and velocity to initiate the iterative estimation process (see Chapter 8). GTDS is part of the Trajectory Computation and Orbital Products System (TCOPS) in the GSFC Flight Dynamics Facility (FDF). The TCOPS launch processor provides the capability to propagate an insertion vector through successive burns to obtain an initial on-orbit vector. However, an accurate estimate is frequently unavailable because of large booster injection errors, maneuver errors, or unknown orbits of tracked satellites. Therefore, GTDS provides the capability to determine a starting value of the position and velocity from a limited number of discrete tracking data samples.

Three techniques are optionally provided to perform this function. They are as follows:

- **Gauss Method and Double R-Iteration Method.** These deterministic methods use three sets of chronologically ordered gimbal angle measurement pairs to solve for the six Cartesian position and velocity components at an epoch time equal to that of the second measurement. The gimbal angle measurement sets need not be from the same tracking station. The central angle (from the Earth's center) subtended by the three sets of angles should be less than 60 degrees for the Gauss Method and less than 360 degrees for the Double R Method. Either X and Y or A and E gimbal angle data from the GRARR, ATSR, USB, or C-band systems; ℓ and m direction cosines from the Minitrack System; or geocentric right ascension, α, and declination, δ, measurements can be used.

- **Range and Angles Method.** This method uses multiple (more than two) sets of simultaneously measured range and gimbal angle data from the GRARR, ATSR, USB, or C-band radar systems. Two-body equations are regressively fitted to the transformed data to yield epoch values of the spacecraft position and velocity.

For TDRS tracking, a separate method based on homotopy continuation techniques is used. This method, which is part of the Preliminary Orbit Determination System (PODS) of TCOPS is documented in Reference 1.

This chapter discusses the powered flight propagation techniques available in the TCOPS launch processor and the early orbit methods available in GTDS.

9.1 LAUNCH AND POWERED FLIGHT PROPAGATION TECHNIQUES

During launch support of an expendable launch vehicle, a vector is selected following the first main engine cutoff (MECO-1) of the launch vehicle and is designated the insertion

vector. This vector is propagated through the following burns of the main engine and the second stage burns to provide the orbit trajectory. Exactly how many burns of the main engine and the second stage depends on the specific vehicle and the mission design. The trajectory from the time of liftoff (main engine ignition) to MECO-1 is provided to TCOPS from outside sources. During the launch, telemetry data from the launch vehicle contain accelerometer data, which are integrated at the launch support site to provide either the thrust components of the spacecraft position and velocity that are used in launch support processing or the position and velocity vectors provided directly as Launch Telemetry Acquisition System (LTAS) vectors.

The propagation of an insertion vector through successive burns when the thrust components are provided requires the following:

- The capability to predict the thrust before the events and the inclusion of this predicted thrust in the force model used to propagate an insertion vector to provide a predicted trajectory. (This capability is available in GTDS and is discussed in Section 4.8.4 of this document.)

- The capability to include thrust information extracted from launch telemetry data in the propagation as the launch telemetry data are received. (This capability is available in the TCOPS launch processor.)

The mathematics for propagation through powered flight using the telemetry data received during launch is presented below.

The following items are given:

$(\bar{r}_0, \bar{v}_0)$ = position and velocity vectors at the initial time, t_0 (insertion vector)

m = mass of the satellite/launch vehicle combination at ignition (or at the last burnout)

A = cross-sectional area of the launch vehicle

T_{LO} = time of liftoff (UTC)

α_g = Greenwich hour angle at T_{LO}

λ = longitude of the launch pad

γ_j = ground elapsed time from T_{LO} for the selected Delta Inertial Guidance System (DIGS) station

$\delta\bar{r}_j$, $\delta\bar{v}_j$ = thrust components in terms of position and velocity changes, respectively, in a geocentric body-fixed coordinate system referenced to the launch pad at time t_j, extracted from the launch telemetry data

M = transformation matrix from the geocentric body-fixed coordinate system to the true of date system

where

$$M = \begin{bmatrix} \cos(a_g + \lambda) & -\sin(a_g + \lambda) & 0 \\ \sin(a_g + \lambda) & \cos(a_g + \lambda) & 0 \\ 0 & 0 & 1 \end{bmatrix} \tag{9-1}$$

The position and velocity at time t_j are computed as follows:

$$\bar{r}_j = \bar{r}'_j + \Delta\bar{r}'_j \tag{9-2}$$

$$\bar{v}_j = \bar{v}'_j + \Delta\bar{v}'_j \tag{9-3}$$

where

$$t_j = \gamma_j + T_{LO} \tag{9-4}$$

The quantities $\bar{r}'_j$ and $\bar{v}'_j$ are the result of integrating from t_{j-1} to t_j considering the effects of forces on the spacecraft other than thrust. The integration to produce $(\bar{r}'_j, \bar{v}'_j)$ is done with a low-order Runge-Kutta integrator, described in Section 6.2.2. The initial conditions are $(\bar{r}_{j-1}, \bar{v}_{j-1})$, the position and velocity vectors computed at the previous step, including thrust effects.

The quantities $\Delta\bar{r}'_j$ and $\Delta\bar{v}'_j$, which are the changes in the position and velocity from t_{j-1} to t_j due to thrust, are computed by rotating $(\delta\bar{r}_j, \delta\bar{v}_j)$ from the geocentric body-fixed coordinate system to the true of date system as

$$\Delta\bar{r}_j = M\,\delta\bar{r}_j \tag{9-5a}$$

$$\Delta\bar{v}_j = M\,\delta\bar{v}_j \tag{9-5b}$$

and computing the following differences:

$$\Delta v_1' = \Delta v_1 \tag{9-6a}$$

$$\Delta r_1' = \Delta r_1 \tag{9-6b}$$

$$\Delta\bar{v}_j' = \Delta\bar{v}_j - \Delta\bar{v}_{j-1} \qquad (j > 1) \tag{9-7a}$$

$$\Delta\bar{r}_j' = \Delta\bar{v}_j'\left(\frac{t_j - t_{j-1}}{2}\right) \qquad (j > 1) \tag{9-7b}$$

If there are no thrust data at t_j, then $\Delta\bar{r}_j$ and $\Delta\bar{v}_j$ equal zero.

When LTAS vectors are used, the only processing necessary is the conversion from the geocentric body-fixed coordinate system to the true of date inertial system, using the matrix M given in Equation (9-1).

9.2 ANGLES-ONLY METHODS

Both the Gauss Method and the Double R-Iteration Method use three sets of chronologically ordered gimbal angle measurements from up to three separate tracking stations to determine the Cartesian components of position and velocity. The angle data set can be distributed over an orbital arc of less than 60 degrees in mean anomaly for the Gauss Method and up to 360 degrees in mean anomaly for the Double R-Iteration Method. The epoch for the position and velocity corresponds to the time of the second measurement set. The methods are deterministic since the six measurement components yield the six position and velocity components. Additional descriptions of these methods are presented in Reference 2.

9.2.1 TRANSFORMATION OF TOPOCENTRIC GIMBAL ANGLES TO INERTIAL COORDINATES

All gimbal angles are initially transformed to topocentric station-centered azimuth, A, and elevation, E. The X_{30} and Y_{30} angles corresponding to the GRARR and USB 30-foot antennas are transformed by

$$\sin E = \cos X_{30} \cos Y_{30} \qquad \left(0 \le E \le \frac{\pi}{2}\right) \tag{9-8a}$$

$$\cos E = \sqrt{1 - \sin^2 E} \qquad \left(0 \le E \le \frac{\pi}{2}\right) \tag{9-8b}$$

and

$$\sin A = \frac{\sin X_{30} \cos Y_{30}}{\cos E} \qquad (0 \le A \le 2\pi) \tag{9-9a}$$

$$\cos A = \frac{\sin Y_{30}}{\cos E} \qquad (0 \le A \le 2\pi) \tag{9-9b}$$

The X_{85} and Y_{85} angles corresponding to the USB 85-foot antennas are transformed by

$$\sin E = \cos Y_{85} \cos X_{85} \qquad \left(0 \le E \le \frac{\pi}{2}\right) \tag{9-10a}$$

$$\cos E = \sqrt{1 - \sin^2 E} \qquad \left(0 \le E \le \frac{\pi}{2}\right) \tag{9-10b}$$

$$\sin A = \frac{\sin Y_{85}}{\cos E} \qquad (0 \le A \le 2\pi) \tag{9-11a}$$

$$\cos A = \frac{-\cos Y_{85} \sin X_{85}}{\cos E} \qquad (0 \le A \le 2\pi) \tag{9-11b}$$

The direction cosines, ℓ and m, are transformed by

$$\cos E = \sqrt{\ell^2 + m^2} \qquad \left(0 \leq E \leq \frac{\pi}{2}\right) \tag{9-12}$$

and

$$\sin A = \frac{\ell}{\cos E} \qquad (0 \leq E \leq 2\pi) \tag{9-13a}$$

$$\cos A = \frac{m}{\cos E} \qquad (0 \leq E \leq 2\pi) \tag{9-13b}$$

The C-band radar gimbal angles are directly measured as A and E, and the resulting angle sets are denoted by (t, A, E). The altitude above the reference Earth ellipsoid, the geodetic latitude, and the longitude of the tracking station measuring the angle set are denoted by (h_s, ϕ_s, λ_s). The unit vector directed toward the spacecraft can be written in topocentric local tangent coordinates as follows:

$$\hat{L}_{ll} = \begin{bmatrix} \cos E \sin A \\ \cos E \cos A \\ \sin E \end{bmatrix} \tag{9-14}$$

The tracking station coordinates, expressed in body-fixed axes, are presented in Section 3.3.7 as

$$\bar{r}_{s_b} = \begin{bmatrix} (N_s + h_s) \cos \phi_s \cos \lambda_s \\ (N_s + h_s) \cos \phi_s \sin \lambda_s \\ [N_s + h_s - (2f - f^2) N_s] \sin \phi_s \end{bmatrix} \tag{9-15}$$

where

$$N_s = \frac{R_e}{\sqrt{1 - (2f - f^2) \sin^2 \phi_s}} \tag{9-16}$$

and

R_e = Earth's equatorial radius

f = Earth's flattening coefficient

Both the $\hat{L}_{lt}$ and $\bar{r}_{s_b}$ vectors are transformed to a common inertial Cartesian axes system. The transformations, presented in Sections 3.3.1, 3.3.2, and 3.3.7, follow. The matrix M_{lt}^T from Section 3.3.7 transforms from the topocentric local tangent system to the body-fixed system and is a function of the station's latitude and longitude, i.e.,

$$\hat{L}_b = M_{lt}^T \hat{L}_{lt} \tag{9-17}$$

where

$$M_{lt} = \begin{bmatrix} -\sin \lambda_s & \cos \lambda_s & 0 \\ -\sin \phi_s \cos \lambda_s & -\sin \phi_s \sin \lambda_s & \cos \phi_s \\ \cos \phi_s \cos \lambda_s & \cos \phi_s \sin \lambda_s & \sin \phi_s \end{bmatrix} \tag{9-18}$$

The matrix B^T, from Section 3.3.2.3, transforms from the body-fixed system to the true of date system and is normally a function of the Greenwich sidereal time and polar motion. Polar motion is neglected for early orbit applications (from considerations of precision). The transformation is as follows:

$$\hat{L}_T = \begin{bmatrix} \cos \delta_t \cos \alpha_t \\ \cos \delta_t \sin \alpha_t \\ \sin \delta_t \end{bmatrix} = B^T(\alpha_g) \hat{L}_b \tag{9-19}$$

and

$$\bar{r}_s = B^T(a_g)\,\bar{r}_{s_b} \tag{9-20}$$

where

$$B^T = \begin{bmatrix} \cos a_g & -\sin a_g & 0 \\ \sin a_g & \cos a_g & 0 \\ 0 & 0 & 1 \end{bmatrix} \tag{9-21}$$

and

a_t = topocentric right ascension of the spacecraft from the true-of-date equinox

δ_t = topocentric declination of the spacecraft from the true-of-date equator

a_g = Greenwich sidereal time at measurement time t (see Equation (3-38))

Equations (9-17) and (9-19) can be combined resulting in a single transformation matrix M_{lt} identical to that in Equation (9-18), with λ_s replaced by $(\lambda_s + a_g)$, the longitude measured from the true vernal equinox. The unit vector $\hat{L}_T$ in Equation (9-19) can be solved for the topocentric right ascension, a_t, and declination, δ_t. Should measurements of the topocentric right ascension and declination be available, they can be used to replace the topocentric gimbal angles and determine $\hat{L}_T$ directly from Equation (9-19). The matrix C^T from Section 3.3.1.3 transforms from the true of date system to the mean of B1950.0 or J2000.0 system and accounts for nutation and precession. The resulting transformation is

$$\hat{L} = C^T \hat{L}_T \tag{9-22a}$$

$$\bar{R}_s = C^T \bar{r}_s \tag{9-22b}$$

where C^T is the product of the precession transformation $A(\zeta_0, \theta_p, \xi_p)$ and the nutation transformation $N(\delta\epsilon, \delta\psi)$, as follows:

$$C^T = (N\,A)^T \tag{9-23}$$

The elements of the summation matrix C^T are obtained from a Solar/Lunar/Planetary (SLP) Ephemeris File in GTDS.

Combining the preceding transformations yields

$$\hat{L} = (M_{li}\,B\,C)^T\,\hat{L}_{li} \tag{9-24a}$$

and

$$\bar{R}_s = (B\,C)^T\,\bar{r}_{s_b} \tag{9-24b}$$

Equations (9-24) present the transformations necessary when the computations are performed in the mean of B1950.0 or J2000.0 system. Specifying C = I permits the vectors to be transformed to the true of reference date system.

In the following sections, three sets of gimbal angles, obtained at times t_1, t_2, and t_3, are available from either the same or different stations. Station vectors and unit vectors directed towards the spacecraft, $(\bar{R}_{s_1}, \hat{L}_1)$, $(\bar{R}_{s_2}, \hat{L}_2)$, and $(\bar{R}_{s_3}, \hat{L}_3)$, can be determined from Equations (9-14) and (9-24) for each gimbal angle set.

9.2.2 GAUSS METHOD

The Gauss Method utilizes the geometric properties of the station positions and station-to-spacecraft unit vectors, in conjunction with an approximation of the orbital dynamics, to determine an estimate of the spacecraft's position at time t_2. The orbital dynamics are approximated by the low-order terms of the f and g series, therefore limiting the orbital arc of the angular measurements to be within approximately 60 degrees in mean anomaly. Subsequently, the accuracy of the position vector is iteratively improved, and the velocity vector is determined by the method of Gibbs. This method utilizes the approximately known position vectors at the three measurement times to determine a velocity vector at time t_2. Knowing the velocity allows one higher order term to be included in the f and g series and thereby improves the spacecraft position determination.

The geocentric inertial position vector, $\bar{R}_i$, can be determined from the known vectors, $\hat{L}_i$ and $\bar{R}_{s_i}$, and the unknown slant range, ρ_i, from the station to the spacecraft as follows (see Figure 9-1):

$$\bar{R}_i = \bar{R}_{s_i} + \rho_i \hat{L}_i \quad (i = 1, 2, 3) \tag{9-25}$$

The three vectors $\bar{R}_1$, $\bar{R}_2$, and $\bar{R}_3$ are coplanar since they all lie in the same orbit plane. Therefore, $\bar{R}_2$ can be written as a linear combination of $\bar{R}_1$ and $\bar{R}_3$ as

$$C_1 \bar{R}_1 + C_2 \bar{R}_2 + C_3 \bar{R}_3 = 0 \tag{9-26}$$

where

$$C_2 = -1 \tag{9-27}$$

Substituting Equation (9-25) into Equation (9-26) yields

$$C_1 \rho_1 \hat{L}_1 + C_2 \rho_2 \hat{L}_2 + C_3 \rho_3 \hat{L}_3 = -(C_1 \bar{R}_{s_1} + C_2 \bar{R}_{s_2} + C_3 \bar{R}_{s_3}) \tag{9-28}$$

or, in matrix form,

$$L \begin{bmatrix} C_1 \rho_1 \\ C_2 \rho_2 \\ C_3 \rho_3 \end{bmatrix} = -R_s \begin{bmatrix} C_1 \\ C_2 \\ C_3 \end{bmatrix} \tag{9-29}$$

where

$$L = \left[\hat{L}_1 \mid \hat{L}_2 \mid \hat{L}_3\right] \tag{9-30a}$$

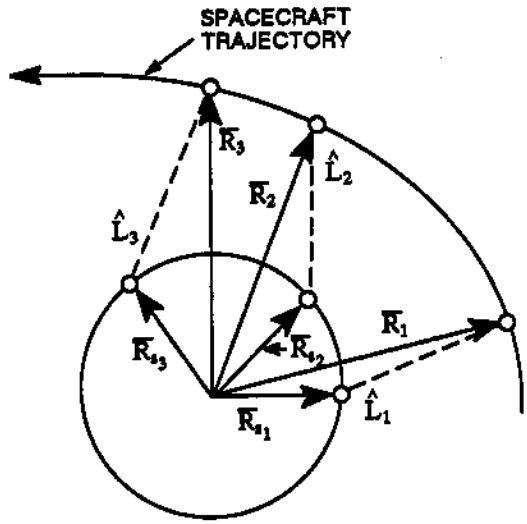

Figure 9-1. Position Vector Geometry

and

$$R_s = \left[\bar{R}_{s_1} \mid \bar{R}_{s_2} \mid \bar{R}_{s_3} \right] \tag{9-30b}$$

Premultiplying Equation (9-29) by L^{-1} yields

$$\begin{bmatrix} C_1 \varrho_1 \\ C_2 \varrho_2 \\ C_3 \varrho_3 \end{bmatrix} = - D \begin{bmatrix} C_1 \\ C_2 \\ C_3 \end{bmatrix} \tag{9-31}$$

where

$$D = L^{-1} R_s \tag{9-32}$$

The preceding three scalar equations involve the five unknown variables C_1, C_2, ϱ_1, ϱ_2, and ϱ_3. Additional conditions must be imposed to determine the slant ranges, ϱ_1, ϱ_2, or ϱ_3. Knowing any one of these ranges, a geocentric position vector, $\bar{R}_1$, $\bar{R}_2$, or $\bar{R}_3$, can be determined from Equation (9-25).

The cross product of $\overline{R}_1$ and $\overline{R}_3$ with Equation (9-26) results in the following equations:

$$\overline{R}_1 \times \overline{R}_2 = C_3 \overline{R}_1 \times \overline{R}_3 \tag{9-33a}$$

$$\overline{R}_3 \times \overline{R}_2 = C_1 \overline{R}_3 \times \overline{R}_1 \tag{9-33b}$$

Forming a dot product between $\hat{k}$, the unit vector normal to the orbital plane in the direction of the angular momentum, and the expressions given in Equations (9-33) yields

$$C_3 = \frac{\hat{k} \cdot (\overline{R}_1 \times \overline{R}_2)}{\hat{k} \cdot (\overline{R}_1 \times \overline{R}_3)} \tag{9-34a}$$

$$C_1 = \frac{\hat{k} \cdot (\overline{R}_2 \times \overline{R}_3)}{\hat{k} \cdot (\overline{R}_1 \times \overline{R}_3)} \tag{9-34b}$$

The position vectors can next be expressed in terms of the f and g series representation for two-body motion (Reference 3). The series is expanded about t_2, the time of the second measurement, as follows:

$$\overline{R}_i = f_i \overline{R}_2 + g_i \dot{\overline{R}}_2 \tag{9-35}$$

where

$$f_i = 1 - \frac{1}{2} u_2 \tau_i^2 - \frac{1}{6} \dot{u}_2 \tau_i^3 - \frac{1}{24} (\ddot{u}_2 - u_2^2) \tau_i^4 - \frac{1}{120} (\dddot{u}_2 - 4u_2 \dot{u}_2) \tau_i^5 - \cdots \tag{9-36a}$$

$$g_i = \tau_i - \frac{1}{6} u_2 \tau_i^3 - \frac{1}{12} \dot{u}_2 \tau_i^4 - \frac{1}{120} (3\ddot{u}_2 - u_2^2) \tau_i^5 - \cdots \tag{9-36b}$$

and

$$\tau_i = t_i - t_2 \tag{9-37a}$$

$$u_2 = \frac{\mu}{R_2^3} \tag{9-37b}$$

where

μ = gravitational parameter for the Earth

Substituting $\overline{R}_1$ and $\overline{R}_3$ from Equation (9-35) into Equations (9-34) yields

$$C_1 = \frac{g_3}{f_1 g_3 - f_3 g_1} \tag{9-38a}$$

$$C_3 = \frac{-g_1}{f_1 g_3 - f_3 g_1} \tag{9-38b}$$

Approximating f_1, f_3, g_1, and g_3 by

$$f_i = 1 - \frac{1}{2} u_2 \tau_i^2 + 0(\tau_i^3) \qquad (i = 1, 2, 3) \tag{9-39a}$$

$$g_i = \tau_i - \frac{1}{6} u_2 \tau_i^3 + 0(\tau_i^4) \qquad (i = 1, 2, 3) \tag{9-39b}$$

Equations (9-38) become

$$C_1 = a_1 + b_1 u_2 \tag{9-40a}$$

$$C_3 = a_3 + b_3 u_2 \tag{9-40b}$$

where

$$a_1 = \frac{\tau_3}{\tau_3 - \tau_1} \tag{9-41a}$$

$$a_3 = -\frac{\tau_1}{\tau_3 - \tau_1} \tag{9-41b}$$

$$b_1 = \frac{\tau_3}{6(\tau_3 - \tau_1)} \left[(\tau_3 - \tau_1)^2 - \tau_3^2\right] \tag{9-41c}$$

$$b_3 = -\frac{\tau_1}{6(\tau_3 - \tau_1)} \left[(\tau_3 - \tau_1)^2 - \tau_1^2\right] \tag{9-41d}$$

Substituting Equations (9-40) into Equation (9-31) gives

$$\begin{bmatrix} (a_1 + b_1 u_2)\,\varrho_1 \\ -\varrho_2 \\ (a_3 + b_3 u_2)\,\varrho_3 \end{bmatrix} = -D \left\{ \begin{bmatrix} a_1 \\ -1 \\ a_3 \end{bmatrix} + \begin{bmatrix} b_1 \\ 0 \\ b_3 \end{bmatrix} u_2 \right\} \tag{9-42}$$

The preceding three scalar equations involve the four unknown variables ϱ_1, ϱ_2, ϱ_3, and u_2.

Dotting Equation (9-25) with itself (for i = 2) yields

$$R_2^2 = \varrho_2^2 + \varrho_2 C_\psi + R_{s_2}^2 \tag{9-43}$$

where

$$C_\psi = 2\hat{L}_2 \cdot \bar{R}_{s_2} \tag{9-44}$$

is known. The second scalar equation of Equation (9-42) is

$$\varrho_2 = d_1^* + d_2^* \frac{\mu}{R_2^3} \tag{9-45}$$

where

$$d_1^* = d_{21} a_1 - d_{22} + d_{23} a_3 \tag{9-46a}$$

$$d_2^* = d_{21} b_1 + d_{23} b_3 \tag{9-46b}$$

and the matrix D contains the elements (d_{ij}).

Substituting Equation (9-45) into (9-43) gives

$$R_2^2 = \left(d_1^* + d_2^* \frac{\mu}{R_2^3}\right)^2 + \left(d_1^* + d_2^* \frac{\mu}{R_2^3}\right) C_\psi + R_{s_2}^2 \tag{9-47}$$

or

$$R_2^8 - [(d_1^*)^2 + d_1^* C_\psi + R_{s_2}^2] R_2^6 - \mu (d_2^* C_\psi + 2 d_1^* d_2^*) R_2^3 - \mu^2 (d_2^*)^2 = 0 \tag{9-48}$$

Solving the preceding equation for its real positive root yields R_2, which, from Equation (9-37b), determines u_2. Equation (9-42) can then be solved for ϱ_1, ϱ_2, and ϱ_3; and, finally, Equation (9-25) can be solved for $\bar{R}_1$, $\bar{R}_2$, and $\bar{R}_3$. This sequence of computations is summarized in Figure 9-2. The resulting position vectors are only approximately correct because of the truncation of the f and g series to obtain Equations (9-39).

The accuracy of the position can be improved and the velocity vector computed by the method of Gibbs (Reference 2). This method utilizes the three approximately known position vectors $\bar{R}_1$, $\bar{R}_2$, and $\bar{R}_3$ to determine the velocity, $\bar{R}_2$. This allows an additional term to be retained in the f and g series.

The position vectors $\bar{R}_1$ and $\bar{R}_3$ can be obtained from a Taylor series expansion about $\bar{R}_2$ as follows:

$$\bar{R}_1 = \bar{R}_2 + \dot{\bar{R}}_2 \tau_1 + \ddot{\bar{R}}_2 \frac{\tau_1^2}{2} + \dddot{\bar{R}}_2 \frac{\tau_2^3}{6} \tag{9-49}$$

The vector differences $(\bar{R}_1 - \bar{R}_2)$ and $(\bar{R}_3 - \bar{R}_2)$ can be obtained from Equation (9-49). Multiplying $(\bar{R}_1 - \bar{R}_2)$ by $-\tau_3^2$ and adding to $(\bar{R}_3 - \bar{R}_2)$ multiplied by τ_1^2 yields

$$\begin{aligned} &-\tau_3^2 \bar{R}_1 + (\tau_3^2 - \tau_1^2) \bar{R}_2 + \tau_2^2 \bar{R}_3 \\ &\quad = -\tau_1 \tau_2 \tau_{13} \left[\dot{\bar{R}}_2 - \tau_2 \tau_3 \frac{\ddot{\bar{R}}_2}{6} - \tau_1 \tau_3 (\tau_3 + \tau_1) \frac{\bar{R}_2^{(IV)}}{24} + \cdots\right] \end{aligned} \tag{9-50}$$

where

$$\tau_{13} = \tau_3 - \tau_1 \tag{9-51}$$

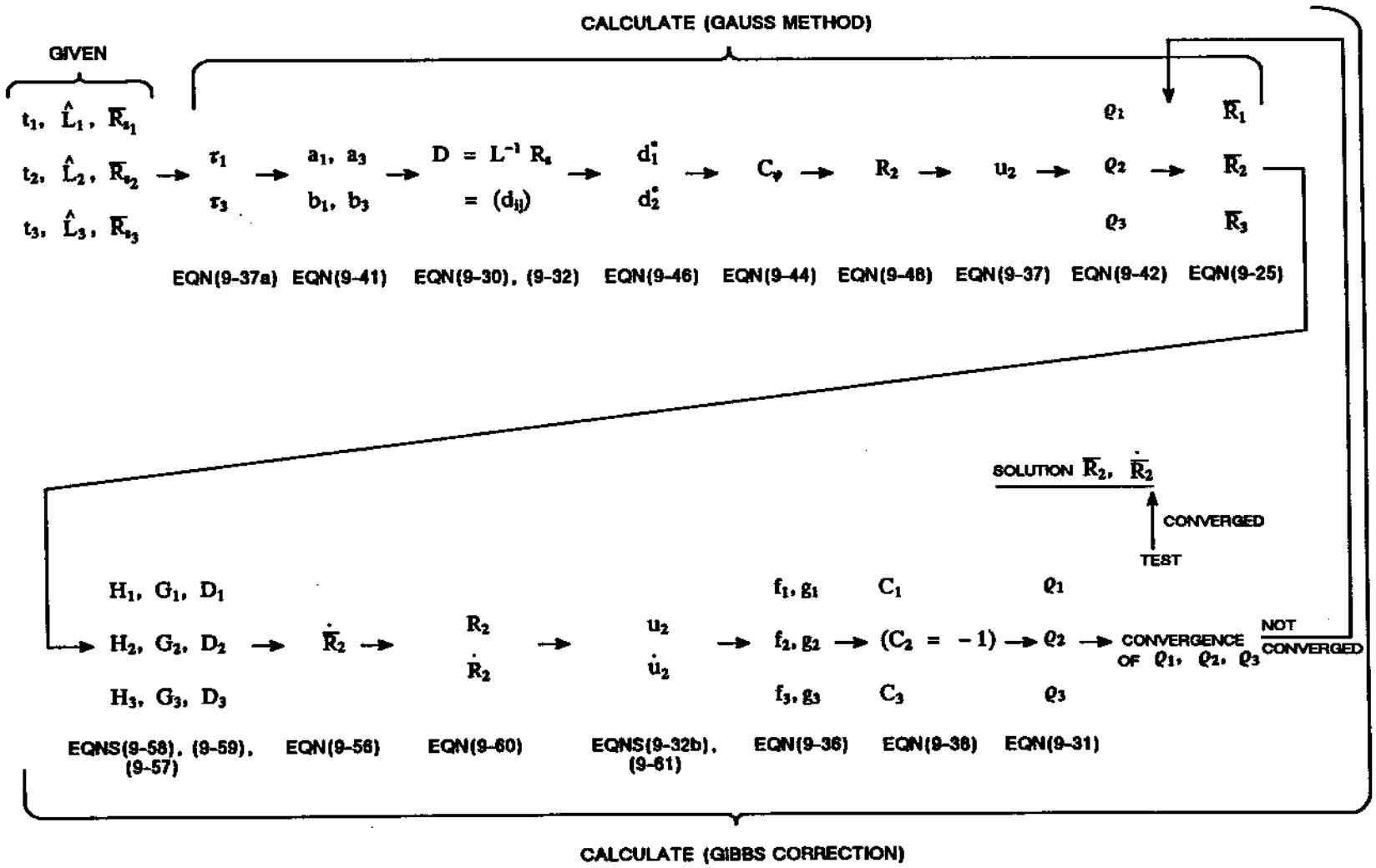

Figure 9-2. Gauss Method Computational Sequence

Differentiating twice gives

$$-\tau_3^2\,\ddot{\bar{R}}_1 + (\tau_3^2 - \tau_1^2)\,\ddot{\bar{R}}_2 + \tau_1^2\,\ddot{\bar{R}}_3 = -\tau_1\,\tau_3\,\tau_{13}\,\dddot{\bar{R}}_2 + 0[\bar{R}_2^{(IV)}] \tag{9-52}$$

Multiplying $(\bar{R}_1 - \bar{R}_2)$ by τ_3 and $(\bar{R}_3 - \bar{R}_2)$ by $-\tau_1$, adding the results, and differentiating twice yields

$$\tau_3\,\ddot{\bar{R}}_1 - \tau_{13}\,\ddot{\bar{R}}_2 - \tau_1\,\ddot{\bar{R}}_3 = -\tau_1\,\tau_3\,\tau_{13}\,\frac{\bar{R}_2^{(IV)}}{2} + 0[\bar{R}_2^{(IV)}] \tag{9-53}$$

Solving Equations (9-52) and (9-53) for $\ddot{\bar{R}}_2$ and $\bar{R}_2^{(IV)}$ and substituting them into Equation (9-50) gives

$$\begin{aligned} &-\tau_3^2\,\bar{R}_1 + (\tau_3^2 - \tau_1^2)\,\bar{R}_2 + \tau_1^2\,\bar{R}_3 \\ &\quad = -\tau_1\,\tau_2\,\tau_{13}\left[\dot{\bar{R}}_2 - \tau_3\,\frac{\dddot{\bar{R}}_1}{12} + (\tau_3 - \tau_1)\,\frac{\dddot{\bar{R}}_2}{12} - \tau_1\,\frac{\dddot{\bar{R}}_3}{12}\right] \end{aligned} \tag{9-54}$$

Substituting the inverse-square law

$$\ddot{\bar{R}}_i = -\mu\,\frac{\bar{R}_i}{R_i^3} \qquad (i = 1, 2, 3) \tag{9-55}$$

into Equation (9-54) and rearranging terms yields

$$\dot{\bar{R}}_2 = -D_1\,\bar{R}_1 + D_2\,\bar{R}_2 + D_3\,\bar{R}_3 \tag{9-56}$$

where

$$D_i = G_i + \frac{H_i}{R_i^3} \qquad (i = 1, 2, 3) \tag{9-57}$$

with

$$H_1 = \frac{\mu\,\tau_3}{12} \tag{9-58a}$$

$$H_3 = -\frac{\mu \tau_1}{12} \tag{9-58b}$$

$$H_2 = H_1 - H_3 \tag{9-58c}$$

$$G_1 = -\frac{\tau_3}{\tau_1 \tau_{13}} \tag{9-59a}$$

$$G_3 = -\frac{\tau_1}{\tau_3 \tau_{13}} \tag{9-59b}$$

$$G_2 = G_1 - G_3 \tag{9-59c}$$

Knowing $\bar{R}_2$ and $\dot{\bar{R}}_2$ from Equations (9-48) and (9-56), R_2 and its time derivative $\dot{R}_2$ are obtained from

$$R_2 = \sqrt{\bar{R}_2 \cdot \bar{R}_2} \tag{9-60a}$$

and

$$\dot{R}_2 = \frac{\bar{R}_2 \cdot \dot{\bar{R}}_2}{R_2} \tag{9-60b}$$

Then u_2 can be determined from Equation (9-37b), and $\dot{u}_2$ can be determined as follows:

$$\dot{u}_2 = -\frac{3\mu}{R_2^2} \dot{R}_2 \tag{9-61}$$

Knowing $\dot{u}_2$ from the preceding equation permits one higher order term to be included in the f and g series in Equations (9-36). An improved determination of $\bar{R}_2$ is thereby obtained by iteratively solving Equations (9-36) for f_i and g_i (including the higher order term); Equations (9-38) for C_1 and C_3; and Equation (9-31) for ϱ_1, ϱ_2, and ϱ_3. After converged values of ϱ_1, ϱ_2, and ϱ_3 are obtained, Equation (9-25) is solved for $\bar{R}_2$ and Equation (9-56) is solved for $\dot{\bar{R}}_2$. The computation sequence is shown schematically in Figure 9-2.

9.2.3 DOUBLE R-ITERATION METHOD

The Double R-Iteration method requires an initial guess of the magnitudes R_1 and R_2. This guess is obtained using the preliminary orbit search technique discussed in Section 9.2.3.1. Then the geometric relations of the three station positions and station-to-spacecraft unit vectors are used in conjunction with the orbital dynamics to determine the time intervals τ_1' (between the first and second measurements) and τ_3' (between the third and second measurements). A standard Newton-Raphson successive approximation scheme is then used to correct R_1 and R_2 to match τ_1' and τ_3' to the known intervals τ_1 and τ_3. These calculations are discussed in Section 9.2.3.2. The computed orbit accuracy determination is described in Section 9.2.3.3, and initiation of the differential correction process is described in Section 9.2.3.4.

The Double R-Iteration method can be used when the angle data are spread out over a considerable arc in eccentric anomaly, whereas the Gauss method is unreliable and may not converge over large arcs. Conversely, when the measurement arc is short, the Double R-Iteration method is not as successful as the Gauss method.

9.2.3.1 Preliminary Orbit Search

During the preliminary orbit search, initial estimates of the spacecraft radius vector magnitudes at the times of the first two measurements (t_1 and t_2) are determined, subject to the constraint that these radius magnitudes be consistent with a trajectory that does not impact the Earth. To accomplish this, an initial estimate of the spacecraft altitude, h_2, at time t_2 is needed. From this initial estimate, potential values of the spacecraft radii, R_1 and R_2, at times t_1 and t_2 are assigned using the cone-masking technique (see Appendix B, Section B.1, of Reference 4 for a discussion of this technique and derivations of the equations used). These R_1 and R_2 estimates are refined until a pair is found that is likely to produce a valid final state vector. These refined values of R_1 and R_2 are then used in the differential correction process, which is discussed later.

The number of such (R_1 ; R_2) pairs so checked is determined by the search level. Each such level determines a specific region in the (R_1 , R_2) space whose perimeter is searched for a good trajectory to match the data.

9.2.3.1.1 Algorithmic Estimation of Upper and Lower Bounds on Spacecraft Heights

For a given search level, L, the upper and lower bounds for R_1 are set, based on the cone-masking technique using the following procedure. Given an initial height estimate, h_2, at time t_2, two possible values of R_2 are tried, i.e.,

$$R_{2+} = R_{\oplus_2} + h_2 K^{+L} \qquad (9\text{-}62a)$$

$$R_{2-} = R_{s_2} + h_2 K^{-L} \tag{9-62b}$$

where R_{s_2} is the magnitude of the station vector $\bar{R}_{s_2}$ and the default value of K is 1.25. For each such value of R_2, the resulting slant range, ϱ_2, and position vector, $\bar{R}_2$, are found from

$$\varrho_2 = \frac{1}{2}\left[-C_{\psi_2} + \sqrt{C_{\psi_2}^2 - 4(R_{s_2}^2 - R_2^2)}\right] \tag{9-63}$$

and

$$\bar{R}_2 = \varrho_2 \hat{L}_2 + \bar{R}_{s_2} \tag{9-64}$$

where

$$C_{\psi_2} = 2\hat{L}_2 \cdot \bar{R}_{s_2} \tag{9-65}$$

Initial estimates for the upper and lower bounds on R_1 are then assigned as

$$R_{1min} = R_{s_1} \tag{9-66a}$$

$$R_{1max} = R_{1up} \tag{9-66b}$$

where R_{1up} is equal to 10^6 kilometers.

Using the following definitions,

$$\beta = \cos^{-1}\left(\frac{R_{s_2}}{R_2}\right) \tag{9-67a}$$

$$\bar{a} = \frac{\bar{R}_2 \cdot \bar{R}_2}{\hat{L}_1 \cdot \bar{R}_2} \tag{9-67b}$$

$$\bar{b} = \frac{\bar{R}_2 \cdot (\bar{R}_2 + \bar{R}_{s_1})}{\hat{L}_1 \cdot \bar{R}_2} \tag{9-67c}$$

$$\bar{a} = \bar{a}\ \hat{L}_1 - \bar{R}_2 \tag{9-67d}$$

$$\bar{b} = \bar{R}_{s_1} + \bar{b}\ \hat{L}_1 - \bar{R}_2 \tag{9-67e}$$

$$d = \bar{a} \cdot \bar{a} - \left(\frac{R_2}{\tan \beta}\right)^2 \tag{9-67f}$$

the quantity Δ can be calculated by

$$\Delta = \bar{a} \cdot \bar{b} - d\,(\bar{b} \cdot \bar{b}) \tag{9-68}$$

If Δ is negative, R_1 can be calculated directly using Equation (9-74) below. Otherwise, the following computations are made:

$$c_1 = -\frac{1}{d}(\bar{a} \cdot \bar{b} - \sqrt{\Delta}) \tag{9-69a}$$

$$c_2 = -\frac{1}{d}(\bar{a} \cdot \bar{b} + \sqrt{\Delta}) \tag{9-69b}$$

$$c_{min} = \cos^2 \beta - 1 \tag{9-69c}$$

For those values of c_j greater than c_{min} (for j = 1 and 2), better values of R_{1min} and R_{1max} can be determined as follows.

If $c_j < 0$, then

$$\varrho_{1min} = \bar{a}\ c_j + \bar{b} \tag{9-70}$$

If $\varrho_{1min} > 0$, then

$$\overline{R}_{1min} = \varrho_{1min} \hat{L}_1 + \overline{R}_{s_1} \tag{9-71a}$$

$$R_{1min} = |\overline{R}_{1min}| \tag{9-71b}$$

If $c_j \geq 0$, then

$$\varrho_{1max} = \bar{a}\, c_j + \bar{b} \tag{9-72}$$

If $\varrho_{1max} \geq 0$, then

$$\overline{R}_{1max} = \varrho_{1max} \hat{L}_1 + \overline{R}_{s_1} \tag{9-73a}$$

$$R_{1max} = |\overline{R}_{1max}| \tag{9-73b}$$

and no upper bound on R_1 has been found for the associated value of R_2 and L.

Next, a value is assigned to R_1 for the current search level, L, and value of R_2, as follows.

If $R_{1min} < R_{s_1}$ and if $R_{1max} > R_{1up}$, then

$$R_1'(L, R_2) = r_{10} \tag{9-74}$$

where r_{10} is equal to the equatorial radius of the Earth, R_e, plus 1000 kilometers (by default), and

$$R_{1u}(L, R_2) = r_{10} - R_{1min} \tag{9-75a}$$

$$R_{1\ell}(L, R_2) = R_{1up} \tag{9-75b}$$

No valid upper and lower bounds have been found.

Otherwise,

$$R_{1mid} = R_{1min} + (R_2 - R_{1min})\left(\frac{r_{10} - R_e}{r_{20} - R_e}\right) \tag{9-76}$$

where r_{20} is equal to r_{10} by default.

If $R_{1mid} > R_{1max}$, then $R_{1mid} = R_2$. Finally,

$$R_1'(L, R_2) = R_{1mid} \tag{9-77a}$$

$$R_{1u}(L, R_2) = R_{1max} - R_{1mid} \tag{9-77b}$$

$$R_{1l}(L, R_2) = R_{1mid} - R_{1min} \tag{9-77c}$$

If $R_{1max} > R_{1up}$, then

$$R_{1u}(L, R_2) = R_{1mid} - R_{1min} \tag{9-78}$$

In this way, upper and lower limits on R_1 are set for each of the two *assumed* values of R_2.

9.2.3.1.2 Preliminary Orbit Search for a Given Level

Upper and lower bounds for R_1 have been set based on the cone-masking technique and on the two trial values of R_2 computed in Equations (9-62). A search is then undertaken to identify values of R_1 and R_2 within the current search level that give the best agreement with the input measurements.

Within the current search level, L, four times L (4L) trial pairs (R_1, R_2) are computed, and an attempt is made to fit an elliptical orbit through each pair. Each (R_1, R_2) pair is determined by selecting values for two integer exponents (E_1, E_2) in the following manner (see Figure 9-3). For the first search level (L = 0), $E_1 = E_2 = 0$ (i.e., the origin) is used. For L = 1, integer exponents are chosen based on the coordinate values of the filled dots on the innermost diamond in Figure 9-3. For L = 2, they are chosen from the

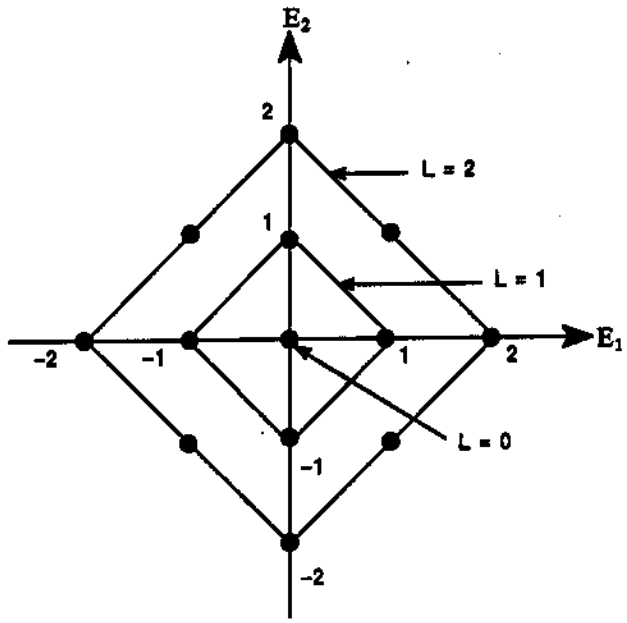

Figure 9-3. Pattern Used in Determining Exponents for the First Three Search Levels (L)

coordinate value of the filled dots on the next diamond, and so forth for each level. The values of E_1 and E_2 for the first three levels are listed in Table 9-1.

For a given value of E_2, R_2 is computed using

$$R_2 = R_{s_2} + h_2 K^{E_2} \tag{9-79}$$

which corresponds to one of the R_2 values found in Equation (9-62). The corresponding value of R_1 is found based on R_2, L, R_{1u}, and $R_{1\ell}$, as follows. First,

$$J = \max\left(\frac{5}{6}, \frac{1}{K}\right) \tag{9-80}$$

where K is the value in Equations (9-62). If $E_1 > 0$ and if an upper bound for R_1 was found previously, then

$$R_1 = R_1'(L, R_2) + R_{1u}(L, R_2)\,(1 - J^{E_1}) \tag{9-81}$$

Table 9-1. Values of E_1 and E_2 for the First Three Search Levels

SEARCH LEVEL (L)	E_1	E_2
0	0	0
1	1	0
	0	1
	-1	0
	0	-1
2	2	0
	1	1
	0	2
	-1	1
	-2	0
	-1	-1
	0	-2
	1	-1

If $E_1 > 0$ and if no upper bound for R_1 was found, then

$$R_1 = R_1'(L, R_2) + R_{1u}(L, R_2)\, K^{-E_1} \tag{9-82}$$

If $E_1 < 0$ and if no upper or lower bound for R_1 was found, then

$$R_1 = R_1'(L, R_2) - R_{1\ell}(L, R_2)\,(1 - J^{-E_1}) \tag{9-83}$$

If $E_1 < 0$ and if valid upper and lower bounds for R_1 were found, then

$$R_1 = R_1'(L, R_2) - R_{1\ell}(L, R_2)\,(1 - K^{-E_1}) \tag{9-84}$$

If the current search level is the first level, the initial orbital parameters and accuracy, Q_0, are determined as in Sections 9.2.3.2 and 9.2.3.3 using the initial estimates of R_1

and R_2 (r_{10} and r_{20}, respectively). The orbital parameters and accuracy, Q, for the current values of R_1 and R_2 are then found, regardless of the search level. If Q is less than Q_0, the current values of R_1, R_2, and Q are

$$Q_0 = Q \tag{9-85a}$$

$$r_{10} = R_1 \tag{9-85b}$$

$$r_{20} = R_2 \tag{9-85c}$$

and the next (R_1, R_2) pair for the current search level is processed.

If $Q > Q_0 > Q_{min}$ ($Q_{min} = 0.2$ by default), then the next (R_1, R_2) pair is processed as above. If $Q_0 < Q_{min}$, then the preliminary orbit search is ended, and the current values of R_1 and R_2 are used as the starting values for the differential correction process discussed in Section 9.2.3.4.

9.2.3.1.3 End-of-Level Search Processing

If, at the end of a given search level, the accuracy, Q, of all the points tried is still not acceptable, the next search level is processed. If all search levels have been processed and the accuracy is still not acceptable, then the best (R_1, R_2) pair found in the orbit search (i.e., the pair that gave the smallest Q value) must be used as the initial estimate for the differential correction process.

9.2.3.2 Computation of Orbital Parameters

The orbital parameters that are consistent with the current values for R_1 and R_2 are determined using the procedure discussed in this section.

From Figure 9-1 and Equation (9-25), the slant range vector from the station to the spacecraft is

$$\bar{\rho}_i = \bar{R}_i - \bar{R}_{s_i} \quad (i = 1, 2, 3) \tag{9-86}$$

Dotting Equation (9-25) with itself yields Equation (9-43) rewritten for the i^{th} measurement as follows:

$$\rho_i^2 + \rho_i C_\psi + (R_{s_i}^2 - R_i^2) = 0 \qquad (i = 1, 2, 3) \tag{9-87}$$

where

$$C_{\psi_i} = 2\hat{L}_i \cdot \bar{R}_{s_i} \qquad (i = 1, 2, 3) \tag{9-88}$$

Solving Equation (9-87) for ρ_1 and ρ_2 by means of the Binominal Theorem gives

$$\rho_i = \frac{1}{2}\left\{-C_{\psi_i} + \sqrt{C_{\psi_i}^2 - 4(R_{s_i}^2 - R_i^2)}\right\} \tag{9-89}$$

where the positive sign on the radical is known to yield the correct root from physical considerations. Initially estimating R_1 and R_2, Equation (9-89) can be solved for ρ_1 and ρ_2 and Equation (9-25) solved for $\bar{R}_1$ and $\bar{R}_2$. Knowing $\bar{R}_1$ and $\bar{R}_2$ merely defines the orbit plane (in terms of Ω and i) and two position vectors in this plane. However, there are numerous orbits (in terms of a and e) that satisfy the two position vectors $\bar{R}_1$ and $\bar{R}_2$. Therefore, a third position vector, along with the orbital dynamics relationships, is necessary to uniquely determine the orbit being measured.

The quantity $\hat{k}$ is defined as the unit vector perpendicular to the orbit plane, i.e.,

$$\hat{k} = \frac{\bar{R}_1 \times \bar{R}_2}{R_1 R_2} \tag{9-90}$$

Then, since the third position vector $\bar{R}_3$ must lie in the orbital plane,

$$\bar{R}_3 \cdot \hat{k} = 0 \tag{9-91}$$

Substituting Equation (9-25) into Equation (9-91) yields

$$\rho_3 = \frac{\overline{R}_{s_3} \cdot \hat{k}}{\hat{L}_3 \cdot \hat{k}} \tag{9-92}$$

Knowing ρ_3, the geocentric vector $\overline{R}_3$ can be obtained from Equation (9-25). Note that when ρ_3 lies in the orbit plane, $\overline{R}_{s_3}$ and $\hat{L}_3$ are perpendicular to $\hat{k}$ and Equation (9-92) is singular. Should such a singularity occur, a different measurement time t_3 must be used. Thus the vectors $\overline{R}_1$, $\overline{R}_2$, and $\overline{R}_3$ have to be determined as functions of the estimated vector magnitudes R_1 and R_2.

The difference in the true anomalies can be determined as follows:

$$\cos (f_j - f_k) = \frac{\overline{R}_j \cdot \overline{R}_k}{R_j R_k} \qquad (j, k = 1, 2, 3) \tag{9-93a}$$

$$\sin (f_j - f_k) = s \sqrt{1 - \cos^2 (f_j - f_k)} \qquad (j, k = 1, 2, 3) \tag{9-93b}$$

where

f = true anomaly

s = orbit direction indicator, determined as described below

If it is not known whether the orbit is direct or retrograde, this is determined as follows. Initially, it is assumed that the orbit is direct ($s = +1$). The quantity T_{min} denotes the period of a spacecraft orbiting at the mean radius of the Earth, where

$$T_{min} = 2\pi \sqrt{\frac{R_e^3}{\mu}} \tag{9-94}$$

If $T_{min} < \tau_3 < -\tau_1$, then s is computed as

$$s = \text{sign} (\overline{R}_2 \times \overline{R}_3)_z \tag{9-95}$$

However, if $-\tau_1 < T_{min}$ and $-\tau_1 < \tau_3$, then s is computed as

$$s = \text{sign}\left(\frac{\bar{R}_1 \times \bar{R}_2}{R_1 R_2}\right)_z = \text{sign}\,(W_z) \tag{9-96}$$

Then the orbit direction, s, is assigned as

$$s = \begin{cases} +1 \text{ direct} \\ -1 \text{ retrograde} \end{cases} \tag{9-97}$$

and the orbital inclination, i, is given by

$$i = \cos^{-1}\left[\frac{W_z}{\sin\,(f_2 - f_1)}\right] \tag{9-98}$$

The quantity W_z appearing in the equations above is the z component of the vector $\bar{W}$. This vector (which is parallel to the angular momentum unit vector), consistent with R_1 and R_2 (assuming a direct orbit), is found using

$$\bar{W} = \frac{\bar{R}_1 \times \bar{R}_2}{R_1 R_2} \tag{9-99}$$

If an orbit has been computed previously and the direction is to be determined, a test for orbit reversal (i.e., direct to retrograde or vice versa) is made by comparing the sign of the current value of W_z from Equation (9-99) with the corresponding value for the previous determination. If the signs are the same, no orbit reversal is assumed to have occurred.

If the signs are not the same, such a reversal *may* have occurred, and this is accommodated as follows. If

$$-\tau_1 < \frac{T_{min}}{2} \tag{9-100a}$$

and

$$\tau_3 < \frac{T_{min}}{2} \tag{9-100b}$$

then such a reversal has already been allowed for through the value of s in Equation (9-97). Otherwise, the following computations are made:

$$f_{min} = \min [\, |f_2 - f_1|,\ |f_3 - f_2|,\ |180° - |f_2 - f_1|\,|,\ |180° - |f_3 - f_2|\,] \tag{9-101}$$

$$\delta = |90° - i| \tag{9-102}$$

The computed orbit direction is assumed to have changed if the inclination, i, is close to 90 degrees and if neither spacecraft position vector pair forms an angle close to 180 degrees. That is, if

$$\delta < 1° \tag{9-103a}$$

and

$$\delta < 0.04\, f_{min} \tag{9-103b}$$

then

$$\sin (f_2 - f_1) = -\sin (f_2 - f_1) \tag{9-104a}$$

$$\sin (f_3 - f_1) = -\sin (f_3 - f_1) \tag{9-104b}$$

$$\sin (f_3 - f_2) = -\sin (f_3 - f_2) \tag{9-104c}$$

and it is assumed that reversal has occurred.

To correct the estimated values of R_1 and R_2, it is necessary to compute the resulting time intervals between $(\overline{R}_3, \overline{R}_2)$ and $(\overline{R}_1, \overline{R}_2)$ to obtain residuals as actual time

differences. The semilatus rectum obtained from Gaussian sector to triangle theory (Reference 2) is

$$p = \frac{R_1 + C_{r3} R_3 - C_{r1} R_2}{1 + C_{r3} - C_{r1}} \tag{9-105}$$

or, dividing the numerator and denominator by C_1

$$p = \frac{C_1 R_1 + C_3 R_3 - R_2}{C_1 + C_3 - 1} \tag{9-106}$$

where

$$C_1 = \frac{R_2}{R_1} \frac{\sin (f_3 - f_2)}{\sin (f_3 - f_1)} \tag{9-107a}$$

$$C_{r1} = \frac{R_1}{R_2} \frac{\sin (f_3 - f_1)}{\sin (f_3 - f_2)} \tag{9-107b}$$

$$C_3 = \frac{R_2}{R_3} \frac{\sin (f_2 - f_1)}{\sin (f_3 - f_1)} \tag{9-107c}$$

$$C_{r3} = \frac{R_1}{R_3} \frac{\sin (f_2 - f_1)}{\sin (f_3 - f_2)} \tag{9-107d}$$

For very short measurement arcs, both Equation (9-105) and Equation (9-106) are poorly determined, and the Gauss Method (Section 9.1.2) should be used. The singularity inherent in Equation (9-105) when $f_3 - f_1 = \pi$ can be avoided, along with other numerical difficulties, by using Equation (9-106) when $f_3 - f_1 \leq |f_3 - f_2|$ and using Equation (9-105) when $f_3 - f_1 > |f_3 - f_2|$.

From Equation (3-222) the conic equation for true anomaly is

$$e \cos f_i = \frac{p}{R_i} - 1 \qquad (i = 1, 2, 3) \tag{9-108}$$

Expanding factors of the form $\sin(f_1 + f_2 + f_3)$ gives the following for $|\sin(f_2 - f_1)| > |\sin(f_3 - f_2)|$:

$$e \sin f_2 = \frac{-e \cos f_2 \cos(f_2 - f_1) + e \cos f_1}{\sin(f_2 - f_1)} \tag{9-109}$$

Otherwise,

$$e \sin f_2 = \frac{e \cos f_2 \cos(f_3 - f_2) - e \cos f_3}{\sin(f_3 - f_2)} \tag{9-110}$$

From Equations (9-108) through (9-110) the eccentricity, e, can be determined as

$$e^2 = (e \cos f_2)^2 + (e \sin f_2)^2 \tag{9-111}$$

and the semimajor axis, a, is determined from

$$a = \frac{p}{1 - e^2} \tag{9-112}$$

For an elliptical orbit ($e < 1$), the following are obtained:

$$n = \frac{1}{a} \sqrt{\frac{\mu}{a}} \tag{9-113}$$

$$T = \frac{2\pi}{60n} \tag{9-114}$$

$$h_p = a(1 - e) - R_e \tag{9-115}$$

$$h_a = h_p + 2a e \tag{9-116}$$

where

a = semimajor axis

n = mean motion

T = orbital period in minutes

h_p = perigee height

h_a = apogee height

The eccentric anomaly, E_i, is given by

$$\sin E_i = \frac{R_i}{p} \sqrt{1 - e^2} \sin f_i \qquad (i = 1, 2, 3) \qquad (9\text{-}117a)$$

and

$$\cos E_i = \frac{R_i}{p}(e + \cos f_i) \qquad (i = 1, 2, 3) \qquad (9\text{-}117b)$$

Equations (9-117) can be written as follows for the second measurement point:

$$S_e \equiv [e \sin E_2] = \frac{R_2}{p} \sqrt{1 - e^2} \, [e \sin f_2] \qquad (9\text{-}118a)$$

$$C_e \equiv [e \cos E_2] = \frac{R_2}{p} (e^2 + [e \cos f_2]) \qquad (9\text{-}118b)$$

The following equations for differences in eccentric anomalies expressed as functions of true anomaly differences can be obtained by expanding Equations (9-117):

$$\sin (E_3 - E_2) = \frac{R_e}{\sqrt{a\,p}} \sin (f_3 - f_2) - \frac{R_3}{p} [1 - \cos (f_3 - f_2)] S_e \qquad (9\text{-}119a)$$

$$\cos (E_3 - E_2) = 1 - \frac{R_3 R_2}{a p} [1 - \cos (f_3 - f_2)] \quad (9\text{-}119b)$$

$$\sin (E_2 - E_1) = \frac{R_1}{\sqrt{a p}} \sin (f_2 - f_1) + \frac{R_1}{p} [1 - \cos (f_2 - f_1)] S_e \quad (9\text{-}119c)$$

$$\cos (E_2 - E_1) = 1 - \frac{R_2 R_1}{a p} [1 - \cos (f_2 - f_1)] \quad (9\text{-}119d)$$

Kepler's equation (Equation (3-178)) is written as

$$M = E - e \sin E \quad (9\text{-}120)$$

where M is the mean anomaly. Mean anomaly differences about the second point can be written as

$$M_3 - M_2 = E_3 - E_2 + 2 S_e \sin^2 \left(\frac{E_3 - E_2}{2} \right) - C_e \sin (E_3 - E_2) \quad (9\text{-}121a)$$

$$M_2 - M_1 = E_2 - E_1 - 2 S_e \sin^2 \left(\frac{E_2 - E_1}{2} \right) - C_e \sin (E_2 - E_1) \quad (9\text{-}121b)$$

where

$$E_3 - E_2 = \tan^{-1} \left[\frac{\sin (E_3 - E_2)}{\cos (E_3 - E_2)} \right] \quad (9\text{-}122a)$$

$$E_2 - E_1 = \tan^{-1} \left[\frac{\sin (E_2 - E_1)}{\cos (E_2 - E_1)} \right] \quad (9\text{-}122b)$$

9.2.3.3 Determination of the Accuracy of the Computed Orbit

A determination can now be made of how well the computed orbit fits the measurements by comparing the times between measurements, as determined from the computed orbit,

with the true measured times. First, using the mean anomaly, the mean time interval between the computed measurements is calculated as follows (not allowing for multiple revolutions between measurements):

$$-\tau_1' = \frac{M_2 - M_1}{n} \tag{9-123a}$$

$$\tau_3' = \frac{M_3 - M_2}{n} \tag{9-123b}$$

Next, the number of full revolutions (λ) between consecutive measurements (if these are not known) are approximated as

$$\lambda_{21} = \text{INT}\left[\frac{-\tau_1 + \tau_1'}{\max\left(T_{min}, \frac{2\pi}{n}\right)}\right] \tag{9-124a}$$

$$\lambda_{32} = \text{INT}\left[\frac{\tau_{32} - T_{32}}{\max\left(T_{min}, \frac{2\pi}{n}\right)}\right] \tag{9-124b}$$

The total computed time between consecutive measurements, T_c, is then computed by

$$T_{21c} = -\tau_1' + \lambda_{21}\left(\frac{2\pi}{n}\right) \tag{9-125a}$$

$$T_{32c} = \tau_3' + \lambda_{32}\left(\frac{2\pi}{n}\right) \tag{9-125b}$$

If a differential correction is currently being performed, the differences between measured and computed time differences are determined as

$$\Delta T_{21} = -\tau_1 - T_{21c} \tag{9-126a}$$

$$\Delta T_{32} = \tau_3 - T_{32c} \tag{9-126b}$$

and the overall accuracy of the fit, Q, is computed as

$$Q = \sqrt{\Delta T_{21}^2 + \Delta T_{32}^2} \tag{9-127}$$

If a differential correction is not currently being performed, the following values are set:

$$T_{21T} = \max\left[\frac{-\tau_1}{T_{21c}}, \frac{T_{21c}}{-\tau_1}\right] \tag{9-128a}$$

$$T_{32T} = \max\left[\frac{\tau_3}{T_{32c}}, \frac{T_{32c}}{\tau_3}\right] \tag{9-128b}$$

and the accuracy of the current fit, Q_1, is computed as

$$Q_1 = \sqrt{(T_{21T} - 1)(1 + 0.5\,\lambda_{21}^2) + (T_{32T} - 1)(1 + 0.5\,\lambda_{32}^2)} \tag{9-129}$$

If both $-\tau_1'$ and τ_3' are greater than 0.5 T_{min}, then the accuracy for the reverse orbit is also determined as above using

$$T_{21}' = \frac{2\pi - (M_2 - M_1)}{n} \tag{9-130a}$$

$$T_{32}' = \frac{2\pi - (M_3 - M_2)}{n} \tag{9-130b}$$

in place of T_{21} and T_{32}, thus generating an accuracy Q_2.

If $Q_1 < Q_2$, then the original orbit fit is accepted, the orbit accuracy, Q, is set equal to Q_1, and T_{21c} and T_{32c} are kept. Otherwise, the reverse orbit direction is accepted as best, Q is set equal to Q_2, and (from Equations (9-130))

$$T_{21c} = T_{21}' \tag{9-131a}$$

$$T_{32c} = T_{32}' \tag{9-131b}$$

In either case, the time differences, ΔT, are determined next using Equations (9-126).

9.2.3.4 Initiation of the Differential Correction Process

Once the parameters for the initial orbit fit have been determined as above, the accuracy of the fit is determined using Equation (9-127). If the accuracy is less than a lower limit, the orbit has been adequately determined. Otherwise, an iterative differential correction process is initiated to refine the orbit (i.e., obtain a better fit to the measurements). Each iteration consists of the following steps:

1. Assuming the current values of R_1 and R_2, a new set of orbital parameters at radius values $(R_1 + \Delta R, R_2)$ (where $\Delta R = 10^{-5}$ kilometer) are determined via the method given in Sections 9.2.3.2 amd 9.2.3.3, yielding the parameters $\Delta T_{21}(R_1 + \Delta R)$, $\Delta T_{32}(R_1 + \Delta R)$, $Q(R_1 + \Delta R)$.
2. Another set of parameters is then determined at radius values $(R_1, R_2 + \Delta R)$, yielding parameters $\Delta T_{21}(R_2 + \Delta R)$, $\Delta T_{32}(R_2 + \Delta R)$, $Q(R_2 + \Delta R)$.
3. Next, one of two methods is used to derive the corrections, δr_i, to the assumed values of R_i. For the first 12 iterations, a simultaneous linear equation method is used; and for the remaining iterations, a Newton-Raphson method is used.

9.2.3.4.1 Method of Simultaneous Linear Equations

In this method, corrections to the assumed radius magnitudes, δr_1 and δr_2, are found by forcing Equation (9-127) to zero. Using a two-dimensional Taylor series expansion and keeping only the linear terms,

$$0 = \Delta T_{21}(R_1, R_2) + \frac{\partial \Delta T_{21}}{\partial R_1} \Delta R_1 + \frac{\partial \Delta T_{21}}{\partial R_2} \Delta R_2 \qquad (9\text{-}132a)$$

$$0 = \Delta T_{32}(R_1, R_2) + \frac{\partial \Delta T_{32}}{\partial R_1} \Delta R_1 + \frac{\partial \Delta T_{32}}{\partial R_2} \Delta R_2 \qquad (9\text{-}132b)$$

The partial derivatives are approximated by

$$\frac{\partial \Delta T_{21}}{\partial R_1} = \frac{\Delta T_{21}(R_1 + \Delta R, R_2) - \Delta T_{21}(R_1, R_2)}{\Delta R} \qquad (9\text{-}133a)$$

$$\frac{\partial \Delta T_{21}}{\partial R_2} = \frac{\Delta T_{21}(R_1, R_2 + \Delta R) - \Delta T_{21}(R_1, R_2)}{\Delta R} \qquad (9\text{-}133b)$$

$$\frac{\partial \Delta T_{32}}{\partial R_1} = \frac{\Delta T_{32}(R_1 + \Delta R,\ R_2) - \Delta T_{32}(R_1,\ R_2)}{\Delta R} \qquad (9\text{-}133c)$$

$$\frac{\partial \Delta T_{32}}{\partial R_2} = \frac{\Delta T_{32}(R_1,\ R_2 + \Delta R) - \Delta T_{32}(R_1,\ R_2)}{\Delta R} \qquad (9\text{-}133d)$$

The determinant (det) of Equations (9-132) is then found as

$$\det = \frac{\partial \Delta T_{21}}{\partial R_1}\,\frac{\partial \Delta T_{32}}{\partial R_2} - \frac{\partial \Delta T_{32}}{\partial R_1}\,\frac{\partial \Delta T_{21}}{\partial R_2} \qquad (9\text{-}134)$$

If $|\det| < 10^{-18}$, then the Newton-Raphson method described in Section 9.2.3.4.2 is used. Otherwise, the corrections δr_1 and δr_2 are found using

$$\det_1 = \frac{\partial \Delta T_{32}}{\partial R_2} \cdot \Delta T_{21}(R_1,\ R_2) - \frac{\partial \Delta T_{21}}{\partial R_2} \cdot \Delta T_{32}(R_1,\ R_2) \qquad (9\text{-}135a)$$

$$\det_2 = \frac{\partial \Delta T_{21}}{\partial R_1} \cdot \Delta T_{32}(R_1,\ R_2) - \frac{\partial \Delta T_{32}}{\partial R_1} \cdot \Delta T_{21}(R_1,\ R_2) \qquad (9\text{-}135b)$$

$$\delta r_1 = \frac{\det_1}{\det} \qquad (9\text{-}136a)$$

$$\delta r_2 = \frac{\det_2}{\det} \qquad (9\text{-}136b)$$

The effective slope of the hyperplane satisfying Equations (9-132), on which the δr_i lie, is found as

$$S = \frac{Q(R_1,\ R_2)}{\sqrt{\delta r_1^2 + \delta r_2^2}} \qquad (9\text{-}137)$$

9.2.3.4.2 Newton-Raphson Method

In this approach, the accuracy, Q, of the solution is forced toward zero by varying the R_i. Using

$$Q_0 = Q(R_1, R_2) \tag{9-138a}$$

$$Q_1 = Q(R_1 + \Delta R, R_2) \tag{9-138b}$$

$$Q_2 = Q(R_1, R_2 + \Delta R) \tag{9-138c}$$

found as described in Section 9.2.3.3 (after Equations (9-130)), the following approximations are made:

$$\frac{\partial Q}{\partial R_1} = \frac{Q_1 - Q_0}{\Delta R} \tag{9-139a}$$

$$\frac{\partial Q}{\partial R_2} = \frac{Q_2 - Q_0}{\Delta R} \tag{9-139b}$$

The corrections δr_i are then found using

$$S = \sqrt{\left(\frac{\partial Q}{\partial R_1}\right)^2 + \left(\frac{\partial Q}{\partial R_2}\right)^2} \tag{9-140}$$

$$\delta r_1 = -\frac{\left(\frac{\partial Q}{\partial R_1}\right)}{S} \cdot \frac{Q_0}{S} \tag{9-141a}$$

$$\delta r_2 = -\frac{\left(\frac{\partial Q}{\partial R_2}\right)}{S} \cdot \frac{Q_0}{S} \tag{9-141b}$$

9.2.3.4.3 Scaling of the Solution

Next the δr_1 are scaled so that they do not exceed the maximum allowed corrections. If $Q_0 = Q(R_1, R_2)$, then the scaling factor S_0 is determined as follows:

$$S_M = \frac{1}{\max\left[\frac{|\delta r_1|}{\frac{3}{4}h_1}, \frac{|\delta r_2|}{\frac{3}{4}h_2}, \frac{|\delta r_1|}{C_{max}}, \frac{|\delta r_2|}{C_{max}}\right]} \tag{9-142}$$

$$S_0 = \min(1.0, S_M) \tag{9-143}$$

where

C_{max} = maximum allowed correction

h_1 = $R_1 - R_{s_1}$

h_2 = $R_2 - R_{s_2}$

R_{s_1} = distance of the station from the center of the Earth for the measurement at t_1

R_{s_2} = distance of the station from the center of the Earth for the measurement at t_2

Next, the solutions are scaled using

$$\delta r_1 = S_0 \cdot \delta r_1 \tag{9-144a}$$

$$\delta r_2 = S_0 \cdot \delta r_2 \tag{9-144b}$$

If the computed slope, S, is not too close to zero, then new values of ΔT_{21}, ΔT_{32}, and Q are found at $(R_1 + \delta r_1, R_2 + \delta r_2)$ using the methods described in Sections 9.2.3.2 and 9.2.3.3. The accuracy, Q, is then set as follows:

$$Q_1 = Q(R_1 + \delta r_1, R_2 + \delta r_2) \tag{9-145}$$

If $Q_1 < Q_0$ (i.e., if the solution with δr_1 and δr_2 is better), the inner loop processing described in Section 9.2.3.4.4 is skipped.

If S is too close to zero or if Q_1 is greater than Q_0, the δr_i are again scaled so that neither exceeds the magnitude of the adjustment on the last loop of the same differential correction type (i.e., Newton-Raphson or linear equations method). This is done using

$$\beta = \sqrt{\delta r_1^2 + \delta r_2^2} \tag{9-146a}$$

$$S_1 = \frac{1}{\max\left(1.0, \frac{\beta}{\beta'}\right)} \tag{9-146b}$$

$$\delta r_1 = S_1 \cdot \delta r_1 \tag{9-146c}$$

$$\delta r_2 = S_1 \cdot \delta r_2 \tag{9-146d}$$

where β' is the value of β from the previous loop of the same differential correction type.

New values of ΔT_{21}, ΔT_{32}, and Q at $(R_1 + \delta r_1, R_2 + \delta r_2)$ are then found using the methods described in Sections 9.2.3.2 and 9.2.3.3. If Q_1 is greater than Q_0, then the inner loop processing described in Section 9.2.3.4.4 is performed, initially halving ($\eta = 1/2$) the δr_i to get better agreement.

If

$$Q_1 < Q_0 \tag{9-147a}$$

but

$$S_1 > 1.0 \tag{9-147b}$$

then inner loop processing is skipped. Otherwise inner loop processing is performed, initially doubling ($\eta = 2.0$) the δr_i to try for better agreement.

9.2.3.4.4 Inner Loop Processing

At this point in outer loop processing, up to 20 inner loops will be performed, each inner loop scaling the δr_i to try to get better accuracy. In this discussion, the following definitions are made:

and

$$\delta r_i' = \eta \cdot \delta r_i \quad (i = 1, 2) \tag{9-148a}$$

$$Q_1 = Q(R_1 + \delta r_1,\ R_2 + \delta r_2) \tag{9-148b}$$

$$Q_0 = Q(R_1,\ R_2) \tag{9-148c}$$

If

$$| \delta r_1 | - | \delta r_1' | < 0.25\ \Delta r \tag{9-149}$$

(where $\Delta r = 10^{-5}\ R_e$), then δr_i is accepted (not $\delta r_i'$), and inner loop processing is terminated. Otherwise, ΔT_{21}, ΔT_{32}, and Q' are recomputed at $(R_1 + \delta r_1',\ R_2 + \delta r_2')$, where

$$Q' = Q(R_1 + \delta r_1',\ R_2 + \delta r_2') \tag{9-150}$$

If $\eta > 1$ and $Q' > Q_1$, then δr_i is accepted (not $\delta r_i'$), and inner loop processing is terminated. Otherwise, more inner loops are performed.

If $\eta < 1$, then

$$| \delta r' | = \sqrt{(\delta r_1')^2 + (\delta r_2')^2} \tag{9-151}$$

If $Q' \geq Q_0$ but $| \delta r' | < 0.5\ \Delta r$, then a solution has been obtained and inner and outer loop processing is terminated. If $Q' \geq Q_0$ but $| \delta r' | > 0.5\ \Delta r$, then the next inner loop is performed.

If $Q' < Q_0$ but the Newton-Raphson differential correction method is being used, then inner loop processing is terminated because a good solution is assumed. If $Q' < Q_0$ but the linear equation method is being used, a parabolic fit is tried using the following:

$$\zeta = \frac{1}{2}\left(\frac{Q_0 - Q_1}{Q_0 - 2Q' + Q_1}\right) \tag{9-152a}$$

$$\delta r_1 = \delta r_1' \tag{9-152b}$$

$$\delta r_2 = \delta r_2' \tag{9-152c}$$

$$\delta r_1' = \delta r_1 (1 + \zeta) \tag{9-152d}$$

$$\delta r_2' = \delta r_2 (1 + \zeta) \tag{9-152e}$$

$$Q_1 = Q' \tag{9-152f}$$

New values of ΔT_{21}, ΔT_{32}, and

$$Q' = Q(R_1 + \delta r_1', R_2 + \delta r_2') \tag{9-153}$$

are found as before at $(R_1 + \delta r_1', R_2 + \delta r_2')$. If $Q' < Q_1$, a good vector has been obtained and inner loop processing is terminated, keeping $\delta r_1'$ and $\delta r_2'$ as the best values. Otherwise, the orbit found using the $\delta r_1'$ was poorer than the one using δr_1; in this case, inner loop processing is terminated, keeping δr_1 and δr_2 as the best values.

9.2.3.4.5 End of Differential Correction Loop Processing

If all inner loops are exhausted with no orbit improvement being found (i.e., if $Q' > Q_0$ at the end of loop processing), then no more loops are performed. Otherwise the new values for R_1 and R_2 are found using

$$R_1 = R_1 + \delta r_1 \tag{9-154a}$$

$$R_2 = R_2 + \delta r_2 \tag{9-154b}$$

If the value of Q corresponding to the R_1 in Equations (9-154) is less than a specified tolerance (whose default value is 0.0005 second), the solution is deemed acceptable and no more iterations are performed.

If Q/Q_0 is less than 0.99, the differential correction process is converging rapidly enough and further iterations are performed. Otherwise, the accuracy improvement is too small and the differential correction on this loop is said to have failed. If a total of three (not necessarily consecutive) loops fail in this way, further corrective measures must be taken.

If the initial estimates of the heights or radius magnitudes were input or the total timespan $(t_3 - t_1)$ is less than 5 minutes, and if the minimum acceptable perigee has not been lowered previously, then the minimum perigee height is lowered by 0.1 R_e, and further loops are attempted. Otherwise a second preliminary orbit search is performed as described in Section 9.2.3.1 using default heights of 20,000 kilometers, and the entire orbit extraction process is reinitiated.

9.2.3.4.6 Determination of Final Orbital Vector

Once the differential correction loops have been completed, the final orbital parameters are determined as before, and the final spacecraft velocity vector, $\dot{\bar{R}}_2$, is generated using

$$f = 1 - \frac{a}{R}[1 - \cos(E_3 - E_2)] \tag{9-155}$$

$$g = \tau_3 - \sqrt{\frac{a^3}{\mu}}[E_3 - E_2 - \sin(E_3 - E_2)] \tag{9-156}$$

$$\dot{\bar{R}}_2 = \frac{1}{g}(\bar{R}_3 - f\bar{R}_2) \tag{9-157}$$

9.3 RANGE AND ANGLES METHOD

The Range and Angles Method determines the spacecraft position and velocity by fitting two-body orbit relations to GRARR, C-band, or USB range and gimbal angle data in a regression manner.

A set of m chronologically ordered radar data vectors are available from the GRARR, C-band, and/or USB systems. Each vector consists of a range measurement and two

gimbal angle measurements. The measurement vectors are first transformed to the station-centered topocentric local tangent Cartesian coordinate system. The GRARR and USB angles, X and Y, are transformed to azimuth, A, and elevation, E, as shown in Equations (9-8) and (9-9). The C-band data vectors and transformed GRARR and USB data vectors are then transformed to local tangent coordinates as follows:

$$\bar{\varrho}_{lt_i} = \begin{bmatrix} x_{lt} \\ y_{lt} \\ z_{lt} \end{bmatrix} = \varrho_i \begin{bmatrix} \cos E_i \sin A_i \\ \cos E_i \cos A_i \\ \sin E_i \end{bmatrix} \qquad (i = 1, 2, \ldots, m) \tag{9-158}$$

The local tangent vectors are then transformed to true of reference date or mean of B1950.0 or J2000.0 inertial coordinate systems as described in Section 9.2.1, i.e.,

$$\bar{\varrho}_i = (M_{lt}\, B\, C)^T\, \bar{\varrho}_{lt_i} \tag{9-159}$$

The station position vector in geocentric inertial Cartesian coordinates, given in Equation (9-24b), is

$$\bar{R}_{s_i} = (B\, C)^T\, \bar{r}_{s_{b_i}} \tag{9-160}$$

where the station coordinates in body-fixed axes are given in Equations (9-15) and (9-16). Vectorially adding the station vectors, $\bar{R}_{s_i}$, and topocentric spacecraft vectors, $\bar{\varrho}_i$, yields the geocentric spacecraft position vector

$$\bar{R}_i = \bar{R}_{s_i} + \bar{\varrho}_i \qquad (i = 1, 2, \ldots, m) \tag{9-161}$$

A two-body orbit is then fitted to the m position vectors by using the f and g series, expanded about a desired epoch time

$$R_i = f_i\, \bar{R}_0 + g_i\, \dot{\bar{R}}_0 \qquad (i = 1, 2, \ldots, m) \tag{9-162}$$

Multiplying the preceding equation by f_1 and then summing on i yields

$$\sum_{i=1}^{m} f_i\, \bar{R}_i = \sum_{i=1}^{m} f_i^2\, \bar{R}_0 + \sum_{i=1}^{m} f_i\, g_i\, \dot{\bar{R}}_0 \tag{9-163}$$

Multiplying Equation (9-162) by g_i and summing on i yields

$$\sum_{i=1}^{m} g_i \bar{R}_i = \sum_{i=1}^{m} f_i g_i \bar{R}_0 + \sum_{i=1}^{m} g_i^2 \dot{\bar{R}}_0 \tag{9-164}$$

Solving Equations (9-163) and (9-164) simultaneously for $\bar{R}_0$ and $\dot{\bar{R}}_0$ yields the desired inertial geocentric position and velocity at epoch:

$$\bar{R}_0 = \frac{\sum_{i=1}^{m} g_i^2 \sum_{i=1}^{m} f_i \bar{R}_i - \sum_{i=1}^{m} f_i g_i \sum_{i=1}^{m} g_i \bar{R}_i}{\sum_{i=1}^{m} f_i^2 \sum_{i=1}^{m} g_i^2 - \left(\sum_{i=1}^{m} f_i g_i \right)^2} \tag{9-165}$$

$$\dot{\bar{R}}_0 = \frac{\sum_{i=1}^{m} f_i^2 \sum_{i=1}^{m} g_i \bar{R}_i - \sum_{i=1}^{m} f_i g_i \sum_{i=1}^{m} f_i \bar{R}_i}{\sum_{i=1}^{m} f_i^2 \sum_{i=1}^{m} g_i^2 - \left(\sum_{i=1}^{m} f_i g_i \right)^2} \tag{9-166}$$

Equations (9-165) and (9-166) are solved iteratively by successively improved approximations for f_i and g_i.

The orbit is initially approximated by a circular orbit with the semimajor axis, a, obtained by averaging the m position vectors as follows:

$$a = \frac{1}{m} \sum_{i=1}^{m} |R_i| \tag{9-167}$$

The mean motion, n, is

$$n = \sqrt{\frac{\mu}{a^3}} \tag{9-168}$$

and the mean anomaly measured from epoch is

$$M_i - M_0 = n\,(t_i - t_0) \tag{9-169}$$

The coefficients f and g for the two-body circular orbit, corresponding to each measurement vector, are (Reference 2)

$$f_i = \cos\,(M_i - M_0) \tag{9-170a}$$

$$g_i = \frac{1}{n}\,\sin\,(M_i - M_0) \tag{9-170b}$$

Substituting the preceding f_i and g_i into Equations (9-165) and (9-166) yields the first approximation for $\bar{R}_0$ and $\dot{\bar{R}}_0$. After the initial iteration, the coefficients f_i and g_i are calculated from the following procedure.

Reference 3 presents a general method for computing f_i and g_i as functions of $\bar{R}_0$ and $\dot{\bar{R}}_0$. The Sundman transformation is used to obtain a new independent variable ψ defined by

$$\dot{\psi} = \frac{1}{R} \tag{9-171}$$

The coefficients f_i and g_i are determined from the relations

$$f_i = 1 - \frac{\mu\, S_2(\psi_i)}{R_0} \tag{9-172a}$$

$$g_i = R_0\, S_1(\psi_i) + \sigma_0\, S_2(\psi_i) \tag{9-172b}$$

The velocity $\dot{\bar{R}}_i$ can be determined by

$$\dot{\bar{R}}_i = \dot{f}_i\, \bar{R}_0 + \dot{g}_i\, \dot{\bar{R}}_0 \tag{9-173}$$

where

$$\dot{f}_i = \frac{-\mu S_1(\psi_i)}{R_i R_0} \tag{9-174a}$$

$$\dot{g}_i = 1 - \frac{\mu S_2(\psi_i)}{R_i} \tag{9-174b}$$

and the time difference between $\bar{R}_i$ and $\bar{R}_0$ is

$$\tau_i = t_i - t_0 = R_0 S_1(\psi_i) + \sigma_0 S_2(\psi_i) + \mu S_3(\psi_i) \tag{9-175}$$

The parameters σ_0 is

$$\sigma_0 = \bar{R}_0 \cdot \dot{\bar{R}}_0 \tag{9-176}$$

and the parameters S_1, S_2, and S_3 are obtained by solving Kepler's equation by successively approximating ψ to satisfy Equation (9-175). The method, described in Reference 3, is summarized below.

After initially estimating a value of ψ, the quantity λ is calculated from

$$\lambda = a \psi^2 \tag{9-177}$$

where

$$a = \dot{\bar{R}}_0 \cdot \dot{\bar{R}}_0 - \frac{2\mu}{R_0} \tag{9-178}$$

If $|\lambda| > 1$, the value is saved as λ_p, and λ is repeatedly divided by 4 (keeping track of the number of divisions, m) until $|\lambda| < 1$.

The parameters C_0, C_1 ..., C_5 are next computed as functions of λ, as follows:

$$35C_5 = \left(1 + \left\{1 + \left[1 + \left(1 + \left\{1 + \left[1 + \left(1 + \frac{\lambda}{19 \cdot 18}\right)\frac{\lambda}{17 \cdot 16}\right]\frac{\lambda}{15 \cdot 14}\right\}\frac{\lambda}{13 \cdot 12}\right)\frac{\lambda}{11 \cdot 10}\right]\frac{\lambda}{9 \cdot 8}\right\}\frac{\lambda}{7 \cdot 6}\right)\Big/40 \tag{9-178a}$$

$$C_4 = \left(1 + \left\{1 + \left[1 + \left(1 + \left\{1 + \left[1 + \left(1 + \frac{\lambda}{18 \cdot 17}\right)\frac{\lambda}{16 \cdot 15}\right]\frac{\lambda}{14 \cdot 13}\right\}\frac{\lambda}{12 \cdot 11}\right)\frac{\lambda}{10 \cdot 9}\right]\frac{\lambda}{8 \cdot 7}\right\}\frac{\lambda}{6 \cdot 5}\right)\Big/24 \tag{9-178b}$$

$$C_3 = \frac{\frac{1}{2} + \lambda(3C_5)}{3} \tag{9-178c}$$

$$C_2 = \frac{1}{2} + \lambda C_4 \tag{9-178d}$$

$$C_1 = 1 + \lambda C_3 \tag{9-178e}$$

$$C_0 = 1 + \lambda C_2 \tag{9-178f}$$

If the initial value of λ has been reduced (i.e., M > 0), then C_0 is compared with the quantity

$$C_0' = \left[\frac{MAX}{2^{(2^{M-1})}}\right]^{2^{-M}} \tag{9-179}$$

where MAX is approximately the maximum positive number representable in the computer (e.g., MAX = 10^{75} for the IBM 4300 series). If $C_0 > C_0'$, then C_0 is set equal to C_0'. Next, C_1 is compared as follows:

$$C_1' = \begin{cases} MAX & (\text{if } C_0 < 1) \\ MAX/(C_0^M) & (\text{if } C_0 \geq 1) \end{cases} \tag{9-180}$$

If $C_1 > C_1'$, then C_1 is set equal to C_1'. With these values of C_0 and C_1, new values are computed by applying the following equations M times:

$$C_1 = C_1 \cdot C_0 \tag{9-181}$$

$$C_0 = 2C_0^2 - 1 \tag{9-182}$$

The new values for C_2, C_3, C_4, and C_5 are found using λ_p from

$$C_2 = \frac{C_0 - 1}{\lambda_p} \tag{9-183}$$

$$C_3 = \frac{C_1 - 1}{\lambda_p} \tag{9-184}$$

$$C_4 = \frac{C_2 - 0.5}{\lambda_p} \tag{9-185}$$

$$3C_5 = \frac{3C_3 - 0.5}{\lambda_p} \tag{9-186}$$

The parameters S_1, S_2, and S_3 are calculated as functions of C_1, C_2, C_3, and ψ as follows:

$$S_1 = C_1 \psi \tag{9-187a}$$

$$S_2 = C_2 \psi \tag{9-187b}$$

$$S_3 = C_3 \psi \tag{9-187c}$$

The time interval between the point corresponding to ψ and the reference epoch, t_0, is determined from Equation (9-175) to be

$$\tau(\psi) = R_0 S_1 + \sigma_0 S_2 + \mu S_3 \tag{9-188}$$

and the geocentric radius corresponding to ψ is

$$R(\psi) = | R_0 C_0 + \sigma_0 S_1 + \mu S_2 | \tag{9-189}$$

The difference between the desired time increment τ_i and $\tau(\psi)$ is

$$\Delta\tau = \tau_i - r_0 S_1(\psi) - \sigma_0 S_2(\psi) - \mu S_3(\psi) \tag{9-190}$$

The successive approximation scheme involves correcting ψ to cause $\Delta\tau$ to vanish. The finite difference form of Equation (9-171)

$$\psi_1 = \frac{t_i - t_0}{R} \qquad (\text{where } \psi \equiv 0 \text{ at } t = t_0) \tag{9-191}$$

aids in determining the iterative correction algorithm

$$\psi_{k+1} = \psi_k - \frac{\Delta\tau}{R(\psi_k)} \tag{9-192}$$

When the solution has converged, the value ψ_i that yields τ_i is obtained. Values of $S_1(\psi_i)$ and $S_2(\psi_i)$ are a by-product and are used to determine f_i and g_i by means of Equations (9-172).

Repeating the preceding process for the data times t_1, t_2, ..., t_m, the values of f_i and g_i (for $i = 1, 2, ..., m$) are obtained for substitution into Equations (9-165) and (9-166), along with data measurements $\bar{R}_1$, $\bar{R}_2$, ... $\bar{R}_m$. These equations yield new estimates of $\bar{R}_0$ and $\bar{\dot{R}}_0$ to commence the next iteration. This computational sequence is shown schematically in Figure 9-4.

9.4 REFERENCES

1. Smith, R., and Huang, C.: 1985, *Study of a Homotopy Continuation Method for Early Orbit Determination With the Tracking and Data Relay Satellite System (TDRSS)*, Computer Sciences Corporation Report CSC/TM-85/6712, June 1985.

2. Escobal, P. R.: 1965, *Methods of Orbit Determination*, John Wiley and Sons, New York.

3. Goodyear, W. H.: 1966, *A General Method for the Computation of Cartesian Coordinates and Partial Derivatives of the Two-Body Problem*, NASA Report NASA-CR-522, September 1966.

4. Cappellari, J. O., Jr., Shanklin, R. E., Jr., and Smith, E. J.: 1983, *Preliminary Orbit Computation System Mathematical Specifications*, Computer Sciences Corporation Report CSC/SD-83/6069, September 1983.

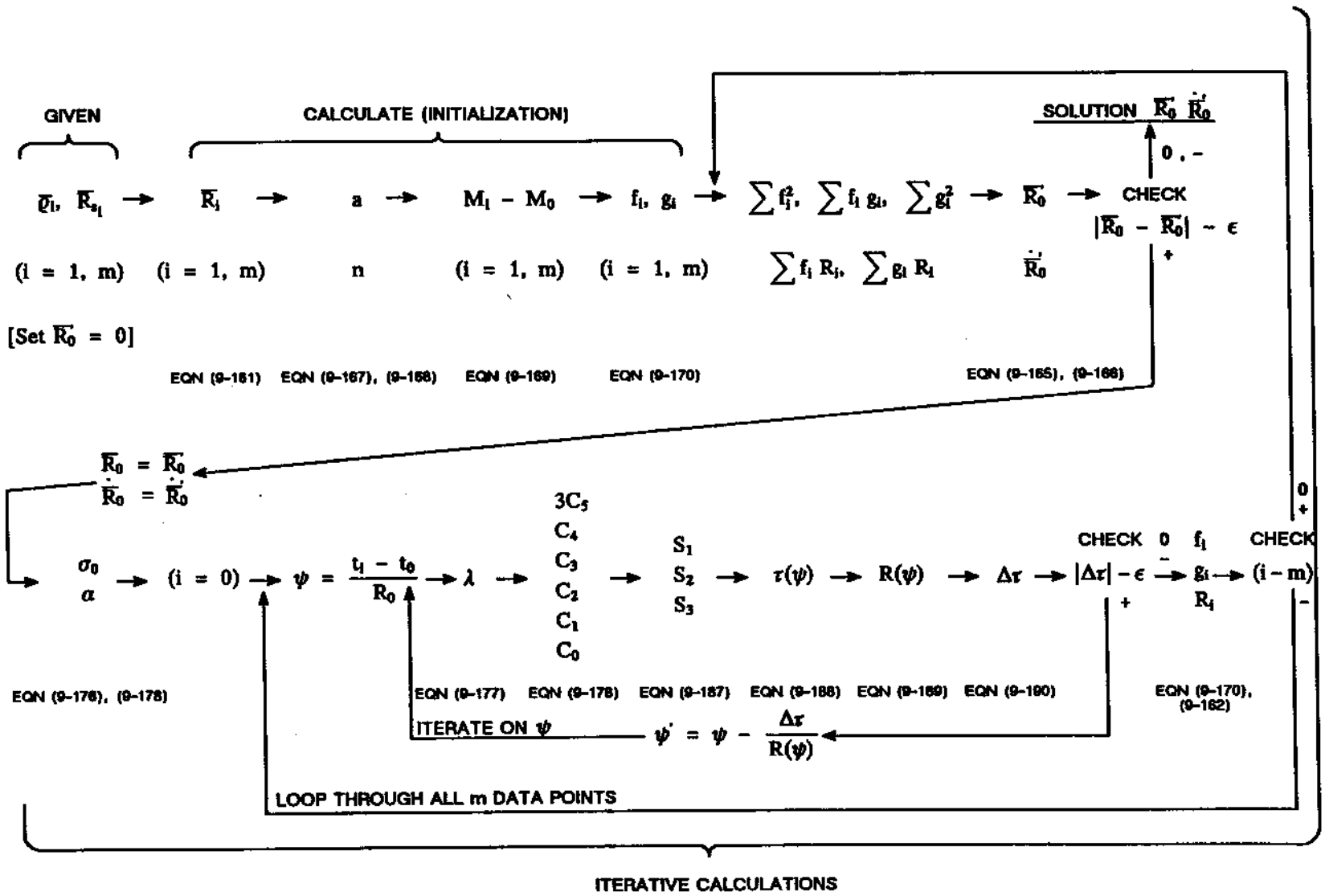

Figure 9-4. Range and Angles Method Computational Sequence

APPENDIX A—TRAJECTORY SENSOR SYSTEMS FUNCTIONAL DESCRIPTIONS AND PREPROCESSING

The trajectory sensor systems measure the various propagation characteristics of electromagnetic or optical signals transmitted between the satellite and tracking stations (or other reference sources). These data are subsequently used to determine the satellite trajectory. The dependence of these measurements upon the relative states of the spacecraft provides the key to the orbit determination process.

This appendix provides a brief functional description of the trajectory sensing systems currently included in GTDS. It also describes the procedures followed in preprocessing the data prior to GTDS processing. (More detailed descriptions are available in References 1 and 2.) The computations given in these descriptions are independent of GTDS and are presented primarily for informational purposes. However, they do provide an insight to the condition of the data at the preprocessor/processor interface which is necessary to understand the processor measurement models described in Chapter 7.

A.1 GODDARD RANGE AND RANGE-RATE (GRARR) SYSTEM AND APPLICATIONS TECHNOLOGY SATELLITE RANGING (ATSR) SYSTEM (No Longer Operational)

The functional and preprocessing descriptions for the GRARR and ATSR systems are given in the following subsections.

A.1.1 FUNCTIONAL DESCRIPTION

The GRARR System (References 1 through 7) and the ATSR System (References 1, 6, and 7) determine and record the spacecraft range, radial velocity, and angular position. The GRARR and ATSR systems are located at the tracking sites shown in Table A-4 of Reference 8. These systems transmit a continuous wave signal from the tracking station antenna at a carrier frequency, ν_T, which is modulated by a low-frequency tone, ν_L. This signal propagates to the spacecraft's omnidirectional antenna, where the received frequency, ν_v, appears to be slightly different from that transmitted (ν_T) because of the uplink Doppler shift. The received signal is modified by the spacecraft transponder electronics and retransmitted back to the ground tracking station. Again, the signal experiences a downlink Doppler shift so that the frequency, ν_R, received at the ground, differs from that transmitted to the spacecraft. The 30-foot-diameter ground receiving antenna is automatically steered through two gimbal angles, X_{30} and Y_{30} or A and E (shown in Figure A-1), to maximize the received signal strength. As the signal is processed through the ground electronics system, the spacecraft transponder modification is undone and the

transmitted carrier frequency is subtracted. At the output, the differenced Doppler signal (reflecting the uplink and downlink Doppler shifts) is modified by the addition of a bias signal of known frequency, ν_b.

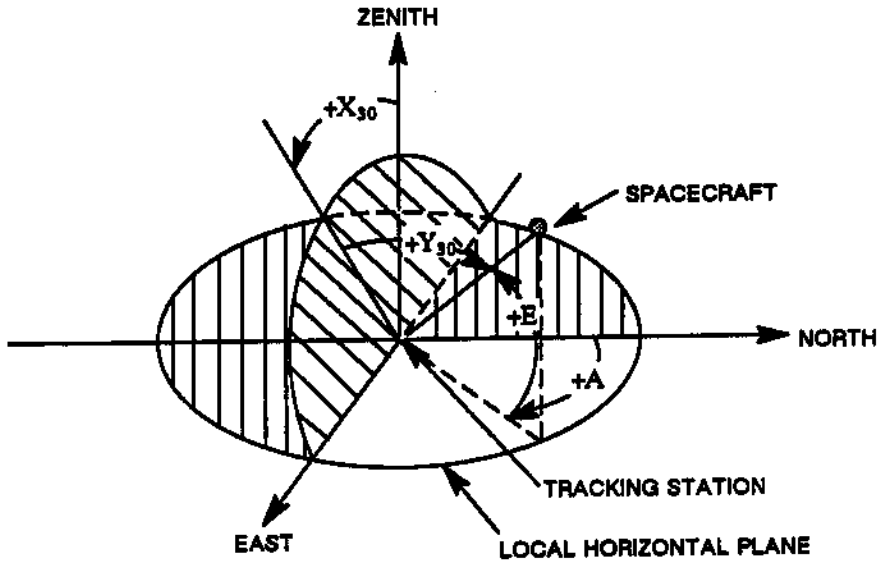

Figure A-1. Schematic of GRARR Gimbal Angles

The following three different types of measurements result from signals received during the frame time interval which begins at frame time t_F:

1. The gimbal pickoff angles, X and Y or A and E, defining the direction of the received signal path at the antenna at time t_F, are recorded in degrees and decimal fractions.

2. The two-way range time delay is measured as a count C_1 of the number of cycles of a reference frequency ν_{R_1} occurring between positive-directed zero crossings of the low-frequency ranging tone (frequency = ν_L) associated with the transmitted and received signals. The counter is started and the frame time, t_F, is signaled simultaneously by a zero crossing of the transmitted signal. The counter is stopped by the next zero crossing of the received signal. Since the lowest sidetone frequency for the GRARR System is 8 hertz, the maximum unambiguous one-way range measurement corresponds to a distance of approximately 18,787 kilometers. Distances greater than this produce phase shifts larger than one cycle of the ν_L signal. When this occurs, the GRARR System utilizes a pseudorandom binary code to determine the range ambiguity

number, ϱ_a, the number of whole cycles to be added to the counter-measured fractional phase shift. The ATSR System does not require an ambiguity resolving system since it is used only in conjunction with ATS synchronous satellites which remain in the same ambiguity period during a pass.

3. The two-way range-rate measurement is made by counting the number of cycles, C_0, of a reference frequency, ν_{R_2}, required to count exactly N cycles of the Doppler-plus-bias signal, $\nu_d + \nu_b$, in the GRARR System and 100 times $\nu_d + \nu_b$ for the ATSR System. The count also is started at the frame time, t_F, and ended after the accumulation of N cycles of the $\nu_d + \nu_b$ signal. All GRARR stations except Santiago have been modified to remove the dependency of C_0 on the independent frequencies ν_b and ν_{R_2}. The modification amounts to deriving the reference and bias frequencies from the same source as the transmitted frequency.

The gimbal angles X_{30} and Y_{30} (or A and E) are measured only at the frame time, t_F; but the range and range-rate measurements are made at the frame time and at three subsequent data sample times t_s within the frame time interval. The spacing of these data samples (and hence the timespan of a data frame) can be varied to give range and range-rate recording rates of four, two, or one samples per second or six samples per minute. ATSR stations can also record at a rate of eight samples per record. The data, one angle sample and four range and range-rate samples for each frame, are punched on paper tape at the tracking station in standard Baudot five-level teletype code and then transmitted to GSFC via teletype to be preprocessed.

A.1.2 PREPROCESSING DESCRIPTION

The GRARR and ATSR data processing procedures and interfaces are obtained from References 1 through 6 and have been revised to reflect subsequent modifications in the software. Emphasis is placed on the preprocessor computations, but the interfaces with the stations and the processor are also included. Figure A-2 summarizes the station/preprocessor/processor interfaces and provides an aid in the ensuing description.

The data are formatted into frames at the station. Each frame contains four sets of range and range-rate measurements, C_0 and C_1, as well as a single set of gimbal angles, X_{30} and Y_{30} (or A and E). Each frame is time-tagged in station time, t_R. Prior to transmission to GSFC, data calibration corrections are applied to the data, and the time tag is corrected for the propagation delay of the WWV radio signal from transmission to its reception at the tracking station, i.e.,

$$t_F = t_R + \Delta t_{WWV} \qquad \text{(A-1)}$$

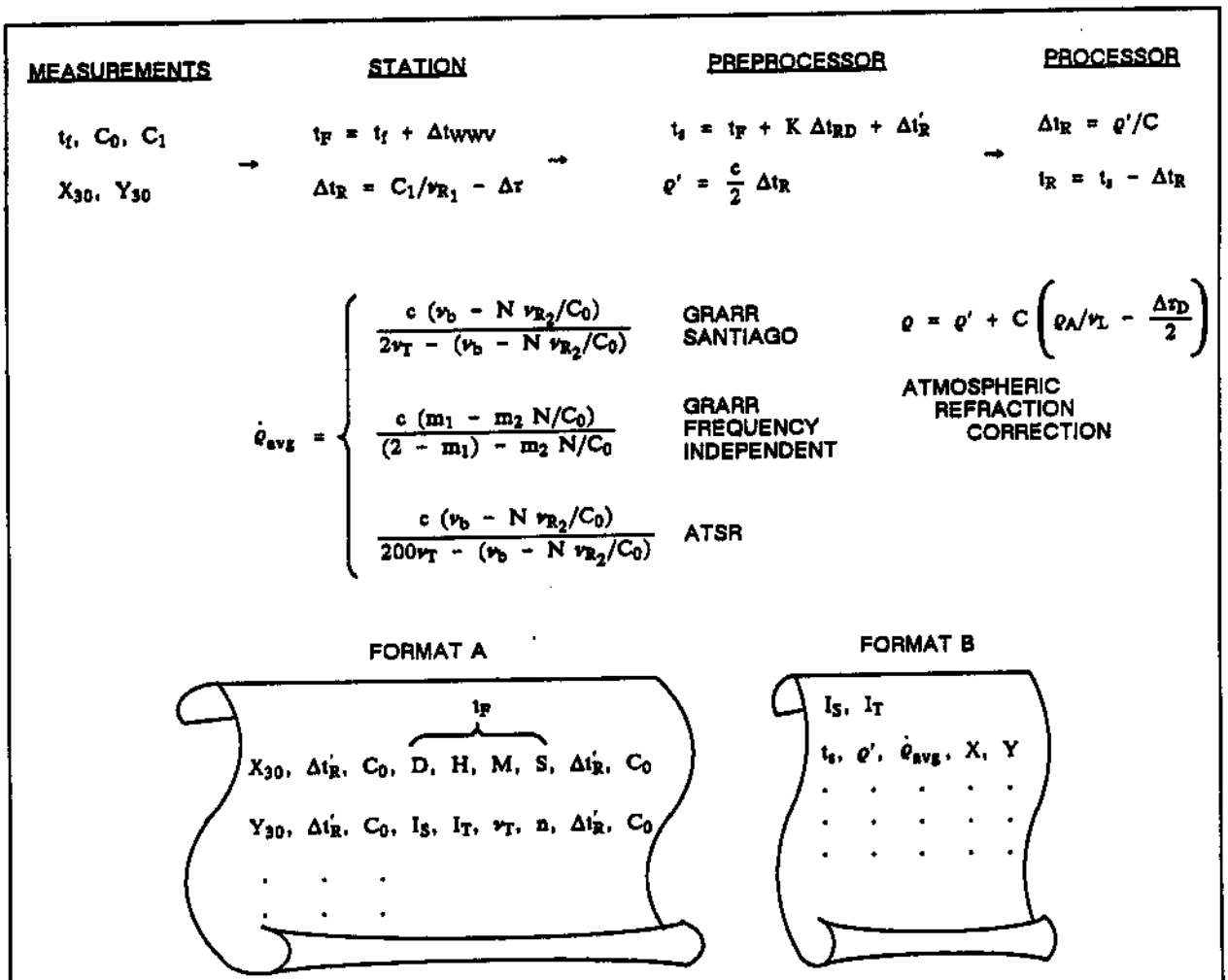

D, H, M, S = DAY, HOUR, MINUTE, AND SECONDS OF TIME t_F

I_S, I_T = SATELLITE AND TRACKER IDENTIFICATION

n = SAMPLING RATE INDICATOR

σ_A = RANGE AMBIGUITY NUMBER

ν_L = LOWEST SIDETONE FREQUENCY

$\Delta\tau$ = STANDARD TRANSPONDER DELAY ($\Delta\tau$ = 17.1 MICROSECONDS FOR VHF AND 0 FOR S-BAND) APPLIED AT THE STATION

$\Delta\tau_D$ = DEVIATION FROM THE STANDARD DELAY APPLIED IN THE PROCESSOR

Figure A-2. GRARR and ATSR Data Preprocessor Computations and Interfaces

Thus, t_F corresponds to the UTC time at initiation of the range counter. Each range measurement, C_1, is divided by the reference frequency, ν_{R_1}, thereby converting it to a time interval, Δt_R, with a standard transponder delay, $\Delta\tau$, accounted for as follows:

$$\Delta t_R = \frac{C_1}{\nu_{R_1}} - \Delta\tau \qquad \text{(A-2a)}$$

where

$$\Delta\tau = \begin{cases} \approx 0 & \text{(for S-band)} \\ \approx 17.1 \text{ microseconds} & \text{(for VHF)} \end{cases} \qquad \text{(A-2b)}$$

Each frame of data is received at GSFC in approximately the format A shown in Figure A-2 (data quality, carriage return, line feed, and figure shift indicators are omitted). These data are then preprocessed as described in the following subsections.

A.1.2.1 Gimbal Angles

The gimbal angles, X_{30} and Y_{30} ($\pm$00.00 to $\pm$90.00 degrees) or A (000.00 to 360.00 degrees) and E (000.00 to 090.00 degrees), are unaltered in the preprocessor. Atmospheric refraction corrections must be applied later in the processor.

A.1.2.2 Range

The range measurement, C_1, is corrected to the two-way propagation time interval, Δt_R, at the station. In the preprocessor, the interval is converted to one-way distance by multiplying by one-half the velocity c of the signal propagation as follows:

$$\varrho' = \frac{c}{2}\Delta t_R \qquad \text{(A-3)}$$

where c is equal to the speed of light.

The preprocessed range, ϱ', always lies in the first ambiguity period and must, therefore, be corrected for range ambiguity in the processor. Furthermore, the transponder delay is a function of the received signal frequency at the spacecraft transponder. Therefore, any deviations from the standard transponder delay deducted in the preprocessor must be accounted for in the processor. The time at each of the four range samples within each frame is

$$t_s = t_F + k\,\Delta t_{RD} \quad (k = 0, 1, 2, 3) \qquad \text{(A-4)}$$

where Δt_{RD} is the reciprocal of the recording rate.

The time t_s is the ground receive time in UTC, corresponding to each range sample. The range and gimbal angles correspond to the spacecraft's position at the time it retransmits the tracking signal. Therefore, the times must be corrected for the one-way light time in the processor. The gimbal angles correspond to the first time (i.e., k = 0 in Equation (A-4) on each frame).

A.1.2.3 Range Rate

The interpretation of the Doppler cycle count, C_0, as a measure of the tracking station-to-spacecraft relative range rate rests upon the following assumptions:

1. The Doppler effect can be adequately represented by the theory of special relativity.
2. A simplification can be made in representing the motion of the tracking station.

Assuming the tracking station motion is uniform in inertial space, it is shown in Appendix C that the average range rate (in the sense of the Theorem of the Mean) over the time interval between t_s and $t_s+\Delta t_{RR}$ is

$$\dot{\varrho}_{avg} = \frac{c\left(\nu_b - \frac{N}{\Delta t_{RR}}\right)}{2\nu_T - \left(\nu_b - \frac{N}{\Delta t_{RR}}\right)} \tag{A-5}$$

where the Doppler-plus-bias count time interval, Δt_{RR}, is

$$\Delta t_{RR} = \frac{C_0}{\nu_{R_2}} \tag{A-6}$$

Equation (A-5) is used for the GRARR station at Santiago. Since ATSR stations count N cycles of 100 times the two-way Doppler-plus-bias frequency, the range-rate equation for the ATSR station data is

$$\dot{\varrho}_{avg} = \frac{c\left(\nu_b - \frac{N}{\Delta t_{RR}}\right)}{200\nu_T - \left(\nu_b - \frac{N}{\Delta t_{RR}}\right)} \tag{A-7}$$

The average range rate, $\dot{\varrho}_{avg}$, in Equations (A-5) and (A-7) is dependent on the three frequencies ν_T, ν_b, and ν_{R_2}. Four of the GRARR stations were modified by driving ν_b and ν_{R_2} with the transmitted frequency ν_T, i.e.,

$$\nu_b = m_1 \nu_T \tag{A-8a}$$

$$\nu_{R_2} = m_2 \nu_T \tag{A-8b}$$

where m_1 and m_2 are the constants given in Table A-1.

Table A-1. GRARR Station Constants

GRARR STATIONS		m_1	m_2
Roseman	VHF crystal	1/5000	1/15
Tananarive	S-band crystal	1/3600	1/180
Carnarvon	S-band PLL*	σ/4500	σ/225
Fairbanks			

*σ = phase locked transponder multiplication constant (Reference 6)

Substituting Equations (A-8) into (A-5) yields the relation for preprocessing Doppler data from these frequency-independent GRARR stations, as follows:

$$\dot{\varrho}_{avg} = \frac{c\left(m_1 - m_2 \frac{N}{C_0}\right)}{(2 - m_1) - \left(m_2 \frac{N}{C_0}\right)} \tag{A-9}$$

A more precise modeling of the Doppler data is provided by the range difference formula in Appendix C. In this optional processing mode, the preprocessor computes

$$\dot{\varrho} = \frac{c}{2\nu_T \Delta t_{RR}} (\nu_b \Delta t_{RR} - N) \tag{A-10}$$

rather than $\dot{\varrho}_{avg}$. The processing program compares $\dot{\varrho}$ with the range difference calculated by Equation (7-41).

A.1.2.4 Smoothing

The range, range-rate, and gimbal angle data are finally smoothed by regressively fitting low-order (third or fourth) polynomials to at least 20 samples each of range and range rate and at least 5 samples each of the gimbal angles. A least-squares method is used for the polynomial fits, and a 2.5σ data rejection criterion is used to eliminate wild data. The midpoint values of the polynomials replace the original data. The smoothed values are stored in a format similar to format B shown in Figure A-2 for subsequent use in the processor.

A.2 C-BAND RADAR TRACKING SYSTEMS

The STDN C-band radar tracking systems are amplitude-comparison monopulse instrumentation systems that measure the range, azimuth, and elevation of spacecraft. The range measurement is unambiguous up to 59,926.118 kilometers.

The NASA C-band radars are of two basic types: the FPS-16 and the FPQ-6, both of which have a low-speed data rate of one per 6 seconds. In addition, there are FPQ-14, FPQ-13, FPQ-15, TPQ-18, and ALCOR C-band radars. Descriptions of all these radar types are as follows:

- **FPS-16 Radar.** This radar has a 3.6-meter diameter parabolic antenna mounted on an azimuth-elevation pedestal. The antenna reflector surface consists of wire-mesh panels supported by radial trusses. The antenna has a four-horn monopulse feed supported on a tetrapod located at the focal point of the antenna reflector.

- **FPQ-6 Radar.** This radar is a second-generation system derived from the FPS-16 and offers several major improvements: tracking capability to greater distances, greater angle tracking precision, and rapid target detection and lock-on. It has a 9-meter diameter, solid-surface, aluminum parabolic antenna with Cassegrain feed. The FPQ-6 antenna is mounted on an azimuth-elevation pedestal.

- **FPQ-14, FPQ-15, FPQ-13, and TPQ-18 Radars.** The FPQ-14 radar is similar to the FPS-16 and offers all of the improvements of the FPQ-6. The radar is computer integrated with the on-axis system. The FPQ-15 radar is functionally identical to, but differs physically from, the FPQ-14. The FPQ-13 radar is similar to the FPS-16, but has a more powerful transmitter, a 6.1-meter diameter

antenna, and is computer integrated with the on-axis system. The TPQ-18 radar is identical to the FPQ-6, except that the electronic equipment is housed in modular shelters, making the entire system transportable.

- **ALCOR Radar.** The Advanced Research Project Agency, Lincoln C-band Observable Radar (ALCOR) is a high-power, narrowbeam, coherent, and chirped C-band monopulse system capable of simultaneous skin and beacon tracking. It provides azimuth, elevation, range, and range-rate data. It has a range accuracy of 0.5 meter in narrowband mode, 0.1 meter in wideband mode, and an angle accuracy of 0.005 degree. The ALCOR has a 12.2-meter diameter parabolic antenna with a gain of 54 decibels and a beamwidth of 0.3 degree. The peak power output of the ALCOR radar is 4 megawatts, with an average power of 10 kilowatts.

The functional and preprocessing descriptions for the C-band radar tracking systems are given in the following subsections.

A.2.1 FUNCTIONAL DESCRIPTION

The pulse radars used most frequently to support NASA satellite tracking are listed in Table A-4 of Reference 8. These radars measure the two-way light time from the antenna to the spacecraft as well as the antenna pointing angles. The antenna gimballing system records the azimuth and elevation angles A and E shown in Figure A-1.

The usual mode of tracking a satellite via a C-band radar is similar to the GRARR System. The two-way light time of a transmitted pulse and associated gimbal angles are measured and time-tagged at the ground receive time of the return pulse. The range measurement is corrected for satellite transponder time delay, and the time tag is corrected for system delays and WWV propagation time delay. The resulting two-way time is converted to units of distance by multiplying by one-half the speed of light. These corrections are performed at the tracking site. There is no range ambiguity or range-rate associated with this type of system.

A.2.2 PREPROCESSING DESCRIPTION

The data received from the C-band tracking site is calibrated, corrected for transponder delay, and time corrected. The preprocessor converts the range data from yards (received from the station) to kilometers (1 meter equals 3.280839895 international feet) and the gimbal angles from mils to degrees (6400 mils equals 360 degrees). The time tag corresponds to the ground receive time.

Capability must be provided in the processor to account for atmospheric refraction and light-time correction of the time tag.

A.3 STDN RANGING EQUIPMENT (SRE) UNIFIED S-BAND (USB) AND VERY HIGH FREQUENCY (VHF) SYSTEMS

The functional and preprocessing descriptions for the SRE USB and VHF systems are given in the following subsections.

A.3.1 FUNCTIONAL DESCRIPTION

The SRE system provides sidetone ranging and coherent Doppler tracking data. The SRE operates with the wideband exciters and the wideband multifunctional receivers (MFRs). The SRE is used with both the USB and VHF systems.

The SRE VHF ranging system operates in the 136- to 155-megahertz band. This system, when measuring the range, uses either basic sidetone ranging techniques or a hybrid ranging mode that uses sidetones and a pseudorandom ambiguity resolving code (ARC). Range-rate measurements are obtained by using coherent Doppler techniques.

The USB System provides Doppler, range, and angle tracking capability, with concurrent transmission and reception of voice, command, television, and telemetry data. The SRE USB system operates in the 2025- to 2300-megahertz band and utilizes a single carrier frequency to provide tracking and communication with the spacecraft. The sidetone range measurement is independent of the Doppler measurement and is unambiguous up to a range of approximately 15,000 kilometers. A pseudorandom ARC extends the unambiguous range measurement to approximately 644,000 kilometers. The USB SRE low-speed data rate is normally one per 10 seconds.

The USB System (References 1, 2, 4, 7, and 9) determines and records the spacecraft range, range-rate, and antenna gimbal angle positions at the globally located tracking sites listed in Table A-4 of Reference 8. The USB System transmits a continuous S-band carrier signal with a modulated pseudorandom code. The nominal uplink signal frequency of 2 gigahertz is multiplied by a constant ($k = 240/221$) at the coherent spacecraft transponder and is retransmitted to the receiving stations.

The USB System range measurement is made by means of an autocorrelation involving a pseudorandom code, which is modulated onto the S-band uplink carrier and coherently turned around by the transponder. The locally generated code at the ground station undergoes a variable delay when compared with the received code, which has undergone a two-way propagation delay. When the inserted ground station delay equals the two-way propagation delay, the autocorrelation has a maximum value and the inserted ground time delay is a measure of the slant range.

With the long code or normal pseudorandom noise code, the USB range measurement is unambiguous to a range of 958,000 kilometers. However, the range word readout size

limits the maximum range readout to 644,000 kilometers. Normally, only one such range acquisition is made over a single tracking station, and subsequent range readouts are obtained by updating the initial measurement by integrating a clock Doppler signal. That is, once range acquisition is made, the ranging code is switched off and a clock modulation is switched on. The relative phase change of the clock signal, as relayed via the spacecraft, is then a measure of the range change.

As presently configured, the clock is not an integral submultiple of the carrier frequency; however, the smallest increment of range change in the tracking format (termed the range unit (RU)) corresponds to approximately 16 cycles of two-way carrier Doppler change. Thus, whenever the vehicle moves a radial distance of approximately 16 half-wavelengths of the carrier frequency relative to the ground station, one RU is recorded. One RU corresponds to 1.0496936 meters of range. The range update is done at the tracking site and, from an equipment standpoint, is essentially independent of the carrier Doppler tracking information which is also contained in the raw USB data format. Only the receiver radio frequency and intermediate frequency stages are common to the range and range-rate channels.

The raw time tag associated with the range corresponds to the UTC ground receive time and includes an onsite correction for the WWV propagation time delay. Typically, all USB remote site clocks are synchronized to the U.S. Naval Observatory master clock to within 50 microseconds. The USB dish antennas employ an X-Y gimbal mounting system (see Figure A-1). The 30-foot diameter antennas employ an X_{30} axis aligned north-south, whereas the 85-foot antenna X_{85} axis is aligned east-west. The X axis is always contained in the local tangent plane.

The basic measurement of the range rate in the USB System is that of carrier frequency Doppler phase change. The downlink carrier from the spacecraft is coherently tracked by a phase-locked ground receiver. The essential system functions are the following:

1. The uplink carrier has a nominal fixed frequency of 2 gigahertz derived from a cesium clock source.

2. The transponder receiver onboard the spacecraft is phase-locked to the uplink frequency plus the uplink Doppler shift.

3. The transponder transmitter frequency is coherently derived from the uplink carrier plus uplink Doppler shift. A fixed frequency turnaround ratio of 240/221 is used for all USB tracking.

4. The ground receiver is phase-locked to the downlink signal, which is at the transponder output frequency plus the downlink Doppler frequency shift.

5. In the two-way mode, a 1 megahertz signal is subtracted from the ground receiver signal prior to comparison with a signal that is coherent with the

transmitted carrier frequency. The basic output is then the Doppler frequency plus a stable 1 megahertz bias.

The raw data consist of whole cycle counts of the phase change, which is a direct measure of the spacecraft radial change relative to the station. The basic measurement N is a nondestruct cycle count of the carrier phase shift plus bias over a time period Δt_{RR}. It is termed nondestructive since, although the counter is read out at even time intervals, the accumulated count is not destroyed. Thus, the average frequency is obtained by differencing the count in adjacent frames and dividing by the sample time.

The Doppler count, N, is resolved to 0.01 cycle through the implementation of the Time Increment Resolver (TIR). Cycle resolving gives a precise measure of the time between the start of the data interval and the time at which the last positive-directed zero crossing of the biased Doppler signal is counted. This time duration is measured by counting the cycles of a 100-megahertz oscillator. The Doppler count, along with the TIR count, will appear in the same data transmission frame. In the high-speed format, the granularity of the TIR is 10 nanoseconds; while in the low-speed format, the granularity is 40 nanoseconds.

The normal low-speed data rates of the USB System are one frame per six seconds and one frame per 10 seconds. The low-speed data are derived onsite from the high-speed data, which are in a 240-bit format. High-speed data are simultaneously available at a rate of 10 frames per second, 5 frames per second, or 2.5 frames per second, depending on the operator selection at the onsite USB data processor. USB sites are capable of obtaining gimbal angle and range-rate data without ranging, in contrast with the GRARR System, which always provides range data.

A.3.2 USB PREPROCESSING DESCRIPTION

The USB range data are transmitted from the sites in octal, with a granularity of 1.0496936 meters. The output of the data handler is the one-way range in kilometers with no data corrections applied.

The N-count and TIR required to compute the range rate are transmitted in octal with a granularity of 1 cycle and 40 nanoseconds, respectively. The one-way and three-way Doppler data are converted to range rate in kilometers per second through the following equations:

$$FOC = \left[\frac{N(t) - N^*(t - \Delta t_{RR})}{\Delta t_{RR}}\right] 4\, C(t)\, (10^{-8}) \qquad \text{(A-11)}$$

$$N^*(t) = N(t) - FOC \qquad \text{(A-12)}$$

$$\dot{\varrho}_{avg} = \left[\frac{N^*(t) - N^*(t - \Delta t_{RR})}{\Delta t_{RR}} - 10^6\right]\left(\frac{c}{2K\,\nu_T}\right) \qquad \text{(A-13)}$$

where

FOC = fractions of a cycle
N(t) = contents of the Doppler counter at time t
$N^*(t)$ = Doppler counter at time t corrected by TIR
C(t) = contents of the TIR counter
Δt_{RR} = sample interval of the Doppler counter
$\dot{\varrho}_{avg}$ = average range rate
c = speed of light
K = transponder turnaround ratio (240/221 for USB)
ν_T = transmitter frequency

The angular measurements are the X and Y gimbal angles, with the 85-foot sites having the $\hat{X}$ axis aligned east-west and the 30-foot sites having the $\hat{X}$ axis aligned north-south. The data are transmitted in octal with a granularity of 6.8664×10^{-4} degree. The data handler outputs the angles in radians.

The time tag associated with all USB angle data is the ground receive time, corrected onsite for WWV propagation delay.

A.4 MINITRACK SYSTEM (No Longer Operational)

The functional and preprocessing descriptions for the Minitrack System are given in the following subsections.

A.4.1 FUNCTIONAL DESCRIPTION

The Minitrack System (References 1, 7, 10, and 11) is basically a radio direction finder which utilizes the interferometer principle to locate a radiating transmitter carried by a spacecraft. The Minitrack network is composed of seven stations, globally located as listed below:

- Quito, Equador
- Santiago, Chile

- Winkfield, England
- Johannesburg, South Africa
- Fairbanks, Alaska
- Orroral Valley, Canberra, Australia
- Tananarive, Malagasy Republic

Each system consists of a series of six horizontal baselines at each station, three oriented east-west (EW) and three oriented north-south (NS), as shown in Figure A-3a. A fixed antenna system is located at each end of each baseline to receive a nominal 136-megahertz signal transmitted continuously from a spacecraft as it passes within view of each station. The spacecraft transmitter frequency can be preset to any of 2000 frequencies between 136.000 and 137.999 megahertz in steps of 1 kilohertz. Each set of three EW or NS baselines consists of a fine, medium, and coarse baseline. The fine baselines are accurately surveyed to be 46 or 57 times the vacuum wavelength of the nominal 136 megahertz signal. The medium and coarse baselines are 4.0 and 3.5 nominal wavelengths, respectively.

The principle underlying the Minitrack System is illustrated by the following simplified two-dimensional case (see Figure A-3b). The spacecraft transmitter is assumed to be located at an elevation angle α and at a very large distance from the station so that received signals appear to be planar wavefronts, e.g., BC and B′C′. The baseline distance AB is a multiple N_B of the nominal 136 megahertz vacuum wavelength. At any given instant, the phase of the signal along the propagation paths AC′ and BB′ is characterized by the two sinusoids shown in Figure A-3b.

The separate signals received by the two antennas at A and B are fed into a phase counter which measures the phase difference between the two signals, normalized to a fractional part of the received signal wavelength, e.g., a_F in the figure. This measurement gives no information concerning the additional number of whole wavelengths that occur between the signal received at antenna A and the signal received at antenna B. This ambiguous integral number, as well as the fractional phase displacement itself, is dependent upon the wavelength of the received signal, λ, the length of the baseline, N_F, and the spacecraft angular geometry, α. Thus, the reason for the multiplicity of parallel baselines (i.e., 46 or 57, 4- and 3.5-wavelength bases) is to resolve the integral cycle count ambiguity on the longer (fine) baseline. This resolution is accomplished by synthesizing a 0.5-wavelength measurement by differencing the 4.0- and 3.5-wavelength baseline phase difference measurements, i.e.,

$$\underline{a}_{0.5} = a_{4.0} - a_{3.5} \qquad \text{(A-14)}$$

where $\underline{a}$ indicates the absolute phase difference.

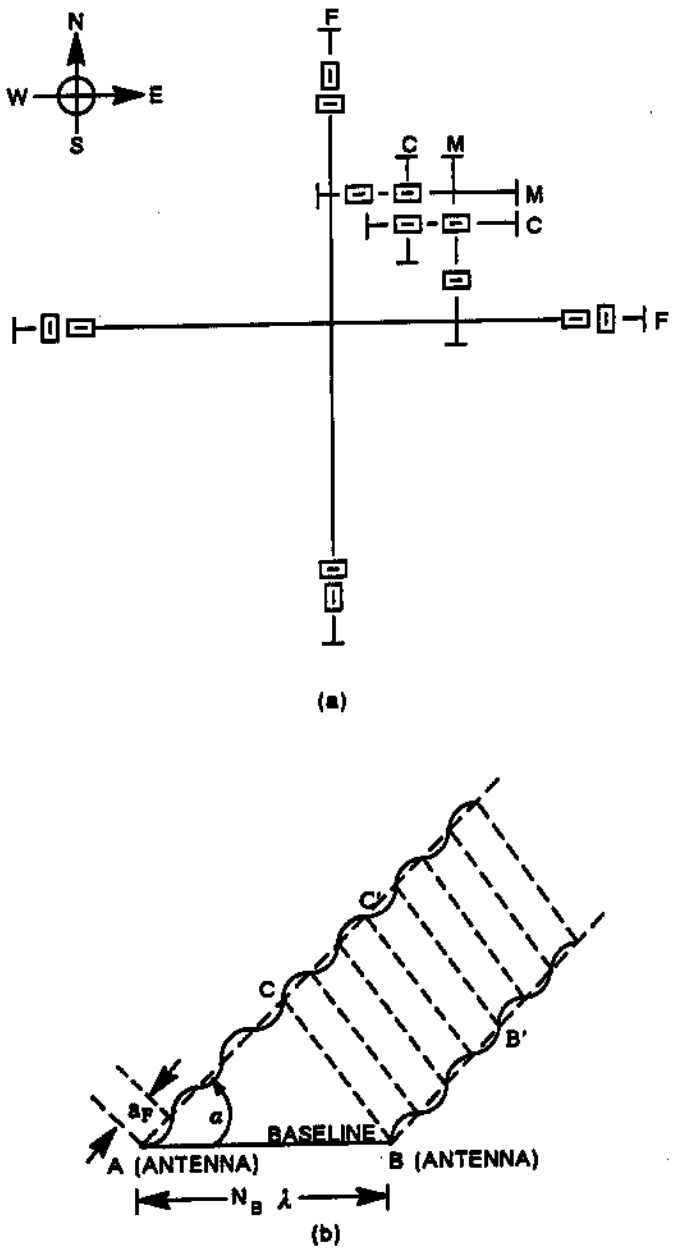

Figure A-3. Minitrack Baseline and Signal Reception Geometry

It would be impractical to build a 0.5-wavelength baseline, since the antennas would physically interfere with each other. The synthesized 0.5-wavelength phase difference, $\underline{a}_{0.5}$, is unambiguous since the extra path length, corresponding to AC in Figure A-3b, is less than one wavelength. By similarity of triangles in the figure, the absolute length of the path AC can be estimated from the 0.5-wavelength value as follows:

$$\underline{a}_F = \frac{N_F}{0.5} \underline{a}_{0.5} \tag{A-15}$$

where $N_F = 46$ or 57

In practice, $\underline{a}_{0.5}$ is not precise enough to be used directly to obtain $\underline{a}_F$. Therefore, a slightly more complicated process is used to determine the unambiguous fine phase difference, $\underline{a}_F$. Knowing $\underline{a}_F$, the direction cosine is

$$\cos \alpha = \frac{AC}{AB} = \frac{\underline{a}_F}{AB} \tag{A-16}$$

For the three-dimensional case, the corresponding ratios obtained from the EW and NS phase difference measurements yield the direction cosines ℓ and m of the signal path at the station.

Each fine baseline has its own phase difference counter; hence, two measurements (EW and NS) are recorded simultaneously. The four ambiguity baselines (EW and NS, medium and coarse baselines) share a single counter through a multiplexed digital recording system. Since all measurements cannot be made simultaneously, the sequence of recordings for each data frame occurs according to the schedule of Table A-2. These data can be recorded at the rate of one frame every 1, 2, 10, 20, or 60 seconds. The fine baseline counter registers a decimal number between 0.000 and 0.999, and the medium and coarse baseline counter registers a decimal number from 0.00 to 0.99.

The frame rate is generally scheduled so that 31 frames give complete coverage of the usable data for a spacecraft pass over a station. A message consisting of up to 31 frames is punched on paper tape at the tracking station in standard Baudot five-level teletype code and transmitted via teletype to GSFC for preprocessing.

A.4.2 PREPROCESSING DESCRIPTION

The Minitrack preprocessing procedures and interfaces are obtained from References 10 and 11 and have been revised to reflect subsequent modifications to the software. Figure A-4 summarizes the station/preprocessor/processor interfaces and provides an aid in the following description.

Table A-2. Minitrack Counter Sequence

TIME REGISTERED BY MINITRACK DATA CLOCK	INITIATION OF BOTH FINE BASELINE COUNTERS	INITIATION OF AMBIGUITY COUNTER AND BASELINE SAMPLED
t_F*	X	EW medium
t_F + 0.2 second	X	EW coarse
t_F + 0.4 second	X	NS medium
t_F + 0.6 second	X	NS coarse
t_F + 0.8 second	X	

*t_F = UTC at the beginning of the frame

At the Minitrack station, the fine, medium, and coarse phase difference measurements are sampled and recorded in frames, as described in Section A.4.1. The time tag, t_F, for each frame is corrected at the station for the propagation delay of the WWV signal from transmission to reception at the tracking station. Thus, t_F corresponds to UTC time at the beginning of each frame. Each frame of data is transmitted to GSFC in approximately format A shown in Figure A-4 (the data signal) (strength indicators are omitted). These data are then preprocessed by rectifying the shift in whole cycle counts between consecutive fine, medium, and coarse phase difference measurements and then least-square fitting low-order polynomials to the data. Electronic system filter delays are corrected in the polynomial time variable, and calibration corrections are applied to the data.

The ambiguity correction for the fine phase data is determined from the medium and coarse data. At each output time, a 0.5-wavelength baseline phase difference, $\underline{a}_{0.5}$, is synthesized from the 4.0-wavelength baseline (medium) data, $a_{4.0}$, and the 3.5-wavelength baseline (coarse) data, $a_{3.5}$. The medium and coarse data are obtained from the smoothing polynomial previously determined.

Because of its short baseline, the synthesized 0.5-wavelength baseline data is an absolute (unambiguous) phase difference (the underscore denotes absolute phase difference). Were it not for inaccuracies in $\underline{a}_{0.5}$, it could be used to determine the ambiguity correction for the fine data. To minimize the amplification of these measurement inaccuracies, $\underline{a}_{0.5}$ is used to correct the ambiguities in $a_{3.5}$ and $a_{4.0}$, which are then used to synthesize $a_{7.5}$, corresponding to a fictitious 7.5-wavelength baseline reading. Finally, $\underline{a}_{7.5}$ is used to correct the ambiguity in the 46- or 57-wavelength baseline fine data. This stepping process is described mathematically in Section A.4.2.3.

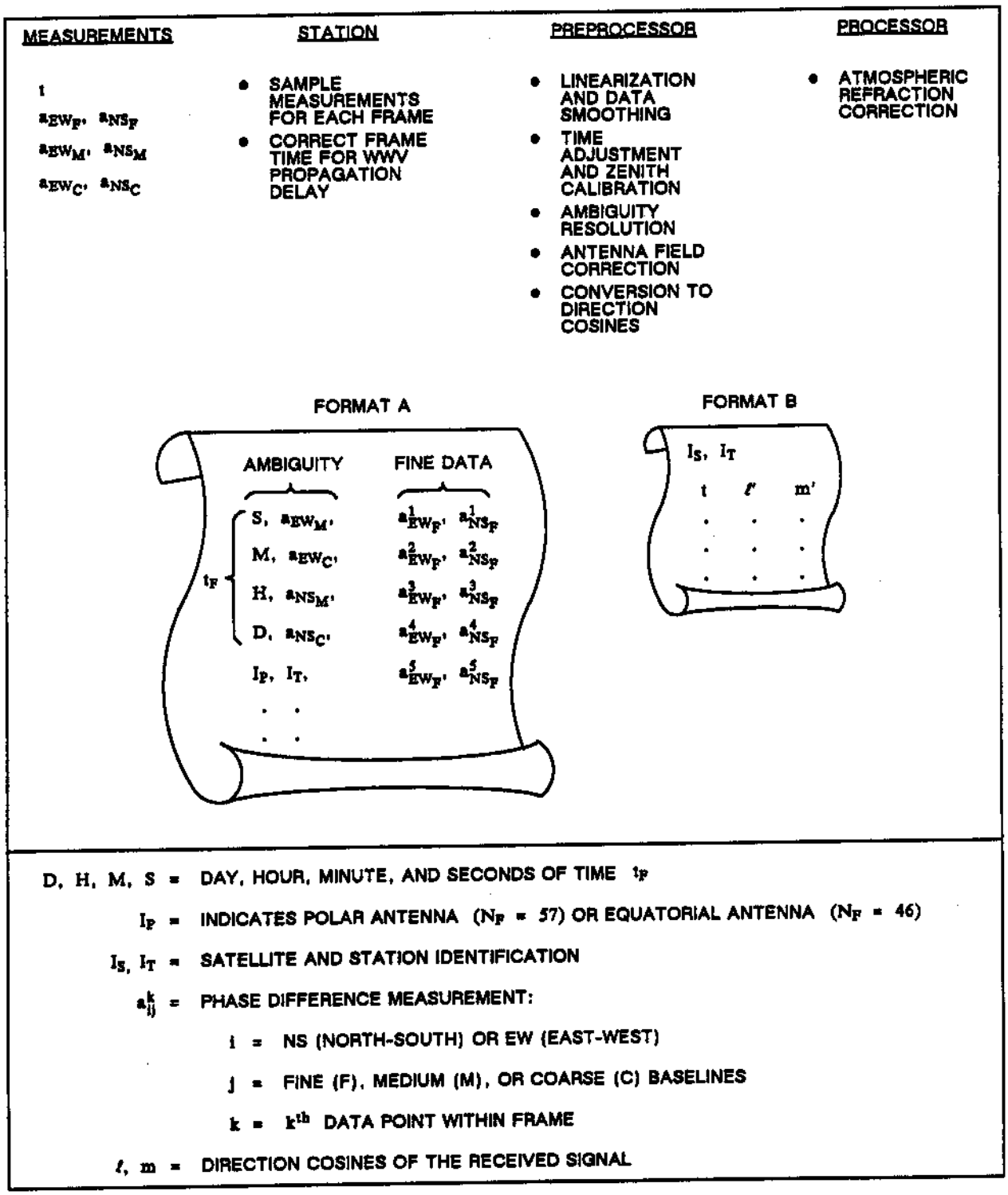

Figure A-4. Minitrack Preprocessor and Interface Schematic

At each output time, the absolute fine phase difference data are corrected for antenna field corrections and converted to direction cosines for use in subsequent processing. Data at different output times from the same station are correlated by means of the smoothing polynomials, which are used to replace the actual measurements.

The preprocessing steps summarized above are described in more detail in the following subsections.

A.4.2.1 Data Linearization and Smoothing

As stated in Section A.4.1, up to 31 frames of data are recorded for each spacecraft pass over a station. Each frame of data contains five fine, one medium, and one coarse baseline phase-difference measurements from each east-west (EW) and north-south (NS) baseline set. Thus, up to 155 fine, 31 medium, and 31 coarse baseline measurements are recorded from each of the EW and NS baseline sets for each spacecraft/station pass.

The fine phase difference counters register only from 0.000 to 0.999. Therefore, it is possible that the absolute value of the difference between consecutive readings can be numerically larger than 0.500. This is assumed to mean that a new cycle crossing occurred between measurements and that the measured data should be rectified by adding or subtracting a full cycle count to one of the points. This process of rectifying the data by converting to nonmodular number sets is called linearization.

A.4.2.1.1 Ambiguity Data

The ambiguity data (medium and coarse baselines) are linearized first since it is less likely that the phase difference will exceed ± 0.50 between consecutive points with these data. The linearization is accomplished as follows:

1. Beginning with the first phase difference measurement, the difference between consecutive points is calculated, i.e.,

$$\delta_i = a_{i+1} - a_i \tag{A-17}$$

2. If δ_i lies within the range $-0.500 < \delta_i < 0.500$, no rectification is necessary. If $\delta_i \geq 0.500$, then integer multiples of 1.000 are subtracted from a_{i+1} until δ_i lies within the range $-0.500 < \delta_i < 0.500$. If $\delta_i \leq -0.500$, then integer multiples of 1.000 are added to a_{i+1} until δ_i lies within the range $-0.500 < \delta_i < 0.500$.

3. The index i is then updated and steps 1 and 2 are repeated until all phase difference measurements have been rectified.

This linearization process is applied separately to each of the EW and NS medium and coarse baseline data sets. The components of the resulting data vectors, $\bar{b}_{EW_M}$, $\bar{b}_{NS_M}$, $\bar{b}_{EW_C}$, and $\bar{b}_{NS_C}$, have the correct relative phase, but the vectors may have an incorrect absolute phase.

After linearizing the medium and coarse baseline data, quadratic smoothing polynomials are least-squares fitted to each of the four data sets. The polynomials are of the form

$$b_n = A_n + B_n \tau + C_n \tau^2 \qquad \text{(A-18a)}$$

where

$$n = EW_M,\ EW_c,\ NS_M,\ NS_c \qquad \text{(A-18b)}$$

and τ is the time measured from t_{FM}, the frame time of the midframe (middle frame of the data sets), i.e., $\tau = t - t_{FM}$. When the polynomial coefficients are determined, the ambiguity data are tagged at their frame times; thus, each of the polynomials is biased in time by the multiplexer time delay. The multiplexer time delay is accounted for later when the polynomial is evaluated. Ambiguity data exhibiting unusually large deviations from the smoothing polynomials are rejected during the fitting process.

A.4.2.1.2 Fine Data

The linearization procedure for the fine baseline data is somewhat more complicated than for the ambiguity data, since the phase change between data in successive frames can exceed one cycle. Therefore, an approximation to the EW and NS data phase change is estimated as follows, using the fine phase rate, $\dot{\bar{a}}_F$:

$$\delta_i = a_{i+1} - a_i - \dot{\bar{a}}_F(t_{i+1} - t_i) \qquad \text{(A-19)}$$

The fine phase rate is determined by averaging the ratioed slopes of the medium and coarse smoothing polynomials at the middle frame time, t_{FM},

$$\dot{\bar{a}}_F = \frac{N_F}{2}\left(\frac{B_C}{3.5} + \frac{B_M}{4.0}\right) \quad (N_F = 46 \text{ or } 57) \qquad \text{(A-20)}$$

The quantities B_C and B_M are the coarse and medium phase rates from Equation (A-18) at the middle frame time, i.e., $\tau = 0$.

The fine phase linearization is accomplished as described in Steps 1, 2, and 3 in the preceding section but using the estimated difference given by Equation (A-19). The components of the resulting data vectors, $\bar{b}_{EW_F}$ and $\bar{b}_{NS_F}$, have the correct relative phase, but the vectors may have an incorrect absolute phase.

After linearizing the fine baseline data, their time tags, t_s, are computed for the appropriate sequential position within each frame by accounting for sequencer delay, Δt_P, and for the counter delay in the phase readout digitizing equipment, Δt_c, as follows:

$$t_s = t_F + \Delta t_P + \Delta t_c \qquad \text{(A-21a)}$$

where

$$\Delta t_P = 0,\ 0.2,\ 0.4,\ 0.6,\ 0.8 \qquad \text{(A-21b)}$$

depending on the relative position of the data point within its frame (see Table A-2), and

$$\Delta t_c = 0.01\, a_F \qquad \text{(A-21c)}$$

Cubic smoothing polynomials are then least-squares fitted to the linearized and time corrected EW and NS fine baseline data. The polynomials are of the form

$$b_m = A_m + B_m \tau_m + C_m \tau_m^2 + D_m \tau_m^3 \qquad (m = EW_F,\ NS_F) \qquad \text{(A-22)}$$

where τ_m is the time measured from the middle point of each data set. The NS and EW midpoint times, t_{M_m}, can differ due to the correction Δt_c. Fine data exhibiting large deviations from the smoothing polynomials are rejected during the fitting process.

A.4.2.2 Time Adjustment and Zenith Calibration

The four ambiguity polynomials and two fine baseline polynomials, in Equations (A-18) and (A-22), are inconsistent in terms of their time variables. The ambiguity polynomials neglect sequencer delay and use a reference time equal to the midframe time, t_{FM}. The fine polynomials use a reference time equal to the time of the midpoint, t_{M_m}, of each data set. Neither of the polynomials accounts for the delays between the time the signal is received at the antennas and the times the phase differences are sampled and tagged, nor do they account for calibrations in the phase difference measurements.

These discrepancies are accounted for by making the following corrections to the fine baseline smoothing polynomials:

$$b_m = [A'_m] + B_m \tau_m + C_m \tau_m^2 + D_m \tau_m^3 \qquad \text{(A-23)}$$

where

$$A'_m = A_m - Z_m \qquad \text{(A-24)}$$

$$\tau_m = t - t^*_m \qquad \text{(A-25)}$$

$$t^*_m = t_{M_m} + \frac{KF_m}{1000} + KI - 0.4 \qquad (m = EW_F, NS_F) \qquad \text{(A-26)}$$

The correction terms are defined as follows:

- Z_m = zenith calibration constant that accounts for internal system changes such as aging and maintenance of electronic components, phase shifts caused by antennas and feed lines, and unequal lengths of cable connecting the antenna pairs
- KF_m = delay of approximately 36 milliseconds caused by the fine filter
- KI = delay of 0.120 second due to the optional 2-hertz bandwidth filter when it is used

The 0.4-second delay in Equation (A-26) accounts for the difference between the time of the middle point, t_{M_m}, and the midframe time, t_{FM}. This term shifts the reference time of the fine polynomials to that of the corrected midframe time. The notation [ ] denotes that the integer part of the number is truncated, leaving only the fractional part. This transforms the phase difference to the first ambiguity period at the reference time.

The ambiguity polynomials are corrected for sequencer and 2-hertz filter delay, their reference times are made equal to those of the fine polynomials, and calibration corrections are applied as shown in the following equations:

$$b_n = [A'_n] + B_n \tau + C_n \tau^2 \qquad \text{(A-27)}$$

where

$$A_n' = A_n + B_n (t_m^* - t_n^*) + C_n (t_m^* - t_n^*)^2 - Z_n \quad \text{(A-28)}$$

$$\tau = t - t_m^* \quad \text{(A-29)}$$

$$t_n^* = t_{FM} + \Delta t_d \quad \text{(A-30)}$$

and

$$m = EW_F \text{ for } n = EW_M \text{ or } EW_C$$
$$m = NS_F \text{ for } n = NS_M \text{ or } NS_C$$

The correction terms are defined as follows:

Z_n = same as Z_m above

Δt_d = correction due to sequencer delay, plus a 0.15-second delay due to a 2-hertz bandwidth filter in the digital recording system,

$$\Delta t_d = \begin{cases} -0.15 \text{ for EW medium} \\ 0.15 \text{ for EW coarse} \\ 0.25 \text{ for NS medium} \\ 0.45 \text{ for NS coarse} \end{cases} \quad \text{(A-31)}$$

The first three terms on the right in Equation (A-28) account (approximately) for the shift in reference time of the ambiguity polynomials.

A.4.2.3 Ambiguity Resolution

The time adjusted and calibrated smoothing polynomials provide the proper relative phase difference (time variation). The phase difference magnitudes are reduced to the first ambiguity period when the constant terms A_n' ($n = EW_F, EW_M, EW_C, NS_F, NS_M, NS_C$) are reduced to their fractional parts in Equations (A-23) and (A-27). Since the time variation of the polynomials is proper, the coefficients B_n, C_n (and D_n for fine polynomials) are

correct and only A_n' needs to be altered to accommodate the ambiguity resolution. Furthermore, $A_n' = b_n\ (\tau = 0) = b_n^*$ is the smooth, time-corrected, and calibrated ambiguous phase difference at approximately the midframe time.

The stepping process, summarized at the beginning of Section A.4.2 and described in detail in References 10 and 11, is then performed to determine the absolute phase differences of the fine baseline polynomials. Throughout the following description, [ ] denotes the fractional part only, and { } denotes the minimum phase difference, i.e., $-0.500 < \{\ \} < 0.500$.

The absolute phase difference for a fictitious north-south and east-west 0.5-wavelength baseline is determined from the medium (4.0-wavelength) and coarse (3.5-wavelength) baseline relative phase differences $b_{4.0}^*$ and $b_{3.5}^*$ as follows:

$$\underline{b}_{0.5} = \{[b_{4.0}^* - b_{3.5}^*]\} \tag{A-32}$$

The absolute phase differences for the medium and coarse baselines are obtained as follows:

$$\underline{b}_{3.5}' = 7\,\underline{b}_{0.5} \tag{A-33}$$

$$\underline{b}_{3.5} = \underline{b}_{3.5}' - \{[\underline{b}_{3.5}' - b_{3.5}^*]\} \tag{A-34}$$

$$\underline{b}_{4.0}' = 8\,\underline{b}_{0.5} \tag{A-35}$$

$$\underline{b}_{4.0} = \underline{b}_{4.0}' - \{[\underline{b}_{4.0}' - b_{4.0}^*]\} \tag{A-36}$$

The absolute phase difference for a fictitious 7.5-wavelength baseline is determined from the absolute medium and coarse data $\underline{b}_{4.0}$ and $\underline{b}_{3.5}$, as follows:

$$\underline{b}_{7.5} = \underline{b}_{3.5} + \underline{b}_{4.0} \tag{A-37}$$

Finally, the absolute phase difference for the fine baseline is determined from the absolute 7.5-wavelength baseline data, as follows:

$$\underline{b}_F' = \underline{b}_{7.5}\left(\frac{N_F}{7.5}\right) \tag{A-38}$$

$$\underline{b}_F = \underline{b}'_F - \{[\underline{b}'_F - b^*_F]\} \tag{A-39}$$

The above process is performed for both EW and NS baseline data. The resulting EW and NS fine baseline absolute phase difference polynomials are

$$\underline{b}_m(\tau) = \underline{b}_m(\tau = 0) + B_m \tau + C_m \tau^2 + D_m \tau^3 \quad (m = EW_F, NS_F) \tag{A-40}$$

where

$$\tau = t - t^*_m \quad (m = EW_F, NS_F) \tag{A-41}$$

A.4.2.4 Antenna Field Correction

The calibration Z_n given in Equation (A-28) is determined as an average over the usable antenna field. There are distortions in the field patterns, however, and they are corrected by the following calibration polynomials operating on the corrected absolute phase differences, $\underline{b}_{NS_F}$ and $\underline{b}_{EW_F}$, obtained from Equation (A-40). These corrections are of the form

$$\begin{aligned}\begin{bmatrix}\underline{b}_{EW_F}\\ \underline{b}_{NS_F}\end{bmatrix}_{\text{corrected}} = {} & \begin{bmatrix}C_1\\ C_2\end{bmatrix} + \begin{bmatrix}C_3 & C_5\\ C_4 & C_6\end{bmatrix}\begin{bmatrix}\underline{b}_{EW_F}\\ \underline{b}_{NS_F}\end{bmatrix} + \begin{bmatrix}C_7\\ C_8\end{bmatrix}\underline{b}_{EW_F}\,\underline{b}_{NS_F}\\ & + \begin{bmatrix}C_9 & C_{11}\\ C_{10} & C_{12}\end{bmatrix}\begin{bmatrix}\underline{b}^2_{EW_F}\\ \underline{b}^2_{NS_F}\end{bmatrix} + \begin{bmatrix}C_{13} & C_{15}\\ C_{14} & C_{16}\end{bmatrix}\begin{bmatrix}\underline{b}^3_{EW_F}\\ \underline{b}^3_{NS_F}\end{bmatrix}\\ & + \begin{bmatrix}C_{17} & C_{19}\\ C_{18} & C_{20}\end{bmatrix}\begin{bmatrix}\sin(2\pi\,\underline{b}_{EW_F})\\ \sin(2\pi\,\underline{b}_{NS_F})\end{bmatrix} + \begin{bmatrix}C_{21} & C_{23}\\ C_{22} & C_{24}\end{bmatrix}\begin{bmatrix}\cos(2\pi\,\underline{b}_{EW_F})\\ \cos(2\pi\,\underline{b}_{NS_F})\end{bmatrix}\end{aligned} \tag{A-42}$$

where the coefficients C_i are obtained by field calibration.

A.4.2.5 Conversion to Direction Cosines

The direction cosines ℓ' and m′ of the corrected phase differences are determined from the corrected absolute fine baseline phase differences by dividing by the distance between the fine antennas, expressed in wavelengths of the received signal. The fine antennas are positioned to be N_F (46 or 57) times the nominal 136.000 megahertz vacuum wavelength.

For transmitted signal frequencies, ν_T, the baseline length in terms of the transmitted frequency is ($N_F\ \nu_T/136.000$). Therefore, the direction cosine of the received signal from the station centered local tangent east-pointing axes is

$$\ell' = (b_{EW_F})_{corrected}\left(\frac{136.000}{N_F\ \nu_T}\right) \tag{A-43}$$

and the direction cosine to the local tangent north-pointing axis is

$$m' = (b_{NS_F})_{corrected}\left(\frac{136.000}{N_F\ \nu_T}\right) \tag{A-44}$$

A.4.2.6 Processor Considerations

Several aspects of the preprocessing procedure influence the accuracy and use of direction cosine data in subsequent orbit determination processing. First, the sampled data are approximated by a cubic polynomial which is used to determine the direction cosines. The cubic polynomial can introduce time-correlated errors into multiple direction cosine pairs obtained from the same station pass. Therefore, the variance of the residuals between the cubic polynomial and the data should be scrutinized, and consideration should be given to limiting the direction cosine data to one pair per station pass. Second, the received signal frequency in Equations (A-43) and (A-44) neglects the downlink Doppler shift and assumes that the transmitted and received signal frequencies are the same (i.e., $\nu_R = \nu_T$). Finally, the direction cosines ℓ' and m' correspond to vacuum signal paths. Thus, atmospheric refraction corrections and light-time delays must be applied in the processor.

A.5 VERY LONG BASELINE INTERFEROMETER (VLBI) (Not Currently Available in GTDS)

As in the Minitrack System, the VLBI System measures the phase differences at two or more ground stations when they simultaneously receive the same radio signal. However, in the VLBI system each terminal is controlled by its own independent frequency standard so that there is no necessity to use cable or microwave links to preserve the phase coherence among these stations. This permits the stations to be separated by arbitrarily large distances, typically on the order of thousands of kilometers. Since the angular resolution of any interferometer is directly proportional to the length of the baseline, the VLBI concept permits the position of the radio source (e.g., satellite) to be determined to a much greater degree of accuracy than is possible with a short baseline system like Minitrack.

The principle underlying the VLBI concept is illustrated by the simplified two-dimensional geometry shown in Figure A-5. The figure shows a signal, characterized as a planar wavefront, being simultaneously received at stations A and B, which are separated by distance D. The phase difference, $\Delta\phi$, between the two received signals is related to the separation of the stations D as follows:

$$\Delta\phi = \left(\frac{D}{\lambda}\right) \cos\theta \qquad \text{(A-45)}$$

where θ is the source direction and λ is the signal wavelength. When the value of θ is such that $\Delta\phi$ is an integral number of half-cycles, i.e., $\theta = \cos^{-1}(n\ \lambda/2D)$ where n is an integer, the signals received at each terminal are in phase or antiphase, and a relative extremum of power is available from the interferometer.

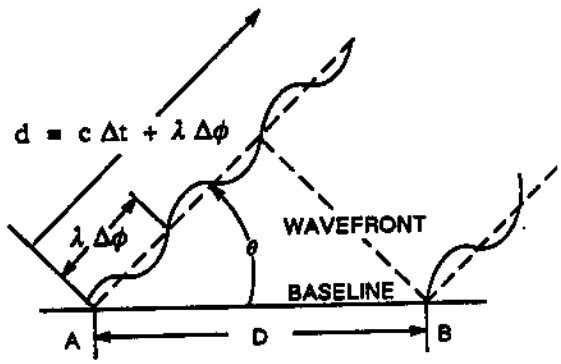

Figure A-5. Simplified Schematic of VLBI

As the source transits the interferometer, a power (or intensity) response such as that shown in Figure A-6 is produced. The abscissa is time, which is related monotonically to the source direction, θ. If the time at which a specific fringe is produced can be determined precisely enough, the relationship for $\Delta\phi$ in Equation (A-45) can be equally precisely specified in terms of source position and baseline parameters. The fringe density is so great, however, that it is very difficult to identify the central fringe (the fringe produced when the source direction is perpendicular to the baseline) and hence very difficult to record accurately the time of passage through any n^{th}-order fringe (i.e., the fringe displaced from the central one by n cycles).

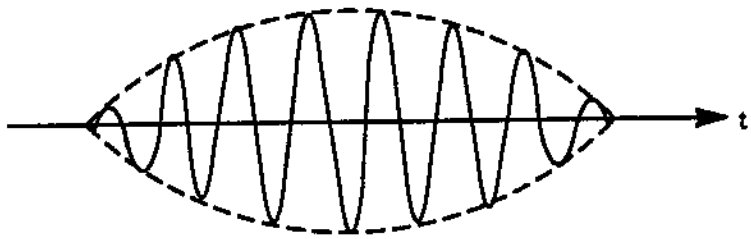

Figure A-6. Interferometer Fringes

The fringe number ambiguity is resolved by recording the received signal onto magnetic tape at as high a bandwidth as possible. These recorded signals are clipped and sampled so that the information is preserved in digital format. Corrections to compensate for the clipping and sampling are applied during preprocessing. Pairs of tapes, one from each station, are crosscorrelated afterwards in a preprocessing program. The correlations are repeated for many trial combinations of relative delay offset and delay-rate offset between the two records. When both digital records are correctly aligned, all of the frequencies within the signal bandwidth will have the same phase, and at this point the superposition of all the harmonic components within the complex correlation function will produce a maximum in its amplitude, as well as in the amplitude of its power spectrum. The delay and delay-rate values that produce this maximum are recorded, and the series of such values form the measurements.

A.6 RADAR ALTIMETER (Not Currently Available in GTDS)

A satellite is assumed to be in a near-Earth orbit, and its attitude is assumed to be stabilized so that the axis $\hat{z}_I$ of an attached pointing instrument is directed along the local vertical or gravity gradient. This can be accomplished by gravity gradient stabilization or other attitude stabilization techniques. Such stabilization allows the use of a directional antenna, pointed along the $\hat{z}_I$ axis, for the radar altimeter. The transmitter onboard the satellite transmits X-band signal pulses, which form a series of spherical wavefronts directed towards the Earth. The antenna beamwidth results in a signal cone with its apex at the transmitter and an axis that coincides approximately with the $\hat{z}_I$ axis of the satellite, as shown in Figure A-7.

As the wavefront of each pulse intersects the sea surface, it is reflected back towards the satellite. The time difference between the time of transmission and the time of reception of the radar pulse is a measure of the height of the satellite above the local surface. If the beamwidth of the transmitted signal is larger than the nominal spacecraft libration in attitude about the local vertical, the first return signal will lie on the transmission path normal to the sea surface and through the satellite. The effective size of the illuminated

spot on the surface is determined by the transmitted pulsewidth, the beamwidth, and the type of return pulse detection utilized. As long as the local vertical from the surface to the satellite lies inside the antenna beamwidth cone, the altimeter measurement will represent the shortest distance between the satellite and the sea surface.

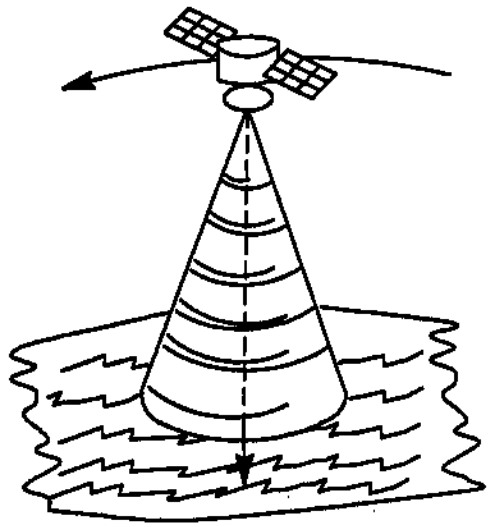

Figure A-7. Radar Altimeter Cone

The satellite timing equipment provides signals for measuring the time interval between the transmitted and received signals and for time tagging discrete measurements. This timing equipment is periodically calibrated from ground stations.

Initial preprocessing of the altimetry data consists of applying calibration and ambiguity corrections to the two-way time difference between transmitted and received signals and converting the result to an altitude by multiplying by one-half the speed of light. The time tag is calibrated and corrected to the midinterval time (i.e., the time that the signal is reflected from the sea surface). After these preprocessing computations, each data element is treated as if it were an instantaneous measurement at the midinterval time.

A.7 STDN LASER SYSTEMS

The STDN laser trackers provide highly accurate range measurements to spacecraft equipped with optical retroreflectors. Range measurements are determined using the propagation time of a laser pulse from the tracker to the spacecraft and back. Corrections for internal system delays and refraction are made on site. Ranging can be performed

during both night and day up to distances of several thousand kilometers; however, atmospheric conditions must be favorable.

Angle data are also provided by the laser trackers. However, the laser telescopes have no autotrack; the laser pointing direction is computer driven according to a priori orbit information. Thus, the angle measurement is only as accurate as the laser beamwidth. The lasers have a half-beamwidth of between 0.006 and 0.009 degree, and the receiving telescopes have a half-beamwidth of approximately 0.015 degree.

The STDN laser data rate is one per second. However, the quick-look (QL) data have a sampling rate of approximately 20 to 50 randomly spaced values per pass.

In the QL laser system, the range to a spacecraft or a fixed target is measured by determining the elapsed time between transmission and reception of a short pulse of intense light. The laser firing is initiated by a one-pulse-per-second signal from the time standard. A sample of the transmitted pulse is fed to a photodiode, which starts the range time interval unit (TIU). Similarly, a pulse from the photomultiplier receiver, which recognizes the return pulse from the target, stops the range TIU. The indication of the TIU is multiplied by the speed of light to determine the range.

With a transmitted pulse on the order of 20 nanoseconds (600 centimeters long), this system is capable of measuring range to an accuracy of approximately 50 to 100 centimeters, because the times of starting and stopping the TIU are dependent upon the height of the laser pulses. System performance is improved by measuring the time of occurrence of the centroid of the transmitted and received pulses and by means of a pulsewidth discriminator and waveform digitizer. When corrections for the time of occurrence of the centroid are applied to the basic range, accuracy of the measurement system is improved to better than 10 centimeters.

The instrumentation developed to perform the laser ranging experiment comprises three major subsystems: tracking pedestal and receiver optics, laser transmitter, and ranging and data control systems. These systems are interconnected to form a digitally controlled optical radar system capable of tracking cooperative spacecraft equipped with retroreflector arrays to within the accuracy of orbit predictions.

A.8 TRACKING AND DATA RELAY SATELLITE SYSTEM (TDRSS)

The functional and processing descriptions for the Tracking and Data Relay Satellite System (TDRSS) are given in the following subsections.

A.8.1 TDRSS FUNCTIONAL DESCRIPTION

TDRSS is a network of geosynchronous relay satellites and a common ground terminal used by NASA for tracking and communications support of low-Earth satellites. TDRSS

comprises two operational satellites and one in-orbit spare. The two operational satellites, TDRS-East at 41 degrees west longitude and TDRS-West at 171 degrees west longitude, are centered about the White Sands Ground Terminal (WSGT) and provide 85- to 100-percent visibility coverage for user spacecraft (Figure A-8).

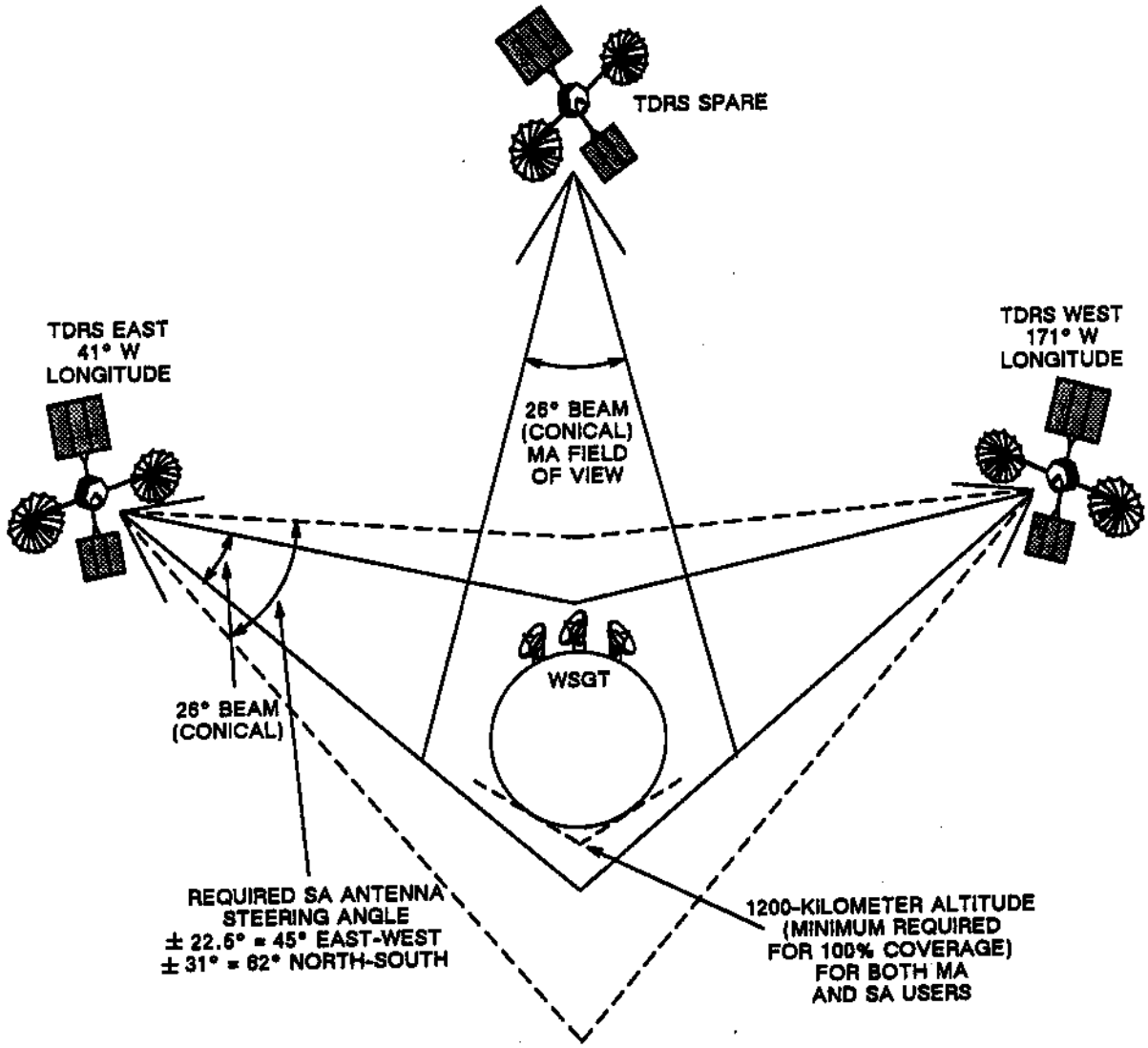

Figure A-8. TDRSS Configuration and Coverage Limits

The Bilateration Ranging Transponder System (BRTS) is used to provide range and Doppler measurements for TDRS. BRTS is a system of four ground-based, unmanned facilities, located at WSGT, Ascension Island, Alice Springs (Australia), and American

Samoa, that contain a total of six transponders similar to those flown on user spacecraft. Since the positions of the BRTS transponders are accurately known, their ranging information is used to determine precisely the trajectories of the TDRSs.

Each Tracking and Data Relay Satellite (TDRS) is equipped with two user service antenna systems. The high-gain system comprises two steerable 5-meter dual S/K-band antennas, known as the Single Access (SA) System (SSA and KSA for S-band and K-band, respectively). The low-gain system consists of a 30-element S-band phased array antenna system, which can provide one forward link and multiple simultaneous pseudorandom noise (PN) code division multiplexed return links. This is known as the Multiple Access (MA) System.

WSGT is configured with three 18-meter K-band elevation-over-azimuth (AZ-EL) antennas; a 6-meter S-band AZ-EL tracking, telemetry, and command (TT&C) antenna; and roof-mounted S-band and K-band simulation/verification antennas. The communications equipment at WSGT can simultaneously support two-way communications for six SSA, six KSA, and three MA services, as well as a total of 20 MA return links.

User tracking equipment can provide nine ranging and 19 Doppler services simultaneously (Figure A-9). The Doppler measurement is a continuous count of a bias plus the Doppler frequency resolved to 0.001 cycle at S-band and to 0.01 cycle at K-band. The range measurement is the four-leg round-trip light time resolved to 1 nanosecond. This range measurement is ambiguous in multiples of the ranging code period, about 0.086 second (13,000 kilometers one way). The measurements are strobed on the whole second, formatted, and transmitted to NASA at selectable sample rates of 1, 5, 10, 60, and 300 seconds.

BRTS (Figure A-10) is used to provide tracking measurements for the relay spacecraft. The BRTS four ground-based unmanned facilities contain transponders similar to those flown on user spacecraft. BRTS provides a set of transponders whose position are accurately known so that ranging information can be used to determine the trajectories of the TDRSs with a high degree of precision. The facilities are located at WSGT (two transponders, three antennas), Ascension Island (two transponders, two antennas), American Samoa (one transponder, two antennas), and Alice Springs, Australia (one transponder, one antenna). TDRS-East (TDRS-E) and TDRS-Spare (TDRS-S) will be supported by BRTS at White Sands and Ascension Island, while TDRS-West (TDRS-W) will be supported by BRTS at Alice Springs, American Samoa, and White Sands.

A detailed functional description of the TDRSS network is available in Reference 12.

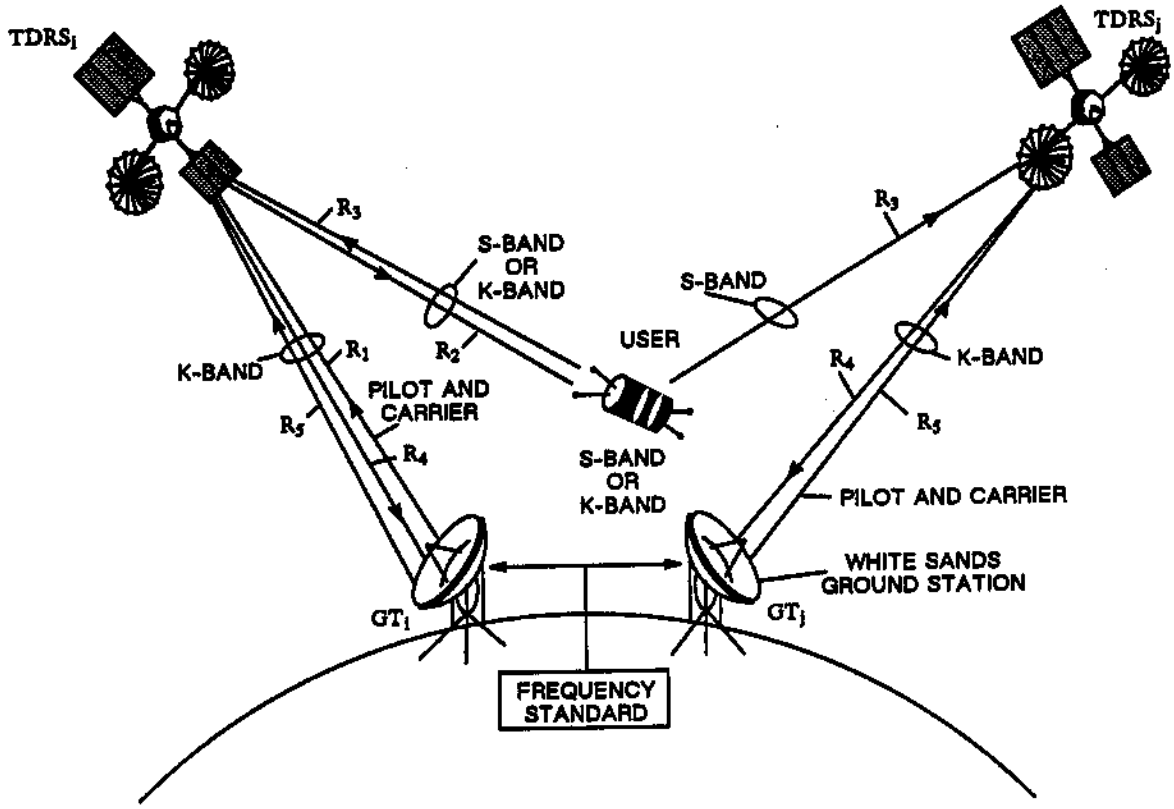

$$\text{RANGE} = \frac{1}{2}(R_1 + R_2 + R_3 + R_4)$$

$$\text{DOPPLER} = -\frac{F_T}{C}(\dot{R}_1 + \dot{R}_2 + \dot{R}_3 + \dot{R}_4) - \frac{F_B}{C}(\dot{R}_4 + \dot{R}_5)$$

Figure A-9. Closed-Loop Tracking Configuration

A.8.2 TDRSS RANGE AND DOPPLER/DIFFERENCED DOPPLER MEASUREMENT PROCESSING

Descriptions of the TDRSS range measurement processing and the Doppler and differenced Doppler measurement processing are given in the following subsections.

A.8.2.1 Range Measurement Processing

The TDRSS range measurement is obtained by measuring the time delay required for a reference time marker (PN code start time determined by autocorrelation of the received PN code with the locally generated PN code) to travel from the White Sands ground tracking station to the TDRS, from the TDRS to the target and back to the same TDRS or

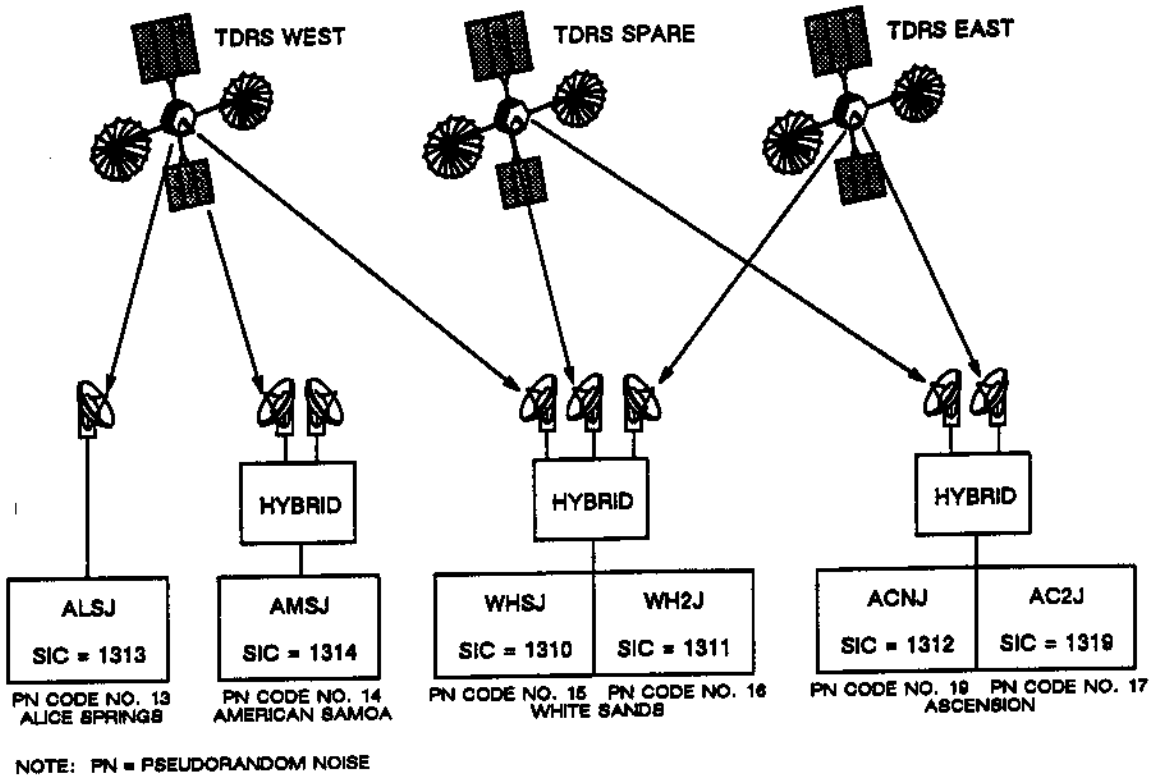

Figure A-10. Bilateration Ranging Transponder System (BRTS) Configuration

to a different TDRS, and to return to the ground station. This time delay measurement has an ambiguity, equal to the integral number of the PN code periods, that must be resolved by the orbit determination process. The algorithm used for processing the range measurements is discussed below.

Raw Data Reduction Algorithm for Range Measurement

The raw data, which are a measure of the signal traveling time, are converted to kilometers. The raw measurement obtained at the ground terminal is a count of the number of chips between the reference and received PN code at a time tag T. This count is converted to a time delay and half-range by the following equations (Reference 13):

$$\Delta t(T) = N \times 2^{-8} \times 10^{-9} \text{ seconds} \tag{A-46}$$

$$\varrho_0(T) = \frac{1}{2} \times c \times \Delta t(T) \text{ kilometers} \tag{A-47}$$

where

Δt = measured round-trip time delay (in seconds) at time tag T between corresponding chips of the reference and received PN code

N = total number of counts (in units of 2^{-8} nanoseconds)

$\varrho_0(T)$ = measured half-range at time tag T (in kilometers)

c = speed of light

The time delay measurement, Δt, given in Equation (A-46) has an ambiguity equal to an integral number of the PN code period. This ambiguity is to be resolved (see Section 7.3.2.3). The range measurement that results from the processing is the half-range of a round trip, since a factor of one-half appears in Equation (A-47). To be consistent, this factor must be included when the range measurement is modeled.

A.8.2.2 Doppler and Differenced Doppler Measurement Processing

Doppler measurements in TDRSS include hybrid, two-way, one-way, and differenced one-way measurements. The raw data measurement consists of a nondestruct Doppler count of a nominal bias frequency, 240 megahertz, over a fixed time interval. The count is cumulative since the counter is not reset to zero between measurements.

A hybrid or a two-way Doppler measurement is performed by transmitting a signal at K-band frequency from a ground transmitting station to a forward-link TDRS. The TDRS coherently translates the signal to the tracking frequency of the user spacecraft in S-band or K-band and transmits it to the user spacecraft. The user coherently turns the signal around at a ratio of either 240/221 for S-band frequency or 1600/1469 for K-band frequency and retransmits it to the return-link TDRS. The TDRS then translates the signal to K-band frequency and transmits it down to the ground receive station.

The one-way Doppler measurement can be generated from either spacecraft or ground transmitters. Any 10 of the 20 MA service antennas of the TDRS can be used simultaneously for one-way Doppler measurements. Although the individual one-way Doppler measurements are dominated by oscillator frequency bias, given a wide-beam antenna system on the autonomous spacecraft, the signal can be received by all three TDRSs with the same frequency bias being measured in each measurement. In differencing the measurements, this bias can be canceled out, thus offering tracking of a spacecraft as accurate as that provided by two-way measurements.

The algorithms used to reduce raw measurements are discussed separately in the following subsections for the Doppler and differenced Doppler measurements.

A.8.2.2.1 Raw Data Reduction Algorithm for Doppler Measurements

In any batch of TDRSS data, the first Doppler measurement of the batch is always invalid because the counter for the Doppler count is not initialized to zero for nondestruct Doppler measurements. Therefore, the first Doppler measurement of a batch is set to zero. The following algorithm is used to preprocess all TDRSS Doppler raw measurements, except differenced one-way Doppler measurements:

$$\begin{aligned} \nu_{d_0}(T_i) &= 0 && \text{(for } i = 1\text{)} \\ &= \frac{1}{L}\left[\frac{(N_i - N_{i-1})}{(T_i - T_{i-1})} - \nu_b\right] && \text{(for } i > 1\text{)} \end{aligned} \tag{A-48}$$

where

$\nu_{d_0}(T_i)$ = measured Doppler shift (in hertz) at time tag T_i, averaged over the time interval between T_i and T_{i-1}

N_i, N_{i-1} = Doppler counter readings (in counts) associated with time tags T_i and T_{i-1}, respectively

L = 1000 for SSA service and MA service and 100 for K-band service

ν_b = bias frequency = 240 megahertz

A.8.2.2.2 Raw Data Reduction Algorithm for Differenced Doppler Measurements

The differenced one-way Doppler measurements are created only when there are two or more batches of one-way Doppler measurements from the same target within the same period of time.

While raw TDRSS data are being processed, pertinent information is stored in an internal table for all one-way Doppler batches that are encountered. After all the raw data have been reduced to 60-byte output format, the table is searched in generating differenced one-way Doppler measurements. The objective is to look for a pair of matching one-way Doppler batches for the same target with overlapping timespans. If an identical time tag is found in the pair, the difference of the already reduced one-way Doppler measurements is computed using the following equation:

$$\Delta\nu_{d_0}(T) = [\nu_{d_0}(T)]_{\text{compare}} - [\nu_{d_0}(T)]_{\text{reference}} \tag{A-49}$$

where

$\Delta\nu_{d_0}(T)$ = measured differenced one-way Doppler measurement at time tag T

$[\Delta\nu_{d_0}(T)]_{reference}$ = reference one-way Doppler measurement

$[\Delta\nu_{d_0}(T)]_{compare}$ = comparison one-way Doppler measurement

When this pair of matched one-way Doppler measurements corresponds to two different return-link TDRS spacecraft, the measurement associated with the lower TDRS number is regarded as the reference. However, if they correspond to the same TDRS spacecraft but have two different access service-link identifications, the measurement encountered first is considered to be the reference (Reference 13). This difference, along with other pertinent information (e.g., time tag, user spacecraft identifier (ID), TDRS ID, and flags), is used for orbit determination.

A.9 REFERENCES

1. Kallmeyer, F. W.: 1980, *Tracking Data Transmission Formats and Reduction Algorithms*, Goddard Space Flight Center STDN Report 721, Revision 6, October 1980.

2. Goddard Space Flight Center: 1989, *Tracking and Acquisition Handbook for the Spaceflight Tracking and Data Network*, STDN Report 724, Revision 5, February 1989.

3. Grenchik, T. J. and Putney, B. H.: 1969, *A Review of Goddard Range and Range-Rate System Measurements and Data Processing Techniques*, Goddard Space Flight Center Report X-551-69-137, April 1969.

4. Schmid, P. E.: 1969, *The Conversion of Fundamental Tracking Data to Metric Form*, Goddard Space Flight Center Report X-551-69-3, January 1969.

5. Watkins, E. R. and Rose, D. H.: 1969, *Description of the Goddard Range-Range Rate Data Processing Program for the CDC-160A*, Goddard Space Flight Center Report X-541-69-322, August 1969.

6. Zillig, D. J.: 1969, *Data Formats of the Goddard Range and Range-Rate System and the Application Technological Satellite Range and Range-Rate System*, Goddard Space Flight Center Report X-571-69-149, April 1969.

7. Scott, J. N.: 1978, *Spacecraft Tracking and Data Network User's Guide (Basic)*, Goddard Space Flight Center STDN Report 101.1, Revision 3, July 1978.

8. Squier, D. and Byers, K.: 1987, *Goddard Trajectory Determination System (GTDS) User's Guide*, Revision 2, Computer Sciences Corporation Report CSC/SD-85/6738, December 1987.

9. National Aeronautics and Space Administration: 1968, *MARK IA Ranging Subsystem*, NASA Report MH-1055, April 1, 1968.

10. Watkins, E. R.: 1969, *Preprocessing of Minitrack Data*, Goddard Space Flight Center Report TND-5042, May 1969.

11. Control System Research, Inc.: 1970, *Minitrack Tracking Function Description*, Control System Research report, March 1970.

12. Goddard Space Flight Center: 1988, *Space Network (SN) User's Guide*, STDN Report 101.2, Revision 6, May 1988.

13. Cowan, D. J.: 1978, *TDRS Data Processing Specifications for the Generalized Data Handler (GDH)*, GSFC Code 572 Memorandum, August 1978.

APPENDIX B—TIME ELEMENTS

The Time-Regularized Cowell system of equations achieves analytic stepsize control through the transformation of the independent variable, time, to a new variable s defined by

$$\frac{dt}{ds} = r^{\alpha} \tag{B-1}$$

where α is called the uniformization constant and r is the magnitude of the radius vector. The physical time, t, is obtained through the integration of Equation (B-1), which involves r. Any linear error in r will propagate into a nearly quadratic error in the time. Time elements are introduced to reduce this nearly quadratic error growth to a nearly linear error growth for perturbed motion. An element in two-body motion is defined as a parameter that is either constant or a linear function of the independent variable.

For perturbed motion (assuming small perturbations), an element varies slowly from the two-body solution. Thus, in deriving a time element τ for the Time-Regularized Cowell method, τ is required to vary linearly with the independent variable s, i.e.,

$$\frac{d\tau}{ds} = c \tag{B-2}$$

where c is a constant; it is also required that τ be related analytically to the physical time, t. This is done via Kepler's Equation

$$t = t_0 + \frac{1}{n}(E - e \sin E) \tag{B-3}$$

which can be rewritten with the introduction of τ as

$$t = t_0 + \tau - \frac{g(\alpha)}{n} + \frac{1}{n}(E - e \sin E) \tag{B-4}$$

where, by definition,

$$\tau = \frac{g(\alpha)}{n} \tag{B-5}$$

and $g(\alpha)$ is a function relating τ to the Kepler element α.

Differentiating Equation (B-5) with respect to s and substituting Equations (B-1) and (B-2) yields

$$\frac{dg}{dt} = n\,c\,r^{-a} \tag{B-6}$$

B.1 UNPERTURBED MOTION

The definition of the function g is obtained for various values of a by utilizing known integrals of the two-body problem.

B.1.1 TIME ELEMENT CORRESPONDING TO THE ECCENTRIC ANOMALY ($a = 1$)

In Keplerian motion, the time derivative of the eccentric anomaly, E, is given by

$$\frac{dE}{dt} = n\,a\,r^{-1} \tag{B-7}$$

where the mean motion, n, and the semimajor axis, a, are constants for two-body motion. Comparing Equations (B-6) and (B-7) for $a = 1$ yields

$$g = E \tag{B-8}$$

and

$$c = a \tag{B-9}$$

Thus,

$$\frac{d\tau}{ds} = \frac{1}{n}\frac{dE}{dt}\,r^{a} = a \tag{B-10}$$

and, from Equation (B-4),

$$t = t_0 + \tau - \frac{e \sin E}{n} \tag{B-11}$$

which is the desired result for two-body motion.

B.1.2 TIME ELEMENT CORRESPONDING TO THE TRUE ANOMALY ($\alpha = 2$)

The time derivative of the true anomaly, f, is given by

$$\frac{df}{dt} = \sqrt{\mu p}\, r^{-2} \tag{B-12}$$

where the semilatus rectum, p, is a constant of the motion for the Kepler problem.

Comparing Equation (B-6) and Equation (B-12) yields

$$g = f \tag{B-13}$$

and

$$c = \frac{\sqrt{\mu p}}{n} \tag{B-14}$$

Thus,

$$\frac{d\tau}{ds} = \frac{1}{n}\frac{df}{dt} r^2 = \frac{\sqrt{\mu p}}{n} \tag{B-15}$$

which is the desired differential equation for τ. Kepler's equation, Equation (B-4), can then be written as

$$\begin{aligned} t &= t_0 + \tau - \frac{f}{n} + \frac{1}{n}(E - e \sin E) \\ &= t_0 + \tau - \frac{(f - E)}{n} - \frac{e \sin E}{n} \end{aligned} \tag{B-16}$$

B.2 PERTURBED MOTION

The extension of the time element equation for perturbed motion is presented for $\alpha = 1$ and $\alpha = 2$, using the approach followed in References 1 and 2.

B.2.1 TIME ELEMENT EQUATION CORRESPONDING TO THE KS FORMULATION (a = 1)

Equation (B-11) can be written as

$$\tau = t + \frac{(\bar{r} \cdot \dot{\bar{r}})}{2h_K} \tag{B-17}$$

where h_K is the negative Keplerian energy

$$h_K = \frac{\mu}{r} - \frac{v^2}{2} \tag{B-18}$$

Differentiating Equation (B-17) with respect to the new independent variable, s, yields

$$\frac{d\tau}{ds} = \frac{dt}{ds} + \left[\frac{(\bar{r} \cdot \ddot{\bar{r}})}{2h_K} + \frac{(\dot{\bar{r}} \cdot \dot{\bar{r}})}{2h_K} - \frac{\bar{r} \cdot \dot{\bar{r}}}{2h_K^2}\,\dot{h}_K\right]\frac{dt}{ds} \tag{B-19}$$

This expression simplifies to

$$\frac{d\tau}{ds} = \frac{\mu}{2h_K} + \frac{r\,(\bar{r} \cdot \bar{P})}{2h_K} + \frac{r\,(\bar{r} \cdot \dot{\bar{r}})(\dot{\bar{r}} \cdot \bar{P})}{2h_K^2} \tag{B-20}$$

where $\bar{P}$ is the perturbing acceleration, i.e.,

$$\ddot{\bar{r}} = \frac{-\mu\,\bar{r}}{r^3} + \bar{P} \tag{B-21}$$

The differential equation for the time element in Equation (B-20) clearly has the desired properties in that the element varies linearly with respect to the independent variable, s, for unperturbed motion ($\bar{P}$ = 0), and for perturbed motion (providing $\bar{P}$ is small) the element varies slowly from the two-body solution. An alternative expression involving the total energy

$$h = h_K - V \tag{B-22}$$

where V is the perturbing potential, can be derived by beginning with the expression

$$\tau = t + \frac{(\bar{r} \cdot \dot{\bar{r}})}{2h} \tag{B-23}$$

Differentiating this equation with respect to the independent variable, s, yields

$$\frac{d\tau}{ds} = \frac{1}{2h}\left[\mu - 2rV - r(\bar{r} \cdot \nabla V) + r(\bar{r} \cdot \bar{P})\right] - \frac{r(\bar{r} \cdot \dot{\bar{r}})}{2h^2}\dot{h} \tag{B-24}$$

where ∇V is the perturbing acceleration due to the perturbing potential function, i.e.,

$$\ddot{\bar{r}} = \frac{-\mu \bar{r}}{r^3} + \bar{P} - \nabla V \tag{B-25}$$

Equation (B-24) can be shown to be the time element equation corresponding to the KS formulation (Equation (5-10a)) by noting that

$$\frac{d}{ds} = 2\omega \frac{d}{dE} \tag{B-26}$$

and

$$\omega = \sqrt{\frac{h}{2}} \tag{B-27}$$

The comparison between Equations (B-20) and the KS equation, Equation (B-24), has been made in Reference 2, and it was found that they give the same amount of accuracy improvement for the tested cases.

B.2.2 TIME ELEMENT EQUATION CORRESPONDING TO THE DS FORMULATION ($\alpha = 2$)

Equation (B-17) can be written as

$$\tau = t + \frac{(\bar{r} \cdot \dot{\bar{r}})}{2h_K} + \frac{\mu(f - E)}{(2h_K)^{3/2}} \tag{B-28}$$

Differentiating Equation (B-28) with respect to the new independent variable s yields

$$\frac{d\tau}{ds} = \frac{dt}{ds} + \frac{r^2}{2h_K}\left[(\dot{\bar{r}} \cdot \dot{\bar{r}}) + (\bar{r} \cdot \ddot{\bar{r}})\right] - \frac{r^2(\bar{r} \cdot \dot{\bar{r}})}{2h_K^2}\dot{h}_K + \frac{\mu r^2}{(2h_K)^{3/2}}(\dot{f} - \dot{E}) - \frac{3\mu r^2 (f - E)}{(2h_K)^{5/2}}\dot{h}_K \tag{B-29}$$

This expression simplifies to

$$\frac{d\tau}{ds} = \frac{\mu}{(2h_K)^{3/2}}\sqrt{\mu p} + \frac{r^2}{2h_K}(\bar{r} \cdot \bar{P}) + \frac{r^2}{2h_K^2}(\bar{r} \cdot \dot{\bar{r}})(\dot{\bar{r}} \cdot \bar{P}) + \frac{3\mu r^2}{(2h_K)^{5/2}}(f - E)(\dot{\bar{r}} \cdot \bar{P}) + \frac{\mu r^2}{(2h_K)^{3/2}}\left[\left(\frac{\partial f}{\partial \dot{\bar{r}}}\right) \cdot \bar{P} - \left(\frac{\partial E}{\partial \dot{\bar{r}}}\right) \cdot \bar{P}\right] \tag{B-30}$$

Noting that the leading term in this equation is a constant and all other terms are a function of the perturbations, it is clear that this differential equation for τ has the desired properties noted previously.

The differential equation for the time element ℓ in the DS formulation (see Equations (5-45), (5-46), and Reference 3) is given by

$$\frac{d\ell}{ds} = \frac{\mu}{(2L)^{3/2}} + V\frac{r}{q}\left(2\frac{\partial r}{\partial \beta_4} - \frac{r}{q}\frac{\partial q}{\partial \beta_4}\right) + \frac{r^2}{q}\frac{\partial V}{\partial L} - P_4 \tag{B-31}$$

where L, the total energy, is one of the elements of the formulation, and s, the independent variable, is the true anomaly. Transforming the independent variable of Equation (B-30) to the true anomaly using the operator

$$\frac{d}{ds} = (G - \Phi)\frac{d}{df} \tag{B-32}$$

(where G is the total angular momentum and Φ is the perturbing energy), and letting Q_1 represent all terms dependent upon perturbations, yields

$$\frac{d\tau}{df} = \frac{\mu}{(2h_K)^{3/2}} + Q_1 \tag{B-33}$$

If Q_2 represents those terms in Equation (B-31) that are dependent upon perturbations, the following equation results:

$$\frac{d\ell}{ds} = \frac{\mu}{(2L)^{3/2}} + Q_2 \qquad \text{(B-34)}$$

As in the case where $a = 1$, the leading term in Equation (B-33) is a function of the Keplerian energy, h_K, whereas the leading term in Equation (B-34) is a function of the total energy, L. This can lead to accuracy improvements for conservative perturbed motion situations, although at present no comparison studies have been performed.

APPENDIX C—DEVELOPMENT OF RANGE-RATE FORMULAS

This appendix presents the development of formulas that relate the tracker and spacecraft relative motion to the Doppler shift in an electromagnetic signal transmitted from one to the other. For a further definition of the mathematical symbols used, refer to Appendix A.

The general relativistic expression relating the frequencies of an electromagnetic signal propagation from a transmitter to a receiver is

$$\frac{\nu_r}{\nu_t} = \frac{a_t}{a_r}\left[\frac{1 - F_r \bar{n}_r \cdot \dot{\bar{r}}_r}{1 - F_t \bar{n}_t \cdot \dot{\bar{r}}_t}\right] \tag{C-1}$$

where

$$a = \sqrt{g_{00} + \frac{2}{c}\sum_{i=1}^{3} g_{0i}\,\dot{x}^i + \frac{1}{c^2}\sum_{i,j=1}^{3} g_{ij}\,\dot{x}^i\dot{x}^j} \tag{C-2}$$

$$F = \frac{1}{c\,g_{00}}\left[\sqrt{\sum_{i,j=1}^{3}(g_{0i}\,g_{0j} - g_{00}\,g_{ij})\frac{dx^i}{dS}\,\frac{dx^j}{dS}} - \sum_{i=1}^{3} g_{0i}\frac{dx^i}{dS}\right] \tag{C-3}$$

and

t, r	=	subscripts indicating that the designated quantities are evaluated at the transmitter and receiver, respectively
ν_t, ν_r	=	frequencies of the transmitted and received signals
$\dot{\bar{r}}_t, \dot{\bar{r}}_r$	=	velocities of the transmitter and receiver, defined as the derivatives of their inertial positions with respect to the coordinate time $\bar{t}$
g_{ij}	=	elements of the metric matrix defining the nature of the space-time frame
x^i	=	components of the space coordinates

S = arc length along the propagation path

$\hat{n}_t$, $\hat{n}_r$ = unit vectors along the local propagation path at the transmitter and receiver, respectively

c = wave propagation speed

The derivatives dx^i/dS are simply the direction cosines of the propagation path, and thus are the components of the local unit vector, $\hat{n}$.

Equation (C-1) is derived under the assumption that the metric elements g_{ij} vary slowly in time compared with the wave propagation speed, c. This is a good approximation since the variations of the g_{ij} elements are due to planetary motions, which are very slow compared with c.

In principle, the g_{ij} should mathematically describe everything that physically affects the propagation of electromagnetic waves in their region of definition, including gravitational influences, the refractive effects of the atmosphere, and any other significant influences. If such a rigorous mathematical description of the space-time frame could be formulated and then solved analytically, propagation paths for specific cases could be computed very accurately as geodesics. However, no such completely general treatment of the problem has yet been produced.

It is generally assumed that the metric coefficients for the case of special relativity are

$$g_{oo} = 1 \tag{C-4a}$$

$$g_{ii} = -1 \qquad (i, j = 1, 2, 3) \tag{C-4b}$$

$$g_{ij} = 0 \quad (i \neq j) \quad (i, j = 1, 2, 3) \tag{C-4c}$$

Equation (C-2) then becomes

$$a = \sqrt{1 - \frac{\dot{\bar{r}} \cdot \dot{\bar{r}}}{c^2}} \tag{C-5}$$

and Equation (C-3) simplifies to

$$F = \frac{1}{c} \tag{C-6}$$

The propagation path, which is the straight relative position vector from $\bar{r}_t$ to $\bar{r}_r$, is given by

$$\hat{n}_t = \hat{n}_r = \hat{n} = \frac{\bar{r}_r - \bar{r}_t}{|\bar{r}_r - \bar{r}_t|} \tag{C-7}$$

Under the preceding conditions, Equation (C-1) reduces to

$$\frac{\nu_r}{\nu_t} = \sqrt{\frac{1 - \frac{\dot{\bar{r}}_t \cdot \dot{\bar{r}}_t}{c^2}}{1 - \frac{\dot{\bar{r}}_r \cdot \dot{\bar{r}}_r}{c^2}}} \left[\frac{1 - \frac{\hat{n} \cdot \dot{\bar{r}}_r}{c}}{1 - \frac{\hat{n} \cdot \dot{\bar{r}}_t}{c}} \right] \tag{C-8}$$

which is the formula from special relativity for the one-way Doppler frequency shift.

The metric coefficients in Equation (C-4) describe straight-line propagation in a vacuum. The neglect of the ray path bending due to gravitational effects is an acceptable approximation, considering the precision of the radar Doppler measuring equipment. However, the refractive bending of the ray by the atmosphere (troposphere and ionosphere) is not negligible and must be taken into account. The special relativistic formula given by Equation (C-8) is modified to replace the unit vector $\hat{n}$ along the idealized straight ray path with the unit vectors

$$\hat{n}_t = \hat{n} + \Delta\hat{n}_t \tag{C-9a}$$

$$\hat{n}_r = \hat{n} + \Delta\hat{n}_r \tag{C-9b}$$

along the actual curved propagation path. The method by which the refraction difference vectors, $\Delta\hat{n}_t$ and $\Delta\hat{n}_r$, are estimated is discussed in Chapter 7. Here the terms will simply be introduced into the equations and formally carried through the derivations. As a result of this substitution, Equation (C-8) becomes

$$\frac{\nu_r}{\nu_t} = \sqrt{\frac{1 - \frac{\dot{\bar{r}}_t \cdot \dot{\bar{r}}_t}{c^2}}{1 - \frac{\dot{\bar{r}}_r \cdot \dot{\bar{r}}_r}{c^2}}} \left[\frac{1 - \frac{\hat{n}_r \cdot \dot{\bar{r}}_r}{c}}{1 - \frac{\hat{n}_t \cdot \dot{\bar{r}}_t}{c}} \right] \qquad \text{(C-10)}$$

where $\hat{n}_r$ and $\hat{n}_t$ are given by Equations (C-9).

The geometry of two-way (or three-way) signal propagation is illustrated in Figure C-1. A continuous wave signal of frequency ν_T is emitted by a ground station at position $\bar{r}_T$ at time t_T. At a later time t_v, the spacecraft at position $\bar{r}_v$ receives this signal along the curved uplink transmission path. Application of Equation (C-10) gives the relationship

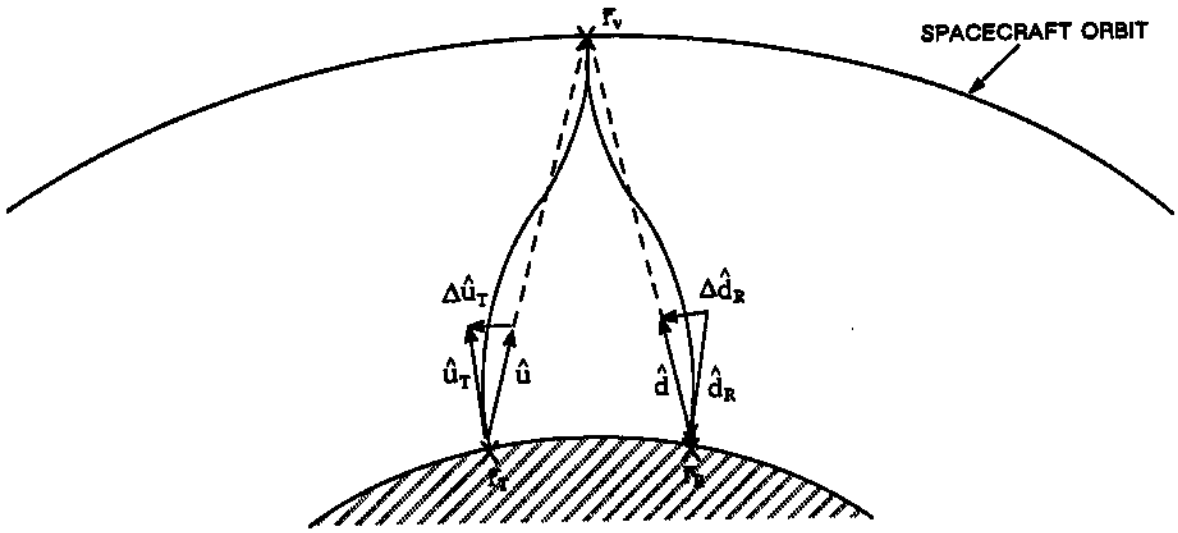

Figure C-1. Signal Propagation Geometry

between the apparent signal frequency at the ground transmitter, ν_T, and at the spacecraft receiver, ν_v, i.e.,

$$\frac{\nu_v}{\nu_T} = \sqrt{\frac{1 - \frac{\dot{\bar{r}}_T \cdot \dot{\bar{r}}_T}{c^2}}{1 - \frac{\dot{\bar{r}}_v \cdot \dot{\bar{r}}_v}{c^2}}} \left[\frac{1 - \frac{\hat{u}_v \cdot \dot{\bar{r}}_v}{c}}{1 - \frac{\hat{u}_T \cdot \dot{\bar{r}}_T}{c}} \right] \tag{C-11}$$

where

$$\begin{aligned} \hat{u}_T &= \hat{u} + \Delta\hat{u}_T \\ \hat{u}_v &= \hat{u} + \Delta\hat{u}_v \\ \hat{u} &= \frac{\bar{r}_v - \bar{r}_T}{|\bar{r}_v \cdot \bar{r}_T|} \end{aligned} \tag{C-12}$$

and the subscript T refers to quantities evaluated at the ground transmitter.

Although it is not rigorously correct to do so, the spacecraft USB transponder can be modeled as though it coherently turns the received signal around and retransmits it at the received frequency, ν_v.* The downlink signal is received by the ground station (either the same station that transmitted the uplink signal or an entirely different station whose oscillator is coherently linked with the transmitter) at position $\bar{r}_R$ at time t_R. The one-way frequency shift that occurs on the curved downlink path is

$$\frac{\nu_R}{\nu_v} = \sqrt{\frac{1 - \frac{\dot{\bar{r}}_v \cdot \dot{\bar{r}}_v}{c^2}}{1 - \frac{\dot{\bar{r}}_R \cdot \dot{\bar{r}}_R}{c^2}}} \left[\frac{1 - \frac{\hat{d}_R \cdot \dot{\bar{r}}_R}{c}}{1 - \frac{\hat{d}_v \cdot \dot{\bar{r}}_v}{c}} \right] \tag{C-13}$$

* The USB uplink frequency capability is 2025 to 2120 megahertz, and the downlink frequency capability is 2200 to 2300 megahertz.

where

$$\hat{d}_v = \hat{d} + \Delta\hat{d}_v$$

$$\hat{d}_R = \hat{d} + \Delta\hat{d}_R \qquad \text{(C-14)}$$

$$\hat{d} = \frac{\bar{r}_R - \bar{r}_v}{|\bar{r}_R - \bar{r}_v|}$$

The relationship between the transmitted and received ground frequencies for this two- or three-way case is computed by multiplying Equations (C-11) and (C-13) together to obtain

$$\frac{\nu_R}{\nu_T} = \sqrt{\frac{1 + \frac{\dot{\bar{r}}_T \cdot \dot{\bar{r}}_T}{c^2}}{1 + \frac{\dot{\bar{r}}_R \cdot \dot{\bar{r}}_R}{c^2}}} \left[\frac{1 - \frac{\hat{u}_v \cdot \dot{\bar{r}}_v}{c}}{1 - \frac{\hat{u}_T \cdot \dot{\bar{r}}_T}{c}}\right]\left[\frac{1 - \frac{\hat{d}_R \cdot \dot{\bar{r}}_R}{c}}{1 - \frac{\hat{d}_v \cdot \dot{\bar{r}}_v}{c}}\right] \qquad \text{(C-15)}$$

The frequencies ν_R and ν_T are defined with respect to the tracking station oscillator. In the language of relativity theory, this clock measures the proper time associated with the inertially moving tracking station. The velocities, on the other hand, are all defined in terms of derivatives with respect to coordinate time, the time system associated with the inertial reference frame. This time can be regarded as the same as uniform time for the present development.

If Equations (C-12) and (C-14) are substituted into Equation (C-15), and the factors within the brackets are expanded in terms of no higher order than $\Delta\hat{u} \cdot (\dot{\bar{r}}/c)$ or $\Delta\hat{d} \cdot (\dot{\bar{r}}/c)$, the following form results:

$$\frac{\nu_R}{\nu_T} = \sqrt{\frac{1 + \frac{\dot{\bar{r}}_T \cdot \dot{\bar{r}}_T}{c^2}}{1 + \frac{\dot{\bar{r}}_R \cdot \dot{\bar{r}}_R}{c^2}}} \left\{\left[\frac{1 - \frac{\hat{u} \cdot \dot{\bar{r}}_v}{c}}{1 - \frac{\hat{u} \cdot \dot{\bar{r}}_T}{c}}\right]\left[\frac{1 - \frac{\hat{d} \cdot \dot{\bar{r}}_R}{c}}{1 - \frac{\hat{d} \cdot \dot{\bar{r}}_v}{c}}\right] + \frac{\Delta\dot{\rho}}{c}\right\} \qquad \text{(C-16a)}$$

where

$$\Delta\dot{\varrho} = \Delta\hat{u}_T \cdot \dot{\bar{r}}_T + \Delta\hat{d}_v \cdot \dot{\bar{r}}_v - \Delta\hat{u}_v \cdot \dot{\bar{r}}_v - \Delta\hat{d}_R \cdot \dot{\bar{r}}_R \qquad \text{(C-16b)}$$

The first term within the braces (the product of the expressions in brackets) represents the vacuum portion of the Doppler shift. The additional term, $\Delta\dot{\varrho}/c$, involving the propagation path unit vector deflections, represents the refraction effects. Equation (C-16) relates the received frequency to the transmitted frequency via the geometry of the round-trip light path.

The continuously transmitted signal is beat against the received signal, resulting in a signal with a frequency equal to the difference between the two, i.e.,

$$\nu_d = \nu_R - \nu_T = \nu_T\left(\frac{\nu_R}{\nu_T} - 1\right) \qquad \text{(C-17)}$$

A fixed frequency bias signal, ν_b, is added to this Doppler signal, and the combination is fed to a Doppler-plus-bias cycle counter. Simultaneously, a reference frequency, ν_{R_2}, is fed to a separate time interval counter. At most tracking stations, the bias and reference frequencies are coherently derived from the same source as ν_T.

The measurement is mechanized in one of two ways, a destruct or a nondestruct count. The destruct count mode (employed in the GRARR and ATSR systems) counts a preassigned fixed number of cycles, N, of the Doppler-plus-bias signal and records the measurement as the (variable) number of cycles, C_0, of the reference frequency required to accumulate the simultaneous N cycle count. The nondestruct mode (employed in the USB System) continually accumulates the count of the Doppler-plus-bias signal in its counter. The measurement consists of recording this continually increasing number whenever a preassigned fixed number of reference frequency cycles has been accumulated. Differences between the recorded values at different sample times gives the number N of the Doppler-plus-bias count over the reference time interval.

Using either technique, the measurement results in a count of some number N of Doppler-plus-bias cycles over a period of time

$$\Delta t_{RR} = \frac{C_0}{\nu_{R_2}} \tag{C-18}$$

This measurement count can be modeled mathematically by the equation

$$N = \int_t^{t+\Delta t_{RR}} (\nu_d + \nu_b)\, dt_R \tag{C-19}$$

If the measurement is made in the destruct mode, the integration time interval, Δt_{RR}, should be varied until the computed value of N exactly matches the fixed cycle count number. In the nondestruct mode, Δt_{RR} is fixed and N, in general, will be some whole number of cycles plus a fractional part. This fractional part should be truncated to simulate more rigorously the actual accumulation of whole cycles.

The integration variable, t_R, in Equation (C-19) is the receiving station clock time, or proper time. The significance of this point will become evident during the evaluation of the integral.

Substitution of Equation (C-17) into Equation (C-19) yields

$$\begin{aligned} N &= \int_t^{t+\Delta t_{RR}} \left[\nu_T\left(\frac{\nu_R}{\nu_T}\right) + \nu_b - \nu_T\right] dt_R \\ &= (\nu_b - \nu_T)\,\Delta t_{RR} + \nu_T \int_t^{t+\Delta t_{RR}} \frac{\nu_R}{\nu_T}\, dt_R \end{aligned} \tag{C-20}$$

and Equation (C-16) can be substituted for the remaining integrand

$$N = (\nu_b - \nu_T)\,\Delta t_{RR} + \nu_T \sqrt{\frac{1 + \dfrac{\dot{\bar{r}}_T \cdot \dot{\bar{r}}_T}{c^2}}{1 + \dfrac{\dot{\bar{r}}_R \cdot \dot{\bar{r}}_R}{c^2}}}$$

$$\times \int_t^{t + \Delta t_{RR}} \left[\frac{1 - \dfrac{\hat{u} \cdot \dot{\bar{r}}_v}{c}}{1 - \dfrac{\hat{u} \cdot \dot{\bar{r}}_T}{c}}\right]\left[\frac{1 - \dfrac{\hat{d} \cdot \dot{\bar{r}}_R}{c}}{1 - \dfrac{\hat{d} \cdot \dot{\bar{r}}_v}{c}}\right] dt_R \qquad \text{(C-21)}$$

$$+ \nu_T\,\Delta t_{RR}\left(\frac{\Delta \dot{\varrho}_{avg}}{c}\right) \sqrt{\frac{1 + \dfrac{\dot{\bar{r}}_T \cdot \dot{\bar{r}}_T}{c^2}}{1 + \dfrac{\dot{\bar{r}}_R \cdot \dot{\bar{r}}_R}{c^2}}}$$

In writing Equation (C-21), it is assumed that the squares of the inertial speeds, $\dot{\bar{r}}_T \cdot \dot{\bar{r}}_T$ and $\dot{\bar{r}}_R \cdot \dot{\bar{r}}_R$, are constant, since the motion of the tracking stations is due to the nearly uniform rotation of the Earth. The refraction integral is evaluated by the trapezoidal rule, yielding

$$\Delta \dot{\varrho}_{avg} = \frac{\Delta \varrho_{t+\Delta t_{RR}} + \Delta \varrho_t}{2} \qquad \text{(C-22)}$$

The remaining integral in Equation (C-21) will not be considered. The geometries of the uplink and downlink ranges are related to the light times by

$$\varrho_u = |\bar{r}_v - \bar{r}_T| = c(\bar{t}_v - \bar{t}_T) \qquad \text{(C-23)}$$

and

$$\varrho_d = |\bar{r}_R - \bar{r}_v| = c(\bar{t}_R - \bar{t}_v) \tag{C-24}$$

The derivatives of these ranges with respect to the coordinate time $\bar{t}$ at the receiver are given by

$$\frac{d\varrho_u}{d\bar{t}_R} = \hat{u} \cdot \left(\dot{\bar{r}}_v \frac{d\bar{t}_v}{d\bar{t}_R} - \dot{\bar{r}}_T \frac{d\bar{t}_T}{d\bar{t}_R}\right) = c\left(\frac{d\bar{t}_v}{d\bar{t}_R} - \frac{d\bar{t}_T}{d\bar{t}_R}\right) \tag{C-25}$$

$$\frac{d\varrho_d}{d\bar{t}_R} = \hat{d} \cdot \left(\dot{\bar{r}}_R - \dot{\bar{r}}_v \frac{d\bar{t}_v}{d\bar{t}_R}\right) = c\left(1 - \frac{d\bar{t}_v}{d\bar{t}_R}\right) \tag{C-26}$$

Explicit solution for the coordinate time derivatives gives

$$\frac{d\bar{t}_v}{d\bar{t}_R} = \frac{1 - \hat{d} \cdot \frac{\dot{\bar{r}}_R}{c}}{1 - \hat{d} \cdot \frac{\dot{\bar{r}}_v}{c}} = 1 - \frac{1}{c}\frac{d\varrho_d}{d\bar{t}_R} \tag{C-27a}$$

$$\frac{d\bar{t}_T}{d\bar{t}_R} = \frac{1 - \hat{u} \cdot \frac{\dot{\bar{r}}_v}{c}}{1 - \hat{u} \cdot \frac{\dot{\bar{r}}_T}{c}} \left(\frac{d\bar{t}_v}{d\bar{t}_R}\right) = \frac{1}{c}\left(\frac{d\varrho_d}{d\bar{t}_R} + \frac{d\varrho_u}{d\bar{t}_R}\right) \tag{C-27b}$$

Equations (C-27) show that a coordinate time increment of a given length at the receiving station corresponds to increments of different lengths at the spacecraft and at the transmitter, considering that the arrival of corresponding phases at $\bar{t}_T$ and $\bar{t}_T + d\bar{t}_T$ marks the interval.

Substitution of Equations (C-27) into the integrand in Equation (C-21) yields the expression for the integral term

$$\nu_T \sqrt{\frac{1 + \frac{\dot{\bar{r}}_T \cdot \dot{\bar{r}}_T}{c^2}}{1 + \frac{\dot{\bar{r}}_R \cdot \dot{\bar{r}}_R}{c^2}}} \int_t^{t_R + \Delta t_{RR}} \left[1 - \frac{1}{c}\left(\frac{d\varrho_d}{d\bar{t}_R} + \frac{d\varrho_u}{d\bar{t}_R}\right)\right] dt_R \qquad \text{(C-28)}$$

At the receiving station, the relationship between coordinate and proper time is

$$dt_R = \sqrt{1 - \frac{\dot{\bar{r}}_R \cdot \dot{\bar{r}}_R}{c^2}}\, d\bar{t}_R \qquad \text{(C-29)}$$

Therefore,

$$\left(1 - \frac{\dot{\bar{r}}_R \cdot \dot{\bar{r}}_R}{c^2}\right) \frac{d\varrho}{d\bar{t}_R} = \frac{d\varrho}{dt_R} \qquad \text{(C-30)}$$

and, since it was assumed that $\dot{\bar{r}}_R \cdot \dot{\bar{r}}_R$ = constant, Equation (C-21) becomes

$$N = \nu_b \Delta t_{RR} - \frac{\nu_T}{c} \Delta\varrho_c + \frac{\nu_T}{c} \Delta t_{RR} \Delta\dot{\varrho}_{avg} \qquad \text{(C-31)}$$

Terms higher than first order in $|\dot{\bar{r}}|/c$ have been neglected, and the computed quantity

$$\Delta\varrho_c = (\varrho_u + \varrho_d)_{t_R + \Delta t_{RR}} - (\varrho_u + \varrho_d)_{t_R} \qquad \text{(C-32)}$$

is the range difference. Since the quantities N, Δt_{RR}, ν_b, and ν_T are known, the preprocessor program can compute the measurement

$$\dot{\varrho}_0 = \frac{c}{2\nu_T}\left(\nu_b - \frac{N}{\Delta t_{RR}}\right) \qquad \text{(C-33)}$$

and Equation (C-31) can be written as

$$\frac{\Delta\varrho_c}{2\Delta t_{RR}} = \dot{\varrho}_0 + \frac{\Delta\dot{\varrho}_{avg}}{2} \qquad \text{(C-34)}$$

where the division by $2\Delta t_{RR}$ causes the range difference to approximate the one-way range rate. Equation (C-34) mathematically describes the modeling of the USB Doppler measurement in GTDS. The quantity on the left side of the equation is the computed measurement and is calculated by means of Equations (C-32), (C-23), and (C-24). The latter two equations require that two iterative light-time solutions be determined to correspond to the round-trip propagation paths terminating at the receiving station at the start and at the end of the Doppler-plus-bias count interval, Δt_{RR}. The first term on the right side of Equation (C-34) represents the actual measurement and is calculated in the preprocessor from the basic measurement data according to Equation (C-33). The second term on the right in Equation (C-34) is the refraction correction term. It is computed by Equations (C-22) and (C-16), where the appropriate $\Delta\hat{u}$ and $\Delta\hat{d}$ path deflection vectors are computed as described in Section 7.6.3.3.

The GRARR and sidetone ATSR Doppler measurement model in GTDS is very simple. The Doppler measurements made with the GRARR and ATSR systems differ from those made using the USB System in terms of the hardware details. The GRARR VHF System operates with a nominal uplink carrier frequency of 148.98 megahertz and a nominal downlink frequency of 136.89 megahertz. The ATSR System, operating in the sidetone Doppler mode, uses C-band frequencies of approximately 6000 and 4000 megahertz on the uplink and downlink legs, respectively.

The simple model for these data types is derived by further restricting the assumptions made in deriving Equation (C-15). As given, that expression for the two-way Doppler-shifted frequency ratio is valid under the assumptions that special relativity holds and that the origin of the inertial coordinate frame is at the center of the Earth. If it is assumed instead that the tracking station moves with uniform velocity, i.e.,

$$\dot{\bar{r}}_R = \dot{\bar{r}}_T = \text{constant (inertially)}$$

then the origin of the coordinate system can be considered to be fixed at the tracking station and moving with it. Then,

$$r_R = \dot{\bar{r}}_T = 0 \tag{C-35}$$

and Equation (C-15) becomes

$$\frac{\nu_R}{\nu_T} = \frac{1 - \dfrac{\hat{u}_v \cdot \dot{\bar{r}}_v}{c}}{1 - \dfrac{\hat{d}_v \cdot \dot{\bar{r}}_v}{c}} \tag{C-36}$$

Substituting Equations (C-12) and (C-14) into this expression, expanding, eliminating higher order terms, and noting that in this case $\hat{u} = -\hat{d}$,

$$\frac{\nu_R}{\nu_T} = \frac{1 - \frac{\hat{u} \cdot \dot{\bar{r}}_v}{c}}{1 + \frac{\hat{u} \cdot \dot{\bar{r}}_v}{c}} + \frac{\Delta\dot{\rho}}{c} \qquad \text{(C-37)}$$

where

$$\Delta\dot{\rho} = 2\,\Delta\hat{u}_v \cdot \dot{\bar{r}}_v \qquad \text{(C-38)}$$

Since the tracking station is motionless in this coordinate frame, the unit vector $\hat{u}$ can be defined in terms of the instantaneous position vector of the vehicle relative to the station at the vehicle turnaround time $\bar{t}_v$ as

$$\hat{u} = \frac{\bar{r}_v(\bar{t}_v)}{|\bar{r}_v(\bar{t}_v)|} \qquad \text{(C-39)}$$

The instantaneous relative range at this time is

$$\rho = |\bar{r}_v(\bar{t}_v)| \qquad \text{(C-40)}$$

and the rate of change with respect to coordinate time is

$$\dot{\rho} = \bar{u} \cdot \dot{\bar{r}}_v \qquad \text{(C-41)}$$

If Equation (C-41) is substituted into Equation (C-37) and the result then substituted into Equation (C-20), the following results:

$$N - \nu_b \Delta t_{RR} = \nu_T \int_t^{t+\Delta t_{RR}} \left[\frac{1 - \frac{\dot{\varrho}}{c}}{1 + \frac{\dot{\varrho}}{c}} - 1 - 2 \frac{\Delta \hat{u}_v \cdot \dot{\bar{r}}_v}{c} \right] dt_R \qquad (C\text{-}42)$$

$$= -2\nu_T \int_t^{t+\Delta t_{RR}} \left[\frac{\dot{\varrho}}{c + \dot{\varrho}} + \frac{\Delta \hat{u}_v \cdot \dot{\bar{r}}_v}{c} \right] dt_R$$

Applying the Theorem of the Mean gives

$$N - \nu_b \Delta t_{RR} = -2\nu_T \left(\frac{\dot{\varrho}}{c + \dot{\varrho}} \right)_{avg} \Delta t_{RR} - 2\nu_T \left(\frac{\Delta \hat{u}_v \cdot \dot{\bar{r}}_v}{c} \right)_{avg} \Delta t_{RR} \qquad (C\text{-}43)$$

The last term on the right is the refraction correction, and it will be assumed that the mean value can be approximated with sufficient accuracy by evaluating $\Delta \hat{u}_v$ and $\dot{\bar{r}}_v$ at the vehicle turnaround time, $\bar{t}_v^*$, corresponding to the counting interval midpoint. With this understanding, the subscript avg will be dropped from this term. Writing $\dot{\varrho}_{avg}$ for the value of the range rate which produces the correct average value in Equation (C-43) and solving explicitly for $\dot{\varrho}_{avg}$ gives

$$\dot{\varrho}_{avg} = \frac{c \left(\nu_b - \frac{N}{\Delta t_{RR}} - 2\nu_T \frac{\Delta \hat{u}_v \cdot \dot{\bar{r}}_v}{c} \right)}{2\nu_T - \left(\nu_b - \frac{N}{\Delta t_{RR}} - 2\nu_T \frac{\Delta \hat{u}_v \cdot \dot{\bar{r}}_v}{c} \right)} \qquad (C\text{-}44)$$

Expanding this expression in terms of the small parameter $\Delta\hat{u}_v \cdot \dot{r}_v$ and eliminating higher order terms in this parameter, as well as terms involving this parameter divided by c, yields

$$\dot{\varrho}_{avg} = \frac{c\left(\nu_b - \frac{N}{\Delta t_{RR}}\right)}{2\nu_T - \left(\nu_b - \frac{N}{\Delta t_{RR}}\right)} - \Delta\hat{u}_v \cdot \dot{r}_v \qquad \text{(C-45)}$$

It is again assumed that the correct average value for $\dot{\varrho}_{avg}$, the instantaneous relative range rate, is given by Equation (C-41) evaluated at t_v^*, the vehicle turnaround time corresponding to the count interval midpoint at the ground station. Equation (C-45) therefore represents the model of the GRARR and sidetone ATSR Doppler measurements in the form of an instantaneous relative range rate. The term on the left is the computed value obtained by evaluating Equation (C-42) for the current estimate of the spacecraft ephemeris. The first term on the right side of Equation (C-45)

$$\dot{\varrho}_0 = \frac{c\left(\nu_b - \frac{N}{\Delta t_{RR}}\right)}{2\nu_T - \left(\nu_b - \frac{N}{\Delta t_{RR}}\right)} \qquad \text{(C-46)}$$

is the algorithm in current use in the preprocessing of the GRARR and ATSR Doppler data (References 3 through 6 in Appendix A) and represents the given measurement. The second term on the right side of Equation (C-45), $\Delta\hat{u}_v \cdot \dot{r}_v$, is the refraction correction. The vehicle velocity is taken at the time t_v^* defined above, and $\Delta\hat{u}_v$ is evaluated as described in Section 7.6.3.3.

APPENDIX D—MEASUREMENT WEIGHTING

Tables D-1 and D-2 define typical dynamic weighting factors and a priori standard deviations for several measurement types that are processed in GTDS. The dynamic weighting factors are used as described below.

If σ^2 is the a priori variance for a given measurement type and ϱ_F is the dynamic weighting factor, then the data weight for a measurement is formed as

$$w = \frac{\varrho_F}{\sigma^2} \tag{D-1}$$

For those measurements where a dynamic weighting factor is not specified, the data weight takes the form

$$w = \frac{1}{\sigma^2} \tag{D-2}$$

Table D-1. Dynamic Weighting Factors

MEASUREMENT TYPE	DYNAMIC WEIGHTING FACTOR*
Minitrack direction cosine ℓ	$\sqrt{1 - \ell^2}$
Minitrack direction cosine m	$\sqrt{1 - m^2}$
Range	C_1 sin (elevation) + C_2
Range rate	C_1 sin (elevation) + C_2
Elevation	C_1 sin (elevation) + C_2
Azimuth	C_3 cos (elevation) + C_4

* C_1, C_2, C_3, and C_4 are user-supplied constants.

Table D-2. Typical A Priori Data Standard Deviations

MEASUREMENT TYPE	A PRIORI STANDARD DEVIATION
Range (VHF)	500 meters
Range rate (VHF)	30 centimeters/second
X_{30} orientation angle (VHF)	3600 seconds of arc
Y_{30} orientation angle (VHF)	3600 seconds of arc
Minitrack direction cosine ℓ	0.3 mil
Minitrack direction cosine m	0.3 mil
Range (S-band)	100 meters
Range rate (S-band)	10 centimeters/second
Azimuth (C-band)	54 seconds of arc
Elevation (C-band)	54 seconds of arc
Range (USB)	15 meters
Range rate (USB)	5 centimeters/second
X_{30} (USB)	720 seconds of arc
Y_{30} (USB)	720 seconds of arc
X_{85} (USB)	54 seconds of arc
Y_{85} (USB)	54 seconds of arc

APPENDIX E—MATRIX IDENTITIES ASSOCIATED WITH SEQUENTIAL ESTIMATION

This appendix presents the derivations of a recursive form of the covariance matrix of error and an alternative form of the optimal linear gain. The results of these derivations are used in Section 8.4.1 to simplify the expressions for the covariance matrix of error and the updated state correction vector.

The following symbols are used in the derivations:

- P = symmetric, positive definite matrix
- I = identity matrix
- w_{m+1} = weight of the $(m+1)^{st}$ measurement; its inverse is equal to the variance of the measurement noise
- F = matrix of partial derivatives (see Equation (8-6))

E.1 DERIVATION OF THE RECURSIVE FORM OF THE COVARIANCE MATRIX OF ERROR, $P_{\Delta x\, m+1}$

From Equation (8-80b), the covariance matrix of error is given as

$$P_{\Delta x_{m+1}} = P_{\Delta x_m} + \Delta P \tag{E-1}$$

To find an expression for ΔP, Equation (E-1) is substituted into

$$P^{-1}_{\Delta x_{m+1}} P_{\Delta x_{m+1}} = I \tag{E-2}$$

yielding

$$P^{-1}_{\Delta x_{m+1}} (P_{\Delta x_m} + \Delta P) = I \tag{E-3}$$

Inverting Equation (8-79b), the following expression is obtained:

$$P^{-1}_{\Delta x_{m+1}} = (P^{-1}_{\Delta x_m} + F^T_{m+1} w_{m+1} F_{m+1}) \tag{E-4}$$

Substituting Equation (E-4) into Equation (E-3) gives

$$P_{\Delta x_m}^{-1} \Delta P + F_{m+1}^T w_{m+1} F_{m+1} P_{\Delta x_m} + F_{m+1}^T w_{m+1} F_{m+1} \Delta P = 0 \qquad \text{(E-5)}$$

Premultiplying Equation (E-5) by $P_{\Delta x_m}$ yields

$$\Delta P + P_{\Delta x_m} F_{m+1}^T w_{m+1} F_{m+1} P_{\Delta x_m} + P_{\Delta x_m} F_{m+1}^T w_{m+1} F_{m+1} \Delta P = 0 \qquad \text{(E-6)}$$

Solving this expression for ΔP yields

$$\Delta P = -(I + P_{\Delta x_m} F_{m+1}^T w_{m+1} F_{m+1})^{-1} P_{\Delta x_m} F_{m+1}^T w_{m+1} F_{m+1} P_{\Delta x_m} \qquad \text{(E-7)}$$

Premultiplying by $P_{\Delta x_m} P_{\Delta x_m}^{-1}$ results in the following:

$$\Delta P = -P_{\Delta x_m} (I + P_{\Delta x_m} F_{m+1}^T w_{m+1} F_{m+1})^{-1} F_{m+1}^T w_{m+1} F_{m+1} P_{\Delta x_m} \qquad \text{(E-8)}$$

Multiplying $F_{m+1}^T w_{m+1} F_{m+1}$ into the term in parentheses in Equation (E-8) and factoring forward yields

$$\Delta P = -P_{\Delta x_m} F_{m+1}^T w_{m+1} F_{m+1} (I + P_{\Delta x_m} F_{m+1}^T w_{m+1} F_{m+1})^{-1} P_{\Delta x_m} \qquad \text{(E-9)}$$

Equation (E-9) is not the best form for ΔP. From the definition of the inverse of a matrix, the following expression can be obtained:

$$(w_{m+1}^{-1} + F_{m+1} P_{\Delta x_m} F_{m+1}^T)^{-1} (w_{m+1}^{-1} + F_{m+1} P_{\Delta x_m} F_{m+1}^T) = I \qquad \text{(E-10)}$$

Postmultiplying Equation (E-10) by $w_{m+1} F_{m+1}$ and then factoring out F_{m+1} yields

$$(w_{m+1}^{-1} + F_{m+1} P_{\Delta x_m} F_{m+1}^T)^{-1} F_{m+1} (I + P_{\Delta x_m} F_{m+1}^T w_{m+1} F_{m+1}) = w_{m+1} F_{m+1} \qquad \text{(E-11)}$$

If Equation (E-11) is then postmultiplied by $(I + P_{\Delta x_m} F_{m+1}^T w_{m+1} F_{m+1})^{-1}$, the following is obtained:

$$(w_{m+1}^{-1} + F_{m+1} P_{\Delta x_m} F_{m+1}^T)^{-1} F_{m+1} = w_{m+1} F_{m+1} (I + P_{\Delta x_m} F_{m+1}^T w_{m+1} F_{m+1})^{-1} \qquad \text{(E-12)}$$

Substituting Equation (E-12) into Equation (E-9) gives

$$\Delta P = -P_{\Delta x_m} F_{m+1}^T (w_{m+1}^{-1} + F_{m+1} P_{\Delta x_m} F_{m+1}^T)^{-1} F_{m+1} P_{\Delta x_m} \tag{E-13}$$

and substituting Equation (E-13) into Equation (E-1) gives

$$P_{\Delta x_{m+1}} = P_{\Delta x_m} - P_{\Delta x_m} F_{m+1}^T (w_{m+1}^{-1} + F_{m+1} P_{\Delta x_m} F_{m+1}^T)^{-1} F_{m+1} P_{\Delta x_m} \tag{E-14}$$

or

$$P_{\Delta x_{m+1}} = (I - K F_{m+1}) P_{\Delta x_m} \tag{E-15}$$

where

$$K \equiv P_{\Delta x_m} F_{m+1}^T (w_{m+1}^{-1} + F_{m+1} P_{\Delta x_m} F_{m+1}^T)^{-1} \tag{E-16}$$

E.2 DERIVATION OF AN ALTERNATIVE FORM OF THE OPTIMAL LINEAR GAIN

From Equation (8-79), the covariance matrix of error is given as

$$P_{\Delta x_{m+1}} = (P_{\Delta x_m}^{-1} + F_{m+1}^T w_{m+1} F_{m+1})^{-1} \tag{E-17}$$

Postmultiplying this equation by $F_{m+1}^T w_{m+1}$ and factoring out $P_{\Delta x_m}^{-1}$ gives

$$P_{\Delta x_{m+1}} F_{m+1}^T w_{m+1} = (I + P_{\Delta x_m} F_{m+1}^T w_{m+1} F_{m+1})^{-1} P_{\Delta x_m} F_{m+1}^T w_{m+1} \tag{E-18}$$

Premultiplying Equation (E-18) by $F_{m+1}^T w_{m+1} F_{m+1}$ and substituting Equation (E-12) into the result yields

$$\begin{aligned} &F_{m+1}^T w_{m+1} F_{m+1} P_{\Delta x_{m+1}} F_{m+1}^T w_{m+1} \\ &\quad = F_{m+1}^T (w_{m+1}^{-1} + F_{m+1} P_{\Delta x_m} F_{m+1}^T)^{-1} F_{m+1} P_{\Delta x_m} F_{m+1}^T w_{m+1} \end{aligned} \tag{E-19}$$

Moving the factor $F_{m+1} P_{\Delta x_m} F_{m+1}^T w_{m+1}$ inside the brackets and factoring out w_{m+1} gives

$$F_{m+1}^T w_{m+1} F_{m+1} P_{\Delta x_m} F_{m+1}^T w_{m+1} = F_{m+1}^T w_{m+1} [w_{m+1}^{-1} (F_{m+1} P_{\Delta x_m} F_{m+1}^T)^{-1} + I]^{-1} \quad \text{(E-20)}$$

Factoring out $F_{m+1} P_{\Delta x_m} F_{m+1}^T$ from this expression and premultiplying by $(F_{m+1}^T w_{m+1} F_{m+1})^{-1}$ gives

$$P_{\Delta x_{m+1}} F_{m+1}^T w_{m+1} = P_{\Delta x_m} F_{m+1}^T (w_{m+1}^{-1} + F_{m+1} P_{\Delta x_m} F_{m+1}^T)^{-1} \quad \text{(E-21)}$$

Finally, substituting Equation (E-21) into Equation (E-16) yields the following expression for K:

$$K = P_{\Delta x_{m+1}} F_{m+1}^T w_{m+1} \quad \text{(E-22)}$$

GLOSSARY OF ACRONYMS

Definitions of the acronyms used throughout this document are given in this glossary. The acronyms are listed in alphabetical order.

ALCOR	Advanced Research Project Agency, Lincoln C-band Observable Radar
ARC	Ambiguity resolving code
ATS	Applications Technology Satellite
ATSR	Applications Technology Satellite Ranging
AZ-EL	Azimuth-elevation
A.1	Atomic time
BRT	Bilateration Ranging Transponder
BRTS	Bilateration Ranging Transponder System
CCIR	International Radio Consultative Committee
CSC	Computer Sciences Corporation
DC	Differential correction
DDNA	Divided Difference Noise Analysis
DIGS	Delta Inertial Guidance System
DMC	Dynamic model compensation
DODS	Definitive Orbit Determination System
DS	Delaunay-Similar
EKF	Extended Kalman Filter
ET	Ephemeris time
EW	East-west

FDF	Flight Dynamics Facility
FOC	Fractions of a cycle
GCI	Geocentric equatorial inertial
GHA	Greenwich hour angle
GMT	Greenwich Mean Time
GRARR	Goddard Range and Range-Rate
GSFC	Goddard Space Flight Center
GTDS	Goddard Trajectory Determination System
ID	Identifier
JPL	Jet Propulsion Laboratory
KS	Kustaanheimo-Stiefel
KSA	K-band single access
LTAS	Launch Telemetry Acquisition System
MA	Multiple-access
MECO-1	Main engine cutoff (first)
MEKF	Modified Extended Kalman Filter
MFR	Multifunctional receiver
MJD	Modified Julian date
NASA	National Aeronautics and Space Administration
NS	North-south
O-C	Observed-minus-computed
OCS	Orbit Computation System

PECE	Predict, evaluate, correct, pseudoevaluate
PN	Pseudorandom noise
PODS	Preliminary Orbit Determination System
QL	Quick look
RA	Radar Altimeter
R&D	Research and Development
RF	Radio frequency
RMS	Root mean square
RMSP	Predicted root mean square
RSS	Root sum square
RU	Range unit
SA	Single-access
SAO	Smithsonian Astrophysical Observatory
SGLS	Space Ground Link Subsystem
SLP	Solar/Lunar/Planetary
SOR	Statistical Output Report
SRE	STDN Ranging Equipment
SSA	S-band single-access
ST	Station time
STDN	Spaceflight Tracking and Data Network
TCOPS	Trajectory Computation and Orbital Products System
TDRS	Tracking and Data Relay Satellite

TDRSS	Tracking and Data Relay Satellite System
TDRS-E	TDRS-East
TDRS-S	TDRS-Spare
TDRS-W	TDRS-West
TIR	Time Increment Resolver
TIU	Time interval unit
TT&C	Tracking, telemetry, and command
USB	Unified S-band
USNO	United States Naval Observatory
UT, UT1, UT2	Universal time
UTC	Coordinated universal time
UT0	Uncorrected universal time
UT1	Universal time, corrected for polar motion
VDNA	Variate Difference Noise Analysis
VHF	Very high frequency
VLBI	Very Long Baseline Interferometer
VOP	Variation of Parameters
WSGT	White Sands Ground Terminal

GLOSSARY OF MATHEMATICAL SYMBOLS

The following pages contain a glossary of the mathematical symbols used throughout this document. Symbols are given in alphabetical order, with Greek symbols following the Roman symbols. Definitions of the major subscript, superscript, and operational symbol conventions are given following the Greek symbols. For each symbol, the corresponding definition is given. If a symbol has multiple definitions, the primary definition is generally given first and/or definitions are listed in section-number order, with the pertinent section number(s) for a specific definition given in parentheses.

A	Azimuth angle
	Rotation matrix for precessing between the mean equator and equinox of two epochs (Section 3.3.1)
	Reference satellite area for aerodynamic drag (Section 4.5)
	Satellite area exposed to direct solar radiation (Section 4.6)
	Cross-sectional area of the launch vehicle (Section 9.1)
	Precession transformation matrix from mean of B1950.0 or J2000.0 to mean of date coordinates (Section 3.3.1)
	Effective transmit frequency from the user (Section 7.3.4)
A, B, C	Matrices of time-varying coefficients in variational differential equations (Sections 4.1, 6.1.4, and 6.3)
A_m, B_m, C_m, D_m	Coefficients of the polynomial fitted to Minitrack fine baseline rectified data (Appendix A)
A_n, B_n, C_n	Coefficients of the polynomial fitted to Minitrack coarse and medium baseline rectified ambiguity data (Appendix A)
A_p	Solar paddle area (Section 4.5.2)
A.1	Atomic time
A_1', A_2', A_1, .., A_{26}	Auxiliary parameters defined in Equations (5-184)
AZ	Azimuth angle (Section 7.3.7)
a	Semimajor axis of the satellite orbit
	Semimajor axis of the reference ellipsoid (Section 7.4)
	Magnitude of the spacecraft thrust acceleration (Section 4.8)

$\dot{a}$	Minitrack fine baseline fractional phase rate (Section A.4)
$\bar{a}_b$	Inertial acceleration vector in body-fixed coordinates (Section 4.3)
$\bar{a}_E(M)$	Inertial acceleration of the point-mass Earth due to the Moon's oblateness (Section 4.4)
a_F, $\underline{a}_F$, $\underline{a}'_F$	Minitrack fine baseline fractional phase difference (Section A.4)
a_l	Drag scale parameter coefficients (Sections 4.5.2 and 4.5.3)
a_{ij}	Polynomial coefficients of polar motion (Section 3.3.2.2)
	Time difference polynomial coefficients (Section 3.5.2)
	Terms used in the evaluation of the Chebyshev polynomial coefficients (b_i) (Section 3.6)
a_i, b_{ij}, c_i	Shank's coefficients used in the Runge-Kutta integration method (Section 6.2.1)
$\bar{a}_j$	Represents the j^{th} row of the matrix of measurement partial derivatives, F (Chapter 8)
a_j, $b_{j\ell}$, c_j	Coefficients for the Hull Runge-Kutta 3(4+) method (Section 6.2.2)
$\bar{a}_m$	Acceleration vector in the nominal dynamical model (Section 8.4.2)
a_p	Planet radius (Section 4.6.1)
$\bar{a}_u$	Vector of unknown or unmodeled accelerations (Section 8.4.2)
a_x, a_y, a_z	Coefficients of the polynomial characterizing the attitude control system acceleration (Section 4.7.1)
a_0, a_1, ..., a_4	Coefficients of the polynomial characterizing the spacecraft thrust acceleration (Section 4.8)
a_1, a_2, a_3	Parameters in the topside electron density profile (Section 7.6)

a_{11}, a_{12}, a_{13}, ..., a_{33}	Elements of the transformation matrix A (Section 3.3.1.1)
B	Transformation matrix from the true equator and equinox of date coordinate system to body-fixed coordinates (Sections 3, 4, and 9)
	Pilot-tone frequency translation from the return-link TDRS (Section 7.3.4)
B, C, A	See A, B, C above
B_C, B_F, B_M	Minitrack coarse, fine, and medium phase rates (Section A.4)
B_1	Transformation matrix from true of date to pseudo body-fixed coordinates (Section 3.3.2)
B_2	Simplified transformation matrix from pseudo body-fixed to body-fixed coordinates (Section 3.3.2)
B_1, ..., B_{15}	Auxiliary parameters defined in Equations (5-185) (Section 5.10)
b	Measurement bias, which depends on the measurement type and the tracking station (Sections 7.1 and 8.2)
$\underline{b}_F$	Absolute phase difference for the Minitrack fine baseline (Section A.4)
b_i	Chebyshev coefficients of the interpolating polynomial (Section 3.6)
b_j, c_j	Numerical coefficients (Section 5.6)
b_m	Polynomial fitted to Minitrack fine baseline rectified data (Section A.4)
b_n	Polynomial fitted to Minitrack coarse and medium baseline rectified ambiguity data (Appendix A)
b_x, b_y, b_z	Coefficients of the linear term of the polynomial characterizing the attitude control system acceleration (Section 4.7.1)
C	Transformation matrix from the mean equator and equinox of B1950.0 or J2000.0 coordinate system to the true of date coordinate system (Section 3.3.1 and Chapters 4 and 9)
	Calibration factor (Section 4.8.3)
	Noise estimation convergence criterion (Section 8.7.4)

C, A, B	See A, B, C above
C_{Ac}	Force coefficient for the force along the cylinder axis (Section 4.5.2) (see Table 4-1)
C_D, C_{D0}	Aerodynamic drag coefficient with and without systematic error corrections (Section 4.5)
C_F	Nondimensional force coefficient (Section 4.5.2)
C_{max}	Maximum allowed correction (Section 9.2.3)
C_{Nc}	Force coefficient for the force normal to the cylinder axis (Section 4.5.2) (see Table 4-1)
C_{Np}	Force coefficient for the force normal to the plate (Section 4.5.2) (see Table 4-1)
C_R	Nondimensional force coefficient for solar radiation pressure (Section 4.6)
C_{Tp}	Force coefficient for the force tangent to the plate (Section 4.5.2) (see Table 4-1)
C_l, C_l'	Comparison parameters (Section 9.3)
C_j^i	Harmonic coefficients of the Earth's nonspherical potential (Section 4.4)
C_n^m	Gravitational harmonic coefficients
$C_{\Delta s \Delta u^*}$	Correlation between errors in $\bar{s}$ and $\bar{u}^*$ (Chapter 8)
$C_{\Delta x \Delta z}$	Correlation between errors in $\bar{x}$ and $\bar{z}_0$ (Chapter 8)
$C_{\Delta x_0 n}$	Correlation between errors in $\bar{x}_0$ and $\bar{n}$ (Chapter 8)
$C_{\Delta x_0 \Delta z}$	Correlation between errors in $\bar{x}_0$ and $\bar{z}_0$ (Chapter 8)
$C_{\Delta z n}$	Correlation between errors in $\bar{z}$ and $\bar{n}$ (Chapter 8)
C_ψ	Dot product (Chapter 9)
C_0, C_1	Count of the number of cycles of the GRARR and ATSR Doppler reference frequency and the range reference frequency (Chapter 7, Appendices A and C)

c	Vacuum speed of light
c_g, c_p	Group speed and phase speed of propagation of an electromagnetic signal (Section 7.6)
c_l^j	Harmonic coefficients of the Moon's nonspherical potential (Section 4.4)
c_j	Coefficients in the expression for $Y_m(t)$ (Section 3.6)
c_x, c_y, c_z	Coefficients of the quadratic term of the polynomial characterizing the attitude control system acceleration (Section 4.7.1)
D	Transformation matrix from true of date to local plane coordinates (Section 3.3.4)
	Parameter obtained from Barker's equation for parabolic motion (Section 3.3.8.1)
	Parameter used to determine if the spacecraft is within the cylindrical shadow of a celestial body (Section 4.6)
	Linear differentiation operator (Sections 6.1.1 and 6.1.4)
D, D_{ij}	Matrix and its elements (Section 5.5)
D_j	Transponder delay at node j (Section 7.3.2)
D_n	Quantity used to solve Kepler's equation for elliptical motion (Section 3.3.8)
DCI	Doppler count interval (seconds) (average Doppler count interval if it is not constant throughout the batch) (Section 8.7.4)
d	Spacecraft diameter (Sections 4.5.2 and Appendix C)
$\hat{d}$	Unit vector pointing down along the vacuum downlink path from the spacecraft to the tracking station (Section 7.6.3 and Appendix C)
d_e	Number of ephemeris days past 0^h January 1, 1950 ET (Section 3.3.3)

E	Eccentric anomaly of an orbit
	Transformation matrix from body-centered true of date inertial Cartesian coordinates to orbit plane coordinates (Section 3.3.5)
	Elevation angle measured from the reference plane to the station-to-spacecraft position vector (Section 3.2.4, Chapter 7, Section 9.2, and Appendix A)
	Matrix of partial derivatives of the nonlinear measurement equations f(x,z) with respect to consider variables z (Section 8.2)
E_a	Measured elevation angle (Section 7.6)
E_{max}	Predetermined maximum of the relative truncation error, E_{rel} (Section 6.2.2)
E_{rel}	Relative truncation error (Section 6.2.2)
E^s	Linear shifting operator (Section 6.1.1)
E_1, E_2	Reference epochs (Section 3.3.1.1)
	Integer exponents in preliminary orbit search (Section 9.2.3)
EL	Elevation angle (Section 7.3.7)
ET	Ephemeris time
e	Orbital eccentricity
	Eccentricity of the central body (Section 3.3.1.3)
	Eccentricity of the planet's figure (Section 3.3.6)
$\bar{e}$	Eccentricity vector (Sections 3.2.6 and 3.3.10)
e_x, e_y, e_z	Herrick eccentricity vector components (Section 3.3.11.2)
em	Exponential multiplier (Section 7.6.3)
F	Hyperbolic anomaly (Section 3.3.8)
	Eccentric longitude (Section 3.3.9); equals the sum of the eccentric anomaly, argument of perigee, and right ascension of the ascending node

F (Cont'd)	Total force acting on the spacecraft (Chapter 4)
	Perturbed Hamiltonian (Section 5.5)
	Matrix of partial derivatives of measurements with respect to solve-for variables (Chapter 8 and Appendix E)
F'	Augmented matrix of partial derivatives (Section 8.2)
$F'(t_i)$	Table entry for the thrust magnitude value (kilonewtons) (Section 4.8.3)
F_B	Aerodynamic acceleration per unit density (Section 4.5.2)
F_R	Receive frequency (hertz) (Section 8.7.4)
F_{rec}	Frequency received at the return-link TDRS from a target (hertz) (Section 7.3.2.3)
F^TWF	Normal matrix (Chapter 8)
$\bar{F}^T W \bar{F}$	Expanded state normal matrix (Chapter 8)
F_t, F_r	Parameters used in the general relativistic expression (defined in Appendix C)
F_0	Unperturbed Hamiltonian (Section 5.5)
F_1, F_2, F_3, F_4	Functions used in the evaluation of the density (Section 4.5.4)
$F_{10.7}$	Daily average of the 10.7-centimeter solar flux (Section 4.5)
$F_{10.7}^{avg}$	81-day running average of $F_{10.7}$ (Section 4.5)
F	Augmented measurement matrix (Section 8.4)
f	Orbital true anomaly (Sections 3.3.8.1, 4.9, 5.9, 6.1.1.2, 9.2.3, and Appendix B)
	Planet's flattening coefficient (Sections 3.3.6.1, 4.5.6, 7.2, and 9.2)
	Inverse flattening coefficient of the central body (Section 3.3.13)

f (Cont'd)	General time–varying function (Chapter 6)
	Function arising from the equations of motion or the variational equations in the Runge-Kutta integrators (Section 6.2)
f	Function (Section 3.3.8)
f, g	Series used to predict spacecraft positions (Chapter 9)
$\hat{f}$, $\hat{g}$, $\hat{w}$	Equinoctial unit vectors along the equinoctial coordinate directions x_{ep}, y_{ep}, and z_{ep}, respectively (Sections 3.2.5 and 3.3.9.1)
$f(t_i)$	Measurement model (Section 4.9)
f_i	Functions used in the Runge-Kutta integration method (Section 6.2)
f_0	Geometric relationship defined by the measurement type at time t + δt (Sections 7.1 and 8.2)
$f_0 F_2$	Critical frequency of the F2 layer (Section 7.6)
G	Universal gravitational constant
	Total angular momentum (Section 5.5 and Appendix B)
GHA	Greenwich hour angle
GM	Gravitational constant of the central body (Sections 3.3.14 and 6.2.3)
g	Argument of the pericenter (Section 5.5)
g, g′	Mean anomaly of the Moon and Sun, respectively (Section 3.3.3)
$g(a)$	Function relating τ and a in the time element formulation (Appendix B)
g_i	Nonlinear functional form of $\hat{\Delta}s_i$ (Section 8.2.3)
g_{ij}	Elements of the metric matrix defining the nature of the space-time frame (Appendix C)

g_s	Sea-level acceleration due to gravity (Section 4.5.4)
H	Local hour angle of the Sun (Section 4.5.4)
	z component of the angular momentum (Section 5.5)
	Matrix used for expressing the Cowell corrector formula in matrix form (Chapter 6)
H_I	Ionospheric scale height in the expression for refractivity (Section 7.6)
H_M, H_m	Maximum and minimum scale heights (Section 4.5.6)
H, h	Transformations of the covariance matrix, $P_{\Delta s}$, and the estimated state, $\bar{s}$, respectively (Chapter 8)
H_s	Height above the mean spheroid, normal to the ellipsoidal surface (Section 3.3.1.3)
H_T	Tropospheric scale height in the expression for refractivity (Section 7.6)
h	Altitude measured as the perpendicular distance from the surface of the ellipsoidal planet model to the point being measured (Sections 3.2.2, 3.3.6, and Chapter 4)
	Energy of the orbit (Section 5.4 and Appendix B)
	Longitude of the ascending node (Section 5.5)
	Integration stepsize (Chapter 6)
h, h_r	Projection of the vector $\bar{e}$ on the $\hat{y}_{ep}$ axis (equinoctial elements) (Chapter 3)
h, $\bar{h}$, h_x, h_y, h_z	Orbital angular momentum vectors and Cartesian components (Section 3.3.8)
h_a, h_p	Apofocal and perifocal altitude (Sections 3.3.8.3, 9.2.3)
h_K	Negative Keplerian energy (Appendix B)
h_L	Lower altitude limit for the ionosphere (Section 7.6)

h_m	Altitude corresponding to the maximum electron density (Section 7.6)
h_r	Runge-Kutta stepsize hour (Section 6.2.3)
h_s	Height of the tracking station above the reference ellipsoid (Sections 3.3.7, 7.6, and 9.2)
h_0, h_1, h_2	Parameters in the topside electron density profile (Section 7.6)
I	Orbital inclination (Section 5.5)
	Linear identity operator (Section 6.1.1)
	Abbreviation used in the ray angular deflection formula (Section 7.6.3) (Equation (7-175))
	Identity matrix (Chapter 8 and Appendix E)
I, I_M	Inclination of the mean lunar equator to the ecliptic of date (Section 3.3.3)
${}^{I}P_n$, ${}^{II}P_n$; ${}^{I}S_n$, ${}^{II}S_n$	Summation symbols (Chapter 6)
i	Orbital inclination
	Local incidence angle between an electromagnetic ray and a radius vector (Section 7.6)
i_p	Incidence angle between the spacecraft axis and the paddle surface (Section 4.5.2)
i_s	Inclination of the Moon's equatorial plane to the Earth's equatorial plane (Euler angle used in the transformation from selenocentric to selenographic coordinates.) (Section 3.3.3)
J_n	Zonal harmonic coefficients ($J_n = -C_n^0$) (Chapter 4)
J_2, J_3, J_4, J_5	Zonal harmonic coefficients (Chapter 5)
JD	Julian day number
JE	Julian epoch (Section 3.3.1)

JED	Julian ephemeris date (Section 3.3.1)
K	Kalman filter gain matrix (Chapter 8)
K	Augmented gain matrix (Section 8.4)
K_p	Geomagnetic planetary index (Section 4.5.4)
k	Solar pressure model parameter (Section 4.6.2)
	Factor used in defining the average Doppler frequency (Section 7.3)
$\hat{k}$	Unit vector normal to the orbital plane (Section 9.2)
k, k_r	Projection of the vector $\bar{e}$ on the $\hat{x}_{ep}$ axis (equinoctial elements) (Chapter 3)
k_i	Functions used in the Runge-Kutta integration method (Section 6.2)
k_1, k_2	Gain constants used to compute measurement variances (Section 8.1)
k_1, k_2, k_3	Decay constants for the lower, middle, and upper third, respectively, of the topside electron density profile (Section 7.6)
k_2, k_3, k_4, k_5	Auxiliary parameters (defined in Section 5.9)
L	Cylinder length (Section 4.5.2)
	Luminosity of the Sun (Section 4.6)
	Magnitude of the angular momentum vector (Section 4.8.2)
	Total energy of the orbit (DS element) (Chapter 5 and Appendix B)
	KS matrix (Section 5.4)
	Length of pseudorandom code (chips) (Section 7.3.2.3)
	Search level (Section 9.2.3)
L, L_b, L_H, L_T	Unit vector directed toward the spacecraft from a tracking station in mean of B1950.0 or J2000.0, body-fixed, local tangent, or true of date coordinates, respectively (Section 9.2)

L_i	Components of the angular momentum vector (Section 4.8.2)
L_1	Libration point, lying on the vector between the Sun and the Earth-Moon barycenter (Section 3.3.14)
$(L^TP)_1$, $(L^TP)_2$, $(L^TP)_3$	Transformed components of perturbing accelerations (Section 5.4)
ℓ	Parameter in Robert's temperature profile (Section 4.5.4)
	Mean anomaly in Delaunay elements (Chapter 5 and Appendix B)
	Direction cosine of the angle between the station-spacecraft vector and the local tangent east-pointing axis; this angle is measured by the Minitrack System (described in Section 7.2.3)
	Number that scales the hyperellipse of constant (normal) probability in terms of the standard deviations (Section 8.5.2)
	Direction cosine of the corrected phase difference from the east-pointing axis at the station (Appendix A)
$\vec{\ell}$, ℓ_x, ℓ_y, ℓ_z	Herrick angular momentum vector and its components (Sections 3.2.6, 3.3.10, and 3.3.11)
M	Orbital mean anomaly
	Transformation matrix from the geocentric body-fixed coordinate system to the true of date system (Section 9.1)
$\overline{M}$	Maneuver parameters (Section 4.8.4)
$M(t_i)$	Table entry for the mass (kilograms) (Section 4.8.3)
M(Z)	Mean molecular mass of atmosphere (Section 4.5.4)
M, M′	Transformation matrices from selenocentric to selenographic coordinates (Sections 3.3.3 and 4.4)
M, M_{ij}, m_{ij}	Notation used in describing the matrix inversion procedure (Section 8.6)
M_{C_i}	Final unedited batch calibration residual mean from the i^{th} batch (Section 8.7.3)

M_c	Final unedited batch calibration mean value (Section 8.7.4)
M_E	Mass of the Earth (Section 3.3.14)
M_e	Final edited batch validation residual mean (Section 8.7.3)
M_i	Molecular mass of atmospheric constituents (Section 4.5.4)
M_{lt}	Transformation matrix from body-fixed coordinates, centered at a tracking station, to local tangent coordinates at the station (Section 3.3.7 and Chapter 9)
M_k	Mean of the unedited residuals (Section 8.7.2)
M_{k-1}	Mean of the unedited residuals from the previous edit loop (Section 8.7.2)
M_M	Mass of the Moon (Section 3.3.14)
	Mean of the unedited batch calibration residual mean values (Section 8.7.3)
M_S	Mean of the unedited batch calibration residual standard deviations (Section 8.7.3)
M_s	Sea-level mean molecular mass (Section 4.5.4)
M_u	Final unedited batch validation residual mean (Section 8.7.3)
M_0	Mean of unedited residuals (Section 8.7.2)
MAX	Maximum (approximately) positive number representable in the computer (Section 9.3)
MJD, MJD_i	Modified Julian date and tabular modified Julian date (Section 3.5)
MUF(3000)F2	Highest frequency usable for a 3000-kilometer single-hop propagation via the F2 layer (Section 7.6)
M-factor	Ratio of MUF(3000)F2 to the critical frequency f_0F_2 (Section 7.6)
m	Mass of a body (Chapter 4)
	Direction cosine of the angle between the station-spacecraft vector and the local tangent north-pointing axis; this angle is measured by the Minitrack System (Section 7.2.3)

m (Cont'd)	Sigma multiplier for the noise analysis "m-sigma" edit (Section 8.7.4)
	Mass of the satellite/launch vehicle combination at ignition (or at the last burnout) (Section 9.1)
$\overline{m}$	Mean value of each residual group (Section 8.6)
m'	Direction cosine of the corrected phase difference from the north-pointing axis at the station (Appendix A)
m_{bo}	Vehicle mass at burnout time (Section 4.8.4)
m_{ig}	Vehicle mass at ignition time (Section 4.8.4)
N	Distance along the normal vector from the intersection of the normal and the ellipsoid to the z_b axis (Figure 3-15 and Section 3.3.6)
	Nutation transformation matrix from mean of date to true of date coordinates (Sections 3.3.1 and 9.2.1)
	Number of unedited residuals available for noise estimation (Section 8.7.4)
	Total number of counts (Section A.8)
$\overline{N}$	Ascending nodal vector in the equinoctial system (Figure 3-5 and Section 3.2)
N, N_1, N_0	Number of cycles of the Doppler-plus-bias signal counted over the Doppler counting cycle (Appendix A and Appendix C)
N_{CNTR}	Doppler count VDNA noise estimate (Section 8.7.4)
$N_{\overline{D}}$	Averaged Doppler VDNA noise estimate (Section 8.7.4)
N'_D	Doppler DDNA noise estimate (Section 8.7.4)
N_e, N_m	Electron density and maximum electron density (Section 7.6)
N_F	Minitrack fine baseline lengths in terms of vacuum wavelengths of the nominal 136.0 megahertz frequency signal (Appendix A)

N_I, N_T	Ionospheric and tropospheric refractivity (Section 7.6)
N_i, N_{i-1}	Doppler counter readings (in counts) associated with time tags T_1 and T_{i-1}, respectively (Section A.8.2)
N_{pq}	Brouwer drag parameters (Section 4.9)
$N_{\dot{R}}$	Averaged range-rate VDNA noise estimate (Section 8.7.4)
$N'_{\dot{R}}$	Intermediate range-rate DDNA noise estimate (Section 8.7.4)
N_s	Magnitude of the normal vector to the surface of the reference ellipsoid at the tracking station (Sections 3.3.7 and 9.2)
	Surface refractivity (Section 7.6)
N_0, N_1, N_2	Parameters in the topside electron density profile (Section 7.6)
n	Keplerian mean motion
	Adjustable parameter exponent of the cosine variation between the Harris-Priester maximum and minimum density profiles (Sections 4.3.5 and 5.3)
	Uniformization constant (Section 5.1)
	Number of accelerations in the backpoints table (Section 6.1.5)
	Variable local index of refraction (Section 7.6)
	Measurement noise (Section 7.8)
	Sigma multiplier (Section 8.7.2)
	Mean motion (Section 9.2.3)
	Total number of counts (Section A.8.2)
$\hat{n}$	Unit vector along the idealized straight signal propagation path (Appendix C)
	Random noise vector (Chapter 8)
$\hat{n}$, $\hat{n}'$	Unit vectors normal to the reference ellipsoid and the geoid, respectively (Section 7.4)

$n(T)$	Integer number of ambiguity intervals for a measured range at time tag T (Section 7.3.2)
n_b	Number of batches of either two-way or hybrid range data for each ground transponder user (Section 8.7.3)
n_s	Total number of residuals for a tracking station and data type (Section 8.6)
$\hat{n}_t$, $\hat{n}_r$	Unit vectors along the local signal propagation path at the transmitter and receiver, respectively (Appendix C)
n_0	Number of remaining unedited residuals in the category validation statistics (Section 8.7.2)
O_c	Computed measurement (Sections 7.1, 7.3, and 8.2)
P	Transformation matrix from orbital rectangular coordinates to true of date coordinates (Sections 3.3.8.1 and 3.3.8.2)
	Orbital period (Section 3.3.8.3)
	Pitch angle (Section 4.8.4)
	PN code period (seconds) (Section 7.3.2.3)
	Ionospheric term used in the equation for atmospheric time delay (Section 7.6.3)
	Order of the variate differences (Section 8.7.4)
	Symmetric positive definite matrix (Appendix E)
$\bar{P}$	Perturbative accelerations additional to the primary body's inverse square gravity (Chapter 5 and Appendix B)
P	Augmented error covariance matrix (Section 8.4)
P_A, P_T	Adopted and true pole, respectively, of the Earth (Section 3.3.2.2)
$\hat{P}_c$	Computed spatial beam vector (Section 7.3.7)
$\hat{P}_c'$	Computed unit vector from the return-link TDRS to the user spacecraft or transponder (Section 7.3.7)

$P_i(\cos\theta)$	Legendre functions (Section 4.2)
P_{ig}	Pitch angle at ignition (Section 4.8.4)
$\dot{P}_{ig}$	Pitch angle rate (assumed constant) (Section 4.8.4)
P_n^m	Legendre functions (Section 4.3.1)
$\hat{P}_o$	Measured spatial beam vector (Section 7.3.7)
P_s	Force on a perfectly absorbing surface due to solar radiation pressure at one astronomical unit (Section 4.6)
P_T, Y_T	Pitch and yaw angles, respectively, defining the thrust direction (Section 4.8)
$P_{\Delta a}$	Covariance matrices (Chapter 8)
$P_{\Delta s}$, $P'_{\Delta s}$	Covariance matrix of the estimated state variable errors (Chapter 8)
$P_{\Delta u}$	Covariance matrix of the state and model parameter errors (Section 8.2.3)
$P_{\Delta x}$	Covariance matrix of estimated solve-for variable errors (Chapter 8)
$P_{\Delta x_0}$	Covariance matrix of a priori solve-for variable errors (Chapter 8)
$P_{\Delta z}$	Covariance matrix of consider variable errors (Chapter 8)
$P_{\Delta z_0}$	Covariance matrix of a priori consider variable errors (Chapter 8)
${}^{I}P_n$, ${}^{II}P_n$	Summation matrices (Section 6.1.4)
P_1, P_2, P_3	Components of the perturbing accelerations (Section 5.4)
p	Semilatus rectum of the orbit
	Dimension of the solve-for vector (Chapter 8)
$\bar{p}$	Dynamic parameters in the equations of motion that can be estimated; these include variables related to the position and velocity, gravitational harmonic coefficients, drag parameters, etc. (Section 7)

$\bar{p}^*$	Components of $\bar{p}$ remaining after excluding satellite position and velocity variables; these components include constant model parameters pertaining to drag, gravitational harmonic coefficients, etc. (Section 4.1)
$\hat{p}$, $\hat{q}$	Unit vectors in the orbit plane (Section 4.9)
p, p_r	Projection of vector $\bar{N}$ on the $\hat{y}_{ep}$ axis (equinoctial elements) (Sections 3.2.6, 3.3.9.1, and 3.3.11.1)
$p_M(\xi)$	Interpolating polynomial representing a component of acceleration as a function of normalized time (Section 5.6)
p_x	Normal probability density function (Section 8.5)
Q	Transformation matrix from spacecraft vehicle-fixed axes to true of date coordinates (Section 3.3.12 and Chapter 4)
	Difference between ephemeris data and the function $Y_m(t)$ (Section 3.6)
	Ionospheric term used in the equation for atmospheric time delay (Section 7.6.3)
	Least-squares loss function (Sections 8.1 and 8.2)
	Covariance of the state noise (Section 8.4)
Q'	Linearized least-squares loss function (Sections 8.1 and 8.2)
Q, Q_i	Orbital accuracy (Section 9.2.3)
q	Pericentric distance (Section 3.3.8.1)
	Scaling factor defining time transformation (Section 5.5 and Appendix B)
	Dimension of the consider vector (Chapter 8)
$\bar{q}$	Total parameter vector of all candidate solve-for variables (Chapter 7)
q, q_r	Projection of the vector $\bar{N}$ on the $\hat{x}_{ep}$ axis (equinoctial elements) (Sections 3.2.5, 3.3.9.1, and 3.3.11.1)

R	Universal gas constant (Section 4.5.4)
	Magnitude of the position vector (Section 6.2.3)
	Rate of pseudorandom code (chips per second) (Section 7.3.2.3)
	Covariance matrix of the measurement noise (Section 8.4)
	Maximum residual multiplier in preliminary residual editing (Section 8.6.2)
$\bar{R}$	Position vector in mean equator and equinox of B1950.0 or J2000.0 coordinates (Chapter 3)
	Column vector of vehicle position coordinates (Chapter 4)
	Epoch state elements (Section 7.2.3)
$\bar{\bar{R}}$	Vector from the center of an inertial coordinate system to the satellite (Section 4.2.1)
$\dot{\bar{R}}$	Velocity of the spacecraft (Sections 4.5.2 and 7.1)
$\bar{R}'$	Satellite position vector relative to the shadowing body (Section 4.6.1)
$\ddot{\bar{R}}$	Total acceleration vector expressed in an inertial Cartesian coordinate system (Section 4.1)
$\ddot{\bar{R}}(t_i)$	Thrust acceleration vector at a tabular point t_i (Section 4.8.3)
R_s	Polar radius of the Earth (Section 4.5.4)
$\bar{R}_B$, $\bar{V}_B$	Inertial position and velocity vectors, respectively, of the barycenter with respect to the Sun (Section 3.3.14)
$\ddot{\bar{R}}_D$	Acceleration due to aerodynamic forces expressed in an inertial Cartesian coordinate system (Chapter 4)
$\bar{R}_E$	Inertial position vector of the Earth with respect to the Sun (Section 3.3.14)
$\ddot{\bar{R}}_E$	Inertial acceleration of the Earth in an inertial Cartesian coordinate system (Section 4.4)

$\ddot{\bar{R}}_E(M)$	Inertial acceleration of the point-mass Earth due to an oblate Moon (Section 4.4)
R_e, R_p	Equatorial and polar radii, respectively, of the Earth or reference body
$\bar{R}_{IO}$	Acceleration due to the mutual nonspherical gravitational attraction of the Earth and Moon in an inertial Cartesian coordinate system (Chapter 4)
$\bar{R}_I$	Geocentric inertial spacecraft position vectors (Chapter 9)
R_{kp}	Vector from the k^{th} body to the satellite (Chapter 4)
$\bar{R}_M$	Inertial position vector of the Moon with respect to the Sun (Section 3.3.14)
$\ddot{\bar{R}}_M$	Inertial acceleration of the Moon in an inertial Cartesian coordinate system (Chapter 4)
$\ddot{\bar{R}}_M(E)$	Inertial acceleration of the point-mass Moon due to an oblate Earth (Section 4.4)
R_m	Equatorial radius of the Moon (Section 4.4)
r_{max}	Maximum position tolerance (Section 4.8.4)
$\dot{r}_{max}$	Maximum velocity tolerance (Section 4.8.4)
$\ddot{\bar{R}}_{NS}$	Gravitational acceleration due to the nonsphericity of the gravitational potential in an inertial Cartesian coordinate system (Chapter 4)
$\ddot{\bar{R}}_{PM}$	Gravitational acceleration due to n-point masses in an inertial Cartesian coordinate system (Chapter 4)
R_p	See R_e, R_p above
$\ddot{\bar{R}}_{SR}$	Acceleration due to solar radiation pressure expressed in an inertial Cartesian coordinate system (Chapter 4)
$\bar{R}_s$	Position vector of the Sun in the inertial mean of B1950.0 or J2000.0 coordinate system (Section 4.6.1)

$\bar{R}_{s_i}$	Magnitude of the tracking station position vectors (Chapter 9)
R_{sun}	One astronomical unit (Section 4.6.1)
$\ddot{\bar{R}}_T$	Acceleration due to thrusting of the spacecraft engines in an inertial Cartesian coordinate system (Chapter 4)
$\ddot{\bar{R}}_{TAC}$	Acceleration due to attitude control system corrections in an inertial Cartesian coordinate system (Chapter 4)
R_u	Right ascension of the fictitious mean Sun on the mean equator of date and measured from the mean equinox of date (Section 3.4.3)
R_{vs}	Distance from the spacecraft to the Sun (Section 4.6.1)
R_x, R_y, R_z	Rotational transformations about the $\hat{x}$, $\hat{y}$, and $\hat{z}$ axes, respectively (Section 3.3)
R_X, R_Z	Rotations to transform between two mean of date coordinate systems (Section 3.3.1)
$\bar{R}_1$, $\bar{r}_2$	Initial and final coordinates, respectively (Section 3.3.1.1)
R_1, R_2	Values of the spacecraft radii at times t_1 and t_2, respectively, in preliminary orbit search (Section 9.2.3)
R_{1max}	Upper bound on R_1 (Section 9.2.3)
R_{1min}	Lower bound on R_1 (Section 9.2.3)
RF_c	Measurement correction due to refraction, light-time, transponder delay, antenna mount errors, etc. (Chapter 7)
RMS	Actual root mean square error (Section 8.6)
RMSP	Predicted root-mean-square error (Section 8.6)
RMSB	Smallest RMS over all prior iterations (Section 8.6)
r	Radial distance from the origin to the satellite or point being measured

r (Cont'd)	Magnitude of the satellite position vector in inertial geocentric coordinates (Sections 3.3.13, 4.5.6, and Appendix B)
	Geocentric radius (Section 7.4)
$\bar{r}$	Position vector
	Satellite position vector in inertial geocentric coordinates (Section 4.5.6)
	Radius vector of the spacecraft center of mass (Section 7.7.4)
	Position vector in true of date coordinates (Sections 3.2, 3.3, and 8.4.2)
$\bar{r}$, $\dot{\bar{r}}$, $\ddot{\bar{r}}$	Position, velocity, and acceleration vectors in the inertial Cartesian coordinate system (Chapter 5)
r_a	Magnitude of the apofocal radius vector (Section 3.3.8)
$\bar{r}_b$, $\bar{r}'_b$	Position vector expressed in body-fixed and pseudo body-fixed coordinates, respectively
$\bar{r}_E$	Position vector in Cartesian coordinates referred to the mean equator and equinox of date (Sections 3.2.1 and 3.3.1.2)
	Position vector of the Earth in selenographic coordinates (Section 4.4)
$\ddot{\bar{r}}_E(M)$	Acceleration of the point-mass Earth due to the oblate Moon in selenographic true of date coordinates (Section 4.4)
$\bar{r}_{EM}$	Position vector of the Moon in geocentric coordinates (Section 4.4)
$\bar{r}_j(t_j)$	Position of node j at time t_j (Section 7.3.2)
$\bar{r}_{j+1}(t_{j+1})$	Position of node j + 1 at time t_{j+1} (Section 7.3.2)
$\bar{r}_{lp}$	Position vector referred to the local plane coordinate system (Section 3.3.4.1)
$\bar{r}_{lt}$	Position vector referred to the local tangent coordinate system (Sections 3.2.4 and 3.3.6)

$\bar{r}_M$	Position vector of the Moon in true of date coordinates (Section 4.4)
$\ddot{\bar{r}}_M(E)$	Acceleration of the point-mass Moon due to the oblate Earth in goecentric true of date coordinates (Section 4.4)
$\bar{r}_{ME}$	Position vector of the Earth in selenocentric coordinates (Section 4.4)
r_{max}	Maximum position tolerance (Section 4.8.4)
$\dot{r}_{max}$	Maximum velocity tolerance (Section 4.8.4)
$\bar{r}_{op}$	Position vector referred to the orbit plane coordinate system (Sections 3.2.5 and 3.3.4)
r_p	Magnitude of the perifocal radius vector (Section 3.3.8.3)
$\bar{r}_p$	Position vector referred to the orbital rectangular coordinate system with the $\hat{x}_p$ axis directed toward perifocus (Section 3.3.8)
$\bar{r}_R$	Position vector of the tracking station at signal reception in inertial Cartesian coordinates (Chapter 7)
$\bar{r}_r$, $\bar{r}_t$	Position vectors of the generalized receiver and transmitter in inertial Cartesian coordinates (Appendix A)
r_s	Geocentric radius of a point (tracking station) on the surface of the ellipsoidal planet (Sections 3.3.6 and 7.6) Ellipsoidal radius of the central body (Section 3.3.13) Radius of the Earth (Section 4.5.6)
$\bar{r}_S$	Inertial position vector of the user spacecraft or transponder (Section 7.3.3)
$\bar{r}_s$	Location in Earth-fixed coordinates of the transmitting and receiving stations, as well as the Bilateration Ranging Transponder (BRT) locations in the case of TDRSS Bilateration Ranging Transponder System (BRTS) tracking
$\bar{r}_T$	Position vector of the return-link TDRS at the measurement time (Section 7.3.7)

$\bar{r}_T$ (Cont'd)	Position vector of the tracking station at signal transmission in inertial Cartesian coordinates (Chapter 7, Appendix A, and Appendix C)
$\ddot{\bar{r}}_T$	Acceleration due to thrust of the spacecraft engines (Section 4.8)
$\ddot{\bar{r}}_{TAC}$	Acceleration due to attitude control effects (Section 4.7)
$\bar{r}_v$	Vector in vehicle-fixed coordinates (Section 4.7.1)
	Position vector of the spacecraft in inertial Cartesian coordinates (Chapter 7 and Appendix C)
$\bar{r}_0$	Earth-centered position vector (Section 3.3.5)
$(\bar{r}_0, \bar{v}_0)$	Position and velocity vectors at the initial time, t_0 (insertion vector) (Section 9.1)
$\bar{r}_2$, $\bar{R}_1$	Final and initial coordinates, respectively (Section 3.3.1.1)
S	Mean solar flux at one astronomical unit (Section 4.6)
	Orbital period in a regularized time system (Section 6.4)
	Series involved in atmospheric signal propagation time delay (Section 7.6.3)
	Epoch sensitivity matrix (Section 8.2.3)
	Eigenvector transformation from basic coordinate frame to principal axes (Section 8.5)
	Sum of the squares of the residuals about the mean in each residual group (Section 8.6)
	Computed slope (Section 9.2.3)
	Arc length along the signal propagation path (Appendix A)
$\bar{S}_{bo}$, $\bar{\dot{S}}_{bo}$	State vector at burnout (Section 4.8.4)
S_{C_i}	Final unedited batch calibration standard deviation from the i^{th} batch (Section 8.7.3)
S_c	Projection of the spacecraft position vector onto the plane normal to the Sun vector in the shadow model (Section 4.6)

S_c (Cont'd)	Final unedited batch calibration standard deviation (Section 8.7.4)
S_c, S_e, S_p, S_s	Coefficients in the aerodynamic force equations (Section 4.5.2)
S_e	See S_c, S_e, S_p, S_s above
	Final edited batch validation residual standard deviation (Section 8.7.3)
$\overline{S}_f$	Postburnout state vector (Section 4.8.4)
$\overline{S}_i$	Preignition state vector (Section 4.8.4)
S_l^j	Harmonic coefficients of the Earth's nonspherical potential (Section 4.4)
$\overline{S}_{ig}$	State vector at ignition (Section 4.8.4)
S_k^2	Variance of the unedited residuals in the category validation statistics (Section 8.7.2)
S_{k-1}	Standard deviation of the unedited residuals from the previous edit loop (Section 8.7.2)
S_M	Standard deviation of the unedited batch calibration residual mean values (Section 8.7.3)
S_n^m	Gravitational harmonic coefficients (Section 4.3)
S_p	See S_c, S_e, S_p, S_s above
S_S	Standard deviation of the unedited batch calibration residual standard deviations (Section 8.7.3)
S_s	See S_c, S_e, S_p, S_s above
S_u	Greenwich hour angle of the fictitious mean Sun (Section 3.4.3)
	Final unedited batch validation residual standard deviation (Section 8.7.3)

$^{I}S_n$, $^{II}S_n$	First and second ordinate sums, respectively, in the Adams-Cowell formulas (Chapter 6)
S_0	Scaling factor (Section 9.2.3)
S_1, S_2, S_3	Components of the unit vector to the Sun in true of date coordinates (Section 4.5)
ST	Station time (defined in Section 3.4.8)
SV	Universal time correction due to seasonal variations in the rotation of the Earth (Section 3.4.6)
s	New independent variable in the time-regularized equations of motion (Chapters 5 and 6 and Appendix B)
	Dynamic solve-for parameter (Section 7.3.3)
	Orbit direction indicator (direct or retrograde) (Section 9.2.3)
$\bar{s}$, $\bar{s}'$	State vector (Chapters 7 and 8)
s_l^j	Harmonic coefficients of the Moon's nonspherical potential (Section 4.4)
T	Time in Julian centuries (of 36525 days) between the reference epoch and epoch J2000.0 (Section 3.3.1)
	Time in tropical centuries (of 36524.2198 mean solar days) elapsed from the B1950.0 epoch to the date specified (Section 3.3.1.3)
	Thrust magnitude (Section 4.8.4)
	Time tag (Sections 7.3 and A.8)
	Orbital period (minutes) (Section 9.2.3)
T_A	Average orbital period defined in terms of the average value of the semimajor axis (Section 5.8)
T_{ac1}, T_{ac2}	Epoch times at which the attitude control acceleration polynomials are turned on and turned off (Section 4.7.1)
T_b	Rocket motor's effective burn time (Section 4.8.1)

T_c	Nighttime minimum global exospheric temperature for zero geomagnetic activity (Section 4.5.4)
	Total computed time between consecutive measurements (Section 9.2.3)
T_E	Time in Julian centuries (36525 Julian days) measured from 1900 January 0^d 12^h ET (JD 2415020.0) to the specified date (Section 3.3.1.2)
T_e	Number of Julian centuries of 36525 Julian ephemeris days past 0^d January 1, 1950 ET (Section 3.3.3)
T_f, T_0	Effective termination and initiation times, respectively, of the spacecraft motor burn (Section 4.8.1)
T_i	Specified time to which the covariance and correlation matrices are propagated (Chapter 8)
T_{ig}	Thrust magnitude at ignition (Section 4.8.4)
$\dot{T}_{ig}$	Thrust rate (assumed constant) (Section 4.8.4)
T_j	Chebyshev polynomials (Sections 3.6 and 5.6)
T_{LO}	Time of liftoff (UTC) (Section 9.1)
T_{min}	Period of a spacecraft orbiting at the mean radius of the Earth (Section 9.2.3)
T_U	Time in Julian centuries (of 36525 Julian days) from B1950.0 (Section 3.3.1.2)
T_u	Number of Julian centuries elapsed from 12 hours UT1 January 0, 1900 (JD = 2415020.0) to the UT1 time of date [B1950.0 system] (Sections 3.3.2 and 3.4.3)
	Number of UT Julian centuries elapsed from epoch J2000.0 to 0 hours UT1 of the date [J2000.0 system] (Section 3.3.2.1)
T_x	Inflection point temperature (Section 4.5.4)
T(Z)	Atmospheric temperature profile (Section 4.5.4)

T_0, T_f	See T_f, T_0 above
T_1	Uncorrected exospheric temperature (Section 4.5.4)
T_1, T_2, T_3	Numerical integration error bounds (Section 6.1.7)
T_∞	Corrected exospheric temperature (Section 4.5.4)
t	Coordinate time measured in seconds from epoch; the independent variable of the equations of motion
	Time in Julian centuries between the reference epoch and the data epoch (Section 3.3.1)
	Universal time (UT) measured in seconds from 0 hours UT1 of the date of the computations (Section 3.3.2.1)
	Request time (Section 6.1.5)
	Independent variable in the Runge-Kutta integrators (Section 6.2)
	Time tag of the measurement (Section 7.1)
	Variable used for testing residuals to determine the confidence interval for the group mean (Section 8.6)
$\bar{t}$	Coordinate time (Appendix C)
t^*	Reference date (Section 3.3.1.4)
t_B	Clock bias (Section 7.3.3)
t_{bo}	Maneuver end (burnout) time (Section 4.8.4)
t_F	Time commencing the frame time interval for the GRARR and Minitrack systems (Appendix A)
t_{FM}	Midframe time for the Minitrack System (Appendix A)
t_f	Time of the postburnout state vector (Section 4.8.4)
	Time of the final measurement (Section 8.4)
t_i	Time of the preignition state vector (Section 4.8.4)

t_{ig}	Maneuver start (ignition) time (Section 4.8.4)
t_j	Signal retransmission time from node j (Section 7.3.2)
t_j'	Signal reception time at node j (Section 7.3.2)
t_j^n	n^{th} approximation for t_j (Section 7.3.2.1)
t_j^{n+1}	$(n+1)^{th}$ approximation for t_j (Section 7.3.2.1)
t_m^*	Corrected midframe time of the Minitrack System (Appendix A)
t_n	Time associated with the most recent entry in the backpoints table (Section 6.1.5)
t_q	Reference time associated with the Brouwer drag parameters (Section 4.9)
t_R	Devised output time in the fourth-order Runge-Kutta integrator (Section 6.6.3)
	Time at which the ground station receives the return signal (Chapter 7 and Appendix A)
	Time tag of the C-band range data (Section 7.2.3)
	Proper time at the receiving station (Appendix C)
t_r, t	Requested time in multistep interpolation with fixed-step integration (Section 6.1.5)
t_s	Sample time of the tracker range and range-rate data (Appendices A and C)
t_T	Signal transmission time at the ground station (Chapter 7 and Appendix A)
t_v	Signal turnaround time at the spacecraft (Chapter 7 and Appendix A)
t_0	Epoch time (Chapter 4 and Section 8.2.3)
	Epoch of the estimated solution (Section 7.3.2)

t_1, t_2	Times of the first two measurement in preliminary orbit search (Section 9.2.3)
U	Geoidal undulation (Section 7.4)
$\hat{U}$	Unit vector directed at the satellite and referred to the geocentric inertial Cartesian coordinate system (Sections 3.3.5 and 4.8.2)
U, V	Tropospheric delay terms (Section 7.6.3)
$\hat{U}_B$	Unit vector directed toward the apex of the diurnal bulge expressed in inertial geocentric coordinates (Section 4.5.6)
U_{B_x}, U_{B_y}, U_{B_z}	Components of the unit vector $\hat{U}_B$ (Section 4.5.6)
$\hat{U}_N$	Unit vector normal to the orbital plane in the direction of the angular momentum vector (Section 3.3.4.2)
$\hat{U}_s$	Unit vector directed at the Sun from a shadowing body (Section 4.6.1)
$\hat{U}_T$	Unit vector directed along the thrust axis and referred to the geocentric inertial Cartesian coordinate system (Section 4.8.1)
UT	Universal time
UTC	Coordinated universal time
UT0	Uncorrected universal time
UT1	UT0 corrected for polar motion; Greenwich universal time measured from midnight (epoch) to time t; UT1 is positive for t after midnight and negative for t before midnight
UT2	UT1 corrected for periodic seasonal variations
$\hat{U}_{z_{lp}}$	Unit vector in the local plane $\hat{z}_{lp}$-axis direction and referred to the geocentric inertial Cartesian system (Section 3.3.4.2)
$\hat{U}_\alpha$, $\hat{U}_\delta$	Partial derivatives of $\hat{U}_T$ with respect to the right ascension, α, and declination, δ (Section 4.8.2)

$\hat{u}$	Unit vector pointing along the vacuum uplink signal propagation path from the station to the spacecraft (Section 7.6.3 and Appendix C)
	Expanded state vector containing as components the merged vectors $\bar{x}$ and $\bar{z}$ (Section 8.2)
	Best estimate of uncertain state and model parameters (Section 8.2.3)
	Vector of Gaussian noise (Section 8.4)
u^*	Uncertain model parameters in $\hat{u}$ (Section 8.2.3)
u, u'	Transformed position and velocity vectors (Section 5.4)
$\hat{u}_j$	Unit vector along the leg between nodes j and j + 1 (Section 7.3.3)
$\hat{u}_x$, $\hat{u}_y$, $\hat{u}_z$	Unit vectors in the body-centered true of date Cartesian coordinate system (Section 3.3.8.3)
V	Spacecraft's velocity vector magnitude
	Magnitude of the velocity with respect to a medium producing an aerodynamic force (Section 4.5)
	Perturbing potential function (Section 5.4 and Appendix B)
$\hat{V}$	Unit vector normal to the geocentric position vector and lying in the orbital plane (Sections 3.3.5 and 4.8.2)
∇_B	Inertial velocity vector of the barycenter with respect to the Sun (Section 3.3.14)
	Relative wind velocity in the spacecraft body axes coordinate system (Section 4.5.2)
∇_E	Inertial velocity vector of the Earth with respect to the Sun (Section 3.3.14)
∇_{rel}	Velocity of the spacecraft relative to the atmosphere (Section 4.5)
∇_M	Inertial velocity vector of the Moon with respect to the Sun (Section 3.3.14)

v	Local vertical at the ground station (Section 7.6.3) Magnitude of spacecraft velocity (Appendix B)
$\bar{v}$	Velocity vector
$\hat{v}$	Unit velocity vector (Section 4.8.3)
v_n	Quantity denoting the Cowell velocity integrator for linear systems (Section 6.1.3)
W	Weighting matrix in the least-squares loss function (Chapter 8)
$\bar{W}$	Vector parallel to the angular momentum unit vector (Section 9.2.3)
$\hat{W}$	Unit vector directed normal to the orbit plane in the direction of the angular momentum vector (Sections 3.3.5 and 4.8.2)
W'	Augmented weighting matrix (Chapter 8)
W_{ij}^{P}	Weighting factor for the P^{th}-order divided differences (Section 8.7.4)
w_{jj}	Component of the measurement weight matrix, W, corresponding to the j^{th} measurement (Section 8.6.2)
w_{m+1}	Weight of the $(m+1)^{st}$ measurement (Chapter 8 and Appendix 8)
X, Y, Z	Inertial Cartesian components of spacecraft position in the mean of B1950.0 or J2000.0 coordinate system (Section 3.2.1)
$\hat{X}_B$	Unit vector along the cylinder axis (Section 4.5.2)
X_b, Y_b, Z_b	Components of the TDRS spacecraft vehicle-fixed position (Section 7.3.7)
X_1, Y_1	Position coordinates in the equinoctial coordinate system (Sections 3.3.9.1 and 5.7)
X_{30}, Y_{30}	Gimbal angles for the GRARR, ATSR, and SRE USB systems (Section 7.2.3)

X_{85}, Y_{85}	Gimbal angles for the SRE USB system (Section 7.2.3)
X	Augmented state matrix (Section 8.4)
x	Transformed time variable (Section 3.6)
$\bar{x}$	State vector Vector of slow osculating orbital elements (Section 5.8)
$\bar{X}$, $\bar{X}_1$	Vector of the dependent variables and its value at time t_1, respectively, in the Runge-Kutta integrators (Section 6.2)
$\ddot{x}$	Accelerations in the backpoints table (Section 6.1.5)
$\bar{x}$, $\hat{\bar{x}}_i$, $\bar{x}_i$, $\bar{x}_0$	Epoch values of the solve-for or expanded state vector of p-dimension: the vector $\hat{\bar{x}}_i$ is the best estimate of $\bar{x}$ obtained on the i^{th} iteration; the vector $\bar{x}_{i+1}$ is the reference solution on the i^{th} iteration; the vector $\bar{x}_0$ is the a priori estimate of the reference state (Chapter 8)
x, y, z	Inertial Cartesian components of spacecraft position in the true of date coordinate system
$\hat{x}'$, $\hat{y}'$, $\hat{z}'$	Axes of the rotating libration point coordinate system (Section 3.3.14)
$\dot{\hat{x}}'$, $\dot{\hat{y}}'$, $\dot{\hat{z}}'$	Rate of change of the libration coordinate axes (Section 3.3.14)
x_b, y_b, z_b	Rectangular Cartesian components of spacecraft position in body-fixed (rotating) coordinates of the principal gravitating body
x_b', y_b', z_b'	Components of spacecraft position in the pseudo body-fixed coordinate system (Section 3.3.2)
x_E, y_E, z_E	Inertial components of spacecraft position in the mean of date coordinate system (Section 3.2.1)
x_{ep}, y_{ep}, z_{ep}	Components of spacecraft position in the equinoctial coordinate system (Section 3.2.5)
x^i	Components of the space coordinates (Appendix C)

$\bar{X}_j(t_j)$	Instantaneous state vectors of node j at time tag t_j (Section 7.3.5)
$\bar{X}_j(t_0)$	State vector (position and velocity) of node j at epoch t_0 (Section 7.3.5)
x_{lp}, y_{lp}, z_{lp}	Components of spacecraft position in geocentric local plane coordinates (up, east, north) (Section 3.2.3)
x_{lt}, y_{lt}, z_{lt}	Components of spacecraft position in topocentric local tangent coordinates (east, north, up) (Section 3.2.4)
x_n	Quantity denoting the Cowell position integrator for linear systems
x_{op}, y_{op}, z_{op}	Components of spacecraft position in geocentric orbit plane coordinates (Sections 3.2.5 and 7.7.4)
x_p, y_p	Instantaneous angular coordinates of the polar motion (Section 3.3.2.2) (see Figure 3-11)
x_p, y_p, z_p	Keplerian Cartesian components of spacecraft position in orbital coordinates, i.e., x_p is directed toward perigee and z_p in the direction of the angular momentum (Sections 3.2.5 and 5.7)
$\hat{x}_p$, $\hat{y}_p$, $\hat{z}_p$	Keplerian unit vectors (Sections 3.2.5 and 5.7) Spacecraft orbit frame unit vectors (Section 4.8.4)
x_s', z_s'	Components used in the two-dimensional analysis of an ellipsoid to indicate that the y component is omitted (Section 3.3.6)
x_s, y_s, z_s	Coordinates of a point s on the surface of an ellipsoidal planet expressed in body-centered rotating coordinates (Section 3.3.6)
$\hat{x}_T$, $\hat{y}_T$, $\hat{z}_T$	TDRS track-oriented coordinate axes (Section 7.3.7)
x_v, y_v, z_v	Components of spacecraft position in the vehicle-fixed coordinate system (Sections 3.2.7 and 4.7.1)

Y	See X, Y, Z above
	Yaw angle (Section 4.8.4)
	Dependent variable vector in the second-order linear differential system of variational equations (Sections 4.1 and 6.1.4)
Y_{ig}	Yaw angle at ignition (Section 4.8.4)
$\dot{Y}_{ig}$	Yaw angle rate (assumed constant) (Section 4.8.4)
Y_T, P_T	Yaw and pitch angles, respectively, defining the thrust direction (Section 4.8)
$Y(t)$, $\dot{Y}(t)$	Matrices obtained by integrating the variational equations (Section 4.1)
	Matrices of position partial derivatives and velocity partial derivatives, respectively (Section 6.1.4)
$Y(t_{j+1} \mid t_j)$	Predicted measurement residual uncertainty (Section 8.4)
$Y_m(t)$	Linear combination of functions used in the interpolation of ephemeris data (Section 3.6)
y	See x, y, z above
	Fast osculating orbital elements (Section 5.8)
$\bar{y}$	m-dimensional vector of measurement data (Chapter 8)
y_b	See x_b', y_b', z_b' above
y_b'	See x_b', y_b', z_b' above
y_E	See x_E, y_E, z_E above
y_{ep}	See x_{ep}, y_{ep}, z_{ep} above
y_i	JPL ephemeris function value at time t_i (Section 3.6)
y_{lp}	See x_{lp}, y_{lp}, z_{lp} above
y_{lt}	See x_{lt}, y_{lt}, z_{lt} above

y_m	Half-thickness of the bottomside layer of the electron density profile (Section 7.6)
y_p	See x_p, y_p, z_p above
y_s	See x_s, y_s, z_s above
y_v	See x_v, y_v, z_v above
y_{op}	See x_{op}, y_{op}, z_{op} above
Z	See X, Y, Z above Altitude (Section 4.5.4)
Z_m, Z_n	Zenith calibration constants (Appendix A)
z	See x, y, z above Nondimensional altitude used in the Chapman profile for electron density (Sections 7.6.2 and 7.6.3)
$\bar{z}$	q-dimensional consider vector containing as components all model parameters whose values are known with limited certainty but are not to be estimated (Chapter 8)
z_b	See x_b, y_b, z_b above
z_b'	See x_b', y_b', z_b' above
z_E	See x_E, y_E, z_E above
z_{ep}	See x_{ep}, y_{ep}, z_{ep} above
z_l	z_b-axis intercept of the vector normal to the surface of the ellipsoidal planet model (Section 3.3.6)
z_{lp}	See x_{lp}, y_{lp}, z_{lp} above
z_{lt}	See x_{lt}, y_{lt}, z_{lt} above
z_{op}	See x_{op}, y_{op}, z_{op} above
z_p	See x_p, y_p, z_p above

z_s	See x_s, y_s, z_s above
z_v	See x_v, y_v, z_v above
z_0	A priori value of z (Chapter 8)

Greek Symbols

α	Right ascension of the spacecraft relative to the true of date system
	Rotation matrix (Section 3.3.1.1)
	Right ascension in spherical coordinates (Section 3.3.13)
	Geocentric angle between the ground station and the sub-ionospheric point (Section 7.6.3)
	Uniformation constant (Appendix B)
$\hat{\alpha}$	Unit vector normal to the orbit plane (Section 4.9)
α, β	Slow and fast elements, respectively (Section 5.7)
$\overline{\alpha}$, $\overline{\beta}$	Four-vectors (Section 5.4 and Appendix B)
α_g	True of date right ascension of Greenwich (also called the true Greenwich sidereal time or true Greenwich hour angle) (Sections 3 and 9)
α_{GM}	Mean Greenwich sidereal time, i.e., right ascension of the fictitious mean Sun minus 12 hours plus the time of day in UT1 (Section 3.3.2.1)
α_i	Thermal diffusion coefficient (Section 4.5.4) (see Table 4-2)
	DS elements vector (Section 5.5)
α_i, β_i; α_i^*, β_i^*	Coefficients of the Adams-Cowell predictor formulas (ordinate form) (Chapter 6)
α_s	Right ascension of the Sun (Section 4.5.6)
α_T	Right ascension of the spacecraft's thrust axis (Section 4.8.1)

α_t	Topocentric right ascension of the spacecraft (Section 9.2)
α_v	Right ascension of the spacecraft's longitudinal axis (Section 3.3.12)
α_τ	Estimated thrust variation coefficient (Section 4.8.3)
$\alpha_0, \ldots, \alpha_4$	Coefficients of polynomial characterizing the thrust axis right ascension (Section 4.8.1)
$\alpha_1, \ldots, \alpha_8$	DS elements vector (Section 5.5)
β	Flight path angle measured from the geocentric position vector to the velocity vector (Section 3.2.3)
$\hat{\beta}$	Unit vector lying in the orbit plane (Section 4.9)
Γ	Flight path angle (Section 3.3.13)
Γ_n^T	Vector containing powers of the thrust burning time (Section 4.8.2)
γ	Normal gravity at a point (Section 7.4)
$\hat{\gamma}$	Unit vector forming right-hand system with $\hat{\alpha}$ and $\hat{\beta}$ (Section 4.9)
γ_e	Normal equatorial gravity (Section 7.4)
$\gamma_i, \gamma_i', \gamma_i''$	Coefficients in the Adams-Cowell formulas (Section 6.1.1)
γ_j	Ground elapsed time from T_{LO} for the selected Delta Inertial Guidance System (DIGS) station (Section 9.1)
$\gamma_2, \gamma_3, \gamma_4, \gamma_5$	Auxiliary parameters (Section 5.9)
$\gamma_2', \gamma_3', \gamma_4', \gamma_5'$	Auxiliary parameters (Section 5.9)
Δ	Auxiliary angle used in determining the transformation from true of date selenocentric to selenographic coordinates (Section 3.3.3)
$\Delta\bar{d}_R, \Delta\bar{d}_v$	Correction vectors used in the determination of refraction correction (Section 7.6.3)

ΔE	Atmospheric elevation correction (Section 7.6.3)
Δf_{cesium}	Correction to the frequency f_{cesium} = 9,192,631,770 cycles of cesium per ephemeris second (Section 3.5.1)
ΔH	Correction to the mean right ascension to account for nutation (Section 3.3.2.1)
$\Delta\ell_{DRAG}$, ΔM_{DRAG}	First-order correction to the mean anomaly (Sections 5.9 and 4.9), respectively
$(\Delta \log_{10} \varrho)_G$	Geomagnetic activity correction to the standard density calculation (Section 4.5.4)
$(\Delta \log_{10} \varrho)_{He}$	Density correction for the seasonal latitudinal variation of helium (Section 4.5.4)
$(\Delta \log_{10} \varrho)_{LT}$	Density correction for the seasonal latitude variation of the lower thermosphere (Section 4.5.4)
$(\Delta \log_{10} \varrho)_{SA}$	Semiannual atmospheric density variation (Section 4.5.4)
$\Delta\overline{M}$	Correction to the maneuver parameters (Section 4.8.4)
Δr	Radius of the error hypersphere (Section 8.5.2)
Δr, $\Delta \dot{r}$	Range and range-rate antenna mount corrections (Section 7.6.3)
$\Delta \dot{\bar{r}}$	Velocity difference (Section 4.8.4)
Δr_a	Antenna offset vector (Section 7.7.4)
$\Delta\overline{S}$	Miss vector (Section 4.8.4)
Δs, $\hat{\Delta s}$	First six components of $\hat{\Delta x}$ and $\overline{\Delta x}$ (Chapter 8)
ΔT, ΔT_i	Time differences (Section 9.2.3)
ΔT_∞	Correction to the exothermic temperature (Section 4.5.4)
ΔT_{1958}	Difference ET—UT2 on January 1, 1958, $0^h0^m0^s$ UT2, minus the periodic terms in the ET-to-A.1 transformation (Section 3.5.1)

Δt	Step size
	Measured round-trip time delay (in seconds) at time tag T between corresponding chips of the reference and received PN code (Section A.8.2)
Δt_c	Counter delay in the phase readout digitizing equipment (Appendix A)
Δt_d	Correction to the sequencer delay (Appendix A)
Δt_{max}	Maximum value for the integration step (Section 9.1)
Δt_P	Sequencer delay (Appendix A)
Δt_R	Two-way light time corresponding to the range measurement (Section A.1)
Δt_{RD}	Reciprocal of the data recording rate (Section A.1)
Δt_{RR}	Doppler count time interval (Chapter 7 and Appendices A and C)
$\overline{\Delta u}$	Perturbations about $\bar{u}$ (Section 8.2.3)
$\hat{\Delta u}$	Best estimate of $\overline{\Delta u}$ in a weighted least-squares sense (Chapter 8)
$\Delta \hat{u}_T$, $\Delta \hat{u}_v$	Correction vectors used in the determination of refraction correction (Section 7.6.3)
$\Delta^P V_i$	i^{th} variate difference of order P (Section 8.7.4)
$\overline{\Delta x_i}$	Perturbation in the solve-for vector about the i^{th} iterated estimate, $\hat{x}_i$ (Section 8.2)
$\hat{\Delta x}_i$	Best estimate of $\overline{\Delta x}$ in a weighted least-squares sense (Section 8.2)
$\bar{\Delta x}_i$	Deviation of the a priori from the i^{th} iterated estimate of $\bar{x}$ (Section 8.2)
$\hat{\Delta x}_{i+1,n}$	State correction computed in the n^{th} residual editing iteration (Section 8.6.2)

$\overline{\Delta y_i}$	Vector of deviation between the actual measurements and the i^{th} iterated estimate of the measurements. (Note: $\overline{\Delta y} = \overline{\Delta y_0}$) (Sections 8.1 and 8.2)
$\Delta y(t_j)$	Measurement residual for the j^{th} measurement (Section 8.6.2)
$\Delta y^*(t_j)$	Predicted weighted measurement residual (Section 8.6.2)
$\overline{\Delta z}$	Perturbations of the consider vector $\overline{z}$ about its a priori value (Section 8.2)
Δz_i	Components of transformed state vector which constitute the coordinates of a hypersphere (Section 8.5.2)
$\Delta\lambda$	Difference between the adopted and true longitude (Section 3.3.2.2)
$\Delta\nu_{d_0}(T)$	Measured differenced one-way Doppler measurement at time tag T (Section A.8.2)
$\Delta\varrho$	Atmospheric range correction (Section 7.6.3)
$\Delta\dot{\varrho}$	Atmospheric range-rate correction (Section 7.6.3)
$\Delta\varrho_c$	Density correction factor (Section 4.5.5)
	Computed range difference (Appendix C)
$\Delta\varrho_\ell(T)$	Difference between the full long-path range at times T and T – ΔT (Sections 7.3.4)
$\Delta\varrho_s(T)$	Difference between the full short-path range at times T and T – ΔT (Sections 7.3.4)
$\Delta\tau$	Spacecraft transponder time delay (Chapter 7 and Appendix A)
$\Delta\phi$	Difference between the adopted and true latitude (Section 3.3.2.2)
δ	Declination angle measured north from the equator
	Declination in spherical coordinates (Section 3.1.13)

δ (Cont'd)	Quantity used in determining the atmospheric refraction correction to the elevation angle (Section 7.6.4)
	Dirac delta function (Section 8.4)
δ_i', δ_i''	Coefficients of the ordinate form of the Adams-Cowell formulas (Section 6.1.6)
δ_{ij}	Polynomial coefficients in the density calculation (Section 4.5.4)
	Kronecker delta function (Sections 4.8.2 and 8.4)
δ_j	Error coefficients (Section 6.2.2)
δ_s	Declination of the Sun
δ_T	Declination of the spacecraft's thrust axis (Section 4.8.1)
δ_t	Topocentric declination of the spacecraft (Section 9.2)
δ_v	Declination of the spacecraft's longitudinal axis (Section 3.3.12)
δ_0, ..., δ_4	Coefficients of polynomial characterizing the thrust axis declination (Section 4.8.1)
δi, $\delta\Omega$, $\delta\omega$	Perturbations in the orbit inclination, right ascension of the ascending node, and argument of perigee, respectively (Section 4.9)
$\delta\bar{r}_j$, $\delta\bar{v}_j$	Thrust components in terms of position and velocity changes, respectively, in a geocentric body-fixed coordinate system referenced to the launch pad at time t_j, extracted from the launch telemetry data (Section 9.1)
δr_1, δr_2	Corrections to the assumed radius magnitudes (Section 9.2.3)
δt	Timing bias in the measurement data (Sections 7.1 and 8.2)
$\delta^P V_i$	i^{th} divided difference of order P (Section 8.7.4)
$\delta\alpha$, $\delta\beta$, $\delta\gamma$	Rotational perturbations around $\hat{\alpha}$, $\hat{\beta}$, and $\hat{\gamma}$, respectively (Section 4.9)

$\delta\epsilon$	Difference between the true and mean obliquity (Section 3.3.1.3)
$\delta\psi$	Nutation in longitude (Section 3.3.1.3)
ϵ	Small parameter proportional to the perturbing acceleration (Section 5.8)
	Tolerance (Sections 7.3.2 and 8.6.2)
	Improvement ratio criterion specified for least-squares iteration convergence (Section 8.6.3)
$\bar{\epsilon}(t)$	First-order Gauss-Markov process representing the unmodeled acceleration, $\bar{a}_u$ (Section 8.4.2)
ϵ_m, ϵ_t	Mean and true obliquity (Sections 3.3.1 and 3.3.2)
ϵ_n	Local error of the numerical integration (Section 6.1.7)
ϵ_t	See ϵ_m, ϵ_t above
$\mathcal{E}(\,)$	Denotes the expected value
ζ_0	Precession angle (Section 3.3.1)
ν	Surface reflectivity coefficient (Section 4.6)
	Auxiliary parameter (Section 5.9)
θ	Flight path angle (Section 4.9)
	Auxiliary parameter (Section 5.9)
	Transition matrix between perturbations in solve-for variables and perturbations in consider variables (Section 8.2.3)
θ, θ_M	Orbital angle and mean orbital angle, respectively, measured along the lunar equator from the descending node of the Earth's orbit to the lunar prime meridian (Section 3.3.3)
θ_p	Precession angle (Section 3.3.1)
Λ	Euler angle used in the transformation from selenocentric to selenographic coordinates (Section 3.3.3)

λ	Longitude measured east from the prime meridian
	Equinoctial and Herrick mean longitudes (Sections 3.2.6 and 3.3.9.1)
λ, λ_1	Number of full revolutions between consecutive measurements (Section 9.2.3)
λ_A, λ_T	Adopted and instantaneous (true) longitudes, respectively (Section 3.3.2.2)
λ_E	Geographic east longitude measured positive west (Section 3.3.13)
	Selenographic longitude of the Earth (Section 4.4)
λ_{lag}	Lag angle between the Sun line and the apex of the diurnal bulge (Section 4.5.6)
λ_M	Geocentric mean longitude of the Moon (Section 3.3.3)
	True right ascension of the Moon (Section 4.4)
λ_p	Longitude of the magnetic north pole (Section 7.6)
λ_r	Mean longitude for retrograde orbit (Section 3.3.11.1)
λ_s	Longitude of the tracking station (Sections 3.3.7 and 9.2)
μ	Gravitational parameter of the reference body, i.e., the product of the universal gravitational parameter and the mass of the body
ν	Bank angle in spherical coordinates (Section 3.1.13)
	Eclipse factor (Section 4.6.1)
	Electromagnetic signal frequency (Section 7.6)
ν_b	Bias frequency on the Doppler signal (Appendices A and C)
ν_d	Doppler signal frequency (Appendices A and C)
$\nu_d(T)$	Computed full Doppler measurement at time tag T (Section 7.3.5)

$\nu_{d_c}(T)$	Computed average Doppler shift tagged at time T (Section 7.3.4)
$[\nu_{d_0}(T)]_{compare}$	Comparison one-way Doppler measurement (Section A.8.2)
$[\nu_{d_0}(T)]_{reference}$	Reference one-way Doppler measurement (Section A.8.2)
$\nu_{d_0}(T_i)$	Measured Doppler shift (in hertz) at time tag T_i, averaged over the time interval between T_i and T_{i+1} (Section A.8.2)
ν_n	High frequency modulation (ranging) tone (Appendix A)
ν_L	Low frequency modulation (ranging) tone (Appendix A)
ν_ℓ	Doppler-shifted carrier frequency via the long-trip path (Section 7.3.4)
ν_R	Signal frequency received at the ground station (Appendices A and C)
ν_{R_1}, ν_{R_2}	Reference frequency for the GRARR and ATSR range and range-rate measurements (Appendices A and C)
ν_s	Doppler-shifted pilot-tone frequency for the short-trip path (Section 7.3.4)
ν_T	Frequency of the signal transmitted at the tracking station (Appendices A and C)
ν_t, ν_r	Frequencies of the transmitted and received signals (Appendix C)
ν_v	Frequency of the signal received at the spacecraft (Appendices A and C)
$(\nu_0)_\ell$	Unshifted carrier frequency via the long-trip path (Section 7.3.4)
$(\nu_0)_s$	Unshifted pilot-tone frequency (Section 7.3.4)
ξ	Normalized time (Section 5.6)
ξ_p	Precession angle (Section 3.3.1)

ϱ	One-way range measurement from the tracking station to the spacecraft (Chapters 3, 7, and Appendix A)
	Planet's mass density (Section 4.3)
	Atmospheric density (Section 4.5)
	Average of the uplink and downlink propagation distances (Section 7.2)
ϱ, η, θ	Oblate spherical coordinates (Section 5.12)
$\varrho(T)$	Computed range at time tag T (kilometers) (Section 7.3.2)
ϱ_A	Range ambiguity interval (kilometers) (Section 7.3.2)
ϱ_a	Atmospheric density (Section 4.5.2)
ϱ_a, ϱ_b	Range ambiguity numbers (Appendix A)
$\dot{\varrho}_{avg}$	Average range rate over the uplink and downlink paths (Chapter 7 and Appendices A and C)
ϱ_F	Dynamic weighting factor (Appendix D)
ϱ_i	Atmospheric constituent densities (Section 4.5.4)
	Slant range from the tracking station to the spacecraft (Section 9.2.2)
ϱ_{ij}	Correlation coefficient (Section 8.5)
ϱ_j	Distance traversed by a tracking signal between nodes j and j + 1 (Section 7.3)
$\dot{\varrho}_\ell$	Time rate of change of the long-trip full range (Section 7.3.4)
ϱ_{lt_l}	Measurement vector in station-centered topocentric local tangent coordinates (Section 9.3)
ϱ_M	Hayn's physical libration in the inclination of the mean lunar equator (Section 3.3.3)
ϱ_M, ϱ_m	Maximum and minimum densities (Section 4.5.6)

ϱ_s	Summed atmospheric density (Section 4.5.4)
$\dot{\varrho}_s$	Time rate of change of the short-trip full range (Section 7.3.4)
ϱ_u, ϱ_d	One-way range distance corresponding to the uplink and downlink signal path (Section 7.2.3 and Appendix C)
$\varrho_0(T)$	Measured range at time tag T (kilometers) (Section 7.3.2)
	Measured half-range at time tag T (kilometers) (Section A.8.2)
ϱ_1	Drag scale factor (Section 4.5.2)
ϱ_1, ϱ_2	Ranges from the first and second stations to the satellite in VLBI tracking (Section 7.4)
ϱ_1, ϱ_2, ϱ_3	Systematic error coefficients in the atmospheric density model (Section 4.5)
ϱ_1', ϱ_2', ϱ_3', ϱ_4'; ϱ_1, ϱ_2, ϱ_3, ϱ_4	Distances between nodes (Section 7.3.2)
ϱ_2	Slant range (Section 9.2.3)
σ	Sample standard deviation (Section 8.6.4)
σ^2_{E-1}	Variance estimate for unedited differences on the $(E-1)^{st}$ edit loop of the same order (Section 8.7.4)
σ_i	i^{th}-order final noise estimate (Section 8.7.4)
σ_i^2	Variance of the measurement noise component n_i (Chapter 8)
σ_k	Standard deviation of the k^{th} measurement (Chapter 8)
$\bar{\sigma}_k$	A priori standard deviation of the noise on the k^{th} measurement (Section 8.1)
$\bar{\sigma}_k$	Standard deviation of the data reduction curve fit obtained during preprocessing of the k^{th} measurement (Section 8.1)
σ_M	Hayn's physical libration in the mean right ascension of the ascending node of the lunar orbit (Section 3.3.3)

σ_{P_D}	DDNA noise estimate (Section 8.7.4)
σ^2_{P-1}	Final variance for the P^{th}-order noise estimate (Section 8.7.4)
$\sigma_1, \ldots, \sigma_6$	Eigenvalues of $P_{\Delta x}$ (Section 8.5)
$\sigma^2_{\Delta s_i}$	Estimate of the variance of Δs_i (Section 8.2.3)
$\sigma^2_{\Delta z_i}$	Estimate of the variance of Δz_i (Section 8.2.3)
τ	Auxiliary angle used in the calculation of the uncorrected exospheric temperature (Section 4.5.4)
	Time measured from effective ignition of the thruster (Section 4.8.1)
	Independent variable (time element) for the transformed time-regularized system (Sections 5.4, 6.4, and Appendix B)
	Runge-Kutta stepsize (Section 6.2.2)
	Phase difference time interval in VLBI tracking (Section 7.4)
τ_{opt}	Optimum stepsize in the Hull Runge-Kutta 3(4+) integrator (Section 6.2.2)
τ_M	Hayn's physical libration in mean longitude (Section 3.3.3)
Φ	Perturbing energy (Section 5.5 and Appendix B)
	State transition matrix (Sections 6.3, 7.3.3, and 7.3.5)
	Augmented state transition matrix (Section 8.4)
ϕ, ϕ'	Geodetic and geocentric latitudes, respectively (Chapters 3, 4, and 7)
	Geocentric and geodetic latitudes, respectively (Chapter 4)
$\phi(T_i, t_0)$	State transition matrix relating state perturbations at time t_0 to state perturbations at time T_i (Chapter 8)
$\phi(t, t_0)$	Transition matrix relating perturbations about $\varpi(t)$ at times t and t_0 (Chapter 8)
ϕ_A, ϕ_T	Latitude corresponding to the adopted and true poles, respectively (Section 3.3.2.2)

ϕ_E	Selenographic latitude of the Earth (Section 4.4)
ϕ_M	Geocentric latitude (declination) of the Moon (Section 4.4)
ϕ_p	Geodetic latitude of the magnetic north pole (Section 7.6)
ϕ_s, ϕ_s'	Geodetic and geocentric latitude of the tracking station (Sections 3.3.7 and 9.2)
ϕ_T	See ϕ_A, ϕ_T above
ϕ_v	Roll angle of the spacecraft (Section 3.3.12)
ψ	Gravitational potential (Sections 4.3.1 and 4.4)
	Angle between the satellite position vector and the apex of the diurnal bulge (Section 4.5.6)
	Generalized true anomaly (Section 5.5)
	Geopotential function (sum of the normal geopotential ψ_N and the disturbing potential ψ_D) (Section 7.4)
	Abbreviation for the covariance matrix of the estimated state in the absence of consider variables (Section 8.3)
ψ_D	Disturbing potential (Section 7.4)
ψ_N	Normal geopotential (Section 7.4)
Ω	Right ascension of the orbital ascending node
	Skew matrix whose elements are components of the Earth's rotation vector (Section 4.5.3)
Ω'	Euler angle used in transformation from selenocentric to selenographic coordinates (Section 3.3.3)
Ω_M	Mean right ascension of the ascending node of the lunar orbit (Section 3.3.3)
ω	Argument of perigee of the satellite orbit
	Frequency related to the negative of the total energy (Section 5.4 and Appendix B)
	Rotation rate of the Earth (Sections 3.3.2.1 and 7.4)

$\bar{\omega}$	Angular rotation vector of the Earth expressed in mean of B1950.0 or J2000.0 coordinates (Section 4.5.2)
	State noise (Chapter 8)
ω_M	Moon's argument of perigee (Section 3.3.3)

Subscripts

$( )_A$	Adopted quantity; averaged quantity; or model replacement
$( )_a$	Apofocus; atmospheric; or apparent
$( )_{ac}$	Attitude control
$( )_{avg}$	Average
$( )_B$	Spacecraft axis
$( )_b$	Body-centered; body-fixed; burn; or bias
$( )_C$	Correction; or coarse baseline (Minitrack)
$( )_c$	Computed; cylinder; or minimum exospheric
$( )_D$	Drag; aerodynamic; deviation; or disturbing
$( )_d$	Doppler; or downlink
$( )_E$	Earth; or mean of date
$( )_{E-W}$	East-west
$( )_e$	Equatorial; ephemeris; end plate; or electron density
$( )_{ep}$	Equinoctial system
$( )_F$	Frame; force; or fine baseline (Minitrack)
$( )_{FM}$	Midframe
$( )_f$	Final
$( )_{GM}$	Greenwich mean value

$( )_g$	Geomagnetic; Greenwich true value; or group
$( )_I$	Ionospheric
$( )_{IO}$	Mutual nonspherical gravitational attraction of Earth and Moon
$( )_i$	Initial node of the measurement (Section 7.3.3)
$( )_{in}$	Counter input
$( )_j$	Reference (central) body
$( )_K$	Keplerian
$( )_k$	Body k
$( )_L$	Four-way ranging; or low frequency
$( )_{lp}$	Local plane
$( )_{lt}$	Local tangent
$( )_M$	Moon; maximum; or medium baseline (Minitrack)
$( )_{M_m}$	Midpoint
$( )_m$	Minimum; maximum (Chapter 7); mean (Section 3.3.3); or middle point
$( )_N$	Normal
$( )_{NS}$	Nonspherical
$( )_{N\text{-}S}$	North-south
$( )_{of}$	Orbital frame
$( )_{op}$	Orbit plane
$( )_{PM}$	Point-mass
$( )_p$	Polar; perifocus; precession; solar paddle; geomagnetic; planetary; orbital rectangular coordinates; or phase

$( )_R$	Ground receiver; or reference
$( )_{RR}$	Doppler count
$( )_{RT}$	Round-trip
$( )_r$	Generalized receiver (Appendix C)
$( )_{rel}$	Relative to the atmosphere
$( )_S$	Two-way ranging
$( )_{SA}$	Semiannual
$( )_{SR}$	Solar radiation
$( )_s$	Tracking station; solar; sample; selenographic; surface; spherical; or sea level
$( )_T$	Ground transmitter; thrust; tropospheric; or true (instantaneous) pole
$( )_{TAC}$	Attitude control system
$( )_t$	Time; topside; topocentric; true (Section 3.3.3); or generalized transmitter (Appendix C)
$( )_u$	Uplink
$( )_v$	Spaceccraft; or vehicle fixed
$( )_x$	Inflection point
$( )_x$, $( )_y$, $( )_z$	Corresponding axis
$( )_0$	Mean elements at epoch; Earth-centered; initial conditions; actual; or a priori (Chapter 8)
$( )_{30}$	GRARR and SRE USB 30-foot antennas
$( )_{85}$	SRE USB 85-foot antennas
$( )_\infty$	Corrected exospheric

Superscripts

$( )^{avg}$	Average value
$( )^{c}$	Corrected values
$( )^{d}$	Day
$( )^{h}$	Hour
$( )^{m}$	Minute
$( )^{p}$	Predicted values
$( )^{s}$	Second
$( )^{T}$	Transpose
$( )^{*}$	Perturbed initial conditions (Section 5.7.3)

Operational Symbols

∇	Linear gradient; or backward difference operator
$( ) \times ( )$	Vector cross product
$( ) \cdot ( )$	Vector dot product
E^{s}	Shifting operator (Section 6.1)
D	Differential operator (Section 6.1)
I	Identity operator
$(\dot{})$	First derivative with respect to time
$(\ddot{})$	Second derivative with respect to time
$(\hat{})$	Unit vector
$(\bar{})$	Vector
$(\_)$	Absolute phase difference (Section A.4)

$\mathcal{E}(\ )$	Expected value (expectation operator)
cov( )	Covariance
det	Determinant
var( )	Variance
$(\ )'$	First derivative with respect to the variable s (Chapter 5)
$(\ )''$	Second derivative with respect to the variable s (Chapter 5)
$(\ )^*$	Perturbed initial conditions (Section 5.7.3)
$f(\ )$	Function (Section 3.3.8)

INDEX

The index given on the following pages consists of an alphabetical list of significant topics contained in this document. Cross-referencing is used where appropriate. The notation appearing in parentheses after certain topics refers to the section or chapter primarily concerned with that topic. The hyphenated numbers refer to the pages where the specified topic is mentioned. A page number immediately following a section or chapter number indicates the beginning page of that section or chapter. For example, the following entry

Mean of estimate, (8.2.1) 8-6, 8-52

indicates that the "mean of estimate" is discussed in Section 8.2.1, which begins on page 8-6, and that it is also mentioned on page 8-52.

A

B

C

D

E

F

G

H

I

J

K

L

M

N

O

P

R

S

T

U

V

W